Forschungszentrum Jülich

Institut für Kernphysik
COSY

Stochastic Cooling of 10^{10} Protons at 3.24 GeV/C

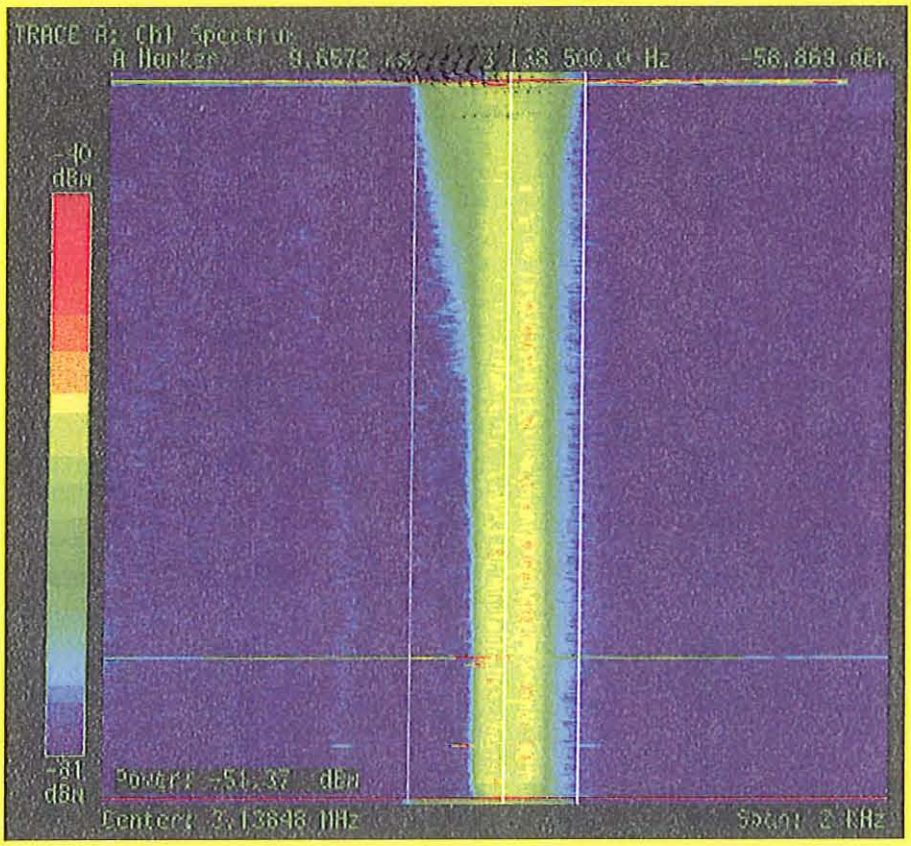

ANNUAL REPORT 1998

Jül-3640

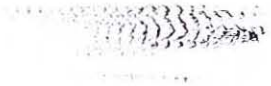

Forschungszentrum Jülich

Institut für Kernphysik
COSY

ANNUAL REPORT 1998

Berichte des Forschungszentrums Jülich ; 3640
ISSN 0944-2952
Institut für Kernphysik Jül-3640

Zu beziehen durch: Forschungszentrum Jülich GmbH · Zentralbibliothek
D-52425 Jülich · Bundesrepublik Deutschland
☎ 02461/61-6102 · Telefax: 02461/61-6103 · e-mail: zb-publikation@fz-juelich.de

Annual Report 1998

Institut für Kernphysik and COSY Research

Cover Picture

Graph of a spectrum analyser presenting information on energy and energy spread versus time of stochastically cooled beam during an internal experiment run. The time axis runs vertically from top to bottom displaying the behaviour over the full one-hour period after which the beam is dumped and a new cycle starts. Beam intensity is color coded spanning 40 dB from dark blue to red for highest values. It is evidenced how the brillance of the beam is raised dramatically after about 15 minutes of cooling. The measurement was taken during a COSY-11 run at a proton momentum of 3.24 GeV/c and 10^{10} protons in the ring. The plot demonstrates convincingly that effects of beam heating in the longitudinal and vertical phase space and energy degrading all resulting from beam-target interaction are fully compensated after reaching equilibrium. This state of affair constitutes an ideal situation to investigate reaction processes close threshold. An article on longitudinal stochastic cooling is contained in the report.

Professor O.W.B.Schult (right) and his successor Professor H. Ströher on the occasion of the colloquium in honor of Professor Schult on March 31,1998.

Professor O.W.B. Schult retired on March 31, 1998 as director of the Institute of Nuclear Physics II. During the more than 25 years serving in that position he has made key contributions to many fields. His early work on high precision gamma ray spectroscopy with high resolution crystal spectrometers was followed by nuclear structure investigations with a gas-filled magnetic separator (JOSEF) that was directly linked to the Juelich research reactor DIDO to study neutron rich spallation products. Among these was for example the double magic nucleus ^{132}Sn one of the few such nuclei which lie far from stability. He had been instrumental in the development of the magnetic spectrograph BIG KARL which was the largest experimental installation at the isochronous cyclotron JULIC and served for many years in the field of high resolution particle spectroscopy. Ideas to raise the luminosity and resolution of this instrument further spurred a series of evolutionary design concepts which ultimately culminated in the construction of COSY. With ANKE, a large magnetic spectrometer residing inside the accelerator ring specialized for zero to small angle spectroscopy with internal targets, he added a new chief experimental facility to the COSY ring.

Preface

This jointly prepared report compiles the activities of the year past of our institute, our partners from CANU and other international collaborations at COSY as well as experiments of our scientists that have been carried out at other laboratories.

Let me first mention a most notable event for our institute, the retirement of Professor O.W.B. Schult who had been in charge as director for the Institute of Experimental Nuclear Physics II for more than 25 years. With deep gratitude we remember his many contributions and scientific visions which have helped the institute to obtain with COSY and ANKE new powerful research instruments. We are fortunate that he will be still at our institute which allows us to benefit also in the future from his distinguished experience.

At the same time it is a great pleasure for me to welcome Professor Ströher, who seamlessly took over the now vacant position. His past activities had been centered at the University of Mainz doing research on electro- and photo-production of mesons and his name was closely connected with the installation and use of the TAPS spectrometer were he had been for three years the speaker for the international collaboration using this instrument. Fundamental work had been carried out with this spectrometer at the accelerators of GSI and MAMI. The research he is going to perform now at COSY, although different, is in many aspects complementary to his former field. He has taken over the responsibility for the scientific use of the new large spectrometer ANKE. The commissioning of this new instrument under his guidance, which was performed in three runs, has been very successful and first data is under analysis.

Top priorities for the accelerator team were the commissioning of the internal spectrometer ANKE, the optimization of stochastic cooling, stochastic extraction and the acceleration of polarized protons. Reliability scores of COSY have been as good as in the year before and the percentage of beam time for experiments has been further extended.

Beam stability problems induced by the new magnetic chicane of ANKE have all been solved and the accelerator has been verified to work up to the specified deflection angle of 10.6° of the spectrometer. Longitudinal stochastic cooling profited tremendously by a new optical notch filter system which has been routinely used for the ongoing research program at COSY-11. The effectiveness of stochastic extraction at higher energies was successfully boosted to over 65%, a crucial requirement for the MOMO K^+K^- low cross section measurement. We also succeeded to accelerate polarized protons up to the full energy of COSY conserving a high degree of polarization despite the crossing of several depolarizing resonances. First polarized beams were delivered to external experiments.

The time of flight spectrometer TOF has been fully mended by replacing about 50% of the scintillators of the ring detector which had prematurely deteriorated. Through the addition of the barrel detector, built in Rossendorf, TOF can now be operated with three big hodoscopes and a distance between target and "quirl"-detector of 3.3 m . TOF was in December the first experiment to use extracted polarized protons for the investigation of bremsstrahlung.

COSY-11 which made optimal use of stochastically cooled stored beam has been again very productive shedding light to the threshold production of η' and comparing the production of Λ and Σ° at low energies.

The GEM-collaboration succeeded in measuring for the first time $p\,d \rightarrow t\,\pi^+$ and $p\,d \rightarrow He\,\pi^\circ$ simultaneously over a large angular range at BIG KARL.

The EDDA collaboration has completed their unpolarized excitation function measurements and started their first measurements with a polarized atomic beam target. Their support has also been essential for optimizing the acceleration of polarized beams.

The MOMO collaboration was able for the first time to collect in a single run about 1800 K^+K^--events from the reaction p d $\rightarrow$ ^{3}He K^+ K^- in an exclusive measurement.

The efforts of the theoretical group were in consonance with the work carried out by the experimenters. Precise predictions for the threshold parameters of pion-nucleon scattering have been obtained in the framework of chiral perturbation theory, as well as an observable which is sensitive to isospin violation. In addition, a parameter-free prediction for the strange magnetic formfactor of the proton has been made. The meson-exchange model has allowed predictions for Phi-meson production in proton-proton scattering. A non-perturbative structure function of the nucleon has been developed enabling a unified description of the flavour asymmetry of the sea antiquarks and proton production in deep inelastic scattering.

The EUROBALL-collaboration studied options for gamma-ray tracking. It was found that the signal shapes of Ge-detectors depend on crystal orientation. This finding has direct implications with respect to the design of position sensitive germanium detectors for gamma rays.

Work on the European Spallation Source (ESS) has been intensified. A super conducting linac cavity was ordered to allow tests for its application in a super conducting linear accelerator. Furthermore, a fundamental physics program has been pursued on this matter and new experiments TETHYS and JESSICA have been proposed. To avoid restriction of the ongoing physics program we are looking for a possible extension of the experimental area.

The accomplishments summarized in this report would not have been possible without the dedication of our technicians and engineers, the IKP service groups, the colleagues of the infrastructure of the Forschungszentrum Juelich, and the students that have advanced the scientific case with their diploma and PhD-theses. The fruitful and amicable collaboration with CANU and the outside users is gratefully acknowledged, that has been a key element for the common success.

We also like to express our gratitude for the advice and help we have obtained by our advisory committees and for the commitment of the board of directors for COSY.

Rudolf Maier

INSTITUTE FOR NUCLEAR PHYSICS

Managing director:	Prof. Dr. R. Maier
Experimental Nuclear Physics I, director:	Prof. Dr. K. Kilian
Accelerator division, head of the:	Prof. Dr. R. Maier
Experimental Nuclear Physics II, director:	Prof. Dr. O. Schult (until March 31st, 1998) Prof. Dr. H. Ströher (since April 1st, 1998)
Theoretical Physics, director:	Prof. Dr. J. Speth

Forschungszentrum Jülich GmbH

D-52425 Jülich, Germany

CONTENTS

1.2 Experiments at External Facilities

2. Nuclear Spectroscopy

II. Theoretical Nuclear Physics

3. MEDIUM AND HIGH ENERGY PHYSICS

4. NUCLEAR STRUCTURE AND REACTION MECHANISM

III. Accelerator Division

5. COOLER SYNCHROTRON COSY

IV. EUROPEAN SPALLATION NEUTRON SOURCE (ESS)

9. TARGET PHYSICS

10. ACCELERATOR COMPONENTS

V. Technical Developments

11. DATA ACQUISITION; ELECTRONICS; SEMICONDUCTOR DETECTRORS; TARGETS

I. Experimental Nuclear Physics

1. MEDIUM ENERGY PHYSICS

1.1 Experiments at COSY

1.2 Experiments at External Facilities

2. NUCLEAR SPECTROSCOPY

1.1 Experiments at COSY

Status of the Technical Development of the TOF - Detector

R. Bilger[3], H. Clement[3], K. Döring[2], A. Erhardt[3], D. Filges[1], H. Hadamek[1], G. Hansen[2], H. Kämmerling[2], R. Klein[1], K. Kilian[1], J. Kress[3], C. Meixner[2], N. Paul[1], W. Renftle[2], E. Roderburg[1], H. Stechemesser[2], H. Wyrwich[2], for the TOF-Collaboration
[1] Institut für Kernphysik, [2]Zentralabteilung Technologie, [3]Physikalisches Institut Universität Tübingen

1. The new "Ring –Detector"

a) Manufacturing the new scintillator layers.

The new high class scintillator material BC 408 had been delivered from BICRON. The scintillators which have to replace the two useless layers of the "Ring-Detector" are complete manufactured at the Forschungszentrum Jülich workshop. The scintillator material had been cut and milled with special diamond tools and finished by polishing with polishing tools plus polishing paste. Every step of this very sensitive process are made under conditions to avoid stress to the scintillator material. The result are scintillators with best surface and high light output (see figure 1).

b) Assembling of the "Ring-Detector"

To assemble the "Ring-Detector" without giving stress to the scintillator-elements we constructed and build in cooperation with ZAT of FZ-Jülich two support rings of low density material. These rings are placed between layer 1 and layer 2 respectively layer 2 and layer 3 of the detector. Short 0.3 mm thick carbon fiber foils are inserted in CNC laser cuted slits. These foils support the long scintillators and held it in positions.

The new assembled "Ring-Detector" is now a high precision part of the TOF-Detector scintillator hodoscope (see figure 2) build of excellent scintillator material.

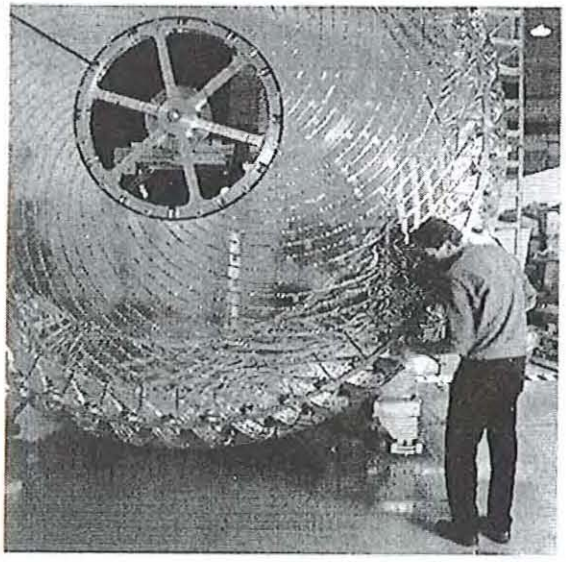

Fig. 1: The new build "Ring-Detector" with the nave support for mounting still inside.

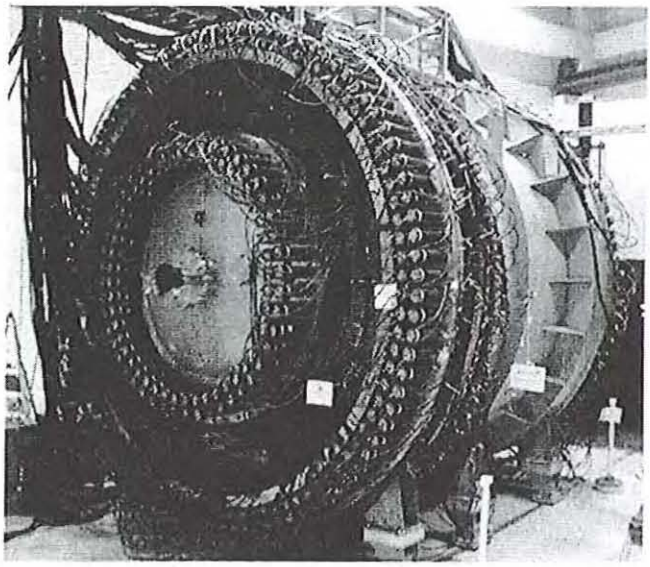

Fig. 2: The completed "One Barrel TOF-Detector" with "Ring-Detector" and "Quirl-Detector"

2. Progress "Three Layer Barrel Detector"

To start producing the scintillators for the "Three Layer Barrel Detector" several questions have to be answered before.

The ZAT of FZ-Jülich made investigations to find out the influence of heating up and cooling down the scintillators for different temperature ranges and temperature gradients. The change of the physical properties and dimensions are recorded. Also the quality of the surface of each scintillator strip has to be checked when it is delivered and also after heating procedure and bending. Therefore a new optical system has been developed to give quantitative information about the surface and to compare different scintillators. The search for the right material surface on which the heated up and soften scintillators can be bend was an other point of investigation. An air oven with fine regulating temperature ramps and very small temperature differences inside has been ordered. This oven is big and long enough to handle the 4.40 m long scintillators inside. A few original shaped scintillator strips are ordered to start first bending tests in 1999.

3. Energy Detector

To get additional information about the particles, which are produced in the TOF-target, we constructed a detector to measure the energy of these particles. With the additional stop signal we can calculate the mass of it for example.

In cooperation with a group of the University of Tübingen a detector concept of 84 hexagonal shaped scintillator bulks are developed, placed directly behind the "Quirl-Detector", but still in the vacuum region of the TOF-Detector. Figure 4 shows the detector arrangement. Each of the detector bulks has a width over the flats of 140 mm and a length of 450 mm. (s. fig. 3) The design of the detector is ready. The scintillators are delivered from BICRON and tested in Tübingen.

The making of the detail construction is given to the ZAT of FZ-Jülich, to make the drawings for manufacturing the pieces. Finite Elements – (FE) calculations have been made for the complete TOF-Detector installation including the new "Energy-Detector". These calculations shows the stress in the material and also the deformation of all pieces coming from the outer atmospheric pressure and the additional load of the 80 mm thick end cap with 85 big holes in it, the 84 scintillators, the supporting construction and the magnetic shield outside. To bring the scintillators of the "Energy-Detector" as close as possible to the "Quirl-Detector", the physics of the measuring system make it necessary, the whole "Quirl-Detector" has to be reassembled and the nave of it reconstructed. The complete system will be installed and tested in 1999.

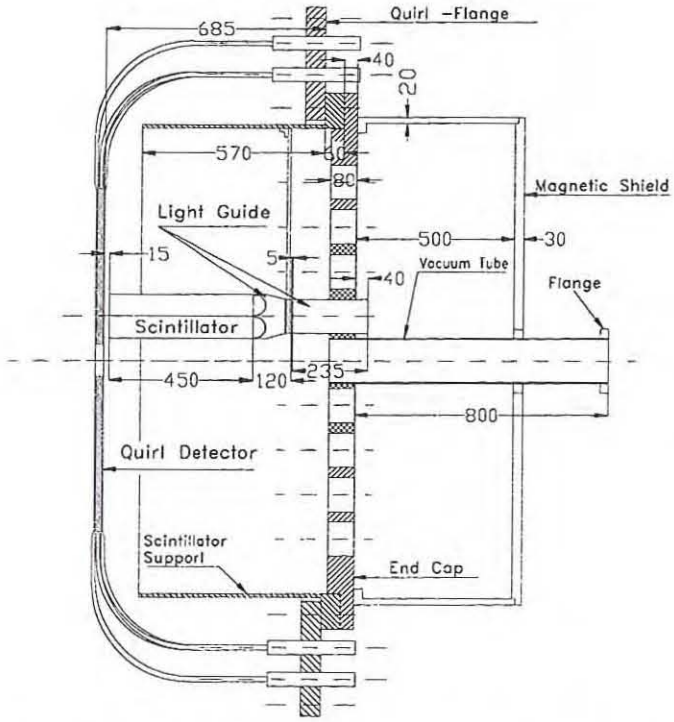

Fig. 3: Cross Section of the "Quirl-Detector" including the "Energy-Detector" with only one Scintillator installed.

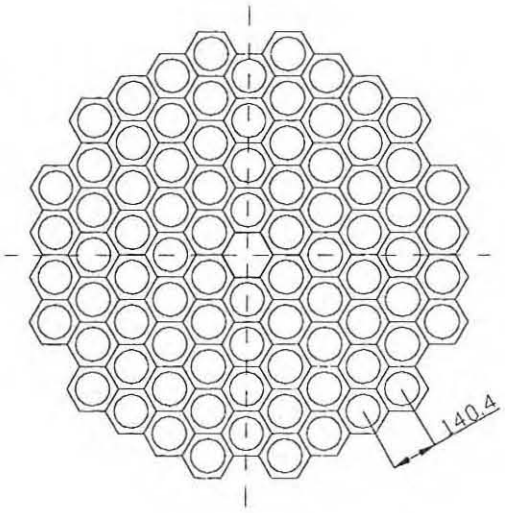

Fig. 4: Arrangement of the 84 Scintillator Bulks, seen from the Back Side

Associated Strangeness Production at COSY-TOF*

The COSY-TOF Collaboration

Experiment E7 (Spokesperson: W. Eyrich)

The associated strangeness production in elementary reactions like pp → KYN close to reaction thresholds is one of the main topics to be investigated at COSY-TOF. In case of the channel pp → $K^+\Lambda p$ several measurements at beam momenta of 2.50, 2.59, 2.68, 2.75 and 2.85 GeV/c have been performed. The concept of the event reconstruction is based on the identification of the delayed decay of the Λ-hyperon into two charged particles p and π^-, which gives a unique signature. Since the highly granulated detector covers almost the full phase space all differential distributions as well as total cross sections and the Λ-polarization can be extracted from the data. The results of the 1996 runs at beam momenta of 2.50 and 2.75 GeV/c have already been published in parts in [1]. For the 1998 measurements at 2.59, 2.68 and 2.85 GeV/c we expect a total yield of about 10000 completely reconstructed Λ-events giving a strongly improved database for further analysis. As an example, the missing mass distribution of reconstructed Λ-hyperons for a subsample of the 2.85 GeV/c data is given in figure 1.

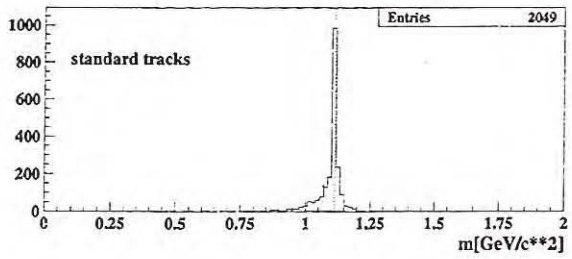

Fig. 1: Missing mass distribution of reconstructed Λ-hyperons at p_{beam} = 2.85 GeV/c

In order to improve precision and redundancy in event reconstruction and to get access to other reaction channels like pp → $K^+\Sigma^+n$ or $K^0\Sigma^+p$, the startdetector system has been extended for the 1998 runs by two new components:

- a double sided silicon ring microstrip detector with 128 segments on the back in addition to the existing 100 concentric rings
- an intermediate fiber hodoscope with 2 layers of 192 scintillating fibers each

Especially, the additional information of the microstrip detector is necessary to measure the short tracks of the Σ^+-hyperons near the target before they decay into $p\pi^0$ or $n\pi^+$, which (in contrast to the Λ-decay) only gives a kink in the charged track. Furthermore,

- a large area scintillator wall

has been added behind TOF for the measurement of both primary and decay neutrons appearing in the Σ^+-channel (see figure 2).

* supported by BMBF and FZ Jülich

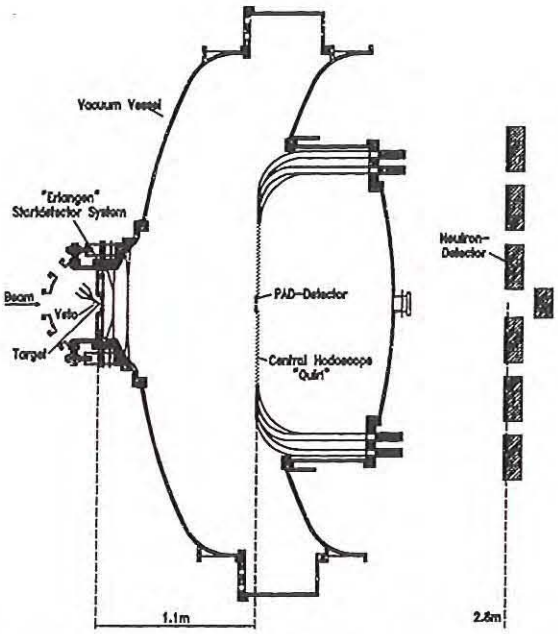

Fig. 2: Scheme of the TOF setup 1998

The analysis of the 2.85 GeV/c data is in progress, a first event of the type $K^0\Sigma^+p$ could be extracted and is shown together with the startdetector scheme in figure 3.

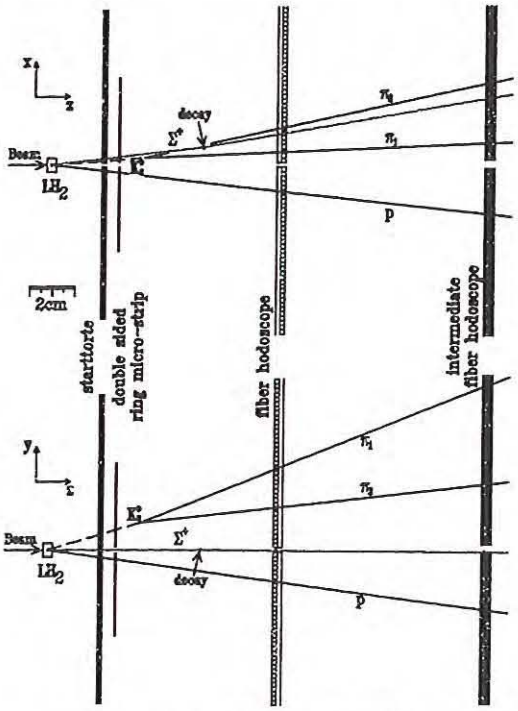

Fig. 3: Side view of the first identified $K^0\Sigma^+p$-event

Future measurements with an extended TOF version will also allow to investigate the Σ^0-production. Moreover, a polarized beam will be used at COSY-TOF.

[1] R. Bilger et al., Phys. Lett. **B 420** (1998), 217

Two Step Mechanism for Meson Production

A. Hassan*, K. Kilian, T. Sefzick

The meson production in the proton-deuteron system at proton momenta below the threshold of the free nucleon-nucleon collisions should allow to distinguish different reaction mechanisms. At these beam momenta the energy necessary for production of the corresponding meson can be gained in a single step reaction from the internal motion of nucleons inside the deuteron or by a two step reaction. The simplest example might be: $pd \rightarrow {}^3He\,\eta$ divided into step **A**: $pp \rightarrow d\pi^+$ and step **B**: $\pi^+ n \rightarrow \eta p$.

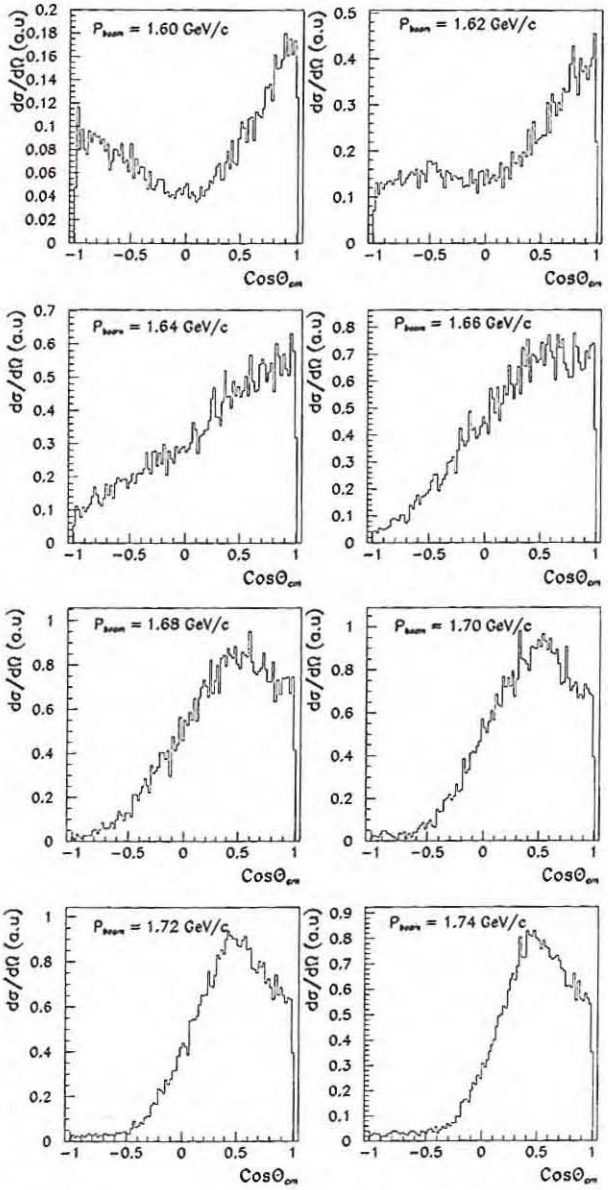

Figure 1: Shape of the angular distribution of ^3He predicted by the two step model in $pd \rightarrow {}^3He\,\eta$.

It was shown by Kilian and Nann [1] that the meson production in the two body proton deuteron interaction ($pd \rightarrow {}^3He\,X$ or $pd \rightarrow {}^3H\,X^+$) might be enhanced in a narrow beam energy and angular range if it proceeds by a two step mechanism due to a selective fusion of the three outgoing baryons because they are matched in velocity. Experimental proof of such an enhancement in the cross section of $pd \rightarrow {}^3He\,\eta$ would proof the importance of the two step reaction. The contribution of the two step mechanism alone to the cross section of the reaction $pd \rightarrow {}^3He\,\eta$ is simulated. An approach is used which is relativistically correct. For the first time the folding process includes the angular and energy dependence of the two subsequent steps and the correct off mass shell situation also in the ^3He fusion and not only as in [1] with the bound reaction partners from the original target deuteron. The angular distribution predicted by the two step process (Fig. 1) shows a forward peak of ^3He in the center of mass system and it enhances the cross section in a rather narrow energy range (Fig. 2). It has its maximum contribution to the total cross section at approximately 50 MeV excess energy [2]. The forward peak of ^3He is in contrast to the direct single step reaction which is known to create a rise of ^3He in the backward direction. An experimental search for this effect is planned at COSY [3].

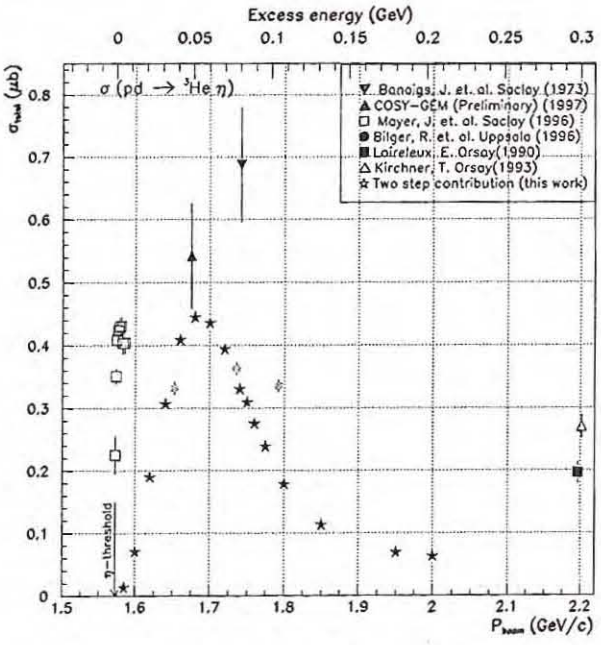

Figure 2: Shape of the cross section contribution of the two step model to the reaction $pd \rightarrow {}^3He$ as a function of beam momentum and excess energy. The calibration may not be precise.

References:

[1] K. Kilian and H. Nann, contribution to the workshop on "Particle production near threshold", Nashville, 1990, AIP conference proceedings 22, 185 (1990)

[2] Hassan A., Thesis Zagazige Univ. Cairo, Egypt, 1998

[3] COSY Proposal Nr. 7

* permanent address: Atomic Energy Authority, NRC Cairo, Egypt

Improving the cool down time of the liquid H_2 /D_2 target using aluminum in comparison with copper

S. Abdel-Samad*, U. Goldmann, K. Kilian, R. Klein

The liquid hydrogen/deuterium target [1,2] is used in the external COSY experiments TOF, GEM and MOMO. The time during the experiment is one of the most valuable parameters. It is important to save time during cool down the target to the working temperature or heat it up to the room temperature or for purposes of evaporating condensates. The time needed depends on the available cooling power, heat conductivity and the heat capacity of the arrangement [3,4]. At liquid hydrogen temperature aluminum has three times higher thermal conductivity than copper. By calculations we found that in our apparatus the cool down time with an aluminum conductor is about 0.7 of that for a version with copper conductor used so far.

Experimental results are shown in Figure 1, for copper or aluminum conductor of 275 mm length and 16 mm diameter (350 gCu, 110 gAl). Figure 1 shows that the cool-down time of the target to 16 K using copper is 160 minutes and by using aluminum it is only 100 minutes. Aluminum saves 60 minutes in cool down time and a similar time also in warming up to room temperature.

Note that aluminum gives faster cooling down even at higher temperatures where its thermal conductivity is less than copper. This is due to the lower heat capacity of Aluminum.

Figure 2 shows the measured results for the thermal conductivity of our copper and aluminum conductors as a function of temperature. As shown, at low temperatures the thermal conductivity of our aluminum material is nearly three times higher than that for our copper. This means that at the working conditions of the target (liquid hydrogen/ liquid deuterium) we have a faster response of the temperature stabilization system.

Aluminum instead of copper might allows for much longer conductors between the cooling machine and the target cell. This could be important for the future.

Silver remains to be tested. It has even higher thermal conductivity than aluminum.

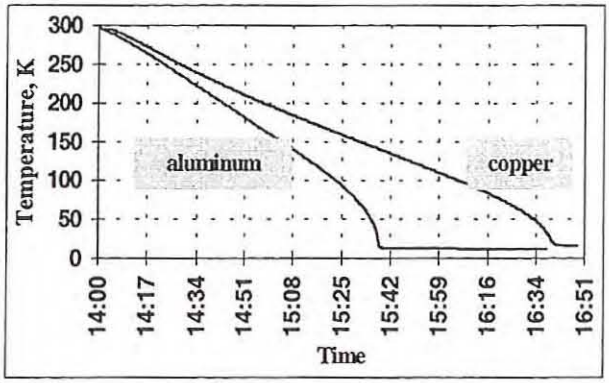

Fig. 1: Comparison between the cool-down time of copper and aluminum.

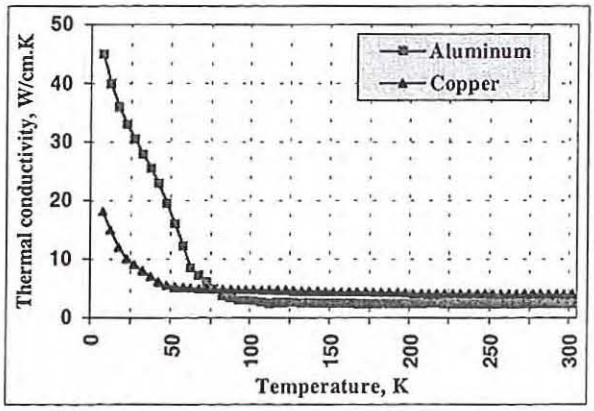

Fig. 2: Thermal conductivity of copper and aluminum as a function of temperature.

References:

1. V. Jaeckle et al., "A liquid hydrogen/ deuterium target with very thin windows" Nucl. Instr. And Meth. A347 (1994) 15.
2. Hassan et al.," The target area of the external COSY experiments" Nuclear Physics A626 (1997) P 435-438.
3. F. Pobell "Matter and methods at low temperatures" second edition, Springer (1996).
4. P.G. Klemens "Low temperature thermal conductivity in solid" Cryogenics (1995).

* NRC, AEA, Egypt.

Status of the development of a straw-tracker for the TOF experiment

C.Fanara, D.Filges, R.Geyer, K.Kilian, K. Nünighoff, M.Schmitz

The studies of the properties of a straw detector prototype went on. The gas leakage of a single tube was determined to be $1.0*10^{-5}$ mbar*l/s, which is in agreement to the theoretical expectation for the diffusion through the 30 µm thick mylar foil. No changes were found during four weeks under vacuum conditions. The requiered pressure of 10^{-3} mbar in the TOF vacuum system can be achieved even with the complete tracker with its 3,000 channels.

The influence of the gravitation on a horizontal tube led to a deflection of about 2 mm. It was found that overpressure inside the tubes has a minor effect on this deflection.

A special crimping technique was developed to fix and center the 20 µm thick anode tungsten wires under a tension of 0.4 N. 1 mm thick copper tubes with an inner hole of 100 µm are being used as crimp sleeves. The maximum load the wire fixation holds was tested for different adjustments of the crimping tool. As a parameter the smallest thickness of the sleeve after crimping was used (Fig. 1). The crimping method was tested more than 100 times in a range between 610 µm and 690 µm. In all tests a wire tension of larger than 0.8 N was reached which is just below the tensile strength of the wire itself.

The concept of the readout electronics has been further completed. The signals of the anodes will be forwarded via very thin kapton-cables (thinner than 100 µm) to the preamplifier. The ASD8B chip [1] will be used. This chip contains amplifier, shaper and discriminator for 8 channels and is a special development for straw-detectors of the university of Pensylvania. The sensitivity of the amplifier allows for thresholds of 2-3 fC which is low enough to operate the straw detectors at moderate gas amplification of a few 10^4. The drift time information will be digitalized by VME TDC modules. We are still testing two different types of CAEN (CAEN 767 [2] and CAEN 673 [3]). Both modules use a deadtimeless conversion method and have a high integration density. First results show that with both of them a minimum of 1,000 events per second can be converted which fullfills the needs of the TOF experiment.

The first 200 straw tubes for the first complete double plane are nearly finished. The frame and readout-electronics are under construction. This plane will be the basis for last tests and optimizations for the final version of the detector.

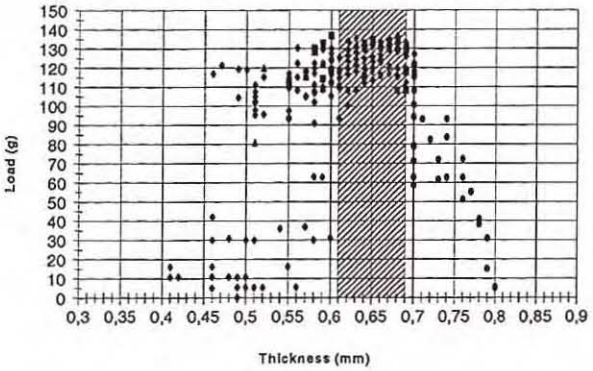

Fig.1 The diagram shows the maximum load before the wire breaks or slides as a function of the smallest thickness after crimping. On the right side of the marked area the wire will slip through the sleeve and on the left side the wire will break.

References:

[1] F.M. Newcomer et al., *A Fast, Low Power, Amplifier-Shaper-Discriminator for High Rate Straw Tracking Systems*

[2] J.Christiansen, *32 channel general purpose time to digital converter*, draft version 0.3, CERN/ECP-MIC

[3] M.Passaseo et al., *A TDC integrated circuit for drift chamber read out*, Nucl. Inst. and Meth. A 367 (1995) 418-421

First Research with ANKE

K. Sistemich for the ANKE collaboration

The magnetic spectrometer ANKE for the detection of products from proton-induced reactions at internal targets has been installed in May 1998 in the COSY accelerator ring. The commissioning of COSY with this additional installation, the tests of the facility with its detectors as well as its calibration have been carried out. First investigations of the production of K^+-mesons in proton-carbon collisions at projectile energies above and below the free nucleon-nucleon threshold of 1.6 GeV have also been performed.

ANKE consists of three magnets (D1, D2, D3), see fig. 1, which, in the straight cooling section, guide the circulating COSY beam through a thin target and allow the separation of ejectiles, emitted in forward and backward direction, from the beam and their analysis with respect to emission angle and momentum. Present research goals at ANKE are studies of nuclear medium effects on elementary processes as in the subthreshold K^+- and K^- - production and in the deuteron break-up. Also phenomena associated with the production of mesons like π, ω, ϕ and a_0^+, in proton-proton and proton-neutron interactions, will be investigated.

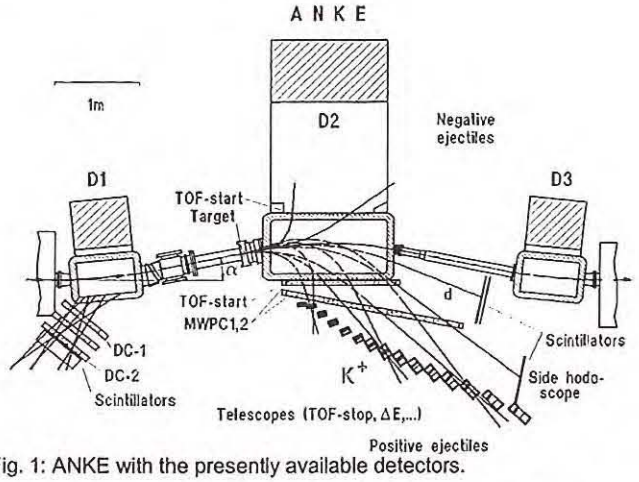

Fig. 1: ANKE with the presently available detectors.

The first step towards the scientific use of ANKE was the development of the COSY acceleration procedure with these new components inside the ring. The facility affects the acceleration because of a change of the orbit, the occurrence of eddy currents (in particular in the vacuum chambers of the dipoles) and the presence of higher multipole components in the magnetic dipole fields. The change of the orbit length does not exceed the acceptable variation of orbits in COSY, in spite of the fact that deflections with angles up to $\alpha = 10.6°$ are used at D1. (Nota bene: the deflection angle can be optimized for each experiment through a convenient choice of the field strengths in the ANKE magnets and a displacement of D2 together with the target!). Thus it could be accounted for by a proper setting of the COSY parameters. The eddy currents, although small because of a special construction of thin vacuum chambers, and the multipole components caused more serious problems which were overcome through the development of a new tune for the components of COSY's straight section and the use of back-leg windings. Acceleration of high intensity ($n \leq 4 \cdot 10^{10}$) proton beams up to energies of 2.3 GeV as well as with the maximum deflection angle in ANKE is now routinely achieved.

The next tasks of the preparation of ANKE for experiments were the development of procedures to optimize the overlap of the beam with the target and tests of the detector performance. Strip targets of carbon and polyethylene with typical dimensions of 2 x 20 mm^2 and thicknesses between 40 and 200 $\mu g/cm^2$ have been used. It turned out that the best procedure is to move the beam after acceleration towards the target. Sufficiently constant reaction rates at luminosities of up to about 10^{32} cm^{-2} s^{-1} could be achieved: the beam is moved swiftly to a touching position and then slowly further with varying speed.

The detector properties have been tested with protons and pions from pC interactions and with mono-energetic pions from the two body reaction $pp \rightarrow d\pi^+$ induced at polyethylene strips. Various energies of pions were used with a change of projectile energies between about 320 and 520 MeV. The detector system which has been used during the studies in 1998 consisted of the side detector system near D2 and two hodoscopes in more forward direction. The ejectiles which leave the vacuum chamber through 0.5 mm thick Al-windows at the side and at the far end can be studied. The ejectiles reaching the side detector system are horizontally focused according to their momentum. This detector system is particularly demanding since it is made to allow, in the subthreshold studies, the identification of K^+-mesons in an up to 10^6 times more intense background of pions and protons. The forward hodoscopes detected the fast deuterons from the $pp \rightarrow d\pi^+$ reaction.

Particles reaching the same side telescope have the same momentum provided they originate from the target. Hence, flight times and energy losses discriminate K^+-mesons from pions and protons. The ΔE difference between pions and kaons is enlarged through the use of Cu degraders which slow down the latter so that their energy loss in the scintillator behind it, is increased. The detector dimensions have been developed on the basis of laboratory tests and of results of extended Monte Carlo calculations. It was to be confirmed under the experimental conditions at COSY that the detector components have the desired specifications, in particular that a time resolution of about 600 ps between the thin and long start detectors, placed in the strong stray field of D2, and the stop scintillator counters can be achieved. The tests had also to check the performance of the two multiwire proportional chambers which are used for the identification of particles stemming from the target and the determination of their momenta and emission angles.

The measurements on K^+ production with carbon targets have been performed at projectile energies of T_p = 2.3, 2.2, 1.8, 1.5 and 1.2 GeV and hence above and below the free nucleon-nucleon threshold. While the measurements above threshold, because of the larger cross sections, served mainly for tests of the K^+-detection system, the ones below were „production runs" for the determination of inclusive momentum spectra for forward emitted kaons in the range from about 150 to 600 MeV/c. The tests showed that the detector system largely fulfils the demands, where mending was needed and improvements could be made. The production runs, according to the present status of the data analysis, were successful. K^+-mesons could be identified also at the lowest value of T_p where the production cross section is low, but where the co-operative effects of the nucleons inside the carbon nucleus must be especially pronounced. The results suggest that a measurement even at T_p=1.0 GeV should be possible at ANKE; it is scheduled for June 1999.

The experiments at ANKE have also been used to test and improve the electronical set-up, the data acquisition and the data analysis software. The data acquisition system must allow the handling of very high rates, since otherwise the intense background would hamper an efficient use of the available luminosity for meaningful K^+-studies. In fact, rates of more than 5000 events/s can be stored. The installation of a fast trigger system which suppresses background through the selection of allowed start-stop detector combinations is still necessary for the measurement at T_p=1.0 GeV.

Parallel to these studies, the ANKE collaboration has continued the development of additional detectors: multi-wire chambers for the forward detector system and backward detectors near D1 (tests), considerations concerning spectator and vertex detectors close to the target and detectors for the study of K^--mesons which can be investigated at the side of D2 opposite the K^+ system. Also additional targets are being set up and built: a cluster jet target for H_2 and D_2 which is in the test phase outside the COSY ring, and a pellet target for H_2 and D_2 but also for heavier gases, as well as a storage cell target with an atomic beam source for polarized protons and deuterons. Finally the development of the scientific program for ANKE has been continued. A proposal to study the ω and ϕ production in pd interactions has been accepted by the PAC.

Detailed descriptions of the activities of the ANKE collaboration are presented in separate contributions to this report.

First test of the angular acceptance of the spectrometer dipole D2 at ANKE

M. Büscher, H. Junghans and V. Koptev[1]

Data taken during the first ANKE beam times were used to determine the angular acceptance and momentum resolution [1] of the spectrometer dipole D2. The goal of the first data analyses presented here is to proof that the design values for the horizontal angular acceptance $\Delta\vartheta = \pm 10°$ can be verified under experimental conditions.

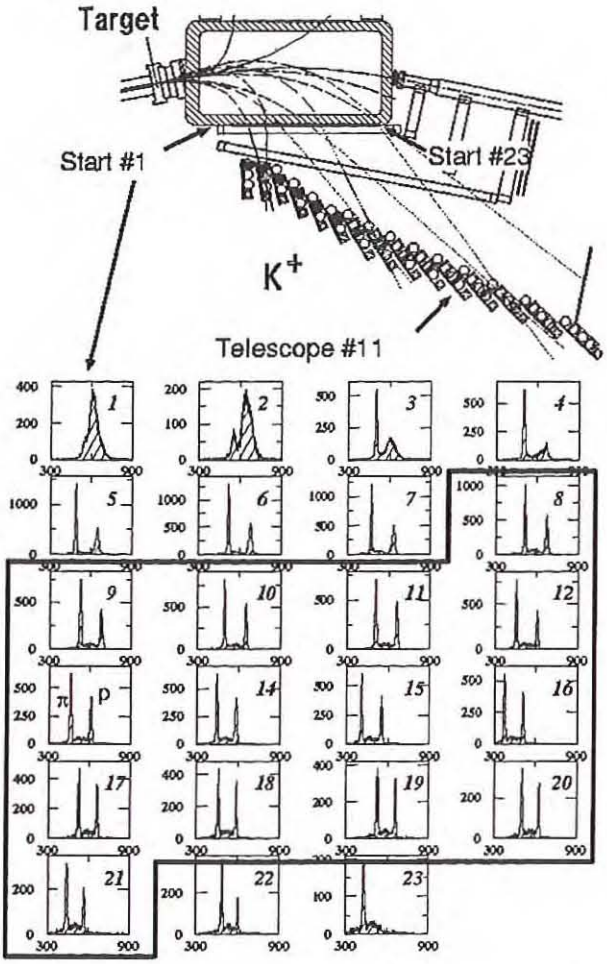

Figure 1: Time-of-flight spectra for telescope #11 and all 23 start counters. Indicated by the box are spectra with narrow TOF peaks for protons indicating a well defined momentum of these particles.

Fig. 1 shows 23 time-of-flight spectra for ejectiles passing through the TOF-start counters which are located close to the exit window of the vacuum chamber of D2 and the TOF-stop counter in telescope #11. In most of the spectra one can see two narrow peaks stemming from pions and protons produced in the target and deflected in D2 onto the telescope. Within the angular acceptance of D2 all ejectiles hitting a certain telescope should have a well defined momentum since all telescopes are located in the focal surface of D2. In case of telescope #11 the stop counter should be reached by ejectiles with momenta $p = 419 \ldots 454$ MeV/c for a field strength of $B = 1.54$ T in D2 which was used during the measurements. Thus, the TOF distributions for these particles show narrow peaks with a width of ~ 600 ps which is basically given by the intrinsic counter resolution. Such peaks are visible e.g. for start counter #13 which corresponds to an emission angle at the target of $\vartheta \approx 0°$.

For emission angles larger than $|\vartheta| \approx 10°$ the focussing properties of D2 deteriorate and ejectiles with momenta outside the nominal values reach the telescopes. Thus, one expects that the two clear peaks first smear out and finally vanish when leaving the angular acceptance of D2. This can be seen in Fig. 1 for start counters with low and high numbers. The box in the figure (start counters #8–21) indicates spectra where the width of proton TOF distribution is ~ 600 ps. Our analysis showed that for start #7 and #22 this width already increases. It should be noted that the width of the pion peaks is less effected since the speed of pions (due to their lower mass) depends weaker on their momenta than in the case of protons.

The start counters indicated by the box in Fig. 1 correspond to emission angles at the target of $\vartheta \approx -10 \ldots +14°$. For different telescopes in the focal surface and hence for ejectiles with different momenta similar angular ranges with good momentum separation were found in our analysis. Thus, we conclude that D2 meets the design values of the horizontal angular acceptance.

References:

[1] G. Borchert et al., *contribution to this report*, p.

[1] St. Petersburg Nuclear Physics Institute

First analysis of the reaction pp $\rightarrow$ pnπ^+ measured at ANKE

G. Borchert, M. Büscher, S. Dymov*, V. Komarov*, A. Kulikov*, V. Kurbatov*, S. Yaschenko*

The calibration of the ANKE setup is being done using the reaction pp $\rightarrow$ dπ^+. In this process also data on the reaction pp $\rightarrow$ pnπ^+ are obtained which allows the study of the two-nucleon system at small effective mass [1]. Here we give a short summary of the analysis of data obtained during a beam-time in July 1998. The data were obtained under the following conditions: beam momentum $p_{\mathrm{beam}} = 1.036$ GeV/c, deflection angle of the COSY beam in ANKE 10.5°, one run with a carbon target, a second with a polyethylene target. The trigger conditions in both runs were $(\sum_4^{23}\mathrm{START}) \cdot (\sum(\mathrm{STOP_i} \cdot \Delta \mathrm{E_i}))$. These conditions were chosen such that the peak from π^+ mesons produced in the calibration reaction pp $\rightarrow$ dπ^+ was located in STOP telescope 13 [2]. Thus, for normalization purposes (subtraction of CH_2 and C data) we used STOP telescope 15 where only pions from carbon can be detected [3]. Only events with one charged particle in the Side Detector were used for the analysis.

In Fig. 1 the spectrum of the reduced missing mass squared is shown for particles hitting telescope 13 where in coincidence a fast particle was detected in the Forward Hodoscope [3]. The spectrum is the difference between the corresponding spectra obtained for CH_2 and C targets.

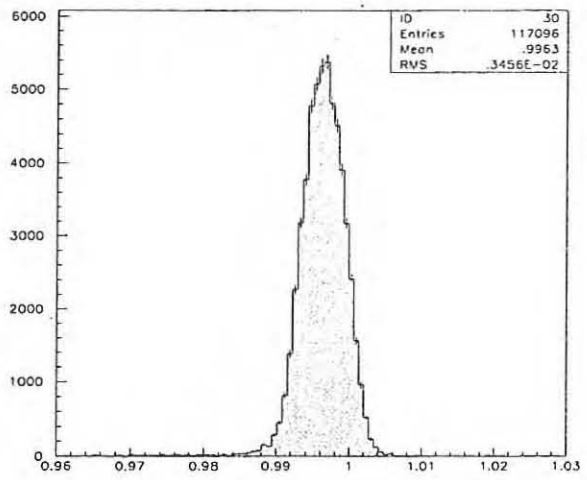

Figure 1: Reduced missing mass squared spectrum for STOP13

The reduced missing mass squared was calculated according to the formula

$$M_{\mathrm{x}}^2 = [(E_{\mathrm{beam}} + m_{\mathrm{p}} - E_\pi)^2 - (\vec{p}_{\mathrm{beam}} - \vec{p}_\pi)^2]/{m_{\mathrm{d}}}^2,$$

where E_{beam}, $\vec{p}_{\mathrm{beam}}$ are the energy and momentum of the proton beam, E_π, $\vec{p}_\pi$ the same for the ejectile pion. m_{p}, m_{d} are the masses of the proton and deuteron, respectively.

Under the conditions required, only pions can be detected in the Side Detector and a proton or deuteron hits the Forward Hodoscope. It is seen that there is a clear peak at ${M_{\mathrm{x}}}^2/{m_{\mathrm{d}}}^2$ slightly less than 1. The reasons for the small shift is still under investigation. In Fig.2 the reduced missing mass squared spectra for STOP11 and STOP12 are shown under the same conditions as for Fig. 1.

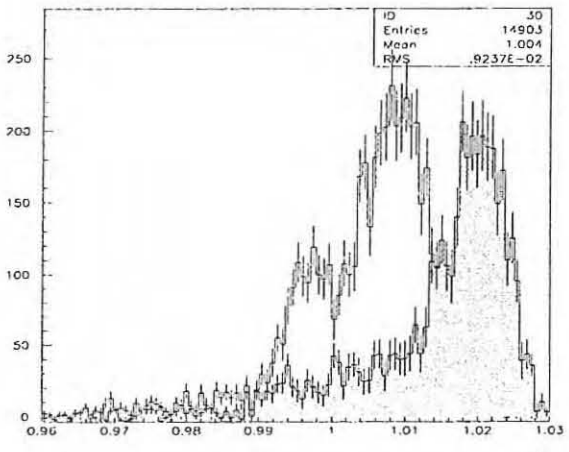

Figure 2: Reduced missing mass squared spectrum for STOP11 (filled) and STOP12

The small peak at missing mass below 1 for STOP12 stays at the same position as for STOP13 and corresponds to pions from the calibration reaction pp $\rightarrow$ dπ^+. Events with a missing mass larger than 1 can be attributed to the one-pion production reaction pp $\rightarrow$ pnπ^+.

The accuracy of the reconstructed missing mass in the region of the deuteron mass is equal to $\sigma_{M_{\mathrm{x}}} = 1.7$ MeV/c^2. The accuracy in the pion momentum at $p_{\pi+} \approx 282$ MeV/c is estimated to be $\sigma_{(\delta p_\pi / p_\pi)} = 1.0$ %. These numbers are in good agreement with estimates obtained from simulation calculations [4].

References:

[1] COSY Proposal #38, "Nucleon-nucleon Final State Interactions in Single Pion Production", IKP FZ Jülich 1997

[2] M. Büscher et al, IKP Ann. Rep. 1996, FZ Jülich, (1997)

[3] G. Borchert et al., *contribution to this report*, p.

[4] V.A. Artemov et al, IKP Ann. Rep. 1996, FZ Jülich, (1997)

* JINR, Dubna, Russia

The work is supported by grant RFBR N 96-02-17215

Detection of η-, η'-, ω- and a_0^0- mesons with ANKE via their decays containing photons in the final state

M. Büscher*, Ye.S. Golubeva[1,*], L.A. Kondratyuk[2,*] and H. Ströher

It was proposed recently [1] to study at ANKE the reaction $pd \to d\omega p_{sp}$ (1) detecting the final deuteron and proton-spectator and identifying the ω-meson in the missing mass distribution. This method can be applied if the signal-to-background ratio is not too small. The momentum distribution of proton-spectators has a sharp maximum at about 60 MeV/c. If events with spectator momenta 30–90 MeV/c are considered then there is a clean signal of reaction (1) because of the comparatively large cross section of the reaction $pn \to d\omega$ ($\sim 10 - 20$ μb at 1.9–1.95 GeV). It can be measured even with a moderate resolution of about 5–10 MeV/c^2 for the missing mass. A different situation arises if one wants to measure the $\omega - p$ elastic cross section by selecting events with fast final protons that receive a significant recoil from the elastic collision with the ω. The relative contribution of the rescattering term is about a few percent as compared to the spectator term. Therefore, the selection of reaction (1) is more difficult because the relative contribution of the background due to the misidentification of protons as deuterons will be larger by about two orders of magnitude. Moreover, the efficiency to detect fast scattered protons is lower. Therefore, it will be important to identify the ω-meson by measuring its radiative decay $\omega \to \pi^0\gamma \to 3\gamma$ (B.R. 8.5%).

Other interesting reactions which can be studied at ANKE are, for example, $pd \to d\eta(\gamma\gamma)p_{sp}$ (2), $pd \to d\eta'(\gamma\gamma)p_{sp}$ (3), $pd \to da_0^0(\pi^0\eta)p_{sp} \to d(4\gamma)p_{sp}$ (4), $pp \to ppa_0^0(\pi^0\eta) \to pp(4\gamma)$ (5). The cross section of η' production in the reaction $pn \to d\eta'$ can be about 200 nb at 2.6 GeV [2]. The cross section of a_0^0 production in the reaction $pn \to da_0^0$ is expected to be comparably large [3]. This means that for the discrimination of reactions (3)-(4) (and apparently (5)) against background particles it is also desirable to directly identify the η'- and a_0^0-mesons by measuring their decays $\eta' \to \gamma\gamma$ (B.R. 2.11%) and $a_0^0 \to \pi^0\eta \to 4\gamma$ (dominant decay), which contain photons in the final state.

The development of a detector for neutral particles for ANKE has begun. It could consist of $PbWO_4$, a fast and compact scintillator material with a radiation length of only 9.38 mm [4]. For acceptance estimates we have assumed a detector in the shape of a hollow cylinder with an inner diameter of 12 cm, a thickness of 15 cm and a length of about 20 cm. It covers an angular range of $\vartheta_\gamma \approx 20° \ldots 100°$. It could be combined with a high acceptance spectator counter. The detection of the deuterons in the forward detectors of ANKE is described in [1].

A typical result of our simulations for reaction (1) at 2 GeV is presented in Figs.1 a and b. In Fig.1 a we show a two-dimensional plot which describes the correlation between the photon angle and momentum. It is seen that the main part of photons can hit the detector. The solid curve in Fig.1 b describes the probability that all three photons hit the detector as a function of the maximal value of the backward angle Θ_b, covered by the detector. The dashed curve describes the same probability with a cut on the deuteron forward angle $\Theta_d \leq 5°$ corresponding to the angular acceptance of ANKE. In case of the dotted curve a second cut has been applied: $\Theta_d \leq 5°$ and $p_{sp} \geq 50$ MeV/c. The maximal value of the probability is about 0.5 for $\Theta_b \approx 100°$. In the case of two photons (reactions (2) and (3)) the maximal value of the probability is 0.6 and in the case of four photons (reaction (4)) it is about 0.3.

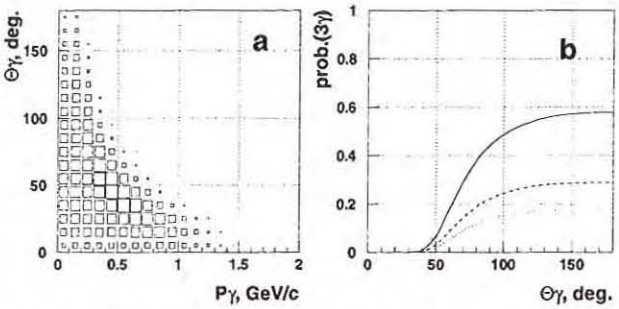

Figure 1: Angular and momentum distribution of decay photons from the reaction p(2 GeV)$d \to d\omega p_{sp}$ (a) and detection probabilities for all three γ's as a function of the maximum detectable backward angle(b). See text for details.

Therefore, a photon detector covering only the forward angular region is sufficiently effective for measurements of η-, η'-, ω- and a_0^0-mesons with ANKE through their decays containing photons in the final state.

References:

[1] M.Büscher et al., COSY proposal No.75 "Study of ω- and ϕ-meson production in the reactions $pd \to dVp_{sp}$ at ANKE" (1998)

[2] V.Grishina, contribution to this report, p.

[3] L.A.Kondratyuk et al., Preprint ITEP 19-97, Moscow (1997); V.Tchernyshev et al., COSY proposal No.55: "Study of a_0^+ mesons at ANKE" (1997)

[4] K.Mengel et al., IEEE Transactions on Nuclear Science, Vol. 45, No. 3, (1998) and references therein

[1] Institute for Nuclear Research, 60th October Anniversary Prospect 7A, 117312 Moscow, Russia

[2] Institute of Theoretical and Experimental Physics, B. Cheremushkinskaya 25, 117259 Moscow, Russia

* Supported by DFG and RFFI

η- and η'-meson production in the reaction pn $\to$ dM near the threshold

V.Yu. Grishina[1,*], L.A. Kondratyuk[2,*], M. Büscher*, C.Hanhart, J.Haidenbauer and J.Speth

The total cross section of the reaction $pn \to d\eta$ has recently been measured near the threshold at CELSIUS [1]. In this report we present results of our calculations of this cross section within the framework of the two-step model (TSM), which was previously applied to the description of the Pontecorvo reactions $\bar{d} \to pM$ (see, e.g., Ref. [2] and references therein). We give also predictions for the cross section of the reaction $pn \to d\eta'$.

In the TSM the reaction $pn \to dM$ proceeds in two steps: i) the initial nucleons produce an η- or η'-meson (denoted as M) via the virtual π-meson exchange; ii) the proton and neutron form a deuteron via a final-state interaction.

Near threshold the amplitude $A(pn \to dM)$ can be expressed through the S-wave amplitude of the reaction $\pi^- p \to nM$ and the structure factor M_{SF}, which contains the integral over the deuteron wave function in momentum space, the propagator of the virtual meson and the πNN form factor $F(q^2)$.

The values of the S-wave cross sections,

$\sigma_{\pi^- p \to n\eta} = (21.2 \pm 1.8) p^*$ μb and

$\sigma_{\pi^- p \to n\eta'} = (0.35 \pm 0.03) p^*$ μb,

(where p^* is the c.m. momentum of the final meson in MeV/c) are taken from [3]. The form factor $F(q^2)$ is taken to be of monopole form with a cutoff mass $\Lambda^2 = 0.7 - 1$ (GeV/c)^2 (see, e.g., [4] and references therein). According to [2] the contributions from exchanges of heavier virtual mesons such as ω and ρ should be relatively small as compared with the π-meson exchange. We found that this is indeed true in the present case. The D-wave part of the deuteron wave function can also be neglected.

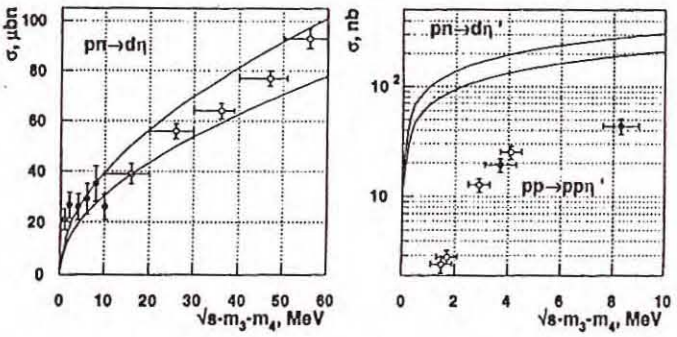

Figure 1: Cross sections of the reactions $pn \to d\eta$ (left part) and $pn \to d\eta'$ (right part) as a function of the c.m. excess energy. Upper and lower curves correspond to the cutoff mass squared $\Lambda^2 = 1$ and 0.7 (GeV/c)^2. Experimental points in the left part are taken from [1]. In the right part data for the reaction $pp \to pp\eta'$ are show which are from [5] (open circles) and [6] (filled circles), respectively.

The calculated total cross sections are show in Fig. 1 as a function of the c.m. excess energy $Q = \sqrt{s} - m_3 - m_4$. The results for the reaction $pn \to d\eta$ are shown on the left side and the ones for $pn \to d\eta'$ on the right side. The upper and lower curves correspond to a cutoff mass squared $\Lambda^2 = 1$ and 0.7 (GeV/c)^2. The experimental points for reaction $pn \to d\eta$ lie in most cases between those two curves. Initial state interaction might give a damping factor of about 0.5. Clearly such a big correction would destroy the agreement with the data. One would think that there is an essential compensation of the initial and final state interaction corrections.

We note that the TSM predicts that the near-threshold cross section of the reaction $pn \to d\eta'$ is much larger than the cross section of the reaction $pp \to pp\eta'$, which was recently measured at COSY [5] (cf. the open circles in the right part of Fig. 1) and SACLAY [6] (black circles in the right part of Fig. 1). The ratio of the cross sections $R(\eta') = \sigma_{pn \to d\eta'} / \sigma_{pp \to pp\eta'}$ is about 6-10 at $Q = 4 - 8$ MeV and increases to a factor of about 30 at $Q \simeq 2$ MeV. This is in qualitative agreement with the near threshold behaviour of $R(\eta) = \sigma_{pn \to d\eta} / \sigma_{pp \to pp\eta}$ [1].

Due to a comparatively large cross section of the reaction $pn \to d\eta'$ it looks quite feasible that this reaction can be measured at ANKE when the photon detector described in [7] will be installed there.

References:

[1] H.Calén et al., Phys.Rev.Lett. **79**, 2642 (1997); ibid. **80**, 2069 (1998)

[2] L.A. Kondratyuk et al., Yad. Fiz.**61**,1670 (1998)

[3] D.M. Binnie et al., Phys. Rev., **8**, 2789 (1973)

[4] G. Janssen, K.Holinde, and J.Speth, Phys. Rev., C**54**, 2218 (1996)

[5] P. Moskal et al., Phys.Rev.Lett. **80**, 3202 (1998)

[6] F. Hibou et al., Phys.Lett. B **438**,41 (1998)

[7] M. Büscher et al., contribution to this report, p.

[1] Institute for Nuclear Research, 60th October Anniversary Prospect 7A, 117312 Moscow, Russia

[2] Institute of Theoretical and Experimental Physics, B. Cheremushkinskaya 25, 117259 Moscow, Russia

* Supported by DFG and RFFI

Possibility to study fast nuclear fragment production at ANKE

G.Borchert[a], A.K.Kacharava[b,c], V.I.Komarov[c], A.V.Kulikov[c], M.S.Nioradze[b], G.G.Macharashvili[b,c], H.Müller[d], A.Yu.Petrus[c], S.V.Yaschenko[c]

The feasibility of inclusive studies of the production of fast nuclear fragments in proton-nucleus interactions at ANKE is investigated. The physical goals of such experiments are elucidated in [1]. Studies of such processes require measurements of the momentum of fast light nuclei produced in pA reactions at small forward angles. We constrain the considerations here to characteristics of the scintillation-counter part of the detector system excluding the track detection part (multiwire chambers).

All the characteristics are discussed here for the specific case of the process $p + {}^{12}C \rightarrow (p, d, {}^3H, {}^3He, {}^4He) + X \ldots (1)$, at $T_p = 800$ MeV.

The ANKE facility is presently equipped with three groups of detectors: the Side Detector (SD) for positively charged reaction products, the forward systems consisting of the Forward Detector (FD) itself and a Side Hodoscope (SH) which is positioned between SD and FD, and the Backward (BD) detectors. The possibilities to identify the particle type (π^+, p, d, ^{3}H, ^{3}He, ^{4}He) in the SD and FD of scintillation counters have been considered in [1],[2]. The geometrical acceptances of the Forward Hodoscope (FH) (which forms part of the FD) and SH for an incident energy of $T_p = 800$ MeV and an deflection angle $\alpha = 10.6°$ of the COSY beam in D1 are shown in **Fig. 1(a,b)**. They have been obtained with ejectiles uniformly distributed in the momentum range $p_{ejec} = 0 \div 2000$ MeV/c and emission angles $\vartheta \leq 20°$ with respect to the circulating COSY beam. Particles were considered as detected if they passed any of the detector systems and reached the second plane of the FH or the first counter plane of SH. It is seen that the hodoscopes provide a significant momentum-angular acceptance. It is essential that acceptances of the two hodoscopes which are complementary to each other, provide measurements of the momentum and angular dependences of the cross sections of the particles emission in a rather wide (p, ϑ) range.

The momentum-angle intervals given by several separate elements of the Forward Hodoscope (FH: #1 – 9), and some SH modules (SH: #1 – 6) in coincidence with several Start counters (ST: #12 – 22), are shown in **Fig. 1(c,d)**. These distributions have been calculated taking into account background from particle interaction with the spectrometer components. The mean values of momentum and angle for the single charged particles detected in the corresponding areas of the acceptance are listed in **Table 1**. It is seen, that the Side Hodoscope together with the Start Counters enables the measurement of momentum and angle of the emitted particles with a rather high accuracy ($\Delta p/p \approx 1.5 - 4.0\%$; $\Delta\vartheta \approx 0.6 - 0.8°$). For the Forward Hodoscope counters alone the accuracy is much worse ($\Delta p/p \approx 10$ – 15%) since there are no Start counters in the FD. Therefore, if to study the processes like (1) at the high luminosity levels, where multiwire chambers operation can be hampered, using only information from the hodoscopes, it would be appropriate to arrange the FH behind the SH and to use them together. This should improve the accuracy of the momentum measurement (because of the higher accuracy of the coordinate measurements) and reliability of the particle type identification (for ΔE-measurements in 3 or 4 planes of the scintillation counters which are then available).

Estimations of the expected cross sections of the fragment production and the counting rates of the detectors have been performed using the Rossendorf Collision Model (ROC-Model) [3]. The first line of **Table 2** lists inclusive differential cross sections $\sigma_i(\Delta\Omega)$, integrated over the angle ($\vartheta < 20°$), obtained within the ROC model for various types of particles produced in the reaction (1). The second line lists the cross sections ($\Delta\sigma_i$) for the production of the same particles, detected in the Forward and Side Hodoscope.

Table 2.. ROC model-differential cross sections for particles from the reaction (1) at $T_p = 800\,MeV$.

particle(i)	π^+	p	d	^{3}H	^{3}He	^{4}He
$\sigma_i(\Delta\Omega)$ mb	1.065	34.350	3.330	0.126	0.180	0.1700
$\Delta\sigma_i$ (mb) FH	0.001	3.780	0.350	0.010	0.013	0.0004
$\Delta\sigma_i$ (mb) SH	0.045	0.720	0.063	0.005	0.012	0.0010

The expected counting rates n_i can be found multiplying the cross sections $\Delta\sigma_i$ by the beam-target luminosity L. For example at a luminosity $L = 1.0 \cdot 10^{31}$ cm^{-2} s^{-1}, the total counting rate for ^{4}He in the Side Hodoscope is equal to $n_{^4He} = 0.001$ mb$\cdot L \approx 10 \cdot$ s^{-1}.

The obtained values show that the processes under consideration can be measured with a good statistical accuracy during a reasonable beam-time at ANKE.

References:

[1] G.Borchert et al., JINR report, E1-xx-xxx, Dubna (1998)

[2] A.K.Kacharava et al., JINR report, E1-97-324, Dubna (1997)

[3] H.Müller, Z.Phys., A353, (1995), p.103; A353, (1995), p.237

[a] IKP, FZ-Jülich, Germany
[b] HEPI TSU, Tbilisi, Georgia *
[c] JINR, Dubna, Russia *
[d] IKPH, FZ-Rossendorf, Dresden, Germany

* The work is supported by the grants RFBR No. 96-02-17215, WTZ No. RUS-667-97, INTAS-Georgia No. 98-505.

SH/ST	#1	#2	#3	#4	#5	#6
#12	496.6± 11.5					
$\vartheta \pm \Delta\vartheta$	-10.71± .71					
$\Delta p/p$	2.3%					
#13	493.9± 11.5	537.5± 13.8				
$\vartheta \pm \Delta\vartheta$	-8.84± .71	-10.40± .73				
$\Delta p/p$	2.33%	2.57%				
#14	491.8± 10.9	531.4± 12.9	581.7± 17.3			
$\vartheta \pm \Delta\vartheta$	-7.05± .70	-8.58± .72	-10.23± .73			
$\Delta p/p$	2.21%	2.42%	2.98%			
#15	489.8± 10.2	526.5± 13.0	573.3± 15.1	633.9± 20.1		
$\vartheta \pm \Delta\vartheta$	-5.33± .72	-6.82± .73	-8.49± .68	-10.22± .69		
$\Delta p/p$	2.09%	2.47%	2.64%	3.17%		
#16	487.1± 9.4	523.6± 11.7	568.7± 14.4	625.4± 18.6	696.5± 24.8	
$\vartheta \pm \Delta\vartheta$	-3.54± .66	-5.13± .69	-6.89± .72	-8.64± .72	-10.42± .68	
$\Delta p/p$	1.93%	2.24%	2.53%	2.97%	3.56%	
#17	486.1± 9.0	520.8± 10.8	562.6± 13.2	614.5± 17.7	685.4± 23.3	776.8± 32.6
$\vartheta \pm \Delta\vartheta$	-1.87± .67	-3.53± .69	-5.22± .71	-6.99± .72	-8.89± .73	-10.86± .74
$\Delta p/p$	1.85%	2.08%	2.35%	2.88%	3.40%	4.20%
#18	485.8± 8.2	517.6± 10.2	557.8± 12.8	607.1± 15.9	672.1± 21.1	758.2± 29.9
$\vartheta \pm \Delta\vartheta$	-.30± .60	-1.90± .66	-3.63± .70	-5.43± .69	-7.36± .69	-9.37± .74
$\Delta p/p$	1.69%	1.97%	2.30%	2.62%	3.13%	3.94%
#19	487.6± 8.1	515.5± 9.6	552.6± 12.1	599.9± 15.1	661.4± 20.2	739.5± 26.6
$\vartheta \pm \Delta\vartheta$	1.02± .70	-.32± .61	-1.99± .67	-3.88± .71	-5.81± .74	-7.84± .76
$\Delta p/p$	1.66%	1.87%	2.19%	2.52%	3.05%	3.59%
#20	485.3± 8.2	516.9± 9.4	547.8± 11.0	593.2± 14.7	649.0± 19.0	723.0± 25.8
$\vartheta \pm \Delta\vartheta$	2.76± .70	.93± .71	-.41± .63	-2.28± .71	-4.24± .74	-6.29± .78
$\Delta p/p$	1.69%	1.82%	2.00%	2.47%	2.93%	3.57%
#21	483.2± 7.2	512.9± 9.2	548.2± 10.8	583.8± 13.3	639.4± 17.8	708.8± 24.0
$\vartheta \pm \Delta\vartheta$	4.48± .65	2.64± .68	.78± .70	-.63± .67	-2.72± .76	-4.80± .77
$\Delta p/p$	1.49%	1.79%	1.97%	2.28%	2.79%	3.38%
#22	480.4± 7.3	507.8± 9.0	541.7± 11.2	583.5± 12.4	624.0± 17.2	693.9± 22.4
$\vartheta \pm \Delta\vartheta$	6.21± .75	4.44± .71	2.53± .75	.50± .66	-.93± .77	-3.25± .77
$\Delta p/p$	1.53%	1.77%	2.06%	2.12%	2.75%	3.23%

Table 1. Mean momentum (MeV/c) and angle (degree) with their RMS, and $\Delta p/p$ of the particles (Z=1) passed through the Start and Side Hodoscopes (ST is a module number of the Start Hodoscope and SH of the Side Hodoscope).

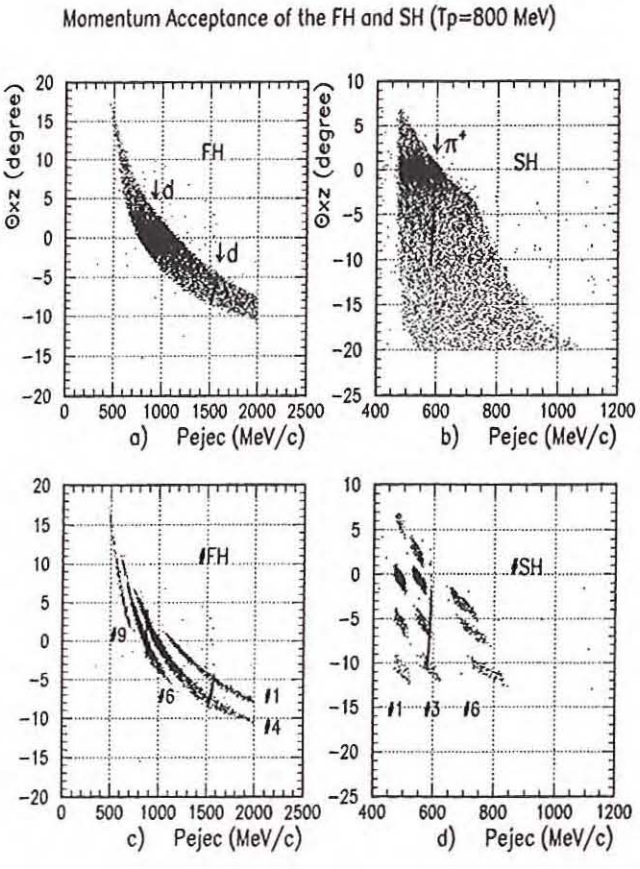

Fig. 1. Angular-momentum acceptance of the Forward (a,c) and Side Hodoscopes (b,d). ϑ_{xz} - projection of the polar angle ϑ of the ejectile with momentum P_{ejec} at the median-plane XZ of the spectrometer. Arrows denote the kinematical boundary for the deuteron and pion from the reaction $pp \rightarrow d\pi^+$

Drift Chambers of the ANKE Backward Detector

V.Abazov[a], V.Artemov[a], G.Borchert[b], H.Ohm[b], A.Petrus[a], I.Potrap[a], A.Rudenko[a], B.Zalikhanov[a]

The multipurpose spectrometer ANKE at the accelerator COSY (Jülich, Germany) is built up for the investigation of proton-proton and proton-nucleus reactions in the intermediate energy region (subthreshold and near-threshold meson production, investigation of few-nucleon system etc.) [1]. It consists of three major detector groups: Forward, Side and Backward detectors (see figure on p. of this report). A set of drift chambers forms part of the Backward Detector along with a hodoscope of scintillation counters. The drift chambers are designed for the track reconstruction of ejectiles with momenta of $150-650$ MeV/c at angles $165°-180°$ relative to the beam direction. TDC LeCroy 3377 are used for time coding of the signals from drift chambers.

The set of drift chambers of the Backward Detector consists of three packages. Each of these packages is made up of two independent modules: one of them to measure the X-coordinate of the track and another for the Y-coordinate. Each module contains two sensitive planes which are placed inside a common gas volume. The drift cells of these planes are shifted relative to each other by half the length of a drift cell (2cm) to get rid of "left-right" ambiguities. The chambers have been constructed using a new technology [2] which differs from the usual design based on fiberglass frames. The new design is more compact, simpler for manufacturing and maintenance. A gas mixture of $80\%\,\mathrm{Ar} + 20\%\,\mathrm{iC_4H_{10}}$ is used.

The chambers were tested with a collimated ^{90}Sr β-source in front of the chamber window. The electrons crossing the chamber volume and passing through another collimator were detected by a scintillation counter.The scintillator was viewed by PMTs from both sides and the signal formed by coincidence of the signals from both PMTs was used as a "common stop" for the TDC.

The dependence of the detection efficiency on the high-voltage at a 2 μA threshold exhibits a plateau from 2.3 kV up to at least 3.2 kV. The measurement also showed that the efficiency has a plateau with respect to changing of the threshold at the fixed high voltage. For instance, at 2.8 kV the registration efficiency retains at the 99% level up to 45 μA threshold. The measurements have also shown a high identity of the characteristics for all the chambers.

Fig. 1 shows the result of the drift velocity measurement by the shadow method based on scattering of a narrow electron beam on the 100 μm diameter field forming wires (see description of the method and references in [3]). The measurements show that the detection efficiency is highly homogeneous along the drift cell. The drift velocity is also constant along the cell except the vicinity of the sensitive wire. The drift velocity is 50 μm/ns in the plateau of its field dependence [4]. Thus stable calibration of the chamber is guaranteed.

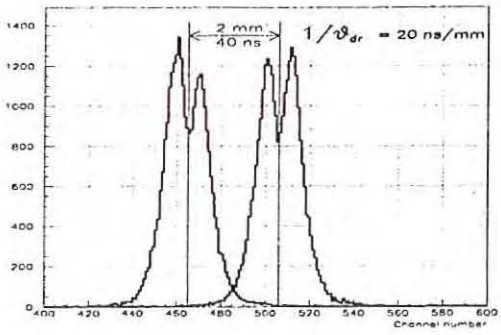

Fig. 1. The drift velocity measurements by the shadow method.

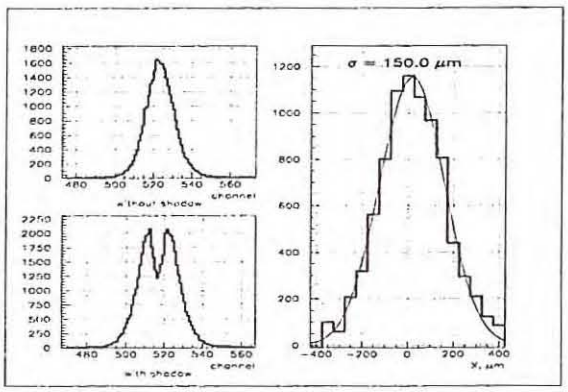

Fig. 2. The drift length distributions at two beam axis positions: with and without wire in the beam, and the deduced difference distribution for the shadow.

Fig. 2 indicates the observed spacial resolution of 150 μm. With corrections for scattering of the β-particles on the entrance window of the chamber it is 140 μm (see [3] for correction procedure).

Thus, the obtained performance completely meets the requirements for operation at ANKE.

The authors are grateful to W.Ermer and N.Lebedev for their valuable help during different stages of the work.

References:

[1] M.Büscher et al., Physica Scripta **48**, 50 (1993)

[2] H.Kalmar et al., NIM **A303**, 298 (1991)

[3] V.Krasnov et al., INR, Moscow, P-0038 (1976)

[4] A.Peisert and F.Sauli, CERN 84-08 (1984)

[a] JINR, Dubna, Russia *
[b] IKP, FZ-Jülich, Germany

* The work was supported by the grants RFFI 96-02-17215 and DFG 436 RUS 113/337.

Fast Multiwire Proportional Chamber with Dielectric Foil of the ANKE Forward Detector

G.Borchert[a], W.Erven[b], R.Koch[a], S.Mikirtichyants[c], H.Ohm[a], S.Yaschenko[d], B.Zalikhanov[d]

The ANKE facility includes at present three groups of detectors: Positive Side (PS), Forward (FD) and Backward (BD) Detector systems. Three proportional chambers will form the coordinate part of the FD system to be installed at the forward exit window of D2 (see figure on p. of this report). They have to operate at a high particle flux (counting rates as large as $5 \cdot 10^7 s^{-1}$ per plane and up to $3 \cdot 10^5 s^{-1}$ per wire). The signal-wire distance has to be 1 mm at a maximum length of 550 mm in order to reach high momentum resolution. The space limitations by the COSY-beam pipe and the side detectors on the one hand and the aim to cover a maximum momentum range on the other hand necessitate a lean frame construction.

These features can be realized with chambers using a new technology [1], see fig. 1. The chamber contains four coordinate planes. The sensitive area of the chamber is 327x261 mm^2. Signal wires made of 20 μm diameter gold-plated W+Re lie on a 100 μm thick dielectric foil with a resistivity of 10^9 Ohm·cm. The signal wire tension is 60 g, the step of the signal wires is 1.041 mm. The step of the strips is 3.25 mm, the distance between the strips is 0.2 mm, the thickness of strips is 0.05 mm (silver paint). The break-through voltage of the dielectric foil is 2600 V. The cathode plane, made of 0.025 mm thick carbon plated mylar, is at 2.0 mm from the wires plane. The total number of signal channels is 821 including 314 X wires, 128 U strips (X + 18^0), 251 Y wires, 128 V strips (X - 18^0). The gas mixture is 80% CF_4, 20% i-C_4H_{10}.

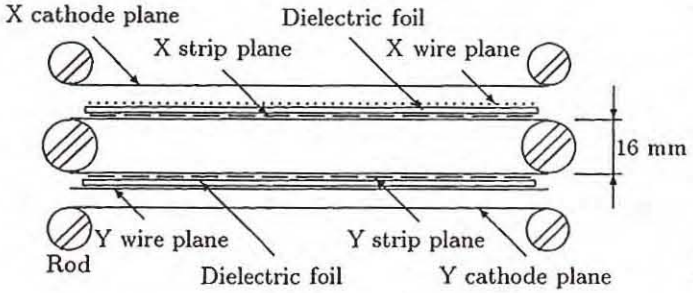

Fig. 1. Schematic drawing of the chamber.

Stable operation at 1 mm signal-wire distance and 550 mm length is possible since the signal wires are pressed to the dielectric foil by forces created by the strong electric field to the strips. These forces are two orders of magnitude stronger than the forces between the wires. Conductivity of the dielectric foil is necessary for the movement of the anode avalanche to the strip electrodes of the chamber.

The first chamber has been built and was tested with a ^{90}Sr β-source using front-end electronics designed and produced by the ZEL [2]. For the strips a signal inverter with a gain of ~3 was used. It allows to use the same electronics for the strip and wire signals. The amplification is needed because the induced signal on the strips is twice less than that of the anode. The time and amplitude spectra and the efficiency characteristics were measured both for wires and strips. The intensities were $2 \cdot 10^5$ $s^{-1}cm^{-2}$. The efficiency curves for the X and Y wires and strips are shown in fig. 2a. The plateau begins at about 1600 V which is very important because the break-through voltage of the dielectric foil is 2600 V. The amplitude spectra from the chamber (see fig. 2b) are ~3 times wider than for the standard chambers. The cause of this phenomenon is a peculiarity of the avalanche formation. The time spectra for the X and Y wires and strips are practically the same. In fig. 2c one time spectrum is shown. The threshold of the discriminator was 20 mV. It corresponds to 2μA threshold of the amplifier entrance. The noise characteristics of the chamber are 6 signals per second per wire for the voltage on the strips U=1700 V, and 50 signals per second per wire for U=1750 V.

The chamber fulfils the requirements at ANKE.

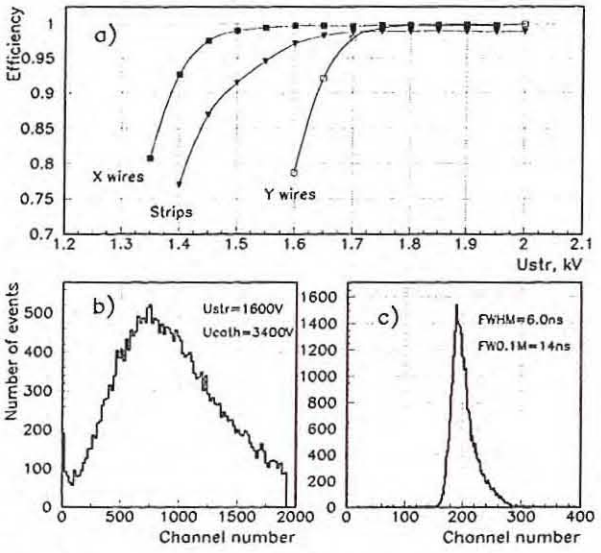

Fig. 2. Efficiency of X and Y wires and strips as a function of the voltage on the strip plane (a). Amplitude spectrum of signals from Y wires (b). Time spectrum of signals from a single wire. One channel corresponds to 0.25ns (c).

References:

[1] H. Kalmar et al., Nucl. Instr. and Meth. A **307**, 279 (1991)

[2] G. Borchert et al., IKP/COSY Annual Report 1997, FZ Jülich, 61 (1998)

[a] IKP and [b] ZEL, FZ-Jülich, Germany
[c] PNPI, Gatchina, Russia
[d] JINR, Dubna, Russia *

* The work is supported by the grants RFBR No. 96-02-17215, DFG 436 RUS113/337.

ANKE Forward Hodoscope: first beam measurements.

G.Borchert[a], W.Borgs[a], S.Dymov[b], M.Hartmann[a], V.Komarov[b], A.Kulikov[b], V.Kurbatov[b], G.Macharashvili[b,c], H.Müller[d], M.Nioradze[c], A.Petrus[b], B.Prietzschk[d], B.Rimarzig[d], R.Schleichert[a], A.Volkov[b], N. Zhuravlev[b]

The Forward Hodoscope (FH) consists of two planes of vertically oriented scintillators viewed by PMs from both ends. The FH design and its performance in cosmic ray tests have been described earlier [1]. Here we present the first results of its use in ANKE beam runs.

In the data analysis we treated as "'a hit in the counter"' events where the time signal was present (in the meantimer channel) and the amplitudes from both PMs exceeded the threshold values. For amplitude analysis we used the normalized sum A_N of two pulse heights defined as:

$$A_N = C \cdot (\frac{A_U}{A_{Um.p.}} + \frac{A_L}{A_{Lm.p.}}),$$

here A_U and A_L are the amplitudes from the upper and lower PMs of the counter, $m.p.$ denotes "'most probable"' values of pulse height distributions, C is the normalization constant. The amplitude corrections for the longitudinal hit coordinate were not included here, so the obtained pulse height resolution can be improved further.

The data taken with a 1.036 GeV/c proton beam and two different targets, CH_2 and C, were analysed with the final aim to observe the $pp \to d\pi^+$ process with the well-known '$CH_2 - C$' method. The ANKE data acquisition system was triggered by a coincidence of an OR signal from the Side Detector (SD) Start counters [2] with OR of any SD telescope [3]. This trigger was tuned for detection of pions but could accept also part of the protons. The π^+ counting rate was concentrated for the CH_2 target in telescope 13, and for triggers with this telescope the response from FH counters 2–6 was present, as expected with deuterons from the $pp \to d\pi^+$ reaction. In general, a clear correlation between the number of the SD start counter and the number of FH counter was observed.

From the time and amplitude spectra of the signals it is confirmed that deuterons constitute the main part of particles detected in FH at these conditions. Indeed, the time spectrum received with a SD signal as START and FH signal as STOP (Fig. 1) shows a single peak when only SD telescope 13 contributes to the trigger (shaded spectrum). A small background is observed when all SD telescopes participate in the trigger (clear histogram). The width of 600 ps (FWHM) of the deuteron peak is defined by the time resolution of the FH and SD counters, by the time of flight dispersion of π^+ and mainly d (due to momentum spread).

The amplitude spectra of the FH counters also display a distinct peak of deuterons. Such a peak (for counter 2) is seen in Fig. 2 in channels 750–1000, its width is FWHM= 25 %. The peak near channel 225 is caused by fast accidental protons as has been confirmed in measurements with a C-target.

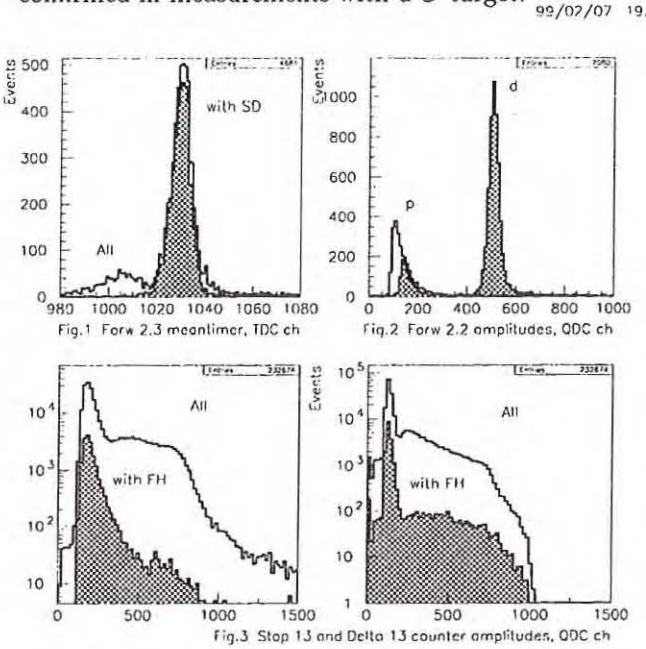

Fig.1 Forw 2.3 meantimer, TDC ch
Fig.2 Forw 2.2 amplitudes, QDC ch
Fig.3 Stop 13 and Delta 13 counter amplitudes, QDC ch

Fig. 3 is a typical picture demonstrating how the inclusion of FH data improves the quality of data in SD for the $pp \to d\pi^+$ process. There are shown the amplitude spectra in Stop and ΔE counters of SD telescope 13. The clear spectra are taken for all particles detected in this telescope and the shaded ones for the particles accompanied by hits in FH. The background is essentially decreased in the last case.

To summarize, the beam measurements have demonstrated a proper performance of the Forward Hodoscope in conditions of the $pp \to d\pi^+$ and $pC \to \pi^+(K^+) + p + X$ processes and the advantages of its use in data analysis.

References:

[1] V. Komarov et al., IKP Ann. Rep. 1997, FZ Jülich, 69 (1998)

[2] R. Esser et al., IKP Ann. Rep. 1993, FZ Jülich, 41 (1994)

[3] Th. Grande et al., IKP Ann. Rep. 1996, FZ Jülich, 63 (1997)

[a] IKP, FZ Jülich, Germany
[b] JINR, Dubna, Russia *
[c] HEPI TSU, Tbilisi, Georgia *
[d] IKPH, FZ Rossendorf, Dresden, Germany

* This work is supported by WTZ Grant RUS-667-97 and INTAS-Georgia Grant No.98-505.

Optimization of the degrader thicknesses in the K^+ telescopes at ANKE

M. Büscher, H. Junghans, V. Koptev[1] and I. Zychor[2]

During the first ANKE beam times data on K^+ production in proton-carbon interactions were taken at beam energies $T = 1.2, 1.5, 1.8, 2.2$ and 2.3 GeV. It is well known that the cross section for K^+ production in proton-nucleus collisions strongly increases with beam energy whereas the background rate of pions and protons stays almost constant. At 2.2 and 2.3 GeV the expected background-to-K^+ ratio on the side-detection system used for kaon identification is ~ 100 [1]. The data taken at this high energy were used to test the detection efficiency of the detectors and, in particular, to tune the thicknesses of degraders located in the K^+ telescopes.

Fig. 1 shows a sketch of a telescope used for kaon identification. The properties of the telescopes are described in detail in [2, 3]. Ejectiles leaving the target after a hadronic interaction are deflected in the spectrometer dipole D2 of ANKE. The telescopes are located in the focal surface of the dipole and, thus, ejectiles hitting a particular telescope have well defined momenta [4]. Typically, the momentum spread on one telescope is around 5% and is defined by the momentum dispersion of the spectrometer. The ejectile momenta increase from left to right on each telescope.

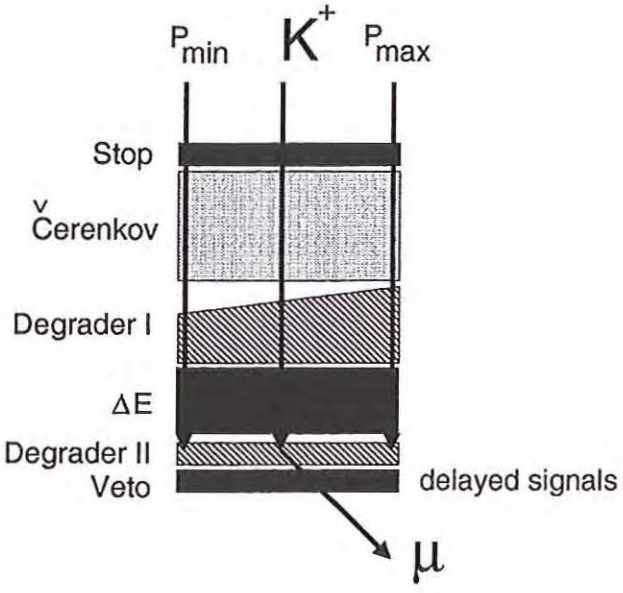

Figure 1: Sketch of a telescope used for the detection of K^+ mesons. Kaons can be identified by their energy losses in the scintillation counters or by detecting delayed signals in the veto counter stemming from e.g. decay muons.

Each telescope consists of a TOF-stop counter, a Čerenkov counter (in telescopes 7–15 only), a ΔE counter and a veto counter for the rejection of fast particles like pions. For a given momentum, the ejectile ranges in the detector material decreases with the ejectile mass. Thus, protons are stopped in each telescope between the stop and ΔE counter and can easily be rejected. Pions have larger ranges and can pass through all telescope components without significantly loosing energy. In order to identify kaons a degrader made from copper is installed in front of the ΔE counter. Here they are slowed down such that they are stopped at the end of the ΔE counter or in the second degrader. The thicknesses of the first degraders and the ΔE counters were optimized with the help of simulation calculations in order to give a maximum energy loss in this counter.

It is foreseen to identify kaons based on TOF measurements as well as on the determination of their energy losses in the scintillation counters. In addition, one can make use of the fact that kaons decay into charged particles with a decay time of 12.4 ns. Fig. 2 shows the time difference between detection of particles in the ΔE and veto counters summed over all 15 telescopes. Since the spatial separation of the two counters is less than 5 cm, pions are expected to give prompt signals. They were rejected using a software cut $\Delta t \gtrsim 4$ ns.

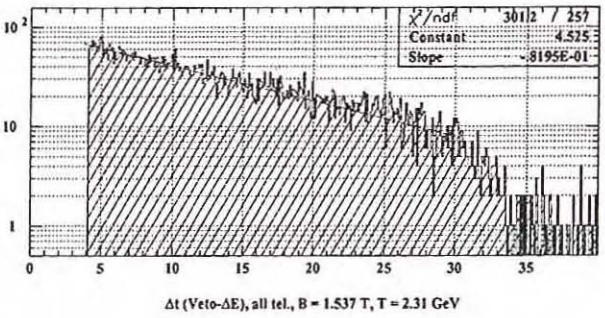

Figure 2: Time difference (in ns) between detection of particles in the ΔE and veto counters for $T = 2.3$ GeV. Prompt signals ($\Delta t < 4$ ns) were rejected by an off-line software cut.

It can be seen from the figure that the remaining events show an exponential slope which corresponds to 12.2 ns. We conclude that most of the events with $\Delta t(\text{veto} - \Delta\text{E}) > 4$ ns are, in fact, kaons. In the following they are used to test the predictions of the simulation calculations on the range of kaons in the telescopes. Note that for kaon identification basically only the time information from the ΔE and veto counters was used except for very mild cuts on the amplitudes in the scintillation counters.

The upper spectrum in Fig. 3 shows the energy loss of the kaon events in the ΔE counter of telescope #15. The data were taken at beam energies $T = 2.2(2.3)$ GeV and field strengths in D2 of $B = 1.4751(1.5370)$ T. Corresponding to the different settings of the magnetic field the ejectile mo-

menta on each telescope differ by 4%. The mean momenta covered by the telescope in the two cases are 560 and 583 MeV/c, respectively. From range tables we deduce a range difference of $\sim$ 1 cm in copper. One can see from the spectra that at 2.3 GeV the kaon energy loss is significantly smaller and already close to the expected peak of pions which was deduced from simulations and is shown in the lower spectrum. At 2.2 GeV the kaons deposit a much larger fraction of their energy in the counter. This can be interpreted such that the degrader thickness in this telescope is well suited for measurements at $B = 1.4751$ but that for higher field strengths in D2 approx. 1 cm of copper should be added to the first degrader. Since it is planned to continue the kaon measurements in spring '99 at $B = 1.5370$ T the modification of the degraders has already been started.

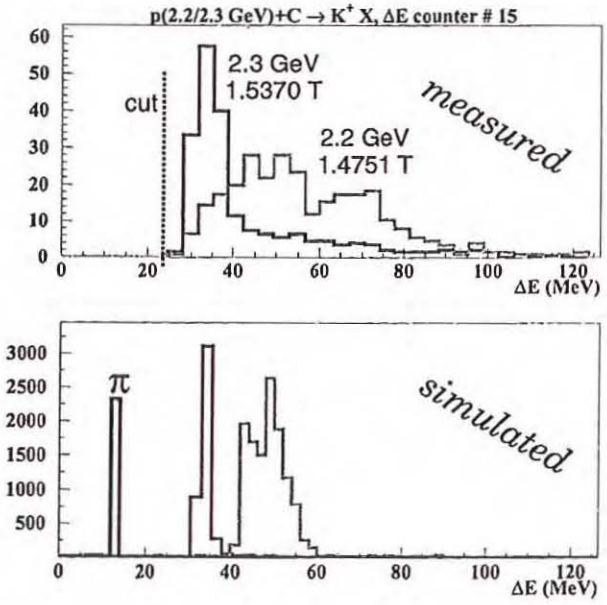

Figure 3: Measured (upper) and simulated (lower) energy-loss spectrum of kaons in ΔE counter #15 for the two different field strengths in D2. For comparison, the expected location of pion events was also simulated. These events were rejected during data taking by setting corresponding thresholds and during data analysis by software cuts.

The lower spectrum of Fig. 3 shows the result of simulation calculations for the two different settings of D2. The simulation can reproduce the location of the peaks for both cases. The width of the simulated distributions is smaller since in the simulation slightly simplified conditions (e.g. no hadronic interactions) were assumed. The simulations allow to determine the location were the kaons are stopped in the telescope and it turned out that the degraders are slightly too thin for the higher energy. The analysis for the remaining 14 telescopes is in progress.

Summarizing, we have developed one possible scheme to identify K^+ mesons at ANKE based on the detection of delayed charged particles from kaon decay. Furthermore, these kaon events are used to optimize the thicknesses of the degraders needed to stop kaons in the telescopes. Measured and simulated ΔE spectra were compared and a good agreement was found. This is important for the continuation of our kaon studies far below the free NN-threshold since here the background conditions are much worse and a well understood detection system is mandatory.

References:

[1] H. Müller, *private communication*;

[2] R. Eßer et al., Annual Report of the IKP 1994, *Berichte des FZ Jülich*, 3035, ISSN 0944-2952, p.52 ff;

[3] M. Büscher et al., Z.Physik A, **355**, 93 (1996);

[4] M. Büscher et al., *contribution to this report*, p.

[1] St. Petersburg Nuclear Physics Institute
[2] Soltan Institute for Nuclear Studies

Polarized Atomic Beam Source for the ANKE-Spectrometer.

R.Baldauf[1], R.Engels[2], S.Geisler, H.Kleines[1], N.Koch[3], V.Koptev[4], A.Kovalev[4], P.Kravtsov[4], S.Lorenz[3], M.Mikirtytchiants[5], S.Mikirtytchiants[4], M.Nekipelov[5], V.Nelyubin[4], H.Paetz gen Schieck[2], F.Rathmann, U.Rindfleisch, J.Sarkadi[1], O.Schult[6], H.Seyfarth, E.Steffens[3], A.Vassiliev[4], K.Zwoll[1]

Future experiments at the ANKE spectrometer like those on deuteron break-up [1,2], non-strange [3,4] and strange [3,5] meson production will make use of polarized hydrogen and deuterium gas targets. For that purpose a polarized atomic beam source (ABS) is being built by the ANKE collaboration. All components of the ABS, shown in Fig. 1, have been designed, have been already built [6] or are presently under construction. In the following we describe the status of the project.

Vacuum System

The complete vacuum system of the ABS has been assembled and tested. One of the main restrictions for the flux of atoms from the nozzle is the limited pumping speed in the first chamber (I). Therefore for this stage an optimization of the pumping system has been carried out [7]. Two different schemes, shown in Fig. 2, have been tested. The pumping speed of the system with the additional turbo pump (Fig. 2a) stays constant up to a hydrogen gas flow of ~ 5 mbar l/s, while for scheme 2b a reduction in pumping speed is already observed at 2.4 mbar l/s. The additional pump significantly increases the compression ratio of the system and therefore leads to an improved performance at higher flows.

RF Dissociator

The design of the rf dissociator allows us to vary and optimize the operating conditions of the gas discharge. The distance between the plasma in the Pyrex tube and the nozzle can be changed online, while the plasma is burning.

For easy access the complete dissociator can be extracted from the ABS chamber while the nozzle and its cooling system stay in place. The cooling water of the dissociator is guided by coaxial glass tubes.

Nozzle Cooling System

The cooling system of the nozzle is based on the results described in ref. [8]. The most critical part is the connection of the Pyrex discharge tube to the nozzle. The metal support components are designed such that no forces are exerted on the Pyrex tube.

Sextupole Magnets

A set of six permanent NdFeB sextupole magnets with pole-tip fields of 1.5 T has been ordered from Vakuumschmelze Hanau. Three materials differing in remanence and coercivity (VACODYM 510HR, 383HR, 400HR) are used to produce the magnets

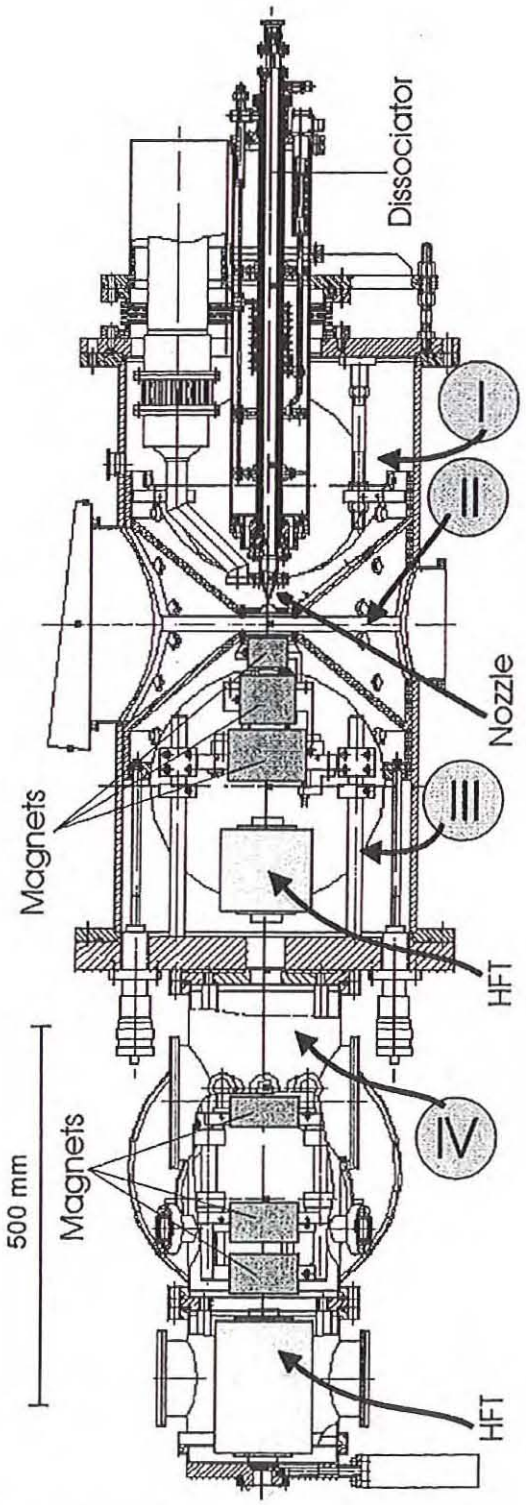

Figure 1. Layout of the ABS.

consisting of 24 segments. Highest remanence and lowest coercivity is used for segments magnetized radially with respect to the magnet surface (510HR) while highest coercivity and lowest remanence is used for segments magnetized tangentially (400HR). For other magnetization directions a material with medium remanence and coercivity (383HR) is used.

Transition Units

The hyperfine transition (HFT) units (labelled HFT in Fig.1) necessary to obtain vector and tensor polarization of hydrogen and deuterium are under development at Universität Erlangen-Nürnberg (diploma thesis S.L.).

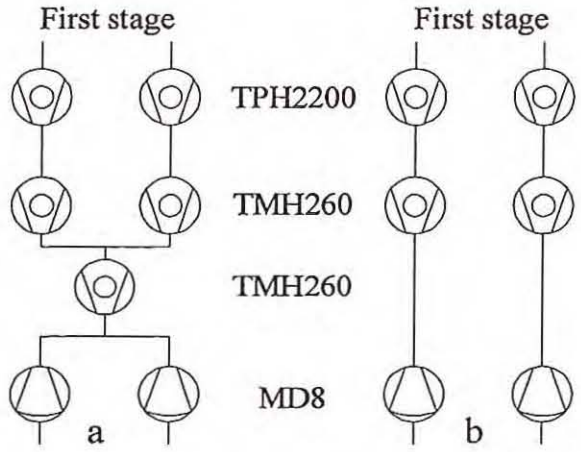

Figure 2. Different schemes with Pfeiffer turbomolecular (TPH2200 and TMH260) and diaphragm pumps investigated for use in the first ABS chamber.

Tools for optimization

For the optimization of the atomic beam source different tools are under development.

For the measurements on the degree of dissociation in a framework of a diploma thesis (M.M.) a device with a crossed-beam quadrupole mass spectrometer has been designed and is presently manufactured. It will be mounted on a two dimensional manipulator which allows us to measure the degree of dissociation of the beam and also to determine the beam profile.

Another diploma thesis (M.N.) aims at absolute intensity measurements based on the use of a compression tube. For that purpose the compression tube will be placed at the same location as the feeding tube of the storage cell (300 mm from the exit of the last magnet). It is planned to measure the intensity in a plane perpendicular to and along the beam axis (z) using a combination of xy- and z-manipulators. A special calibrated unpolarized gas system will permit to measure the absolute beam intensity with an accuracy of a few percent.

For measurements of the beam profile a two-dimensional monitor of the atomic flow has been developed [9]. The monitor is based on the recombination heat transferred to the surface of thin tungsten wires.

It is anticipated to use a Lamb-shift polarimeter which is under construction (Ph.D. thesis, R.E.) at the Universität zu Köln to measure the polarization of hydrogen or deuterium atoms injected into or emerging from the storage cell.

Slow Control System

For a reliable operation of the ABS during the optimization phase and later operation in the COSY ring a modular control system is used. This system, based on the Siemens S7-300 modular line by Simatic [10], is connected to a PC via a MultiPoint Interface (MPI). Another PC, connected by a PROFIBUS interface and operated under WinCC, provides remote control, visualization, and recording of all necessary parameters of the ABS.

[1] Zentrallabor für Elektronik, FZ Jülich
[2] Institut für Kernphysik, Universität zu Köln , D-50937 Köln, Germany
[3] Universität Erlangen-Nürnberg, D-91058 Erlangen
[4] High Energy Physics Department, St. Petersburg Nuclear Physics Institute, 188350 Gatchina, Russia
[5] St. Petersburg State Technical University, St. Petersburg, Russia
[6] professor emeritus, former director at IKP

References:

[1] Spokesperson V.I.Komarov, COSY Exp. Prop. No. 20 (1992)
[2] V.I.Komarov, Proc. 105th Int. WE-Heraeus-Seminar on Hadronic Processes at Small Angles in Storage Rings, Bad Honnef, Feb. 1993 (Konferenzen des Forschungszentrum Jülich, Vol.12, 1993), p.281
[3] S.L.Belostotski, as [2], p.253
[4] COSY Exp. Prop. No.38 (1997), Spokesperson V.Koptev
[5] O.Grebenyuk and V.Koptev, IKP Ann. Rep. 1994 (report Jül-3035, 1995), p.49
[6] H.Seyfarth et al., IKP Ann. Rep. 1997 (report Jül-3505, 1998), p.65
[7] V.P. Koptev, A.I. Kovalev, P.A. Kravtsov, F. Rathmann, H. Seyfarth, A.A. Vassiliev, Preprint PNPI, EP-52-1998, no. 2266
[8] A. Vassiliev, V. Koptev, S. Kotov, H. Seyfarth, Proc. 7th Int. Workshop on "Polarized Gas Targets and Polarized Beams", Urbana/Illinois 1997 (AIP Conf. Proc. 421, 1997), p.479
[9] A. Vassiliev, Preprint PNPI, EP-46-1998, no. 2260
[10] Siemens AG, Automatisierungssysteme S7-300, M7-300 Baugruppendaten EWA 4NEB 710 6067-01

Cluster targets for COSY

H.H. Adam*, A. Khoukaz*, T. Lister*, C. Quentmeier*, R. Santo*, C. Thomas*

Cluster beams are of growing interest for internal accelerator experiments. Produced in Laval-nozzles, they can be used as windowless targets of very high purity. The absolute density can easily be varied by orders of magnitude by changing the nozzle temperature or the gas input pressure. Different to gas-jet beams they provide a spatially well defined target beam with a homogeneous density distribution.

In the IKP at Münster extensive studies on cluster beam production, especially of hydrogen, have been performed in the framework of designing optimized cluster targets for storage ring experiments [1]. Two cluster targets have been build up for the COSY storage ring at the FZ-Jülich. The first one was installed in 1995 at the target place TP3 as part ot the COSY-11 installation. Several months of beam time have been carried out using hydrogen cluster beams with areal densities up to 10^{14} atoms/cm^2. Detailed information about this target can be found in [2, 3].

For experiments at the ANKE installation the second cluster target for COSY was build up in 1998 in the IKP at Münster and moved to FZ-Jülich in the same year. A sketch of the mechanical assembly of this cluster target is shown in Fig. 1. Test measurements with the ANKE target have been performed at Münster and the FZ-Jülich and confirmed the expected performance comparable to the COSY-11 target. The installation of the cluster target is scheduled for week 31 in 1999, thus first experiments within the ANKE installation are planned for fall 1999.

For control purposes via ethernet a slow control system based on a LINUX PC-system was designed and built up in the IKP at Münster. This cluster target-remote control allows to switch devices on or off and displays pressure values in the different pumping stages, nozzle temperature and gas input pressure as well as the status of target components like pumps, sutter and valves. Furthermore, two identical switch boards, one forseen at the target place and one outside of the storage ring, enable the manual control of the cluster target. The complete system was already successfully set into operation.

During several test runs of the COSY-11 cluster target it was shown that also deuterium can be used as target material which, with the use of proton-spectator detectors, provides neutrons as targets in the quasi free scattering. To avoid high operation costs during future beam times using the more expensive deuterium, a recuperation system is under construction in the IKP at Münster by collecting the gas after the pumping system. After cleaning the gas by means of absorption filters it is compressed ($\leq$ 20 bar) and fed back to the existing gas supply system, which includes a hydrogen/deuterium palladium purifier for the final cleaning of the gas.

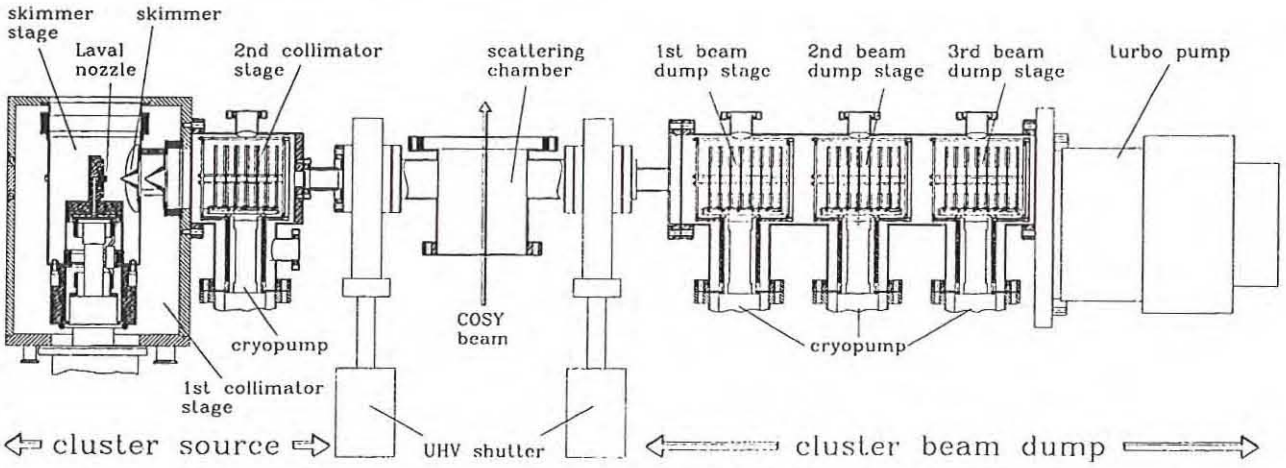

Fig. 1. Construction of the cluster target for the ANKE experiment at COSY.

References:

[1] A. Khoukaz, T. Lister, C. Quentmeier, R.Santo, and C. Thomas, accepted by Eur. Phys. Jour. D

[2] H. Dombrowski, D. Grzonka, W. Hamsink, A. Khoukaz, T. Lister, R.Santo, Nucl. Phys. **A 386**, 228 (1997)

[3] S. Brauksiepe et al., Nucl. Phys. **A 376**, 397 (1996)

* Institut für Kernphysik, Universität Münster, 59399 Münster, Germany

Study of the reactions $p + d \rightarrow^3 H + \pi^+$ and the $^3He + \pi^0$ reactions in the transition region

The GEM Collaboration

For the understanding of pion production on nuclei the knowledge of the elementary process is mandatory. We, therefore, have completed existing cross section data for the reaction $pp \rightarrow d\pi^+$ close to threshold where so far no data existed [1]. These studies close to threshold were performed by using only the magnetic spectrometer. It was also used in a study of the precision of the absolute accelerator momentum calibration. There, we made again use of the above mentioned reaction. Around a momentum of 1930 MeV/c are the laboratory momenta of the forward emitted pions nearly those of the backward emitted deuterons in the centre of mass system. Both could be measured in coincidence and from their momentum difference was the absolute beam momentum calculated [2].

The next logical step to study meson production in nuclei is the measurement on a deuterium target, i.e. $pd \rightarrow^3 H\pi^+$.

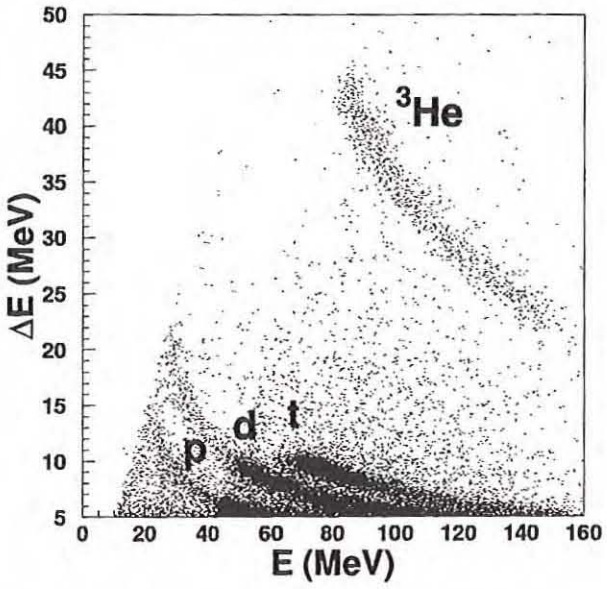

Figure 1: The response of the Ge-wall. Shown as a scatter plot are the energies deposited in the quirl detector (ΔE) versus energy in the first pizza detector (E). The different particle types are indicated next to the appropriate bands.

because deuterons are very extended objects with rather small binding energies the process is usually treated as a $pp \rightarrow d\pi^+$ reaction with the additional neutron acting as a spectator. However, in calculating the cross section one has now to include a form factor, which is the probability to have a deuteron formed in an $A = 3$ system. This leads to strong forward - backward asymmetries. The measurements were performed in a transitional region between the near threshold region, where systematic data from Saclay were recently published [3], and the resonance region. In the latter only some inconsistent scatter of data exists so far. In order to perform such measurements the larger acceptance of the Germanium Wall with respect to the magnetic spectrograph was mandatory. The details of this detector complete with its electronics is described elsewhere [4].

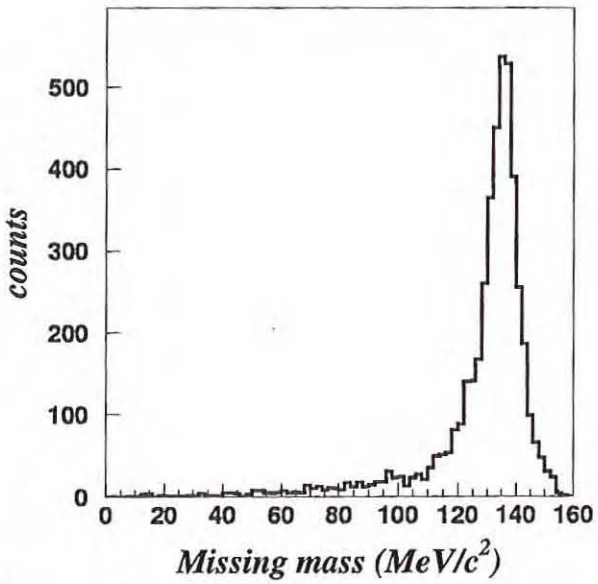

Figure 2: The reconstructed missing mass of neutral pions from the coincident measurements of two protons from the reaction $pp \rightarrow 2p\pi^0$ at 850 MeV/c beam momentum.

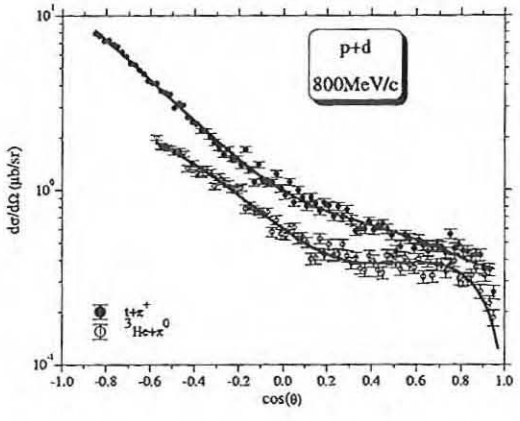

Figure 3: The measured centre of mass system differential cross sections for the reactions $pd \rightarrow^3 H\pi^+$ and $pd \rightarrow^3 He\pi^0$as function of the centre of mass system emission angle of the pion for an incident beam with 800 MeV/c momentum. The solid curves represent fits by Legendre polynomials to the data.

To shortly summarize the main features of the system: it consists of up to four annular planar strip detectors made of HP Germanium. The first has 200 Archimedes' spirals left and right bended on the front and rear side, respectively. It is called quirl and served as tracker as well as ΔE detector. It is followed by up to three E detectors with 32 wedges on the surface (called pizzas). A scatter plot of the events as function of the energies deposited in quirl and the first pizza is shown in Fig. 1. One can clearly identify the different particle types. In addition to the above mentioned reaction it was possible at 850 MeV/c beam momentum to also analyze the $pp \rightarrow d\pi^+$ and the $pp \rightarrow 2p\pi^0$ reactions. In Fig. 2 is the reconstructed missing mass after measurement of two protons shown. In Fig. 3 are angular distributions shown for the two reactions with A=3 plus pion in the final state. The strong backward peaking of the recoiling nucleus corresponds to strong forward peaking of the meson emission. The distribution of the ^3He nuclei is truncated for backward angles, corresponding to small energies because these low energy particles are already stopped in the quirl detector. These will become measurable in the future by either employing a thinner quirl detector made of Silicon or by applying the reversed reaction, i.e. $d + p \rightarrow (A = 3) + meson$ reaction using a deuteron beam. This leads to larger momenta of the recoiling A=3 nuclei which can not be bent in all cases to the focal plane of the magnetic spectrograph because of limited magnetic fields. However, an exit in the side yoke of the first dipole magnet was installed and studied wether it can serve as a focal plane [5]. The present data are also an ideal testing ground for isospin symmetry, since for such a study almost all systematical errors cancel out.

References

[1] M. Drochner et al., Nucl. Phys. **A 643** (1998) 55

[2] M. Bettigeri et al., Nucl. Instr. and Methods in Phys. Research **A** in press

[3] V. N. Nikulin et al., Phys. Rev. **54** (1996) 1732

[4] M. Bettigeri et al., Nucl. Instr. and Methods in Phys. Research **A** in press

[5] *Second focal plane of the Big Karl spectrometer*, cqontribution in this Annual Report

Efficiency of Germanium detectors

The GEM Collaboration

The efficiency of a solid state detector is influenced by mainly two effects: particles can be scattered out of the detector volume and during stopping they can undergo nuclear collisions. The first effect has been simulated for the Germanium wall and it was found that a maximal emission angle being up to 1.4 degree smaller than the maximal geometrical angle is sufficient to stop 100% in the detector volume. The efficiency ϵ due to the second effect can be calculated according to

$$\epsilon = -\frac{L}{A}\int_0^E \frac{\sigma(e)}{\frac{dE}{dx}(e)}de \qquad (1)$$

with L Avogadro's number, A the mass number of the target material, σ the nuclear reaction cross section and $\frac{dE}{dx}$ the electronic stopping power. The latter quantity can be calculated applying the Bethe–Bloch theory. In an earlier study the nuclear reaction cross section for deuterons impinging on germanium was calculated for small energies from a global optical potential and for high energies from nucleon-nucleon scattering in terms of Glauber theory [1]. Unfortunately, for tritium and ^3He no such global optical potential exist. We, therefore choose another way to derive at the necessary reaction cross section. In summary we applied the following prescription: we start from a formula, which described well absorption cross sections in heavy ion collisions. This formula is corrected for proton absorption. The final equation is tested against data for α–particle absorption. Since this procedure leads to satisfactory results we assumed the equation to be also valid for other light ion absorptions.

The first step is the equation valid for ion-ion reactions. Kox et al. [2] found

$$\sigma = \pi r_0^2[A_p^{1/3} + A_t^{1/3} + a\frac{A_p^{1/3}A_t^{1/3}}{A_p^{1/3} + A_t^{1/3}} - c(E/A_p)]^2(1 - \frac{V_{Coul}}{E/A_t}) \qquad (2)$$

with $r_0 = 1.1\ fm$, $a = 1.85$ and $c(E/A_p)$ given for some energy intervals. With V_{Coul} is the Coulomb

barrier denoted. The first part accounts for the geometry, the second for the overlap of the two surfaces and the energy dependent variable for the nuclear transparency. Since the parameters are optimized for heavy ion absorption they are not optimal for light ions as is the present interest. On the other hand Carlson [3] found when analysing proton absorption cross section from a few MeV up to 1 GeV that the quantity $\sqrt{(\sigma/\pi)}$ shows always a linear dependence on $A_t^{1/3}$. However, slope and intercept are energy dependent. Employing these parameters one can calculate the energy dependence of the proton absorption cross section for any nucleus. We used such values and - by applying the Kox formula - we can extract the transparency function which also contains the necessary correction for the target mass number. Since our detector is made of Germanium [4] we are interested in $A = 72$ and hence fit the function $c(E, A_t = 72)$. Then the assumption that $c(E_p, A_t = 72) = c(E_\alpha/4, A_t = 72)$ is tested. Because the A-dependence was found to be weak around $A \approx 72$ we choose the system $\alpha + ^{58}Ni$ for comparison where data exist.

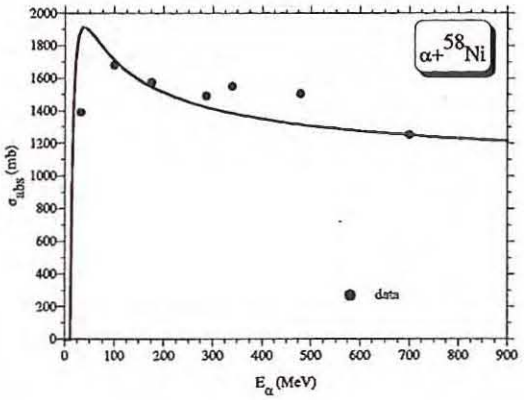

Figure 1: The predicted absorption cross section for the indicated reaction (curve) is compared with data.

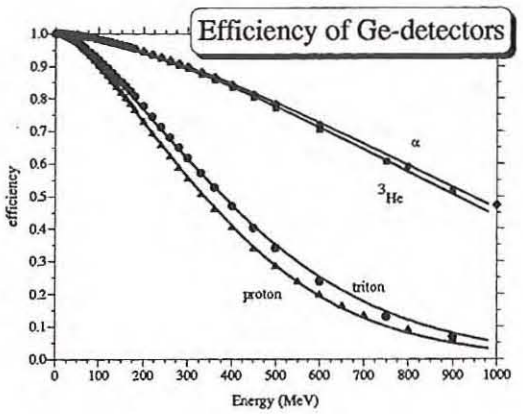

Figure 2: The efficiency for the indicated particles in Germanium as function of the energy.

It is found that the decrease in the cross section which is due to transparency effects is sufficiently reproduced. Therefore, we proceed and calculate the efficiency according to Eq. 1. The results are shown in Fig. 2. The results fall into two bands: one for hydrogen isotopes and one for helium isotopes. The similarity for isotopes of one element was already found earlier [1]. Helium isotopes have a much larger efficiency than hydrogen isotopes due to their larger stopping power.

References

[1] H. Bojowald et al., Nucl. Instr. and Methods in Phys. Research **A 253** (1987) 298

[2] S. Kox et al., Phys. Lett. **B 159** (1985) 15

[3] R. F. Carlson, Atomic Data and Nuclear Data Tables **63** (1996) 93

[4] M. Betigeri et al., Nucl. Instr. and Methods in Phys. Research **A** in press

Second focal plane of the Big Karl spectrometer

The GEM Collaboration

The GEM collaboration is working on several projects dealing either with meson production or meson–nucleus interactions. For a lot of this projects the use of a deuteron beam will be favourable. As mentioned in Ref. [1] use of the $dp \rightarrow ^3 He\pi^0$ reaction will allow the measure the low energy ^3He ions because of the higher momenta compared to the normal reaction employing a proton beam. In reactions producing a meson at rest to study the meson–nucleus interaction, inverse reactions like $dn \rightarrow ^3 He\pi^-$ or $dp \rightarrow ^3 He\eta$ as elementary reactions lead to larger cross sections (see Fig. 3 in Ref. [1]. Also the study of isospin symmetry breaking by comparing the p+d$\rightarrow^3$H+π^+ and p+d$\rightarrow^3$He+π^0 reactions in the vicinity of the η production threshold [2] will benefit from the inverse kinematics. However, in almost all cases have the recoiling ions then so large momenta that they can not more be bent to the focal plane by the magnetic dipoles of the spectrograph BIG KARL. Therefore, it was proposed to use the

hole in Big Karl's first dipole side yoke to extract reaction products: this will be called the second focal plane. The dipole yoke hole allows for exit of particles with the rigidity from 2 to 4 times larger than particles reaching the standard focal plane since it was foreseen as the beam dump exit. In order to use this exit it is first necessary to find out the optical properties and the acceptance of the new focal plane. For this purposes the reaction p+p→ d+π^+ at the proton beam momentum of 1.206 GeV/c was used. At this beam momentum the reaction products have the momentum ratio equal 2 (deuteron – 0.804 GeV/c, π^+ – 0.402 GeV/c) resulting in the ratio of magnetic rigidities equal 2, thus allowing a kinematical coincidence measurement between the pion in the normal focal plane and the deuteron in the new focal plane . The direct proton beam was also used to check the performance of the new detection system mounted at new focal plane position. The new detection system mounted at the first dipole yoke hole (see Fig. 1) consists of two sets of drift chambers mounted 40 cm apart and two scintillator layers. The drift chambers with double sense wires and active area of 32x32 cm^2 [3] were used. The first scintillator layer was mounted just behind the drift chambers and the second at a distance of about 3.5 m. The first scintillator layer consists of 4 paddles and the second of 16 paddles, with the individual paddle area of 10x20 cm^2 and thickness of 6 mm. The drift chambers allow the track determination, the scintillators are used to start the drift time measurements and enable the particle identification by means of energy loss and time of flight measurements. During tests it was found that with a count rate of 10^4 per second the drift chambers operate very well. Very good particle identification was obtained, as it is shown in Fig. 2, where the time of flight spectrum is presented with a clearly visible deuteron peak.

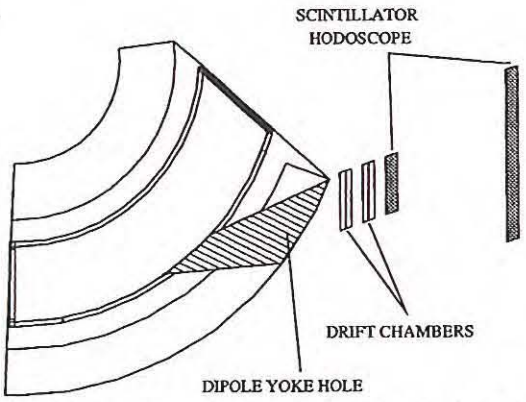

Figure 1: Schematic view of the first Big Karl dipole with side yoke hole and new detection system consisting two sets of drift chambers and two scintillator hodoscopes.

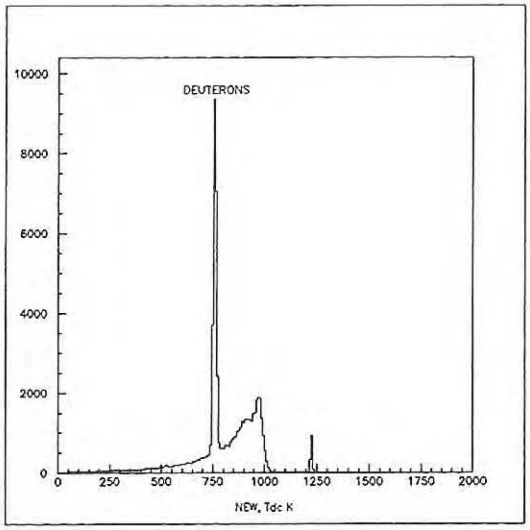

Figure 2:Time of flight spectrum for the detection system mounted at the Big Karl dipole yoke hole. The sharp peak in the spectrum corresponds to the deuterons emerging from the reaction pp→dπ^+.

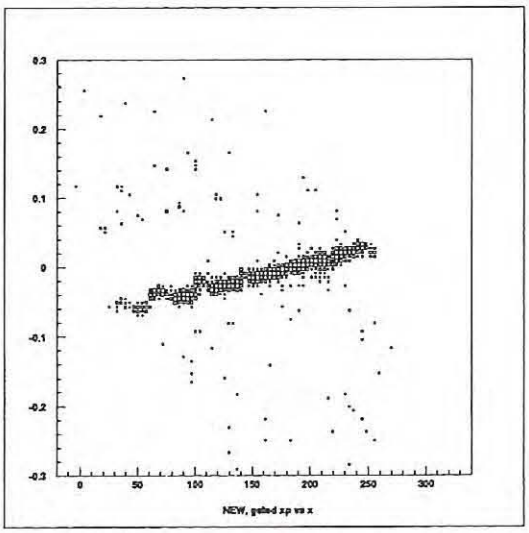

Figure 3: Horizontal angle vs. horizontal position for deuterons detected at the dipole hole in coincidence with pions detected at the focal plane. The density of the points corresponds to the number of counts and varies logarithmically.

As a first step the direct beam was used in order to check the optics of the part of Big Karl that transmits particles to the first dipole yoke hole. It was found that by varying the fields of the first two quadrupole magnets it is possible to obtain good focus at the dipole yoke hole. With optimal quadrupole setting the direct beam at this position has a diameter of 3 mm in both directions. It should be pointed out that such a setting will be very useful for all future Big Karl experiments, since it allows a beam intensity calibration in the case when the beam cannot be bent to the focal plane. Further tests were performed using the pp→dπ^+ reaction at the beam momentum

of 1.206 GeV/c. The pions and deuterons were detected in the focal plane and at the dipole yoke hole, respectively. The relative acceptance at these two detection positions was measured using the kinematical coincidences between the deuterons at the dipole yoke hole and the pions in the focal plane. In order to find the optimal setting for the Big Karl magnets, the acceptance measurements were performed for various quadrupole and dipole magnetic fields. It was found that the maximum relative acceptance is obtained with the standard Big Karl setting. With such a setting the acceptance at the dipole yoke hole is by factor 14 smaller than that for the focal plane. The online spectrum of the horizontal angle vs. horizontal position for the deuterons detected at the dipole hole in coincidence with pions detected at the focal plane is shown in Fig. 3. The horizontal acceptance cut on the right side is due to the edge of the magnet, while on the left side the horizontal acceptance is limited by the dimensions of the drift chambers. It has been determined that it is possible to increase the acceptance at the dipole yoke hole by varying the fields of the first two quadrupole magnets. Then the acceptance at the dipole hole is by factor of 1.6 larger than the focal plane acceptance. Such a setting may be used in any future experiment when the bending of high momenta particles to the focal plane is impossible.

References

[1] The GEM collaboration, *Study of the reactions $p + d \rightarrow {}^3H + \pi^+$ and the ${}^3He + \pi^0$ reactions in the transition region*, contribution to this Annual Report.

[2] A. Magiera, COSY - Proposal No. 59 (1997).

[3] COSY-11-Collaboration, Annual Report 1995, KFA-IKP, 1996, p. 44.

Investigations of isospin symmetry breaking in the $p + d \rightarrow {}^3H + \pi^+$ and the ${}^3He + \pi^0$ reactions at the η production threshold

The GEM Collaboration

Isospin and charge symmetry breaking of strong interaction is one of the most basic problems of nuclear and particle physics. Studies of those effects are hindered by difficulties caused by much stronger isospin and charge symmetry breaking signals originating from the electro–weak sector of the interaction. Therefore there are only few attempts to attack experimentally the genuine strong interaction isospin conservation violation (see Ref. [1] for a recent review). It is believed that on the quark level charge symmetry breaking of the strong interaction is due to the mass difference between the up and down quarks. Information on this mass difference cannot be obtained directly. It could be, however, extracted from isospin and charge symmetry breaking on hadronic level e.g. taking into account mesons mixing ($\pi^0 - \eta$ and $\rho^0 - \omega$). It was proposed [2] to study the isospin symmetry breaking in the p+d$\rightarrow{}^3$H+π^+ and p+d$\rightarrow{}^3$He+π^0 reactions. The measurements of the ratio R of the cross sections:

$$R = \frac{d\sigma/d\Omega(p + d \rightarrow {}^3H + \pi^+)}{d\sigma/d\Omega(p + d \rightarrow {}^3He + \pi^0)}$$

should deliver information about isospin symmetry breaking. Under assumption of isospin conservation theory delivers R=2, with small electromagnetic corrections due to different three nucleon wave functions [1]. Coulomb effects present in those reactions lead to modifications of R value, which are however, weakly energy dependent in the limited energy range. On the contrary, the isospin symmetry breaking introduces strong oscillations of R value with energy. In the backward direction $\theta^{\pi}_{c.m.} = 180^0$ in the interval of a few MeV around the incident proton energy of 900 MeV the magnitude of the R variations can reach about 10% [3].

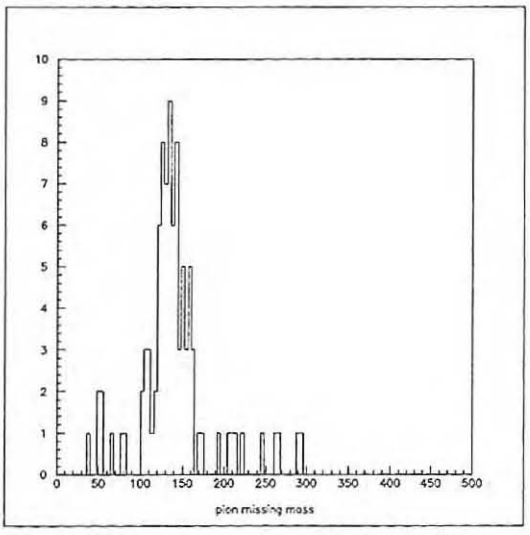

Figure 1:Missing mass spectrum for the ^{3}He events detected in the Big Karl focal plane. The peak corresponds to the events originating in the p+d$\rightarrow{}^3$He+π^0 reaction at the proton beam energy of 850 MeV. Very small background underlying the π^0 peak proves that this reaction can be identified almost

background free.

Such incident energy corresponds to the threshold for the p+d→^{3}He+η reaction and it is expected that strong $\pi^0 - \eta$ mixing might lead to the large isospin symmetry breaking. The most suitable detection system for the measurements at small angles is the Big Karl spectrometer. In order to obtain sufficient accuracy allowing isospin symmetry breaking studies, the simultaneous detection of emitted ^{3}H and ^{3}He is required. In this case most of the systematical errors cancel and the accuracy of the R-ratio is limited by the statistical error. The simultaneous measurement of outgoing ^{3}H and ^{3}He may be achieved by using the Big Karl focal plane for ^{3}He detection and first dipole yoke hole for ^{3}H detection (for details see ref. [4]). The feasibility studies of the proposed investigations were performed in test measurements. It was found that the interesting reaction ^{2}H(p,^{3}He)π^0 can be singled out almost background free by identifying ^{3}He in the focal plane detection system and by selecting a clearly visible π^0 peak in the missing mass spectrum shown in Fig. 1. With the beam intensity of $7 \cdot 10^7$ protons/s the observed counting rate for ^{3}He was 7 per hour. It was found that the geometrical acceptance ratio of the detection systems at the focal plane and at the first dipole yoke hole is equal 14 [4]. Unfortunately large background in the detectors placed at the first dipole yoke hole was observed, which originates from the beam dump located close to this detection system. Nevertheless the observed counting rate and the acceptance ratio of the two applied detection systems allows to estimate that the ratio R can be measured with the accuracy of about 3%, which should be compared with expected 10% variation due to the isospin symmetry breaking. In order to obtain such accuracy reduction of the background at the first dipole yoke hole detectors is necessary. It may be achieved by measurements with inverse kinematic i.e. deuteron beam incident on the proton target, since the beam dump is than located at a different, more favourable position. Also a possibility of measurements at an angle slightly different from zero is considered. This will move the beam dump significantly further from the detection system. Monte-Carlo simulations and test measurements will be performed in order to optimize the experimental conditions.

References

[1] G.A. Miller, B.M.K. Nefkens, I. Slaus, Phys. Rep. 194 (1990) 1.

[2] A. Magiera, COSY - Proposal No. 59 (1997).

[3] C. Wilkin, Phys. Lett. B331 (1993) 275.

[4] The GEM Collaboration, *Second focal plane of the Big Karl spectrometer*, contribution to this Annual Report.

Analysis of the $pp \to pp\eta'$ reaction measured at COSY - 11

Paweł Moskal* for the COSY - 11 Collaboration

* Institute of Physics, Jagellonian University, Cracow, Poland

Recently the total cross section for the $pp \to pp\eta'$ reaction was determined at a few beam energies [1, 2, 3]. The data allows for the first comparisons with theoretical models [4, 5], and indicates that the proton-η' interaction may have an repulsive character [6], in contrary to the proton-η interaction.

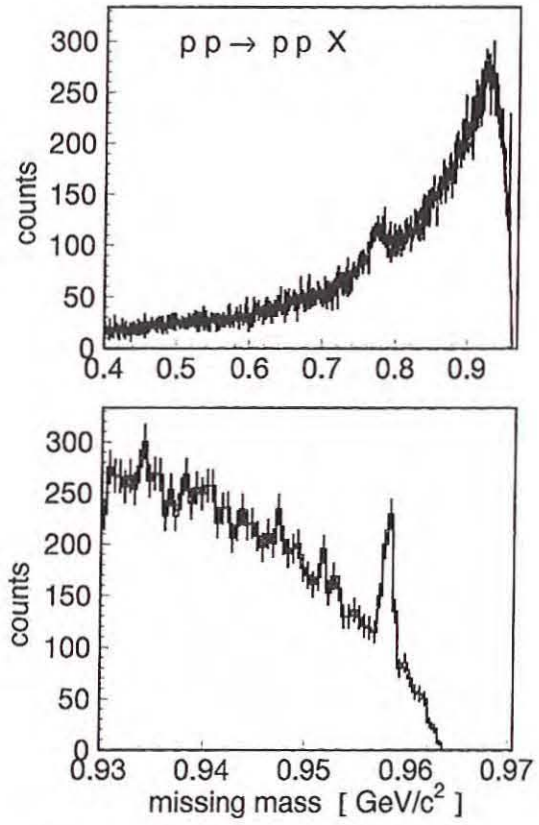

Figure 1: Missing mass in the $pp \to ppX$ reaction

In order to determine precisely the energy dependence for the $pp \to pp\eta'$ total cross section, the COSY - 11 Collaboration has continued the measurement at seven excess energies ranging between Q = 3 MeV and Q = 20 MeV. During the experiment the proton beam was cooled stochastically enlarging the luminosity and diminishing the beam momentum spread. Consequently, in comparison to the former measurements [1] the missing mass resolution was improved making the signal to the background ratio more pronounced, which is very important as far as the study of the differential cross section is concerned. The analysis of the data is in progress.

Figure 1 depicts the missing mass spectrum obtained for the $pp \to ppX$ reaction at the excess energy value of Q = 6 MeV. The upper picture shows the missing mass distribution at a broad mass range, where the clear peak corresponding to the production of the ω meson is visible at a mass value of 780 MeV/c^2. The very sharp peak originated in the η' production can also be seen at a mass value of 958 MeV/c^2. The signal of the $pp \to pp\eta'$ reaction is better to be seen in the lower picture, where the missing mass distribution only in vicinity of the kinematical limit is presented.

The evaluation of the cross section values is in progress.

[1] P. Moskal et al.,
Phys. Rev. Lett. **80** (1998), 3202

[2] F. Hibou et al.,
Phys. Lett. **B 438** (1998), 41

[3] Y. Bedfer,
Acta Phys. Pol. **B 29** (1998), 2973

[4] A. Sibirtsev and W. Cassing,
Eur. Phys. J. **A 2** (1998), 333

[5] C. Wilkin, e-Print nucl-th/9810047

[6] P. Moskal et al.,
Acta Phys. Pol. **B 29** (1998), 3091

Measurement of near Threshold Σ^0-and Λ-Production

S.Sewerin and G.Schepers for the COSY-11 Collaboration

As an extension of the COSY-11-measurements of the reaction $pp \longrightarrow pK^+\Lambda$ close to threshold, which have been puplished in [1], the hyperon production at the $pK^+\Sigma^0$ threshold was investigated. The comparison of the Λ and the Σ^0 production yield at the same excess energies, relative to their respective thresholds, provides useful information for the understanding of the coupling constants and the production mechanisms in the presence of strong channel couplings.

At the COSY-11 facility the four-momenta of the positively charged p and K^+ are determined directly, whereas the neutral hyperon is identified using the missing mass method. In figure 1 the detected invariant mass of the second particle with the first particle being an identified proton is plotted versus the missing mass for a beam energy above the $pK^+\Sigma^0$ -threshold. A band in the K^+-mass region is visible which shows enhancements at the Λ- and the Σ^0-masses.

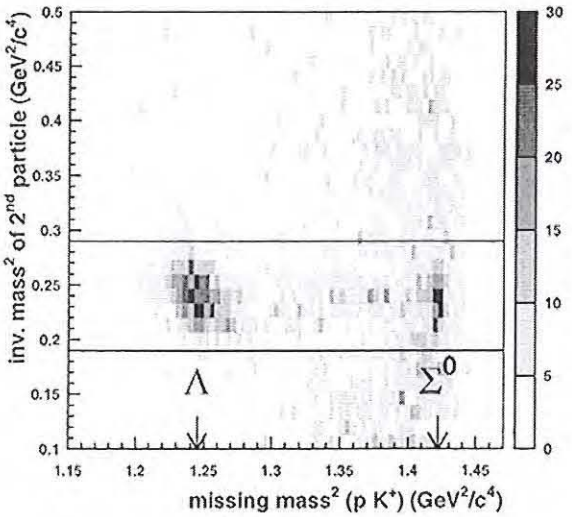

Fig. 1: Squared inv. mass of the K^+ versus the missing mass of the (pK^+) subsystem

Comparing the results of the first run for Σ^0-production with data from [1] has shown a large difference of the cross section between Λ- and Σ^0-production. To optimize for equal experimental conditions COSY was used in the supercycle mode, which allows a repetition of a sequence of spills of different energy. We used 10 or 20 spills at beam momenta equivalent to one excess energy above the Σ^0-threshold followed by one spill equivalent to the same excess energy for Λ-production. The length of the spills was 5 minutes. The value of the missing mass of the hyperon can be determined with an accuracy of 0.4 MeV. In figure 2 the determined cross section values are presented graphically.

Near threshold the following cross section ratio for the two hyperon productions is obtained:

$$R(Q) = \frac{\sigma(pp \longrightarrow pK^+\Lambda)}{\sigma(pp \longrightarrow pK^+\Sigma^0)} \approx 28. \qquad (1)$$

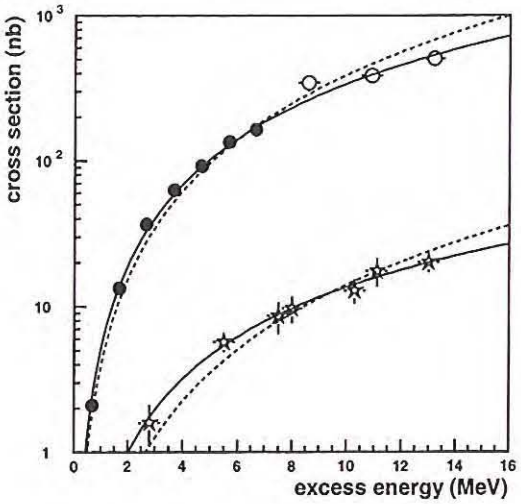

Fig. 2: Cross section of $pp \longrightarrow pK^+\Lambda$ (circles) and $pp \longrightarrow pK^+\Sigma^0$ (stars) [2]. The data of the filled circles have been puplished in [1]. The dashed curves show phase-space fits to the data. The solid curves are fits, which also include proton-hyperon final state interaction.

Both π^0 and K^+ exchange diagrams can contribute to the hyperon production. Assuming only K^+ exchange, the value of the SU(6) prediction of 27/1 for the ratio $R(Q)$ is in very good agreement the measured one. In reality one has to consider significant π^0 exchange, which favours the Σ^0 above the Λ production [2]. However, the measured ratio can be explained, if virtually produced Σ's are converted into Λ's due to strong $\Sigma N \longrightarrow \Lambda p$ final state interaction. Evidences for these effects are well known in the literature. K^- absorption in deuteron $K^-d \longrightarrow \pi^-\Lambda p$ [3] shows a very clear indication for the following two-step process $K^-d \longrightarrow \pi^-(\Sigma N \longrightarrow \Lambda p)$. An additional hint might be the clearly visible irregularity in the mass spectrum of the pΛ at the Σ threshold in the $pp \longrightarrow pK^+\Lambda$ reaction measured at COSY-TOF [4].

References:

[1] J. Balewski et al., Phys. Lett. **B 420** (1998) 211
[2] submitted to Phys. Rev. Lett.
[3] T.H. Tan, Phys. Rev. Lett. **23** (1969) 395
[4] R. Bilger et al., Phys. Lett. **B 420** (1998) 217

Measurement of the $pp \rightarrow pp\phi$ reaction at COSY - 11

Paweł Moskal* and Georg Schepers for the COSY - 11 Collaboration

* Institute of Physics, Jagellonian University, Cracow, Poland

The COSY-11 collaboration measured the $pp \rightarrow pp\phi$ reaction using a proton beam momentum of 3481 MeV/c corresponding to an excess energy of about 24 MeV. The improvement of the data analysis program during the last years and especially the more realistic treatment of the magnetic field used in the momentum reconstruction [1] encouraged us to reanalyze the data.

Figure 1 shows the missing mass spectrum for the $pp \rightarrow ppX$ reaction, where the outgoing protons were identified by reconstructing their mass from the measured momentum and velocity [2]. Most of the entries in this spectrum originate from the multi-pion production and the production of broad mesons like $f_0(980)$ or $a_0(980)$. The clear peak at the mass value of 780 MeV/c^2 above the background corresponds to the production of the ω meson, however, no indication shows up at a mass of 1020 MeV/c^2, which is the mass of the ϕ meson.

Considering that the ϕ meson decays with 49% into the K^+K^- mesons, and that the mesons $f_0(980)$ and $a_0(980)$ decay predominantly into $\pi\pi$ and $\eta\pi$, respectively [3], it is possible to augment the relative signal of ϕ production by the requirement that additionally to the two protons also a K^+ meson was detected. The missing mass distribution obtained under this condition is shown in figure 2. The requirement of a coincident identification of two protons and a K^+ reduces the number of events significantly . However, now an enhancement at the missing mass value corresponding to the mass of the ϕ meson is clearly visible. The run for the ϕ meson production was only 60 hours, since it was regarded as a feasibility test. An extraction of cross section is in progress.

In 1999 further experiments on the ϕ meson production will be performed, which should allow us to improve the statistics, to identify unambiguously the production of ϕ mesons in the proton-proton collisions, and to determine the cross section at different excess energies.

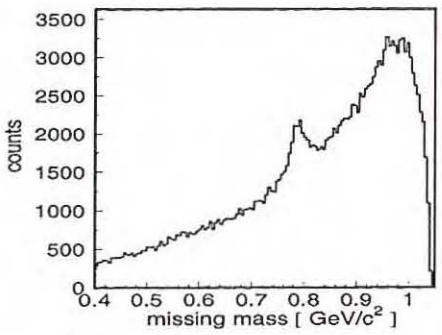

Fig. 1: Missing mass in the $pp \rightarrow ppX$ reaction

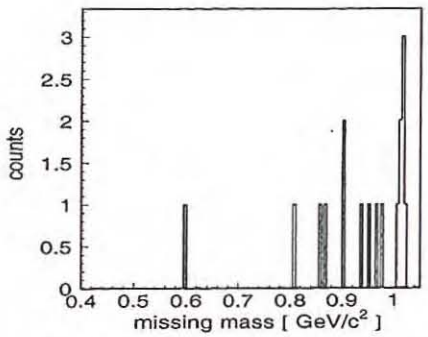

Fig. 2: Missing mass in the $pp \rightarrow ppX$ reaction with the additional condition that a third particle with the mass correspondig to a kaon is registered

References:

[1] COSY - 11 collaboration, Annual Report 1995, IKP, FZ Jülich (1996) p. 38

[2] S. Brauksiepe et al., Nucl. Instr. & Meth. **A 376** (1996), 397

[3] C. Caso et al., Eur. Phys. J. **C 3** (1998)

Production amplitude for the $pp \to pp\eta'$ reaction

Pawel Moskal* for the COSY - 11 Collaboration

* Institute of Physics, Jagellonian University, Cracow, Poland

The cross section for the reaction $pp \to pp\eta'$ can be expressed as:

$$\sigma_{pp\to pp\eta'} = \frac{\int phase\ space \cdot |M_{pp\to pp\eta'}|^2}{flux\ factor} \quad (1)$$

where $M_{pp\to pp\eta'}$ denotes the transition matrix element for the $pp \to pp\eta'$ reaction. In analogy with the *Watson-Migdal* approximation [1] for two body processes, it can be assumed that the complete transition amplitude of a production process $M_{pp\to pp\eta'}$ factorizes approximately as [2]:

$$M_{pp\to pp\eta'} \approx M_0 \cdot M_{FSI} \quad (2)$$

where, M_0 accounts for all possible production processes, and M_{FSI} describes the elastic interaction of protons and η' meson in the exit channel. Assuming that the primary production amplitude does not change with the excess energy, and that only the proton-proton interaction is present in the exit channel the M_0 was calculated estimating the proton-proton interaction according to the Cini-Fubini-Stanghellini formula as described in reference [3].

Figure 1 compares the extracted absolute values for the modulus of amplitudes for the near to threshold production of the π^0 (triangles), η (circles) and η' (squares) mesons. It can be seen that $|M_0|$ stays nearly constant with the tendency of larger values at small Q for the η meson. Whereas very close to threshold it decreases for the pion production with the similar tendency for the η'

The behaviour of the extracted $|M_0|$ can be attributed to the attractive interaction of the proton-η and repulsive interaction of the proton-pion and proton-η' or to the actual variation of the primary production amplitude very close to the reaction threshold.

The large difference between the absolute values of the obtained modulus of the production amplitude for η and η' mesons, may suggests that the production mechanisms for these mesons are different. And since it is known that the η is produced via the excitation of the baryonic resonance, thus probably it is not the case for the η' production.

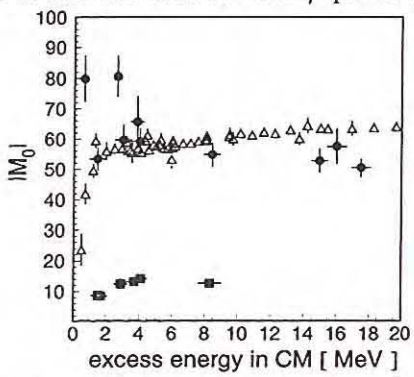

Figure 1: Symbols show the results extracted from the exprimental data for the reactions $pp \to pp\pi^0$ (open triangles) [4], $pp \to pp\eta$ (filled circles) [5, 6], and $pp \to pp\eta'$ (filled squares) [5, 7].

[1] K.M. Watson, Phys. Rev. **88** (1952), 1163

[2] A. Moalem et al., Nucl. Phys. **A 589** (1995), 649 and also hep-ph/9505264

[3] P. Moskal for the COSY-11 Collaboration Ann. Rep. 1996, IKP FZ Jülich 1997, p.37

[4] A. Bondar et al., Phys. Lett. **B356**(1995),8
H.O. Meyer et al.,
Nucl. Phys. **A 539** (1992), 633
Phys. Rev. Lett. **65** (1990), 2846

[5] F. Hibou et al., Phys. Lett. **B438**(1998),41

[6] H. Calèn et al., Phys. Lett. **B366**(1996),39
A.M. Bergdolt et al.,
Phys. Rev. **D 48** (1993), R2969
E. Chiavassa et al.,
Phys. Lett. **B 322** (1994), 270
COSY-11 Collaboration, Ann. Rep. 1995, IKP FZ Jülich 1996 p. 39

[7] P. Moskal et al.,
Phys. Rev. Lett. **80** (1998), 3202

Reactions of the Type pp → ppK⁺X near the (K^+K^-)-Threshold

T. Lister*, C. Quentmeier*, M. Wolke for the COSY-11 Collaboration

Studies of the $K\bar{K}$ channel in the proton–proton interaction may contribute to disentangle the structure of the scalar objects $f_0(980)$ and $a_0(980)$. Their nature has been subject of incessant discussions [1, 2, 3, 4] and is still being controversely interpreted from recent experimental data [5].

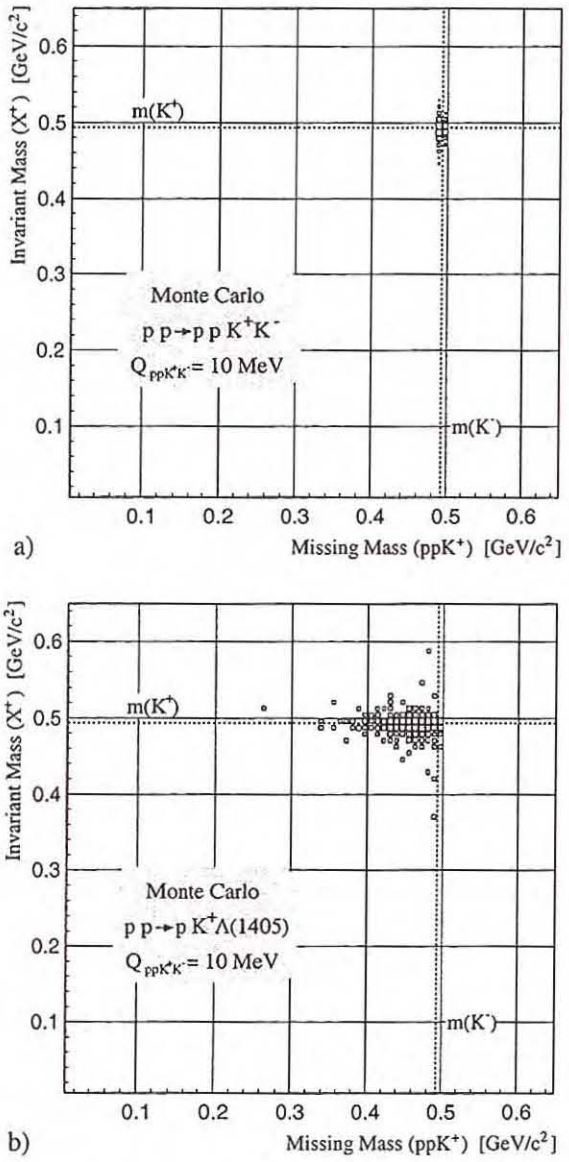

Fig. 1: Invariant mass of a third positively charged ejectile besides two identified protons in the exit channel versus the missing mass with respect to the (ppK^+) subsystem at 10 MeV excess energy above the (K^+K^-) threshold according to Monte Carlo simulations of the reactions $pp \to ppK^+K^-$ (a) and $pp \to pK^+\Lambda\,(1405)$ (b).

Results obtained within the framework of the Jülich meson exchange model [4] closely relate a $K\bar{K}$ molecule structure of the $f_0(980)$ with the strength of the $K\bar{K}$ interaction, which determines both shape and absolute value of the $\pi\pi \to K\bar{K}$ excitation functions [6]. A similar effect on kaon pair production cross sections in the proton–proton interaction is conceivable.

At the COSY-11 installation the four-momenta of positively charged particles are directly experimentally available. In addition, negative particles can be detected with reduced acceptance, which e.g. remains for the K^- detection at a level of more than 40 per cent at excess energies of 30 MeV with respect to the (K^+K^-) threshold. Details of the experimental technique in case of the (ppK^+K^-) final state are given in [7, 8, 9].

With no additional signal from a negatively charged particle being required the identification of a (ppK^+) subsystem leads to the reaction type

$$pp \to ppK^+X. \qquad (1)$$

In this case the underlying reaction mechanism is not unambigous, as one of the identified protons may originate from the decay of a previously produced hyperon Y in $pp \to pK^+Y \to pK^+pX$. Thus, in reaction type (1), X denotes a system of one or more undetected particles.

In consequence, the missing mass with respect to the identified (ppK^+) subsystem may shift to values too small for a (ppK^+K^-) hypothesis as demonstrated by the simulations in figure 1. An experimental acceptance decreasing with increasing excess energy favours final states close to threshold, thus a dominant influence of the hyperons $\Sigma^0\,(1385)$ and $\Lambda\,(1405)$ is expected [9]. Furthermore, reactions of the type $pp \to pK^+\Lambda x \to pK^+p\pi^-x$ might contribute, i.e. reactions with up to two additional pions or a number of gammas (x) produced along with a hyperon.

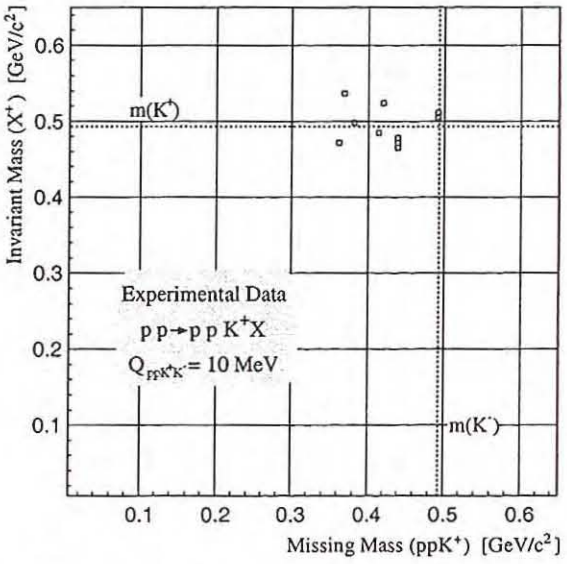

Fig. 2: Experimental data at an excess energy of 10 MeV with respect to the (K^+K^-) threshold. Axes are the same as in figure 1.

Experimental data at Q = 10 MeV in excess of the (K^+K^-) threshold, when compared to the simulations

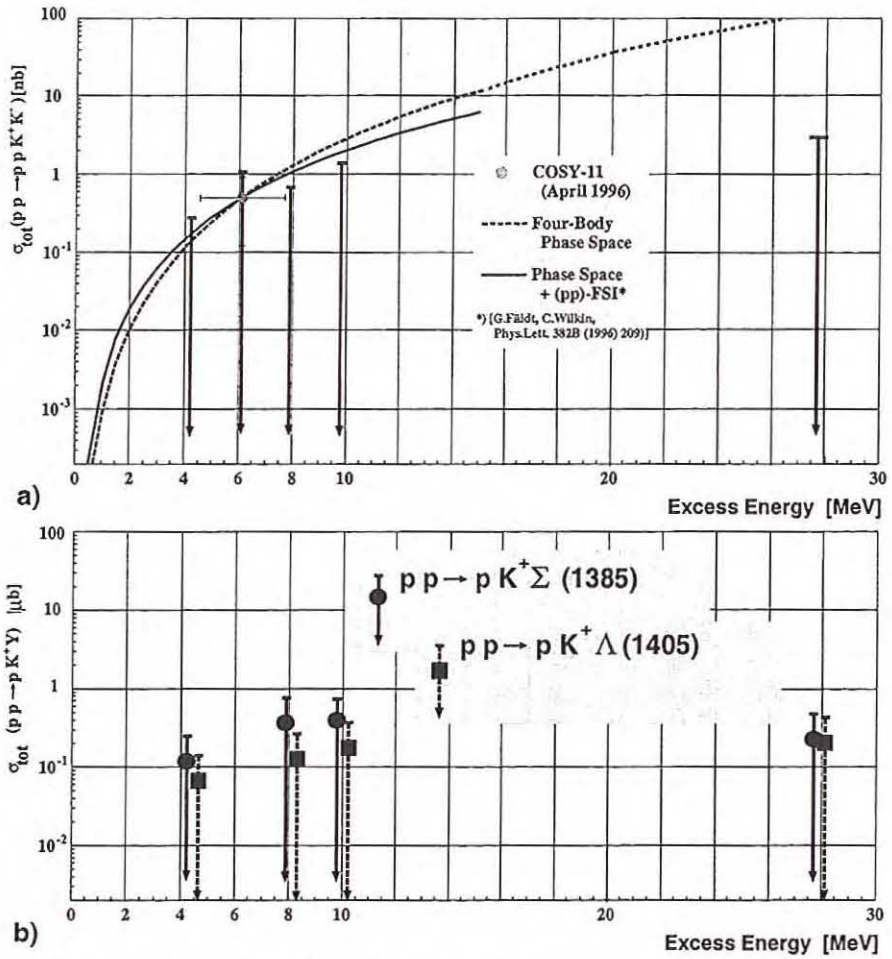

Fig. 3: Upper limits on the total cross section for the final states ppK^+K^- (a) and $pK^+\Sigma\,(1385)\,/\Lambda\,(1405)$ (b) at a confidence level of 95 %. Only events within a range of $3\,\sigma = 6\,\mathrm{MeV/c^2}$ around the kaon mass are accepted as (ppK^+K^-) candidates, based on a typical missing mass resolution $\leq 2\,\mathrm{MeV/c^2}$ at COSY–11. In (a) predictions of the energy dependence from four–body phase space and phase space including proton–proton FSI are fixed at the data point at Q = 6.1 MeV.

of figure 1, show a clear hint of the significance of the hyperon channels on the (ppK^+) system (fig. 2). The lack of at least 50 per cent of the expected number of hits which are consistent with a K^- interpretation in the data provides another piece of evidence.

With only a few ten events of the type (1) being identified in total, data taken at five different beam momenta up to excess energies of 30 MeV show no enhancement that can be considered a clear exclusive signal of one of the reaction channels previously discussed. Thus, at this stage of the analysis only upper limits of the total cross section for the charged kaon pair production and the hyperon channels of the $\Sigma\,(1385)$ and $\Lambda\,(1405)$, respectively, are available (fig. 3) [8, 9].

To unravel this situation, additional data have been taken at excess energies of $Q = -3\,\mathrm{MeV}$ and $Q = +3\,\mathrm{MeV}$, i.e. below and above the (K^+K^-) threshold, as well as at a higher Q value of 17 MeV in September 1998, the latter filling the obvious gap in figure 3.

A preliminary analysis of the data at $Q = 17\,\mathrm{MeV}$ suggests several events with additionally detected K^- mesons. Further evaluation of these data may result in an absolute value for the total cross section of the exclusive $pp \to ppK^+K^-$ channel in the vicinity of the $f_0(980)$.

References:

[1] R. L. Jaffe, Phys. Rev. **D 15**, 267 (1977)

[2] J. Weinstein, N. Isgur, Phys. Rev. **D 41**, 2236 (1990)

[3] D. Morgan, M. R. Pennington, Phys. Rev. **D 48**, 1185 (1993)

[4] D. Lohse, J. W. Durso, K. Holinde, J. Speth, Nucl. Phys. **A 516**, 513 (1990)

[5] HADRON'97 conference contributions by A. Kirk, G. D. Lafferty and P. Lebrun, AIP Conf. Proc. Vol. **432**, pp 361, 504, 715 (1998)

[6] O. Krehl, R. Rapp, J. Speth, Phys. Lett. **B 390**, 23 (1997)

[7] Annual Report 1996, IKP, Forschungszentrum Jülich, **Jül–3365**, 42 (1997)

[8] M. Wolke, PhD thesis (1997), Rheinische Friedrich–Wilhelms–Universität Bonn, **Jül–3532**, Forschungszentrum Jülich

[9] T. Lister, PhD thesis (submitted 1998), Westfälische Wilhelms–Universität Münster

* Institut für Kernphysik, Westfälische Wilhelms–Universität Münster, 48149 Münster, Germany

Note on the glue content in the η' meson

Paweł Moskal* for the COSY - 11 Collaboration

* Institute of Physics, Jagellonian University, Cracow, Poland

The investigations of the η' meson aim in a better understanding of its structure and its interaction with nucleons. The η' meson being predominantly an flavour singlet state may be built out not only of the quarkonium but also out of the gluonium state, making it an very interesting object. The possible gluonium contents implies that the creation of this meson in the proton-proton collisions may proceed via a fusion of gluons emitted from the colliding protons [1].
Similarly, the creation of the η' in the fusion of gluons is considered when trying to explain the large branching ratios of B and D mesons decay into the η' meson observed by the CLEO Collaboration [2, 3]. Without assuming the significant gluonium [4] or charmonium content in the η' meson it is also not possible to explain its large mass in comparison to the masses of its counterpart mesons from the pseudoscalar flavour octet.

Recently it is discussed whether the "gluon rich" states are more copiously produced for small transverse momentum transfer in the reaction $pp \to ppX$ where the conventional quarkonium states are supposed to be suppressed [5, 6, 7]. The central particle production in the $pp \to ppX$ reaction has been studied by the CERN WA102 Collaboration [8] for the high incident beam momenta ranging between 85 and 450 GeV/c. There are examples shown in reference [9], that considering only a large transverse momentum transfer $\Delta P_T > 500$ MeV/c, the usual $q\bar{q}$ states like ρ are clearly seen in the $\pi\pi$ invariant mass spectrum, whereas they disappear at a small ΔP_T ($\Delta P_T < 200$ MeV/c). In contrary, the Θ/f_J state which is supposed to be dominantly a glueball appears at a small ΔP_T.

The performed and planned COSY - 11 experiments on η and η' production in the $pp \to ppX$ reaction close to the kinematical threshold may also be analysed in view of the cross section distribution as a function of the transverse momentum transfer. For example at an excess energy Q = 10 MeV the transverse momentum transfer range from zero to about 100 MeV/c, which is of the same order as a small momenta studied at high incident beam energies at CERN.
The η is predominantly a flavour octet state and hence its coupling to gluonium is expected to be much weaker than in the case of the η' meson. Therefore if the gluon-gluon fusion mechanism is to be taken seriously it is expected to observe the enhancement at a small ΔP_T value for the η' meson production relative to the η.
The study of the transverse momentum transfer distributions may be performed with a very good momentum accuarcy of 1 MeV/c achieved at the COSY - 11 experiments.

[1] N. Nikolaev, CosyNews **No. 3** May 1998,

[2] C. P. Jessop et al., hep-ex/9801010

[3] B. H. Behrens et al., hep-ex/9801012

[4] F. Lenz, Nucl. Phys. **B 279** (1987), 119

[5] A. Kirk et al., hep-ph/9810221

[6] F. E. Close and A. Kirk, hep-ph/9701222 Phys. Lett. **B 397** (1997), 333

[7] J. -M. Frére, hep-ph/9810227

[8] D. Barberis et al., hep-ex/9803029

[9] M. R. Pennington, hep-ph/9811276

Angular and momentum distributions of the $pp \rightarrow pp\eta$ reaction products.

J. Smyrski and P. Wüstner for the COSY-11 collaboration

The S-wave interaction of η-mesons with nucleons influences substantially the energy dependence of the $pp \rightarrow pp\eta$ total cross section as observed by H. Calén et al.[1]. In angular and momentum distributions of the $pp \rightarrow pp\eta$ reaction products these final state interactions should be more sensitive. In order to search for such effects, we analysed experimental data collected in the near–threshold $pp \rightarrow pp\eta$ measurements performed at the COSY–11 facility. These measurements were done for nominal beam momenta varied continuously in the range from Q = - 9.6 MeV/c below to Q = 20.4 MeV/c above the threshold momentum equal to 1981.6 MeV/c. The nominal beam momentum, calculated from the synchrotron frequency and the beam orbit length, was corrected by -2 MeV/c based on the difference between the measured missing mass of the two outgoing protons and the known mass of the η–meson.
Figures 1 and 2 show examples of CM angular distributions of the η momentum vector and the proton–proton relative momentum vector, respectively, determined for the beam momenta range from 1993 to 1996 MeV/c, which is equivalent to an excess energy range of Q = 4 MeV to Q = 5 MeV. These distributions were obtained by correcting the experimental counts for the detection acceptance calculated from Monte Carlo simulations with phase space distribution of the reaction products weighted by the (p–p)-FSI. The angular distributions are flat indicating dominant S-waves in the exit channel.
Figure 3 shows the distribution of the event yield as a function of the relative momentum of the two outgoing protons again determined for beam momenta in the range from 1993 to 1996 MeV/c. The solid line indicates the result of a Monte Carlo calculation with phase space distribution weighted by the (p–p)-FSI whereas the dashed line represents calculations with a uniform phase space distribution. The solid line is normalized to the data points at small relative momenta, where (p–p)-FSI is particularly strong. With this normalization, the data points at higher relative momenta are underestimated. This can be caused by the $(\eta - N)$-FSI which has not been taken into account. Theoretical calculations describing the three body ppη final state with inclusion of (p–p)-FSI and (p–η)-FSI would be very useful for testing this hypothesis.

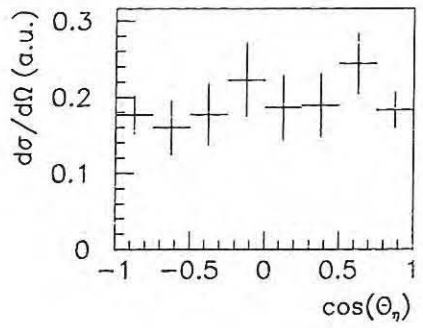

Figure 1: Angular distribution of the η momentum vector in the CM system.

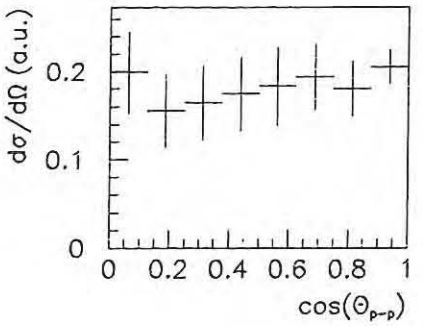

Figure 2: Angular distribution of the relative momentum vector of two protons the in CM system.

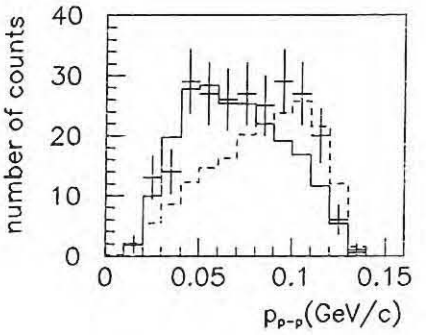

Figure 3: Distribution of the relative proton - proton momentum. Histograms are described in text.

References:

[1] H. Calén et al., Phys. Lett. **B366**(1996)39

Development and Test of the Three Threshold Discriminator

J. Majewski, A. Misiak for the COSY-11 and the TOF collaboration

The solution of a three-threshold discriminator using a two-point constant-level method has been presented in the IKP Annual Report 1996 [1]. A first discriminator of this type was realised as a hybrid on a printed-circuit board with the dimensions 25.5mm × 73.2mm. The unit, tested with pulses from a generator (t_{rise} = 1ns, t_{width} = 3ns), effectively reduced the time walk in a wide range of pulse amplitudes (±50ps for a 300:1 dynamic range). However, when using this discriminator with (attenuated) pulses from a photomultiplier triggered by a light emitting diode (LED) system [2] (PM+LED) the results were not satisfactory anymore. The time walk reached values up to ±200ps for a 10:1 dynamic range (with pulses of t_{rise} = 3ns, t_{width} = 7ns). It was found that the worsening of the timing characteristics was caused by the photoeffect from the first dynode of the photomultiplier which disturbed the leading edge of the output signals and thus did not allow to set a very low threshold value.

In order to still improve the characteristics of this discriminator, the input circuit was modified to enable constant-fraction shaping of the input pulses. The new printed-circuit board of the discriminator (model MΛM06) has the dimensions 24.8mm × 77.2mm. Test measurements with pulses of t_{rise} = 3ns and t_{width} = 7ns have shown an improvement of the timing characteristics of the discriminator after the modifications. Figure 1 presents timing characteristics of the modified discriminator for different settings of the three thresholds. The thresholds were chosen the following way: the highest threshold (THR3) was set to the minimum required signal amplitude (i.e. particle identification in the experiment), the lowest threshold (THR1) arbitrarily to the half of it. The middle threshold (THR2) was adjusted for minimum time walk over the whole possible amplitude range. The comparison of the THR1 timing, which acts as a leading edge discriminator, and the resulting output of the whole discriminator circuit shows the timing improvement. The time walk is about ±100ps for a 120:1 dynamic range.

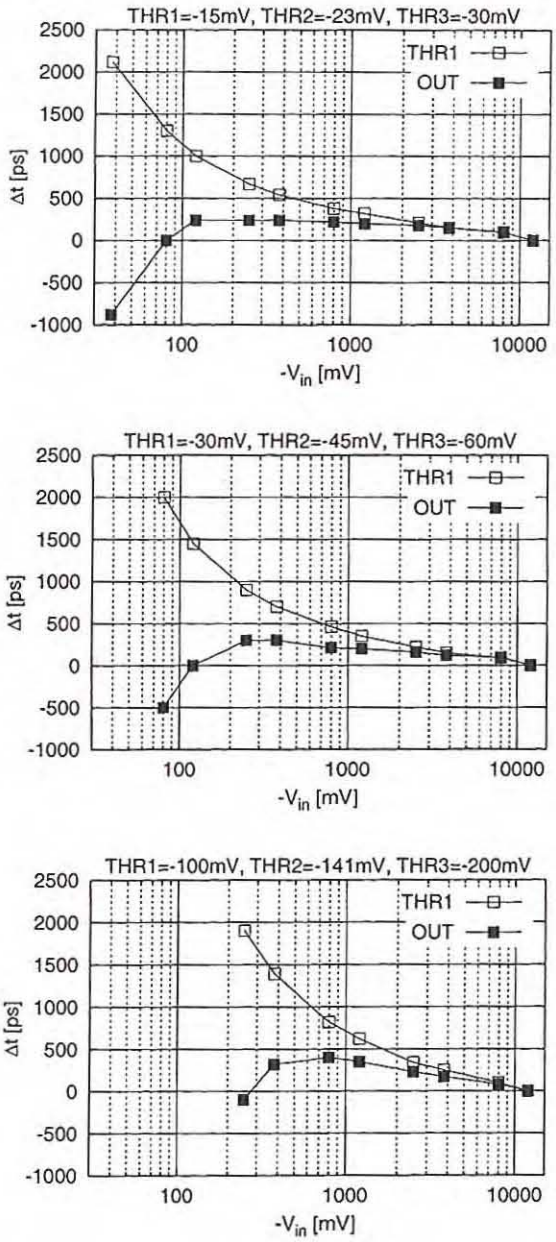

Fig. 1: Time walk measurements for different threshold settings with: input pulse source = PM+LED, t_{rise} = 3ns, t_{width} = 7ns, fraction = 0.2, delay = 2.5ns, clamping at +0.4V and −10V. The open squares show the timing characteristics of the lower threshold (THR1), the filled squares represent the time walk of the discriminator output.

References:

[1] J. Majewski, A. Misiak: "Multi-Point Methods for the Time Walk Reduction of Discriminators", IKP Annual Report 1996, p.39-41

[2] T. Sefzick et al.: "A System for Simulation of Scintillator Light Signals", Nucl. Inst. and Meth. A288 (1990) 571-573

Additional drift chamber for the COSY–11 facility

J. Smyrski for the COSY-11 collaboration

The COSY–11 facility uses two planar drift chambers for measurements of trajectories of positively charged reaction products which are deflected in one of the COSY dipole magnets towards the center of the COSY ring. The chambers cover only the upper range of momenta of the outgoing particles. It is planned, therefore, to install along the dipole magnet an additional drift chamber extending the momentum acceptance of the COSY–11 spectrometer towards smaller momenta. This chamber will allow one to measure for example the π^+–momenta in the reaction $pp \to pp\pi^+\pi^-$ near threshold. It will also increase the detection efficiency for kaons, due to its smaller distance to the target.

The new chamber contains hexagonal cells (see Fig. 1), identical with the ones which are used in the central drift chamber of the SAPHIR detector [1]. The drift field in this type of cells has approximately cylindrical symmetry, and thus the distance to drift time relation is independent of the particles' angles of incidence. In order to minimize the multiple scattering on wires, gold–plated aluminium [2] is used for the 110 μm–thick field wires. The sense wires are made of 20 μm–thick gold–plated tungsten. As chamber gas a mixture of 50% argon and 50% ethane at atmospheric pressure is used. The sense wire potential is about +1800 V, whereas the field wires are all grounded.

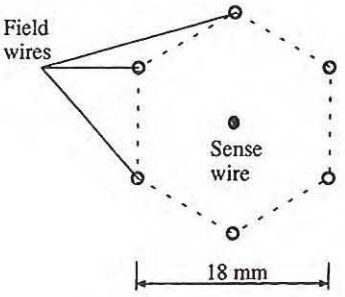

Figure 1: Cell structure.

The cells are arranged in the detection plane as shown in Fig. 2. The chamber consists of three detection planes with vertical wires, two planes with wires inclined at -10^o and two with wires inclined at $+10^o$. This arrangement makes it possible to reconstruct particle trajectories in three dimensions, also in cases of multi-track events. The chamber contains 3x80=240 and 4x77=308 cells with vertical and inclined wires, respectively.

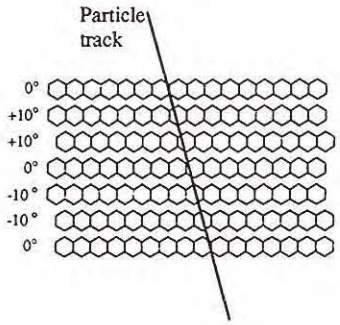

Figure 2: Orientation of wires in the seven detection planes of the chamber.

The wires are stretched between two aluminium plates and are positioned by means of sockets with inner openings of $\phi = 50$ μm and $\phi = 150$ μm for the sense and field wires, respectively. The wires are fixed in the sockets by means of small wedges. The sockets are inserted in ϕ=2 mm holes drilled in the aluminium plates. The plates are supported by two U-shaped frames (see Fig. 3). More stable rectangular frames were excluded due to space limitations, however, the applied frames are rigid enough to hold the total load of 290 kg originating from the mechanical tension of all wires. The active area of the chamber is 1500 mm wide and 400 mm high. The installation of the chamber at the COSY–11 facility is foreseen for summer of 1999.

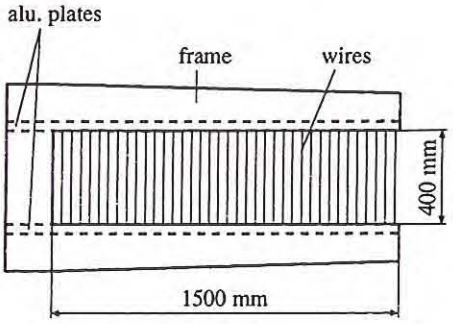

Figure 3: Front view of the chamber.

References:

[1] W. J. Schwille et al., Nucl. Instr. and Meth. A 344(1994)470

[2] California Fine Wire Company, Grover Beach, California, USA

The EDDA Experiment: Excitation Functions of Proton-Proton Scattering at Intermediate Energies

J. Bisplinghoff, F. Hinterberger and W. Scobel for the EDDA collaboration [1]

1 Motivation and General Description

The EDDA experiment [2] is designed to provide a high precision measurement of proton-proton elastic scattering excitation functions ranging from 0.5 to 2.5 GeV of laboratory kinetic energy, T_p. It utilizes the proton beam of the cooler synchrotron COSY [3] operated by Forschungszentrum Jülich. The proton-proton elastic scattering [4] is fundamental to the understanding of the strong interaction. Excitation functions for cross sections and polarization observables of the pp interaction, in particular the elastic channel, provide the data base for phase shift analyses serving as input to calculations concerning nuclei and the test of meson exchange models [5]. The experimental data base is rather poor [6] for energies $T_p > 1.2$ GeV and there is a need for exclusive data in narrow energyy increments and over a large angular range. Such data is also suitable to either detect dibaryonic resonances or to place upper limits on their existence in case of their coupling to the elastic channel.

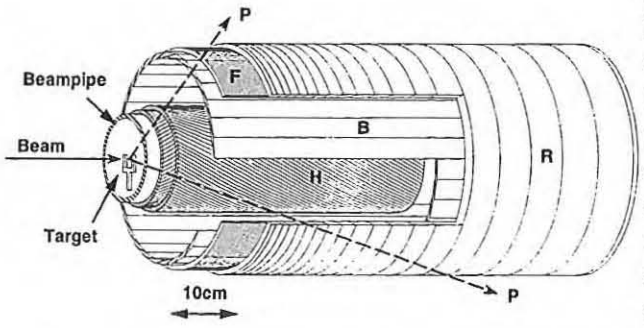

Figure 1: The EDDA detector (not to scale)

Both for a phase shift analysis as such and for its use in identifying dibaryonic resonances, it is mandatory to measure not only spin-averaged cross sections, but also spin observables such as analyzing powers (A_N) and spin correlation coefficients (A_{NN}, A_{SS},A_{SL}). This requires a polarized COSY beam and a polarized EDDA target. EDDA was conceived as an experiment using the internal recirculating COSY beam in order to obtain luminosities high enough for use of a polarized atomic beam target [2]. Data collection proceeds during synchrotron acceleration in a multipass technique, so that a full excitation function is measured in each acceleration cycle. Statistical accuracy is obtained by averaging over many cycles. This technique requires (and has demonstrated) a very stable and reproducable operation of COSY.

The EDDA detector was designed for large solid angle coverage in a cylindrical geometry, and it provides a fast and efficient trigger on low multiplicity events of a given kinematic signature. Elastic events are identified by coplanarity with the beam ($\varphi_1 - \varphi_2 = 180°$) and the elastic scattering kinematics, which impose $\tan\Theta_{1,lab} \cdot \tan\Theta_{2,lab} = 2m_pc^2/(2m_pc^2 + T_p)$ These conditions are employed – with different degrees of stringency – both in triggering and in event identification during off-line analysis. The EDDA detector is shown in Fig. 1 in a schematic fashion. It consists of two cylindrical double layers covering 30° to 150° in Θ_{cm} for the elastic pp channel and about 85 % of the full solid angle. The inner layers are composed of scintillating fibers which are helically wound in opposing directions. They are not required and were not installed when measuring spin-averaged cross sections with a CH_2 fiber target, but are essential for measuring spin observables with the polarized atomic beam target, as they provide for vertex reconstruction. The outer layers consist of 32 scintillator bars which are running parallel to the beam axis and which are read out at both ends. They are surrounded by scintillator semirings. The scintillator cross sections were designed so that each particle traversing the outer layers

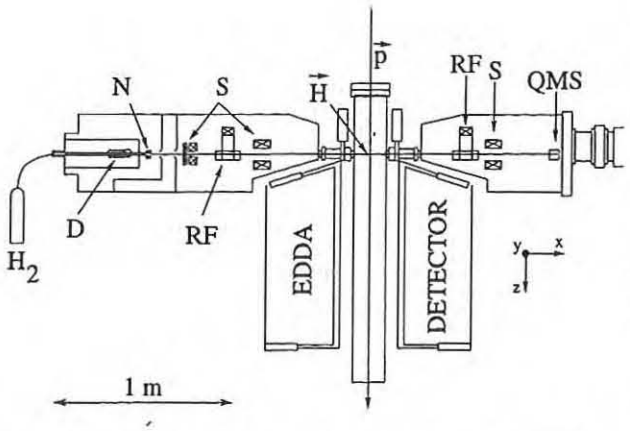

Figure 2: Polarized atomic beam target with dissociator D, cooled nozzle N, permanent sextupole magnets S, RF transitions and Breit-Rabi polarimeter in the beam dump

produces a signal in two neighbouring bars and rings. Analysis of the fractional light output is used to determine the angles of incidence much more accurately (by a factor of 5) than would be possible on the basis of detector granularity alone. Combined with the spatial resolution of the 2.5 mm scintillator fibers, this provides for vertex reconstruction to a precision of about 2 mm. Details are given in Ref.[2].

2 Status and Recent Progress

Taking unpolarized data with outer detector layer alone using CH_2 fiber targets and C fiber targets for background subtraction was completed in 1996, and cross sections resulting from the data published [7]. During the run in November 1997, commissioning of the inner detector layer and of the polarized atomic beam target [8] (see fig. 2) was completed as scheduled. The polarized hydrogen atoms are prepared using an atomic beam source with dissociator D, cooled nozzle N, permanent sextupole magnets S, and RF transition units. In the beam dump the polarization is continuously monitored using a Breit-Rabi polarimeter consisting of RF transition, permanent sextupole magnet S and quadrupole mass spectrometer QMS. Preparing a polarized hydrogen beam in a pure hyperfine state yields a peak polarization of about 85 % with an effective target density of $2.5 \cdot 10^{11}$ atoms/cm^2. Taking the unpolarized hydrogen background in the target region into account the effective polarization amounts to about 60 %. The FWHM diameter at the target point is about 12 mm. The installation of the polarized atomic beam target does not preclude the use of fiber targets for tuning and referencing.

Two runs in June and November 1998 were devoted almost exclusively to the collection of analyzing power data using the unpolarized COSY beam and the polarized atomic beam target. With $1.5 \cdot 10^6$ turns/s and $3 \cdot 10^{10}$ protons in the ring a luminosity of about 10^{28}/cm^2/s was achieved. Data were taken during acceleration as well as during deceleration of the COSY beam. The time period of one cycle was about 20 s. The direction of the target polarization was changed from cycle to cycle between $\pm x$ and $\pm y$ thus allowing a proper spin flip correction of false asymmetries [9]. Since the target polarization is constant during an acceleration/deceleration cycle the analyzing power excitation function can be measured with a high relative accuracy. The absolute calibration is established with reference to angular distributions measured at the IUCF cooler ring near 1000 MeV/c and at Los Alamos near 1500 MeV/c with a high absolute accuracy. The data analysis is underway. Now preparations for measuring excitation functions of polarization correlation observables A_{NN}, A_{SS} and A_{SL} are underway.

The EDDA collaboration wishes to acknowledge the great support it has been receiving from the COSY team.

References

[1] The EDDA collaboration: M. Altmeier[1], F. Bauer[2], J. Bisplinghoff[1], T. Bissel[1], R. Bollmann[2], M. Busch[1], K. Büßer[2], T. Colberg[2], L. Demirörs[2], O. Diehl[1], F. Dohrmann[2], H.P. Engelhardt[1], P.D. Eversheim[1], O. Felden[1], R. Gebel[3], M. Glende[1], J. Greiff[2], A. Groß[2], R. Groß-Hardt[1], F. Hinterberger[1], R. Jahn[1], E. Jonas[2], H. Krause[2], R. Langkau[2], T. Lindemann[2], J. Lindlein[2], R. Maier[3], R. Maschuw[1], T. Mayer-Kuckuk[1], A. Meinerzhagen[1], M. Pfuff[2], D. Prasuhn[3], H. Rohdjeß[1], D. Rosendaal[1], P. von Rossen[3], B. Sanz[2], N. Schirm[2], M. Schulz-

Rojahn[1], V. Schwarz[1], W. Scobel[2], S. Thomas[1], H.J. Trelle[1], E. Weise[1], A. Wellinghausen[2], K. Woller[2], R. Ziegler[1], Spokesmen: J. Bisplinghoff[1], F. Hinterberger[1] and W. Scobel[2],
(1)Inst. f. Strahlen- und Kernphysik, Univ. Bonn,
(2) I. Inst. f. Experimentalphysik, Univ. Hamburg,
(3) Inst. f. Kernphysik, FZ Jülich.

[2] J. Bisplinghoff, and F. Hinterberger, *Particle Production Near Threshold, AIP Conf. Proc.* **221**, 312 (1991); W. Scobel, *Phys. Scr.* **48**, 92 (1993); H. Rohdjeß, *Proc. Int. Conf. on Physics with GeV-Particle Beams, Jülich, 1994* Singapore: World Scientific, 1995, p. 334.

[3] R. Maier, *Nucl. Instr. and Meth. in Phys. Res.* **A 390**, 1 (1997).

[4] C. Lechanoine-Leluc, and F. Lehar, *Rev. Mod. Phys.* **65**, 47 (1993).

[5] R. Machleidt, *Adv. in Nucl. Phys.* **19**, 189 (1989).

[6] R.A. Arndt, et al., *Phys. Rev.* **C 56**, 3005 (1997), SAID solution SM97.

[7] D. Albers, et al. *Phys. Rev. Lett.* **78**, 1652 (1997).

[8] P.D. Eversheim, *Nucl. Phys.* **A626**, 117c (1996).

[9] G.G. Ohlsen and P.W. Keaton, Jr., *Nucl. Instr. and Meth.* **109**, 41 (1973).

The Storage Cell for the EDDA-Experiment at COSY

M. Glende, U. Bechstedt, P.D. Eversheim, O. Felden, R. Gebel, U. Rindfleisch, D. Rosendaal

The EDDA experiment measures excitation functions of polarization observables from 0.5 to 2.5 GeV at COSY. It uses a polarized atomic beam target which provides the expected polarization and density distribution[1][2]. For a further increase of the target density a storage cell was installed.

For a high gain in luminosity the aperture of a storage cell should be as small as possible to get a high target density and wide enough to let the full accelerator beam pass. With the present cell aperture of 12 mm height and 29 mm width a gain factor of 56 in target thickness is expected for experiments using the whole cell length. For the EDDA experiment the region where interactions can be evaluated is limited by the angular acceptance of the detector to ± 15 mm. Thus the gain in target thickness by the storage cell is reduced to a factor 9.6 for the EDDA experiment.

Since the storage cell reduces the acceptance of the accelerator the optimal aperture for the given situation was determined in several steps:
i) By scrapers [3] and the given β-functions the beam losses for given apertures at the EDDA experiment were estimated.
ii) These predictions were tested by real apertures at the EDDA experiment. For the envisioned aperture the beam intensity was reduced to 43 % in accordance with the prediction of the scraper test.
iii) The storage cell was built. The small variation of the β-functions allows to choose a length of 300 mm without a perceptible additional beam loss.
If the cell is not in use it can be raised to the top of the beam pipe to let the beam pass undisturbed for other experiments.

For a high target density the cell is cooled to about 80 K – 100 K. Lower temperatures will cause depolarization of the stored target gas [4]. Evaluating the results of [4] for several coatings $P^2 \cdot I$ can be increased by 25 % with a Teflon coating. Another 25 % could be achieved with a Fomblin oil coating. (Pressure of Fomblin oil Y-VAC 3: $5 \cdot 10^{-13}$ Torr at 293 K).
The present cell is coated with PTFE 3170, a polytetrafloruetylene form of Teflon, by a proper tempering proceeding. It is expected to be more resistant as the flourinated ethylene propylene copolymer form of Teflon and delivers the same conservation of polarization [4].

The present storage cell (see figure 1) is made of aluminium manufactured of a single piece to maintain a high heat conductance. Based on calculations for simulated particle trajectories [5] the part of the cell that is seen by the detector has a wall thickness of 0.2 mm in order to minimise multiple straggling.

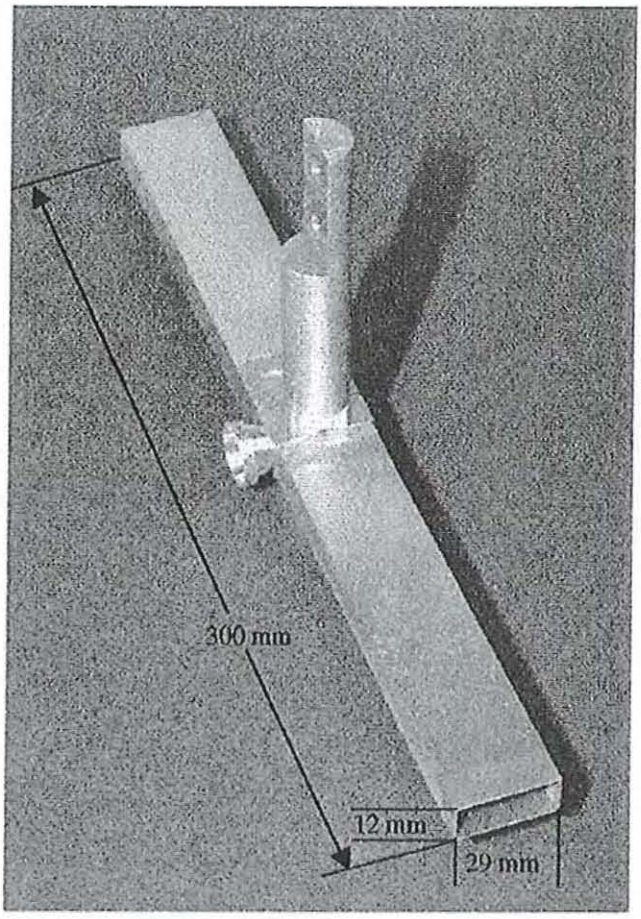

Figure 1:
The storage cell with an aperture of 12x29 mm^2 and 300 mm length installed in the beam pipe at TP2
In front: The cell part with 0.2 mm wall thickness.
Aside: Mount for the feeding tube
At the top: Connection to the cold finger

Since the detector adjoin very close to the interaction zone, the cold head for the cell had to be positioned 60 cm above the beam pipe. Cell and cold head were linked by an appropriate cold finger. When the cold head is warmed up, an additional turbo molecular pump cares for conservation of a good vacuum quality.
The storage cell is operated with a feeding tube fastened at the funnel shaped opening at the side of the cell. A spring mounting cares for a sufficient pressure between the cell and the feeding tube to achieve a high heat conductance between them.

References:

[1] M. Altmeier, Ph.D. thesis 1998
[2] O. Felden, Ph.D. thesis 1998
[3] M. Glende, An. Rep. 97, p 151
[4] J.S. Price, W. Haeberli, NIM, A349 (1994) 321-333
[5] E. Weise, private communication

Determination of the Λ lifetime in hypernuclei produced in the 1.9 GeV p + Bi reaction

I. Zychor for the COSY-13 Collaboration

The lifetime of the heavy Λ hypernuclei was measured by the observation of delayed fission using the recoil shadow method in the p + Bi reaction. The measurements were performed at 1.9 GeV proton energy and the background was determined at 1.0 GeV. From the distribution of the fission fragments in the shadow region the lifetime

$\tau = [\ 161 \pm 7\ (\text{statist.}) \pm 14\ (\text{system.})]$ ps

was obtained.

Details of the experiments are given in Ref. [1] and [2].

In Fig. 1 the experimental and calculated distributions are shown for the p + Bi reaction.

We have used two different targets in our measurements. The hypernucleus lifetime τ was calculated from the experimental event distributions in the shadow region using the maximum likelihood method applied for the Poisson distribution. In the wire range from 1 to 54 we have recorded 1604 events at 1.9 GeV and in the corresponding normalized background spectra at 1.0 GeV we measured 146 events. In the wire range from 41 to 54 we have recorded 1418 events at 1.9 GeV and 140 events at 1.0 GeV. This gives a statistical error in the lifetime determination equal to 7 ps.

The shape of the drop-off around the shadow edge is predominantly caused by absorption of fission fragments in the target and by small-angle scattering of fission fragments in a window foil at the bottom of the experimental chamber. These effects were simulated assuming a Gauss distribution with $ó_{Gauss}$ as parameter. The parameter was varied until the drop-off curve (dashed line in Fig.1) fitted the data points. The target deformation was a parameter in our lifetime calculations and it was assumed that the lower edge of the target was shifted up to 0.4 mm in the direction of the proton beam.

The following contributions were included to the systematic error of the lifetime:

1. target deformation: 2 ps,
2. different wire ranges: 3 ps,
3. small angle scattering described by the Gauss distribution: 5 ps,
4. the error of measured lengths and distances in the experimental set up (e.g. a target length, a distance from the detectors to the shadow edge etc.) 6 ps,
5. uncertainty in the recoil momentum distribution and its modification caused by the absorption in the target: 8 ps,
6. uncertainty where the COSY protons hit the target in vertical direction: 6 ps,
7. four different cuts in the event selection during the track reconstruction for 1 σ, 1.5 σ, 2 σ and 3 σ values for both horizontal directions: 2 ps,
8. normalizing and shifting of spectra from different runs: 1 ps.

Assuming independent contributions from different errors we get a total systematic error equal to 14 ps.

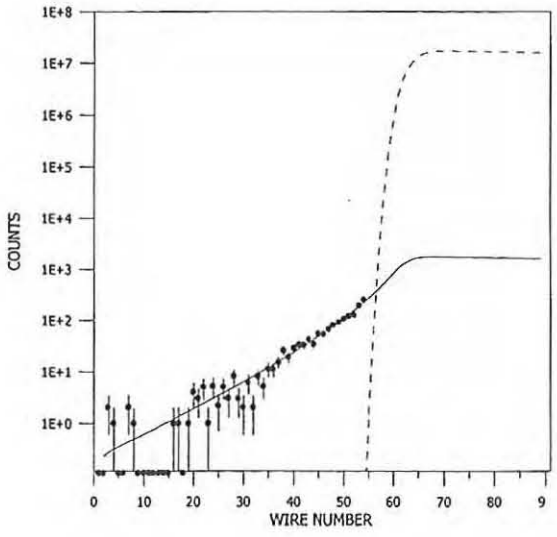

Fig.1. The experimental points shown for channels 54 (the shadow region) were obtained by subtracting the normalized background measured at 1.0 GeV. The full line presents the result of the fit of delayed fission fragments for a hypernucleus lifetime of 161 ps. The dashed line is the distribution of prompt fission events modelled taking into consideration absorption and scattering of fission fragments in the target and in window foils. The abscissa is the distance (in 1 mm wide channels) along the lower MWPC, parallel to the COSY beam direction

[1] P.Kulessa et al., Phys. Let. B427 (1998) 403

[2] K.Pysz et al., NIM A420 (1998) 356

Influence of the background shape on hypernucleus lifetime measured in the 1.9 GeV p + Bi reaction

I.Zychor for the COSY-13 Collaboration

The background in the COSY-13 experiments, using the recoil shadow technique, is measured at 1.0 GeV proton energy. At this energy hypernucleus production in reactions induced on heavy targets is very small.

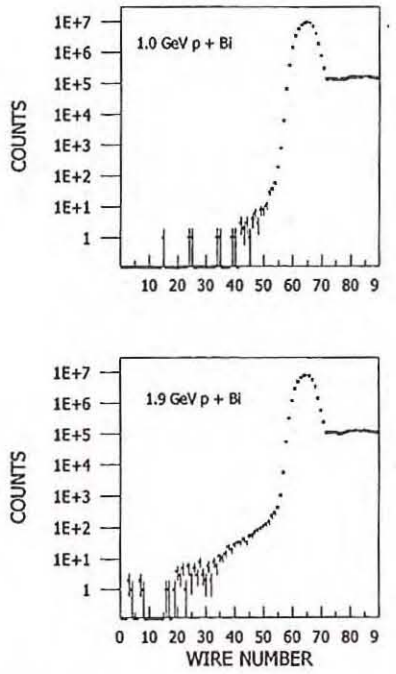

Fig.1 Position distributions obtained in the lower MWPC for collisions of 1.0 GeV and 1.9 GeV protons with a Bi target. The abscissa is the distance (in 1 mm wide channels) along the lower multiwire proportional chamber, parallel to the COSY beam direction.

After normalization of the 1.0 GeV spectrum to the 1.9 GeV spectrum in the plateau region (for wire numbers > 70) the background was subtracted from the 1.9 GeV spectrum in the shadow region (< 55). The lifetime τ of the Λ hyperon was then obtained from a fit to the number of net events in the shadow region. It was found to be equal to

$$\tau = [\ 161 \pm 7\ (\text{statist.}) \pm 14\ (\text{system.})]\ \text{ps}.$$

Details of the experiments and lifetime calculations are given in Ref. [1-3]. Spectra measured in the p + Bi reaction are shown in Fig. 1.

To check the background influence on the calculated lifetime two shapes of background were assumed: a constant background and a "step background" in the shadow region (Fig. 2).

For the "step background" the number of counts in the fitted wire range was kept constant and within the error bars equal to the measured number of counts at 1.0 GeV (after normalization).

For calculations with the constant background the total number of counts in the wire range from 1 to 54 was varied from 5.4 (0.1 count/wire) up to 54 (1 count/wire) events. The lifetime decreases with the increasing number of subtracted background counts from 158 to 149 ps.

For different shapes of the "step background" (in steps of 10 wires) we have got the lifetime values from 156 to 161 ps.

So, the largest difference between lifetime values obtained for different shapes of the included background is 12 ps, then it differs less than 7.5 % from the value obtained with normalized background subtracted wire by wire.

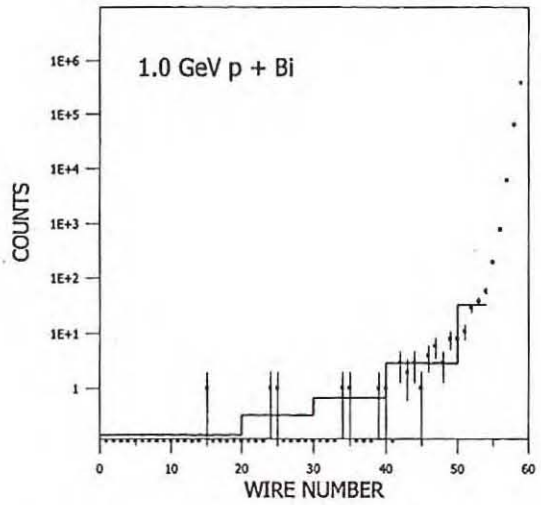

Fig.2. An example of the "step background" (solid line) shown in the shadow region for wire numbers from 1 to 54

[1] P.Kulessa et al., Phys. Let. B427 (1998) 403
[2] K.Pysz et al., NIM A420 (1998) 356
[3] I.Zychor, contribution to this Report

First Results on Two - Kaon Production at MOMO

F. Bellemann[1], A. Berg[1], J. Bisplinghoff[1], G .Bohlscheid[1], J. Ernst[1],F. Hinterberger[1], R. Ibald[1], R. Jahn[1], L. Jarczyk[2], R. Joosten[1], A. Kozela[3], H. Machner, A. Magiera[2], R. Maschuw[1], T. Mayer-Kuckuk[1], G. Mertler[1], J.Munkel[1], P. v. Neumann-Cosel[4], D. Rosendaal[1], P. v. Rossen, H. Schnitker[1], J. Smyrski[2], A. Strzalkowski[2], R. T Ile, and C. Wilkin[5]

The MOMO experiment focuses on near threshold meson production via the reactions pd 6 ^{3}He $\pi^+\pi^-$ and pd 6 ^{3}He K^+ K^-. It takes advantage of the high quality of the cooled external COSY beam and the existing spectrometer BIG KARL. The setup consists of a high granularity scintillating fibers meson detector near the target with a $\forall$ 45 deg. opening angle, and the spectrometer, which is used for ^{3}He-identification. The large solid angle and high resolution of this detection method will yield precision data on the low energy (T<80 MeV) meson-meson interaction and probe into questions like meson-nucleon resonances and KK-molecule.

The MOMO vertex detector consists of 672 scintillating fibers (round, 2.5 mm diameter) arranged in three planes tilted 60 deg. versus each other. Each plane is subdivided into two identical modules. The fibers are read out by 16-fold photomultipliers. The total efficiency was measured to be better than 99% for minimal ionizing particles. The BIG KARL spectrometer is also fully operational. Its status is described in detail elsewhere in this annual report. The MOMO scattering chamber houses the 4mm LD2 target as well as a remotely steerable ladder for beam viewers and solid targets. The 5 mm thin Al front end of the chamber faces the vertex detector on the outside and keeps straggling of the mesons at a small level.

Until 1997, the MOMO collaboration measured the pd 6 ^{3}He $\pi^+\pi^-$ reaction at three different proton beam momenta (1060 MeV/c, 1150 MeV/c, 1200 MeV/c), corresponding to 28 MeV, 70 MeV and 92 MeV center of mass energy above the reaction threshold. In total, some 30 000 kinematically complete $\pi^+\pi^-$ - events were observed. The obtained two - pion invariant mass spectra showed a strong deviation from phase space at all three energies, whereas the $\pi - ^3$He missing mass spectra followed phase space. The pion angular distributions displayed a remarkable sidewise peaking (in the c.m.s.) and a preferential back to back emission of the two pions. This behaviour can be well described by calculations assuming a p-wave between the two pions and s - waves in the $\pi - ^3$He system. Several articles on theses results have been submitted for publication.

In two beam times in 1998 the MOMO - collaboration measured two kaon production via the reaction pd 6 ^{3}He K^+ K^- at a beam momentum of 2.62 GeV/c (Q = 56 MeV). In the first beam time (one week) data taking was severely limited by the then available beam intensity of 3 x 10^7 protons per second and only some 30 two kaon events were obtained. But at least the feasibility of this experiment with the MOMO setup was clearly demonstrated. The beam time in August (two weeks) was a major breakthrough for MOMO as well as for COSY. For the first time, an extraction rate larger than 60% was obtained at this high beam momentum. In addition, new beam line optics and various other improvements resulted in a beam intensity of about 10^9/s. The beam cycle was 12 s beam on and 8 s beam off. Furthermore, for the first time the beam halo was negligible (< 10^{-4}). The count rate of the newly implemented halo veto counter was only some 80 K/s. During the first five days the beam intensity was limited to about only 10^8/s due to the neutron monitors next to our counting room. After implementation of an additional concrete block wall at the entrance of the BIG KARL area this problem disappeared so that we could use the maximal available beam intensity.

The reaction pd 6 ^{3}He K^+ K^- was measured at four largely overlapping BIG KARL momentum settings, so that the full phase space of the reaction was obtained.

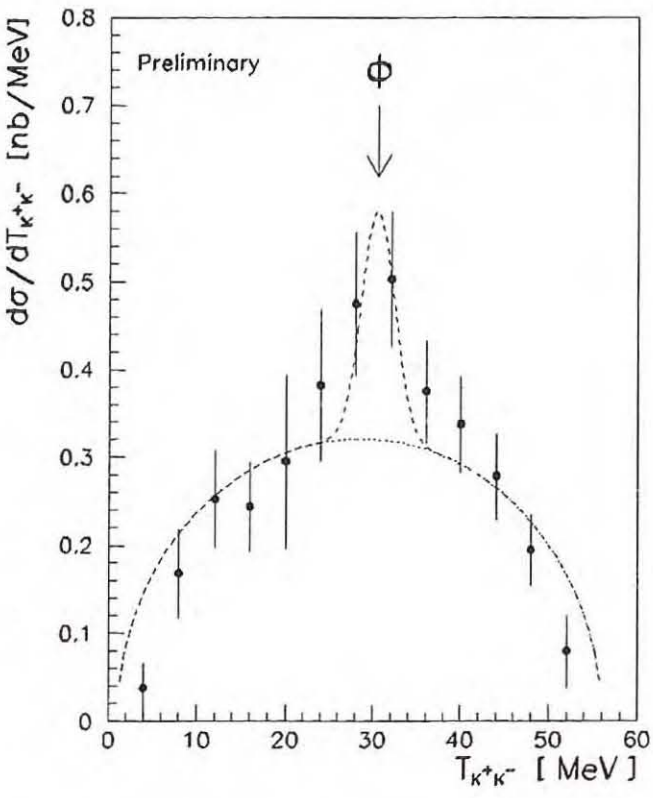

The ^{3}He particles could be unambiguously identified by

Fig. 1: K^+K^- invariant mass spectrum from the reaction

pd 6 ^{3}He K^+ K^- at 56 MeV above reaction threshold plotted in units of K^+ K^- relative energy. See text.
time of flight and energy loss measurements. The two - kaon hits on the vertex wall were uniquely identified by their hit patterns and energy loss. Good events must be coplanar in respect to the total meson momentum axis, which is defined by the beam and the ^{3}He momenta. The newly implemented 16 – fold circular scintillator hodoscope behind the vertex detector enables good kaon identification and pion separation. In total, some 1500 two kaon events were observed. The (still preliminary) results of our data analysis are displayed in the figures.

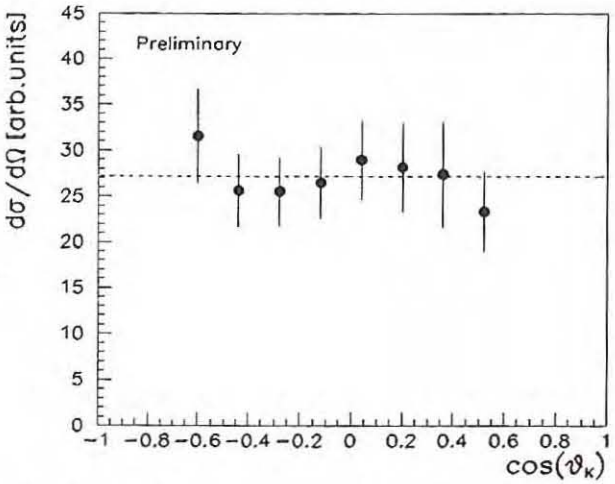

Fig 2: Angular distributions of the individual kaons in the c.m.s. at 56 MeV above threshold. See text.

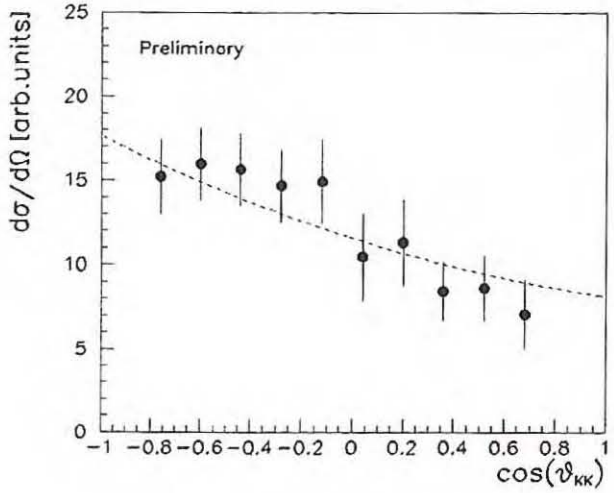

Fig.3 Distribution of the relative angles between the two kaons in the c.m.s.. See text.

Fig.1 shows the obtained two kaon invariant mass spectrum. A clear signal of the phi meson is evident. Figure 2 and figure 3 show the kaon angular distributions, and figure 4 the kaon – helium invariant mass spectrum. In all figures, the dashed lines correspond to phase space. In contrast to our two pion data, no significant deviation from phase space can be observed. Data analysis is in good progress and further measurements of this reaction at different beam energies near threshold will be interesting.

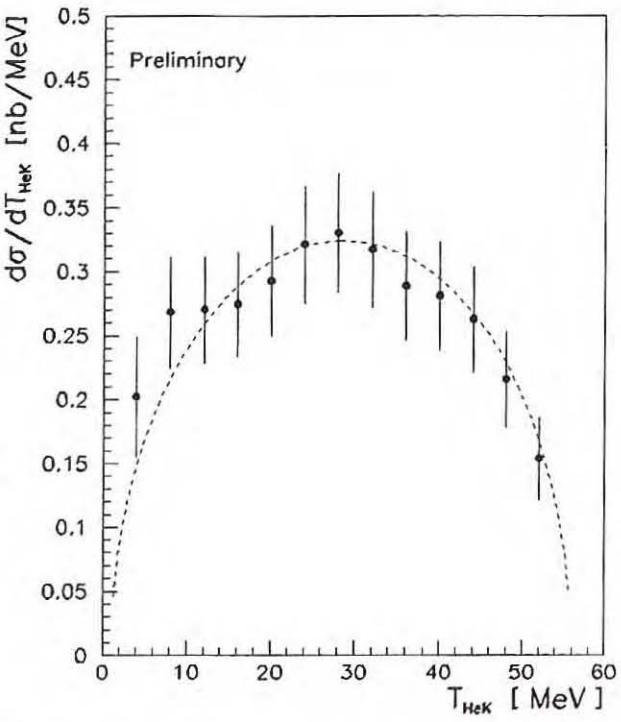

Fig. 3: K– ^{3}He invariant mass spectrum from the reaction pd 6 ^{3}He K^+ K^- at 56 MeV above reaction threshold plotted in units of K – ^{3}He relative energy. See text.

[1] Institut fηr Strahlen- und Kernphysik, Universitεt Bonn
[2] Institute of Physics, Jagellonian University, Cracow, Poland
[3] Institute of Nuclear Physics, Cracow, Poland
[4] Institut fηr Kernphysik, Technische Hochschule Darmstadt
[5] Physics & Astronomy Department, University College London, UK

1.2 Experiments at External Facilities

Strong-interaction effects in the 2p states of antiprotonic hydrogen and deuterium

D. Anagnostopoulos[1], M. Augsburger[2], G. Borchert, C. Castelli[3], D. Chatellard[2], P. El-Khoury[4], J.-P. Egger[2], H. Gorke, D. Gotta, P. Hauser[5], P. Indelicato[4], K. Kirch[5], S. Lenz, N. Nelms[3], K. Rashid[6], O.W.B. Schult, Th. Siems, L.M. Simons[5]

LEAR experiment PS207 used the high quality antiproton beam to investigate the characteristic X-radiation from antiprotonic hydrogen and deuterium. In order to achieve sufficiently high line yields the cyclotron trap was used to stop the antiproton beam in dilute hydrogen gas of 20 mbar pressure. The energy resolution necessary to be sensitive to the hyperfine structure in the 2p states was achieved with a focussing Bragg crystal specrometer [1].

The energy calibration was obtained from fluorescence X-rays and the spectrometer resolution was determined with the narrow $\bar{p}\,^3$He and $\bar{p}\,^{20}$Ne lines, which are not affected by the strong interaction [2,3]. To measure the Lα transition from $\bar{p}$H with high statistics, the crystal spectrometer was set up as a twin system, where three spherically bent quartz crystals (arm I, arm II top and bottom) were installed. Each crystal reflected X-rays to its own CCD detector.

To compare the theoretical predictions with the experimental results (Figure 1), the line shape was constructed for each model by folding the Lorentzian line shape of the 2p hyperfine components with the experimental resolution. The energy differences of the sublevels were fixed according to the pure electromagnetic (QED) and the predicted hadronic shifts. A statistical population of the hyperfine levels was assumed. In a χ^2 analysis for the various predictions, the total intensity and the height of the (almost negligible) background were free parameters.

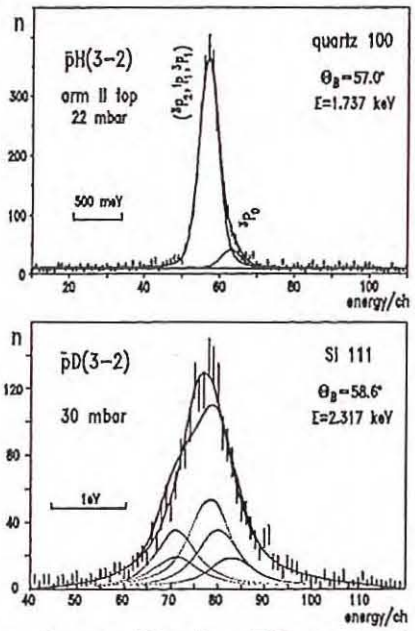

Figure 1: Top - Lα transition from $\bar{p}$H, measured with one crystal-detector pair. The high energy tail was identified to be the 2^3P_0 state. The three close-lying states 2^3P_2, 2^1P_1, and 2^3P_1 were not resolved. Bottom - Lα line shape from $\bar{p}$D.

Taking into account only the hyperfine splitting from QED, a bad description of the line shape was obtained as was the case for a model predicting strongly bound states close to threshold. Best agreement between theory and experiment was obtained for the models based on meson exchange to construct the real part of the antiproton-proton potential and adding a strong phenomenolgical annihilation potential („Dover-Richard potential" [4]).

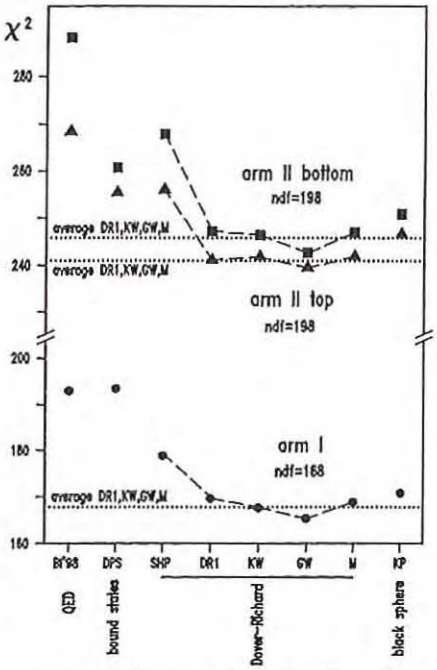

Fig. 2: Comparison of the measured Lα line shape of $\bar{p}$H with theoretical predictions.

For $\bar{p}$D, the measured line shape could not be described when the 2p hyperfine splittings were used as predicted by [5,6] (Fig.1 – bottom: skewed line shape). This provoqued a recalculation of the QED levels both for $\bar{p}$H and $\bar{p}$D [7], the results of which deviate significantly from the earlier approaches [5,8] especially for the deuterium case. The new calculation yielded much smaller QED splittings, which is consistent with experiment, where no substructure was observed (Fig. 1 – bottom: one line Lorentzian fit).

[1] Dep. of Physics, University of Ioannina, Greece
[2] Inst. de Physique, Université de Neuchâtel,Switzerland
[3] Dep.of Physics & Astronomy,University of Leicester,England
[4] Inst.du Radium, Université P.et M.Curie, Paris,France
[5] Paul-Scherrer-Institut (PSI) Villigen, Switzerland
[6] Quad-I-Azam University, Islamabad, Pakistan

[1] LEAR experiment PS207, CERN/PSCC/90-9/P124, 1990
[2] Annual report, 1997, p. 87 and ref. therein
[3] D. F. Anagnostopoulos et al., Nucl. Phys. B 56 A (1997) 84c and ref. therein
[4] J. Carbonell, G. Ihle, and J.-M.Richard, Z. Phys. A 344 (1989) 329 and ref. therein
[5] S. Barmo, H. Pilkuhn, and G. Schlaile, Z. Phys. A 301 (1981) 283
[6] S. Wycech, A. M. Green und J. A. Niskanen, Phys. Lett. 152 B (1985) 308
[7] S. Boudard and P. Indelicato, priv. comm.
[8] E. Borie, Proc. Erice 1982, Plenum Cor., NY, 1984

Preparations for the ATRAP Experiment: Production and Spectroscopy of trapped Anti-Hydrogen

J. Bojowald, W. Erven*, D. Grzonka, H. Hadamek, M. Hofmann, M. Köhler*, R. Nellen, W. Oelert, G. Schepers, T. Sefzick, K. Zwoll*.
for the ATRAP collaboration (AD-2) at AD/CERN

The "ATRAP" (Anti-Hydrogen TRAP) experiment at the new Antiproton-Decelerator "AD" at CERN will be carried out by an international collaboration. First measurements are scheduled for late spring 1999. The motivation for the experiments is the chance to perform a model independent test of CPT invariance when comparing the spectroscopy of hydrogen (H^0) and anti-hydrogen ($\bar{H}^0$). For this aim $\bar{H}^0$ atoms should be produced in a combined $\bar{p}$ and e^+ trap arrangement. The trap will be placed in the center of a superconducting magnet. For the evidence of trapped $\bar{H}^0$ as well as for optimizing the experimental parameters for the magnetic fields a detection system is essential which will make use of the annihilation products emitted, in case $\bar{H}^0$ gets in contact to normal matter as of the trap walls or residual gas. A detailed concept of the detection system within the experimental set-up was designed and first test measurements were performed. It consists of Si-μ-strip detectors and scintillating fibers surrounding the trap which allows for an annihilation vertex reconstruction. Investigations - concerning the choice of individual components - have been completed and lead to the following results:

1. Scintillating fibers
   The fiber material BICRON BCF-12 has been chosen with diameters of 1.5 mm to 2.5 mm. The fibers will be mounted onto a very thin plastic support, where pre-shaped grooves will define the exact position.

2. Photomultiplier
   Tests of the 16-fold photomultiplier Hamamatsu H6568 concerning gain, dark current, single electron signal amplitude, and cross talk showed expected and satisfactory results. For large veto-detectors around the magnet the photomultipliers Hamamatsu R-2238 were selected because of their high efficiency in the environment of the magnetic field.

3. Silicon detectors
   Both the detailed construction and the choice of the supplier for these detectors will be done in 1999. Tests of rather large silicon pad counters with respect to the detector performance at low temperatures and high magnetic fields have been carried out and demonstrated that the detector conditions are negligibly influenced down to temperatures of 20 K and magnetic fields up to 8 T. A test of Si-μ-strip detectors at equivalent conditions is in preparation.

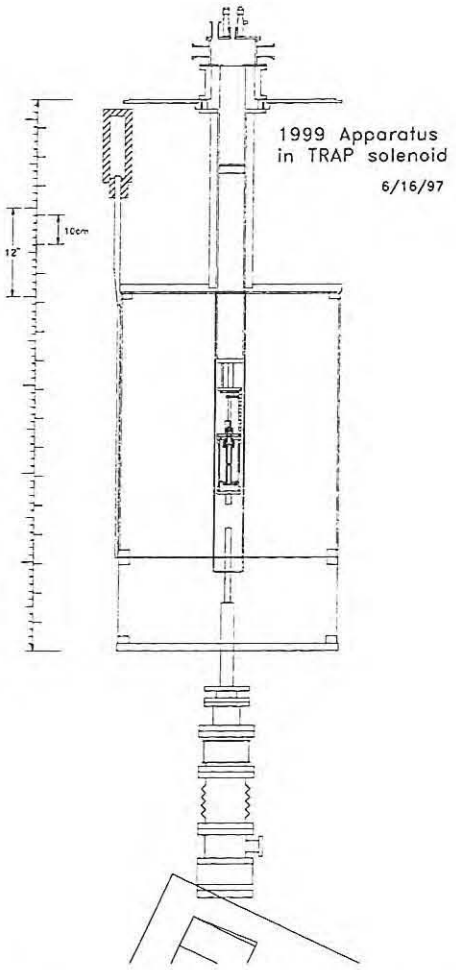

Figure 1: **Overall experimental set-up of the ATRAP arrangement. The trap in the centre of the magnet will be surrounded by scintillating fibers and Si-μ-strip detectors.**

4. Electronics and data acquisition
   The numerous detector channels require a high intergrated data acquisition system. Directly behind the photomultipliers integrated preamplifier stage will be placed. For further signal processing discriminators and digital RAL111 chips will be used which will be read out via CAMAC and PC based front end computers. For the read-out of the silicon-μ-strip detectors a highly integrated system will be developed based on VA-1 chips.

* ZEL - Forschungszentrum Jülich

The possibility of detecting Anti-Hydrogen in the Phase-One Apparatus of ATRAP

D. Grzonka, H. Hadamek, M. Hofmann, W. Oelert, G. Schepers, T. Sefzick, S. Sewerin
for the ATRAP collaboration (AD-2) at AD/CERN

Though a magnet with a larger bore is under construction, in the start-up phase of the ATRAP experiment [1] the collaboration will use an existing superconducting magnet which has a bore of only 10 cm diameter. This is just enough space to install one cylindrical fiber hodoscope consisting of three layers of scintillating fibers. With this arrangement we will not be able to i) perform a track reconstruction and therefore a determination of the annihilation vertex is excluded and ii) to identify eventually produced anti-hydrigen atoms which needs the measurement of two back to back 511 keV γ's resulting from the positron annihilation with an electron. Presently a reduction of the trap dimensions is under discussion to allow an insertion of an additional layer of BGO crystals placed between the trap for anti-hydrogen and the scintillating fiber hodoscope, as indicated in Fig. 1.

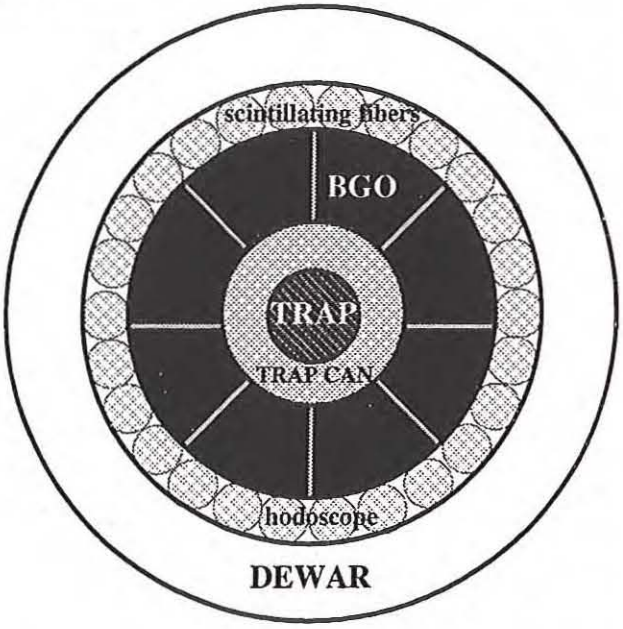

Figure 1: **Schematic view of the phase-one ATRAP apparatus.**

For this geometry Monte Carlo calculations were performed for several segmentations of the BGO ring. Signals due to charged pions from the proton - antiproton annihilation can be well distinguished from the 511 keV γ's since mostly the energy deposit from the pions is much larger. Further it has been checked that the straggling of the pions in the BGO material is sufficiantly small and the fibers behind the BGO segments can provide a veto signal for the crystals. The anti-hydrogen trigger in the calculations was based on the following conditions:

1. two signals in opposite BGO segments
2. the signals in the BGO crystals should be in an energy range of 500 keV to 520 keV
3. no signals from the fibers behind these BGO segment
4. at least two signals in the fibers are consistent with the energy loss of charged pions

For the case of an eight-fold segmented BGO ring (see Fig. 1) from 11.000 simulated events about 3.600 events are left which are consistent with the 511 keV signal after background subtraction, see Fig. 2.

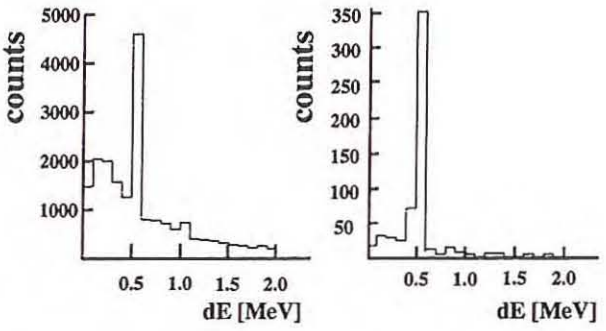

Figure 2: **Energy losses of reaction products from hydrogen - anti-hydrogen annihilation in the BGO crystals, left side**
rate when using the anti-hydrogen trigger conditions 1., 3. and 4., right side

Finally, 355 anti-hydrogen triggers were accepted when using the above listed conditions 1., 3., and 4. with a background rate of 25 events.
When increasing the segmentation of the BGO ring to 16 crystals the Monte Carlo calculations indicate an increase of the acceptance by about a factor of two. A further increase of the granulation of the BGO ring does not increase the acceptance significantly due to the limited size of the BGO elements.

References

[1] G. Gabrielse et al.,ATRAP proposal - AD-2 - SPSC 97-8/P306

Light losses and performance of scintillating fibers by interrupted light guides

U.Seddik[1] for the ATRAP Collaboration(AD-2) at AD/CERN
[1]NRC, Atomic Energy Authority, P.O. 13759, Cairo, Egypt

An array of three coaxial cylinders of scintillating fibers is part of the vertex detector which will be used for the detection of antihydrogen via the antiproton annihilation inside the trap of the ATRP(AD-2) experiment [1] at the new Antiproton Decelerator (AD) at CERN. The purpose of this vertex detector is:
a) the particles identification and
b) to determine the vertex of the annihilation in order to optimise the trap parameters.

The vertex detector will be located in vacuum since it should operate at low temperature. Therefore, the scintillator light which passes through the fibers may cross a gap for technical reasons.

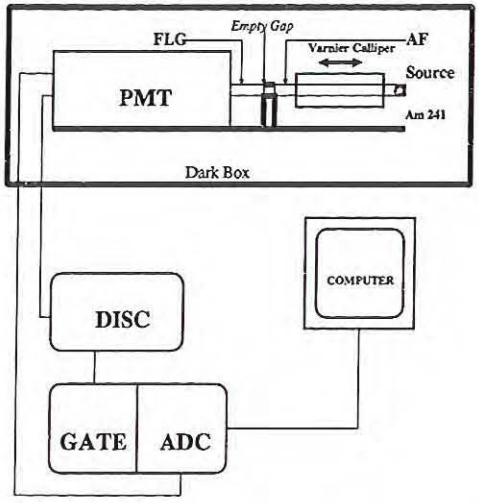

Figure 1: Schematic drawing of the used apparatus.

The effect of such a gap is investigated here by using an ^{241}Am activated fiber (AF) which is mounted in the front of a 5 cm long fiber light guide (FLG) through a hole in a dark plastic support. A photomultiplier tube (PMT) is coupled to the FLG with silicon oil. The distance between AF and FLG (the gap) was measured using a calliper with an accuracy up to 0.01 mm, where the AF was fixed on the movable part of the calliper. The whole apparatus is kept in darkness inside a tightly closed large box, see fig.1.
Up to a gap width of about 1.5 mm within the experimental errors no intensity losses are observed. A further increase of the gap width results in a

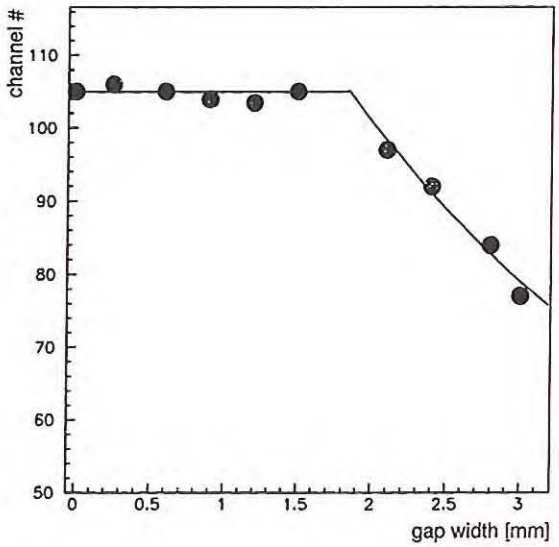

Figure 2: A plot of the gaussian mean values of the α peak versus the gap widths (mm) for a scintillation fiber with a diameter of 2.2 mm at room temperature.

steady decrease of the intensity. The light emitted from the activated fibre can be considered as a light cone with a certain opening angle and homogenious intensity. In a simple model with increasing gap width only a part of this cone is covered by the FLG, i.e. the intensity decreases proportional to the ratio of the FLG area to the light cone area. A relation like: $I/I_0 = (1 + c(x - x_0))^{-2}$ with the constant c and x denoting the gap width with the offset x_0 is expected which is consistent with the observed behaviour. The line in fig. 2 is a fit to the data starting at $x_0 = 1.85$.
In conclusion, the gap distance should not exceed 1.0 mm to avoid large light losses and therefore to get a high detection efficiency.

References:

[1] G. Gabrielse et al., Proposal presented to the CERN SPSDC on 25 March 1997 (SPSC978/P306)

The Structure of the Roper Resonance

H. P. Morsch and P. Zupranski[1]

Data on the N*(1440 MeV) resonance excitation in α-p scattering were reanalysed assuming projectile and target excitation and their interference. Assuming threshold modified Breit-Wigner shapes with momentum dependent widths, a quantitative description of the spectrum is obtained. However, the resonance parameters deduced do not describe the resonance seen in π-N scattering. A consistent description of the data on α-p and π-N can be achieved only assuming two structure in this resonance, with only the lower one excited in α-p. The nature of the second structure is discussed.

The first N* resonance (Roper resonance) at about 1440 MeV is in many respect a very interesting resonance. A well established P_{11} resonance has been deduced from phase shift analyses[1] of elastic π-N scattering. Its mass distribution is quite different from a Breit-Wigner form and has an unusually large width. The P_{11} resonance is dominant in the elastic π-N channel; the inelasticities into 2π(s)-N (2π coupled to isospin=0) and π-Δ, studied in the π-N$\rightarrow \pi\pi$N reaction[2], are in the order of 10-20 %.

More recently, a resonance at this mass has been observed[3] in α-p scattering. The excitation of this N*(1/2,1/2)$^+$ resonance with α-particles corresponds to a monopole excitation (L=0) which exhausts a large fraction of the energy weighted operator sum rule[4]; therefore, it has been interpreted as a compression or breathing mode of the nucleon, from which the nucleon compressibility has been deduced.

Theoretically, a N*(1/2,1/2)$^+$ at low excitation energy is of particular interest. In the constituent quark model such a resonance corresponds to a 1s$\rightarrow$2s quark excitation which should lie at an excitation energy of about 1 GeV. However, in Skyrmion models this resonance is much lower in excitation energy, in the order of 400-500 MeV.

We calculated energy loss spectra for α-p$\rightarrow \alpha'$+X, using the Monte-Carlo method and fitting the N* mass distribution. We assumed two contributions in the spectrum, (1) the excitation of the N* in the proton and (2) Δ-excitation in the projectile (which decays by coherent pion emission). The importance of the interference of these contributions has been pointed out in ref.5 and has been included in our calculations. Other reaction graphs have been estimated[5] to be almost two orders of magnitude smaller and have therefore been neglected.

To obtain a consistent description of the resonance forms for α-p scattering and the π-N system we used a 1 or 2π-threshold modified Breit-Wigner shape with momentum dependent width, further a small background term necessary to describe the real π-N amplitudes. A good fit of the resonance observed in α-p scattering is obtained (see fig.1) using values of M and Γ of about 1380 MeV and 200 MeV, respectively. The small resonance energy and width is not consistent with the Roper resonance seen in π-N scattering which has a higher centroid and a much larger width.

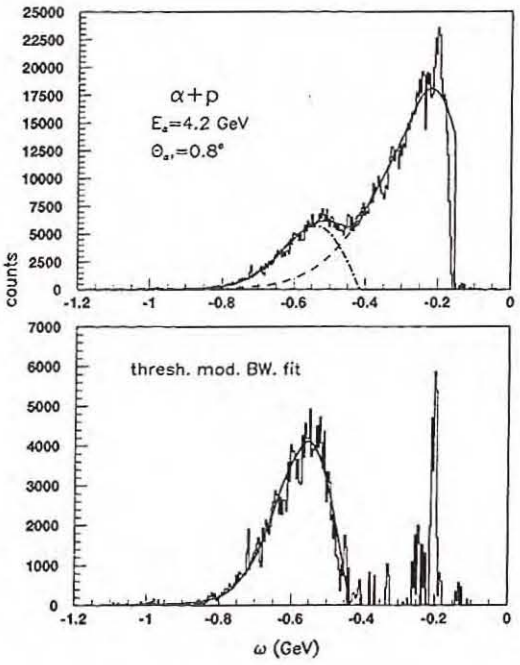

Figure 1: Missing energy spectrum of α-p scattering from ref.3 (with instrumental background subtracted) in comparison with our calculations

The above results suggest that the structures observed in the different systems are not identical. The scattering of α-particles is very selective, exciting only isoscalar, non-spin-flip structures. Differently, π-N scattering is a resonant reaction which shows very little selectivity. Indeed, in this system the decay of the Roper resonance into $\pi\Delta$ is quite strong at higher mass, which may indicate a coupling to a double Δ excitation, Δ_Δ, a structure which should not be observed in α-p scattering.

The different results may be reconciled in a two-resonance picture assuming that in α-p scattering only the lower resonance is excited. Because of its strong excitation in α-p this should have a strong decay into the 2π(s)-N channel.

Using the above resonance forms, a good description of the π-N data is obtained. The different observables (amplitudes, speed, total and partial cross sections) fix quite unambiguously the threshold cut-offs, the momentum dependence and the resonance parameters. A quantitative description of the various observables is obtained. For the total π-N cross section and the speed, derivative of the scattering amplitudes T with respect to the mass $|dT/dW|$, this is shown in fig.2. The dashed line in the upper part corresponds to the shape of the first resonance seen in α-p scattering.

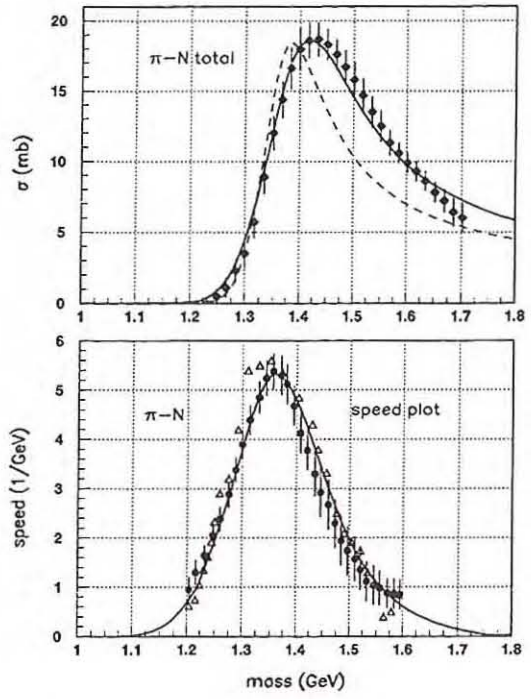

Figure 2: Total P_{11} π-N cross sections and speed

The second resonance is seen almost entirely in the decay of the Roper resonance into the $\pi\Delta$ channel. This suggests an interpretation in terms of a Δ_Δ structure (Δ excitation of the Δ). For such a double Δ excitation, there are certain constraints on the mass and width which have to be fulfilled. The mass difference between Δ_Δ and Δ should be about the same as between Δ and nucleon; further, the Δ width should be folded over the Δ decay width. This gives:

$$\frac{M_{\Delta_\Delta} - M_N}{M_\Delta - M_N} \sim 2 \text{ and } \frac{\Gamma_{\Delta_\Delta}}{\Gamma_\Delta} > 2. \qquad (1)$$

From the resonance parameters extracted for the second resonance we obtain

$$\frac{M_{(2.res)} - M_N}{M_\Delta - M_N} = 1.8 \pm 0.1 \text{ and } \frac{\Gamma_{(2.res)}}{\Gamma_\Delta} = 3.1 \pm 0.30.$$

This is in agreement with the above requirements (1) and shows that this structure may be well understood by a Δ_Δ mode, supporting the importance of the spin-isospin degree of freedom in baryons. In a static picture, as the constituent quark model, a double Δ excitation of this form is not possible. However, it is well supported in dynamical or collective models.

The present results can be tested in exclusive α-p scattering which should exhibit a N* decay branching ratio quite different from π-N.

[1]Soltan Institut for Nuclear Studies, Pl-00681 Warsaw, Poland

References:

1. R. A. Arndt, I. I. Strakovsky, R. L. Workman and M. M. Pavan, Phys. Rev. C 52, 2120 (1995), and refences therein

2. D.M. Manley, R.A. Arndt, Y. Goradia and V.L. Teplitz, Phys. Rev. D 30, 904 (1984)

3. H. P. Morsch et al., Phys. Rev. Lett. 69, 1336 (1992)

4. H.P. Morsch, W. Spang and P. Decowski, Z. Phys. A 348, 45 (1994); and H.P. Morsch, Z. Phys. A 350, 61 (1994)

5. S. Hirenzaki, P. Fernandez de Cordoba and E. Oset, Phys. Rev. C 53, 277 (1996)

2. Nuclear Spectroscopy

Study of shape coexistence in nuclei around ^{142}Gd with EUROBALL

R.M. Lieder, T. Rzaça-Urban[1], H. Brands, W. Gast, H.M. Jäger, L. Mihailescu, Z. Pytel[1], W. Urban[1], D. Bazzacco[2], G. Falconi[2], R. Menegazzo[2], S. Lunardi[2], C. Rossi-Alvarez[2], G. de Angelis[3], E. Farnea[3], A. Gadea[3], D.R. Napoli[3], Z. Podolyak[3]

Extensive studies of high-spin rotational bands in the mass regions with $A \approx 130$ and $A \approx 150$ have shown the existence of highly-deformed bands ($\beta_2 \approx 0.35$) in the former and superdeformed bands ($\beta_2 \approx 0.50$) in the latter region. The nucleus ^{142}Gd lies in the intermediate region and no bands built on states of large quadrupole deformation are known in this nucleus, from which one could learn how the transition between these two regions takes place. Theoretical calculations for ^{142}Gd in the framework of the cranked Woods-Saxon-Strutinsky approach predict a coexistence of superdeformed ($\beta_2 = 0.49$) and highly-deformed ($\beta_2 = 0.27$) shapes. Furthermore, oblate shapes ($\beta_2 = 0.15$) are predicted. Previous knowledge on the level scheme of ^{142}Gd results from investigations of Starzecki et al. [1] and Sugawara et al. [2].

A study of high-spin states in nuclei around ^{142}Gd has been carried out with the γ-detector array EUROBALL III. A ^{99}Ru target (enrichment 95%) consisting of four self-supporting metal foils with a total thickness of 0.84 mg/cm^2 was bombarded with a ^{48}Ti beam of 240 MeV produced by the XTU tandem – linear accelerator (ALPI) combination of the Laboratori Nazionali di Legnaro, Italy. The recoil velocity was $v/c = 3.38\%$. In this reaction ^{142}Gd is populated with a maximum cross section through the 2p3n channel but neighbouring Tb, Gd, Eu and Sm nuclei are also populated very strongly. In order to allow for an isotopic separation and to increase thus the selectivity of EUROBALL III the charged-particle detector array ISIS, consisting of 40 Si-detector telescopes, has been mounted in the center of the γ-detector array. Events were recorded when either ≥ 7 unsuppressed Ge detectors or ≥ 6 unsuppressed Ge detectors and ISIS fired. The total trigger rate was 12000 events/s for a beam current of 6 particle-nA. Approximately $4.5 \cdot 10^9$ high-fold γ-events have been collected, $\approx 60\%$ of which are associated with one or more detected particles. On average ≈ 4.5 γ-rays have been observed in an event after Compton suppression.

In the analysis of the data set a full as well as one- and two-proton-gated γ-γ-γ cubes have been sorted. It is possible to expand considerably the level schemes of ^{140}Eu, ^{140}Gd, ^{142}Gd and ^{143}Tb. Furthermore, the level scheme of ^{142}Tb can be established, the high-spin states of which are completely unknown. A preliminary level scheme of ^{142}Gd is shown in fig. 1. It has been considerably extended in excitation energy, spin and the number of observed cascades. The previously known [2] three dipole bands in ^{142}Gd have been extended and a fourth one has been found. The order of the transitions deviates in the present work from that proposed previously [2]. A dipole band with an irregular level spacing has also been observed in ^{144}Gd [3]. It has been interpreted as an oblate rotational dipole band with a $\nu h_{11/2}^{-2} \otimes (\pi h_{11/2}^2)_{K=10+}$ configuration for the lowest band members. The irregular level spacings result from additional particle-hole excitations which increase the alignment. Following the proposal of Frauendorf [4] these bands represent the rotation of a magnetic dipole. Regular bands of this type have first been oberved in nuclei around ^{200}Pb.

The long stretched E2 cascade labelled $(+,0)_1$ in fig. 1, extending to $I^\pi = 34^+$, is a candidate for a highly-deformed band. In order to determine its character, the total aligned angular momentum I_x has been plotted in fig. 2 as function of the rotational frequency $\hbar\omega$. For comparison the triaxial band in ^{144}Gd of $\pi h_{11/2}^2 \nu h_{11/2}^{-1} \nu h_{9/2}$ configuration at low spins ($\beta_2 = 0.20, \gamma = -18°$) [3] and the highly-deformed bands involving $\nu i_{13/2}$ configurations in ^{139}Gd ($\beta_2 \approx 0.35$) [5, 6] and ^{141}Gd ($\beta_2 = 0.29$, $\gamma = 20°$) [7] are included. The $(+,0)_1$ sequence in ^{142}Gd behaves similarly to that in ^{144}Gd but quite different from the bands in ^{139,141}Gd. Hence, it must be concluded that the $(+,0)_1$ sequence corresponds to a triaxial nuclear shape and not to a highly-deformed shape. The analysis, especially the search for bands of large deformation, is continued for the nuclei around ^{142}Gd.

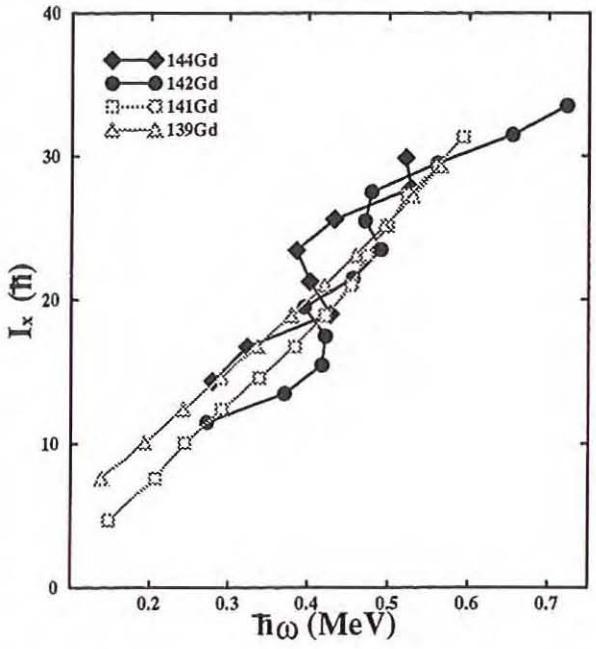

Figure 2: Total aligned angular momentum vs. rotational frequency for the $(+,0)_1$ cascade in ^{142}Gd, the triaxial band in ^{144}Gd and the highly-deformed bands in ^{139,141}Gd.

The work was in part funded by the EU under the contract ERBFMRXCT970123, by the Volkswagen Foundation under the contract number I/71 976, by the the Foundation for Polish Science and by the KBN Grant No. 2P03B 05312.

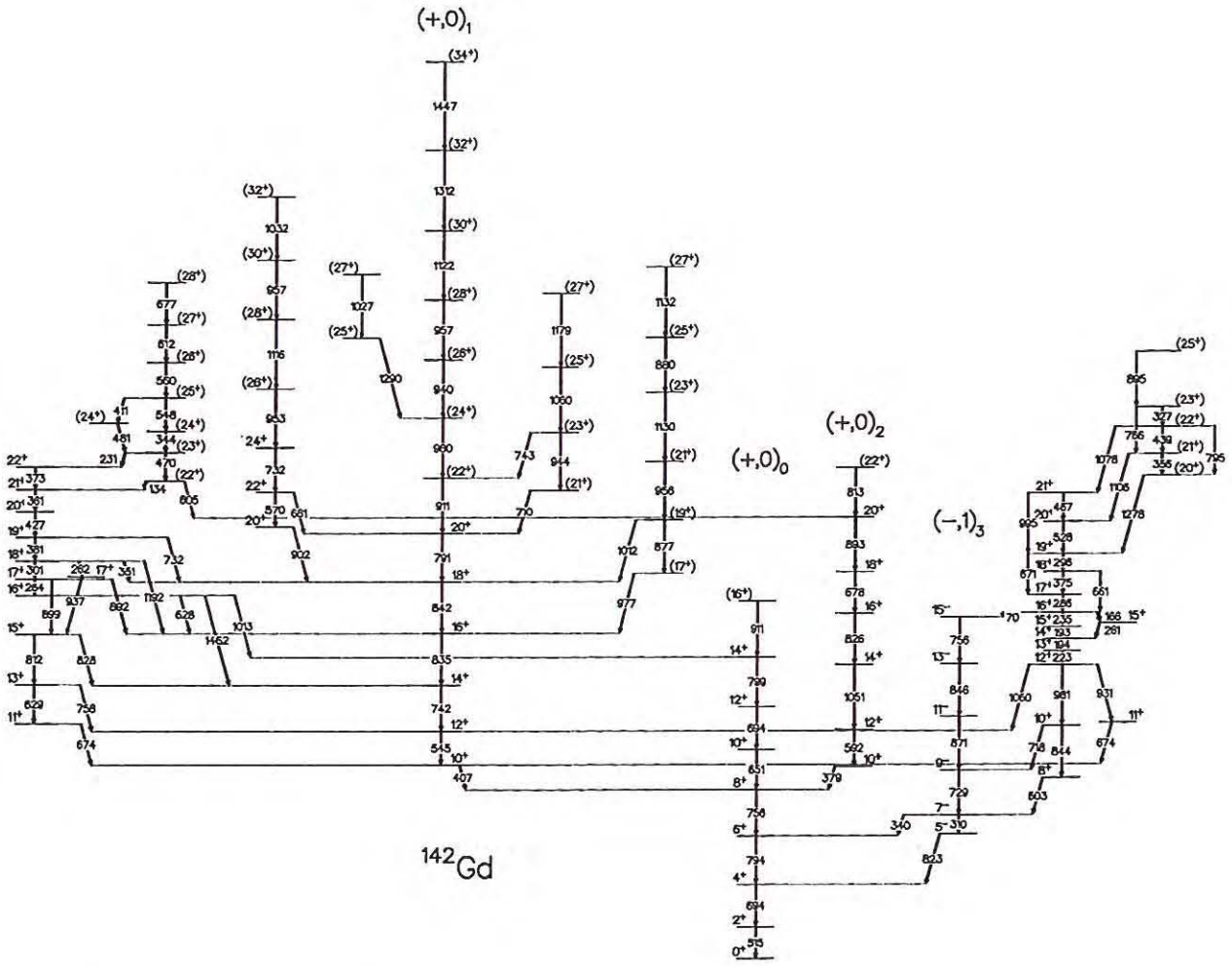

Figure 1: Partial level scheme of ^{142}Gd.

[1] Institute of Experimental Physics, University of Warsaw, PL-00-681 Warszawa, Poland
[2] Dipartimento di Fisica dell'Universita and Istituto Nazionale di Fisica Nucleare, Sezione di Padova, I-35131 Padova, Italy
[3] Istituto Nazionale di Fisica Nucleare, Laboratori Nazionali di Legnaro, I-35020 Legnaro, Italy

References:

[1] W. Starzecki et al., Phys. Lett. B 200 (1988) 419
[2] M. Sugawara et al., Z. Phys. A358 (1997) 1
[3] T. Rząca-Urban et al., Nucl. Phys. A579 (1994) 319
[4] S. Frauendorf, Z. Phys. A358 (1997) 163
[5] R. Ma et al, J. Phys. G 16 (1990) 1233
[6] E.S. Paul et al, Phys. G 18 (1992) 121
[7] S.M. Mullins et al, Phys. Rev. C 47 (1993) R2447

Experimental Study of the Influence of Crystal Orientation on Ge Detector Pulse Shapes

H. Brands, L. Mihailescu, W. Gast, R.M. Lieder, H.M. Jäger and M.J. Rossewij

In the framework of the TMR project:"The Development of γ-ray tracking Detectors for 4π γ-ray arrays" the influence of the anisotropy of the charge carrier drift velocity in different crystallographic directions on the pulse shapes of Ge detectors has been investigated. For the development of a γ-tracking detector the pulse shape characterizes the radius where the γ-ray interacted.
The orientation of the Ge crystal inside the semihexagonal detector capsule has been determined by means of neutron scattering. The Neutron Reflectometer HADAS installed at the FRJ-2 Research Reactor has been used. The (220) crystallographic direction was determined for an angle of $\theta = 90°$ between the neutron beamline and the neutron detector direction and a neutron wave length of $\lambda = 2.828$Å. The (001) direction is found to be almost parallel to the cylinder axis of the detector. A deviation of $(1.6 \pm 0.1)°$ was found.
The aim of the experiment has been to extract the pulse

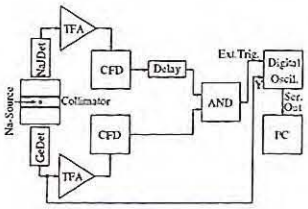

Figure 1: Experiment with ^{22}Na Source

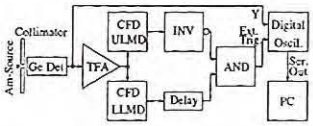

Figure 2: Setup with ^{241}Am Source

lengths from the differentiated preamplifier signals (current signals) as function of the radius and the azimuthal angle in steps of 15 degrees. This information is equivalent to the charge collection time if the parameter time-to pulse-end is analysed. The experimental setups are reflected in the block digrams of Fig.1 and Fig.2 respectively. In the first experiment a 1" NAJ scintillator has been placed in front of an encapsulated, semihexagonal, closed-end n-type Ge detector. Both detectors were irradiated by the 511 keV annihilation radiation of a collimated ^{22}Na source. Pulse shapes from the Ge detector were recorded using a digital oscilloscope with a sampling rate of up to 1 Gsps/s and 8 bit resolution. An external trigger signal was provided by the coincidence circuit when both detectors registered a 511 keV γ-ray at the same time. Since it is of interest to investigate also the pulse shapes of γ-rays interacting in the first millimeters of the Ge detector volume, the front face and the cylindrical part at the rear end of the Ge-detector were irradiated by 60 keV γ-rays of a collimated ^{241}Am source. The external trigger signal was generated by setting a window on the 60 keV line.

The parameters characterizing the pulse shapes

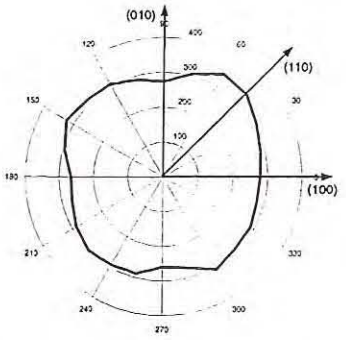

Figure 3: Average Time-to-Pulse-End obtained with^{22}Na at $r = 25$mm

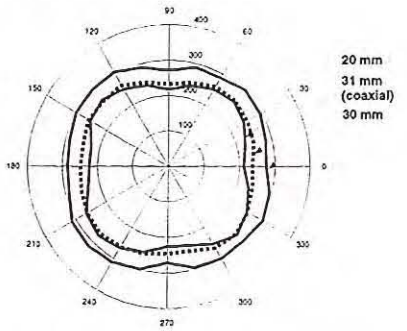

Figure 4: Time-to-Maximum Values measured with ^{241}Am at different radii

(e.g. time-to-maximum, time-to-steepest-slope or time-to-pulse-end) were extracted by analysing the current signals of the preamplifier. In Fig.3 the polar plot of the average time-to-pulse-end as obtained with the ^{22}Na source is shown. The time-to-maximum values for different radial positions measured with ^{241}Am are plotted in Fig.4. The influence of the crystal orientation on the pulse shapes is evident in both diagrams. The largest times correspond to the crystallographic direction (110) while the shortest times belong to the direction (100). Quantitatively there is a time-to-maximum difference of 20ns ($\approx$ 10%) observed in Fig.4 moving from the (100) to the (110) direction. Moreover Fig.4 indicates different pulse shapes between the front- and the rear- (coaxial) regions of the detector. The time-to-maximum values differ approximately 50ns ($\approx$ 25%).
For the development of a γ-tracking detector based on semihexagonal Ge detectors the different regions of the crystal can e.g. be separated by segmentation of the outer and inner contacts to improve the radial position resolution. An azimuthal segmentation of the outer contact should be in multiples of four to consider the crystal symmetry. A segmentation of the inner contact separates the front part from the coaxial-like part.

Estimation of the Anisotropy of the Drift Velocity for the Development of Ge γ-Ray Tracking Detectors

L. Mihailescu, H. Brands, W. Gast, H.M. Jäger, R.M. Lieder, M.J. Rossewij

The development of γ ray tracking detectors opened new problems in the design of these detectors and in the electronics for the read-out. By a shape analysis of the detector signals, new information can be obtained such as the position the γ ray hits the detector. For the processing of these pulse shapes it is essential to know the mobilities of the charge carriers in each particular position inside the detector. In this respect, the anisotropy of the conductivity in Ge plays an important role.

Due to the band structure, in HPGe, similarly to any cubic semiconductor, the conductivity of the charge carriers at high electric fields and at low temperature is anisotropic. As a consequence of this anisotropy, the drift velocity of the charge carriers has different values for different orientations of the applied electric field with respect to the crystallographic axes. At the same time, the direction of the drift velocity will have an angle $\phi \neq 0$ with the applied electric field, if the electric field is not along a crystallographic rotation axis.

Since the drift velocity does not have a simple analytical form with respect to the electric field and the temperature, we followed a phenomenological approach [2] to calculate these dependencies using the experimental data of the electrons drift velocity at a temperature of 78 K, for the (100) and (111) directions [3], and taking into account the expressions for the drift velocity of Reik and Risken [1]. In the present calculations, the dependence of the electron drift velocity on the applied electric field is taken in the following form:

$$v_d = \mathcal{A}(|E|) \sum_i \frac{n_i}{n} \frac{(\gamma_i E_0)^{-1/2}}{E_0 \gamma_i E_0} \qquad (1)$$

where γ_i is the effective mass tensor for the i-th conduction band, n_i/n is the ratio of the carriers in the i-th band, $\mathcal{A}$ is a parameter which depends on the argument of the electric field vector. The present phenomenological approach avoids the need to know the complex dependencies of the scattering mechanism which influences the population of the conduction bands by estimating this population from the experimental data of the drift velocity taken as a function of electric field for a fixed temperature. For an experimental determination of the amplitude of the repopulation, deviation from the uniform distribution value of the population is considered to vary with the electric field strength as:

$$\frac{n_i}{n} = \mathcal{R}(|E|) \left[\frac{(E\gamma_i E)^{-1/2}}{\sum_l (E_0 \gamma_l E_0)^{-1/2}} - \frac{n_e}{n} \right] + \frac{n_e}{n} \qquad (2)$$

Since it does not exist any repopulation of the conduction bands if the electric field is equivalently oriented with respect to all the (111) directions, an electric field applied along the (100) direction assures the terms n_i/n to be all equal, at any electric field strength. Therefore, using the experimental drift velocity in (100) direction, the value of the parameter $\mathcal{A}$ can be determined using eq. (1). Furthermore, the amplitude of the repopulation effect can be approximated from the experimental data of the drift velocity taken with the electric field along the (111) direction, by determining the parameter $\mathcal{R}$ from eq. (2). Knowing $v_d(E)$, the electric field values are obtained by calculating the numerical solutions of the Poisson's equation inside the detector. The experimental drift velocity dependencies on the applied electric field for the (100) and (111) directions, as well as the calculated drift velocity values for an applied electric field in the (110) direction in the range of the detector field are represented in fig. 1. The simulated pulse shapes in a closed end detector considering photoelectric hits at the detector surface, for different interaction radii, at 0° ((100) for the coaxial region) and 45° azimuthal angles , are shown in fig. 2.

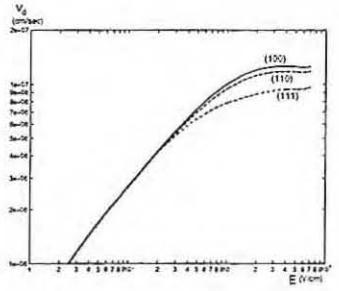

Figure 1: *Experimental* curves for the (111) and (100) directions; *calculated* curve for (110)

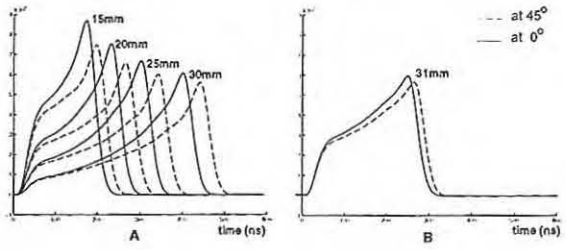

Figure 2: Simulated pulses. left: hits in the front part of the detector; right: hits in the coaxial region.

The presented method to carry out 3D simulations of the charge carrier trajectories offers a tool for simulating realistic pulse shapes for Ge detectors in various designs. In this way, the drift velocity anisotropy can be correctly estimated in future developments of Ge detectors and pulse shape analysis methods for γ-ray tracking.

References:

[1] H. G. Reik et al., Phys. Rev. 126, 1737(1962);
[2] M. I. Nathan, Phys. Rev. 130, 2201(1963);
[3] G. Ottaviani et al. IEEE Trans. Nucl. Sci. NS-22, 192(1975);

II. Theoretical Nuclear Physics

3. MEDIUM AND HIGH ENERGY PHYSICS

4. NUCLEAR STRUCTURE AND REACTION MECHANISM

3. MEDIUM AND HIGH ENGERGY PHYSICS

Semi-inclusive Pion Production and the d/u Ratio

W. Melnitchouk, J. Speth and A. W. Thomas*

The d/u ratio contains important information about the flavor structure of the proton. In particular, its asymptotic behavior at large x can tell us which mechanism is responsible for the breaking of $SU(2)_{spin} \times SU(2)_{flavor}$ symmetry. Given that there are firm predictions for this behavior, it constitutes a serious test of perturbative QCD [1].

So far, a direct measurement of the d/u ratio has been rather difficult, mainly because the cross sections decrease rapidly in the extreme kinematics near $x \sim 1$. Previous analyses have used inclusive deep-inelastic scattering data on proton and deuteron targets to obtain the neutron to proton structure function ratio, from which d/u can be extracted at large x. However, the neutron structure function is obtained from data on the deuteron, which suffer from the fact that nuclear effects, even in the deuteron, become quite significant at large x [2]. In particular, whether one corrects for Fermi motion only, or in addition for binding and nucleon off-shell effects, the extracted neutron structure functions for $x < 0.7$ can differ rather dramatically [2].

In order to avoid the problem of the uncertainty in the extraction procedure introduced by nuclear effects, we explore the feasibility of directly extracting the large-x valence d/u ratio through a measurement of pions in the current fragmentation region of semi-inclusive deep-inelastic scattering from protons. In the parton model the number of pions in a given x and z bin can be written as a product of a quark distribution function, $q^h(x)$, in the hadron h, and a fragmentation function giving the probability of the scattered quark q producing a pion:

$$N_h^\pi \sim \sum_q e_q^2 \, q^h(x) \, D_q^\pi(z). \qquad (1)$$

Taking the ratio of the π^- to π^+ proton cross sections, $R^\pi = N_p^{\pi^-}/N_p^{\pi^+}$, one finds:

$$R^\pi(x,z) = \frac{4\bar{D}(z)/D(z) + d(x)/u(x)}{4 + d(x)/u(x) \cdot \bar{D}(z)/D(z)} \qquad (2)$$

where $D(z) \equiv D_u^{\pi^+} = D_d^{\pi^-}$ is the leading fragmentation function, and $\bar{D}(z) \equiv D_d^{\pi^+} = D_u^{\pi^-}$ is the non-leading fragmentation function. The fragmentation functions D and $\bar{D}$ have been measured by the EMC [3]. In the limit $z \to 1$, the leading fragmentation function dominates, $D(z) \gg \bar{D}(z)$, in which case the ratio $R^\pi \to (1/4)d/u$, although the point $z = 1$ cannot be reached experimentally.

In the realistic case of smaller z, the $\bar{D}/D$ term in Eq.(2) will contaminate the yield of fast pions originating from struck primary quarks, diluting the cross section with pions produced from secondary fragmentation picking up $q\bar{q}$ pairs from the vacuum. Nevertheless, one can estimate the yields of pions using the empirical fragmentation functions [3]. Integrating the differential cross section over a range of z, as is more practical experimentally, the resulting ratios for cuts of $z > 0.3$ and $z > 0.5$ are shown in Fig. 1. One sees that decreasing the lower limit for z has the effect of raising the cross section ratio significantly, because of the larger integrated contribution from the non-leading fragmentation, which is more important at smaller z. Although the relative difference between the ratios for the two forms of asymptotic d/u behavior then becomes smaller, the absolute difference between these remains relatively constant, and should be measurable with the high luminosities available at current facilities.

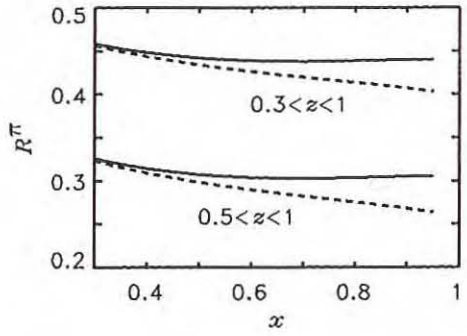

Figure 1: Ratio R^π as function of x, integrated over z between $0.3 < z < 1$ and $0.5 < z < 1$. The dashed line represents the ratio constructed from the CTEQ4 parameterization, while the solid includes the modified d distribution according to Ref.[4] and pQCD.

In summary, we reiterate the importance of an accurate experimental determination of the behavior of the valence d/u ratio as $x \to 1$. Not only are the present fits to world data in clear disagreement with the predictions of perturbative QCD (unlike the reanalysis of Ref.[2]), but the discrepancy is extremely important when it comes to estimating event rates for charged current events at the large values of x and Q^2 accessible at HERA.

* Department of Physics and Mathematical Physics, and SRCSSM, University of Adelaide, Australia.

References:

[1] G.R. Farrar and D.R. Jackson, Phys. Rev. Lett. 35 (1975) 1416.

[2] W. Melnitchouk and A.W. Thomas, Phys. Lett. B 377 (1996) 11.

[3] J.J. Aubert et al., Phys. Lett. 110B (1982) 73.

[4] W. Melnitchouk and J.C. Peng, Phys. Lett. B 400 (1997) 220.

Dynamics of Light Antiquarks in the Proton

W. Melnitchouk, J. Speth and A. W. Thomas*

The recent Drell-Yan experiment by the E866/NuSea Collaboration at Fermilab [1], in which $\mu^+\mu^-$ Drell-Yan pairs were detected in pp and pD collisions, provides the best information yet on the x-dependence of the $\bar{d}/\bar{u}$ ratio in the proton.

In the parton model, the Drell-Yan cross section is proportional to:

$$\sigma^{ph} \propto \sum_q e_q^2 \left(q^p(x_1)\, \bar{q}^h(x_2) + \bar{q}^p(x_1)\, q^h(x_2) \right) \quad (1)$$

where $h = p$ or D, and x_1 and x_2 are the light-cone momentum fractions carried by partons in the projectile and target hadron, respectively. Assuming that the deuteron is composed of two bound nucleons, and utilizing isospin symmetry, in the limit $x_1 \gg x_2$ the ratio of the deuteron to proton cross sections can be written:

$$\frac{\sigma^{pD}}{2\sigma^{pp}} = \frac{1}{2}\left(1 + \frac{\bar{d}(x_2)}{\bar{u}(x_2)}\right) \times \frac{4 + d(x_1)/u(x_1)}{4 + d(x_1)/u(x_1) \cdot \bar{d}(x_2)/\bar{u}(x_2)} \quad (2)$$

so that the ratio would be unity if $\bar{d} = \bar{u}$. The relatively large asymmetry found in these experiments (see Fig.1) implies the presence of non-trivial dynamics in the proton sea which does not have a perturbative QCD origin.

From the symmetry properties of QCD, we know that one source of non-perturbative quark-antiquark pairs is the pion cloud associated with dynamical chiral symmetry breaking. One can model the effects of the pion cloud by hypothesising that the physical nucleon state can be expanded in a series involving bare nucleon and two-particle, meson–baryon states. The relative probabilities of finding the meson–baryon fluctuation in the nucleon are determined by the strengths of the meson-baryon-nucleon vertex functions, parameterised by a smooth form factor with a cut-off mass parameter Λ. In practice, the most important fluctuations are those involving πN and $\pi\Delta$ states.

Our analysis suggests that a quantitative description of the entire region of x covered in the experiment requires a delicate balance between several competing mechanisms. The best fit, within the pion cloud framework, to the data on both the sum and difference of $\bar{u}$ and $\bar{d}$ at large x accounts for around half of the integrated asymmetry, leaving room for possible other, non-pionic, mechanisms to provide the missing strength at smaller x.

Aside from the flavor-asymmetric πN and $\pi\Delta$ components of the nucleon, there is no *a priori* reason why the 'bare' (non–pion-dressed) nucleon state itself cannot have an intrinsic asymmetric sea associated with it. In fact, this is actually what is expected from the Pauli exclusion principle, as anticipated long ago by Field and Feynman on the simple basis that the u and d valence quark sectors are unequally populated in the proton ground state. Although more difficult to estimate model-independently, the contribution to the $\bar{d}$–$\bar{u}$ difference from antisymmetrization has been calculated within a non-perturbative model of the nucleon [3]. Along the lines of the model estimates, we find that the effects of antisymmetrization are most relevant at small x, with normalization such that they can account for most of the remaining half of the integrated asymmetry. Indeed, our analysis suggests that the best fit to the E866 data is obtained when both mechanisms play a role, Fig.1.

Finally, we note that it would be helpful to have more data at large x, where the error bars are largest, to verify the downward trend of $\bar{d}/\bar{u}$.

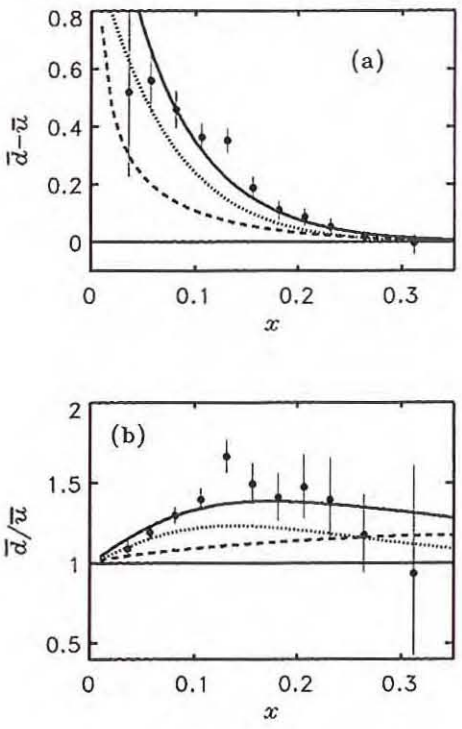

Figure 1: Contributions from pions with $\Lambda_{\pi N} = 1$ GeV and $\Lambda_{\pi\Delta} = 1.3$ GeV (dashed) and from antisymmetrization (dotted) to the (a) $\bar{d} - \bar{u}$ difference and (b) $\bar{d}/\bar{u}$ ratio, and the combined effect (solid).

* Department of Physics and Mathematical Physics, and SRCSSM, University of Adelaide, Australia.

References:

[1] E.A. Hawker et al., Phys. Rev. Lett. 80 (1998) 3715.

[2] W. Melnitchouk et al., Phys. Rev. D, in press.

[3] A.W. Schreiber et al., Phys. Rev. D 44 (1991) 2653.

Strange Asymmetries in the Nucleon

M. Malheiro*, W. Melnitchouk and J. Speth

The question of "how much" strangeness there is in the nucleon has been quite topical for at least the last decade. One of the earlier indicators of a non-negligible strangeness presence in the nucleon came with measurement of the strange axial matrix elements in polarised deep-inelastic scattering. Subsequently, parity-violating electron scattering experiments at MIT/Bates [1] and more recently at Jefferson Lab [2] have sought to measure the strange electromagnetic form factors of the nucleon at low Q^2.

Any reasonable model of the non-perturbative sea quark content of the nucleon must be compatible with the symmetries of QCD. One symmetry which has proved to be quite important in the study of hadronic structure and interactions is chiral symmetry. Applied to the SU(3) sector, it predicts a number of novel effects for the strange quark distributions in the nucleon, at both high and low energy scales [3]. In particular, each of these predictions is consistent with what is currently known from experiment.

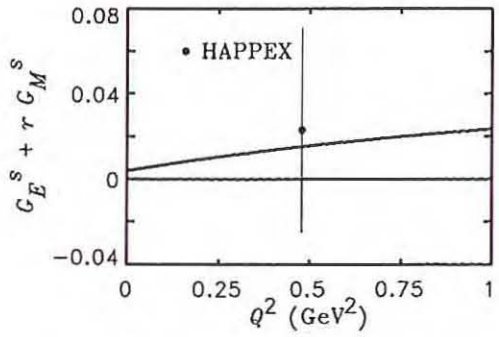

Figure 1: Strange electric and magnetic form factor combination as extracted from the HAPPEX data [2].

In Fig.1 the latest result from the HAPPEX experiment on the strange electromagnetic form factors is shown. The kinematics of the experiment determine a combination of G_E^s and G_M^s at $Q^2 \approx 0.5$ GeV^2, with a relative factor $r \approx 0.39$ between them. The kaon cloud model agrees with the data quite well, for a cut-off mass of $\Lambda = 1$ GeV.

The strange axial charge, g_A^s, can be measured in both elastic neutrino-nucleon scattering, as the axial form factor at $Q^2 = 0$, or in polarised deep-inelastic charged lepton-nucleon scattering, as the first moment of the spin-dependent strange quark distribution, Δs. Within the simple kaon cloud model, the strange axial charge arises through the dissociation of the nucleon into a spin-0 kaon and a spin-1/2 hyperon (contributions from spin-3/2 hyperons are quite small numerically). This is shown in Fig.2 by the solid line, as a function of the kaon-nucleon-hyperon vertex function cut-off mass, Λ. The couplings and form factors are correlated with those from hyperon-nucleon scattering data [4].

Because the axial matrix elements are evaluated on the light-cone (or in the infinite-momentum frame), care must be taken to ensure preservation of Lorentz covariance, as the usual prescription of using only "+" components of currents in the impulse approximation is known to violate rotational symmetry [5]. The dashed curve in Fig.2 corresponds to a calculation of the axial charge taking "+" components of currents, without correcting for the symmetry breaking — as one can see, the difference is quite large numerical compared with the full calculation. One finds fairly good agreement with the deep-inelastic data for $0.5 < \Lambda < 1$ GeV.

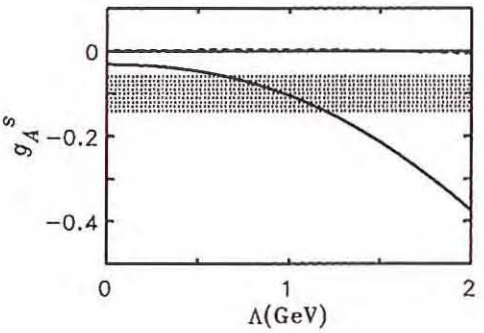

Figure 2: Strange axial charge of the proton as a function of the hadronic vertex function cut-off mass, Λ. The shaded area corresponds to the value of $\Delta s = -0.10 \pm 0.04$ from deep-inelastic scattering.

In future we intend to quantify in addition the contributions of the vector K^* mesons to both the deep-inelastic structure functions and elastic strangeness form factors. Furthermore, using coherent state techniques [6] we will be able to develop a systematic estimate of the importance of higher order, multi-meson contributions, which so far have been omitted in the one-loop calculations.

* Instituto de Física, Universidade Federal Fluminense, 24210-340, Niterói, R. J., Brazil.

References:

[1] B. Mueller et al., Phys. Rev. Lett. 78 (1997) 3824.

[2] K.A. Aniol et al., nucl-ex/9810012.

[3] W. Melnitchouk et al, Phys. Rev. C 55 (1997) 431.

[4] J. Haidenbauer et al, nucl-th/9805014.

[5] M. Malheiro et al, Phys. Rev. C 56 (1997) 2373.

[6] P. Alberto et al., Z. Phys. A 336 (1990) 449.

Renormalization of the effective chiral pion–nucleon Lagrangian to fourth order

Ulf-G. Meißner, G. Müller (Wien) and S. Steininger

In the effective meson–baryon low–energy theory of QCD, one encounters the problem that to one (or higher) loop order in the chiral expansion divergences appear. This problem has been considered to third order in external momenta and meson masses collectively denoted $\mathcal{O}(p^3)$, i.e. one loop graphs with insertions entirely from the lowest order meson–baryon Lagrangian, for the two–flavor case in [1] and for SU(3) in [2]. We have extended these works and analyzed the divergence structure of the one–loop generating functional to order p^4 [3], which are one–loop diagrams with exactly one insertion from the dimension two effective Lagrangian. This is mandated by the fact that it not only completes the full one loop generating functional but also is based on the phenomenological observation that one loop graphs with exactly one dimension two insertion are often important (like e.g. in the calculation of the nucleons electromagnetic polarizabilities of neutral pion photoproduction off nucleons or light nuclei). These divergences can be extracted in a chiral invariant manner by making use of the heat kernel representation of the propagators in d-dimensional Euclidean space. The first class of divergent graphs are the so–called tadpoles, which can be treated by standard methods. In the case of the self–energy contribution the divergences are due to the singular behaviour of the product of the meson and the baryon propagators in the conincidence limit. To order p^4, however, we can have an additional insertion on the intermediate nucleon line. This is the so–called *eye graph*. These various graphs are depicted in fig.1.

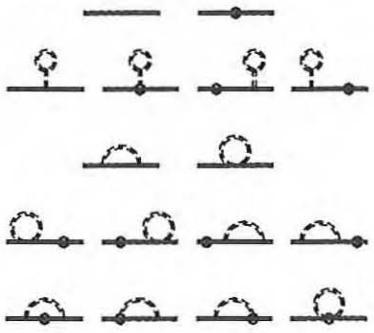

Figure 1: Contributions to the one–loop generating functional at order q^4. In the lowest line, the irreducible graphs quadratic in pion fluctuations are shown. These are (from left to right) the eye, the two vertex–corrected self–energy and the tadpole diagram. The circle–cross denotes a dimension two insertion and the solid (dashed) double lines the baryon (meson) propagator in the presence of external fields.

Therefore, we have to deal with a triple coincidence limit which has not yet been treated in heavy baryon chiral perturbation theory. We have developed a new method to treat such triple coincidences and more generally, one loop diagrams with an arbitrary number of insertions on the internal fermion line (hedgehog graphs). We also have shown how the heat kernel method has to be extended for operators that are not parallel to the heavy fermion four–velocity. A lengthy calculation of the (irreducible) tadpole, self–energy, vertex–corrected self–energy and eye graphs results in the complete counterterm Lagrangian,

$$\mathcal{L}_{\pi N}^{(4)\,\mathrm{ct}} = \frac{1}{(4\pi F)^2} \sum_{i=1}^{199} d_i\, \bar{N}_v(x)\, \tilde{O}_i^{(4)}(x)\, N_v(x)$$

for the velocity–dependent heavy nucleon fields N_v and in terms of the operators $\tilde{O}_i^{(4)}$, which can be found in table 1 of ref.[3]. This table constitutes the central result of this work. To facilitate comparison and checks, we have also listed in the appendices of that paper the resulting operators and β–functions for the tadpole, self–energy and eye graphs, respectively. The pertinent β–functions depend on the finite LECs g_A, $c_{1,\ldots,6}$ and the inverse of the nucleon mass. The values of these LECs are all well determined. The renormalized LECs $d_i^r(\mu)$ are measurable quantities. They satisfy the renormalization group equations

$$\mu \frac{d}{d\mu} d_i^r(\mu) = -\delta_i \ .$$

Therefore, the choice of another scale μ_0 leads to modified values of the renormalized LECs,

$$d_i^r(\mu_0) = d_i^r(\mu) + \delta_i \log \frac{\mu}{\mu_0} \ .$$

We remark that the scale–dependence in the counterterm Lagrangian is, of course, balanced by the scale–dependence of the renormalized finite one–loop functional for observable quantities.

As applications and checks of the rather involved algebra, we have studied the isoscalar magnetic moment and the scalar form factor of the nucleon to fourth order in small momenta based on Feynman diagrams. The resulting divergences can exactly be cancelled by using the pertinent operators from table 1 of ref.[3] and their β–functions. We have also studied the divergence structure of the elastic pion–nucleon scattering amplitude and are presently constructing the complete effective Lagrangian at fourth order including the minimal set of finite terms.

References:

[1] G. Ecker, Phys. Lett. B336 (1994) 508.

[2] G. Müller and Ulf-G. Meißner, Nucl. Phys. B492 (1997) 379.

[3] Ulf-G. Meißner, G. Müller and S. Steininger, hep-ph/9709446, accepted for publication in Ann. Phys. (NY).

Pion–nucleon scattering in chiral perturbation theory to one loop

N. Fettes, Ulf-G. Meißner and S. Steininger

A detailed investigation of pion–nucleon scattering based on the existing πN partial wave amplitudes has been performed for the first time in ref.[1]. This is the first step in a bigger program of investigating isospin violation in low energy processes involving pions, nucleons and photons.

1. We have constructed the minimal pion–nucleon Lagrangian at third order in the chiral expansion, including all corrections arising from the expansion in the inverse nucleon mass (with fixed coefficients as well as dimension two LECs). We have also enumerated the purely divergent terms which arise from the evaluation of the one–loop generating functional to one loop and order q^3. At third order, the effective Lagrangian has 23 terms with LECs,

$$\mathcal{L}_{\pi N}^{(3)} = \mathcal{L}_{\pi N}^{(3),\,\mathrm{fixed}} + \sum_{i=1}^{23} d_i \, \bar{H} \tilde{O}_i H \ ,$$

Only 14 of these have a non–vanishing β–function. This extends the result obtained in [2]. In addition, there are 8 terms which are only necessary for the renormalization (eqaution of motion terms).

2. Based on this Lagrangian, we have constructed the complete amplitude for elastic pion–nucleon scattering to third order in small momenta and pion masses. Our loop contribution agrees exactly with the one given previously. For the tree graphs, we have shown the exact equivalence between the $1/m$ expansion of the result obtained in the relativistic theory and the one calculated directly in the heavy baryon approach, provided one does not expand the normalization factor of the nucleon spinors.

3. We have fitted the two S– and four P–wave partial wave amplitudes for three different sets of available pion–nucleon phase shifts at intermediate energies (typically in the range of 50 to 100 MeV pion momentum in the laboratory frame), a typical fit is shown in fig.1. This allows to predict the phases at *lower* and at *higher* energies, in particular the (sub)threshold parameters (scattering lengths and effective ranges). By this fitting procedure we can determine the four dimension two LECs $c_{1,2,3,4}$ and five (combinations) of dimension three LECs. The numerical values for the LECs $c_{2,3,4}$ are in good agreement with previous determinations from threshold and subthreshold parameters alone. Consequently, the numerical values of these LECs can be understood by resonance exchange saturation. The LEC c_1, which is directly related to the pion–nucleon σ–term, comes out larger than before. We show, however, that the fits are not very sensitive to its actual value and one thus can not pin down the σ–term at this order in the chiral expansion. The dimension three LECs have "natural" size.

4. We have evaluated the threshold parameters using the one–loop amplitude for the extrapolation. The

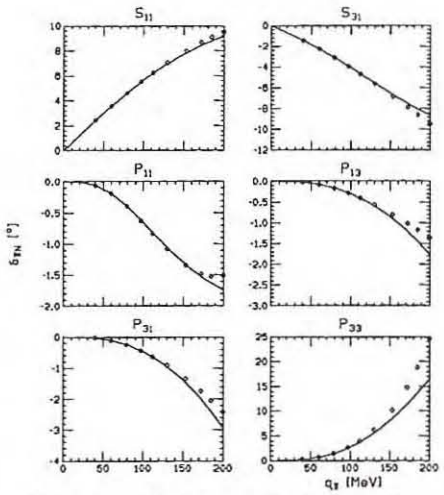

Figure 1: Fit to the Karlsruhe phase shifts.

results are fairly stable for the various fits and, if applicable, comparable to the results based on dispersion theory. As already known, the isoscalar S–wave scattering length can not be determined precisely to this order, but we give an improved prediction for the isovector one, $0.083\, M_\pi^{-1} \leq a_{0+}^- \leq 0.093\, M_\pi^{-1}$. This value is in good agreement with recent determinations from the strong interaction level shift in pionic atoms measured at PSI and with values extracted from phase shift analyses, compare fig.2

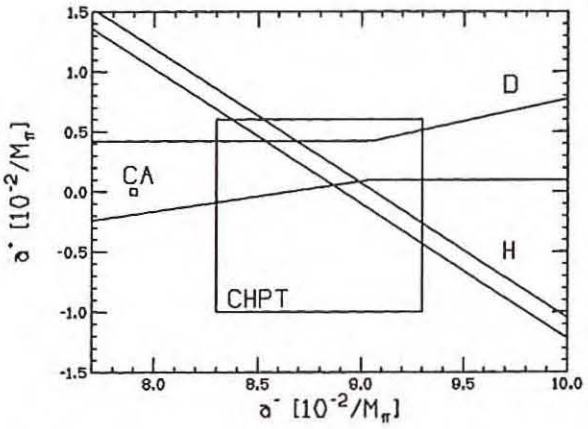

Figure 2: Isovector (a^-) and isoscalar (a^-) S–wave scattering lengths compared to results from pionic hydrogen (H band) and deuterium (D band) measurements.

References:

[1] N. Fettes, Ulf-G. Meißner and S. Steininger, Nucl. Phys. A640 (1998) 199.

[2] G. Ecker and M. Mojžiš, Phys. Lett. B365 (1996) 312.

Wave function renormalization in heavy fermion effective field theories

N. Fettes, Ulf-G. Meißner and S. Steininger

We consider effective field theories with massive spin–1/2 degrees of freedom, like heavy baryon chiral perturbation theory (HBCHPT) or heavy quark effective field theory (HQEFT). In such theories, the massive degrees of freedom behave essentially non–relativistically and it is thus not obvious how to extend the notion of wave function renormalization to such a situation. In relativistic baryon CHPT, this is not an issue since one can apply standard quantum field theoretical methods. In the work of ref. [1], the wave function renormalization was defined via the derivative of the nucleon self–energy at $\omega = 0$, leading to a momentum independent result for Z_N, the heavy nucleon Z–factor. A more detailed analysis of this particular aspect was performed by Ecker and Mojžiš [2], who argued that the Z–factor can not be a constant but rather depends (in momentum space) on the chosen frame via the baryon momentum. They for the first time stressed the role of the heavy fermionic sources and within their scheme, the contribution from these sources is entirely given by Z_N and one thus does not have to perform any explicit calculation for terms involving these heavy sources (once the Z–factor is determined). Note that the Z–factor given in that paper for the "BKKM" approach is not correct, it should be momentum–independent. This momentum dependence is, however, also present in the treatment à la ref.[1]. In that approach, the tree graphs are calculated from the *relativistic* tree level Lagrangian and then expanded in inverse powers of the nucleon mass up to the needed accuracy. More precisely, one has to include all relativistic tree level Lagrangian terms $\mathcal{L}_{\pi N}^{(1)} + \mathcal{L}_{\pi N}^{(2)} + \ldots$ which, when expanded, can contribute to the order of M_π/m_N one is after. This procedure contains automatically the momentum dependent pieces through the spinor normalization, as explicitely shown for the case of elastic pion–nucleon scattering in [3]. A general proof that this method always leads to the correct results has been given in ref.[4]. In that paper a very simple scheme for wave function renormalization in heavy fermion effective field theories which parallels as closely as possible the conventional quantum field theory approach was set up. This scheme is also very useful to elucidate the interrelationship between the various approaches found in the literature. It also provides us with the proof that expanding the relativistic tree graphs indeed leads to the correct result, as first conjectured in [5]. The method developed should also be of interest for HQEFT, since to our knowledge this issue has not been addressed in detail there.

The most natural and economic way of defining wave function renormalization in heavy fermion effective field theories rests on the interpretation of the light components of the heavy fields (like e.g. the nucleons) as *Dirac* spinors. In that way, one can define the heavy fermion Z–factor, also denoted by Z_N, that fulfills the following four conditions: 1) The definition of Z_N should be independent of the choice of the four–velocity vector v. 2) Its definition should only involve the physical fields. 3) At tree level, one should have $Z_N^{\rm tree} = 1$. 4) The definition of Z_N should be independent of the way one approaches the physical on–shell momentum, $p \to p_N$. In particular, the so–defined Z–factor is momentum–independent and its tree graph contribution is equal to one. Furthermore, this prescription can be extended to higher orders, i.e. beyond one loop, without problems. Such an interpretation is mandated by the correct matching of the heavy fermion EFT to its relativistic counterpart. Note that all calculations performed so far in HBCHPT have been done under the assumption that the light components of the heavy fields are to be interpreted as *Pauli* spinors. We have shown the equivalence between such an approach and the Dirac spinor interpretation, provided one works in the rest–frame $v = (1, \vec{0})$ in the Pauli case. This allows to *justify* a posteriori the methods employed by BKKM [1] ($1/m_N$ expansion of the relativistic tree graphs independent of the spinor interpretation) and by FMS [3] (inclusion of the explicit four–dimensional spinor normalization in the tree graphs calculated from HBCHPT). When applied correctly, all these different schemes lead to the same physics. As an example, one can show how the tree result for the proton charge form factor, $G_E^{\rm tree}(k^2) = e = \text{constant}$, with e the proton charge and k^2 the photons' four–momentum squared, emerges in the various calculational schemes. Furthermore, we have studied the nucleon mass shift to fourth order in the pion mass. Apart from an unspecified counter term contribution, which formally amounts to a quark mass correction of a dimension two operator, these corrections are tiny.

References:

[1] V. Bernard, N. Kaiser, J. Kambor and Ulf-G. Meißner, Nucl. Phys **B388** (1992) 315.

[2] G. Ecker and M. Mojžiš, Phys. Lett. **B410** (1997) 266.

[3] N. Fettes, Ulf-G. Meißner and S. Steininger, Nucl. Phys. **A640** (1998) 199.

[4] S. Steininger, Ulf-G. Meißner and N. Fettes, J. High Energy Phys. **09** (1998) 008.

[5] V. Bernard, N. Kaiser and Ulf-G. Meißner, Z. Phys. **C 70** (1996) 483.

Isospin violation in the pion–nucleon scattering lengths

N. Fettes, Ulf-G. Meißner and S. Steininger

Pion–nucleon scattering is one of the prime reactions to test our understanding of the spontaneous and explicit chiral symmetry breaking QCD is supposed to undergo. During the last years, there has been considerable interest in using πN scattering data to extract information about the violation of isospin symmetry, some analyses indicating effects as large as 7% [1]. In both these analyses, the source of this rather large effect remains mysterious. Microscopically, there are two competing sources of isospin violation, which are generally of the same size, namely the strong effect due to the light quark mass difference $m_d - m_u \simeq m_u$ and the electromagnetic (em) one caused by virtual photons. For neutral pion scattering off nucleons, these effects can be dramatically enhanced due to the smallness of the isoscalar pion–nucleon amplitude [2, 3]. This spectacular effect in the difference of the $\pi^0 p$ and $\pi^0 n$ scattering lengths is, however, at present not amenable to a direct experimental verification. It is therefore mandatory to include also the channels with charged pions in any analysis of isospin violation. To do this in a consistent fashion, one has to develop an effective field theory (EFT) of pions, nucleons and virtual photons. The corresponding effective Lagrangian was developed in ref.[3] extending the standard πN EFT. The pertinent power counting of the EFT is based on the observation that besides the pion mass and momenta, the electric charge e should be counted as an additional small parameter, given the fact that $e^2/4\pi \simeq M_\pi^2/(4\pi F_\pi)^2 \simeq 1/100$ (with M_π and F_π the pion mass and decay constant, respectively). Similar information can also be obtained from precise data on pion photoproduction. In ref.[4] we have given a first systematic study of the expected size of isospin violation in the πN amplitude in the threshold region based on a set of relations, which vanish in the limit of exact isospin. In that paper, only the strong and em isospin violating operators of dimension two were retained and it was assumed that the hard em (Coulomb) effects can be factored out.

Isospin violation is best characterized in terms of quantities which are exactly zero in the isospin limit of equal quark masses and vanishing em coupling. With the three pion $(\pi^\pm, \pi^0)$ and two nucleon (p, n) fields, we have ten reaction channels, which in the case of isospin symmetry are entirely described in terms of two amplitudes. Employing time reserval invariance, one thus can write down six isospin relations

$$R_1 = 2\,\frac{T_{\pi^+p\to\pi^+p} + T_{\pi^-p\to\pi^-p} - 2T_{\pi^0p\to\pi^0p}}{T_{\pi^+p\to\pi^+p} + T_{\pi^-p\to\pi^-p} + 2T_{\pi^0p\to\pi^0p}}$$

$$R_2 = 2\,\frac{T_{\pi^+p\to\pi^+p} - T_{\pi^-p\to\pi^-p} - \sqrt{2}T_{\pi^-p\to\pi^0n}}{T_{\pi^+p\to\pi^+p} - T_{\pi^-p\to\pi^-p} + \sqrt{2}T_{\pi^-p\to\pi^0n}}$$

$$R_3 = 2\,\frac{T_{\pi^0p\to\pi^+n} - T_{\pi^-p\to\pi^0n}}{T_{\pi^0p\to\pi^+n} + T_{\pi^-p\to\pi^0n}}$$

$$R_4 = 2\,\frac{T_{\pi^+p\to\pi^+p} - T_{\pi^-n\to\pi^-n}}{T_{\pi^+p\to\pi^+p} + T_{\pi^-n\to\pi^-n}}$$

$$R_5 = 2\,\frac{T_{\pi^-p\to\pi^-p} - T_{\pi^+n\to\pi^+n}}{T_{\pi^-p\to\pi^-p} + T_{\pi^+n\to\pi^+n}}$$

$$R_6 = 2\,\frac{T_{\pi^0p\to\pi^0p} - T_{\pi^0n\to\pi^0n}}{T_{\pi^0p\to\pi^0p} + T_{\pi^0n\to\pi^0n}}$$

From these, R_1 and R_6 only involve isoscalar amplitudes and are thus particularly sensitive to isospin violation. R_6 has been previously been considered in refs.[2, 3]. For the novel ratio R_1 we expect an even larger effect,

$$R_6 \simeq 37\% \,.$$

This ratio involves scattering of charged and neutral pions off the proton. The $\pi^0 p$ scattering length can be determined from a precise neutral pion photoproduction target asymmetry measurement below the secondary $\pi^+ n$ threshold, see e.g. [5]. The ratios involving the isovector scattering amplitude are all of the order of one percent.

	R_2 [%]	R_3 [%]	R_4 [%]	R_5 [%]
Fit 1	0.9	−0.5	−0.7	1.1
Fit 2	1.1	−0.6	−0.9	1.1
Fit 3	0.9	−0.5	−0.8	1.0

Table 1: Values of the ratios R_i for the various parameter sets as given by the fits of FMS [6].

Also given in [4] are predictions for the (in some cases complex–valued) scattering lenghts. Further work to systematically include hard photons (Coulomb corrections) and higher order operators related to soft virtual photons are underway.

References:

[1] W.R. Gibbs, Li Ai and W.B. Kaufmann, Phys. Rev. Lett. 74 (1995) 3740; E. Matsinos, Phys. Rev. C58 (1997) 3014.

[2] S. Weinberg, Trans. N.Y. Acad. of Sci. 38 (1977) 185.

[3] Ulf-G. Meißner and S. Steininger, Phys. Lett. B419 (1998) 403.

[4] N. Fettes, Ulf-G. Meißner and S. Steininger, hep-ph/9811366.

[5] A.M. Bernstein, hep-ph/9810376.

[6] N. Fettes, Ulf-G. Meißner and S. Steininger, Nucl. Phys. A640 (1998) 199.

Effective theory for the two–nucleon system

E. Epelbaum, W. Glöckle (Bochum), A. Krüger (Bochum) and Ulf-G. Meißner

Chiral perturbation theory is hoped to provide insight into the nuclear force problem and possibly even lead to a quantitative framework. Chiral symmetry imposes constraints on possible momentum and spin dependences of the nuclear forces but the framework is restricted to momenta below a certain scale. Only in this regime one can set up a power counting scheme which limits the number of interaction terms in the nuclear Hamiltonian. Whether this scheme works quantitatively and is applicable to interacting nucleons seems not yet fully established, despite a large number of investigations and considerable progress over the last few years. We therefore think that a model study based on a simplified nuclear force which, however, captures the essential features of the nucleon–nucleon interaction (long/intermediate–range attraction and short–range repulsion) can provide useful insights.

In refs.[1, 2] we have shown how to construct an effective low energy theory for nucleons based on the method of unitary transformations [3, 4] starting from a realistic two–nucleon potential (in momentum space). This unitary transformation can be parametrized by an operator A, which obeys a nonlinear integral equation. This equation can be solved numerically and any observable can then be calculated in the space of small momenta only. To the best of our knowledge such an exact momentum space projection has never been done before. While the method is interesting *per se*, we have also made contact to chiral perturbation theory (CHPT) approaches to the two–nucleon system by studying a series of questions, which can be addressed unambigouosly within the framework of our exact low momentum theory. Clearly, this should not be considered a substitute for a realistic CHPT calculation but might be used as a guide. The main results of this study can be summarized as follows:

1. We have demonstrated that the theory projected onto the subspace of momenta below a given momentum space cut–off Λ leads to exactly the same S–matrix as the original theory in the full (unrestricted) momentum space provided appropriate boundary conditions for the scattering states are chosen. In particular, the components of the transformed scattering states with initial momenta below the cut–off Λ in the subspace of momenta above the cut–off Λ are strictly zero. It is important to stress that the exact projection leads to non–localities in momentum space.

2. Starting from an S–wave NN potential with an attractive light ($\mu_L \simeq 300$ MeV) and repulsive heavy meson exchange ($\mu_H \simeq 600$ MeV), we have numerically solved without *any* approximation the nonlinear equation for the operator A and demonstrated that the bound and scattering state spectrum of the effective and the full theory agree exactly up to the

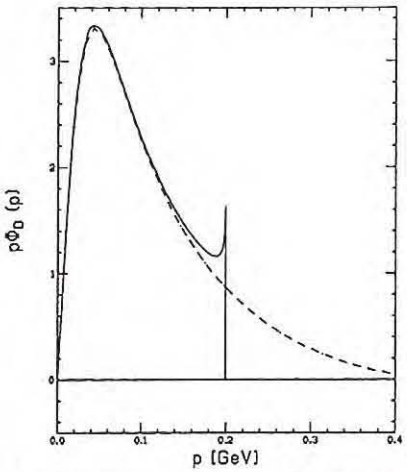

Figure 1: Deuteron wave function $p\,\Phi_D(p)$ versus the momentum p from the effective potential (solid line) and the original potential (dashed line) for $\Lambda = 200$ MeV.

cut–off Λ. In particular, we have exactly one bound state with a binding energy of 2.23 MeV. The corresponding deuteron wave function is shown in fig.1. These results are independent of the value of the cut–off, which was varied from 200 MeV to 5.5 GeV. We have argued that the most natural choice is Λ about 300 MeV. The effective potential can differ substantially from the original one (for values of Λ on the small side of the range mentioned before, cf. fig.2).

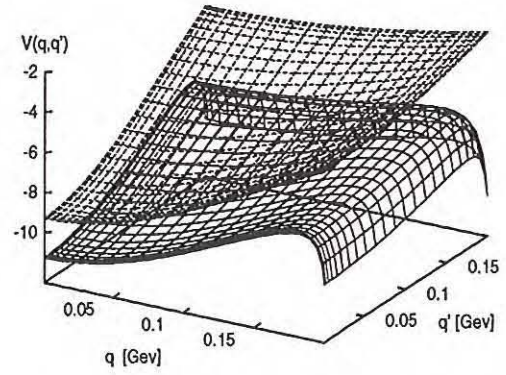

Figure 2: Effective two–nucleon potential (green hatched area with solid lines) in comparison with the original potential (blue hatched area with dashed lines), for momenta less than 200 MeV.

3. We have expanded the heavy meson exchange term in a string of local operators with increasing dimension but kept the light meson exchange explicitely,

$$V'(q',q) = V'_{\rm light}(q',q) + V'_{\rm contact}(q',q)\ ,$$
$$V_{\rm contact} = V^{(0)} + V^{(2)} + V^{(4)} + \dots\ ,$$

$$V^{(0)} = C_0 \ , \quad V^{(2)} = C_2(q'^2 + q^2) \ ,$$
$$V^{(4)} = C_4(q'^2 + q^2)^2 + C_4' q'^2 q^2 \ .$$

The corresponding coupling constants accompanying these local operators, which are monomials of even power in the momenta, can be determined precisely from the exact solution. We have shown that they are of "natural" size, i.e. of order one, with respect to the mass scale $\Lambda_{\rm scale} = 600$ MeV. We have also discussed the relation of this scale to the mass of the heavy meson, which is integrated out, and the convergence properties of such type of expansion. In particular, to recover the binding energy within a few percent, one has to retain terms of rather high order in this expansion. This is to be expected due to the unnatural smallness of this energy on any hadronic mass scale. The $^3S_1$ scattering phase shift can be well reproduced up to kinetic energies $T_{\rm lab} \simeq 120$ MeV with the first three terms in the contact term expansion.

4. Based on the expanded heavy meson exchange term, we have also determined the constants C_i directly from a fit to the phase shifts. This is equivalent to the procedure performed in an effective field theory approach. We could show that as long as one does not include polynoms of order six (or higher), the resulting values of these constants are close to their exact ones. Furthermore, the binding energy is reproduced within 2%. Including dimension six terms, the fits become unstable. This can be traced back to the fact that the contribution of such terms to the phase shifts are very small (at low and moderate energies) and thus can not really be pinned down.

5. We have also studied the quantum averages of the expanded potential in the bound and scattering states. For $\Lambda = 300$ MeV, the expansion parameter is of the order of 1/2 and we find fast convergence for the bound and the low-lying scattering states. As expected, for scattering states with higher energy, the convergence becomes slower, as shown in the tables 1,2.

$\langle\Psi\|V^{(0)}\|\Psi\rangle$	$\langle\Psi\|V^{(2)}\|\Psi\rangle$	$\langle\Psi\|V^{(4)}\|\Psi\rangle$
25.94 MeV	-4.23 MeV	1.07 MeV
31.34 GeV^{-2}	-6.19 GeV^{-2}	1.64 GeV^{-2}
11.54 GeV^{-2}	-3.28 GeV^{-2}	1.11 GeV^{-2}
7.79 GeV^{-2}	-3.09 GeV^{-2}	1.40 GeV^{-2}

Table 1: The quantum averages of the operators $V^{(0)}$, $V^{(2)}$, $V^{(4)}$ and $V^{(6)}$ for the bound (second row) and the scattering states (third to fifth rows, $E_{\rm lab} = 10, 50, 100$ MeV) for $\Lambda = 300$ MeV in the $^3S_1$ channel.

6. To study the $^1S_0$ channel, we had to slightly readjust the parameters of the model potential. The phase shift can be well reproduced with the terms up-to-and-including fourth order in the contact term expansion of the heavy meson exchange. For the scattering states, the quantum averages of the expanded potential show convergence properties similar to the $^3S_1$ case. There is no bound state in the $^1S_0$, but a virtual one just above threshold. Therefore, the pertinent scattering length is unnaturally large and it shows a similar slow convergence as does the binding energy in the $^3S_1$ channel.

$\langle\Psi\|V^{(0)}\|\Psi\rangle$	$\langle\Psi\|V^{(2)}\|\Psi\rangle$	$\langle\Psi\|V^{(4)}\|\Psi\rangle$
37.42 GeV^{-2}	-4.68 GeV^{-2}	0.90 GeV^{-2}
11.72 GeV^{-2}	-2.56 GeV^{-2}	0.68 GeV^{-2}
8.82 GeV^{-2}	-2.98 GeV^{-2}	1.18 GeV^{-2}

Table 2: Quantum averages of the operators $V^{(0)}$, $V^{(2)}$ and $V^{(4)}$ for the scattering states ($E_{\rm lab} = 10, 50, 100$ MeV) with $\Lambda = 300$ MeV in the $^1S_0$ channel.

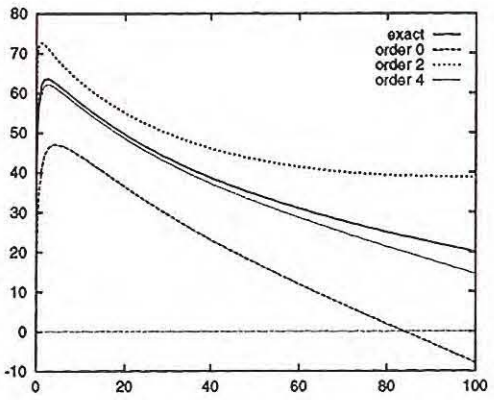

Figure 3: Phase shifts from the effective potential V' (solid green line) and the truncated expansion to zeroth, second and fourth order as a function of the kinetic energy in the lab for the $^1S_0$ channel for $\Lambda = 300$ MeV.

7. In the model space of small momenta only, one can also study the non-localities in the coordinate space representation. We have shown that for typical cut-off values, the effective potential $V(x, x')$ is highly non-local and looks very different from the original one. For very large values of the cut-off, one recovers the original local potential.

We hope that this study might be useful for derivation of NN-forces based on chiral Lagrangians in the low-momentum regime. It should also provide new insights into a consistent and convergent treatment of relativistic effects in few- and many-nucleon systems.

References

[1] E. Epelbaum, W. Glöckle and Ulf-G. Meißner, Phys. Lett. B439 (1998) 1.

[2] E. Epelbaum, W. Glöckle, A. Krüger and Ulf-G. Meißner, `nucl-th/9809084`, Nucl. Phys. A, in press.

[3] S. Okubo, Prog. Theor. Phys. 12, 603 (1954).

[4] N. Fukuda, K. Sawada and M. Taketani, Prog. Theor. Phys. 12, 156 (1954).

The nucleons electroweak form factors at low energies

V. Bernard (Strasbourg), H.W. Fearing (TRIUMF), T.R. Hemmert and Ulf-G. Meißner

The chiral symmetry of the light flavor sector of QCD is spontaneously broken at low energies leading to the existence of Goldstone boson modes. In the light (u,d) quark sector, one identifies the pions with these Goldstone bosons. All low energy dynamics is governed by these lightest hadronic degrees of freedom and the chiral symmetry puts very strict constraints on their interactions among themselves, with external sources and on their coupling to matter fields (baryons, etc.). This Goldstone-boson dominated regime of *non-perturbative* QCD at low energies can be formulated exactly in an effective lagrangian formalism called Chiral Perturbation Theory (CHPT). With the pions being the lightest degrees of freedom in the hadron spectrum, CHPT suggests that the long range structure of baryons and its leading momentum dependence is governed by the chiral symmetry of the pion interaction.

The electro–weak structure of baryons is parameterized via form factors. In the case of the nucleon they have been analyzed in one–loop relativistic baryon CHPT [1] and in a "non–relativistic" approach called HBCHPT [2] in the past. Recently [3], we have repeated this analysis utilizing a phenomenological extension of CHPT called the "small scale expansion" [4]. In this approach one includes the first nucleon resonance $\Delta(1232)$ as an explicit degree of freedom in a phenomenologically resummed chiral expansion. In [3] all six form factors of the nucleon are discussed, here we will focus on the isovector Pauli form factor $F_2^v(q^2)$.

Consider the nucleon matrix element of the isovector component of the quark vector current $V_\mu^i = \bar{q}\gamma_\mu(\tau^i/2)q$, which involves a vector (Dirac) and a tensor (Pauli) form factor,

$$\langle N(p_2)|V_\mu^i(0)|N(p_1)\rangle = \bar{u}(p_2)\left[F_1^v(q^2)\,\gamma_\mu + \frac{i}{2M_N}F_2^v(q^2)\,\sigma_{\mu\nu}q^\nu\right]u(p_1)\,,$$

where $u(p)$ is a Dirac spinor and $q^2 = (p_2 - p_1)^2$ is the invariant momentum transfer squared. The radii of these form factors should be determined by the extension of the pion cloud. *E.g.* for the radius of $F_2^v(q^2)$ one finds to leading order in HBChPT [2], [SSE [3]]

$$(r_2^v)^2 = \frac{g_A^2 M_N}{8F_\pi^2\kappa_v\pi m_\pi} + \left[\frac{g_{\pi N\Delta}^2 M_N}{9F_\pi^2\kappa_v\pi^2\sqrt{\Delta^2-m_\pi^2}}\log\left[\frac{\Delta}{m_\pi}+\sqrt{\frac{\Delta^2}{m_\pi^2}-1}\right]\right] = 0.52\text{fm}^2\,[+\,0.09\text{fm}^2]\,,$$

compared with the empirical value, $(r_2^v)^2 = 0.80\text{fm}^2$ [5]. The only parameters are the pion decay constant (mass) F_π (m_π), the πNN $(\pi\Delta N)$ couplings g_A $(g_{\pi N\Delta})$, the nucleon mass M_N, the mass-splitting $\Delta = M_\Delta - M_N$ and the anomalous isovector magnetic moment κ_v. All these parameters are well determined. One can see that already the *leading* HBCHPT result for the extension of the pion cloud provides a good estimate for the size of the nucleon in this channel. Inclusion of explicit delta components in the nucleon wavefunction around which the pions can fluctuate provides a 17% correction in the right direction [3]. In the chiral limit, we recover the well known $1/m_\pi$ singularity, which is not touched by the resonance contribution in accord with general decoupling requirements. This singularity is a consequence of the infinite range of a cloud of massless pions. Other form factor results (also for the two form factors related to the weak axial current) are discussed in [3].

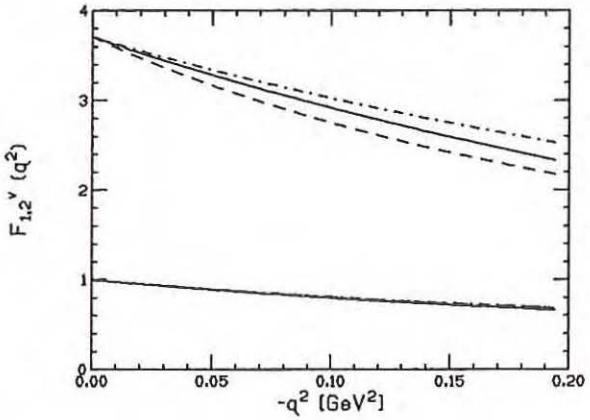

Figure 1: Isovector form factors of the nucleon. SSE: solid lines, HBCHPT: dot-dashed lines, empirical parametrization of ref.[5]: dashed lines. The lower (upper) set of curves refers to $F_1^v(q^2)$ $(F_2^v(q^2))$.

References:

[1] J. Gasser, M.E. Sainio and A. Švarc, Nucl. Phys. **B307**, 779 (1988).

[2] V. Bernard, N. Kaiser, J. Kambor and Ulf-G. Meißner, Nucl. Phys. **B388**, 315 (1992); V. Bernard, N. Kaiser and Ulf-G. Meißner, Int. J. Mod. Phys. **E4**, 193 (1995).

[3] V. Bernard, H.W. Fearing, T.R. Hemmert and Ulf-G. Meißner, Nucl. Phys. **A635**, 121 (1998).

[4] T.R. Hemmert, B.R. Holstein and J. Kambor, Phys. Lett. **B395**, 89 (1997); J. Phys. **G24**, 1831 (1998).

[5] P. Mergell, Ulf-G. Meißner and D. Drechsel, Nucl. Phys. **A596**, 367 (1996).

Strange magnetism in the nucleon

T.R. Hemmert, Ulf-G. Meißner and S. Steininger

The strangeness content of the nucleon has been much discussed in the last years, like e.g. in the analysis of the pion–nucleon Σ–term or the spin content of the proton. Another sector where explicit strange degrees of freedom figure prominently concerns the strangeness vector current of the nucleon to be measured in parity–violating electron–hadron scattering at MAMI and JLAB. It is defined as

$$\langle N|\, \bar{s}\, \gamma_\mu\, s\, |N\rangle = (1/3) J^0_\mu - (1/\sqrt{3}) J^8_\mu\,, \qquad (1)$$

in terms of the conventional singlet and octet currents. These can be written in terms of form factors as

$$J^{0,8}_\mu \sim \left[F_1^{(0,8)}(q^2)\gamma_\mu + F_2^{(0,8)}(q^2)\frac{i\sigma_{\mu\nu}q^\nu}{2M_N} \right] . \qquad (2)$$

Here, $q_\mu = p'_\mu - p_\mu$ corresponds to the four–momentum transfer to the nucleon by the external singlet ($v^{(0)}_\mu = v_\mu \lambda^0$) and the octet ($v^{(8)}_\mu = v_\mu \lambda^8$) vector source v_μ, respectively. The strangeness Dirac and Pauli form factors are defined via

$$F^{(s)}_{1,2}(q^2) = \frac{1}{3} F^{(0)}_{1,2}(q^2) - \frac{1}{\sqrt{3}} F^{(8)}_{1,2}(q^2)\,, \qquad (3)$$

subject to the normalization $F_1^{(s)}(0) = 0, F_2^{(s)}(0) = \kappa_B^{(s)}$, with $\kappa_B^{(s)}$ the (anomalous) strangeness moment. In the following we concentrate our analysis on the "magnetic" strangeness form factor $G_M^{(s)}(q^2)$, which in analogy to the (electro)magnetic Sachs form factor is defined as

$$G^{(s)}_M(q^2) = F_1^{(s)}(q^2) + F_2^{(s)}(q^2)\,. \qquad (4)$$

In the case of a nucleon $G^{(s)}_M(0) \equiv \mu^{(s)}_N$ defines the so called "strange magnetic moment" of the nucleon whose sign and/or size is heavily contested in theoretical analyses. Furthermore, it is precisely this form factor at $q^2 = -0.1\mathrm{GeV}^2$ which has been analyzed in the recent Bates measurement [1]. As shown in ref.[2], the evolution of this form factor with q^2 can be predicted in terms of well-known low energy quantities. To $\mathcal{O}(p^3)$ in SU(3) HBCHPT one finds

$$G^{(s)}_M(Q^2) = \mu^{(s)}_N + \frac{\pi M_N m_K}{(4\pi F_\pi)^2} \times \frac{2}{3}\left(5D^2 - 6DF + 9F^2\right) f(Q^2)\,, \qquad (5)$$

with $Q^2 = -q^2, D \simeq 3/4, F \simeq 1/2, F_\pi \equiv (F_\pi + F_K)/2 \simeq 102\mathrm{MeV}$ the average pseudoscalar decay constant and m_K being the kaon mass. The momentum dependence is given entirely in terms of the function $f(Q^2)$, which for small and moderate Q^2 rises almost linearly with increasing Q^2, see fig.1. Eq.(5) only contains the leading order chiral contribution which stems exclusively from the kaon-cloud of the nucleon. It will be interesting to calculate the next-to-leading order (*i.e.* $\mathcal{O}(p^4)$) correction to this result in order to check possible contributions from vector mesons which are usually assumed to dominate this form factor [3]. However, already at $\mathcal{O}(p^3)$ one can implicitly include some of the higher order corrections if one analyzes the magnetic isoscalar form factor $G_M^{I=0}(Q^2)$ and the strange magnetic form factor $G_M^{(s)}(Q^2)$ simultaneously[2]. One obtains the *model-independent* connection

$$G^{(s)}_M(Q^2) = \mu^{(s)}_N + \mu^{I=0}_N - G^{I=0}_M(Q^2) + \mathcal{O}(p^4)\,, \qquad (6)$$

where $\mu^{I=0}_N$ denotes the isoscalar magnetic moment of the nucleon. To $\mathcal{O}(p^3)$ one therefore predicts that the low Q^2 behavior of the strange magnetic form factor of the nucleon is *exactly* controlled by the well-known isoscalar form factor of the nucleon, see fig.1.

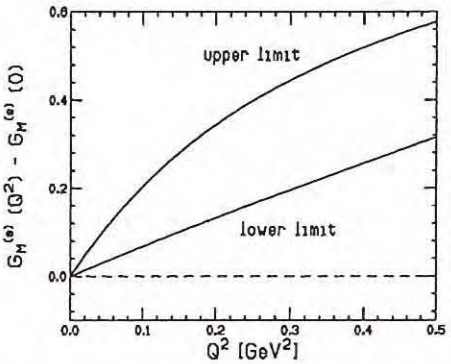

Figure 1: Lower and upper bound for the Q^2–evolution of the strange magnetic form factor setting $G^{(s)}_M(0) = \mu^{(s)}_N = 0$.

Eqs.(5,6) can be considered as a lower, upper bound on the q^2 evolution of the strange magnetic form factor at low momentum transfer [2]. Both relations can be used to extrapolate from the experimentally determined values for $G^{(s)}_M(Q^2)$ at $Q^2 > 0$ to the sought after strange magnetic moment $\mu^{(s)}_N$ of the nucleon at $Q^2 = 0$. Clearly, with improving experimental accuracy on $G^{(s)}_M(Q^2)$ one also needs to calculate the $\mathcal{O}(p^4)$ corrections to both relations. Furthermore, comparing Eqs.(5,6) we are also looking forward to the mapping of the low Q^2 dependence of $G^{(s)}_M(Q^2)$ by the G0 collaboration at J-Lab [4].

References:

[1] B. Mueller et al., Phys. Rev. Lett. **78**, 3824 (1997).

[2] T.R. Hemmert, Ulf-G. Meißner and S. Steininger, Phys. Lett. **B437**, 184 (1998).

[3] R.L. Jaffe, Phys. Lett. **B229**, 275 (1989); H.-W. Hammer, Ulf-G. Meißner and D. Drechsel, Phys. Lett. **B367**, 323 (1996).

[4] TJNAF experiment E91-017 (D. Beck, spokesperson).

Muon capture on the proton

V. Bernard (Strasbourg), T.R. Hemmert and Ulf-G. Meißner

Ordinary ($\mu^- p \to \nu_\mu n$) and Radiative ($\mu^- p \to \nu_\mu \gamma n$) Muon Capture (OMC, RMC) on a proton are venerable subjects in nuclear physics. After having served for decades as a testing ground for the symmetries and structure of the weak interaction, today these reactions can also be regarded as unique tests of the axial structure of the nucleon as mandated by the explicitly and spontaneously broken chiral symmetry of QCD at low energies. In particular, they can give us access to the elusive pseudoscalar form factor $G_P(q^2)$ of the nucleon. We have started therefore a systematic analysis of OMC and RMC in the framework of the "small scale expansion" (SSE), which is a phenomenologically inspired extension of heavy baryon chiral perturbation theory (HBCHPT) including also the $\Delta(1232)$ as a dynamical degree of freedom. OMC and RMC indeed are low energy hadronic processes where a good convergence behavior of HBCHPT (or SSE) can be expected [1]. In the Fermi approximation of a static W_μ^- field, the invariant matrix element of ordinary muon capture can be written as the product of a leptonic and an hadronic matrix element. The leptonic matrix element $\langle \nu_\mu | W_\mu^+ | \mu \rangle$ is uniquely fixed by the electroweak vertices of the Standard Model, utilized here as the source of well-understood external fields that probe the hadronic structure of a nucleon of mass M_N and isovector magnetic moment μ_v at low energies. Now one calculates the charge-changing hadronic vector $\langle n | V_\nu^- | p \rangle$ and axial-vector $\langle n | A_\nu^- | p \rangle$ currents in the SSE to the order desired. Assuming that the initial muon-proton system constitutes the ground-state of a bound system described by a 1s Bohr-wavefunction $\Phi(x)_{1s}$ of a muonic atom one finds the *spin-averaged* capture rate to second order [1]

$$\begin{aligned}
\Gamma_{\rm OMC} &= \frac{\alpha^3 G_F^2 V_{ud}^2 m_\mu^5}{2\pi^2 (m_\pi^2 + m_\mu^2)^2} \Big\{ (2g_A^2 + 1) m_\mu^4 \\
&+ (4g_A^2 + 2) m_\mu^2 m_\pi^2 + (3g_A^2 + 1) m_\pi^4 \\
&+ \frac{2m_\mu}{(m_\pi^2 + m_\mu^2) M_N} \big[(g_A \mu_v - 5g_A^2 - 2) \\
&\times (m_\mu^6 + 3m_\mu^4 m_\pi^2) \\
&+ (3g_A \mu_v - 16 g_A^2 - 6) m_\mu^2 m_\pi^4 \\
&+ (g_A \mu_v - 7 g_A^2 - 2) m_\pi^6 \big] \Big\} \\
&= (247 - 59) \times s^{-1} + \mathcal{O}(1/M_N^2) \\
&= 188 \times s^{-1} + \mathcal{O}(1/M_N^2) ,
\end{aligned}$$

with $G_F = g_2^2 \sqrt{2}/(8 M_W^2)$ the Fermi constant, m_π (m_μ) the pion (muon) mass, g_A the axial coupling constant, α the fine structure constant and V_{ud} the pertinent CKM matrix element. Note that the second order contribution amounts to a correction of less than 25% of the leading term. The expectation that OMC has a well behaved chiral expansion is also supported by the observation that in the case of no explicit chiral symmetry breaking (i.e. $m_\pi = 0$) the spin-averaged capture rate is only changed by 10%,

$$\begin{aligned}
\Gamma_{\rm OMC}^\chi &= (214 - 46) \times s^{-1} + \mathcal{O}(1/M_N^2) \\
&= 168 \times s^{-1} + \mathcal{O}(1/M_N^2) .
\end{aligned}$$

The physical reason for the nice stability of perturbative calculations for OMC is of course the fact that contributions of order n are suppressed [1] by $(m_i/\Lambda_\chi)^{n-1}$, with $i = \pi, \mu$ and $\Lambda_\chi \sim M_N \sim$ 1GeV. Analogous suppression effects are at work for RMC [1]. We therefore note that at $\mathcal{O}(1/M_N^2)$—when the calculation becomes sensitive to the internal structure of the nucleon beyond just the isovector magnetic moment μ_v and the leading pion pole—the new structure effects are strongly suppressed and therefore present a formidable challenge for the required precision of muon capture experiments.

We have also started to take a closer look at RMC. Several HBCHPT calculations of RMC have been performed, the most elaborate one by Ando and Min [2]. They found that the third order effects are small. However, in our opinion there is one point left to be examined in detail regarding the contribution of $\Delta(1232)$ in muon capture. In HBCHPT these effects are incorporated via third order counterterms, leading only to a small effect, consistent with previous phenomenological analyses. While this result is reassuring it is also surprising from the viewpoint of effective field theories. Introducing $\Delta(1232)$ into the theory leads to a new scale $\Delta = M_\Delta - M_N \sim$ 300MeV, which would suggest that the resulting effects (m_i/Δ), $i = \pi, \mu$ could be of the order of 30%. We have started to investigate [1] this problem to identify the origin of this strong suppression of $\Delta(1232)$. First numerical results confirm the smallness of the contributions, but the *analytical* structure and the physics behind this suppression is hard to pin down. Its origin lies in the fact that due to the atomic structure of the μp system both OMC and RMC are very sensitive to spin structure of the initial state which seems to act as filter mechanism [1].

References:

[1] V. Bernard, T.R. Hemmert and Ulf-G. Meißner, "Radiative Muon Capture and the Pseudoscalar Form Factor of the Nucleon", forthcoming and hep-ph/9811336.

[2] T. Meissner, F. Myhrer, and K. Kubodera, Phys.Lett. **B416** (1998) 36; S.-I. Ando and D.-P. Min, Phys.Lett. **B417** (1998) 177; H. W. Fearing, R. Lewis, N. Mobed, and S. Scherer, Nucl.Phys. **A631** (1988) 735c.

The parity–violating pion–nucleon coupling

Ulf-G. Meißner and H. Weigel (MIT)

There has been considerable interest and controversy about the parity–violating pion–nucleon coupling constant G_π over the last years, triggered on one side by new experimental results and on the other by fresh theoretical ideas. The measurement of the anapole moment in ^{133}Cs, which allows to get a bound on G_π, seems to contradict the bounds from the anapole moment measured in ^{205}Tl and the bound from the circular polarization asymmetry measurement of ^{18}Fl. To be precise, these data are analyzed in the framework of parity–violating (pv) one–boson exchange and are thus sensitive to the products of the weak and the strong (parity–conserving) couplings. The latter are, however, sufficiently well known for the present accuracies one is dealing with. On the theoretical side, the chiral perturbation theory analysis of Kaplan and Savage [1] seems to indicate a large enhancement of the weak pion–nucleon coupling due to strangeness. More precisely, the underlying four–fermion current–current Hamiltonian has a piece of the form $(\bar{q}q)(\bar{s}s)$, which contributes sizeably to G_π. Here, q (s) denotes the light (strange) quarks. In ref. [1], numerical estimates where given based on factorization and dimensional analysis. On the other hand, the two–flavor topological chiral soliton model had been used to study parity–violating meson–nucleon couplings [2] and interaction regions [2], including also the $N\Delta$ and $\Delta\Delta$ vertices. This model gives a successful description of many nucleon observables as reviewed in ref. [3]. In this approach, the weak pion–nucleon coupling comes out to be very small, typically $G_\pi \simeq 0.3 \cdot 10^{-7}$. Note that in the SU(2) Skyrme model without vector mesons, the weak pion–nucleon coupling vanishes due to a particular symmetry between the currents. This symmetry is absent in the presence of vector mesons or realistic three flavor version (we thus always compare to the vector meson stabilized Skyrmion when we talk about SU(2)). Clearly, in the two–flavor approch one is not sensitive to operators involving strange quarks and also strange components in the nucleon wave function. It appears therefore mandatory to extend the soliton model calculations to the three flavor case. We have therefore calculated G_π in a realistic SU(3) Skyrme model [4], which gives a fair description of many observables, like the mass splittings of the low-lying $1/2^+$ and $3/2^+$ baryons, magnetic moments, hyperon deacys and many others (for a review, see ref. [5]). Within this approach, we can quantify the role of the four–quark operators involving strange quark pairs as well as the role of strangeness in the nucleons' wave function.

The pertinent results of this study are now summarized. As input, we use for the Skyrme parameter values in the range $e = 4.0 \ldots 4.5$, which reasonably reproduces the baryon spectrum. The results for a large number of hyperon properties for these parameters can be found in the literature [5]. In fig.1 we show the weak pion–nucleon coupling constant as a function of the kaon mass, i.e. as a function of the symmetry breaking. For the physical value of m_K, we get

$$G_\pi = \{0.8, 1.3\} \cdot 10^{-7} \quad \text{for} \quad e = \{4.0, 4.5\} \,, \quad (1)$$

which is considerably bigger than the SU(2) generalized Skyrme result of $0.2 \ldots 0.3 \cdot 10^{-7}$ [2]. However, as one freezes out the kaon degrees of freedom, the value of G_π approaches zero as indicated in fig.1. The values given in eq.(1) are in fair agreement with most recent quark model calculations in which $G_\pi = 2.0 \ldots 2.7 \cdot 10^{-7}$ [6, 7]. The typical range of values in the quark model calculations is $G_\pi = 0 \ldots 3 \cdot 10^{-7}$ [6]. This large enhancement of the weak pion–nucleon coupling compared to the SU(2) calculations is largely due to the induced kaon fields (due to the collective quantization). Our study underlines the importance of four–quark operators involving strange quarks.

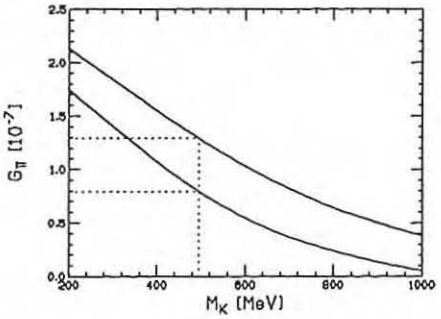

Figure 1: The weak πN coupling as a function of the kaon mass. Upper (lower) solid curve: $e = 4.5\,(4.0)$.

References:

[1] D.B. Kaplan and M. Savage, Nucl. Phys. A556 (1993) 653.

[2] N. Kaiser and Ulf-G. Meißner, Nucl. Phys. A499 (1989) 699; *ibid* A510 (1990) 759.

[3] Ulf-G. Meißner, Phys. Rep. 161 (1988) 213.

[4] Ulf-G. Meißner and H. Weigel, nucl-th/9807038, to appear in Phys.Lett.B.

[5] H. Weigel, Int. J. Mod. Phys. A11 (1996) 2419.

[6] B. Desplanques, Nucl. Phys. A335 (1980) 147; Phys. Rep. 297 (1998) 1.

[7] G.B. Feldman, G.A. Crawford, J. Dubach and B.R. Holstein, Phys. Rev. C43 (1991) 863.

Effective field theory approach to meson production in proton–proton collisions

V. Bernard (Strasbourg), N. Kaiser (München), Ulf-G. Meißner

Over the last years, very precise data on pion, η and η' meson production in proton-proton collisions in the threshold region have been obtained at IUCF, CELSIUS and COSY. The basic process is thus $pp \to pNM$, where N denotes the nucleon and M denotes a pseudoscalar meson, in our case the π^0, π^+, η or the η'. At the respective threshold, the produced meson is soft, i.e. has vanishing three momentum. Consequently, in the case of the pions, which are believed to be the Goldstone bosons related to the spontaneous chiral symmetry breaking QCD is assumed to undergo, this process appears to be a good testing ground for chiral perturbation theory methods. To be specific, at threshold one has only S–waves and thus the pertinent T–matrix for the specific case of π^0 production is parametrized in terms of one single amplitude,

$$T^{\rm cm}_{\rm th}(pp \to pp\pi^0) = \mathcal{A}\,(i\,\vec\sigma_1 - i\,\vec\sigma_2 + \vec\sigma_1 \times \vec\sigma_2)\cdot\vec p\,.$$

The $\vec\sigma_{1,2}$ are the spin–matrices of the two protons. The value of the proton cm momentum to produce a neutral pion at rest is given by

$$|\vec p\,| = \sqrt{M_\pi(m + M_\pi/4)} = 362.2\ \text{MeV}\ ,$$

with $m = 938.27$ MeV the proton and $M_\pi = 134.97$ MeV the neutral pion mass, respectively. Obviously, $|\vec p\,|$ vanishes in the chiral limit of zero pion mass. Therefore the soft–pion theorem which requires a vanishing threshold T–matrix in the chiral limit $M_\pi = 0$ is trivially fulfilled (as long as $\mathcal{A}$ does not become singular). Furthermore, it is known that the energy dependence in the threshold region the strong final–state interactions (FSI) governs the energy dependence. In the approaches we developed [1] the complete amplitude is written as

$$T = T^{\rm ISI}\cdot T^{\rm Prod}\cdot T^{\rm FSI}\ ,$$

where ISI denotes the initial–state interaction and the microscopic approaches are applied to the production amplitude $T^{\rm Prod}$. Clearly, such a separation induces a priori some model dependence. Based on the observation that the heavy baryon approach is not expected to converge, in ref.[1] a different approach was pursued. Consider first the process $pp \to pp\pi^0$. Approximating the near threshold T–matrix by the T–matrix exactly at threshold one gets for the unpolarized total cross section

$$\sigma_{\rm tot}(T_{\rm lab}) = |\mathcal{A}|^2 \int dW\, KF(W)\, F_p(W)\ ,$$

where the flux and three-body phase space factors, denoted as $KF(W)$, can be approximated by an analytical expression which is accurate within a few percent in the threshold region. $F_p(W)$ is the correction factor due the final–state interaction. It evaluated it in the effective range approximation. This is of course a very strong assumption but it allows to explain the energy dependence of the experimental total cross sections very accurately in terms of a single constant amplitude $\mathcal{A}$. In fact, one can derive this particular treatment of the FSI from an effective field theory (EFT) approach. Separating off the final–state interaction in that way, one can then pursue a diagrammatic approach to the (on-shell) production amplitude $\mathcal{A}$. This allows to investigate in a simple fashion the role of one-pion exchange and chiral loop effects together with shorter range exchanges due to heavier mesons. In a similar fashion, one can investigate the other processes $pp \to pn\pi^+$, $pp \to pp\eta$ and $pp \to pp\eta'$ (see below).

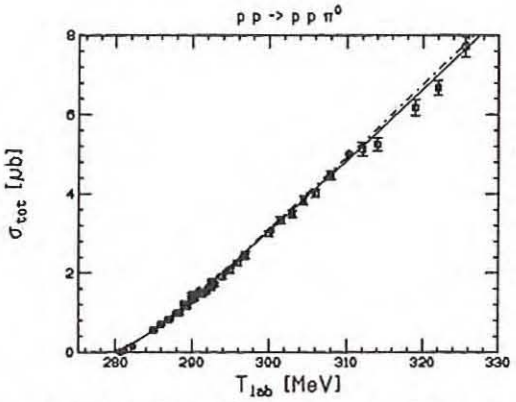

Figure 1: Fit to the total cross section for $pp \to pp\pi^0$ as described in the text (solid line). The data are from IUCF (boxes) and CELSISU (crosses). The dashed line is result of the diagrammatic approach.

Consider first the $pp\pi^0$ reaction. The S–wave threshold amplitude can be extracted from the data, $\mathcal{A}^{(\rm exp)} = (2.7 - i\,0.3)\ \text{fm}^4$, as shown by the solid line in the figure. The imaginary part is due to the ${}^3P_0$ pp phase shift taken at the threshold energy in the lab frame, $T^{\rm lab}_{\rm th} = 279.65$ MeV, where $\delta({}^3P_0) = -6.3°$. Thus the imaginary part $\mathrm{Im}\,\mathcal{A}$ is about $-1/9$ of the real part $\mathrm{Re}\,\mathcal{A}$ and contributes negligibly to the total cross section near threshold. This number can be well understood in terms of chiral π^0 exchange (including chiral π^0 rescattering) and heavy meson (ω, ρ^0, η) exchanges based on a relativistic Feynman diagram calculation with all parameters being fixed from reliable methods, like forward NN dispersion relations for the ω and a dispersion–theoretical analysis of $\bar NN \to \pi\pi$ for the ρ. Interestingly, in the relativistic approach the rescattering contribution interferes constructively with the direct production term, different from the heavy baryon approach and in agreement with the meson–exchange models. One can also evaluate some classes of one-loop graphs and finds that they lead to small corrections of the order of a few percent. Therefore chiral loops do not seem to play any significant role in the processes

$NN \to NN\pi$, which are dominated by one–pion exchange and short–range physics. I remark also that both the long range π^0 exchange and the short range vector meson exchange lead to contributions to the threshold amplitude $\mathcal{A}$ which do not vanish in the chiral limit $M_\pi \to 0$. There is no chiral suppression of the reaction $pp \to pp\pi^0$ compared to other $NN\pi$ channels. In all cases the respective threshold amplitudes are non-zero (and finite) in the chiral limit. This is in contrast to the widespread believe that $pp \to pp\pi^0$ is suppressed for reasons of chiral symmetry.

Within the same approach, one can investigate the threshold behavior of the process $pp \to pn\pi^+$. It is given in terms of $\mathcal{A}$ and the triplet threshold amplitude $\mathcal{B}$,

$$\mathrm{T}_{\rm th}^{\rm cm}(pp \to pn\pi^+) = -\sqrt{2}\mathcal{B}i(\vec{\sigma}_1 + \vec{\sigma}_2)\cdot\vec{p} + \mathcal{A}/\sqrt{2}(i\,\vec{\sigma}_1 - i\,\vec{\sigma}_2 + \vec{\sigma}_1 \times \vec{\sigma}_2)\cdot\vec{p}\,.$$

From the IUCF data, one can determine the empirical value of the triplet amplitude, $\mathcal{B}^{\rm emp} = (2.8 - i1.5)\,\mathrm{fm}^4$. The large imaginary part is related to the strong ISI in the $^3P_1$ entrance channel, which naturally can not be explained by tree graphs only. The value of the $^3P_1$ phase at the threshold energy for $pn\pi^+$ is $-28.1°$. The corresponding real part Re $\mathcal{B}$ is well reproduced by chiral one–pion exchange and short–range vector meson physics. For the same parameters as used in the study of $pp\pi^0$, one gets Re $\mathcal{B} = 2.74\,\mathrm{fm}^4$. Clearly, this channel deserves further study.

Let me now turn to η production. The threshold matrix element takes the form as in the case of $pp \to pp\pi^0$ in terms of the (complex) threshold amplitude $\mathcal{C}$. The η–production threshold is reached at a proton laboratory kinetic energy $T_{\rm lab}^{\rm th} = M_\eta(2 + M_\eta/2m) = 1254.6$ MeV, where $M_\eta = 547.45$ MeV denotes the eta–meson mass. In the case of η–production near threshold it is also important to take into account the ηp final–state interaction, since the ηN–system interacts rather strongly near threshold. In fact recent coupled–channel analysis of the $(\pi N, \eta N)$-system finds for the real part of the ηN scattering length Re $a_{\eta N} = (0.717 \pm 0.030)$ fm. For comparison, this value is about six times than the $\pi^- p$ scattering length, $a_{\pi^- p} = 0.125$ fm, as measured e.g. in pionic hydrogen. In ref.[1], it is assumed that the correction due to the S–wave ηp FSI near threshold can be treated in effective range approximation analogous to the S–wave pp FSI. The further assumption that the FSI in the pp subsystem and in the two ηp subsystems do not influence each other and that they factorize is made. The corresponding from of the unpolarized total cross section in terms of the S–wave amplitude $\mathcal{C}$ the various FSI functions $F_p(W)$, $F_\eta(s_\eta)$ can be foind in ref.[1]. Note that the ηp FSI function is complex–valued. From the CELSIUS data, one finds for the modulus of the threshold amplitude $|\mathcal{C}| = 1.32\,\mathrm{fm}^4$. The resulting energy dependent cross section from threshold up to $T_{\rm lab} = 1375$ MeV is shown in the figure together with the data from CELSIUS. It is rather astonishing that one can describe the total cross section data up to 100 MeV above threshold with a constant threshold amplitude $\mathcal{C}$ and a simple factorization ansatz for the three–body FSI. The relativistic Feynman graphs contributing to

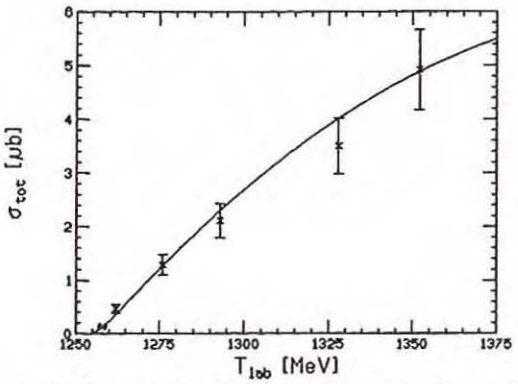

Figure 2: The cross section $\sigma_{\rm tot}(pp \to pp\eta)$ as a function of $T_{\rm lab}$. The data are taken from CELSIUS.

the threshold amplitude $\mathcal{C}$ can be easily evaluated. To account for the strong ηN S-wave rescattering, which is often attributed to the nucleon resonance $S_{11}(1535)$, one has to introduce a local $NN\eta\eta$ contact term, $\mathcal{L}_{\eta N} = K\bar{N}(x)N(x)\eta^2(x)$. Its strength K can be obtaiend from fitting the scattering length $a_{\eta N}$. With $g_{\eta N} = 5.3$, which is close to flavor SU(3) estimates and determinations from boson–exchange models, one can exactly reproduce the value of $\mathcal{C}$. It is worth to point out that ρ^0 exchange is the dominant contribution, because it is enhanced by factors of $M_\eta/m \simeq 0.6$ quite in contrast to the neutral pion case, where ω and π exchange are the dominant mechanisms. This ρ–meson dominance has in the mean time been *verified* by analyzing angular distributions measured at CELSIUS

At COSY, η' production very close to threshold has been measured for the first time, at much smaller excess energies than the few data points from the now defunct SATURNE facility. Within the diagrammatic approach of ref.[1] the empirical S–wave amplitude can be obtained with $g_{\eta' NN}\,(1 - 1.28\varepsilon) = 1.12$, with $g_{\eta' NN}$ the so far undetermined $\eta' - N$ coupling constant and ε the pseudoscalar to pseudovector mixing parameter. Interestingly, only the tensor interaction of the ρ–exchange ($\sim \kappa_\rho$) is sensitive to the parameter ε. Combining this result with constraints from deep inelastic lepton–nucleon scattering

$$g_{\eta' NN} = 2.5 \pm 0.7\,, \quad \varepsilon = 0.4 \pm 0.1\,. \qquad (1)$$

It remains to be seen whether other η'–production processes (e.g. photoproduction $\gamma p \to \eta' p$) are consistent with these values.

References:

[1] V. Bernard, N. Kaiser and Ulf-G. Meißner, nucl-th/9806013.

[2] P. Moskal et al., Phys. Rev. Lett. 80 (1998) 3202.

Chiral and dispersive description of πN scattering

Paul Büttiker

Chiral perturbation theory (ChPT) is the effective theory of the Standard Model at low energies. As it is a non renormalizable theory, additional low energy constants (LEC) enter the calculation at each order of the chiral expansion.

One possible chiral description of πN scattering is given by heavy baryon chiral perturbation theory (HBChPT) [1]. In this frame to order $O(p^3)$, the isoscalar and the isovector amplitudes $A^{\pm}(s,t,u)$ and $B^{\pm}(s,t,u)$ (s, t and u are the Mandelstam variables) are parametrized by the LEC's c_1, c_2, c_3, c_4 and $\bar{d}_1, \bar{d}_2, \bar{d}_3, \bar{d}_5, \bar{d}_{14}, \bar{d}_{15}, \bar{d}_{18}$ [2].

These quantities can not be fixed by the theory only. One possibility to obtain values for the above LEC's is to fit the chiral amplitudes to the experimental data [2]. However, ChPT is known to yield the most reliable predictions for s and t lying inside the Mandelstam triangle. As this region is unphysical, there is no direct access by experimental data.

By the use of dispersion relations this problem can be circumvented. Dispersion relations for πN scattering have been studied in great detail in axiomatic field theory in the last thirty years [3]. By using analyticity, unitarity, and crossing symmetry one obtains dispersive relations for the scattering amplitudes:

$$\mathrm{Re}\, A^{\pm}(s,t,u) = \frac{1}{\pi} P \int_{s_{th.}}^{\infty} ds' \mathrm{Im}\, A^{\pm}(s',t,u') \cdot \left\{ \frac{1}{s'-s} \pm \frac{1}{s'-u} \right\}$$

$$\mathrm{Re}\, B^{\pm}(s,t,u) = \frac{g^2}{m_N^2 - s} \mp \frac{g^2}{m_N^2 - u} + \frac{1}{\pi} P \int_{s_{th.}}^{\infty} ds' \mathrm{Im}\, B^{\pm}(s',t,u') \left\{ \frac{1}{s'-s} \mp \frac{1}{s'-u} \right\},$$

where g is the pion-nucleon coupling constant, $s_{th.} = (m_N + M_\pi)^2$, and m_N and M_π are the nucleon and the pion mass, respectively.

The advantage of the above relations is obvious: as the range of integration is restricted to the physical domain of s, the integrands of the dispersion integrals can be calculated from the available experimental data. On the other hand, the dispersion relations are valid for any s and t, i.e. by using the data in the *physical* domain one is able to calculate the amplitudes $A^{\pm}(s,t,u)$ and $B^{\pm}(s,t,u)$ in the *unphysical* region, where a comparison with the chiral amplitudes yields the most accurate values for the LEC's. Furthermore, by projecting the scattering amplitudes onto partial waves, one obtains sum rules for the threshold parameters, for which HBChPT gives predictions, too. A comparison of these chiral values with the dispersive quantities may be viewed as a probe into the validity in energy of chiral predictions.

As a third application of dispersion relations, we plan to study the dispersive description of the pion-nucleon σ-term when isospin symmetry is violated: according to the Ward-Takahashi identity, the σ-term, $\sigma(t=0)$, can be related to the elastic πN scattering amplitude $\bar{D}^{+}(s,t,u)$ at $u=s$, $t=2M_\pi^2$:

$$F_\pi^2 \bar{D}^{+}(s, t=2M_\pi^2, u=s) = \sigma(0) + \Delta_\sigma + \Delta_R,$$

where Δ_σ and Δ_R are quantities that can be worked out in the framework of ChPT.

On the other hand the σ-term can be expressed in terms of physical masses and the matrix element $\langle p|\bar{s}s|p\rangle$. Therefore the πN scattering amplitude may be used to calculate the strange quark content of the nucleon. Again, dispersion relations are the suitable tool to determine the scattering amplitude.

In the isospin symmetric case this has been done by several authors [4]. However, as pointed out by Meißner and Steininger [5], isospin breaking effects lower the value of the σ-term by about 8 %, strongly suggesting a new dispersive analysis of the σ-term, taking into account the violation of isospin symmetry.

References:

[1] V. Bernard, N. Kaiser, U.-G. Meißner, Int. J. Mod. Phys. E4 (1995) 193

[2] N. Fettes, U.-G. Meißner and S. Steininger, Nucl. Phys. A 640 (1998) 199

[3] J. Hamilton and W. S. Woolcock, Rev. Mod. Phys. 35, 737 (1963); G. Höhler, Pion–Nucleon Scattering, Landolt–Börnstein I/9b2, Springer 1983, ed. H. Schopper

[4] R. Koch, Z. Phys. C 15 (1982), 161; J. Gasser et al., Phys. Lett. B 213 (1988) 85

[5] U.-G. Meißner, S. Steininger, Phys. Lett. B 419 (1998) 403

Low Energy Hadron Dynamics and Virtual Compton Scattering

D. Drechsel (Mainz), T.R. Hemmert (IKP), B.R. Holstein (IKP & UMASS) and G. Knöchlein (Mainz)

One of the primary goals of contemporary particle/nuclear physics is to understand the structure of the nucleon. Indeed this is being pursued at the very highest energy machines such as SLAC and HERMES, at which one probes the quark/parton substructure, as well as at lower energy accelerators such as MAMI and BATES, wherein one studies the behavior of the nucleon in terms of a three quark system surrounded by a pion cloud. In recent years one of the important low energy probes has been Compton scattering, by which one can study the deformation of the nucleon under the influence of quasi-static electric and/or magnetic fields.[1] For example, in the presence of an external electric field $\vec{E}$ the quark distribution of the nucleon becomes distorted, leading to an induced electric dipole moment

$$\vec{p} = 4\pi\alpha_E \vec{E} \tag{1}$$

in the direction of the applied field, where α_E is the electric polarizability. The interaction of this dipole moment with the field leads to a corresponding interaction energy

$$U = -\frac{1}{2} 4\pi\alpha_E \vec{E}^2. \tag{2}$$

Similarly in the presence of an applied magnetizing field $\vec{H}$ there will be in induced magnetic dipole moment

$$\vec{\mu} = 4\pi\beta_M \vec{H} \tag{3}$$

and an interaction energy

$$U = -\frac{1}{2} 4\pi\beta_M \vec{H}^2. \tag{4}$$

For wavelengths large compared to the size of the system, the effective Hamiltonian for the interaction of a system of charge e and mass m with an electromagnetic field is, of course, given by the simple form

$$H^{(0)} = \frac{(\vec{p} - e\vec{A})^2}{2m} + e\phi \tag{5}$$

As the energy increases, however, one must take into account also polarizability effects and the effective Hamiltonian becomes

$$H_{\rm eff} = H^{(0)} - \frac{1}{2} 4\pi(\alpha_E \vec{E}^2 + \beta_M \vec{H}^2) \tag{6}$$

The Compton scattering cross section from such a system (taken, for simplicity, to be spinless) is given then by

$$\begin{aligned} \frac{d\sigma}{d\Omega} &= \left(\frac{\alpha_{em}}{m}\right)^2 \left(\frac{\omega'}{\omega}\right)^2 [\frac{1}{2}(1+\cos^2\theta) \\ &- \frac{m\omega\omega'}{\alpha_{em}} [\frac{1}{2}(\alpha_E + \beta_M)(1+\cos\theta)^2 \\ &+ \frac{1}{2}(\alpha_E - \beta_M)(1-\cos\theta)^2 + \ldots], \end{aligned} \tag{7}$$

where α_{em} is the fine structure constant and ω, ω' are the initial, final photon energies respectively. It is clear from Eq. 7 that from careful measurement of the differential scattering cross section extraction of these structure dependent polarizability terms is possible provided that i) the energy is large enough that these terms are significant compared to the leading Thomson piece and ii) that the energy is not too large that higher order corrections become important. In this way the measurement of electric and magnetic polarizabilities for the proton has recently been accomplished using photons in the energy range 50 MeV $< \omega <$ 100 MeV, yielding[2] #1

$$\begin{aligned} \alpha_E^p &= (12.1 \pm 0.8 \pm 0.5) \times 10^{-3}\text{fm}^3 \\ \beta_M^p &= (2.1 \mp 0.8 \mp 0.5) \times 10^{-3}\text{fm}^3 \end{aligned} \tag{9}$$

From these results which say that the polarizabilities of the proton are nearly a factor of a thousand smaller than the corresponding volume we learn that the nucleon is a rather rigid object when compared to the hydrogen atom, for example, for which the electric polarizability and volume are comparable.
Additional structure probes are possible if we exploit the feature of nucleon spin.[4] Thus, for example, the presence of a time varying electric field in the plane of a rotating system of charges will lead to a charge separation and induced electric dipole moment

$$\vec{p} = -\gamma_1 \vec{S} \times \frac{\partial \vec{E}}{\partial t} \tag{10}$$

and corresponding interaction energy

$$U_1 = -\vec{p} \cdot \vec{E} = \gamma_1 \vec{E} \cdot \vec{S} \times (\vec{\nabla} \times \vec{B}), \tag{11}$$

where we have used the Maxwell equations in writing this form. (Note that the "extra" time or spatial derivative is required by time reversal invariance since $\vec{S}$ is T-odd.) Similarly other possible structures are

$$\begin{aligned} U_2 &= \gamma_2 \vec{B} \cdot \vec{\nabla} \vec{S} \cdot \vec{E} \\ U_3 &= \gamma_3 \vec{E} \cdot \vec{\nabla} \vec{S} \cdot \vec{B} \\ U_4 &= \gamma_4 \vec{B} \cdot \vec{S} \times (\vec{\nabla} \times \vec{E}) \end{aligned} \tag{12}$$

and the measurement of these various "spin-polarizabilities" γ_i via polarized Compton scattering provides a rather different sort of probe for nucleon structure. Because of the requirement for polarization not much is known at present about such

#1 Note that in practice one generally exploits the strictures of causality and unitarity as manifested in the validity of the forward scattering dispersion relation, which yields the Baldin sum rule[3]

$$\begin{aligned} \alpha_E^{p,n} + \beta_M^{p,n} &= \frac{1}{2\pi^2} \int_0^\infty \frac{d\omega}{\omega^2} \sigma_{\rm tot}^{p,n} \\ &= \begin{cases} (13.69 \pm 0.14) \times 10^{-4}\text{fm}^3 & p \\ (14.40 \pm 0.66) \times 10^{-4}\text{fm}^3 & n \end{cases} \end{aligned} \tag{8}$$

as a constraint because of the small uncertainty associated with the photoabsorption cross section $\sigma_{\rm tot}^p$.

spin-polarizabilities, although from dispersion relations the combination[5]

$$\gamma_0^p \equiv \gamma_1^p - \gamma_2^p - 2\gamma_4^p \approx -1.34 \times 10^{-4}\mathrm{fm}^4 \quad (13)$$

has been determined and from a global analysis of unpolarized Compton data, to which it contributes in higher orders, one has found the so-called backward polarizability to be [6]

$$\begin{aligned} \gamma_\pi &= \gamma_1 + \gamma_2 + 2\gamma_4 \\ &= (27.1 \pm 2.2 \pm 2.8) \times 10^{-4}\mathrm{fm}^4\,, \end{aligned} \quad (14)$$

which disagrees by as much as 50% with the most recent calculations from chiral lagrangians [4] as well as with dispersion relation analyses [7]. Clearly high precision measurements with polarized photons and polarized hydrogen targets are called for to resolve this low-energy spin puzzle.

At the same time it has been come to be realized that a high resolution probe of nucleon structure is available, in principle, via the use of *virtual* Compton scattering—VCS—wherein virtual photons produced from scattered electrons are scattered from a nucleon target into real final state photons. The outcome of such measurements is, in principle, a q^2-dependence in the polarizabilities (usually termed "generalized polarizabilities" [8]), which can be thought of as the Fourier transforms of *local* polarization densities in the nucleon. At the present time there exist approved VCS experiments at MAMI, at BATES, and at TJNAF. The results of the first pioneering VCS experiment at MAMI have been reported at Baryons 98 [9] and agree very well with a recent calculation [10, 11] in chiral perturbation theory (ChPT), ruling out traditional Born model analyses with resonances + form factors [12] as well as simple constituent quark models of the nucleon (*e.g.* [8]). The Mainz analysis indicates that the q^2-dependence is governed by the low-energy dynamics of the pion cloud—which can be described very precisely via ChPT—and contains physics different from the standard monopole or dipole q^2-variation of the Born models. Some aspects of this particular q^2-variation due to the pion cloud can also be seen in the linear sigma model [13] and the Skyrme model [14]. The advantage of VCS therefore lies in the possibility of an *independent* variation of photon energy and momentum, thus enabling us to distinguish between theoretical descriptions with quite different dynamical content at finite q^2—even if they all agree at $q^2 = 0$.

In view of the intense interest in these quantities, we have revisited the (numerical) chiral calculation [10] of the 10 generalized polarizabilities of Guichon [8] and now managed to find *closed form analytical expressions of their* q^2*-dependence* at $\mathcal{O}(p^3)$ [15]. Furthermore we have analyzed the leading modification of the chiral $\mathcal{O}(p^3)$ predictions due to explicit propagation of the first nucleon resonance $\Delta(1232)$, utilizing the recently developed "small scale expansion" formalism [16]. In contrast to the Born models we only find a weak modification of the chiral results. This work is presently being written up for publication.

[1] See, *e.g.* A. L'vov, Int. J. Mod. Phys. **A8**, 5267 (1993); B.R. Holstein, Comm. Nucl. Part. Phys. **20**, 301 (1992).

[2] *e.g.* B.E. MacGibbon et al., Phys. Rev. **C52**, 2097 (1995).

[3] D. Babusci, G. Giordano, and G. Matone, Phys. Rev. **C57**, 291 (1998).

[4] T.R. Hemmert, B.R. Holstein, J. Kambor and G. Knöchlein, Phys. Rev. **D57**, 5746 (1998); D. Babusci et al., Phys. Rev. **C58**, 1013 (1998).

[5] A.M. Sandorfi et al., Phys. Rev. **D50**, R6681 (1994).

[6] J. Tonnison, A. M. Sandorfi, S. Hoblit and A. M. Nathan, Phys. Rev. Lett. **80**, 4382 (1998).

[7] A.I. L'vov and A.M. Nathan, preprint no. nucl-th/9807032; submitted to Phys. Lett. **B**.

[8] P.A.M. Guichon, G.Q. Liu, and A.W. Thomas, Nucl. Phys. **A591**, 606 (1995) and Aust. J. Phys. **49**, 905 (1996).

[9] N. d'Hose, Talk given at BARYONS 98, Bonn (Germany), Aug 1998.

[10] T.R. Hemmert, B.R. Holstein, G. Knöchlein and S. Scherer, Phys. Rev. Lett.**79**, 22 (1997).

[11] T.R. Hemmert, B.R. Holstein, G. Knöchlein and S. Scherer, Phys. Rev. **D55**, 2630 (1997).

[12] *e.g.* M. Vanderhaeghen, Phys. Lett. **B368**, 13 (1996).

[13] A. Metz and D. Drechsel, Z. Phys. **A356**, 351 (1996) and **A359**, 165 (1997).

[14] M. Kim and D.-P. Min, preprint no. hep-ph/9704381.

[15] D. Drechsel, T.R. Hemmert, B.R. Holstein, and G. Knöchlein, in preparation.

[16] T.R. Hemmert, B.R. Holstein, and J. Kambor, Phys. Lett. **B395**, 89 (1997) and J. Phys. **G24**, 1831 (1998).

Chiral symmetry and the $N\Delta$-transition form factors

G.C. Gellas[a], T.R. Hemmert, C.N. Ktorides[a] and G.I. Poulis[a]
[a] Dept. of Physics, Univ. of Athens, Greece

1. Introduction

We have performed a calculation [1] of the ΔN transition form factors at low momentum transfer $t \equiv q^2$ in an effective chiral lagrangian framework. In our calculation a scale $\varepsilon = \{p, m_\pi, \delta\}$ denoting, collectively, small momenta, the pion mass and the Delta-nucleon mass splitting is used to establish a systematic power-counting, thus telling us precisely which diagrams/vertices have to be included if we want to calculate up to a certain order in ϵ. This approach allows for an efficient inclusion of $\Delta(1232)$ degrees of freedom consistent with the underlying chiral symmetry of QCD and is referred to as the "Small Scale Expansion" (SSE) [2], constituting a phenomenological extension of Heavy Baryon Chiral Perturbation Theory. So far, we have performed the calculation to third order in ϵ and in the process have also established a new relation for the matching of the non-relativistic microscopic calculation to the relativistic transition current. We find that the q^2 evolution of the three complex form factors is completely determined by the dynamics of the nucleon's pion cloud governed by chiral symmetry. Finally, utilizing previous calculations performed at $q^2 = 0$ we discuss the role of relevant low energy parameters for the sought after multipole ratios EMR(q^2) and CMR(q^2).

2. The $\Delta \to N\gamma^*$ Vertex

Demanding Lorentz covariance, gauge invariance and parity conservation the most general form of the $\Delta \to N\gamma^*$ radiative decay amplitude is described by three form factors $G_i(q^2)$, i=1,2,3,

$$\begin{aligned} i\mathcal{M}_{\Delta N\gamma} &= \frac{e}{2M_N}\bar{u}(p)\gamma_5 \left[G_1(q^2)(\not{q}\epsilon_\mu - \not{\epsilon} q_\mu)\right. \\ &+ \frac{G_2(q^2)}{2M_N}(p\cdot\epsilon\, q_\mu - p\cdot q\, \epsilon_\mu) \\ &\left. + \frac{G_3(q^2)}{2(M_\Delta - M_N)}(q\cdot\epsilon\, q_\mu - q^2\epsilon_\mu)\right] \\ &\times u^\mu_\Delta(p_\Delta)\,. \end{aligned} \tag{1}$$

Here $M_N\,(M_\Delta)$ is the nucleon (Delta) mass, p^μ, p^μ_Δ denotes the four-momentum of the nucleon, Delta and q^μ, ϵ^μ represent the photon four-momentum and polarization vectors, respectively. A SSE calculation of the radiative vertex to $\mathcal{O}(\varepsilon^3)$ entails a restriction to $\mathcal{O}(1/M_N^2)$ accuracy [2]. The calculation of the relevant Feynman diagrams must then be matched to Eq.(1), which is done in the $\Delta(1232)$ rest frame [1]. One finds that to $\mathcal{O}(\epsilon^3)$ one is sensitive to the first two orders in the chiral expansion of G_1, whereas the quadrupole form factors G_2, G_3 only start at $\mathcal{O}(\epsilon^3)$ and therefore only their leading behavior is determined in this calculation. Note that one has to introduce a particular mass dependence proportional to $(M_\Delta - M_N)^{-1}$ accompanying the form factor $G_3(q^2)$ in Eq.(1) in order to achieve consistency with the chiral $\mathcal{O}(\epsilon^3)$ calculation [1].

3. The Calculation

The calculation involves one-loop diagrams with $\mathcal{O}(\varepsilon)$ vertices and tree level vertices up to $\mathcal{O}(\varepsilon^3)$ coming from four counterterms. Independent of any choice of gauge one finds that even for finite q^2 only two one-loop diagrams—the well known $\Delta \to N\gamma$ triangle diagrams [3] where the photon couples to two pions and the intermediate baryon state is nucleon, Delta respectively—contribute to this order. Due to the fact that the $\Delta \to N\gamma^*$ transition starts with a magnetic dipole amplitude M1, one finds no tree-level $\mathcal{O}(\varepsilon)$ vertex but has to take into account all $\mathcal{O}(\varepsilon^2)$ and $\mathcal{O}(\varepsilon^3)$ tree contributions. Matching the general expression of the $\Delta N\gamma^*$ vertex Eq.(1) to the 1-loop chiral calculation one obtains a representation for the three form factors which is valid at small momentum transfer. We note that each form factor has a real and an imaginary part as a direct consequence of chiral symmetry [1]. With the complete set of $N\Delta$ form factors $G_i(q^2)$, $i = 1, 2, 3$ now known to $\mathcal{O}(\epsilon^3)$ we have also calculated [1] the M1, E2, C2 $N\Delta$ multipole transitions of interest at recent electron-scattering experiments at Bonn, Mainz and MIT-Bates. For the moment we have utilized input from dispersion relation analyses [4] to get information on unknown couplings at $q^2 = 0$. The q^2-evolution of the electric and coulomb multipole ratios EMR(q^2), CMR(q^2) is then obtained as prediction by SSE to $\mathcal{O}(\epsilon^3)$.

References:

[1] G.C. Gellas, T.R. Hemmert, C.N. Ktorides and G.I. Poulis, preprint FZJ-IKP(Th)-1998-14 [hep-ph/9810246]; submitted to *Phys. Rev.* D.

[2] T.R. Hemmert, B.R. Holstein and J. Kambor, *Phys. Lett.* B **395**, 89 (1997); *J. Phys.* G. **24**, 1831 (1998).

[3] M.N. Butler, M.J. Savage and R.P. Springer, *Phys. Lett.* B **304**, 353 (1993); M. Napsuciale and J.L. Lucio, *Nucl. Phys.* B **494**, 260 (1997).

[4] O. Hanstein, D. Drechsel and L. Tiator, *Nucl. Phys.* A **632**, 561 (1998).

The reaction $pp \to pp\phi$ and the validity of the OZI rule

K. Nakayama[1], J.W. Durso[2], J. Haidenbauer, C. Hanhart and J. Speth

Recently the DISTO collaboration presented results for the cross section ratio $\sigma_{pp\to pp\phi}/\sigma_{pp\to pp\omega}$ at T_{lab} = 2.85 GeV [1]. The experimental ratio turned out to be about 8 times larger than the estimation based on the OZI rule. We carried out a model analysis of the DISTO data with the aim of extracting the $NN\phi$ coupling constant [2]. Specifically we wanted to see whether the observed enhancement over the OZI estimate in the cross section implies a $g_{NN\phi}$ that is likewise enhanced and therefore at variance with the OZI rule.

We describe the $pp \to pp\phi$ reaction within a relativistic meson-exchange model, where the transition amplitude is calculated in Distorted Wave Born Approximation in order to take the NN final state interaction into account. (See Ref. [3] for the details of the formalism.) We do not consider the initial state interaction explicitly. Its effect is accounted for via an appropriate adjustment of the (phenomenological) form factors at the hadronic vertices.

In a previous study of the reaction $pp \to pp\omega$[3] we found that the dominant production mechanisms are the nucleonic and $\omega\rho\pi$ mesonic currents, as depicted in Fig. 1. We also found that the angular distribution of the produced ω meson provides a unique and clear signature of the magnitude of these currents, thus allowing one to disentangle these two reaction mechanisms. The situation is quite similar for the reaction $pp \to pp\phi$. In this case the nucleonic current and the $\phi\rho\pi$-exchange current provide the dominant contributions to the production amplitude[2]. Therefore, it is possible to fix uniquely the magnitudes of the nucleonic and the meson-exchange current by analyzing the angular distribution of the ϕ meson measured by the DISTO collaboration[1]. Furthermore, since the $NN\phi$ coupling constant enters only in the nucleonic current it is possible to extract its value from such an analysis. It is determined by the requirement of getting the proper contribution of the nucleonic current needed to reproduce the angular distributions.

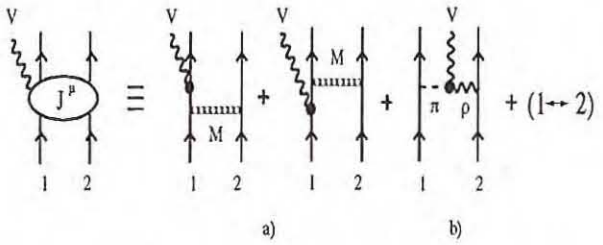

Fig. 1: ω and ϕ meson production mechanisms: a) nucleonic current; b) $V\rho\pi$ meson-exchange current.

The parameters of the model (coupling constants, cutoff masses of the vertex form factors) are mostly taken over from the employed NN model. The $\phi\rho\pi$ coupling constant is obtained from the measured decay width of $\phi \to \rho + \pi$. However, besides the $g_{NN\phi}$ that we want to extract from the analysis, there are still some more free parameters: The cutoff mass of the $\phi\rho\pi$ vertex form factor of the meson-exchange current, and the form factor and tensor- to vector coupling constant ratio $\kappa_\phi \equiv f_{NN\phi}/g_{NN\phi}$ of the nucleonic current (cf. Ref. [2] for details). Thus in order to determine these remaining four parameters we need at least four independent ϕ-meson production data. In view of the more limited data set presently available, we decided to perform a combined analysis of ϕ- and ω-meson production. This means that we use the data from both reactions and we assume relations between corresponding parameters in the production amplitudes. Specifically, we assume that the form factors at the $\phi\rho\pi$- and $\omega\rho\pi$ vertices are the same. This is a reasonable choice because the off-shell particles (ρ, π) are the same in both cases. Likewise we assume that the form factor at the meson production vertices in the nucleonic current are the same. The $NN\omega$ coupling constant is fixed to the SU(3) value, $g_{NN\omega} = 9$, based on $g_{NN\rho}$ of Ref. [4]. Furthermore we assume that $\kappa_\phi = \kappa_\omega$, as also suggested by SU(3) symmetry, and $-0.5 \leq \kappa_\omega \leq 0.5$.

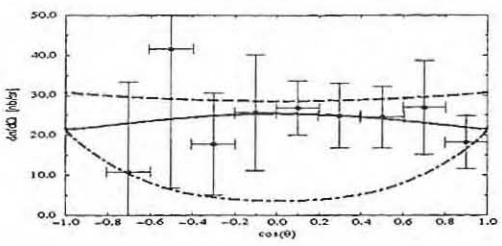

Fig. 2: Angular distribution of the ϕ meson at T_{lab} = 2.85 GeV. The dashed (dash-dotted) curve is the result with the mesonic (nucleonic) current alone. The solid curve is the total result. The data points are from Ref. [1], normalized as discussed in the text.

Concerning the data we use the total cross sections of Ref. [5] for the reaction $pp \to pp\omega$ and the ϕ-meson angular distribution at $T_{lab} = 2.85$ GeV measured by the DISTO collaboration [1]. The latter is given without absolute normalization in Ref. [1]. But since the DISTO group has also measured the ratio $\sigma_{pp\to pp\phi}/\sigma_{pp\to pp\omega}$ at this energy we can estimate $\sigma_{pp\to pp\phi}$ by multiplying this ratio with the total cross section for ω-meson production interpolated from the existing data. This yields a value of $\sigma_{pp\to pp\phi} \approx 0.3\ \mu b$.

Our strategy for fixing the various parameters is outlined in detail in Ref. [2]. Here we only want to mention that the lack of a more complete set of data prevents us from achieving a unique determination of $g_{NN\phi}$. Rather we get a set of values which range

from $g_{NN\phi} = -0.163$ to $g_{NN\phi} = -1.40$. Nevertheless, it is encouraging to see that the extracted values all lie within fairly narrow bounds. This clearly indicates to us that the dependence on the model parameters is not very strong, and that the magnitude of $g_{NN\phi}$ is primarily determined by the experimental information used.
The values of $g_{NN\phi}$ obtained may be compared with those resulting from SU(3) flavor symmetry considerations and imposition of the OZI rule,

$$g_{NN\phi} = -3g_{NN\rho}\sin(\alpha_v) \cong -(0.60 \pm 0.15) ,$$

where the factor $\sin(\alpha_v)$ is due to the deviation from the ideal $\omega - \phi$ mixing. The numerical value is obtained using the values of $g_{NN\rho} = 2.63 - 3.36$[4] and $\alpha_v \cong 3.8°$. Comparing this value with the ones extracted from our model analysis, we conclude that the preliminary data presently available can be described with using a $NN\phi$ coupling constant that is compatible with the OZI rule.

References:

References:

[1] Y. Bedfer, Acta Phys. Pol. B29, (1998), in press.
[2] K. Nakayama et al., in preparation; J. Haidenbauer et al., `nucl-th/9810069`.
[3] K. Nakayama, A. Szczurek, C. Hanhart, J. Haidenbauer, and J. Speth, Phys. Rev. C57, 1580, (1998).
[4] G. Höhler and E. Pietarinen, Nucl. Phys. B95, 210, (1975).
[5] Collaboration CRN Strasbourg, IPN Orsay, LNS Saclay, in *Nouvelles de Saturne no. 19*, p.51 (Saclay 1995)

[1] Department of Physics and Astronomy, University of Georgia, Athens, GA 30602, USA
[2] Physics Department, Mount Holyoke College, South Hadley, MA 01075, USA

Polarization in the reaction $NN \to NN\pi$

C. Hanhart, J. Haidenbauer, O. Krehl and J. Speth

Recently we accomplished a comprehensive model calculation for pion production in nucleon-nucleon collisions [1]. In this model direct production, pion rescattering and contributions from pair diagrams involving heavy-meson exchanges are taken into account, see Fig. 1. Furthermore also production mechanisms involving the $\Delta(1232)$ are included explicitly. The amplitudes for the elementary reaction processes are taken from well established meson-exchange models for nucleon–nucleon and pion–nucleon scattering.

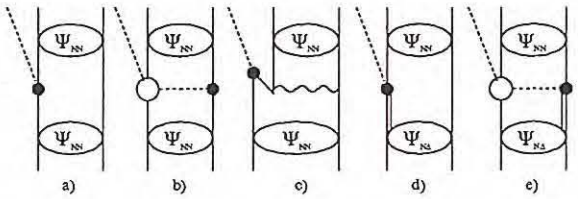

Fig. 1: Pion production diagrams included in our model calculation. Note that those diagrams where the Δ is exited after the emission of the pion are included as well.

For the first time all experimentally accessible reaction channels ($pp \to pp\pi^0$, $pp \to d\pi^+$, $pp \to pn\pi^+$ and $pn \to pp\pi^-$) were investigated simultaneously and consistently in a microscopic model. Our model yields an overall satisfactory agreement with available data on total and differential cross sections from pion production threshold up to the Delta resonance region [1]. As an example we show in Fig. 2 the total cross-section for all four reaction channels. We have now employed our model for calculating predictions for various spin-dependend observables of the reaction $NN \to NN\pi$. Such observables are particularly interesting because they reflect the spin-dependence of the production processes and therefore should be very useful in discriminating between different production mechanisms.

Analyzing powers for the reactions $pp \to pp\pi^0$, $pp \to d\pi^+$, and $pp \to pn\pi^+$ were presented in Ref. [1]. It turned out that our model predictions are in rather nice agreement with all available data in the threshold region. This is a clear indication that our model reproduces the proper onset of higher partial waves. Here we show results for some double polarization observables of the reaction $pp \to pp\pi^0$, namely the spin-dependent total cross section $\Delta\sigma_T/\sigma_{tot} = -(A_{xx} + A_{yy})$ and the spin correlation coefficient $A_{xx} - A_{yy}$, as well as the integrated analyzing power A_y, which have recently been measured at IUCF [2]. As expected the $\Delta(1232)$ resonance plays a crucial role over the whole energy range. But also the non-resonant production mechanisms contribute significantly to these polarization observables. Thus, our

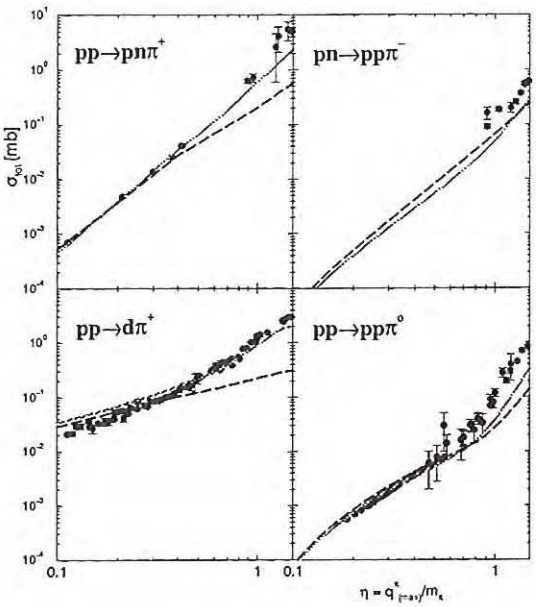

Fig. 2: Results for the different reaction channels. The solid line is the full result whereas for the dashed line the Delta contributions are switched off.

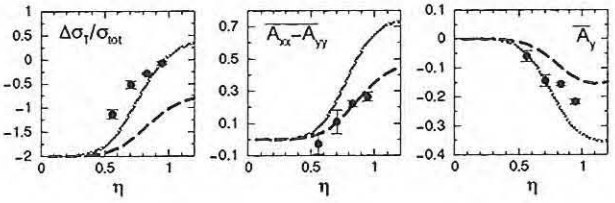

Fig. 3: Results for different polarisation observables for the reaction $pp \to pp\pi^0$. Curves as in figure 2. The data are taken from ref. [2]

results suggest that pion production near threshold is an ideal testing ground for resonant and non-resonant production mechanisms. Specifically polarization experiments seem to be crucial to distinguish between different production mechanisms.

References:

References:

[1] C. Hanhart, J. Haidenbauer, O. Krehl and J. Speth, Phys. Lett. B 444, 25 (1998).

[2] H.O. Meyer et al., Phys. Rev. Lett. **81**, 3096 (1998).

On the treatment of NN interaction effects in meson production in NN collisions

C. Hanhart and K. Nakayama

We clarify under what circumstances the nucleon-nucleon final state interaction fixes the energy dependence of the total cross-section for the reaction $NN \to NNx$ close to production threshold, where x can be any meson whose interaction with the nucleon is not too strong.

In ref. [1] Watson argues that if there is a strong and attractive force between two of the outgoing particles, as is the case for the reactions under consideration, the energy dependence of the total cross-section is determined by the phase space and the energy dependence of the relevant attractive interaction, i.e.,

$$\begin{aligned} \sigma_{NN\to NNx} &\propto \int d\rho(q')|T(p',p')|^2 \\ &\propto \int d\rho(q') \left(\frac{\sin\delta(p')}{p'}\right)^2 . \end{aligned} \quad (1)$$

In the above equation $T(p',p')$ is the on-shell NN T-matrix, ρ the three particle phase-space and $\delta(p')$ denotes the NN phase shifts at the energy, $2E(p')$, of the final NN subsystem (here restricted to s-waves), where $E(p') \equiv \frac{p'^2}{2m}$, with m denoting the nucleon mass. Very accurate measurements for π production indeed proved eq. (1) to be valid. Several authors [2] concluded from this observation that it is appropriate to calculate the transition $NN \to NNx$ to lowest order in perturbation theory and just include the final state interaction (FSI) by using a formula of the type in eq. (1); they implement the FSI by use of just the on-shell NN T-matrix, not only to get the right energy dependence of the cross-section, but also to get the strength of the matrix elements. In a recent preprint [3] we criticize this procedure. We shall demonstrate that the observation that the energy dependence of the cross-section is given by the *on-shell* FSI does not necessarily imply that the strength of the matrix elements is also determined by the on-shell NN interaction.

Based on unitarity alone one can rewrite the matrix element A that describes the $NN \to NNx$ transition in the following way

$$\begin{aligned} A(E,p') &= -M(E,p')e^{i\delta(p')}\left(\frac{\sin(\delta(p'))}{ap'}\right) \\ &\times \left[\mathcal{P} + 1 - \frac{1}{2}ar_o p'^2 - \ldots\right] , \end{aligned} \quad (2)$$

where a and r_o denote the scattering length and the effective range of the NN interaction respectively. All the off-shell effects are hidden in $\mathcal{P}$, defined as

$$\mathcal{P} = \frac{ap'}{\kappa(p')}\mathbf{P}\int_0^\infty dk \frac{k^2 f(E,k)}{E - 2E(k)} , \quad (3)$$

where

$$f(E,k) = \frac{T(p',k)}{T(p',p')}\frac{M(E,k)}{M(E,p')} , \quad (4)$$

with M as the (short range) production operator, where the FSI was separated off [3]. Eq. (2) shows that the energy dependence of the amplitude is indeed determined by the on-shell NN parameters, as long as $\mathcal{P}$ does not introduce an additional energy dependence. This is the case as long as the Nx-interaction is considerably weak for small energies as it is the case for π production. Note, however, that the overall normalization is determined by the actual value of $\mathcal{P}$. Since $\mathcal{P}$ is the overlap integral of the production matrix element and the final state T-matrix its value is model dependent. This observation calls for a consistent calculation of both the FSI as well as the production operator in order to achieve physically meaningful results. It is this argument that shows the inapplicability of the methods presented in refs. [2].

A similar calculation that leads to eq. (2) can be used to derive an expression that allows one to estimate the effect of the initial state interaction (ISI) on the reaction $NN \to NNx$, with x any meson heavier than the pion, in terms of the (on-shell) NN scattering phase shifts and inelasticities. We derived the following suppression factor introduced by the ISI:

$$\begin{aligned} \lambda &= \left|\frac{1}{2}e^{i\delta_L(p)}\left(\eta_L(p)e^{i\delta_L(p)} + e^{-i\delta_L(p)}\right)\right|^2 \\ &= \eta_L(p)\cos^2(\delta_L(p)) + \frac{1}{4}[1-\eta_L(p)]^2 \\ &\leq \frac{1}{4}[1+\eta_L(p)]^2 . \end{aligned} \quad (5)$$

The necessary assumption for the derivation of the above factor is that the ISI only weakly depends on the energy – this is not justified for the energies necessary for pion production. At energies required in the initial state for η production, however, the NN phase-shifts show only a very weak variation with energy and thus we expect the above formula to give a proper estimate of the effect of the ISI on the production cross section.

This work was supported by COSY FFE–Project Nr. 41324880.

References:

[1] K. Watson, *Phys. Rev.* 88, 1163 (1952).

[2] A. Moalem et al., *Nucl. Phys.* A **589**, 649 (1995), R. Shyam and U. Mosel, *Phys. Lett.* B **426**, 1 (1998), A. Sibirtsev and W. Cassing, nucl-th/9802025, A. Sibirtsev and W. Cassing, nucl-th/9806022, E. Gedalin et al., nucl-th/9803028, V. Bernard, N. Kaiser and Ulf-G. Meißner, nucl-th/9806013.

[3] C. Hanhart and K. Nakayama, submitted to Phys. Lett. B and nucl-th/9809059.

On the momentum dependence of the reaction $\pi^- p \to \omega n$ near threshold

C. Hanhart[a,b] and A. Kudryavtsev[b,c]

The reaction $\pi^- p \to \omega n$ near threshold was studied relatively long ago in refs. [1]. The authors of those papers claimed to have found an abnormal behavior of the production amplitude for this reaction near threshold that is not yet understood theoretically [2]. The conclusion was based on a comparison of the measured cross-section with the one for the production of a stable particle. To be concrete, the authors found that the production cross section is proportional to $P^{*\,2}$ instead of the expected P^* dependence, where P^* denotes the momentum of the outgoing neutron in the center of momentum system. Recently a behavior of the cross section analogous to the one of the reaction under discussion was also found in the reaction $pd \to \omega\, ^3He$ [3].

The experiments listed above were all performed in an unusual kinematical situation: instead of measuring the momentum distribution of the final state for a fixed beam energy, the excitation function for a fixed neutron momentum versus initial energy was measured.

In our work [4] we analyzed the general expression for the production cross-section of unstable particles in near threshold binary reactions. We shall demonstrate that the dependence of the count rates on the outgoing center of mass momentum changes controlled by an order parameter χ to be defined below. We conclude that the behavior of the ωn-amplitude is quite normal – it is a decreasing function of energy in the near threshold region.

The cross section for the production of omega or any other resonance with finite width Γ is

$$\frac{d\sigma}{d\Omega} \propto \int_{(P^*,\Delta P)} \frac{\Gamma/2\pi \mid T(E,\vec{k}) \mid^2}{(E_{kin} - k^2/2\mu)^2 + \Gamma^2/4} k^2 dk \ ,$$

where $E_{kin} = E - M - \bar{m}$ We introduced for simplicity a Breit-Wiegner representation for the spectral density. Here we already imposed the experimental condition of refs. [1] to constrain the outgoing relative momentum to values in a small band around some given P^*. The range of integration, denoted by $(x_0, \Delta x)$, is to be interpreted as an integration from $x_0 - \Delta x/2$ to $x_0 + \Delta x/2$.

It is easy to show, that the parameter that controls the momentum dependence of the count rates is $\chi(P^*) \equiv \frac{2P^*\Delta P}{\mu\Gamma}$.

Let us discuss the different regimes and start with the situation typical for close to threshold measurements, namely $\chi(P^*) \ll 1$. In this limit it is easy to estimate the remaining integral as the denominator under the integral is practically constant. So we get

$$I(E_{kin}) \approx \frac{2}{\pi\Gamma} \frac{P^{*2}\Delta P}{(y^* - y_0)^2 + 1}, \qquad (1)$$

where $y^* = P^{*2}/\mu\Gamma$ and $y_0 = 2E_{kin}/\Gamma$. The authors of refs. [1] additionally performed an integration over the beam energy (still keeping P^* fixed) to remove the width dependence from eq. (1). Indeed, since the spectral density is normalized, integrating over the beam energy gives

$$\int_{(E_0,\Delta E)} dE_{kin} I(E_{kin}) \simeq P^{*2}\Delta P \ ,$$

Therefore, we find a P^{*2} dependence of the count rates even for a constant matrix element. We thus conclude that the close to threshold matrix element for $\pi N \to \omega N$ is to be constant close to threshold.

Let us now investigate the second limiting case $\chi(P^*) \gg 1$. To estimate the phase space integral in this case we must distinguish separately two different cases:

i)Consider the case, when the energy parameter y_0 is just within the limits of the phase space integral. In this case $I(E_{kin}) \approx \sqrt{2\mu E_{kin}}$, as should be for the case of production of a stable particle.

ii)In the opposite case, when y_0 is not inside the limits of integration, the integral is strongly suppressed. So in the case of a narrow resonance we get the usual energy behavior for the differential cross section.

Note that the classification of wide and narrow resonances depends on values of ΔP and P^* used in each concrete experimental setup. So the condition $\chi(P^*) \approx 1$ determines the critical value of P^*_{cr} for which the case of wide resonance transforms into the case of narrow resonance. So by measuring the count rate versus P^* one may observe a transition from a P^{*2} behavior of the cross section at low P^* to a linear dependence at high P^* even for a constant matrix element. In the case of the omega this could take place at $P^*_{cr} = \mu\Gamma/2\Delta P \approx 90 MeV/c$ using $\Delta P \approx 20$ MeV as specified in ref. [1].

This work was supported by COSY FFE–Project Nr. 41324880.

[a]Institut für Theoretische Kernphysik, Universität Bonn, D-53115 Bonn, Germany

[b]Institut für Kernphysik, Forschungszentrum Jülich GmbH, D-52425 Jülich, Germany

[c]Institute of Theoretical and Experimental Physics, 117258, B.Cheremushkinskaya 25, Moscow, Russia

References:

[1] D.M.Binnie et al.Phys.Rev.D8, 9(1973)2789, J.Keyne et al.Phys.Rev.D14,1 (1976)28, H.Karami et al. Nucl.Phys.B154 (1979)503.

[2] C. Wilkin, talk presented at the Baryon98 conference and nucl-th/9810047.

[3] R.Wurzinger et al. Phys.Rev.C51 (1995)R443.

[4] C. Hanhart and A.Kudryavtsev, submitted to Phys. Lett. B and nucl-th/9812022.

The role of the rho-meson nucleon channel in pion photo-production

K.Nakayama, S.Krewald, J.Speth

Recently, pion photo-production off nucleons has been investigated by many authors within meson-exchange models of the hadronic interaction which treat the final state interactions dynamically [1, 2]. This approach requires the introduction of so-called formfactors at the hadronic vertices which account for the composite structure of the hadrons. At present, the lack of theoretical understanding of these vertex form factors forces us to introduces phenomenological form factors of e.g. a monopole form:

$$f(\vec{q}^{\,2}) = \frac{\Lambda_\pi^2}{\Lambda_\pi^2 + \vec{q}^{\,2}} \qquad (1)$$

with a cutoff parameter Λ_π which is adjusted to the data. Values of $\Lambda_\pi = 300...450 MeV$ are found [1, 2].
In calculations other than pion photoproduction, one needs values of $\Lambda_\pi = 800 MeV$ [3].
The question arises why pion-photoproduction is so sensitive to the form factors and why it needs so extremely soft form factors.
We suggest that the coupling to the rho-meson nucleon channel may reduce the influence of the final state interaction. In order to investigate this point, we worked out a model for the $\rho + N \to \pi + N$ transition potential which is summarized in Fig.1. In our present study, we omit the final state interaction within the ρN channel.
In Table 1 we show the electric dipole amplitude, E_{0+}, for the $\gamma + p \to \pi^0 + p$ reaction at threshold. The contributions from the individual diagrams displayed in the lower part of Fig.1 are shown separately. The columns (a), (b), (c), and (d) refer to the corresponding diagrams in the lower part of Fig.1. The column labelled "rest" sums the contributions of the other diagrams. One realizes that the coupling to the charged intermediate states, $\pi^+ N$, generates a particularly strong final state interaction in the pionic sector. The coupling to the ρN channel generates contributions which tend to cancel the pionic final state interaction, however. In the present calculation, a cutoff of $\Lambda_\pi = 800 MeV$ has been assumed as suggested by ref.[3]. The cutoff for the ρN intermediate states has been assumed to be $\Lambda_\rho = 1300 MeV$. This number is needed in order to reproduce the experimental cross sections of pion photoproduction. The value $\Lambda_\rho = 1300 MeV$ is in line with what is expected from the nucleon-nucleon interaction. Quantitative results, however, require a more complete calculation than done here.

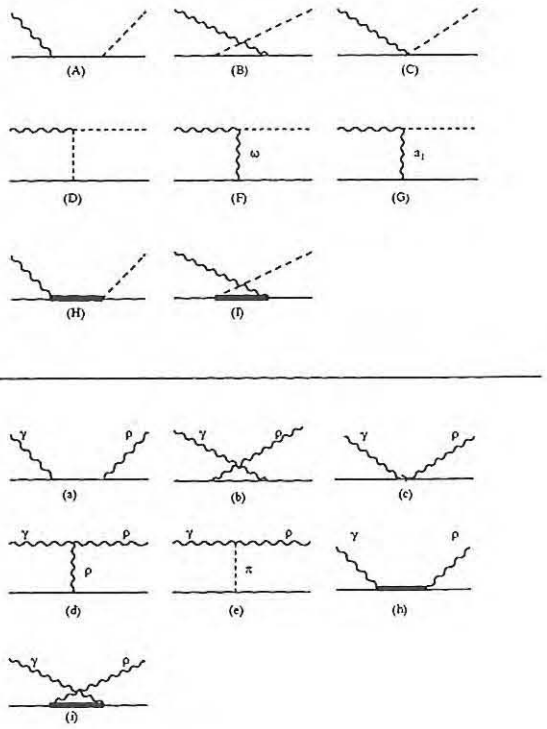

Fig. 1: Diagrams contributing to the πN scattering potential (upper part) and photo-production transition potential (lower part). The solid lines represent the nucleon, dashed lines the pion, and wiggle lines the photon. The internal solid lines may be either nucleon or Δ-isobar, while the internal wiggle line represents ρ-, ω- or a_1-meson.

Table 1: Real part of the E_{0+} amplitude for the threshold π^o photo-production off a proton in units of $10^{-3}/m_{\pi^o}$.

	(a)	*(b)*	*(c)*	*(d)*	*(rest)*	sum
BORN	-1.26	-1.26	-	-	0.66	-1.85
FSI-pion	-1.85	-0.96	8.18	-13.27	0.39	-7.51
FSI-rho	6.13	3.80	-0.67	-2.05	0.23	7.44
SUM	3.02	1.58	7.51	-15.32	1.28	-1.93

1. References

References:

[1] Y. Surya and F. Gross, Phys. Rev. **C53**, (1996) 2422.
[2] T. Sato and T. -S. H. Lee, Phys. Rev. **C54**, (1996) 2660.
[3] K. F. Liu, S. J. Dong, T. Draper, and W. Wilcox, Phys. Rev. Lett. **74**, (1995) 2172.

The $\pi^- p \to \pi^0\pi^0 n$ reaction in the vicinity of the $f_0(980)$ resonance

Zisheng Wang, S.Krewald, J.Speth

The $\pi^- p \to \pi^0\pi^0 n$ reaction has been investigated recently at Brookhaven using incoming pions with a momentum of $P_{LAB} = 18.3 GeV/c$ [1]. In this reaction, invariant masses of the two-pion system up to 3 GeV have been investigated. For small momentum transfers between the incoming proton and the outgoing neutron, the experimental cross sections show a dip in the vicinity of the $f_0(980)$ resonance, whereas for larger momentum transfers, the data clearly show a resonance.

If one assumes that the reaction mechanism is dominated by a one-pion exchange mechanism, the appearance of the resonance at larger momentum transfers cannot be explained [1]. A model independent partial-wave analysis of the $\pi^- \vec{p}$ reaction suggests a possible role of the A_1 meson[2, 3]. A Regge pole model fit can indeed reproduce the resonant behaviour[4].

We analyse the reaction using a meson-exchange model assuming the following reaction mechanism: the incoming proton is allowed to emit a virtual pion, a A_1 meson and a ρ. The virtual meson and the incoming pion are allowed to interact via meson-exchanges. The Jülich model for pion-pion scattering and Kaon-Kaon scattering [5] has been generalized to the full SU(3) sector including vector mesons using a bosonization of an underlying Nambu-Jona Lasinio Lagrangian. We include $\rho - \omega$ mixing thus allowing for a small violation of G-parity conservation. The off-shell T-matrix is generated by solving the Bethe-Salpeter eq.

$$T_{m\pi\to\pi\pi} = V_{m\pi\to\pi\pi} + V_{m\pi\to nn} G_{nn} T_{nn\to\pi\pi}, \quad (1)$$

where m and n denote virtual mesons.

If one allows only one-pion exchange at the proton-neutron vertex, one gets a qualitative description of the data both for small and large momentum transfers, but in the vicinity of 980 MeV, one finds a dip in the cross section, as is displayed in Figs. 1 and 2. Considering the exchange of only an a_1 meson at the proton-neutron vertex, a peak in the cross section is indeed produced at 980 MeV. For momentum transfers below $0.2(GeV/c)^2$, the magnitude of the peak is too small to be seen in the cross section. At larger momentum transfers, however, the peak grows and can be recognized.

The calculation shows that the a model based on a Kaon-Antikaon structure of the f_0 resonance is compatible with the recent two-pion production data.

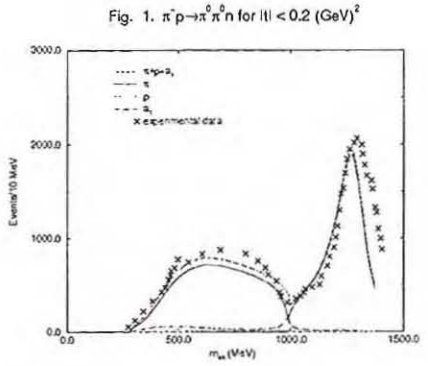

Fig. 1: The cross section for the reaction $\pi^- p \to \pi^0\pi^0 n$, averaged for momentum transfers $\mid t \mid \leq 0.2(GeV/c)^2$ is shown as a function of the invariant two-pion mass.

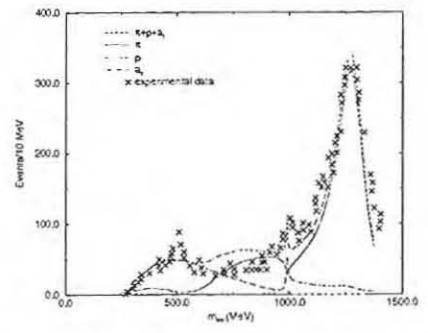

Fig. 2: Same as Fig.1, but for for momentum transfers $\mid t \mid \geq 0.4(GeV/c)^2$.

1. References

References:

[1] A. Dzierba, Nucl. Phys. **A623**, (1997) 142c.
[2] H.Becker et al., Nucl. Phys. **B151**, (1979) 46.
[3] R.Kaminski et al., Z. Phys. **C74** , (1997) 79.
[4] N.N. Achasov, G.N.Shestakov, Phys.Rev.D(in print)
[5] G.Janssen, B.C.Pearce, K.Holinde, and J.Speth, Phys.Rev.**D52**, (1995) 2690.

On production of the η'-meson in pp-collisions close to threshold

V.Baru[a,b], J.Haidenbauer[a], C.Hanhart[a,c], A.Kudryavtsev[a,b], J.Speth[a]

It was shown long ago by Watson [1] that in reactions of the type $NN \to NNx$ the energy dependence of the total cross section should be determined by the strong NN interaction in the final state (FSI), as long as the interaction of the meson x with the nucleons is considerably weaker than the NN interaction. The argument is based on the observation that the meson production in NN collisions requires large momentum transfers of the order of $\sqrt{M_N m_x}$ leading to a production operator that is nearly energy independent. In what follows we will denote the energy dependence introduced by the NN interaction by $\sigma_{NN}(E)$.

Thus any deviation from $\sigma_{NN}(E)$ points to a sizable meson nucleon interaction. Indeed, a series of recent measurements on η production in NN collisions shows, that the ηN interaction has a non negligible influence on the energy dependence of the total cross section leading to an enhancement of the cross section close to threshold [2]. This influence can be traced back to the attractive $N\eta$ interaction due to the presence of the $S_{11}(1535)$ resonance.

Recently the total cross section for the reactio n $pp \to pp\eta'$ close to threshold was measured for the first time [3, 4]. Especially the data of ref. [3] show an energy dependence that strongly deviates from the one given by $\sigma_{NN}(E)$. However, instead of an enhancement close to threshold the data shows a depletion with respect to $\sigma_{pp}(E)$. A natural conclusion from this would be that there is a repulsive η'N interaction of significant strength. In the present work we investigate this question.

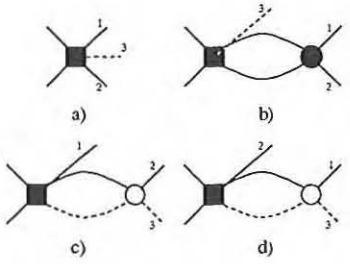

Fig. 1: *Feynman diagrams for the amplitude of the reaction* $pp \to pp\eta'$.

Since in this very first investigation we are only interested in the energy dependence we use the following factorization ansatz for the transition matrix element $pp \to pp\eta'$ [5]

$$M = A\Psi_{FSI} \ , \qquad (1)$$

where A denotes the production operator and Ψ_{FSI} denotes the final state wavefunction. In principle one would have to solve a Faddeev type of equation in order to treat Ψ_{FSI} properly. However, to get a feeling for the effect of the η'N interaction on the energy dependence of the cross section we include the two particle interactions to lowest order only as depicted in figure 1. We are presently working on relaxing this approximation. Thus, the expression for Ψ_{FSI} may be presented in the form:

$$\begin{aligned}\Psi_{FSI} = 1 \ &+ \ (\beta_{pp} + iq_{12}) f^{on}_{pp}(q_{12}) \\ &+ \ (\beta_{\eta' p} + iq_{13}) f^{on}_{\eta' p}(q_{13}) \\ &+ \ (\beta_{\eta' p} + iq_{23}) f^{on}_{\eta' p}(q_{23}), \qquad (2)\end{aligned}$$

where β_{pp} and $\beta_{\eta' p}$ are cut-off parameters and f^{on}_{pp} and $f^{on}_{\eta' p}$ are the on-shell pp- and $\eta' p$-amplitudes. The inclusion of the Coulomb interaction is straight forward and described elsewhere [5, 6]. To get this formula we used the following simple expression for the half-off-shell amplitudes,

$$f^{off}_{ij}(q_{ij}, q) = \frac{q_{ij}^2 + {\beta_{ij}}^2}{q^2 + {\beta_{ij}}^2} f^{on}_{pp}(q_{ij}), \qquad (3)$$

neglecting for the moment the Coulomb pp-interaction. In case of the pp system we find $\beta_{pp} \approx 3/r_{eff}$, where $r_{eff} \approx 2.8$ fm is the pp-effective range. Thus $\beta_{pp} \approx 0.2$ GeV in our case. Note that contrary to β_{pp} the value of $\beta_{\eta' p}$ is not known. If the range of $\eta' p$-effective potential is large, $\beta_{\eta' p}$ may be of the order of β_{pp}. If the range of the $\eta' p$-potential is small, say just $0.2 \div 0.4 fm$, then the parameter $\beta_{\eta' p}$ will be much larger. We varied $\beta_{\eta' p}$ to study its influence on observables.

For the $\eta' p$-amplitude $f^{on}_{\eta' p}(q)$ we use the scattering length approximation,

$$f^{on}_{\eta' p}(q) = \frac{1}{-1/a_{\eta' p} - iq}, \qquad (4)$$

where $\alpha = -1/a_{\eta' p} = \alpha_1 - i\alpha_2$ is complex because of the presence of absorption ($\alpha_2 \geq 0$).

Our formalism contains four parameters, namely α_1, α_2, $\beta_{\eta' p}$ and a normalization constant. For each set $\alpha_1, \alpha_2, \beta_{\eta' p}$ the normalization constant was chosen to provide a best χ^2-fit to the data. We considered separately regions of small ($\beta_{\eta' p}$=2.5 μ) and large ($\beta_{\eta' p}$=5 μ) values for the range parameter of the η'N interaction, where μ is pion mass. We also considered separately regions of small and large α_2, i.e. we checked the sensitivity of the fitting procedure to the fraction of $\eta' p$-absorption.

The function $\chi^2(\alpha_1)$ for $\alpha_2 = 0$ has two separate minima. The first one, which is at $\alpha_1 \approx -250 MeV/c$ may be called a normal solution (I). The second solution (II) corresponds to extremely small values of $\alpha_1, (\alpha_1 \approx -30 MeV/c)$ and hence to extremely large values of the $\eta' p$-scattering length. We may call this solution abnormal. Unfortunately this solution is outside the approximation we used in this paper. Namely if both the $\eta' p$- and pp-scattering lengths

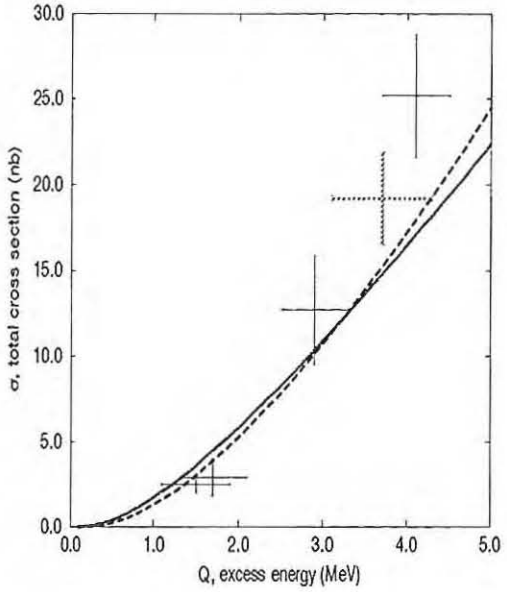

Fig. 2: *Total cross section for the reaction* $pp \to pp\eta'$. *The solid line is the calculation with pp FSI + phase space, the dashed line corresponds to the best* χ^2 *for the solution I with* $\alpha_1 = -240 MeV/c$, $\alpha_2 = 50 MeV/c$ *and* $\beta_{\eta' p} = 2.5\mu$. *The curve for the solution II with* $\alpha_1 = -32 MeV/c$ *and the same values* $\beta_{\eta' p}$ *and* α_2 *is almost identical to the curve for solution I below* $Q = 5 MeV$ *and therefore not shown here. The experimental data are from Refs. [3] and [4].*

are large, we can not limit ourselves to the diagrams of *Fig.* 1 only but should sum up all sets of FSI–diagrams. The behavior of the total cross section for some specific values of α_1, α_2, and $\beta_{\eta' p}$ is presented in *Fig.* 2 as a function of the excess energy Q. Note, that a reasonable fit to the data ($\chi^2 \approx 2$) for points below $Q = 5 MeV$ with both options, the small and the large value of $\beta_{\eta' p}$, can be achieved. The behavior of the total cross section above $Q = 5 MeV$ depends drastically on the parameters used and tends to enhance the cross section in comparison to what follows from the fit without $\eta' p$-FSI. We want to remark that the best χ^2 fit can be improved considerably, if either the lowest two points or the highest point (at 8 MeV, not shown in *Fig.* 2) are removed from the database.

In *Fig.* 3 the pp-effective mass distribution for Q=10 MeV is shown at special values of α_1, α_2 and $\beta_{\eta' p}$. Obviously, experimental information on this observable in the region around $5 - 20 MeV$ could be very useful for improving our knowledge on the η'N interaction.

[a]Institut für Kernphysik, Forschungszentrum Jülich GmbH, D–52425 Jülich, Germany
[b]Institute of Theoretical and Experimental Physics, 117258, B.Cheremushkinskaya 25, Moscow, Russia
[c]Institut für Theoretische Kernphysik, Universität Bonn, D–53115 Bonn, Germany

References:

[1] K.Watson, Phys.Rev, **88**, 1163, 1952
[2] A.Moalem, L.Razdolskaja, E.Gedalin, hep-ph/9505264, 1994
[3] P.Moskal et al.,Phys. Rev. Lett. **80**, 3202,1998
[4] F.Hibou at al., Phys. Lett. B **438**, 41, 1998
[5] B.L.Druzhinin,A.E.Kudryavtsev,V.E.Tarasov, Z.Phys. A **359**, 205, 1997
[6] H.van Haeringen, Nucl.Phys. A **253**, 355, 1975

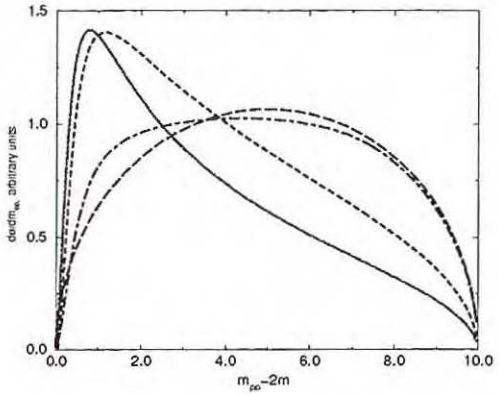

Fig. 3: *Spectra of pp-mass, calculated with* $\alpha_2 = 50 MeV/c$. *The long dashed curve is the phase space factor (arbitrary normalization). The solid and dashed curves are defined in Fig.* 2. *The dot-dashed curve corresponds to the solution II with* $\alpha_1 = -32 MeV/c$. *The normalization for all curves (except the dashed one) is the same as in Fig.* 2.

How important is the ρN channel in πN scattering?

O. Krehl, S. Krewald and J. Speth

We have extended the Jülich $\pi N/\sigma N/\pi\Delta/\eta N$ coupled channel model for πN scattering [1] by adding the ρN reaction channel. The potentials are calculated from an effective Lagrangian based on the one given by Wess and Zumino [2]. Chiral symmetry is realized in a nonlinear way and the ρ and a_1 degrees of freedom are treated as gauge bosons in a local $SU(2) \times SU(2)$ symmetry. The Δ, ω and σ degrees of freedom are added in a phenomenological way.

The $\pi N \to \rho N$ transition potential contains N and Δ u-channel exchange and π, ω and a_1 t-channel exchange diagrams. In addition, a $\pi\rho NN$ contact interaction is taken into account, which emerges as a generalization of the Kroll-Rudermann $\pi\gamma NN$ term in the picture of vector meson dominance.

The $\rho N \to \rho N$ potential is given by N u-channel exchange, ρ t-channel exchange and a $\rho\rho NN$ contact graph. Both, $\rho\rho\rho$ and $\rho\rho NN$ interaction are part of the Wess Zumino Lagrangian and arise from the fact, that the ρ meson is treated as a gauge boson.

After a partial wave decomposition, the potential is iterated in a one dimensional coupled channel scattering equation. In order to ensure the convergence of the scattering equation, a monopole formfactor has to be supplemented to each vertex of a t- or u-channel graph. For the contact interaction we are using a formfactor of the form .

$$\left(\frac{\Lambda^2 - m_i^2}{\Lambda^2 + \vec{p}_i^{\,2}}\right)^2 \left(\frac{\Lambda^2 - m_f^2}{\Lambda^2 + \vec{p}_f^{\,2}}\right)^2$$

where $m_{i,f}$ and $p_{i,f}$ are mass and momentum of the meson in the initial and final state.

All coupling constants in the $\pi N \to \rho N$ and $\rho N \to \rho N$ potentials are fixed form other sources. The 9 cutoffs in the formfactors are treated as free parameters in the fit to the experimental πN partial wave amplitudes and the $\pi N \to \rho N$ transition cross sections. The result of the fit in some πN partial waves is shown in fig.1 and our description of the $\pi N \to \rho N$ cross sections is displayed in fig.2.

The coupling to the ρN channel improves the description of the πN phase shifts especially in the partial waves P_{13} and P_{31}, where the model without ρN channel gives too much repulsion. This is demonstrated in fig.1 where the solid (dashed) curves are calculated with (without) coupling to the ρN channel. Fig.1 also shows the importance of the ρN channel close to threshold: at energies of about $1250 MeV$ almost 50% of the S_{11} phase shift is generated by the ρN intermediate state. In this partial wave parity conservation forces the ρN intermediate state into a relative S-wave where the centrifugal barrier is not present. Furthermore, in analogy to the photoproduction of pions, the most important contribution at

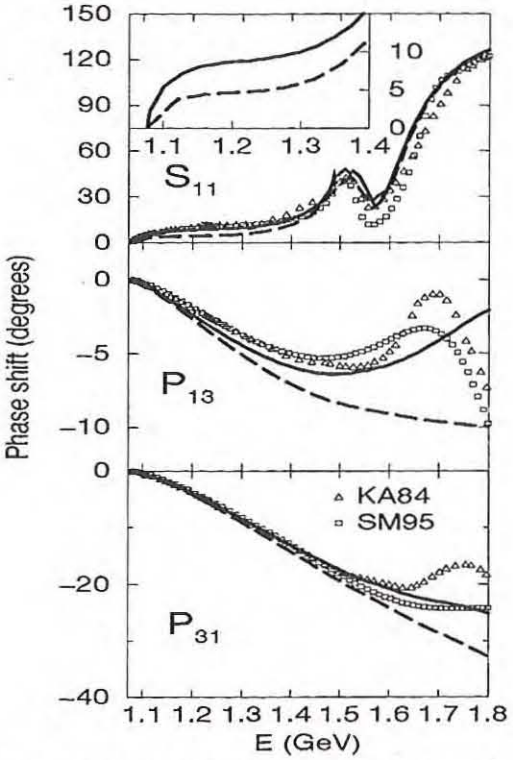

Fig. 1: πN phase shifts in the partial waves S_{11},P_{13} and P_{31}. The solid line is calculated with the full model. For the dashed line, the ρN channel has been switched off by setting $V_{\pi N \to \rho N} = 0$.

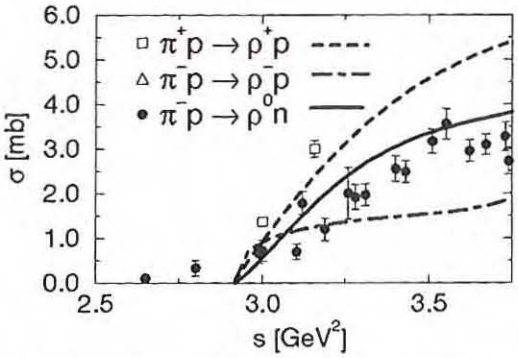

Fig. 2: The $\pi N \to \rho N$ cross sections. Curves are calculated within the full model.

these energies is the $\pi\rho NN$ contact diagram, which acts only in partial waves where the total angular momentum $J = 1/2$. In the P and D waves, the ρN channel influences the πN partial waves only at energies above $1300 MeV$.

References:

[1] C. Schütz, J. Haidenbauer, J.W. Durso and J. Speth, Phys. Rev. C 57 (1998) 1464.

[2] J. Wess and B. Zumino, Phys. Rev. 163 (1967) 1727.

A Microscopic Model for the πNN Formfactor in Time Ordered Perturbation Theory

R. Böckmann*, C. Hanhart, O. Krehl, S. Krewald, and J. Speth

The long range part of the pion nucleon form factor is generated by mesonic interactions such as the ones illustrated in Fig.1. Before interacting with the nucleon, a pion may couple to an intermediate pion-rho or pion-sigma state.

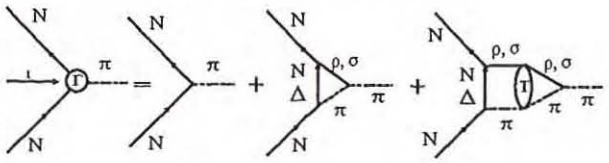

Fig. 1: Contributions to the πNN vertexfunction

A dispersion integral approach allows to determine the vertex function for space-like momentum transfers from the unitarity cuts of the intermediate processes[1].

$$\Gamma(t) = 1 + \frac{1 - m_\pi^2}{\pi} \int \frac{Im(\Gamma(t')dt'}{(t - t')(t' - m_\pi^2)}. \qquad (1)$$

Janssen et al. included the $\pi - \rho$ interaction in the calculation of the vertex function. The form factor they obtained [2] was harder than the phenomenological ones required e.g. in the analysis of pion-nucleon scattering and nucleon-nucleon scattering.

In the present work, we have included the sigma-nucleon states explicitly and have based our work on time-ordered perturbation theory. In contrast to the frequently used three-dimensional reductions of the Bethe-Salpeter equation, such as the Blankenbecler-Sugar model, time-ordered perturbation theory does not suffer from a non-uniqueness of the off-shell behaviour of the scattering matrix. By employing time-ordered perturbation theory, one avoids unphysical singularities which are introduced in some u-channel processes within the Blankenbecler-Sugar model. The off-shell scattering matrix elements generated by time-ordered perturbation theory are in many cases smaller than the corresponding ones obtained within the Blankenbecler-Sugar approach.

As input for the calculation of the πNN formfactor we take into account a coupled channel $\pi\rho - \pi\sigma$ T-Matrix including π, ω and A_1 u-channel exchange diagrams as well as a σ t-channel exchange in the $\pi\sigma$ scattering. Due to its dominant contribution we restricted ourselves to pion exchange in the transition potential $\pi\rho \to \sigma\pi$.

The results are shown in Fig.2. The contributions to the spectral function, i.e. the imaginary part of the form factor, are shown in the left panel. The dashed line corresponds to the uncorrelated pion-rho intermediate state(second diagram in Fig.1). The inclusion of the rescattering diagrams (third diagram in Fig.1) enhances the spectral function(dotted line). The uncorrelated pion-sigma exchange by itself is negligible(dashed-dotted line), as was found already in ref. [3]. The inclusion of the coupling between the rho-pion and the sigma-pion channel strongly enhances the imaginary part(solid line), however. This effect can be traced to the gradient coupling between the sigma and the pion field,

$$\mathcal{L}_{\pi\pi\sigma} = \frac{f}{2m_\pi} \partial_\mu \vec{\pi} \partial^\mu \vec{\pi} \cdot \Phi_\sigma.$$

The maximum of the spectral function coincides with the pion $\pi(1300)$.

The right panel of Fig.2 shows the corresponding form factors for space-like momentum transfers. One sees that the coupling between the sigma-pion and rho-pion intermediate states leads to a significant softening of the microscopically calculated form factor. For comparison, a phenomenological parameterization of the form factor by a monopole, using a cut-off mass of $\Lambda_{\pi NN} = 800MeV$, is also displayed(short-dashed line). The calculation including only the correlated pion-rho exchange gives a form factor corresponding to a cut-off mass of $\Lambda_{\pi NN} = 1500MeV$ (dotted line).

The pion-nucleon form factor derived here agrees well with phenomenological ones [4].

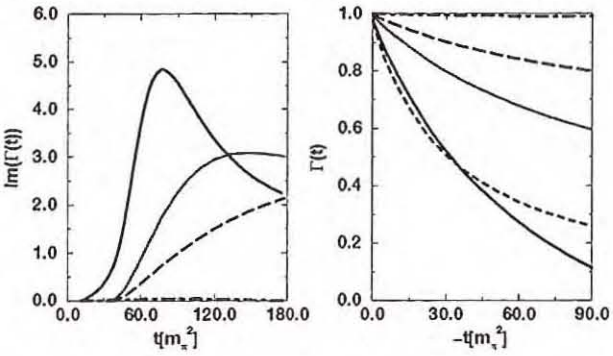

Fig. 2: The spectral function and form factor for various contributions discussed in the text

References:

[1] H.J.Braathen, Nucl.Phys.**B44**, (1972) 93.

[2] G. Janssen, J. W. Durso, K. Holinde, B. C. Pearce and J. Speth, Phys. Rev. Lett. **71** (1993) 1978.

[3] M. Dillig and M. Brack, J. Phys. G: Nucl. Phys. **5** No. 2 (1979) 223.

[4] S.A.Coon et al., Phys.Rev. **C42** (1990) 2256.

*MPI für biophysikalische Chemie, Göttingen

Off-shell behavior of the correlated $\pi\pi$ exchange in πN scattering

O. Krehl, S. Krewald and J. Speth

One of the major problems in calculating correlated two pion exchange potentials for πN scattering via dispersion relations is the unknown off shell behavior, because the dispersion relations only connect on shell amplitudes. But the off shell behavior is important to know when the potential is iterated in a scattering equation. To overcome this problem, we have followed a different way: We calculate potentials for sharp mass σ and ρ exchange and incorporate the $\pi\pi$ dynamics by the use of spectral functions. These spectral functions can be calculated from the pseudophysical $N\bar{N} \to \pi\pi$ amplitudes, which contain all the $\pi\pi$ dynamics.

For the calculation of the correlated $\pi\pi$ exchange in the σ channel we start with an interaction Lagrangian

$$L_{int} = \frac{g_{\sigma\pi\pi}}{2m_\pi}\partial_\mu\vec{\pi}\cdot\partial^\mu\vec{\pi}\sigma + g_{\sigma NN}\bar{\Psi}\Psi\sigma$$

Using this Lagrangian and the standard decomposition into an isospin even amplitude A^+ (see e.g. ref. [1]) we get for the exchange of a fixed mass σ meson:

$$A^+_\sigma = -\frac{g_{\sigma NN}g_{\sigma\pi\pi}}{2m_\pi}2p_2^\mu p_{4,\mu}\frac{1}{t-m_\sigma^2}F_\sigma(p_1,p_3)$$

where we are using the notation $N(p_1)\pi(p_2) \to N(p_3)\pi(p_4)$. The form-factor $F_{\sigma,\rho}(p_1,p_3) = (\frac{\Lambda^2-m^2_{\sigma,\rho}}{\Lambda^2+(\vec{p}_1-\vec{p}_3)^2})^2$ is needed when iterating the potential in a scattering equation. The potential can be constructed from this amplitude via

$$V_\sigma(p,p',\lambda,\lambda') = -\chi\bar{u}(p',\lambda')A^+_\sigma u(p,\lambda)$$

where $\chi = \frac{1}{(2\pi)^3}\sqrt{\frac{m_N m_N}{E_p E_{p'} 2\omega_p 2\omega_{p'}}}$ is multiplied to get a potential suitable for the iteration in the framework of time ordered perturbation theory. Due to the use of a field theoretical approach the off shell behavior of this potential is fixed.

We can now incorporate the width of the σ meson – which we know is a parameterization of an interacting pion pair – by requiring, that the σ does not have a fixed mass. We therefore have to exchange a continuum of σ mesons with a continuous mass m_σ. Of course there has to be a weighting function, which tells us how strong the exchange of a σ with a mass m_σ should be. This weighting function is the spectral function $\rho(m_\sigma)$. The amplitude for the correlated $\pi\pi$ exchange in the sigma channel can then be written as

$$A^+_{2\pi} = \frac{1}{\pi}\int dm_\sigma^2\rho_\sigma(m_\sigma)A^+_\sigma(m_\sigma) \qquad (1)$$

with the normalizing condition

$$\frac{1}{\pi}\int dm_\sigma^2\rho_\sigma(m_\sigma) = 1$$

For constructing the spectral function we use the pseudophysical data on $N\bar{N} \to \pi\pi$ [2]. This reaction is dominated by the $\pi\pi$ final state interaction and therefore contains the information about the σ spectral function. For this purpose, we express the the amplitude A^+_σ in the $N(q_1)\bar{N}(q_2) \to \pi(q_3)\pi(q_4)$ channel in terms of so called Frazer Fulco amplitudes f, which are free of kinematical singularities [3]

$$A^+_\sigma = -\frac{g_{\sigma NN}g_{\sigma\pi\pi}}{2m_\pi}2q_3^\mu q_{4,\mu}D_\sigma(t) = -\frac{4\pi}{p_t^2}f^0_+(t), \quad (2)$$

where $p_t = \sqrt{t/4-m_N^2}$ is the on shell momentum of the nucleon in the $N\bar{N} \to \pi\pi$ channel (where $t = E^2$) and $D_\sigma(t)$ is the dressed σ propagator, which contains the dynamics of the $\pi\pi$ interaction. It is related to the spectral function by

$$\rho_\sigma(m_\sigma) = -Im(D_\sigma(m_\sigma^2))$$

where we identify $t = m_\sigma^2$ as the continuous σ mass. Solving eq.(2) for D_σ we get

$$\rho_\sigma(m_\sigma) = -\frac{4\pi}{p_t^2}Im(f^0_+(m_\sigma^2))\frac{2m_\pi(2q_3^\mu q_{4,\mu})^{-1}}{g_{\sigma\pi\pi}g_{\sigma NN}}$$

After inserting this spectral function into eq.(1) and recalling that $2q_3^\mu q_{4,\mu} = m_\sigma^2 - 2m_\pi^2$ we get

$$\begin{aligned} A^+_{2\pi} &= 16(2p_2^\mu p_{4,\mu})* \qquad (3)\\ &* \int dm_\sigma^2\frac{Im(f^0_+(m_\sigma^2))(m_\sigma^2-2m_\pi^2)^{-1}}{(m_\sigma^2-4m_N^2)(t-m_\sigma^2)}F_\sigma(p_1,p_3)\end{aligned}$$

On shell eq.(3) is the same as the amplitude used in ref. [1], where the factor $-2p_2^\mu p_{4,\mu}$ is replaced by $t-2m_\pi^2$, since on shell $-2p_2^\mu p_{4,\mu} = t-2m_\pi^2$. However, off shell these amplitudes behave quite differently as can be seen in fig.1. Whereas in the S_{11} our sigma potential is of much shorter range (in momentum space), it is of much longer range in the P_{11} as compared to the potential used in ref. [1]. Furthermore, we don't have a change of sign in the P_{11} potential.

The ρ exchange potential can be calculated in the same way. From the Lagrangian

$$\begin{aligned} L_{int} &= g_v\bar{\Psi}(\gamma_\mu\vec{\Phi}^\mu_\rho - \frac{\kappa}{2m_N}\sigma_{\mu\nu}\partial^\nu\vec{\Phi}^\mu_\rho)\frac{1}{2}\vec{\tau}\Psi\\ &+ g_{\rho\pi\pi}(\vec{\Phi}_\pi\times\partial^\mu\vec{\Phi}_\pi)\vec{\Phi}^\mu_\rho,\end{aligned}$$

where $\kappa = \frac{g_t}{g_v}$, one can calculate the amplitudes

$$\begin{aligned} A^-_\rho &= g_{\rho\pi\pi}\frac{g_t}{m_N}(p_1+p_3)^\mu Q_\mu\frac{1}{t-m_\rho^2}F_\rho(p_1,p_3)\\ B^-_\rho &= -g_{\rho\pi\pi}(g_v+g_t)\frac{1}{t-m_\rho^2}F_\rho(p_1,p_3),\end{aligned}$$

with $Q = \frac{1}{2}(p_2+p_4)$.

In the $N\bar{N} \to \pi\pi$ channel, the amplitudes A^- and B^- are connected to the Frazer Fulco amplitudes in

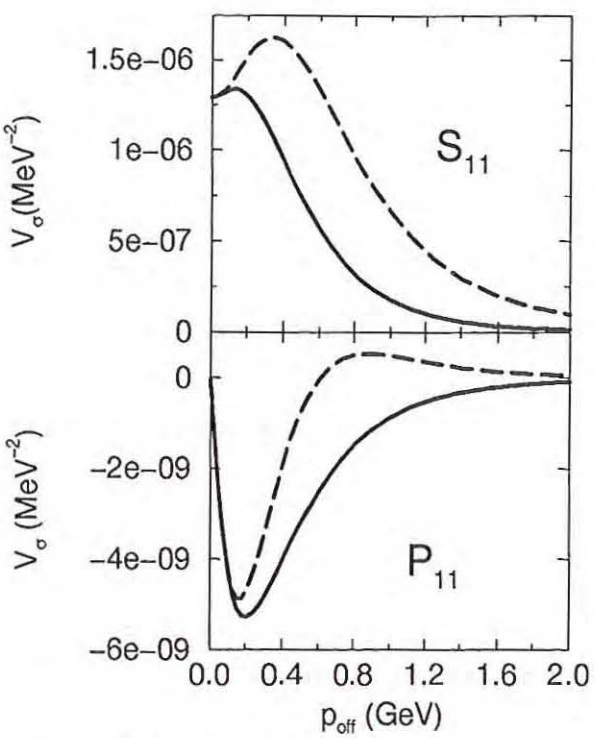

Fig. 1: Half off shell σ exchange potential $V_\sigma^{JLS}(p_{on}, p_{off})$ for $E = 1077MeV$ and $\Lambda = 1150MeV$. The solid line is calculated with the $p_2^\mu p_{4,\mu}$ off shell prescription and the dashed line is calculated with the $t - 2m_\pi^2$ off shell behavior. For the on shell momentum $p_{on} = 3.2MeV$ both potentials agree.

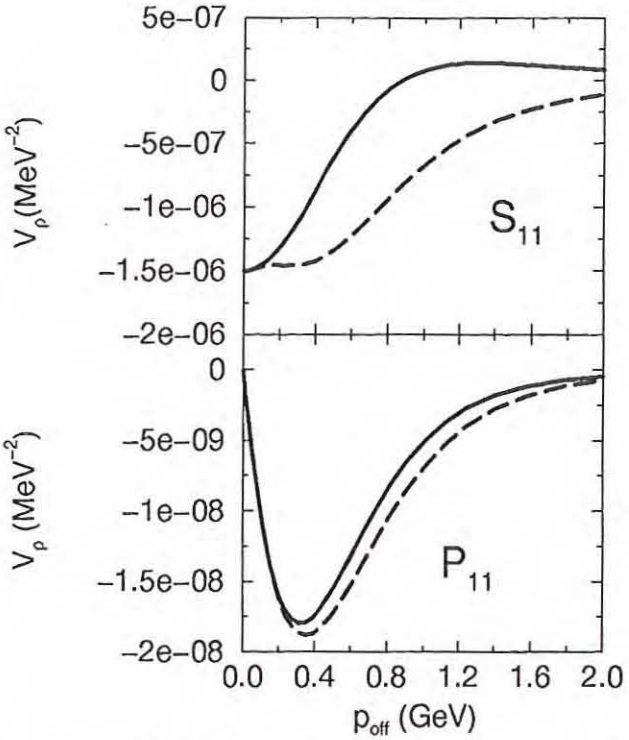

Fig. 2: Half off shell ρ exchange potential $V_\sigma^{JLS}(p_{on}, p_{off})$ for $E = 1077MeV$ and $\Lambda = 1250MeV$. The solid line is calculated with the $(p_1 + p_3)^\mu Q_\mu$ off shell prescription and the dashed line is calculated with the $2p_t q_t x$ off shell behavior. For the on shell momentum $p_{on} = 3.2MeV$ both potentials agree.

the following way:

$$A_\rho^-(t) = \frac{12\pi}{p_t^2} p_t q_t x \left(\frac{m_N}{\sqrt{2}} f_-^1(t) - f_+^1(t) \right)$$
$$B_\rho^-(t) = \frac{12\pi}{\sqrt{2}} f_-^1(t)$$

where $q_t = \sqrt{t/4 - m_\pi^2}$ is the on shell momentum of the pions and $x = cos(\theta)$ is the scattering angle.

The ρNN coupling consists of a vector coupling and a tensor coupling, which can be dressed differently. Therefore we have to assign two different propagators $D_\rho^v(t)$ and $D_\rho^t(t)$ to the vector and the tensor part. From these propagators the spectral functions can be calculated and inserted in equations similar to eq.(1) for A_ρ^- and B_ρ^-. The result reads

$$A_{2\pi}^- = -3(p_1 + p_3)^\mu Q_\mu \int dm_\rho^2 \frac{1}{t - m_\rho^2} \frac{1}{p_{m_\rho^2}^2} *$$
$$* \left(\sqrt{2} m_N Im(f_-^1(m_\rho^2)) - 2Im(f_+^1(m_\rho^2)) \right) F_\rho(p_1, p_3)$$
$$B_{2\pi}^- = -6\sqrt{2} \int dm_\rho^2 \frac{Im(f_-^1(m_\rho^2))}{t - m_\rho^2} F_\rho(p_1, p_3)$$

This is almost the same expression as was calculated by the use of dispersion relations over the formfactors Γ_1 and Γ_2 used by Höhler and Pitarinen [4] (see also the discussion in [1]). The only difference is again the factor $(p_1 + p_3)^\mu Q_\mu$ in front of the integral. In ref. [1] a factor $2p_t q_t x$ was used instead. This is on shell equivalent to $(p_1 + p_3)^\mu Q_\mu$. The difference in the off shell behavior is displayed in fig.2. Again our potential is of much shorter range in the S_{11} and changes sign at $p_{off} \approx 0.8GeV$, whereas the difference in the P_{11} is small.

Our method of constructing the potential for the correlated $\pi\pi$ exchange in the σ and ρ channel reproduces the on shell potentials calculated via dispersion relations. However, due to the field theoretical starting point the off shell behavior is well defined and differs drastically from the one used in the dispersion theoretical approach. The consequences of these changes for the πN scattering amplitudes are under investigation and will be discussed elsewhere.

References:

[1] C. Schütz, J.W. Durso, K. Holinde and J. Speth, Phys. Rev. C 49 (1994) 2671.

[2] G. Höhler in *Pion-Nucleon Scattering*, Vol. I/9b2 of *Landolt-Börnstein*, edited by H. Schopper (Springer-Verlag, New York, 19983).

[3] W.R. Frazer and J.R. Fulco, Phys. Rev. 117 (1960) 1609.

[4] G. Höhler and E. Pitarinen, Nucl. Phys. **B** 95 (1975) 210.

Comments on the reactions $pp \to pK^+\Lambda$ and $pp \to pK^+\Sigma^0$

A. Gasparian[1], J. Haidenbauer, C. Hanhart[2], L. Kondratyuk[3] and J. Speth

Recently the total cross sections for the reactions $pp \to pK^+\Lambda$ and $pp \to pK^+\Sigma^0$ were measured for the first time close to threshold [1]. The most interesting aspect of these new data is that at the same excess energy the cross section for the Σ^0 production is about a factor of 30 smaller than the one for the Λ. In principle, this strong suppression of the Σ^0 production can be understood if one assumes that the hyperon production is solely due to the K-exchange mechanism, depicted in Fig. 1(b). In this case the ratio of Σ^0/Λ production is essentially given by the ratio of the coupling constants at the vertices from which the K meson emerges, i. e. by $g^2_{\Sigma NK}/g^2_{\Lambda NK}$. These coupling constants are not very well known experimentally. However, they can be inferred from SU(3) flavour symmetry - a symmetry which, so far, has been rather successfully employed in investigations of reactions involving hyperons. Specifically according to SU(6) this ratio is 1/27 [2], a value which coincides almost exactly with the experimental cross section ratio.

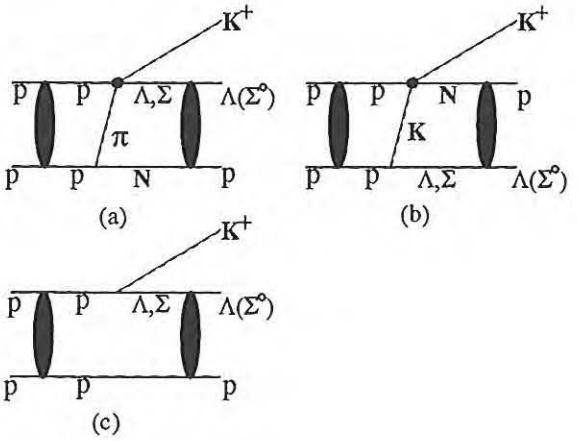

Fig. 1: *Mechanisms for the reaction* $pp \to pK^+\Lambda/\Sigma^0$

None-the-less, most likely the contributions of the π-exchange mechanism (Fig. 1(a)) to hyperon production are not negligible. A simple estimation based on the experimental amplitudes of the elementary scattering processes ($K^+p \to K^+p$ and $\pi^0 p \to K^+\Lambda, K^+\Sigma^0$, respectively) shows that for the Λ production the π–exchange contribution should be roughly a factor of 10 smaller than the K–exchange contribution [1]. In the Σ^0 channel, however, π–exchange might be indeed the dominant production mechanism. Furthermore contributions from direct production (Fig. 1(c)) could be important as well for both hyperon production channels [3]. Therefore a pure K–exchange model is certainly unrealistic and a detailed microscopic calculation including all production diagrams and the full complexity of the ($\Lambda N - \Sigma N$ coupled channel) final state interaction is required for achieving conclusive results. Such investigations are presently under way in our group. As a first result we present here a simple calculation of the energy dependence of the total cross section utilizing the Watson model. In this case he production amplitude $A_{NN\to NKY}$ is given by

$$A_{NN\to NKY} = C_Y \cdot T_{YN} \ ,$$

where T_{YN} is the amplitude of the hyperon–nucleon final state interaction, and C_Y is a constant that is determined by a fit to the experiment for each channel. Results for the Jülich model A [4] and the Nijmegen model [5] are shown in Fig. 2. Note that in the actual calculation an effective range approximation is used for T_{YN} and only s-waves are taken into account. Coupled channel effects are, however, still implicitly included leading to complex effective-range parameters for the ΣN interaction. Evidently both models yield an energy dependence that agrees quite well with the experimental data (Fig. 2).

[1]also at: Moscow Engineering Physics Institute, 115409, Kashirskoe s.31, Moscow, Russia
[2]also at: Institut für Theoretische Kernphysik, Universität Bonn, D-53115 Bonn, Germany
[3]Institute of Theoretical and Experimental Physics, 117258, B.Cheremushkinskaya 25, Moscow, Russia

References:

[1] S. Sewerin et al., nucl-ex/9811004.
[2] J.J. De Swart, Rev. Mod. Phys. **35**, 916 (1963); C.B. Dover and A. Gal, Prog. Part. Nucl. Phys. **12**, 171 (1984).
[3] J.M. Laget, Phys. Lett. B **259**, 24 (1991).
[4] B. Holzenkamp et al., Nucl. Phys. **A500**, 485 (1989).
[5] P.M.M. Maessen et al., Phys. Rev. C **40**, 2226 (1989).

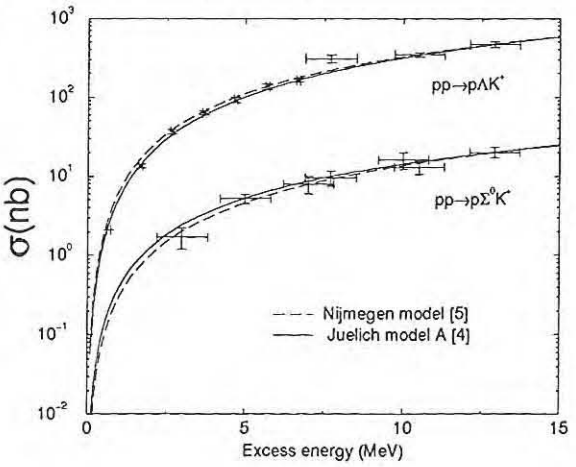

Fig. 2: *Total cross sections for the reactions* $pp \to pK^+\Lambda$ *and* $pp \to pK^+\Sigma^0$.

2π production close to threshold: via an intermediate ρ meson?

C. A. Mosbacher, O. Krehl, C. Hanhart, and J. Speth

We investigate the two pion production in the reactions $n + p \to d\,(\pi\pi)^0$ and $p + d \to {}^3\mathrm{He}\,\pi^+\pi^-$ close to threshold. Corresponding experiments have been performed at LAMPF [1] with a 1.46 GeV/c neutron beam, and by the MOMO group at COSY [2] with a 1.15 GeV/c proton beam. The deuteron spectrum (LAMPF) and the invariant mass distribution of the two pions (COSY) are measured, respectively. In these experiments, the production of $\pi^+\pi^-$ pairs was found to be dominated by a relative p–wave within the 2π system while the $\pi^0\pi^0$ production seems to follow the phase space [3].

In order to explain this different behaviour, C. Wilkin proposed a reaction mechanism where first an intermediate ρ meson is produced, $n + p \to \rho^0 d$, which subsequently decays into two pions, $\rho^0 \to \pi^+\pi^-$ [4]. Three possible Feynman diagrams for the ρ^0 meson production in $n + p$ collisions are shown in fig. 1. The $p + d$ reaction is assumed to proceed in a similar way but with an additional spectator nucleon being involved.

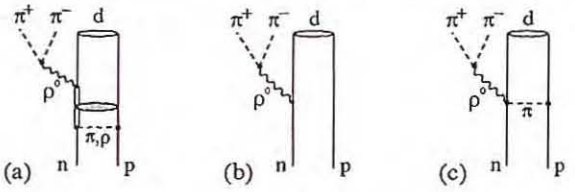

Fig. 1: Different ρ production mechanisms in the $n + p \to \rho^0 d$ reaction. The ρ meson subsequently decays into a $\pi^+\pi^-$ pair.

With the beam momentum denoted by k_{lab}, the deuteron spectrum for the ρ–mechanism is given by

$$\frac{d^2\sigma}{dk_d d\Omega_d} = \frac{1}{(2\pi)^2}\frac{M}{k_{\mathrm{lab}}}\,k_d^2\,\frac{A_\rho(s_\rho)}{\pi}\,|\mathcal{M}|^2\,, \qquad (1)$$

while the two pion invariant mass distribution is found to be

$$\frac{d\sigma}{dT_{\pi\pi}} = \frac{1}{(2\pi)^2}\,\frac{M}{k_{\mathrm{lab}}}\,\frac{\sqrt{s_\rho}}{E_\rho}\,\frac{A_\rho(s_\rho)}{\pi}\int p_\rho^2\,\frac{dp_\rho}{dE}\,d\Omega_\rho\,|\mathcal{M}|^2 \qquad (2)$$

where $T_{\pi\pi} = \sqrt{s_\rho} - 2m_\pi$. The spectral function A_ρ of the ρ meson describes its decay into two pions and is parameterized as given in ref. [5].

From eqs. (1), (2) one easily obtains the phase space for the ρ–production by assuming the matrixelement $\mathcal{M}$ to be constant. Fig. 2 shows this phase space compared to the full three particle phase space and to the MOMO data [2]. It seems that the experiment strongly supports the hypothesis of an intermediate ρ meson.

However, in the case of the $n + p \to d\,(\pi\pi)$ reaction, the explicit calculation of the matrix elements corresponding to fig. 1 yields a cross section which is by

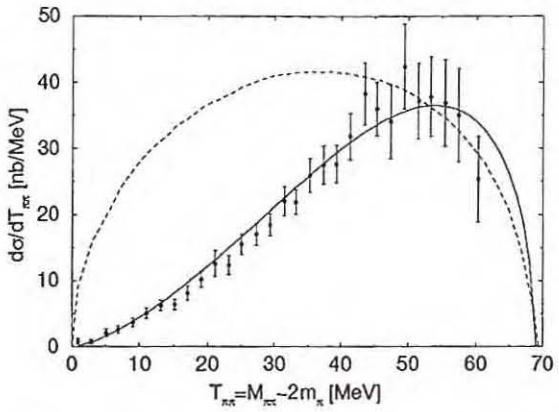

Fig. 2: Experimental cross section $d\sigma/dT_{\pi\pi}$ of the reaction $p + d \to {}^3\mathrm{He}\,\pi^+\pi^-$ at $k_p = 1.15$ GeV/c [2]. Dotted line: three particle phase space, solid line: phase space for the ρ–mechanism (in arbitrary units).

a factor of ≈ 20 smaller than the experimental value [6]. The suppression of the ρ–mechanism close to the 2π threshold is mainly due to the large energy denominator of the ρ propagator at $\sqrt{s_\rho} \approx 2m_\pi$. Moreover, the matrixelements do not show a strong decrease with energy. If one assumes the ρ–mechanism to be dominant at threshold, such a decrease would be needed in order to explain the completly different results in the ABC energy region ($\sqrt{s} \approx 2M_\Delta$) where the pions are found to be in a relative s–wave rather than a p–wave [6, 7].

We draw the conclusion that the production of an intermediate ρ meson is most probably not able to explain the 2π production at threshold. Other mechanisms, e.g. the excitation of the Roper resonance $N^*(1440)$ as recently discussed in ref. [8], may be more important.

References:

[1] C.L. Hollas *et al.*, *Phys. Rev.* C **25**, 2614 (1982)
[2] R. Jahn, private communication.
[3] G. Bohlscheid, phd thesis, Universität Bonn (1998).
[4] C. Wilkin, private communication.
[5] G.J. Gounaris and J.J. Sakurai, *Phys. Rev. Lett.* **21**, 244 (1968).
[6] C. A. Mosbacher, phd thesis, Berichte des Forschungszentrums Jülich, Jül–3609 (1998).
[7] A. Abashian, N. E. Booth, and K. M. Crowe, *Phys. Rev. Lett.* **7**, 35 (1961)
[8] L. Alvarez–Ruso, nucl-th 9811058

Study of $\Delta\Delta$ excitations in the reaction $n + p \to d + \pi\pi$

C. A. Mosbacher and F. Osterfeld†

The deuteron spectrum in $n+p \to d+\pi\pi$ at $k_n = 1.88$ GeV/c and $\theta_d = 0°$ is explained by considering a $\Delta\Delta$ excitation as the reaction mechanism for the 2π production. We study the influence of intermediate $\Delta\Delta$ and ΔN interactions on the spectrum. The angular distribution of the pions is predicted.

1. Introduction

Experimental measurements of the reaction $n + p \to d + \pi\pi$ at neutron momenta of 1.88 GeV/c [1] show a typical cross section structure known as the ABC–effect [2]. The main features of this effect can be explained by assuming a double $\Delta(1232)$ excitation to be the dominant reaction mechanism for the 2π production [3, 4]. Therefore the $n + p \to d + \pi\pi$ reaction allows us to study the influence of direct $\Delta\Delta$ and ΔN interaction potentials. The Feynman diagram corresponding to the $\Delta\Delta$ mechanism is shown in fig. 1.

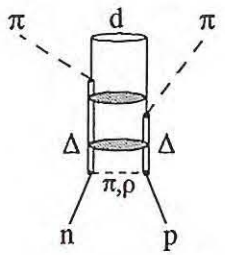

Fig. 1: $\Delta\Delta$ excitation mechanism in the reaction $n + p \to d + \pi\pi$. The shaded areas symbolize the intermediate $\Delta\Delta$ and ΔN interaction, respectively.

2. Theoretical Framework

In order to incorporate the interaction dynamics of the $\Delta\Delta$ system in a proper and efficient way, we apply a coupled channel approach [5] deduced from Δ–hole models. The matrix element is calculated using the source function formalism [6]. By means of detailed balance, the two pions are considered to excite the $\Delta\Delta$ system from the deuteron. The source function is defined to be

$$|\,\rho\,\rangle = F^\dagger(\vec{k}_1)\, G_{\Delta N}\, F^\dagger(\vec{k}_2)\, |\psi_d\rangle \pm (1 \leftrightarrow 2) \qquad (1)$$

where $\vec{k}_1, \vec{k}_2$ denote the momenta of the two pions. The operator

$$F^\dagger(\vec{k}_\pi) = \frac{f_{\pi\Delta N}}{m_\pi}\, e^{i\vec{k}_\pi\cdot\vec{r}} \left(\vec{S}^\dagger \cdot \vec{k}_\pi\right) T^\dagger \qquad (2)$$

describes the pion absorption and excitation of a Δ resonance (whereby $\vec{S}^\dagger$, $T^\dagger$ are the spin and isospin transition operators, respectively). Furthermore, $G_{\Delta N}$ in eq. (1) is the full propagator for the intermediate ΔN system.

The matrix–element corresponding to the $\Delta\Delta$ mechanism can now be written as

$$\mathcal{M} = \langle\psi_{np}|\, V_{NN,\Delta\Delta}\, G_{\Delta\Delta}\, |\,\rho\,\rangle. \qquad (3)$$

with the full propagator

$$G_{\Delta\Delta} = \frac{1}{E + \frac{i}{2}\left(\Gamma(s_{\Delta_1}) + \Gamma(s_{\Delta_2})\right) - \hat{T}_{\Delta\Delta} - \hat{V}_{\Delta\Delta}} \qquad (4)$$

Here $\Gamma(s_\Delta)$ is the energy–dependent width of the Δ resonance. An equation analogous to (4) holds for $G_{\Delta N}$. In particular, the propagators include the interaction potentials $V_{\Delta N}$ and $V_{\Delta\Delta}$, respectively. Therefore, eq. (3) leads to a system of coupled integro–differential equations, which can be solved in an efficient way with the Lanczos method [6]. The interaction potentials (as well as the transition potential $V_{NN,\Delta\Delta}$ in eq. 3) are constructed within a meson exchange model [7]. The exchanged mesons taken into account are the pion (π), the rho (ρ), the omega (ω), and the sigma (σ). The parameters of the potentials are the coupling constants, cutoffs and meson masses given in Table 1.

	$\frac{f^2_{\alpha NN}}{4\pi}$	$\frac{f^2_{\alpha N\Delta}}{4\pi}$	$\frac{f^2_{\alpha\Delta\Delta}}{4\pi}$	Λ_α[GeV]	m_α[MeV]
π	0.08	0.32	0.0031	1.1	138
ρ	5.4	21.6	0.286	1.4	770
ω	8.1	—	8.1	1.7	783
σ	6.9	—	6.9	1.6	580

Table 1: Parameters for the meson exchange model of the interaction potentials.

3. Results and Discussion

Fig. 2 shows the result of our full model calculation compared to the experimental deuteron spectrum for $\theta_d = 0°$. The overall agreement is very good. The cross section exhibits characteristic enhancements at missing masses close to $2m_\pi$ (corresponding to maximal and minimal deuteron recoil momentum in the laboratory frame) and at the largest missing masses possible (the central peak). This structure can be easily understood as follows [3]. Let us define

$$K = k_1 + k_2\,, \qquad k = k_1 - k_2\,, \qquad (5)$$

where k_1, k_2 denote the four–momenta of the two pions. The $\Delta\Delta$ mechanism is most efficient if both Δ's are on–mass shell, which requires

$$s_{\Delta_1} = \frac{1}{4}(k_d + K + k)^2 = \frac{1}{4}(k_d + K - k)^2 = s_{\Delta_2}\,. \qquad (6)$$

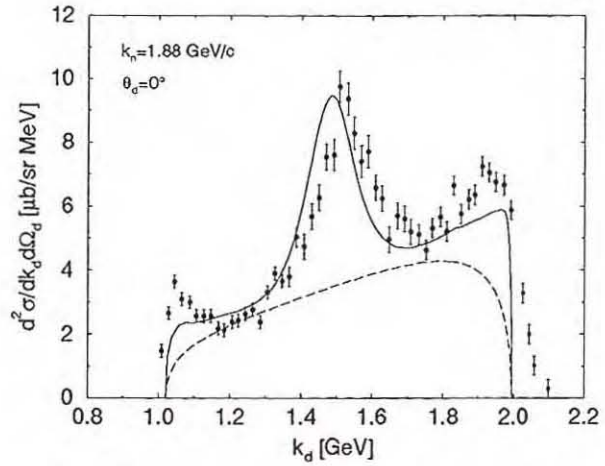

Fig. 2: Theoretical result for the $n+p \to d+\pi\pi$ cross section (full line) and experimental data [1] at $k_n = 1.88$ GeV/c and $\theta_d = 0°$. The dashed line shows the phase space.

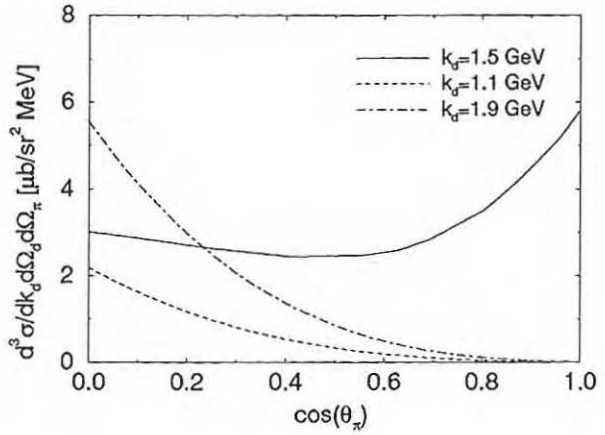

Fig. 3: Angular distribution of the two pions in the deuteron rest frame, given as a function of $\cos(\theta_\pi) = \hat{k} \cdot \hat{k}_n$.

This condition is equivalent to $k_d \cdot k = 0$ and can be satisfied in two ways:

1. $k = 0$ and hence $\sqrt{K^2} = M_{\pi\pi} = 2m_\pi$, or
2. $\vec{k}_d = 0$ in the rest frame of the two pions.

In the latter case, the 2π CMS is identical to the rest frame of the deuteron and hence the overall CMS. The two pions pick up the whole kinetic energy which means $M_{\pi\pi} = \max$. This leads to the high mass enhancement which corresponds to the anti-parallel decay of the two Δ's, while the low mass enhancement ($k = 0$) corresponds to the parallel decay.
These two different kinematical situations are also manifest in the angular distributions shown in fig. 3. For $k_d = 1.5$ GeV/c (in the lab frame), the pions are emitted back to back and any angle between $\vec{k}$ and the beam axis is kinematically possible. The shape of the cross section reflects the spin-structure of the $\Delta\Delta$ excitation [5]. For $k_d = 1.1$ and 1.9 GeV/c, the pions are emitted nearly parallel and have identical

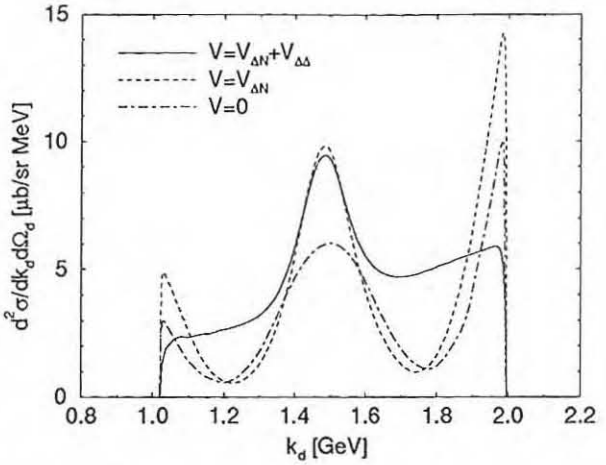

Fig. 4: Influence of the $\Delta\Delta$ and ΔN interaction potentials.

energies, hence $\vec{k}$ is dominantly perpendicular to the beam axis.
Fig. 4 demonstrates the influence of the ΔN and $\Delta\Delta$ interaction potentials in our model calculation. The result for $V = 0$ (dashed-dotted line) clearly shows the three peak structure as discussed above. The potential $V_{\Delta N}$ is attractive and thus results in even more pronounced peaks (dashed line) since it simply lowers the overall excitation energy. Inclusion of $V_{\Delta\Delta}$, however, leads to a redistribution of strength from the peaks towards the kinematical less favored situations between (solid line). This is the case because the optimal configuration with both Δ's on mass-shell can now also be reached if the initial momentum distribution was asymmetric.
To summarize we have shown that 1. the $\Delta\Delta$ excitation is the dominant reaction mechanism in the $np \to d + \pi\pi$ two pion production at $k_n = 1.88$ GeV/c, and 2. the intermediate $\Delta\Delta$ and ΔN interactions play an important role in this reaction which therefore may serve as a tool for closer examination of the interaction potentials.

References:

[1] F. Plouin *et al.*, *Nucl. Phys.* A **302**, 413 (1978)
[2] A. Abashian, N. E. Booth, K. M. Crowe, R. E. Hill, and E. H. Rogers *Phys. Rev.* **132**, 2296 (1963)
[3] T. Risser and M. D. Shuster, *Phys. Lett.* B **43**, 68 (1973)
[4] I. Bar-Nir, T. Risser, and M. D. Shuster, *Nucl. Phys.* B **87**, 109 (1975)
[5] C. A. Mosbacher and F. Osterfeld, *Phys. Rev.* C **56**, 2014 (1997)
[6] T. Udagawa, P. Oltmanns, F. Osterfeld, and S. W. Hong, *Phys. Rev.* C **49**, 3162 (1994)
[7] R. Machleidt, K. Holinde, and C. Elster, *Phys. Rev.* **149**, 1 (1987)

The d(^{3}He,t) charge exchange reaction in the Δ resonance region

C. A. Mosbacher

We adopted the theoretical model of ref. [1], originally designed for the d(p,n)X reaction, in order to calculate inclusive triton spectra in the d(^{3}He,t)X charge exchange reaction at $T_{\rm He} = 2$ GeV. This was accomplished by introducing an additional formfactor for the ^{3}He–t transition at the projectile vertex. From a three–body Fadeev calculation [2], this formfactor is obtained to be

$$f_{\rm He}(t) = \exp[-\alpha_0\, t]\,(1 + \alpha_1\, t + \alpha_2\, t^2), \qquad (1)$$

where in the spin–longitudinal (spin–transversal) channel $\alpha_0 = 0.406$ (0.567) fm^2, $\alpha_1 = -0.014$ (0.036) fm^2 and $\alpha_2 = 0.036$ (0.043) fm^4, respectively. If $(\omega, \vec{q})$ denotes the four–momentum transfer to the target, then $t = \omega^2 - \vec{q}^{\,2}$ in eq. (1).

Possible final states in the Δ energy region are $X = 2p$, $X = \pi d$ and $X = \pi NN$. The feynamn diagrams for the different reaction mechanisms are shown in fig. 1. Special emphasis is given to the residual interaction in the excited ΔN intermediate systems which is included in all orders. The corresponding potential $V_{\Delta N}$ is constructed in a meson exchange model with π, ρ, ω, and σ exchange taken into account [1, 3].

In fig. 2 the result of our calculation is compared to the preliminary experimental data [4]. The overall agreement is very good. Both the quasi–elastic peak and the Δ resonance peak are described correctly,

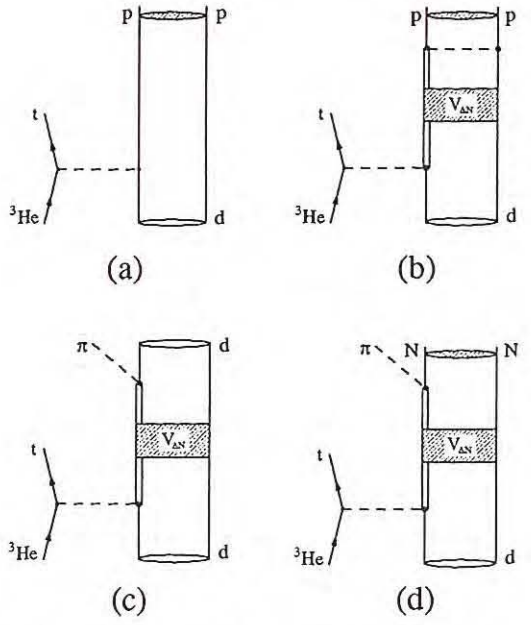

Fig. 1: Reaction mechanisms in the model calculation: (a) impulse approximation, (b) p–wave rescattering, (c) coherent pion production, (d) quasi–free pion production. $V_{\Delta N}$ denotes the residual interaction in the ΔN intermediate system.

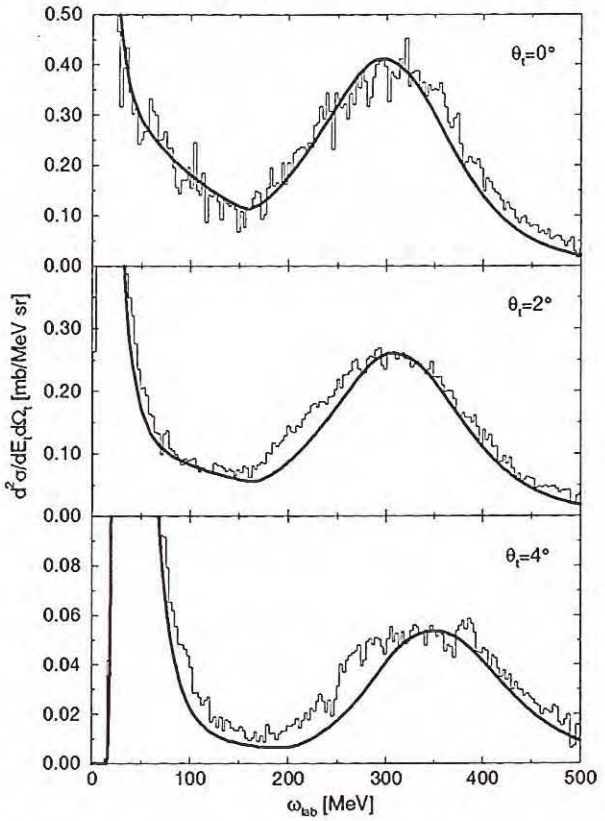

Fig. 2: Inclusive triton spectra $d^2\sigma/dE_t d\Omega_t$ in the reaction d(^{3}He,t) at $T_{\rm He} = 2$ GeV and scattering angles $\theta_t = 0°$, 2° and 4°, respectively. The theoretical result (solid line) is shown as a function of the energy transfer $\omega = E_{\rm He} - E_t$ to the target. The histogram represents the preliminary experimental data [4].

and the right angular dependence of the cross section is obtained. Minor deviations are probably due to the neglection of non–resonant pion production and s–wave rescattering.

References:

[1] C. A. Mosbacher and F. Osterfeld, *Phys. Rev.* C **56**, 2014 (1997)

[2] P. Desgrolard, J. Delorme and C. Gignoux, *Nucl. Phys.* A **544**, 811 (1992)

[3] R. Machleidt, K. Holinde, and C. Elster, *Phys. Rev.* **149**, 1 (1987)

[4] B. Ramstein, IPN Orsay, private communication.

Diffractive production of S and D-wave vector mesons

I.Ivanov[a,b], N.Nikolaev[a,c]

Diffractive virtual photoproduction of vector mesons $\gamma^* + p \to V + p'$, $V = \rho_0, \omega, \phi, J/\Psi, \Upsilon$, in deep inelastic scattering (DIS) at small $x = (Q^2 + m_V^2)/(W^2 + Q^2)$ is a testing ground of ideas on the QCD pomeron exchange and light-cone wave function (LCWF) of vector mesons ([1, 2]). Though theory provides a reasonably accurate qualitative description of the phenomena observed, at some points theoretical predictions seem to systematically deviate from experimental data. In particular, such discrepancy in the value of $R = \sigma_L/\sigma_T$ (L and T stand for the longitudinal and transverse polarizations) has been a long–standing problem. Undoubtedly, the predictive power of theoretical calculations is limited by our inability to treat non-perturbative effects dynamically, however, other sources of disagreement can lurk either in the theoretical approach used or in the data analysis.

One step in this direction has recently been made in [2], where the assumption of the exact s-channel helicity conservation (SCHC), implicitly used in experimental data analysis, was brought under thorough investigation. The full set of helicity amplitudes for transitions $\gamma_L^* \to V_L, \gamma_L^* \to V_T, \gamma_T^* \to V_T, \gamma_T^* \to V_L$ was obtained and significant s-channel non-conserving effects were observed.

In our research we went further and considered another issue, which needed to be improved. Namely, the above approach treated a vector meson as a $q\bar{q}$ Fock state and used to implement the $V\bar{q}q$ vertex in the form $\Gamma_V V_\mu \bar{u}\gamma_\mu u$. Strictly speaking, this type of vertex, being an unjustified assumption, does not reflect the true internal structure of a vector meson LCWF. In other words, this spinor structure describes neither pure S nor pure D-wave vector mesons.

Investigating this issue, we found the way to describe the diffractive production of S and D-wave vector mesons and derived the full sets of helicity amplitudes in both cases.

A general helicity amplitude of a vector meson diffractive production is proportional to

$$A(x, Q^2, \Delta_\perp) \propto \int_0^1 dz \int d^2k_\perp \int \frac{d^2\kappa_\perp}{\kappa^4} \cdot$$
$$\cdot \alpha_S(\max\{\kappa^2, k_\perp^2 + m_V^2\}) \mathcal{F}(x, \kappa_\perp, \Delta_\perp) I(\gamma^* \to V),$$

where k and κ are the internal loop momenta of the quark loop and gluon ladder loop correspondingly and Δ is the momentum transfer. Integration over κ together with $\mathcal{F}(x, \kappa_\perp, \Delta_\perp)$ results in the gluon density. With an appropriate choice of k, the first integration in the above expression can be transformed into integral over $d\mathbf{k}$, where $\mathbf{k}$ is in fact the relative $q\bar{q}$ momentum in the vector meson frame of reference. The only thing by which various helicity amplitudes differ is the integrands $I(\gamma^* \to V)$.

To make the new features of these amplitudes more prominent, we considered the heavy meson case (J/ψ or Υ). In this case, the LCWF of the vector meson which enters $I(\gamma^* \to V)$ varies on a hadronic scale $|\mathbf{k}| \sim R_V^{-1} << m_V$. This means that quarks inside a meson can be safely considered non-relativistic, allowing one to perform the twist expansion in $\overline{Q}^2 = m_q^2 + z(1-z)Q^2$ and analyze the twist structure of the amplitudes.

We found that in the case of S-wave vector mesons, the twist hierarchy repeats that when the $V\bar{q}q$ vertex was naively taken in γ_μ form. However, the quantity σ_L/σ_T differs now from the simple Q^2/m_V^2 dependence.

The similar analysis of a D-wave vector meson uncovers a number of completely novel features. It turns out that after angular averaging over $\mathbf{k}$, the leading contributions cancel out in all amplitudes. Though the reason for such a behavior is quite obvious, the result is that the higher twist contribution begin to play a crucial role in Q^2 dependence of D-wave amplitudes.

Namely, first of all, we found that all four amplitudes become comparable, contrary to the situation known for the γ_μ type of vertex when spin conserving amplitudes dominate.

Then, we found that

$$I(\gamma_L^* \to V_L) \propto \frac{Q}{M} \cdot \frac{1}{15}\left(1 - 8\frac{m_V^2}{Q^2 + m_V^2}\right)$$
$$I(\gamma_T^* \to V_T; \lambda_V = \lambda_\gamma) \propto \left(1 + \frac{4}{15}\frac{m_V^2}{m_V^2 + Q^2}\right),$$

thus making Q^2 dependence of the σ_L/σ_T ratio highly non-trivial. Finally, it is seen that longitudinal transition amplitude changes its sign at moderately large Q^2.

Such a bouquet of new effects looks very intriguing and deserves further careful investigation. In particular, it would be interesting to analyze the truly relativistic ρ system.

[a]Institut für Kernphysik, Forschungszentrum Jülich GmbH,
[b]Novosibirsk University, Novosibirsk, Russia
[c]L. D. Landau Institute for Theoretical Physics, GSP-1, 117940, ul. Kosygina 2, Moscow 117334, Russia

References:

[1] N.N.Nikolaev, *Comments on Nucl. Part. Phys.* **21**(1992) 41; B.Z.Kopeliovich, J.Nemchik, N.N.Nikolaev and B.G.Zakharov, *Phys. Lett.* **B309** (1993) 179; B.Z.Kopeliovich, J.Nemchik, N.N.Nikolaev and B.G.Zakharov, *Phys. Lett.* **B324** (1994) 469.

[2] E.V.Kuraev, N.N.Nikolaev, and B.G.Zakharov, hep-ph/9809539.

SECONDARY REGGEONS IN DIFFRACTIVE DEEP INELASTIC SCATTERING - THE MICROSCOPIC QCD EVALUATION

W. Schäfer, N.N. Nikolaev

The secondary Regge trajectories (f, ω, ρ, A_2) are well known from the phenomenology of soft hadronic reactions at high energies. For example the cross sections for processes that involve the exchange of non-vacuum quantum numbers are governed by the t-channel reggeon-exchanges and exhibit an energy dependence like $d\sigma/dt|_{t=0} \propto (s/s_0)^{2\Delta_R}$, with an almost universal intercept $\Delta_R \simeq -0.5$. Hadronic total cross sections are well described by Regge-parametrizations of the form $\sigma_{tot}(ab) = \sigma_{I\!P}(s/s_0)^{\epsilon_{I\!P}} + \sigma_R(s/s_0)^{\epsilon_R}$ with $\epsilon_R \simeq -0.5, \epsilon_{I\!P} \simeq 0.1$. Also for the inclusive hadronic reactions there exists a successful Regge-phenomenology [1], which has recently been extended to diffractive DIS[2, 3]. For diffraction dissociation of the hadronic projectile $ap \to pX$ the large Regge parameter is $1/x_{I\!P} = s/M^2$, and there appear the forward scattering amplitudes for $a{I\!P} \to a{I\!P}, aR \to aR$, as well as an interference amplitude $a{I\!P} \to aR$. In DIS the projectile a is the virtual photon γ^* and one readily introduces the pomeron and reggeon structure functions $F_{2{I\!P},R}(x, Q^2) = Q^2/(4\pi^2\alpha_{em}) \cdot \sigma(\gamma^* {I\!P}, R)$ and the interference structure function $F_{2R{I\!P}}(x, Q^2) = Q^2/(4\pi^2\alpha_{em}) \cdot \Sigma(\gamma^* R \to \gamma^* {I\!P})$. For $x_{I\!P} > 0.1$ the secondary trajectories take over, and the effective intercept Δ_{eff}, that parametrizes the local $x_{I\!P}$ behaviour approaches the pomeron intercept for $x_{I\!P} \to 0$ and decreases in the region of large $x_{I\!P} > 0.1$ where the secondary exchanges dominate. Such a behaviour has been seen by H1 in diffractive DIS [4]. Not much is known in the literature about the importance of the pomeron-reggeon interference term: Triple-Regge fits to hadronic data are not conclusive. If one adopts the naive point of view that one can attribute the hadronic (particle-) state vectors to the pomeron and reggeon one may be mislead to conclude that such interference amplitudes should vanish. For the orthogonality of state vectors $\langle R|{I\!P}\rangle = 0$ implies vanishing parton number and momentum integrals [2, 6], which suggests a strong suppression of such interference SF's. However we could demonstrate, that such a reasoning is not borne out by pQCD. In a DGLAP approximation we obtain the following result for the diffractive structure function [5]:

$$F_2^{D(3)}(x_{I\!P}, \beta, Q^2) \propto \beta(1-\beta)^2\alpha_S^2(\bar{Q}^2) \times \left|\eta_{I\!P} G(x_{I\!P}, \bar{Q}^2) + \eta_R \frac{C_F}{2\pi\alpha_R} x_{I\!P} v(x_{I\!P}, \bar{Q}^2)\right|^2,$$

where the hardness scale $\overline{Q}^2 = (m_q^2 + \vec{k}_\perp^2)/(1-\beta)$ and for large β one is safe in the pQCD domain [8]. Let us discuss the salient features of this equation: first we see now explicitly that there are no extra suppression factors whatsoever for the $R{I\!P}$–interference. It enters in the *maximal possible way.* Second, the β-dependence is a universal $(1-\beta)^2$ for the pomeron, reggeon and the interference structure function. In particular, the reggeon structure function differs from the common theoretical guesses $F_{2\pi} \sim (1-\beta)$ for the pion structure function in the large β region. Third we encountered the manifest leading twist effect. For the longitudinal photons there will emerge the twist four effect in much the same way as it was discussed first by Genovese et al.[8] for the pomeron. Fourth our knowledge of the valence and gluon structure functions implies that the result is in the correct order in magnitude with what can be expected from the analysis of the H1 data [2, 3].

A final comment on possible applications is in order: the theoretical understanding of the reggeon and inteference contributions has important impact on the theory of the nuclear shadowing of the valence quark densities, a topic which has not been adressed before. Vice versa the phenomenology of nuclear shadowing puts much constraint on the diffractive production mechanisms. For instance we have found that the much discussed hard gluon dominated pomeron favoured by the DGLAP fits to the H1 data yields an unacceptably large shadowing of the deuteron gluon density [9]. A different option for the pomeron structure function where quarks and gluons share the momentum of the pomeron in about equal fractions, as it emerges from the colour dipole calculations of Nikolaev and Zakharov, (which are incorporated in the above presented evaluations of the pomeron contribution) gives the correct amount of gluon shadowing.

References:

[1] A.B. Kaidalov, *Phys. Rep.* **50**, 157 (1979)

[2] N.N. Nikolaev, W.Schäfer, and B.G. Zakharov, hep-ph 9608338.

[3] H1 Collab.:C. Adloff et al., *Z. Phys.* C **76**, 613 (1997)

[4] H1 Collab.:P. Newman, proceedings of DIS96

[5] W. Schäfer, to appear in the proceedings of DIS98, Brussels; N.N. Nikolaev and W. Schäfer, paper in preparation.

[6] M.Kh. Khankhasayev et al. *Z. Phys.* A **359**, 191 (1997)

[7] N.N. Nikolaev and B.G. Zakharov, *Z. Phys.* C **64**, 631 (1994), *Phys. Lett.* B **332**, 177 (1994)

[8] M. Genovese, N.N. Nikolaev and B.G. Zakharov,*Phys. Lett.* B **380**, 213 (1996), M. Bertini et al. *Phys. Lett.* B **422**, 238 (1998)

[9] W. Schäfer; to appear in the proceedings of DIS98(WG4-Spin physics).

Do the E866 Drell Yan data change our picture of the chiral structure of the nucleon ?

N.N. Nikolaev, W. Schäfer, A. Szczurek(Cracow), and J. Speth

The violation of the Gottfried Sum Rule discovered by the NMC collaboration at CERN in muon deep inelastic scattering [1] opened the long ongoing discussion on the $\bar{d} - \bar{u}$ asymmetry in the nucleon. Extending and following the early work of Sullivan [4], the asymmetry can be naturally explained within the framework of the isovector meson cloud model of the nucleon (for recent reviews see [5, 6] and references therein), which uniquely predicted the asymmetry to be placed at large x, in good agreement with the early NA51 Drell-Yan experiment [2]. In the practical evaluation the dominant contribution can be interpreted as due to the admixture of the πN and $\pi\Delta$ Fock-states in the physical proton.

A recent E866 experiment at Fermilab [10] has reported the first high precision mapping of the x-dependence of the $\bar{u} - \bar{d}$ asymmetry from the comparison of the pp and pd Drell-Yan production with the striking finding that the difference of the $\bar{u}$ and $\bar{d}$ distributions seems to vanish at large $x \gtrsim 0.3$

Such a behaviour was not predicted by the earlier meson cloud model calculations (see e.g. [5]), and thus it calls for a more thorough investigation of the finer details of the meson-nucleon Fock state wave functions.

In an extensive analysis [7] we have revisited the evaluation of the pionic mechanism of the $\bar{u} - \bar{d}$ asymmetry in the proton structure function. As in earlier work [8, 9] our strategy is to exploit the close relationship between the hadronic $pp \to hX$ ($h = n, \Delta, \pi$) and deep inelastic $\gamma^* p \to hX$ inclusive production of forward hadrons. The parameters of the nonperturbative production mechanisms (π, ρ, a_2 -exchanges) in DIS are determined through an analysis of the corresponding hadronic reactions.

Here we improve upon the earlier work in several aspects: for example we treat the ρ, a_2-exchanges as reggeized, which is more appropriate than the particle-exchange formalism used in [9]. Apart from allowing a better description of the hadronic inclusive production, there is another crucial property of the secondary Reggeon exchanges with intercept $\alpha(0) \approx 1/2$ (e.g. ρ, a_2). As is argued in [7], despite of the important role of the ρ, a_2-exchanges in the population of the $nX, \Delta X$ inclusive channels, the opening of the nX and ΔX intermediate states via Reggeon exchange leads to a negligible contribution to hadronic total cross section and/or the structure funtions in DIS. This emerges as a consequence of the unitarity relation (the extended AGK [11] rule) and the specific Regge-phase. As a consequence, the isovector Reggeon contribution to the Gottfried Sum Rule violation is also negligible.

There is another issue, which did not receive due attention in the previous work. The application of the Regge phenomenology to the production of forward neutrons and Δ's only allows to constrain the large-z behaviour of the relevant vertex-functions (z is the fraction of the proton's lightcone-momentum carried by the struck meson). For the region of smaller z one must look into another constraint, here the light-cone wave function formalism offers an intimate relationship between the flux of mesons originating from a meson-baryon MB-Fock state and the corresponding flux of baryons. Clearly, if $f_{M/B}(z_M)$ denotes the probability to find in the MB-Fock state a meson M carrying the (light-cone) momentum fraction z_M and if $f_{B/M}(z_B)$ has the analogous meaning of finding the baryon B, carrying momentum z_B, it must hold true that $f_{M/B}(z) = f_{B/M}(1-z)$. Figure (1) shows that the earlier calculation [9] leads to a quite dramatic overprediction of the forward pion production cross section. We show also the results for several options for the πNN -Formfactor, which resolve the contradiction. In figure 2 we show our description of the inclusive neutron production, which includes in addition to the pion exchange also the background contributions from the reggeized ρ, a_2 exchange and from two step processes $p \to \Delta \to n$. A very good agreement is found, this is also true for the $p_\perp^2$-dependent inclusive spectra not shown here [7]. Due to a lack of precision data, the parameters of the $\pi N\Delta$-vertex cannot be detrmined in a satisfactory manner. However one may relate the ρ, a_2-exchange background contributions in the inclusive neutron and Δ channels. This allows one to put some constraints on the strength of the $\pi\Delta$-Fock state contribution. Having determined the relevant parameters in this manner, one may proceed to the calculation of the $\bar{d} - \bar{u}$ asymmetry in the proton structure function, which is entirely exhausted by the nonperturbative πN and $\pi\Delta$ Fock state contributions. In Fig.3 we display $\bar{d}(x) - \bar{u}(x)$ as obtained in the present analysis and compare it to the recent result of the NuSea collaboration [10]. The $\pi\Delta$ contribution (dashed line) becomes important only at rather small values of Bjorken-x which is due to rather soft form factor as suggested by the analysis of leading Δ isobars. Our analysis clearly demonstrates that it is possible to construct the pion flux factor consistent with both hadronic and Drell-Yan data, provided the background processes in hadronic reactions are taken carefully into account.

Let us finally comment on the violation of the Gottfried sum rule. We obtain a number of pions in the proton in the πN Fock state of $n_{\pi N} = 0.21 \div 0.28$. For the $\pi\Delta$ Fock state, we estimate $n_{\pi\Delta} = 0.03$. For the Gottfried integral we obtain correspondingly $S_G = 0.215 \div 0.247$. The value reported by NMC is $S_G = 0.235 \pm 0.026$ [1] which is perfectly consistent with our result.

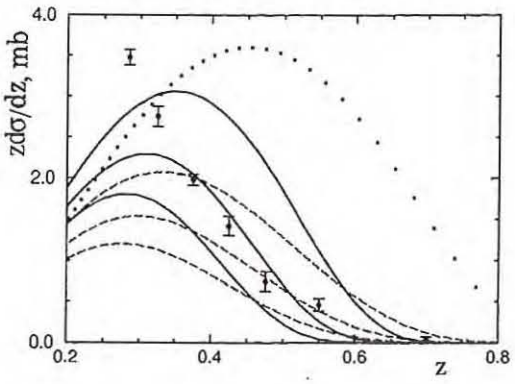

Fig. 1: *Differential cross section* $zd\sigma/dz(pp \to \pi^0 X)$ *at* $p_{LAB} = 400\ GeV/c$. *The data are taken from [12]. The dotted curve shows a prediction of the model [9]. The solid curves were calculated with a 'Gaussian' form factor* $F_{\pi NN}(t) = \exp(-\left[R_G^2(t - m_\pi^2)\right]^2)$. *The curves in the figure correspond to* $R_G^2 = 1.0, 1.5, and\ 2.0\ GeV^{-2}$ *(from top to bottom). The dashed curves were calculated with an exponential form factor* $F_{\pi NN}(t) = \exp(R_E^2(t - m_\pi^2))$. *The curves in the figure are for* $R_E^2 = 1.0, 1.5, and\ 2.0\ GeV^{-2}$ *(from top to bottom).*

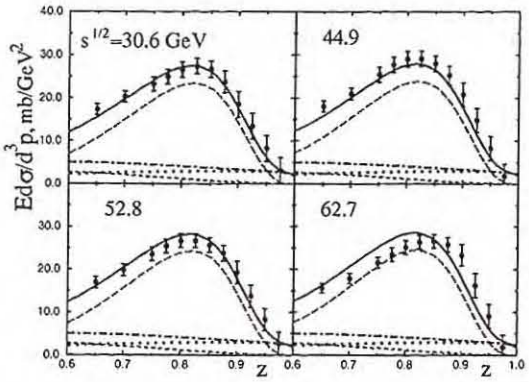

Fig. 2: *Invariant cross section for the reaction* $pp \to nX$ *as a function of* z *for* $p_\perp^2 = 0$. *The long dashed curve shows the contribution from the pion exchange; the dotted curve is the* ρ, a_2*-exchange contribution, and the dashed curve shows the contribution from the two-step process* $p \to \Delta \to n$. *In addition we present the sum of the two background contributions as the dot-dashed line. The solid curve represents the sum of all components. The experimental data are taken from [13].*

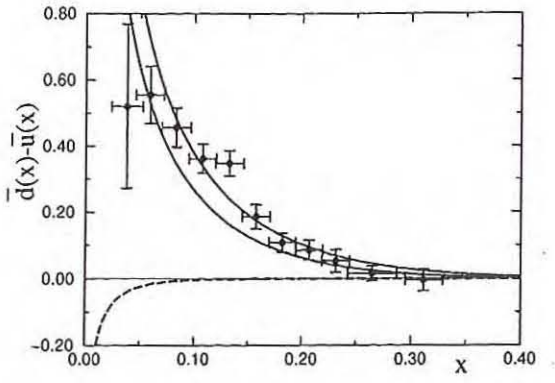

Fig. 3: *Flavour asymmetry* $\bar{d}(x) - \bar{u}(x)$ *at* $Q^2 = 54\ GeV^2$. *Experimental data are from E866 [10]. The solid curves show the contribution from the* πN*-Fock state and were calculated for Gaussian form-factors; the upper curve belongs to* $R_G^2 = 1\ GeV^{-2}$, *the lower one to* $R_G^2 = 1.5\ GeV^{-2}$ *The dashed line shows the contribution of the* $\pi\Delta$*-Fock state, calculated for an exponential form factor with* $R_\Delta^2 = 2\ GeV^{-2}$.

References:

[1] P. Amaudruz et al., Phys. Rev. Lett. **66** (1991) 2712.

[2] A. Baldit et al., Phys. Lett. **B332** (1994) 244.

[3] E.A. Hawker et al., Phys. Rev. Lett. **80** (1998) 3715.

[4] J.D. Sullivan, Phys. Rev. **D5** (1972) 1732.

[5] J. Speth and A.W. Thomas, Adv. in Nuclear Physics Vol.**24** (1998) 84.

[6] S. Kumano, Phys. Rep. **303** (1998) 183.

[7] N.N. Nikolaev, W. Schäfer, A. Szczurek, and J. Speth, 'Do the E866 Drell Yan data change our picture of the chiral structure of the nucleon ?'; e-print archives hep-ph/9812266.

[8] V.R. Zoller, Z. Phys. **C53** (1992) 443.

[9] H. Holtmann, A. Szczurek and J. Speth, Nucl. Phys. **A596** (1996) 631.

[10] E.A. Hawker et al., Phys. Rev. Lett. **80** (1998) 3715.

[11] V.A. Abramovskii, V.N. Gribov and O.V. Kancheli, Sov. J. Nucl. Phys. **18** (1974) 308.

[12] M. Aguilar-Benitez et al., Z. Phys. **C50** (1991) 405.

[13] W. Flauger and F. Mönnig, Nucl. Phys. **B109** (1976) 347.

Diffractive vector mesons beyond the s-channel helicity conservation

E.V. Kuraev[1)], N.N. Nikolaev [2,3)] and B.G. Zakharov[3)]

Diffractive production of vector mesons $\gamma^* + p \to V + p'$, $V = \rho_0, \omega, \phi, J/\Psi, \Upsilon$, in deep inelastic scattering (DIS) at small $x = (Q^2 + m_V^2)/(W^2 + Q^2)$ is a testing ground of ideas on the QCD pomeron exchange and light-cone wave function (LCWF) of vector mesons ([1, 2, 3, 4, 5], for the recent review see [6]). It is a self-analyzing process because the helicity amplitudes can be inferred from vector meson decay angular distributions. The published experimental data analyses suffer from an unwarranted assumption of an exact of s-channel helicity conservation (SCHC) [6], which needs a theoretical scrutiny.

We report here a derivation of the full set of helicity amplitudes for transitions $\gamma_L^* \to V_L, \gamma_L^* \to V_T, \gamma_T^* \to V_T, \gamma_T^* \to V_L$ for all flavours and small to moderate momentum transfer $\vec{\Delta}$ within the diffraction cone. We find substantial s-channel helicity non-conserving (SCHNC) effects similar to the SCHNC LT interference found earlier by Pronyaev and two of the present authors (NNN and BGZ) for diffraction $\gamma^* p \to p' X$ into continuum states X [7].

We treat vector mesons as $q\bar{q}$ states with the Vqq vertex $\Gamma_V V_\mu \bar{u}\gamma_\mu u$, Γ_V is related to the radial LCWF of the $q\bar{q}$ Fock state of the vector meson as

$$\psi_V(z,\vec{k}) = \frac{\Gamma_V(z,\vec{k})}{D(m_V^2, z, \vec{k})}, \qquad (1)$$

where $D(\vec{k}^2) = \vec{k}^2 + m_q^2 - z(1-z)m_V^2$. The corresponding quantity for photons, $\psi_\gamma(z,\vec{k}) = 1/D(-Q^2, z, \vec{k})$ only differs by the substitution $\Gamma_\gamma(z,\vec{k}) = 1$ and $m_V^2 \to -Q^2$. The standard Sudakov technique leads to virtual photoproduction amplitude of the form

$$A(x,Q^2,\vec{\Delta}) = is\frac{C_F N_c c_V \sqrt{4\pi\alpha_{em}}}{2\pi^2}\int_0^1 dz \int d^2\vec{k} \int \frac{d^2\vec{\kappa}}{\kappa^4}\alpha_S \mathcal{F}(x,\vec{\kappa},\vec{\Delta})\psi_V(z,\vec{k}) I_{\lambda_V\lambda_\gamma}, \qquad (2)$$

where $N_c = 3$ is the number of colors, $C_F = \frac{N_c^2-1}{2N_c}$ is the Casimir operator, $C_V = \frac{1}{\sqrt{2}}, \frac{1}{3\sqrt{2}}, \frac{1}{3}, \frac{2}{3}$ for the $\rho^0, \omega^0, \phi^0, J/\Psi$ mesons, α_S and α_{em} are the strong and electromagnetic couplings, respectively. For small $\vec{\Delta}$ within the diffraction cone

$$\mathcal{F}(x,\vec{\kappa},\vec{\Delta}) = \frac{\partial G(x,\kappa^2)}{\partial \log\kappa^2}\exp(-\frac{1}{2}B_{3I\!P}\vec{\Delta}^2). \qquad (3)$$

where $\partial G/\partial\log\kappa^2$ is the conventional unintegrated gluon structure function and, modulo to a slow Regge growth, the diffraction cone $B_{3I\!P} \sim 6$ GeV^{-2} [5].

Notice that $\psi_V(z,\vec{k})$ varies on a hadronic scale $k^2 \sim R_V^{-2}$, where R_V is a radius of the vector meson, whereas $\psi_\gamma(z,\vec{k})$ is a slow function which varies on a large pQCD scale

$$\overline{Q}^2 = m_q^2 + z(1-z)Q^2. \qquad (4)$$

which allows a systematic twist expansion in powers of $1/\overline{Q}^2$ for Δ within the diffraction cone. In all cases but the double helicity flip the dominant twist amplitudes come from the leading $\log\overline{Q}^2$ (LL$\overline{Q}^2$) region of $\vec{k}^2 \sim R_V^{-2}, \vec{\Delta}^2 \ll \vec{\kappa}^2 \ll \overline{Q}^2$. After some algebra we find

$$I_{0L} = -\frac{Q}{m_V}\cdot\frac{8z(1-z)[m_q^2+\vec{k}^2]}{\overline{Q}^4}\cdot\vec{\kappa}^2, \qquad (5)$$

$$I_{\pm\pm} = 2(\vec{V}^*\vec{e})\cdot\frac{m_q^2+2[z^2+(1-z)^2]\vec{k}^2}{\overline{Q}^4}\cdot\vec{\kappa}^2, \qquad (6)$$

$$I_{\pm L} = -8\frac{(\vec{V}^*\vec{\Delta})Q}{\overline{Q}^2}\cdot\frac{z(1-z)(1-2z)^2}{\overline{Q}^4}\cdot\vec{k}^2\cdot\vec{\kappa}^2, \qquad (7)$$

$$I_{L\pm} = -4\frac{(\vec{e}\vec{\Delta})}{M}\cdot\cdot\frac{[m_q^2+\vec{k}^2](1-2z)^2}{\overline{Q}^4}\cdot\vec{\kappa}^2. \qquad (8)$$

$$I_{\pm\mp} = 2(\vec{V}^*\vec{\Delta})(\vec{e}\vec{\Delta})\cdot\frac{z(1-z)}{\overline{Q}^4} \times\left[6(1-2z)^2\frac{\vec{\kappa}^2}{\overline{Q}^2}+1\right]\vec{k}^2. \qquad (9)$$

In all cases when $I(\gamma^* \to V) \propto \kappa^2$ the LL$\overline{Q}^2$ approximation is at work, the gluon structure function enters the integrand in the form

$$\int^{\overline{Q}^2}\frac{d\kappa^2}{\kappa^2}\frac{\partial G(x,\kappa^2)}{\partial\log\kappa^2} = G(x,\overline{Q}^2) \qquad (10)$$

and after the z integration one finds that the helicity amplitudes will be proportional to $\alpha_S(Q_V^2)G(x,Q_V^2)$, where the pQCD hard scale

$$Q_V^2 \sim (0.1-0.2)(Q^2+m_V^2) \qquad (11)$$

can depend on helicities because of the different endpoint contributions from $z \to 0$ and $z \to 1$ where the running hardness $\overline{Q}^2$ is small [2, 4]. This issue and the sensitivity of helicity amplitudes to the LCWF of vector mesons will be discussed elsewhere. Here we cite our results for the dominant twist SCHC and single-flip SCHNC amplitudes $A_{\lambda_V\lambda_\gamma}$ in the helicity basis:

$$A_{0L} \propto \frac{Q}{m_V}\cdot\frac{\alpha_S(Q_V^2)}{(Q^2+m_V^2)^2}\cdot G(x,Q_V^2), \qquad (12)$$

$$A_{\pm\pm} \propto \frac{\alpha_S(Q_V^2)}{(Q^2+m_V^2)^2}\cdot G(x,Q_V^2), \qquad (13)$$

$$A_{\pm L} \propto \frac{\Delta}{m_V}\cdot\frac{\alpha_S(Q_V^2)}{(Q^2+m_V^2)^2}\cdot G(x,Q_V^2), \qquad (14)$$

$$A_{0\pm} \propto \frac{Q}{m_V}\cdot\frac{m_V\Delta}{Q^2+m_V^2}\cdot\frac{\alpha_S(Q_V^2)}{(Q^2+m_V^2)^2}\cdot G(x,Q_V^2), \qquad (15)$$

First, all above amplitudes are pQCD calculable for large Q^2 and/or heavy vector mesons. Second, the

factor Q/m_V in the longitudinal photon amplitudes (12) and (14) is a generic consequence of gauge invariance irrespective of the detailed production dynamics. Third, the longitudinal Fermi momentum of quarks is $k_z \sim \frac{1}{2}m_V(2z-1)$ and eqs. (7),(8) make it obvious that single-helicity flip requires a longitudinal Fermi motion of quarks and vanishes in the nonrelativistic limit. Similarly, double-helicity flip requires the transverse Fermi motion of quarks. Fourth, the leading SCHNC effect is an interference of A_{0L} and $A_{0\pm}$ and the first experimental indications for that have been reported recently [8].

In contrast to the above, the dominant twist double-helicity flip amplitude comes from the non-leading-$\log\overline{Q}^2$ term 1 in the square brackets in (9) and is proportional to

$$\int^{\overline{Q}^2} \frac{d\kappa^2}{\kappa^4}\frac{\partial G(x,\kappa^2)}{\partial \log\kappa^2} \sim \frac{1}{\mu_G^2}G(x,\mu_G^2) \qquad (16)$$

where a soft scale $\mu_G \sim 0.7$-1 GeV is set by the inverse radius of propagation of perturbative gluons. Precisely the same nonperturbative quantity (16) describes the contribution from the $\gamma^* \to V$ transition vertex to the diffraction slope for helicity-non-flip amplitudes, for more discussion see [5]. Then from eq. (8) we find

$$A_{\pm\mp} \propto \Delta^2 \cdot \frac{\alpha_S(Q_V^2)}{(Q^2+m_V^2)^2} \times \left[\frac{6G(x,Q_V^2)}{Q^2+m_V^2}\cdot\frac{\langle k_z^2\rangle}{4m_V^2} + \frac{G(x,\mu_G^2)}{\mu_G^2}\right], \qquad (17)$$

where the leading $\log\overline{Q}^2$ amplitude is of higher twist. Such a mismatch of the twist and leading $\log\overline{Q}^2$ regime in diffractive DIS is déjà vu: the leading twist σ_T is soft-gluon dominated whereas the full fledged $\log\overline{Q}^2$ is at work for the higher twist σ_L [9, 10]. What is new in (17) is that the both regimes mix in one and the same helicity amplitude. The soft-gluon exchange dominance of the leading twist double-helicity flip was noticed recently by Ivanov and Kirschner [11].

Finally, we emphasize that non-vanishing single- and double-helicity flip amplitudes (14) and (16) do not require the applicability of pQCD and can best be searched for in real photo- or electroproduction at small $Q^2 \lesssim m_V^2$.

EAK is grateful to Institute für Kernphysik of Forschungszentrum Jülich for the hospitality. The work of EAK and BGZ has been supported partly by the INTAS Grants 93-0239 and 96-0597, respectively.

[1)]Laboratory for Theoretical Physics, JINR, 141980 Dubna, Moscow Region, Russia

[2]IKP(Theorie), KFA Jülich, D-52428 Jülich, Germany [3]L. D. Landau Institute for Theoretical Physics, GSP-1, 117940, ul. Kosygina 2, Moscow 117334, Russia

References:

[1] N.N.Nikolaev, *Comments on Nucl. Part. Phys.* **21** (1992) 41; B.Z.Kopeliovich, J.Nemchik, N.N.Nikolaev and B.G.Zakharov, *Phys. Lett.* **B309** (1993) 179; B.Z.Kopeliovich, J.Nemchik, N.N.Nikolaev and B.G.Zakharov, *Phys. Lett.* **B324** (1994) 469.

[2] J.Nemchik, N.N.Nikolaev and B.G.Zakharov, *Phys. Lett.* **B341** (1994) 228;

[3] D.Yu.Ivanov, *Phys. Rev.* **D53** (1996) 3564; I.F.Ginzburg, D.Yu.Ivanov, *Phys. Rev.* **D54** (1996) 5523; I. Ginzburg,S. Panfil and V. Serbo, *Nucl.Phys.* **B284** (1987) 685; **B296** (1988) 569.

[4] J.Nemchik, N.N.Nikolaev, E.Predazzi and B.G.Zakharov, *Z. Phys.* **C75** (1997) 71.

[5] J. Nemchik, N.N.Nikolaev, E.Predazzi, B.G.Zakharov and V.R.Zoller, *J. Exp. Theor. Phys.* **86** (1998) 1054.

[6] J. Crittenden, Springer Tracts in Modern Physics, vol.140 (Springer, Berlin, Heidelberg, 1997).

[7] N.N.Nikolaev, A.Pronyaev and B.G.Zakharov, e-Print Archive: hep-ph/9812212

[8] The reports by ZEUS, H1 and HERMES collaborations at 29th International Conference on High Energy Physics (ICHEP-98), 23-29 July 1998 , Vancouver, Canada.

[9] N.N.Nikolaev and B.G.Zakharov, *Phys. Lett.* **B332** (1994) 177; *Z. Phys.* **C53** (1992) 331.

[10] M. Genovese, N.N. Nikolaev and B.G. Zakharov, *Phys.Lett.* **B380** (1996) 213.

[11] D. Ivanov and R. Kirschner, hep-ph/9807324.

Azimuthal asymmetry as a new handle on σ_L/σ_T in diffractive DIS

N.N. Nikolaev[a,b], A.V. Pronyaev[c], B.G. Zakharov[b]

The ratio of (L) longitudinal and (T) transverse cross sections, $R = \sigma_L/\sigma_T$, is a much discussed test of mechanisms of deep inelastic scattering (DIS). The QCD theory of diffractive DIS (DDIS) $ep \to e'p'X$ predicts [1] an unprecedented dominance of higher twist σ_L^D over leading twist σ_T^D in a broad range of $\beta \gtrsim 0.9$ (Hereafter the superscript D stands for "diffractive" and the electron inelasticity y, the $\gamma^* p$ c.m.s. energy W, Q^2, $x = Q^2/(Q^2+W^2)$, the mass M of the diffractive system X, $\beta = Q^2/(Q^2+M^2)$ and $x_{I\!P} = x/\beta$ are the standard DDIS variables). This must be contrasted to leading twist σ_L in small-x inclusive DIS where the theory predicts [2] $R = \sigma_L/\sigma_T \sim 0.2$-$0.3$ in agreement with the experiment [3]. The pQCD calculations of σ_L^D describe the experimental data for large β very well [4] and higher twist σ_L^D found in [1] has become a part of modern parameterizations of DDIS structure functions (SF's) [5]. However, a direct measurement of R^D requires a variable electron/proton energy runs which are not foreseen in the near future at HERA. Here below we show how this experimental limitation can be circumvented by the measurement of the LT interference SF F_{LT}^D which contributes to the observed cross section a term $\propto \cos\phi$, where ϕ is an azimuthal angle ϕ between the electron scattering and proton production planes.

The principal point is as follows. The experimental measurement of the asymmetry $\propto \cos\phi$ amounts to the determination of

$$A_{LT} = \frac{F_{LT}^D}{F_T^D + F_L^D} = \frac{\rho_{LT}}{1+R^D}\,. \qquad (1)$$

If $\rho_{LT} = F_{LT}^D/F_T^D$ were known, then inversion of (1) would yield

$$R^{D(4)} = \frac{\rho_{LT}}{A_{LT}} - 1\,. \qquad (2)$$

We argue that for $\beta \gtrsim 0.9$ of the interest the theoretical evaluations of ρ_{LT} are model-independent and the inversion (2) offers a viable test of the pQCD prediction $R^D \gtrsim 1$ from the experimentally measured azimuthal asymmetry A_{LT}.

The microscopic QCD mechanism of DDIS at $\beta > 0.9$ is an excitation of $q\bar{q}$ Fock states of the photon (we focus on continuum $M^2 \gg 4m_f^2$)[6, 7]. Our new finding is that σ_{LT}^D is dominated by the same aligned jet configurations as σ_T^D. Consequently, we expect similar hard QCD scales

$$\langle\overline{Q}^2\rangle_{LT} \approx \langle\overline{Q}^2\rangle_T\,, \qquad (3)$$

which is a basis for our conclusion on the model-independence of ρ_{LT}:

$$\rho_{LT}(\beta,\Delta) = \qquad (4)$$
$$\frac{24\beta^3(2-3\beta)}{(1-\beta)(3+4\beta+8\beta^2)}\cdot\frac{\Delta}{Q}\cdot\exp(-[B_{LT}-B_T]\vec{\Delta}^2)\,,$$

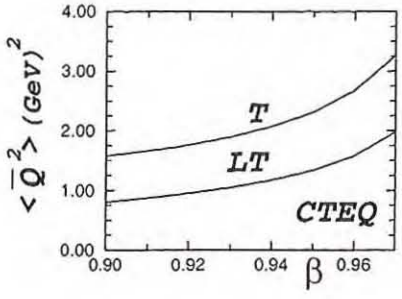

Fig. 1: The average hard scale $\langle\overline{Q}^2\rangle$ for light flavour contribution to the (T) transverse and LT interference diffractive structure functions evaluated for the CTEQ gluon SF of the proton.

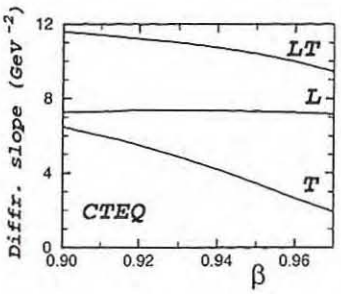

Fig. 2: Our predictions for the diffraction slopes B_T, B_L, B_{LT} of the transverse, longitudinal and LT interference diffractive SF's for the CTEQ gluon SF of the proton ($x_{I\!P} = 10^{-3}$, $Q^2 = 100$ GeV^2).

in which the *r.h.s.* depends on neither $x_{I\!P}$ nor Q^2 (apart from the trivial kinematical factor Δ/Q). The average value of the running hard scale can be estimated calculating the expectation values of $(\overline{Q}^2)^\gamma$. For heavy flavours and weak scaling violations in the gluon structure SF these moments can be evaluated analytically with the result $\langle\overline{Q}^2\rangle_T = \left(\frac{6}{5}\right)^2\langle\overline{Q}^2\rangle_{LT}$ for typical $\gamma = \frac{1}{2}$. Numerical claulations for light flavours give the results shown in fig. 1, the slight inequality $\langle\overline{Q}^2\rangle_T \approx 1.6\langle\overline{Q}^2\rangle_{LT}$ is similar to that for heavy flavours and does not affect our major argument.

The calculation of the diffraction slopes $B_{L,T}$ and B_{LT} can be done following our work [8]. The variations of diffraction slopes from CTEQ to GRV to MRS parameterizations do not exceed ~ 5 per cent and are not shown in fig. 2.

The predicted azimuthal asymmetry A_{LT} for the Δ-intregrated cross section is shown in fig. 3. It is sub-

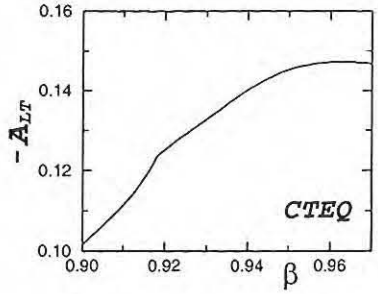

Fig. 3: Our predictions for the β dependence of the azimuthal asymmetry A_{LT} for the Δ-integrated cross sections evaluated using the diffraction slopes of fig. 3 ($x_{\mathbb{P}} = 10^{-3}$, $Q^2 = 100$ GeV^2, CTEQ gluon SF of the proton).

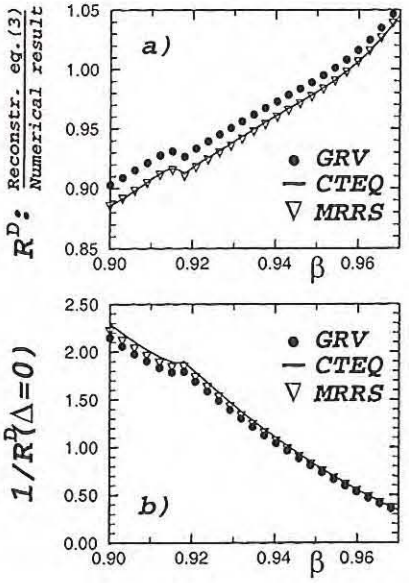

Fig. 4: a) A comparison of the $R^D = \sigma_L/\sigma_T$ reconstructed from azimuthal asymmetry of fig. 3 using eqs. (3) and approximation (17) for ρ_{LT} with the direct numerical evaluation of R^D for the GRV, CTEQ and MRRS gluon SF of the proton. b) Our numerical predictions for $R^D(\Delta = 0)$ in forward DDIS for the same set of gluon SF's of the proton ($x_{\mathbb{P}} = 10^{-3}$, $Q^2 = 100$ GeV^2).

stantial and within the reach of the LPS experiments at HERA. For $Q^2 \sim 50$ GeV^2 for which $\beta \sim 0.95$ does still belong to the continuum, the expected asymmetry is $\approx 50\%$ larger. The cusp-like behaviour at $\beta = \beta_c = Q^2/(Q^2 + 4m_c^2) \approx 0.92$ is due to the open charm excitation at $\beta < \beta_c$.

The accuracy of reconstruction (2) of $R^D = \sigma_L^D/\sigma_T^D$ can be judged from fig. 4a. Here we show the ratio of R^D reconstructed from the numerically calculated azimuthal asymmetry A_{LT} on the basis of analytic approximation (5) for ρ_{LT} to the direct numerical result for R^D presented in fig. 4b (for the convenience of plotting, in fig. 4b we show the inverse quantity $1/R^D(\Delta = 0)$). The reconstruction errors do dot exceed dozen per cent and this accuracy of our reconstruction of R^D is adequate for a reliable check of the pQCD predictions of large R^D at $\beta \gtrsim 0.9$.

We emphasize the Q^2 independence of $\langle\overline{Q}^2\rangle_{LT}$ and $\langle\overline{Q}^2\rangle_T$ by which ρ_{LT} does not depend on Q^2. Consequently, our method allows a reliable experimental determination of the Q^2 dependence of R^D and an unambiguous test of the higher twist nature of σ_L^D.

The work of B.G.Z. has been supported partly by the INTAS grant 96-0597 and the work of A.V.P. was supported partly by the US DOE grant DE-FG02-96ER40994.

[a]IKP(Theorie), FZ Jülich, 5170 Jülich, Germany.
[b]D. Landau Institute for Theoretical Physics, GSP-1, 117940, ul. Kosygina 2, Moscow V-334, Russia.
[c]Virginia Polytechnic Institute and State University, Blacksburg, VA 24061-0435, USA.

References:

[1] Genovese M., N.Nikolaev and B.Zakharov, *Phys.Lett.* **B380**, 213 (1996).

[2] N. N. Nikolaev and B.G.Zakharov, *Phys. Lett.* **B327**, 149 (1994); **B327**, 157 (1994).

[3] H1 Collab., C. Adloff, S. Aid, M. Anderson, V. Andreev, B. Andrieu et al., *Phys. Lett.* **B393**, 452 (1997); E140X Collab., L.H. Tao, L. Andivahis, P. Anthony, R. Arnold et al. *Z. Phys.* **C70** 387 (1996); E143 Collab., K. Abe, T. Akagi, P.L. Anthony, R. Antonov et al., **SLAC-PUB-7927**, Aug 1998, hep-ex/9808028.

[4] Bertini M., M. Genovese, N.N. Nikolaev, A.V. Pronyaev and B.G. Zakharov, *Phys. Lett.* **B422**, 238 (1998).

[5] J. Bartels, J. Ellis, H. Kowalski and M. Wusthoff, hep-ph/9803497; J. Bartels and C. Royon, hep-ph/9809344.

[6] Nikolaev N.N. and B.G.Zakharov, *Phys. Lett.* **B332**, 177 (1994); *Z. Phys.* **C53**, 331 (1992).

[7] Genovese M., N.Nikolaev and B.Zakharov, *Phys. Lett.* **B378**, 347 (1996).

[8] N.N.Nikolaev, A.V.Pronyaev and B.G.Zakharov, JETP Lett. 68, 604 (1998).

Precocious asymptopia for charm from the running BFKL

N.N. Nikolaev[1] and V.R. Zoller[2]

The generalized BFKL [1] equation for the interaction cross section $\sigma(x,r)$ of the color dipole $\vec{r}$ with the target reads [2]

$$\frac{\partial\sigma(x,r)}{\partial\log(1/x)} = \mathcal{K}\otimes\sigma(x,r) \qquad (1)$$

where x is the Bjorken variable. The kernel $\mathcal{K}$ is related to the flux of the Weizsäcker-Williams soft gluons $|\vec{E}(\vec{\rho}_1)-\vec{E}(\vec{\rho}_2)|^2$. The Asymptotic Freedom (AF) dictates that the chromoelectric fields $\vec{E}(\vec{\rho})$ be calculated with the running QCD charge $g_S(r_m)=\sqrt{4\pi\alpha_S(r_m)}$ taken at shortest relevant distance $r_m=\min\{r,\rho\}$ and

$$\vec{E}(\vec{\rho}) = g_S(r_m)\vec{\rho}/\rho^2 \times (\text{screening factor}).$$

Our findings on the running BFKL equation which are of prime importance for the problem under discussion are as follows [3, 4]. The spectrum of the running BFKL equation is a series of moving poles $\mathbb{P}_n$ in the complex j-plane with eigenfunctions

$$\sigma_n(x,r) = \sigma_n(r)\exp(\Delta_n\log(1/x)) \qquad (2)$$

being a solution of $\mathcal{K}\otimes\sigma_n = \Delta_n\sigma_n(r)$.
The leading eigen-function $\sigma_0(r)$ is node free. The sub-leading $\sigma_n(r)$ has n nodes. The intercepts Δ_n closely, to better than 10%, follow the law $\Delta_n = \frac{\Delta_0}{(n+1)}$ suggested earlier by Lipatov [5] . The intercept of the leading pole trajectory, with our specific choice of the infrared regulator, $R_c = 0.27\,\text{fm}$, is $\Delta_0\equiv\Delta_{\mathbb{P}}=0.4$. The sub-leading $\sigma_n(r)$ represented in term of $\mathcal{E}(r)=\sigma_n(r)/r$, to a crude approximation is similar to Lipatov's quasi-classical eigenfunctions [5], $\mathcal{E}_n(r)\sim\cos[\phi(r)]$. With $R_c = 0.27\,\text{fm}$ the node of $\sigma_1(r)$ is located at $r=r_1\simeq 0.05-0.06\,\text{fm}$, for larger n the first node moves to a somewhat larger $r\sim 0.1\,\text{fm}$. Hence, $\sigma(x,r_1)$ is dominated by $\sigma_0(x,r_1)$. This observation explains the precocious asymptopia for the dipole cross section, $\sigma(x,r)\propto(1/x)^{\Delta_{\mathbb{P}}}$, at $r\sim 0.1\,\text{fm}$. Consequently, zooming at $\sigma(x,r_1)$ one can readily measure $\Delta_{\mathbb{P}}$. The point we want to make here is that because $r_1\sim 1/m_c$, the excitation of open charm provides the desired zooming. Indeed, we shall demonstrate that the effect of suppression of the sub-leading BFKL terms in $F_2^{cc}(x,Q^2)$ is remarkably strong.
The color dipole representation for the charm structure function (SF) reads [8]

$$F_2^{cc}(x,Q^2) = \frac{Q^2}{4\pi\alpha_{em}}\int_0^1 dz\int d^2\vec{r}|\Psi^{cc}(z,r)|^2\sigma(x,r), \qquad (3)$$

Starting with the BFKL-Regge expansion

$$\sigma(x,r) = \sigma_0(r)(x_0/x)^{\Delta_0}+\sigma_1(r)(x_0/x)^{\Delta_1}+\sigma_2(r)(x_0/x)^{\Delta_2}+\ldots. \qquad (4)$$

with Δ_n determined in [3, 4] we arrive at the BFKL-Regge expansion for the charm SF

$$F_2^{cc}(x,Q^2) = \sum_n f_n^{cc}(Q^2)(x_0/x)^{\Delta_n}, \qquad (5)$$

where the charm eigen-SF is as follows $f_n^{cc}(Q^2) = \frac{Q^2}{4\pi\alpha_{em}}\langle\sigma_n\rangle$. In conjunction with the explicit form of the $c\bar{c}$ light-cone wave function, $\Psi^{cc}(z,r)$ [8], the eq.(3) show that the integral over r in (3) is dominated by $Q^{-2}\lesssim r^2\lesssim m_c^{-2}$. Indeed, after z-integration one can write

$$f_n^{cc}(Q^2)\propto\int_{1/Q^2}^{1/m_c^2}\frac{dr^2}{r^2}\frac{\sigma_n(r)}{r^2}. \qquad (6)$$

The dipole cross section $\sigma_n(r)$ in (6) is an oscillating function of r with the first node located inside the integration region. Then in a broad range of Q^2 one has strong cancellations in (6) for sub-leading poles which result in the leading pole dominance in charm production. From our analysis of experimental data from H1 [6] and ZEUS [7] it follows that the charm production in a wide range of the photon virtualities, $Q^2\lesssim 10^2\,\text{GeV}^2$, provides the unique opportunity of getting hold of elusive BFKL asymptotics and measuring $\Delta_{\mathbb{P}}$ already at currently available x.
The detailed presentation of these results is published in [9].

[1] Institut für Kernphysik, Forschungszentrum Jülich
[2] Institute for Theoretical and Experimental Physics, Moscow, Russia

References:

[1] E.A.Kuraev, L.N.Lipatov and V.S.Fadin, *Sov.Phys. JETP* **44** (1976) 443; **45** (1977) 199; Ya.Ya.Balitskii and L.N.Lipatov, *Sov. J. Nucl. Phys.* **28** (1978) 822.
[2] N.N. Nikolaev, B.G. Zakharov, V.R. Zoller, *JETP Letters* **59** (1994) 8.
[3] V.R. Zoller in Proc. 5th Int. Workshop on DIS and QCD (DIS 97), Chicago, IL, 1997.
[4] N.N. Nikolaev, B.G. Zakharov, V.R. Zoller,*JETP Letters* **66** (1997) 138.
[5] L.N. Lipatov, *Sov. Phys. JETP* **63** (1986) 904.
[6] H1 collaboration: C.Adloff et al.,*Z. Phys* **C72** (1996) 593.
[7] ZEUS collaboration: J. Breitweg et al., *Phys. Lett.* **B407** (1997) 402.
[8] N.N. Nikolaev and B.G. Zakharov, *Z. Phys.* **C49** (1991) 607.
[9] V.R. Zoller, Report No. FZ-IKP(TH)-1998-5; N.N. Nikolaev and V.R. Zoller, Report No. FZ-IKP(TH)-1998-33.

The running BFKL: resolution of Caldwell's puzzle

N.N. Nikolaev[1] and V.R. Zoller[2]

Caldwell's presentation of the HERA data in terms of the logarithmic derivative $\partial F_2/\partial \log Q^2$ for the proton structure function (SF) $F_2(x,Q^2)$ exhibits the turn-over of the slope towards small x and/or Q^2 up to currently attainable $x \sim 10^{-6}$ and $Q^2 \sim 0.1\,\mathrm{GeV}^2$ [1]. The DGLAP-evolution with GRV input [2] predicts a steady increase of the derivative $\frac{\partial F_2^{DGLAP}}{\partial \log Q^2} \propto \alpha_S(Q^2) G^{DGLAP}(x,Q^2)$ with $1/x$, due to the growth of the gluon structure function $G^{DGLAP}(x,Q^2) = xg^{DGLAP}(x,Q^2)$.

The turn-over point located at $x \sim 5 \cdot 10^{-4}$ and $Q^2 \sim 5\,\mathrm{GeV}^2$, in a commonly believed legitimate pQCD domain. So, the phenomenon occurs on the interface between "soft" and "hard" physics. Its explanation within the color dipole approach is based on two observations:

i) specific smallness of the $\log Q^2$-derivative of sub-leading terms of the BFKL-Regge expansion for F_2 at the turn-over point, which is due to the nodal structure of the running BFKL eigen-SF's;

ii) significant contribution to the small-Q^2 proton SF coming from the non-perturbative component of the BFKL pomeron.

The properties of the running color dipole BFKL equation responsible for the observed Q^2 dependence of $\partial F_2/\partial \log Q^2$ are as follows [4, 5]. The spectrum of the running BFKL equation is a series of moving poles in the complex j-plane with eigen-functions

$$\sigma_n(x,r) = \sigma_n(r) \exp\left[\Delta_n \log(1/x)\right] \qquad (1)$$

being a solution of

$$\mathcal{K} \otimes \sigma_n = \Delta_n \sigma_n(r). \qquad (2)$$

The leading eigen-function $\sigma_0(r)$ is node free. The sub-leading $\sigma_n(r)$ has n nodes. The intercepts Δ_n closely, to better than 10%, follow the law $\Delta_n = \Delta_0/(n+1)$ suggested earlier by Lipatov [6]. The intercept of the leading pole trajectory, with the above specific choice of R_c, is $\Delta_0 \equiv \Delta_{I\!P} = 0.4$. The sub-leading eigen-functions σ_n [4, 5] are very close to Lipatov's quasi-classical solutions [6] for $n \gg 1$. For our specific choice of the infrared regulator, R_c, the node of $\sigma_1(r)$ is located at $r = r_1 \simeq 0.05 - 0.06\,\mathrm{fm}$, for larger n the first node moves to a somewhat larger $r \sim 0.1\,\mathrm{fm}$.

The BFKL-Regge expansion

$$\sigma(x,r) = \sigma_0(r)(x_0/x)^{\Delta_0} + \sigma_1(r)(x_0/x)^{\Delta_1} + \sigma_2(r)(x_0/x)^{\Delta_2} + \ldots \qquad (3)$$

gives the BFKL-Regge expansion for the SF

$$F_2(x,Q^2) = \sum_n f_n(Q^2)(x_0/x)^{\Delta_n}. \qquad (4)$$

Asymptotically, at $1/x \to \infty$, the expansion (4) is dominated by the term $f_0(Q^2)(x_0/x)^{\Delta_0}$. At moderately small x the sub-leading terms are equally important since $\Delta_n \sim 1/n$. However, as it has been pointed out in [4, 5], for $Q^2 \lesssim 10^4\,\mathrm{GeV}^2$ all $f_n(Q^2)$ with $n \geq 3$ are very close in shape to each other. Then we arrive at the truncated expansion

$$F_2(x,Q^2) = \sum_{n=0}^{3} f_n(Q^2)(x_0/x)^{\Delta_n} + F_2^{soft}(Q^2) + F_2^{val}(x,Q^2), \qquad (5)$$

where the term $f_3(Q^2)(x_0/x)^{\Delta_3}$ with the properly adjusted weight factor, a_3, stands for all terms with $n \geq 3$.

The $\log Q^2$-derivative of the non-perturbative term F_2^{soft} levels off at very small $Q^2 \sim 0.15\,\mathrm{GeV}^2$ and does not contribute to the observed growth of $\partial F_2/\partial \log Q^2$.

Because the sub-leading SF's, $f_n(Q^2)$, have node at $Q^2 \sim 20 - 60\,\mathrm{GeV}^2$ [4, 5], their contribution to the slope $\partial F_2/\partial \log Q^2$ vanishes at $Q^2 \sim 5 - 10\,\mathrm{GeV}^2$, which is very close to the turn-over point in the HERA data. Hence $\partial F_2/\partial \log Q^2$ at small Q^2 follows closely $\partial f_0/\partial \log Q^2$. From (??) it follows that at small Q^2, $f_0(Q^2)$ behaves like $\sim Q^2/(\Lambda_0^2 + Q^2)$ with $\Lambda_0^2 \simeq 0.72\,\mathrm{GeV}^2$ coming from (??). Therefore, $\partial F_2/\partial \log Q^2$ rises with Q^2 up to $Q^2 \sim 1\mathrm{GeV}^2$ then levels off. Only at large Q^2, when the sub-leading terms enter the game, $\partial F_2/\partial \log Q^2$ decreases and even becomes negative valued at large x. Our estimates are in good agreement with HERA data [1]. The detailed presentation of these results is published in [7].

[1] Institut für Kernphysik, Forschungszentrum Jülich
[2] Institute for Theoretical and Experimental Physics, Moscow, Russia

References:

[1] A. Caldwell, DESY Theory Workshop, DESY, October 1997; ZEUS Collaboration, J. Breitweg et al., Report No. *DESY-98-162*

[2] M. Glück, E. Reya and A. Vogt, *Z. Phys.* **C67** (1995) 433.

[3] E.A.Kuraev, L.N.Lipatov and V.S.Fadin, *Sov.Phys. JETP* **44** (1976) 443; **45** (1977) 199; Ya.Ya.Balitskii and L.N.Lipatov, *Sov. J. Nucl. Phys.* **28** (1978) 822.

[4] V.R. Zoller in Proc. 5th Int. Workshop on DIS and QCD (DIS 97), Chicago, IL, 1997.

[5] N.N. Nikolaev, B.G. Zakharov, V.R. Zoller, *JETP Letters* **66** (1997) 138.

[6] L.N. Lipatov, *Sov. Phys. JETP* **63** (1986) 904.

[7] V.R. Zoller, in Proc. 6th Int. Workshop on DIS and QCD (DIS 98), Brussels, 1998; Report No. *FZ-IKP(TH)-1998-5*; N.N. Nikolaev and V.R. Zoller, Report No. *FZ-IKP(TH)-1998-32*

Neutrino optics of crystals

V.R. Zoller[1)]

Recently there was much discussion on possible laboratory observations of neutrino electro-magnetic conversion [1]. We show that the crystal converter is able to contribute to the future investigations of the neutrino electrodynamics. The point is that the well known Thomas interaction of atomic theory is proportional to the gradient of the matter density,

$$\sigma \nabla \rho(r)\,,$$

which is large in the impact parameter plane for particles passing through the crystal along the crystallographic axis. Still, for high energy neutrino beam the coherence length is large , $l_{coh} \sim E_\nu/q_\perp^2$, and one can gain from the big number of scatterers, $N \sim l_{coh}/d$, since the coherent conversion cross section is $\sigma \propto N^2$. Hereafter, d is the inter-atomic distance. From the phenomenological transition matrix element [2]

$$\mathcal{M}(\nu_1\gamma \to \nu_2) = i\bar{u}_2\,(\mu_{21} + \gamma_5 d_{21})\,\sigma_{\mu\nu}F^{\nu\mu}u_1\,, \quad (1)$$

where μ_{21} and d_{21} are the transition magnetic and electric dipole moments of the neutrino and $F^{\nu\mu}$ is the electro-magnetic field strength tensor, one readily finds the cross section of the coherent neutrino conversion in crystal

$$\sigma_{21} = 4\alpha Z^2 b_{21}^2 \int dq_\perp^2 \frac{q_\perp^2}{(q_\perp^2+\mu^2)^2} S_L^2(q_z) S_T^2(q_\perp)\,. \quad (2)$$

Here $\mu = a_{TF}^{-1}$ and $a_{TF} = (m_e\alpha Z^{1/3})^{-1}$ is the Thomas-Fermi radius of an atom, $b_{21}^2 = |\mu_{21}|^2 + |d_{21}|^2$ for Dirac neutrinos and $b_{21}^2 = 4\left[(\mathrm{Im}\mu_{21})^2 + (\mathrm{Re}d_{21})^2\right]$ for Majorana neutrinos [2]. Denoted by S_T is the transverse form factor $S_T^2(q_\perp^2) = \exp\left[-\frac{2}{3}\langle \mathbf{u}^2\rangle q_\perp^2\right]$, where $\langle \mathbf{u}^2\rangle$ is the square of amplitude of the lattice thermal vibrations. It is precisely the factor S_T^2 which cuts off $q_\perp^2$ at $q_\perp^2 \gtrsim \langle \mathbf{u}^2\rangle^{-1}$. The longitudinal form factor which involves the structure factor of a crystal is as follows

$$S_L(q_z) = \exp\left[-\frac{1}{6}q_z^2\langle \mathbf{u}^2\rangle\right]\frac{\sin(q_z N_z d/2)}{\sin(q_z d/2)}\,, \quad (3)$$

where the longitudinal momentum transfer is

$$q_z = \frac{\Delta m_{21}^2 + q_\perp^2 + 2\mathbf{p}_\perp\mathbf{q}_\perp}{2p}\,. \quad (4)$$

The term $\mathbf{p}_\perp\mathbf{q}_\perp$ vanishes if the incident neutrino momentum $\mathbf{p}$ is parallel to the chain. The transition coherence length is determined by the inverse longitudinal momentum transfer, $L_c \sim 1/q_z$

The coherent conversion rate $R = \sigma_{21}/d^2$ exhibits the resonance enhancement at the projectile momenta which satisfy the equation $q_z d = 2\pi n$, $n = \pm 1, \pm 2, ...$ As a function of beam momentum R looks like a series of narrow resonances with the width $\sim 1/N$. For the practical purposes, one must focus on the coherent enhancement at $n = 0$. Indeed, for high energy neutrino $q_z d$ is small and the longitudinal form factor $S_L^2 \simeq N^2[1 - N^2/N_c^2 + ...]$ defines the coherence length $L_c = N_c d$, where

$$N_c = \frac{4\sqrt{3}\,p}{(\Delta m_{21}^2 + q_\perp^2)d}\,. \quad (5)$$

If the amplitude of thermal vibrations is large compared to a_{TF}, that is $\xi = (\frac{2}{3}\langle \mathbf{u}^2\rangle\mu^2)^{-1} \ll 1$, the coherent conversion rate vanishes as $R \propto \xi^2$. To be specific we consider the W-crystal converter for which $\xi \simeq 10$ [3]. At $N \sim N_c$ the conversion rate reaches the value

$$R \simeq 2\alpha Z^2 N_c^2 \frac{b_{21}^2}{d^2}\,, \quad (6)$$

which is followed by the logarithmical dependence on N at still larger N.

So, we derive constraints on the $\nu_1\gamma \to \nu_2$ conversion rate

$$\frac{\mu_{21}}{\mu_B} \simeq \frac{m_e d}{2\alpha Z N_c}\sqrt{\frac{R}{\pi}}\,. \quad (7)$$

Note, the upper bound on μ_{21} can be pushed down by the factor $1/\sqrt{K}$ if the neutrino passes successively through a big number, K, of crystal plates of the thickness $\sim N_c$ each. In this case the conversion rate acquires the factor of the incoherent enhancement which equals to K. Evidently, the most straightforward way to lower down the upper bound on μ_{21} would be to increase the neutrino beam energy making use of a muon collider.

The detailed presentation of these results is published in [4].

[1)] Institute for Theoretical and Experimental Physics, Moscow, Russia

References:

[1] M.C. Gonzalez-Garcia, F. Vannucci and J. Castromonte, Phys. Lett. B373 (1996) 153; S. Matsuki and K. Yamamoto, Phys. Lett. B289 (1992) 194; M. Sakuda and Y.Kurihara, Phys. Rev. Lett. 74 (1995) 1284; S. Domokos and S. Kovesi-Domokos, Phys. Rev. D55 (1997) R2526.

[2] J. Schechter and J.W.F. Valle, Phys. Rev. D24 (1981) 1883; P.B. Pal and L. Wolfenstein, Phys. Rev. D25 (1982) 766; J. Nieves, Phys. Rev. D26 (1982) 3152.

[3] D.S. Gemmel, Rev. Mod. Phys., 46 (1974) 1.

[4] V.R. Zoller, Neutrino Optics of Crystals, in Proc. of "Electroweak Interactions and Unified Theories" The XXXIVnd Rencontres de Moriond, Les Arcs, France - March 14-21, 1998. Report No. FZ-IKP(TH)-1998-34.

Scaling transverse flow in Bjorken's scenario for heavy ion collisions

V.E.Fortov[a], P.Milyutin[a] and N.N.Nikolaev[b,c]

Landau's hydrodynamic stage [1] is a part of all scenarios for the evolution of the hot and dense matter (quark-gluon plasma - QGP) formed in ultrarelativistic heavy ion collisions [2]. It is now well understood that Landau's complete stopping of Lorentz-contracted colliding nuclei is not feasible because of the Landau-Pomeranchuck-Migdal (LPM) effect [3], i.e., the finite proper formation time τ_0 and the relativistic growth of the formation time for fast secondary particles. The corollary of the LPM effect in conjunction with the approximate central rapidity plateau is the rapidity-boost invariance of initial conditions. The corresponding solution for a longitudinal expansion in an 1+1-dimensional approximation, neglecting the transverse flow, was found by Bjorken [4]. There is some experimental evidence [5, 6], although a disputed one [7, 8], for a transverse flow which must develop if the lifetime of the hydrodynamical stage is sufficiently long.

We report here a simple analytic solution of the Euler-Landau equation for the velocity of transverse expansion, u, gained in the hydrodynamic expansion of QGP before the hadronization phase transition (published in [9]). It is only marginally sensitive to properties of the hot stage and offers a reliable determination of lifetime of the QGP τ_B if the radial profile of the initial energy density is known. We find that the u-distribution is a scaling function of u/u_m, where u_m is a maximal velocity of expansion.

The collective transverse expansion is driven by the radial gradient of pressure. As we shall see, for uysual estimates for τ_B the radial flow is nonrelativistic (We recall that for central $PbPb$ collisions, for which there is some experimental evidence for the QGP formation [2], the typical estimates are $\tau_B \approx 3$f/c at SPS [10, 11] and $\tau_B \approx 6$f/c at RHIC [2], which are much larger than the standard estimate $\tau_0 \sim 0.5$ f/c.). We start with the familiar Landau relativistic hydrodynamics equations

$$\partial_\mu T_{\mu\nu} = 0\,, \tag{1}$$

for the energy-momentum tensor $T_{\mu\nu} = (\epsilon+p)u_\mu u_\nu - p\delta_{\mu\nu}$, where ϵ and p are the energy density and pressure in the comoving frame, and u_μ is the 4-velocity of the element of the fluid. To the first order in radial velocity u_r, the radial projection of (1) gives the Euler-Landau equation

$$(\epsilon+p)\frac{\partial u_r}{\partial\tau} + u_r\left(\frac{\partial(\epsilon+p)}{\partial\tau} + \frac{(\epsilon+p)}{\tau}\right) + \frac{\partial p}{\partial r} = 0\,, \tag{2}$$

in which we can use the Bjorken's solution for ϵ and EOS $p = c_s^2\epsilon$. Then the Euler-Landau equation can be cast in a simple form

$$\frac{\partial u_r}{\partial\tau} - \frac{c_s^2}{\tau}u_r = -\frac{c_s^2}{(1+c_s^2)}\frac{\partial \log p}{\partial r}\,. \tag{3}$$

According to the lattice QCD studies, the familiar $c_s^2 = \frac{1}{3}$ holds for a velocity of sound c_s in the QGP excepting a negligible narrow region of the hadronization transition temperature $T_h \sim 160$MeV and energy density $\epsilon_h \sim 1.5$ GeV/fm^3 [12, 10]. The important point is that the transverse expansion of the QGP fireball can be neglected which we can justify *a posteriori*. For this reason the time dependence of the logarithmic derivative $D(r,\tau) = \frac{\partial \log p}{\partial r}$ can be neglected, it is completely determined by the initial density profile and depends neither on the temperature nor fugacities of quarks and gluons, which substantially reduces the model-dependence of the transverse velocity. Then the solution of (2) subject to the boundary condition $u_r(\tau_0) = 0$ is

$$u_r(r,\tau) \approx \frac{c_s^2\tau D(r,0)}{1-c_s^4}\cdot\left[1-\left(\frac{\tau_0}{\tau}\right)^{1-c_s^2}\right]. \tag{4}$$

AT RHIC and higher energies of the initial state is expected to be formed by semihard parton-parton interactions for which nuclear shadowing effects can be neglected. Then for central collisions $\epsilon(r,\tau_0) \propto T_A^k(r)$, where $k = 2$ and $T_A(r) = \int dz n_A(\sqrt{z^2+r^2})$ is the density of constituents, $T_A(r) \sim \exp(-\frac{r^2}{R_A^2})$, where $R_A \approx 1.1A^{-1/3}$fm is the nuclear radius. In another extreme scenario of strong shadowing and of strong LPM effect the soft particle production is not proportional to the multiplicity of collisions of fast partons and $k = 1$ is more appropriate. Hereafter we take $k = 2$. In any case, the logarithmic pressure gradient is approximately linear, $D(r,t) \approx 2kr/R_A^2$, and according to the solution (4) the displacement of the fluid element Δr is proportional to the radius, $\Delta r \propto r\tau^2$. Consequently, we have the Hubble-type radial rescaling

$$\lambda(\tau) \approx 1 + \frac{\Delta r}{r} \approx 1 + \left(\frac{\tau}{\tau_T}\right)^2\,, \tag{5}$$

where

$$\tau_T \approx \frac{R_A}{\sqrt{k}c_s}\,. \tag{6}$$

has a meaning of the *lifetime against transverse expansion*. For central $PbPb$ collisions eq. (6) gives $\tau_T \approx 10k^{-0.5}$f/c which is larger than the above cited estimates of τ_B and at SPS and RHIC energies the transverse expansion of the fireball can be neglected.

In a quasi-uniform plasma the hydrodynamic expansion lasts until $\epsilon = \epsilon_h$. For long-lived QGP and $\tau \gg \tau_0$ we can use the Bjorken's solution

$$\epsilon(r,\tau) = \epsilon_h\left(\frac{T_A(r)}{T_A(0)}\right)^k\left(\frac{\tau_B}{\tau}\right)^{1+c_s^2}\,, \tag{7}$$

which gives the position of the hadronization front

$$r_h(\tau) = R_A\sqrt{\frac{1+c_s^2}{k}\ln\frac{\tau_B}{\tau}} \qquad (8)$$

and the radial velocity at the hadronization front

$$u(\tau) = u_r(r_h(\tau),\tau)$$
$$= \frac{c_s^2\tau}{R_A(1-c_s^4)}\sqrt{4k(1+c_s^2)\ln\frac{\tau_B}{\tau}}\left[1-\left(\frac{\tau_0}{\tau}\right)^{1-c_s^2}\right]. \qquad (9)$$

For the usually discussed τ_B and τ_0 we have $\tau_B \gg \tau_0$. For such s long-lived QGP, $\tau_B \gg \tau_0$, the radial velocity takes the maximal value u_m at $t = \tau/\tau_B \approx 1/\sqrt{e}$,

$$u_m = \frac{c_s^2\tau_B}{R_A(1-c_s^4)}\sqrt{\frac{2k(1+c_s^2)}{e}}\left[1-\left(\frac{\tau_0\sqrt{e}}{\tau_B}\right)^{1-c_s^2}\right]. \qquad (10)$$

The large-τ_B approximation (10) is accurate to better than $\sim 4\%$ at $\tau_B = 3$ f/c and better than $\sim 1\%$ at $\tau_B = 8$ f/c. For the above cited estimates for τ_B in central $PbPb$ collisions we find $u_m(SPS) \approx 0.13$ and $u_m(RHIC) \approx 0.28$, consequently the nonrelativistic expansion approximation is justified very well.

The most interesting quantity is a radial velocity distribution which can be evaluated experimentally from the Doppler modifications of the thermal spectrum of particles radiated from the hadronization front. This post-acceleration in the mixed phase is negligible for weakly interacting K^+ and ϕ-mesons, which gives the desired access to the radial flow at the hadronization transition. For the of constant hadronization temperature contribution of the hadronization surface $r_h(\tau)$ to the particle multiplicity is

$$dw \propto r_h(\tau)d\tau\,. \qquad (11)$$

Making use of the solutions (8) and (9), it can readily be transformed into $dw/du \propto r_h(du/d\tau)^{-1}$. Notice, that for a long-lived QGP the hadronization front (8) and $u(\tau)/u_m$ depend only on the scaling variable $t = \tau/\tau_B$, with an obvious exception of the short-time region $\tau \sim \tau_0$. This scaling implies that the hadronization front velocity distribution is a scaling function of $x = u/u_m$:

$$\frac{dw}{du} = \frac{1}{u_m}\frac{f(x,\tau_B)}{\sqrt{1-x}}, \qquad (12)$$

where for a long-lived QGP $f(x,\tau_B)$ does not depend on τ_B. The square-root singularity at $x = 1$ is a trivial consequence of the vanishing derivative $du(\tau)/d\tau$ at $\tau \approx \tau_B/\sqrt{e}$. The numerical calculation show that the approximation $f(x) = 0.5$ is good for all the practical purposes.

The NA49 fits to the proton, kaon and pion transverse mass m_T distribution in central $PbPb$ collisions at SPS assume identical freeze-out temperature for all particle species [5]. For positive particles NA49 finds $T_f = 140 \pm 7$ MeV and the transverse velocity $\langle u\rangle = 0.41\pm0.11$. However, for the K^+ one must take the higher freeze-out temperature $T_f = T_h \approx 160$ MeV given by the lattice QCD. Because of the anti-correlation between the local temperature T_f and $\langle u_T\rangle$, see Fig. 7 in [6], such a fit with larger T_f to the same m_T distribution shall yield smaller $\langle u\rangle$.

Acknowledgements: This work was partly supported by the INTAS grant 96-597 and the Grant N 94-02-05203 from the Russian Fund for Fundamental Research.

[1] High Energy Density Research Center of the Russian Academy of Sciences, IVTAN, Izhorskaya 13/9, 127412 Moscow, Russia;
[2]Institut f. Kernphysik, Forschungszentrum Jülich, D-52425 Jülich,Germany;
[3]L. D. Landau Institute for Theoretical Physics, GSP-1, 117940, ul. Kosygina 2, Moscow V-334, Russia.

References:

[1] L.D.Landau, Izvestiya Akademii Nauk SSSR, Ser. Fiz. 17, 51 (1953)
[2] K.Geiger, Phys. Rep. C258, 237 (1995); J.W.Harris and B.Müller, Ann. Rev. Nucl. Part. Sci. 46, 71 (1996); B.Müller, Nucl. Phys. A630, 461c (1998)
[3] L.D.Landau and I.Ya.Pomeranchuk, Dokl. Akad. Nauk SSSR 92, 525 (1953); 92, 735 (1953)
[4] J.D.Bjorken, Phys. Rev. D27, 140 (1983)
[5] I.G.Bearden et al., Phys. Rev. Lett. 78, 2080 (1997)
[6] H.Appelshäuser et al., Eur. Phys. J. C2, 661 (1998)
[7] P.Braun-Munzinger and J.Stachel, nucl-ex/9803015.
[8] Jan-e Alam, J.Cleymans, K.Redlich and H.Satz, nucl-th/9707042.
[9] P.Milyutin, V.E.Fortov and N.N.Nikolaev, JETP Lett. 68, 191 (1998)
[10] B.R.Schlei, Heavy Ion Phys. 5, 403 (1997)
[11] A.Dumitru et al., Workshop on Hydrodynamics at ECT*, Trento, May 1997, nucl-th/9705056.
[12] C.M.Hung and E.V.Shuryak, Phys. Rev. Lett. 75, 4003 (1995)

Quark energy loss in an expanding quark-gluon plasma

B.G.Zakharov[a]

Study of the induced gluon radiation from a fast quark in a quark-gluon plasma (QGP) is of great importance in connection with the forthcoming experiments on high energy AA-collisions at the RHIC and LHC. It is expected that the energy loss of high-$p_\perp$ jets produced at the initial stage of AA-collision may be an important potential probe for formation of QGP [1, 2]. In [3, 4] the quark energy loss, ΔE_q, was estimated for a homogeneous QGP. Here we present the results of evaluation of ΔE_q in an expanding QGP in the light-cone path integral approach to the induced radiation [5, 6]. We model QGP by a system of static Debye screened scattering centers [1].

We consider a fast quark produced in the central rapidity region with a velocity perpendicular to the axis of AA-collision. We choose the z axis along the initial quark velocity, and the quark production point is assumed to be at $z = 0$. Then, the distance passed by the quark in QGP, $L = z$, is close to the expansion time, τ. For the $\tau(z)$-dependence of the temperature of QGP we use prediction of Bjorken's model [7] $T\tau^{1/3} = T_0\tau_0^{1/3}$.

The probability of radiation of a gluon with the fractional longitudinal momentum x from a fast quark is given by [5]

$$\frac{dP}{dx} = 2\mathrm{Re}\int_0^\infty dz_1 \int_{z_1}^\infty dz_2 \exp\left[\frac{i(z_1-z_2)}{L_f}\right] g(z_1,z_2,x) \times \left[K(0,z_2|0,z_1) - K_v(0,z_2|0,z_1)\right] . \quad (1)$$

Here K is the Green's function for the Hamiltonian (acting in the transverse plane)

$$H = \frac{\mathbf{q}^2}{2\mu(x)} + v(\rho,z) , \quad (2)$$

$$v(\rho,z) = -i\frac{n(z)\sigma_3(\rho,x,z)}{2} , \quad (3)$$

and K_v is the Green's function for the Hamiltonian (2) with $v(\rho,z) = 0$. In (2) the Schrödinger mass is $\mu(x) = E_q x(1-x)$, $L_f = 2E_q x(1-x)/[m_q^2x^2 + m_g^2(1-x)]$ is the gluon formation length, here m_q is the quark mass, and m_g is the mass of the radiated gluon. We introduce the gluon mass to remove the contribution of the unphysical long-wave gluon excitations. In (3) $n(z)$ is the number density of QGP, and σ_3 is the cross section of interaction of color singlet $q\bar{q}g$ system with color center. Summation over triplet (quark) and octet (gluon) color states is implicit in (3). The z-dependence of σ_3 is connected with the one of the Debye screening mass. In (1) $g(z_1,z_2,x)$ is the vertex factor which includes all spin effects.

The Hamiltonian (1) describes evolution of the light-cone wave function of a fictitious $q\bar{q}g$ system [5].

The three-body cross section entering the imaginary potential (3) is given by [8]

$$\sigma_3(\rho,x,z) = \frac{9}{8}[\sigma_2(\rho,z)+\sigma_2((1-x)\rho,z)]-\frac{1}{8}\sigma_2(x\rho,z) , \quad (4)$$

where $\sigma_2(\rho,z)$ is the dipole cross section of interaction with color center of color singlet $q\bar{q}$ system. The latter can be written as $\sigma_2(\rho,z) = C_2(\rho,z)\rho^2$, where $C_2(\rho,z)$ has a smooth (logarithmic) dependence on ρ at small ρ. As in [4] we approximate $C_2(\rho,z)$ by its value at $\rho \approx 1/m_g$. Then the Hamiltonian (2) takes the oscillator form with the z-dependent frequency

$$\Omega(z) = \frac{(1-i)}{\sqrt{2}}\left(\frac{n(z)C_3(x,z)}{E_q x(1-x)}\right)^{1/2} , \quad (5)$$

where

$C_3(x,z) = \frac{1}{8}\left\{9[1+(1-x)^2]-x^2\right\}C_2(1/m_g,z)$.

The coefficient C_2 was calculated in the double gluon approximation. In numerical calculations we evaluated the Green's function K using the approach previously developed in analysis of the vector meson photoproduction [9]

It follows from (5) that even for a thermolized QGP the oscillator frequency is dominated by the gluon contribution. There is every indication [10, 11] that for the RICH and LHC the hot QCD medium produced in AA-collisions at $\tau \sim \tau_0 \sim 0.1$ fm will be thermolized gluon plasma to a first approximation, and for quarks the chemical equilibration is not reached during the expansion of QGP. For this reason we take for the gluon fugacity $\lambda_g = 1$. To take into account the suppression of quarks we use the value $\lambda_q = 1/3$ for the quark fugacity. Numerical calculations were carried out with $\alpha_s = 1/3$. For τ_0 we use the value 0.1 fm [10, 11]. At $z \le \tau_0$ we take $\Omega(z) = \Omega(\tau_0)$. We have evaluated ΔE_q for $T_0 = 1100$ expected for central Pb-Pb collisions at the LHC [10]. To study the dependence of the quark energy loss on T_0 we give also the results for $T_0 = 700$ MeV. The numerical predictions for ΔE_q as a function of E_q for $L = 3$, 6, 9 fm are shown in Fig. 1. The results were obtained for $m_q = 0.2$ GeV. As for a homogeneous QGP [4], our predictions have a weak dependence on m_q. To study the infrared sensitivity of ΔE_q we present in Fig. 1 the results for $m_g = 0.75$ and 0.375 GeV. These values are of the order of the Debye screening mass for QGP in the region $\tau \gtrsim 2-3$ fm, which, as our numerical calculations show, dominates the quark energy loss. For this reason the value of m_g within the above range seems to be a plausible estimate for the infrared cutoff in the considered problem. Note that in the limit $E_q \to \infty$ ΔE_q has only a smooth (logarithmic) m_g-dependence connected with ρ-dependence of the coefficient C_2 [4]. Our numerical calculations really demonstrate that for $E_q \gtrsim 10$ GeV ΔE_q is not very sensitive to m_g. Fig. 1 shows that ΔE_q grows by a factor $\sim 2-3$ as

E_q increases from ~ 10 to ~ 100 GeV. The predictions for $L = 6$ and $L = 9$ fm can be regarded as a plausible estimates for ΔE_q in central collisions of heavy nuclei. We have checked that the effect of the mixed phase (with $T_c \approx 150$ MeV) and the hadronic phase turns out to be relatively small. Comparison of the results for $T_0 = 1100$ and $T_0 = 700$ MeV demonstrates that the T_0-dependence of ΔE_q is not very strong. This is connected with an increase of Landau-Pomeranchuk-Migdal suppression and a decrease of the coefficient C_2 for a high density QGP.

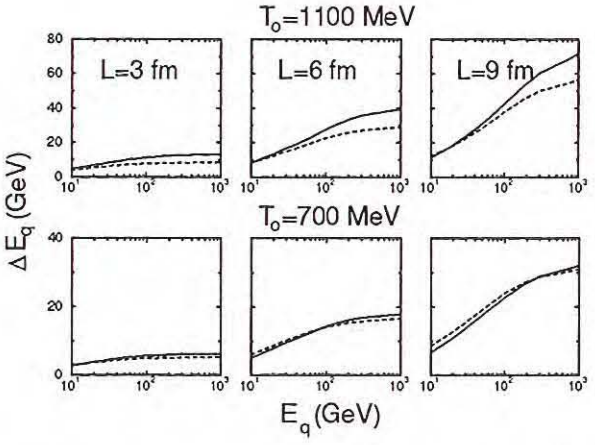

Fig. 1: The quark energy loss as a function of the quark energy for $m_q = 0.2$ GeV, $m_g = 0.75$ GeV (solid line) and $m_g = 0.375$ GeV (dashed line).

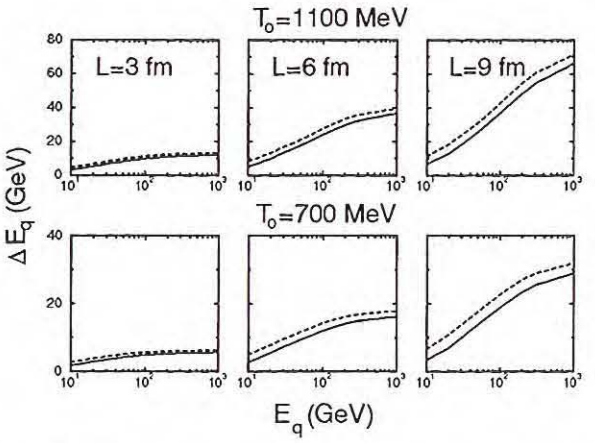

Fig. 2: The quark energy loss as a function of the quark energy for $m_g = 0.75$ GeV, $m_q = 1.5$ GeV (solid line) and $m_q = 0.2$ GeV (dashed line).

To study the sensitivity of ΔE_q to dynamics of QGP at small τ we have also carried out the calculations taking $\Omega(z \lesssim a) = \Omega(a)$ with $a \sim 1 - 2$ fm. The results for these versions do not differ strongly from the ones in Fig. 1. This demonstrates that ΔE_q is insensitive to the dynamics of QGP at $\tau \lesssim 2$ fm. This fact is a consequence of suppression of probability of gluon radiation at small z [4, 6].

To illustrate the quark mass dependence of ΔE_q in Fig. 2 we compare the results for ΔE_q for c-quark ($m_q = 1.5$ GeV) with the ones for light quarks ($m_q = 0.2$ GeV). As one can see the dependence of ΔE_q on m_q becomes weak at $E_q \gtrsim 50 - 100$ GeV.

The rather large values of ΔE_q obtained in the present work show that jet quenching may be an important probe for the formation of QGP in AA-collisions. The Monte-Carlo analysis of jet quenching [2] with ΔE_q close to the estimates of the present work demonstrates that the induced radiation must considerably modify the charged particle spectra. The induced gluon radiation can also lead to other interesting experimental consequences. For instance, fluctuations of the quark energy loss will generate additional transverse momentum (defined with respect to the AA-collision axis) in production of $c\bar{c}$ and $b\bar{b}$ pairs. In the case of $g \to gg$ transitions the production of the gg state in the color decuplet state can increase the cross section for production of baryon-antibaryon pairs through the mechanism analogous to the one previously discussed [12] in connection with $B\bar{B}$ annihilation at high energies.

[a]L. D. Landau Institute for Theoretical Physics, GSP-1, 117940, ul. Kosygina 2, 117334 Moscow, Russia

References:

[1] M. Gyulassy and X.-N. Wang, Nucl. Phys. **B420** (1994) 583; X.-N. Wang, M. Gyulassy and M. Plümer, Phys. Rev. **D51** (1995) 3436.

[2] X.-N. Wang, Prog. Theor. Phys. Suppl. **129** (1997) 45.

[3] R. Baier, Yu.L. Dokshitzer, A.H. Mueller, S. Peigne and D. Schiff, Nucl. Phys. **B483** (1997) 291; **B484** (1997) 265.

[4] B.G. Zakharov, JETP Lett. **65** (1997) 615.

[5] B.G. Zakharov, JETP Lett. **63** (1996) 952.

[6] B.G. Zakharov, Phys. Atom. Nucl. **61** (1998) 838.

[7] J.D.Bjorken, Phys. Rev. **D27** (1983) 140.

[8] N.N. Nikolaev and B.G. Zakharov, JETP **78** (1994) 598.

[9] B.Z. Kopeliovich and B.G. Zakharov, Phys. Rev. **D44** (1991) 3466.

[10] K.J. Eskola, Prog. Theor. Phys. Suppl. **129** (1997) 1.

[11] K.J. Eskola and K. Kajantie, Z. Phys. **C75** (1997) 515.

[12] B.Z. Kopeliovich and B.G. Zakharov, Phys. Lett. **211B** (1988) 221; Sov. J. Nucl. Phys. **48** (1988) 136.

Enhancement of $\pi A \rightarrow \pi\pi A$ Threshold Cross Sections by $\pi\pi$ Final State Interactions

R. Rapp[1], J.W. Durso[2], O. Krehl and J. Speth

The Jülich model of meson-meson scattering [1], based on meson exchange, has been developed and refined over the past decade and gives a good quantitative description of the scattering of two pseudoscalar mesons. The latest version of the model [2,3] builds in constraints on the S-wave $\pi\pi$ scattering lengths imposed by chiral symmetry [4]. This feature turns out to be crucial in preventing a (theoretical) $\pi\pi$ pairing instability in nuclear matter at densities below that of normal nuclear matter observed in many models [5,6,7].

While the chirally improved Jülich model avoids the theoretical problem of $\pi\pi$ pair condensation in low-density nuclear matter, it nevertheless predicts a pronounced shift in the strength of the S-wave isoscalar $\pi\pi$ scattering amplitude to lower energies as the density of the surrounding nuclear medium increases. This enhancement of the low-energy strength is largely absent in the I=2 channel, in which the interaction is purely repulsive. The accumulation of strength in the I=0 S-wave scattering amplitude at energies just above the $\pi\pi$ threshold is substantial even at half normal nuclear matter density [2].

Recent experimental data from the CHAOS collaboration [8,9] at TRIUMF appear to indicate a density-dependence of the in-medium $\pi\pi$ scattering amplitude in the direction predicted by the Jülich model. In the CHAOS experiment a pion beam of nominal kinetic energy T_π=282.7 MeV was directed at various nuclear targets, and two outgoing pions were detected in coincidence. With increasing nuclear mass number, the corresponding invariant mass spectra show a strong enhancement of $\pi^+\pi^-$ pairs just above the two-pion threshold of $M_{\pi\pi}=2m_\pi$. In contrast, only very minor variations are observed for $\pi^+\pi^-$ pairs. This is consistent with what one would expect if the effect is due to the final state interaction of the pions produced at finite nuclear density since the $\pi^+\pi^+$ state is pure I=2, while the $\pi^+\pi^-$ S-wave is two-thirds I=0.

Before we can assert that this view of the process explains the data we need not only the in-medium, off-shell $\pi\pi$ amplitudes, but also a model for the production process $\pi A \rightarrow \pi\pi A$ in order to make quantitative comparisons with the date. Since our emphasis here is on the possible medium effects in the $\pi\pi$ interaction, we treat the pion production process very simply. First, we assume that it always proceeds as an elementary process on a single nucleon. Second, we account only for the two most important contributions [9,10] , which are the one-pion exchange reaction, contributing to both the isoscalar and isotensor channel and the $N^*(1440)$ resonance formation, leading to isoscalar $\pi\pi$ states only. The contribution of the $N^*(1440)$ to the two-pion final state is modeled as proceeding via an intermediate scalar-isoscalar resonance, $\tilde{\sigma}$, of invariant mass $M_{\pi\pi}$, which subsequently decays into two pions; i.e $\pi N \rightarrow N^*(1440) \rightarrow \tilde{\sigma}\, N \rightarrow \pi\pi N$.

Since there is no low-lying genuine σ resonance in the Jülich model, we identify the $\tilde{\sigma}$ with the ε resonance located at $M_{\pi\pi} \approx 1400$ MeV. Its coupling to $\pi\pi$ states is well determined by a satisfactory fit to the $\delta_{\pi\pi}^{00}$ phase shifts above 1 GeV [2].

For the $N^*(1440)N\varepsilon$ vertex we assume scalar coupling,

$$\mathcal{L}_{N^*N\varepsilon} = g_{N^*N\varepsilon}\, \Psi^+_{N^*} \varepsilon \Psi_N + \text{h.c.}$$

and estimate the corresponding coupling constant $g_{N^*N\varepsilon}$ from the experimentally measured branching ratio of 5-10\% for $N^*(1440) \rightarrow N\pi\pi^{I=0}_{\text{S-wave}}$ [11]. Similarly, for the entrance channel, we employ the usual interaction vertex

$$\mathcal{L}_{N^*N\pi} = \frac{f_{N^*N\pi}}{m_\pi} \Psi^+_{N^*} \vec{\sigma}\cdot\vec{q}\,\tau_a \pi_a \Psi_N + \text{h.c.}$$

and adjust the $N^*N\pi$ coupling constant to the branching ratio for $N^*(1440) \rightarrow N\pi$ of 60-70% [11].

In the next step we account for the experimental acceptance of the CHAOS spectrometer via an *acceptance factor* $A(t, M_{\pi\pi}, s_{tot})$ that we evaluate by a Monte Carlo technique (here t is the 4-momentum transfer squared to the nucleon, $M_{\pi\pi}$ is the invariant mass of the final $\pi\pi$ system and s_{tot} is the total c.m. energy squared of the initial πN system). We do this by generating events in the c.m. frame of the final pion pair according to our theoretical scattering amplitude, then transform them to the laboratory frame to see if they fall within the experimental acceptance of the spectrometer.
This yields the differential cross section for pion production on free nucleons,

$$\frac{d\sigma^{\pi^+N^*}}{dM_{\pi\pi}} = \frac{q_{out}}{16\pi^3 p_{lab}^2} \int_{t_{min}}^{t_{max}} dt A(t, M_{\pi\pi}, s_{tot}) \left| \mathcal{M}^{\pi^+N^*} \right|^2$$

where the $\mathcal{M}^{\pi^+N^*}$ is the coherent sum of the one-pion and $N^*(1440)$ amplitudes.

Finally we assume that the production of the pion

pairs occurs at a single nuclear density. We then average the cross-section above over the Fermi sphere appropriate to that density. The results of our calculation are shown in figs 1 and 2.

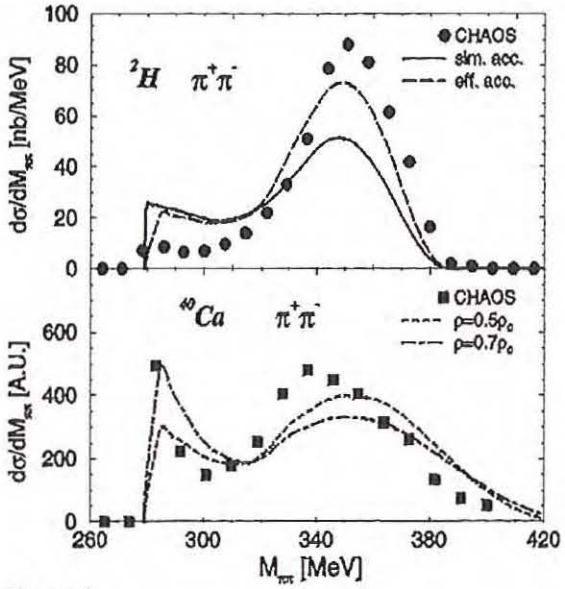

Figure 1.

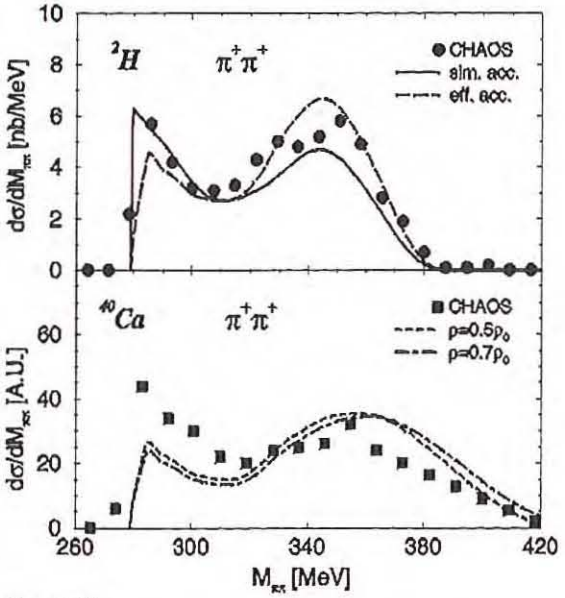

Figure 2.

[1] D. Lohse, J.W. Durso, K. Holinde and J. Speth, Phys. Lett. **B234**, (1989) 235; Nucl. Phys. **A516**, (1990) 513; B.C. Pearce, K. Holinde and J. Speth, Nucl. Phys. **A541**, (1992) 663; G. Janssen, B.C. Pearce, K. Holinde and J. Speth, Phys. Rev. **C52**, (1995) 2690

[2] R. Rapp, J.W. Durso and J. Wambach, Nucl. Phys. **A596** (1996), 436

[3] R. Rapp, PhD thesis Bonn 1996, in *Berichte des Forschungszentrum Jülich* 3195, (Jülich, 1996)

[4] S. Weinberg, Phys. Rev. Lett. **17**, (1966) 616; Phys. Rev. **166**, (1968) 1568

[5] G. Chanfray, Z. Aouissat, P. Schuck and W. Nörenberg, Phys. Lett. **B256**, (1991) 325; V. Mull, J. Wambach and J. Speth, Phys. Lett. **B286**, (1992) 13; Z. Aouissat, G. Chanfray and P. Schuck, Mod. Phys. Lett. **A15**, (1993) 1379

[6] P. Schuck, W. Nörenberg and G. Chanfray, Z. Phys. **A330**, (1988) 199

[7] Z. Aouissat, R. Rapp, G. Chanfray, P. Schuck and J. Wambach, Nucl. Phys. **A581**, (1995) 471

[8] CHAOS Collaboration, F. Bonutti *et al.*}, Phys. Rev. Lett. **77**, (1996) 603

[9] F. Bonutti *et al.*, Nucl. Phys. **A** (1998), in press

[10] E. Oset and M.J. Vicente-Vacas, Nucl. Phys. **A446**, (1985) 584

[11] R. Barnett *et al.*, Phys. Rev. **D54**, (1996) 1

[1] Dept. of Physics and Astronomy, SUNY at Stony Brook, Stony Brook NY 11794-3800, U.S.A.

[2] Physics Department, Mount Holyoke College, South Hadley, MA 01075, U.S.A.

Photon-Photon and Photon-Hadron Interactions in pp and AA Collisions

G. Baur, K. Hencken*, P. Stagnoli*, and D. Trautmann*

In central collisions at relativistic heavy ion colliders like RHIC at Brookhaven and LHC at CERN/Geneva one aims at producing and detecting a new form of hadronic matter, the Quark Gluon Plasma. It is the purpose of [1] to discuss a complementary aspect of these collisions: the very peripheral ones. Due to coherence there are strong electromagnetic fields of short duration in such collisions. They give rise to photon–photon and photon–hadron collisions up to invariant mass regions hitherto unexplored experimentally. Recently it was suggested to use the CMS detector at LHC to do photon–photon physics at LHC [2]. Some aspects of this were discussed in detail in connection with the Letter of Intent for FELIX [3].

Ref. [1] is structured as follows: After a general introduction a survey of peripheral high energy collisions is given. Then impact parameter dependent equivalent photon spectra are discussed. They serve to calculate the γ-γ luminosities relevant for the heavy ion collisions, where strong absorption at small impact parameters is an essential feature. In a chapter on photonuclear reactions the production of vector mesons is discussed among other things. This is of interest for LHC physics, where a new energy regime will be entered and also for RHIC, where the invariant mass region of HERA is relevant [4]. Then photon-photon physics is discussed with applications to LHC [2, 3] and RHIC [4]. Then QED electrons are discussed, with special emphasis to the effects of strong fields, like the multiple pair production. It is concluded that photon-photon physics and, more generally, peripheral collisions are an interesting and fruitful topic of research for future hadron colliders. Shortened and somewhat updated reviews can also be found in the following proceedings [5],[7],and [6]. Calculation of higher order effect in electron-positron pair production in relativistic heavy ion collisions have recently been done in [8]. Whereas the single-pair production cross section is mainly unaffected by these higher order effects, cross section for multiple pair production were found to be rather sensitive.

References:

[1] G. Baur, K. Hencken and D. Trautmann, Journal of Physics G Topical Review 24(1998)1657.

[2] G. Baur, K. Hencken, D. Trautmann. S. Sadovsky and Yu. Kharlov , Photon-Photon Physics with heavy ions at CMS, CMS Note 1998/009, available from the CMS information server at http:/cmsserver.cern.ch,1998 and "Non QGP Physics at CMS" CMS Heavy Ion Chapter, in preparation.

[3] FELIX Letter of Intent, CERN/LHCC97-45, LHCC/I10(1997).

[4] S. Klein and E. Scannapieco, *The Gold Flashlight*, STAR Note 298, 1995.

[5] G. Baur, K. Hencken, and D. Trautmann, Two Photon Physics in pp and AA collisions, invited talk, Proceedings of the Lund workshop on photon interactions and the photon structure, Lund, September 10-13, 1998, edited by G. Jarlskog and T. Sjostrand, hep-ph/9810418.

[6] G. Baur, K. Hencken, and D. Trautmann, Photon-photon and photon-hadron interactions at Relativistic heavy ion colliders,Talk given at the Erice 98 Summer School on Heavy Ion Physics, to be published in the Proceedings, nucl-th/9810078.

[7] D.Trautmann,Z.Halabuka,T.Heim,K.Hencken, H.Meier,and G.Baur Excitation and Ionization of exotic and non-exotic atoms in heavy ion collisions,Denton Conference,November1998

[8] K. Hencken,D. Trautmann, and G. Baur, to appear in Phys. Rev. C, nucl-th/9808035.

*Institut für Theoretische Physik, Universität Basel, Klingelbergstrasse 82, CH 4056 Basel, Schweiz

Bethe-Heitler cross-section for very high photon energies and large muon scattering angles

G.Baur and A.Leuschner*

This work arose out of a practical question. At future Linear Colliders like TESLA [2] electron and positron beams of several hundreds of GeV and high beam powers of some 10 MW have to be absorbed after having passed the interaction region. In this process, high energy photons are produced which in turn give rise to high energy muons. In order to estimate the muon radiation dose at earth surface above the Linear Collider [3] pair production cross-sections for large angles are necessary. This is a well known problem which has been studied many times, most elaborately probably by Y.S.Tsai [4]. An exact lowest order formula is given there, which corresponds to the graphs shown in figs.1 a) and b). The infor-

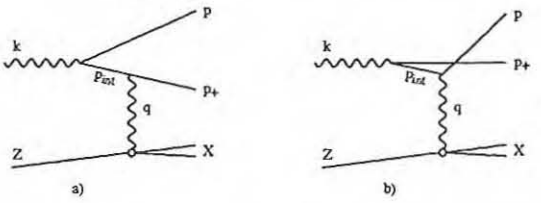

Figure 1: Feynman graphs describing the process $\gamma + A \rightarrow p + p_+ + X$

mation about nuclear structure is fully contained in the electromagnetic structure functions W_1 and W_2. However, this formula is very complicated and hard to evaluate practically, especially if one has to integrate over the unobserved lepton with fourmomentum p_+ (e or μ, we are here concerned only with muons). Therefore practical calculations were done using the Weizsäcker-Williams (or equivalent photon) approximation. This corresponds to the kinematical situation where the square of the momentum of the exchanged photon, $q^2 = -Q^2$, is specially small ($q^2 \approx 0$). In many situations, this is the dominant contribution. In our studies we found another kinematical situation to be important. It corresponds to the muon pole, where the intermediate muon is close to its mass-shell ("equivalent muon approximation"). This has been studied before [5] (see also [6]) and we adopt the formulations of these authors.

Starting from the usual formula for the Bethe-Heitler process (where infinitely heavy point-like nuclei are assumed) we explain the general features of the pair production process and its important limiting cases. Then we discuss the general case, where structure effects are taken into account (along with the effects due to the finite mass, or recoil effects). The information needed as an input is sufficiently well known (see [7]), specially from electron scattering. Then we provide some illustrative examples, together with discussions and conclusions. In fig.2 we show muon inclusive cross-sections for the Bethe-Heitler process off a proton.

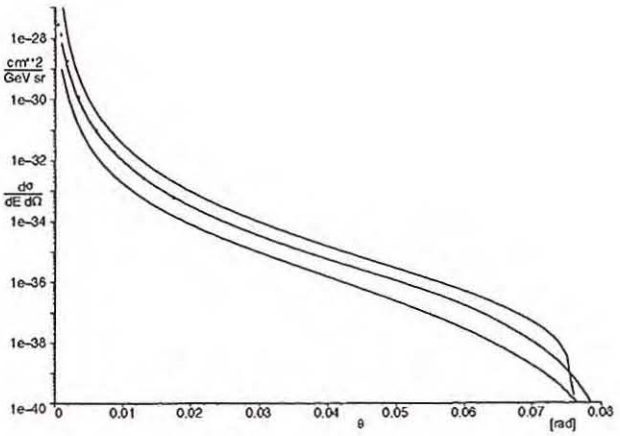

Figure 2: The inclusive muon cross-section in γ-p scattering of 200 GeV photons on a proton as a function of the polar angle θ. The muon energy is 120 GeV. From top to down 3 different curves are shown: deep inelastic, elastic, p-Δ.

References:

[1] G.Baur, A.Leuschner: to be submitted to Eur.Phys.J C

[2] R. Brinkmann et al.: *Conceptual Design of a 500 GeV e^+e^- Linear Collider with Integrated X-ray Laser Facility.* DESY 1997-048, ECFA 1997-182

[3] G. Baur, A. Leuschner, K. Tesch: *Muon doses at earth surface above the Linear Collider: Improved calculations.* Internal Report, DESY D3-91, September 1998

[4] Y.S. Tsai: *Pair production and bremsstrahlung of charged leptons.* Rev.Mod.Phys. 46(1974)815

[5] M. Chen, P. Zerwas: *Equivalent-particle approximation in electron and photon processes of higher-order QED.* Phys.Rev. D12(1975)187

[6] V.N. Baier, V.S. Fadin, V.H. Khoze: *Quasi-real electron method in high energy quantum electrodynamics.* Nucl. Phys. B65(1973)381

[7] *Review of Particle Properties.* Eur.Phys.J. C3(1998)1

*Deutsches Elektronen-Synchrotron DESY
Strahlenschutzgruppe
Notkestrasse 85
22607 Hamburg

Bound-Free Pair Production in Relativistic Heavy Ion Collisions and Relativistic Antihydrogen Production

H.Meier*,Z.Halabuka*,K.Hencken*,D.Trautmann*,and G.Baur

Antihydrogen,the simplest bound state of antimatter,has first been produced and detected in 1995 at CERN in the Low Energy Antiproton Ring(LEAR). [1] We evaluate the matrixelement for bound-free pair production using partial wave decomposition. [2] The same matrixelement is also evaluated in [3] where perturbative wave functions for the leptons are used.In the present method,the validity is not restricted to small values of $Z\alpha$.The charge number of the nucleus,to which the lepton is bound is denoted by Z.We can also apply this method to e+e- bound free transitions in relativistic heavy ion collisions.There are some discrepancies of the present results to those of [3] for small values of the Lorentz factorγ,while the agreement for larger values of γ is good.The reason may lie in the approximations used for the wave functions in [3] .For low values of γ one is sensitive to smaller distances,where the exact wave functions used here differ more from each other than at larger distances,relevant for the larger values of γ.See e.g. Sects.14 and 15 of [4]
Now we apply our methods to bound-free pair production in relativistic heavy ion collisions.Exact Dirac wave functions are used. In Fig.1 we show our results for pair production with e- capture into the K-shell. This is relevant for the heavy ion luminosities at RHIC and LHC. For a general reference see [5]We also calculated capture into higher orbits(2s,2p1/2,2p3/2,3s,..)and compare to the simple $1/n^3$ scaling law.For further details see [6]. .

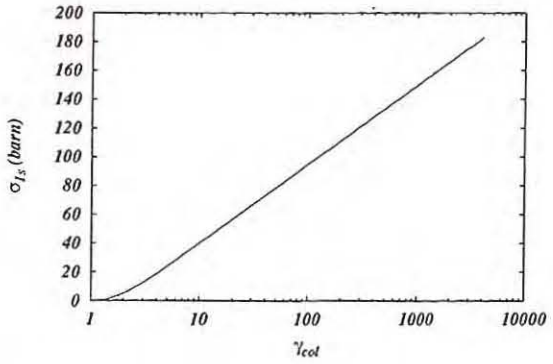

Figure 1: The cross section$\sigma_{1s}$for K-shell bound-free pair production in an Au-Au collision is shown as a function of the Lorentz factor γ in the collider reference frame

References:

[1] PS21 collaboration,W.Oelert,spokesperson,G.Baur et al. Phys.Lett.B368(1996)251

[2] H.Meier,Z.Halabuka,K.Hencken,D.Trautmann and G.Baur,Eur.Phys.J.C5(1998)287,hep-ph/9712461

[3] C.A.Bertulani and G.Baur,Phys.Rev.D58(1998)034005

[4] H.A.Bethe and E.E.Salpeter,Quantum Mechanics of One- and Two-Electron Atoms,1977,Plenum Publishing Corporation,New York

[5] G.Baur,K.Hencken and D.Trautmann J.Phys.G:Topical Review 24(1998)1657

[6] H.Meier et al.,to be published

*Institut für Theoretische Physik Universitaet Basel, Klingelbergstrasse 82 CH4056Basel Schweiz

Bremsstrahlung from Electrons and Positrons in Relativistic Heavy Ion Collisions

K. Hencken*, D. Trautmann*, and G. Baur

The cross-section for electron-positron pair production in relativistic heavy ion collisions is huge, see, e.g., [1] for a general reference. On the other hand, bremsstrahlung in peripheral relativistic heavy ion collisions was found to be small, both for real [2] and virtual [3] bremsstrahlung photons. This is essentially due to the large mass of the heavy ions. Since the cross section for e^+e^- pair production is so large, of the order of 100 kb for RHIC and LHC, one can expect to see sizeable effects from the radiation of these light mass particles. In the soft photon limit (see, e.g., [5]) we can calculate the cross section for soft photon emission of the process as

$$Z + Z \to Z + Z + e^+ + e^- + \gamma$$

as

$$d\sigma(k, p_-, p_+) = -e^2 \left[\frac{p_-}{p_- k} - \frac{p_+}{p_+ k}\right]^2 \frac{d^3k}{4\pi^2\omega} d\sigma_0(p_+, p_-)$$

where $d\sigma_0$ denotes the cross section for the e^+e^- pair production in heavy ion collisions. Using our code [4] for the e^+e^- pair production we can calculate the soft photon emission from the outgoing lepton lines numerically according to this equation. An alternative approach is done by using the DEPA(double equivalent photon approximation) and calculating the exact lowest order matrixelement for the process

$$\gamma + \gamma \to e^+ + e^- + \gamma.$$

In fig.1 we show results of such a calculation for low energy photons.

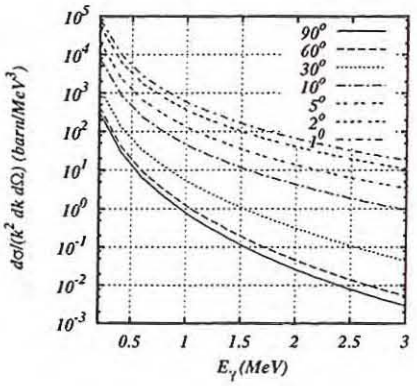

Figure 1: *The cross section for bremsstrahlungsphotons for Au-Au collisions at RHIC are shown as a function of the photon energy for different angles.*

These low energy photons constitute a background for the detectors. Unlike the low energy electrons and positrons, they are of course not bent away by the magnets. Recently the soft bremsstrahlung photons from central ultrarelativistic nucleus-nucleus collisions were suggested to be used to infer the rapidity distribution of the outgoing charge [7]. We note that the presently considered soft photons from peripheral collisions can be a source of background for the considered experiment.

References:

[1] G. Baur, K. Hencken and D. Trautmann J.Phys.G Topical Review 24 (1998) 1657.

[2] C. A. Bertulani, G. Baur Phys. Rep. 163 (1988) 299.

[3] H. Meier, K. Hencken, D. Trautmann, and G. Baur Eur. Phys. J. C2 (1998) 741.

[4] A. Alscher, K. Hencken, D. Trautmann, and G. Baur, Phys. Rev. A55 (1997) 396.

[5] S. Weinberg, The Quantum Theory of Fields Vol. 1, 1995, Cambridge.

[6] V. S. Fadin and V. A. Khoze, JETP17 (1973) 313.

[7] S. Jeon, J. Kapusta, A. Chikanian, and J. Sandweiss, Phys. Rev. C58 (1998) 1666.

[8] "Conceptual design of the relativistic heavy ion collider(RHIC)", Brookhaven National Laboratory, Report BNL51932 (May 1986).

*Institut für Theoretische Physik Universitaet Basel, Klingelbergstrasse 82 CH4056Basel Schweiz

4. NUCLEAR STRUCTURE AND REACTION MECHANISM

There is no missing isoscalar monopole strength in ^{58}Ni.

S.Kamerdzhiev*, J.Speth, G.Tertychny*, and F. Osterfeld

Till very recently there were still many questions connected with properties of the IS E0 giant resonance in nuclei with A<90. An important one being the problem of distribution of E0 strength and small amount of it observed in several nuclei . The most recent ^{40}Ca(α,α') experiments at E_α = 240 MeV at small angles including 0° gave (92 ± 15)% of the IS E0 EWSR in the (8 - 29) MeV interval [1]. But the same experiments and the same analysis for ^{58}Ni gave unexpected results. Only 32% (at best <50%) of the IS E0 EWSR was observed in the (12.0 - 25.0) MeV region [2]. In fact, these ^{58}Ni results increased uncertainties for the A<90 nuclei. The improved analysis of the experimental data [2] in Ref. [3] based upon the most realistic folding models gave about 50% of the IS E0 EWSR in ^{58}Ni.

In our preliminary calculations [6] we compared with the theory *only the form of the experimental spectra* for the ^{58}Ni(α,α') in the observed (12 -25) MeV interval because there were no data about the corresponding absolute values in Ref. [2]. A good agreement with these experiments was obtained but our value of the IS E0 EWSR was equal to 71.4%. We concluded that a considerable part of the strength might be hidden in the experimental background [2].

Recently it was reported by the authors of Ref. [2] that they have extended the observed energy interval up to 35 MeV in several of the A<90 nuclei including ^{58}Ni and found some additional IS E0 strength at higher excitation energy [4]. Thus, due to this fact and also with taking into account a continuum under the monopole peak 75-100% of the EWSR might be present below 35 MeV excitation energy [5]. In addition, some absolute values of experimental spectra are known at present [4].

For the A<90 nuclei the giant resonance strength has a broad distribution, the role of the nuclear surface is more important than for heavier nuclei and (α,α') reactions are very sensitive to the nuclear surface. Therefore, taking into account, in addition to the RPA configurations, more complex 1p1h⊗phonon configurations with surface collective phonons should be rather essential. For these reasons a consistent microscopic nuclear structure model which accounts for both of these kind configurations has been used here [7, 8, 9]. It was shown in Ref. [9] that the microscopic transition densities depend on the energy interval considered especially if the interval is small (we considered 5 MeV bins). In this respect our microscopic transition densities are very different from the phenomenological ones which are not energy dependent and which have been used sofar in conventional analyses. We calculated in the present microscopic approach the distribution of the IS E0 strength and the corresponding (α,α') cross sections for the isotope ^{58}Ni in the both analysed energy regions (12.0 - 25.0) MeV [2] and (12.0 - 35.0) MeV [4, 5].

The comparison of the cross sections with the experiment at the observed angle θ = 1.08° is shown in Fig. 1 and in Fig. 2 at θ = 4.08° The experimental data in Fig. 1 have been taken from Ref. [4] . They were obtained there after substraction of the experimental background. One can see from Figs. 1, 2 that a good agreement with the experiment for absolute values of the total cross sections has been also obtained. The contribution of the IS E0 resonance in our calculations is 71.4% of the IS E0 EWSR in the (12.0 - 25.0) MeV interval. This means that a considerable part of the E0 strength was hidden in the experimental background [2] (see also below).

In the recent ^{58}Ni(α,α') experiment [4] (see also [5]) the authors extended the observed energy interval up to 35 Mev and obtained an additional monopole strength in the (25.0 - 35.0) MeV region. Therefore, it was necessary to substract another background and another additional strength should appear under the previous (12.0 - 25.0) MeV interval. This can be clearly seen from Fig. 1. In Ref. [2] the background was substracted beginning from 25 MeV for the case θ = 1.08° as it is shown by the upper border of the shaded area in Fig. 1. In other words, only the part of the E0 resonance which is higher than this upper border could be observed in Ref. [2]. In the recent experiment [4, 5] the background was substracted beginning from about 35 MeV, to be exact, the experimental data given in our Figs. 1,2 were counted from the new background which corresponds to zero on the vertical axis. So the shaded area in Fig. 1 corresponds to the IS E0 strength which could not be observed in Ref. [2] and was observed in the newest experiments in addition to the old result in Ref. [2]. It is possible to estimate approximately the part of the IS E0 EWSR corresponding to this shaded area. The square of the area which is the sum of the shaded one and that of the E0 resonance upper than the shaded area is about 138.3 mb/sr. This figure corresponds to our 71.4 % of the EWSR. The shaded area gives 42.6 mb/sr which corresponds to 22 % of the IS E0 EWSR and was missed in the Ref. [2] experiment.

We have also performed the calculations like those in Figs. 1,2 for the unstable nucleus ^{56}Ni which is of astrophysical interest. The difference between the corresponding curves in not very noticeable on the whole for the regions beginning from about 10 MeV. Only the maximal values of the double cross sections are more for ^{56}Ni by 12-14%. But for the (5-10) MeV regions the ^{58}Ni values for the total cross sections are

much larger than for ^{56}Ni, especially for $\theta = 4.08°$ this difference is nearly a factor of two.

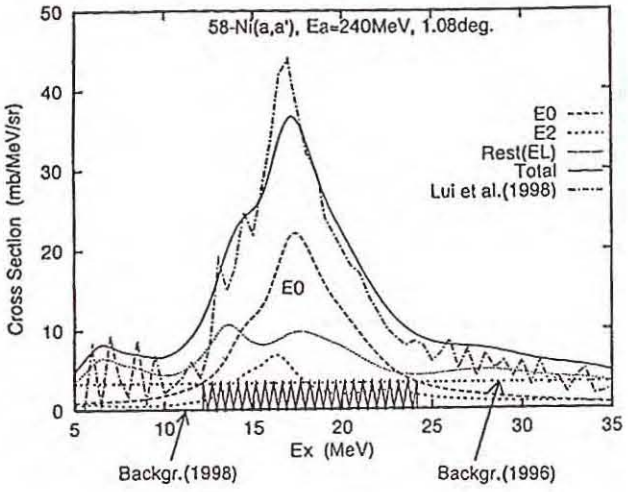

Fig.1. Cross sections of ^{58}Ni(α, α') at $E_\alpha = 240$ MeV and $\theta = 1.08°$. The experimental data (dash-dotted curve) were taken from Ref. [4]. The solid curve gives the total (summed) cross section, the dotted line ("Rest(EL)") corresponds to the sum of the IS and IV E1, and IS E3 and E4 multipoles. The shaded area shows an additional IS E0 strength which could not be observed in the experiments of Ref. [2], see text. This area corresponds to 22% of the IS E0 EWSR.

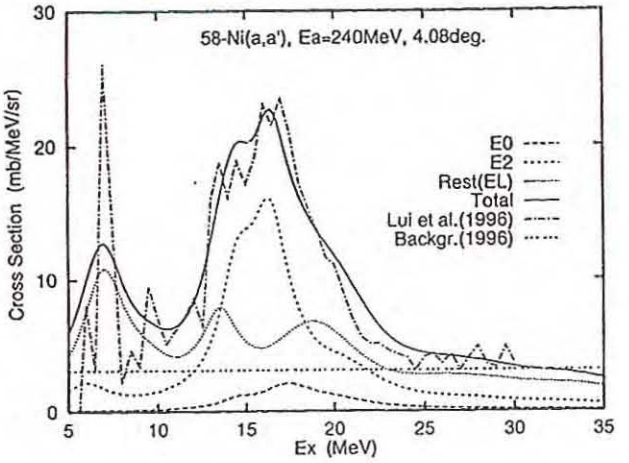

Fig.2. Same as in Fig.1 but for $\theta = 4.08°$. The experimental data were produced by us using the results of Ref. [2].

In conclusion, using a microscopic nuclear structure model that takes into account the continuum RPA and 1p1h⊗phonon configurations we were able to describe the experimental spectra for ^{58}Ni(α, α') in the observed energy interval [2] with the microscopic ρ^L_{tr}s. However, the percentage of the IS E0 EWSR turned out to be equal to 71.4% in the earlier observed (12.0 - 25.0) MeV interval instead of the value of $\leq$50% of the EWSR reported in Refs. [2, 3], where a conventional analysis has been used. In the new (12.0 - 35.0) MeV observed interval we have obtained 89.6% of the EWSR. The latter is confirmed by the newest analyses of the same authors. We have shown that a fraction of the IS E0 strength in ^{58}Ni might be hidden in the experimental background [2]. Theoretically, it is difficult to imagine any mechanism which would reduce so strongly the IS E0 strength in nuclei heavier than ^{40}Ca. Our general conclusion is that for A<90 nuclei it is necessary to use microscopic transition densities.

References:

[1] D.H. Youngblood, Y.-W. Lui, and H.L. Clark, Phys. Rev. C 55, 2811 (1997).

[2] D.H. Youngblood, H.L. Clark, and Y.-W. Lui, Phys. Rev. Lett. **76**, 1426 (1996).

[3] G.R. Satchler and Dao T. Khoa, Phys. Rev. C **55**, 285 (1997).

[4] Y.-W. Lui, D.H. Youngblood, and H.L. Clark, Contribution to the Topical Conference on Giant Resonances, Italy, Varenna, May 1998.

[5] A.van der Woude, Summary talk at the Topical Conference on Giant Resonances, Italy, Varenna, May 11-16 1998, to be published in the Proceedings of the Conference in Nucl. Phys. A.

[6] S. Kamerdzhiev, J. Speth, and G. Tertychny, in Proceedings of the Intern. Conference on Nuclear Structure and Related Topics, edited by S.N. Ershov, R.V. Jolos and V.V. Voronov, Dubna, September 1997, p. 347; in Proceedings of the Workshop on the Structure of Mesons, Baryons and Nuclei, Cracov, May 1998, edited by S. Drozdz and S. Krewald, Acta Phys. Pol. 28, 2231 (1998).

[7] S. Kamerdzhiev, J. Speth, and G. Tertychny, V. Tselyaev, Nucl. Phys. **A555**, 90 (1993).

[8] S. Kamerdzhiev, G. Tertychny, and V. Tselyaev, Phys. Part. Nucl. **28**, 134 (1997).

[9] S.Kamerdzhiev, J. Speth, and G. Tertychny, Nucl. Phys. **A624**, 328 (1997).

*The Institute of Physics and Power Ingineering, 249020 Obninsk, Russia.

Configuration Mixing Effects in Isoscalar Giant Dipole Resonance

M. Wójcik* and S. Drożdż*

We evaluated the isoscalar giant dipole resonance (ISGDR) strength distribution using a prescription described in ref [1]. ISGDR is one of the most interesting nuclear excitation modes. This partly originates from the fact that its centroid energy can directly be related to the nuclear compression modulus [2]. The corresponding one-body isoscalar dipole operator reads:

$$f = r^3 Y_1 - \eta r Y_1,$$

where $\eta = 5\langle r^2 \rangle / 3$. The second term in this equation removes the spurious center of mass motion component from the operator $r^3 Y_1$ [3]. The resulting $3\hbar\omega$ strength distribution in ^{208}Pb on the 1p1h level is located between 20 and 25 MeV. This about corresponds to the energy region where the isoscalar dipole strength can be identified in the present day experiments on ^{208}Pb [4]. The picture changes however significantly when mixing due to the coupling to 2p2h states is allowed. This is illustrated in Fig. 1 which on the three succesive panels indicates a degree of fragmentation for $H_{th} = 0.4, 0.3$ and 0.2 MeV. The number of the 2p2h states (349,1125 and 4374 respectively) included correspond to $|\langle 1|\hat{H}|2\rangle| \geq H_{th}$.

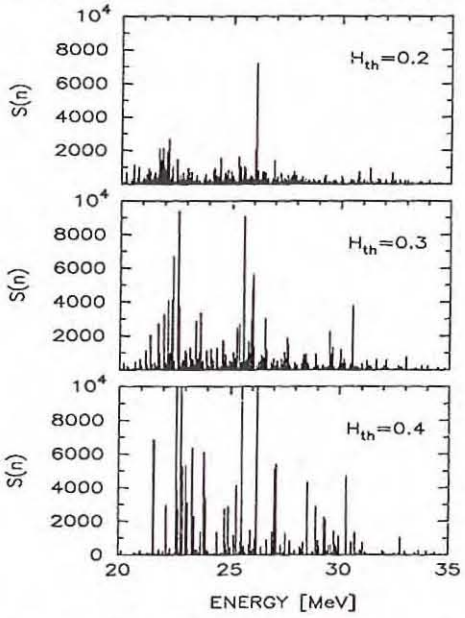

Fig. 1. Isoscalar $3\hbar\omega$ dipole strength distribution in ^{208}Pb calculated in the space of 1p1h and 2p2h states, for three different values of H_{th}.

Consistently with our previous investigations [5] a specific form of the resulting strength distribution strongly depends on many factors and thus also on H_{th}. However, more global characteristics, like a percentage of the total strength in certain sufficiently large energy windows is much more stable. A reasonable convergence of those results, together with a realistic input of the present model, provides quite a convincing indication that one may expect about 50% of the total $J^\pi = 1^-$ isoscalar $3\hbar\omega$ strength in the higher energy region, above 25 MeV, i.e., in the region which is dominated by many other multipoles and thus this portion of the strength escapes an experimental detection. Even above 30 MeV one finds almost 10% of the total strength. The present calculations thus suggest that a recent empirical estimation [4] of the nuclear incompressibility ($K_A = 126 \pm 6$ MeV) for ^{208}Pb may appear much to low.

References:

[1] M. Wójcik, S. Drożdż, Acta Phys. Pol. **B29**, 2239(1998)

[2] S. Stringari, Phys. Lett. **108B**, 232(1982);
R. de Haro, S. Krewald and J. Speth, Phys. Rev. **C26**, 1649(1982)

[3] N. van Giai and H. Sagawa, Nucl. Phys. **A371**, 1(1981)

[4] B.F. Davis *et al.*, Phys. Rev. Lett. **79**, 609(1997)

[5] S. Drożdż, S. Nishizaki and J. Wambach, Phys. Rev. Lett. **72**, 2839(1994);
A. Górski and S. Drożdż, Acta Phys. Polonica **B28**, 1111(1997);
S. Drożdż, S. Nishizaki, J. Speth and M. Wójcik, Phys. Rev. **E57**, 4016(1998)

* Institute of Nuclear Physics, PL-31-342 Kraków, Poland
Institut für Kernphysik, Forschungszentrum Jülich, D-52425 Jülich, Germany

Density dependent relativistic Hartree-Fock theory with isovector mesons

B.Q.Chen*, Z.Y.Ma*, F.Grümmer, S.Krewald

Brockmann and Toki have suggested a method that allows to link the binding energies and radii of finite nuclei to the nucleon-nucleon interaction via a local density dependence approximation to the Dirac–Brückner–Hartree-Fock (DBHF) [1]. Density dependent coupling constants of the meson-nucleon interactions are derived from DBHF calculations in nuclear matter. The relativistic density dependent mean field approach (RDH) with σ, ω as well as ρ mesons gives satisfactory descriptions of ground state properties of a few stable nuclei, although the fit quality cannot match the one achieved in the RMF theories [2]. Investigations of this type are very important for our understanding of properties of finite nuclei in a parameter free way. The model so far has been applied only to a relatively small number of nuclei. Therefore it is of great interest to extend such density dependent relativistic model to deformed and exotic nuclei.

In the RDH the Pauli exchange effects have been neglected. Fritz, Müther and Machleidt [3] pointed out that the nuclear radii are reduced once the Pauli exchange effects are taken into account. On the other hand, after incorporating both π and ρ-exchange (including in particular the tensor part of the ρ-N coupling) into the relativistic density dependent Hartree-Fock approach, larger radii are found [4]. These findings suggest that the effects of Fock terms be investigated more thoroughly.

As an example for our study we choose the Ca isotope chain. In both the relativistic density dependent Hartree- and Hartree-Fock approximation, the ω-N and the σ-N coupling constants are adjusted to reproduce the nucleon self-energy in nuclear matter. Therefore it is not too surprising that both methods reproduce the binding energies of N=Z nuclei with comparable accuracy.

In Fig. 1 we show the binding energies of the Ca isotopes obtained in our model. The effect of the Fock terms on the binding energies in the vicinity of the N=Z nucleus ^{40}Ca is small, as expected. With increasing neutron excess, however, the inclusion of the Fock terms leads to a reduction of the binding energy. One might expect that isovector mesons may contribute significantly for nuclei with large neutron excess. We therefore extend the calculation to include both π and ρ. We find that the inclusion of the π and the ρ makes a perceptible change in the calculated binding energies. Experimentally, the binding energies of the Ca isotopes are known only till A=56 (open circles) [5]. We use the finite range liquid drop model by Möller, Nix and Kratz [6] to extrapolate the binding energies of the exotic nuclei till A=70. The comparison with the experimental data shows that the RDH approach is not able to reproduce the slope of the curve of the experimental binding energies. The slope is properly described as soon as the Fock term is included.

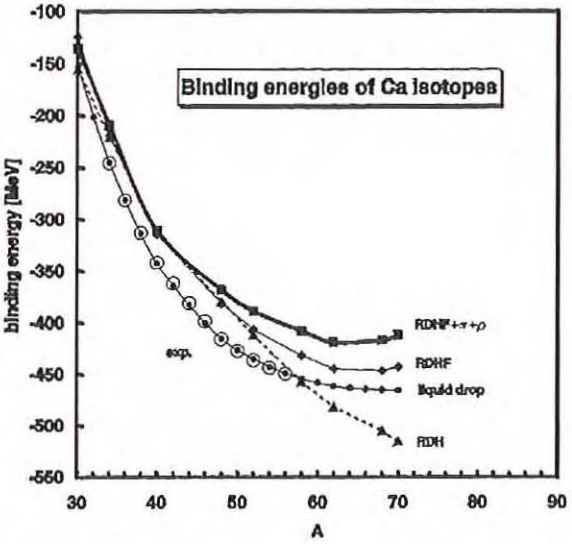

To conclude, the density dependent relativistic Hartree-Fock theory has been employed to investigate properties of neutron rich nuclei. For the first time the effect of Fock exchange terms and isovector mesons on these properties has been studied. It is found that these terms give large contributions to properties of exotic nuclei as compared to the Hartree approach. Especially in the case of very neutron rich nuclei, where e.g. a neutron halo is expected, one has to take into account all additional effects.

[1] R.Brockmann and H.Toki, Phys.Rev.Lett. **68,** 3408 (1992)
[2] P.Ring, Prog.Part.Nucl.Phys. **37**,193 (1996)
[3] R.Fritz, H.Müther and R.Machleidt, Phys.Lett. **71**, 46 (1993); Phys.Rev. **C49**, 633 (1994)
[4] Z.Y.Ma, H.L.Shi and B.Q.Chen, Phys. Rev. **C50** , 3170 (1994); **C52**, 144 (1995)
[5] G.Audi and A.H.Wapstra, Nucl.Phys. **A595**, 409 (1995)
[6] P.Möller, J.R.Nix and K.L.Kratz, Atomic data and nuclear data tables **66**, No 2 (1997)

* China Institute of Atomic Energy, Beijing 102413, P.R.China

A shell model description of high-spin states in rare earth nuclei

R. D. Ratna Raju[a], S. B. Prem Kumar[b], I. Shyam Kishore[a], F.Grümmer

A cluster-rotor weak-coupling model was proposed by Evans and Harris [1] for the description of backbending, approximating the rotating core by a rigid rotor and using a pure pairing force as the residual two-body interaction among abnormal parity particles. This model was later extended by Grümmer and his co-workers [2] by including pair scattering between the core and valence $i_{13/2}$ orbital and Surface Delta Interaction (SDI) instead of pure pairing among valence particles. They studied extensively the behaviour of the moment of inertia varying the particle number as well as the seniority of the valence system

In this work we want to provide a pure shell model description of high-spin states using the pseudo SU(3) truncation scheme [3] in the natural parity configurations of the rare earth nuclei. The usefulness of this truncation scheme for the description of collective properties of heavy deformed nuclei in the low-spin region has already been well established (see e.g. [4]). Our approach in the present work is analogous to the one presented in [2]. But, instead of the rigid rotor states we make use of truncated shell model states to describe the rotating core. The truncation is effected through the pseudo SU(3) scheme.

We chose ^{160}Yb and ^{162}Yb as test cases since a large number of the Yb isotopes exhibit backbending, offering a possibility to test the consistency of the model subsequently. Furthermore, the leading representations that characterise the natural parity proton and neutron configurations are both unique for these isotopes.

In a first stage of calculations the SDI has been used as the proton- and neutron- Hamiltonians of the core. It is then found that the core energies in the yrast band mimic very closely the rigid rotor energies. In order to obtain a more realistic description of the rotational bands we adopted the Hamiltonian (H_{LDR}), introduced by Leschber, Draayer and Rosensteel [5] recently, which is an SU(3) realisation of the quantum triaxial rotor. It can be written as

$$H_{LDR} = C_1\mathbf{J}^2 + C_2X_3 + C_3X_4$$

with

$$X_3 = \frac{1}{6}\sqrt{30}\left[(\mathbf{J}\times\mathbf{Q})^1\times\mathbf{J}^1\right]^0 \text{ and}$$

$$X_4 = \frac{-5}{18}\sqrt{3}\left[(\mathbf{J}\times\mathbf{Q})^1\times(\mathbf{Q}\times\mathbf{J})^1\right]^0.$$

We compare in Figure 1 the theoretical backbend curves obtained with core energies generated using SDI and LDR Hamiltonians for the core with the experimental one for ^{160}Yb. As was pointed out earlier, in the low spin region below the critical angular momentum, the theoretical backbend curve generated with H_{SDI} for the core Hamiltonian, is nearly parallel to the X-axis indicating that the moment of inertia is almost constant. The agreement between theory and experiment is better when H_{LDR} is used to describe the core.

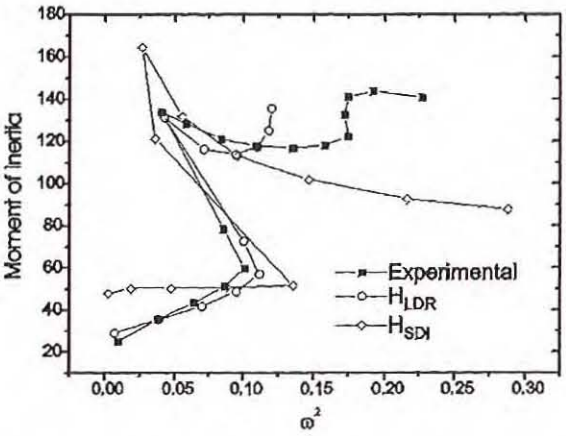

[1] P. J. Evans and S. M. Harris, Nucl. Phys. **A277**, 109 (1977)
[2] F. Grümmer, K. W. Schmid and A. Faessler, Nucl. Phys. **A239**, 289 (1975)
[3] R. D. Ratna Raju, J. P. Draayer and K. T. Hecht, Nucl. Phys. **A202**, 433 (1973)
[4] J. P. Draayer and K. J. Weeks, Ann. Phys. **156**, 41 (1984)
[5] Y. Leschber, J. P. Draayer and G. Rosensteel, J. Phys. G **12**, L179 (1986)

[a] Department of Physics, Andhra University, Visakhapatnam-530 003 AP, India
[b] Currently with Lockhead Martin, NASA space center, Houston, Texas, USA

On Elastic Nucleon-Nucleus Scattering in a Consistent Fermi-Liquid Theory.

V. Klemt

Whereas many-body GREEN'S-function techniques have long been used in nuclear-structure calculations [1][2], they have never become fashionable in reaction theory.

Some of their advantages, in particular inherent proper antisymmetrisation, have early been recognized and described in a review article by VILLARS [3]. However, the whole formalism there, as well as, e. g., in a later article by BRIEVA and NAGARAJAN [4], is developed in terms of the bare nucleon-nucleon interaction, without due consideration of the fact that a force with a strong repulsive core does not generate a suitable HARTREE-FOCK mean field.

An early attempt to describe nuclear reactions consistently in terms of an effective interaction was made by BRENIG [5]. He pointed out that the GREEN'S function method provided a more natural connection to linear-response theory than the more commonly used FESHBACH theory [6]. Additionally, he showed how the S matrix could be expressed, in an RPA-like approximation starting from plausible assumptions on the pole structure of the mass operator, in terms of the many-body T matrix.

Yet, after all, this approach is still rather heuristic. A more systematic connection beteween mass operator and the T matrix was given, for bound states, by the author [7]. Two equations, one of them equivalent to the DYSON equation, another one exploiting particle-number conservation, describe the spectra of even-odd systems, a complementary set of equations generalizes the RPA equations for even-particle systems. The first two of these equations start from the expectation values of the energy and the particle number, respectively. Since this is impossible for continuum states, one has to replace these by matrix elements between incoming and outgoing scattering states. The S-matrix elements formed in this way are restricted to the energy shell. If only the elastic channel is open and the target is a magic nucleus the result becomes particularly simple. Summarizing the quantum numbers of the partial wave in the index s, we get $\left(\delta_{ss'} = \delta_{ll'}\delta_{jj'}\delta(E-E')\right)$

$$e^{2i\delta_s}\delta_{ss'} = \sum_{\nu}\langle\Phi_s^{(-)}|a_\nu^\dagger|\Phi_0\rangle\langle\Phi_0|a_\nu|\Phi_{s'}^{(+)}\rangle$$
$$+\sum_{\nu\nu'}\langle\Phi_s^{(-)}|a_\nu^\dagger|\Phi_0\rangle\langle\Phi_0|a_{\nu'}|\Phi_{s'}^{(+)}\rangle\sum_{\mu\mu'\mu''}\int_{\circlearrowleft}\frac{d\Omega}{2\pi i}$$
$$\times T_{\nu\mu'\nu'\mu}(E,\Omega,0)G_{\mu''\mu'}(\Omega)G_{\mu\mu''}(\Omega)\,.$$

Now the products

$$\langle\Phi_s^{(+)}|a_\nu^\dagger|\Phi_0\rangle\langle\Phi_0|a_{\nu'}|\Phi_s^{(+)}\rangle$$

form a matrix of rank one in the indices ν and ν', so that diagonalization results in one selected single-particle orbit that carries the full overlap strength, while all the others carry none.

Using the relation $|\Phi_s^{(-)}\rangle = e^{-2i\delta_s}|\Phi_s^{(+)}\rangle$ for pure elastic scattering and choosing the index σ for the selected orbit we get on the energy shell

$$\langle\Phi_s^{(+)}|a_\sigma^\dagger|\Phi_0\rangle\langle\Phi_0|a_\sigma|\Phi_{s'}^{(+)}\rangle\big|_{\text{onshell}} = \delta_{ss'}\cos^2(\delta_s-\tilde{\delta}_s)$$

and consequently

$$\tan^2(\delta_s-\tilde{\delta}_s) = \sum_{\mu\mu'\mu''}\int_{\circlearrowleft}\frac{d\Omega}{2\pi i}T_{\sigma\mu'\sigma'\mu}(E,\Omega,0)$$
$$\times G_{\mu''\mu'}(\Omega)G_{\mu\mu''}(\Omega)\,.$$

The quantity δ_s here is the full phase shift of the partial wave s, while $\tilde{\delta}_s$ is (for not too strongly attractive forces) the corresponding maximally possible phase shift generated by a (energy-independent but possibly nonlocal) one-body potential. Usually one may approximately identify this potential with the HARTREE-FOCK mean field.

In the simplest possible case a single pole will give a dominating contribution. Assuming optimal shell closure we get in second order perturbation theory [7] (no angular-momentum coupling carried out for simplicity)

$$\tan^2(\delta_s-\tilde{\delta}_s) = \frac{1}{2}\frac{|V_{\sigma inn'}|^2}{E+\varepsilon_i-\varepsilon_n-\varepsilon_{n'}}$$

with a two-particle one-hole pole. Two special cases are especially interesting: Destructive interference occurs for a pole term that gives $\delta_s = 0$ while a maximal cross section is reached for $\delta_s = \pi/2$ (compare section IV.2 of FESHBACH's book [6]).

The quantity $\cos^2(\delta_s-\tilde{\delta}_s)$ is the exact scattering equivalent to the the single-particle strength factor z_s for bound even-odd states. It remains to be explored whether there are other kinds of correspondence, as e. g. between destructive and constructive interference of scattering states and the single-particle and collectivity dominatated partners with equal quantum numbers among the bound even-odd states.

It is worth mentioning that the equations above give only the magnitude of the difference between the full and the potential phase shift. Full information is, of course, only contained in DYSON's equation.

[1] A. B. Migdal, Theory of Finite Fermi Systems, Interscience Publ. 1967.
[2] J. Speth, E. Werner, W. Wild, Phys. Lett. C (Phys. Rep.) 33 (1977) 127.
[3] F. Villars, in "Fundamentals in Nuclear Theory" (eds. A. DeShalit, C. Villi), IAEA, Vienna 1967.
[4] F. A. Brieva, M. A. Nagarajan, Nucl. Phys. A 452 (1986) 221.
[5] W. Brenig, Zeits. f. Physik 202 (1967) 340.
[6] H. Feshbach, Theoretical Nuclear Physics - Nuclear Reactions, Wiley 1992.
[7] V. Klemt, J. Phys. G 8 (1982) 1547

New applications of Coulomb dissociation for nuclear astrophysics

G. Baur, S. Typel*, and H. H. Wolter*

In nuclear astrophysics radiative capture reactions of the type $b + c \rightarrow a + \gamma$ play a very important role. They can also be studied in the time-reversed reaction $\gamma + a \rightarrow b + c$, at least for those cases where the nucleus a is in the ground state. As a photon beam we use the equivalent photon spectrum which is provided in the fast peripheral collision. Recent reviews, both from an experimental and a theoretical point of view have been given [1], thus we concentrate here on a few points.

Nucleosynthesis beyond the iron peak proceeds mainly by the r- and s-processes (rapid and slow neutron capture) [2, 3]. To establish the quantitative details of these processes, accurate energy-averaged neutron-capture cross sections are needed.

In such a situation, the Coulomb dissociation can be a very useful tool to obtain information on (n,γ)-reaction cross sections on unstable nuclei, where direct measurements cannot be done. Of course, one cannot and need not study the capture cross section on all the nuclei involved; there will be some key reactions of nuclei close to magic numbers. Quite recently, it was proposed [4] to obtain information about (n,γ) reaction cross sections, using nuclei like ^{124}Mo, ^{126}Ru, ^{128}Pd and ^{130}Cd as projectiles. The optimum choice of beam energy will depend on the actual neutron binding energy. Since the flux of equivalent photons has essentially an $\frac{1}{\omega}$ dependence, low neutron thresholds are favourable for the Coulomb dissociation method. Note that only information about the (n,γ) capture reaction to the ground state is possible with the Coulomb dissociation method. The situation is reminiscent of the loosely bound neutron-rich light nuclei, like ^{11}Be and ^{11}Li. In this context the recent Coulomb dissociation experiment of 28.53 MeV/nucleon ^{9}Li is worth mentioning [5]. It is relevant for the ^{8}Li(n,γ) reaction which is of interest for inhomogeneous big bang nucleosynthesis.

A new field of application of the Coulomb dissociation method could be two particle capture reactions. Evidently, they cannot be studied in a direct way in the laboratory. However, sometimes the relevant information about resonances involved can also be obtained by other means (transfer reactions, etc.), like in the triple α-process. Two-neutron capture reactions in supernovae neutrino bubbles are studied in [6]. In the case of a high neutron abundance, a sequence of two-neutron capture reactions, ^{4}He(2n,γ)^{6}He(2n,γ)^{8}He can bridge the $A = 5$ and $A = 8$ gaps. The ^{6}He and ^{8}He nuclei may be formed preferentially by two-step resonant processes through their broad 2^+ first excited states [6]. Dedicated Coulomb dissociation experiments can be useful. Another key reaction can be the ^{4}He(αn,γ) reaction [6]. Also in the rp-process, two-proton capture reactions can bridge the waiting points [7, 8, 9]. From the ^{15}O(2p,γ)^{17}Ne, ^{18}Ne(2p,γ)^{20}Mg and ^{38}Ca(2p,γ) ^{40}Ti reactions considered in Ref. [8], the latter can act as an efficient reaction link at conditions typical for X-ray bursts on neutron stars. A ^{40}Ti $\rightarrow$ p + p + ^{38}Ca Coulomb dissociation experiment should be feasible. The decay with two protons is expected to be sequential rather than correlated ("^{2}He"-emission). In Ref. [9] it is found that in X-ray bursts 2p-capture reactions accelerate the reaction flow into the $Z \geq 36$ region considerably. It is proposed to study the Coulomb dissociation of these nuclei in order to obtain more direct insight into the 2p-capture process [10].

Quantum tunneling processes following Coulomb excitations are studied in a time-dependent approach in [11].

References:

[1] G. Baur and H. Rebel, J. Phys. G: Nucl. Part. Phys. **20** (1994) 1, and Ann. Rev. Nucl. Part. Sci. **46** (1996) 321

[2] C. E. Rolfs and W. S. Rodney, Cauldrons in the Cosmos, The University of Chicago Press, 1988

[3] J. J. Cowan, F.-K. Thielemann and J. W. Truran, Phys. Rep. **208** (1991) 267

[4] M. Gai, ISOL workshop, Columbus/Ohio, July 30 — August 1, 1997

[5] P. Zecher et al.,Phys.Rev.C57(1998)959

[6] J. Görres et al., Phys. Rev. **C52** (1995) 2231

[7] NuPECC Report, Nuclear and Particle Astrophysics, July 16, 1997, I. Baraffe et al., F.-K. Thielemann (convener)

[8] J. Görres, M. Wiescher and F.-K. Thielemann, Phys. Rev. **C51** (1995) 392

[9] H. Schatz et al., Phys. Rep. **294** (1997) 167

[10] G. Baur, S. Typel and H. H. Wolter, Proceedings of the International Workshop XXVI on Gross Properties of Nuclei and Nuclear Excitations, Hirschegg, January 11 - 17, 1998, edited by M. Buballa, W. Nörenberg, J. Wambach and A. Wirzba

[11] H. Utsunomiya et al., Excitation of Continuum States in ^{7}Li and their decay by Quantum Tunneling, contributed paper to INPC98, Paris

* Sektion Physik, Universität München, Am Coulombwall 1, 85748 Garching

Supported partially by grant LMWolT of GSI.

III. Accelerator Division

5. COOLER SYNCHROTRON COSY

6. ION SOURCES AND BEAM TRANSPORT

7. SPECTROMETER BIG KARL

8. RADIATION PROTECTION

5. COOLER SYNCHROTRON COSY

Operating Report of COSY in 1998

U. Bechstedt, J. Dietrich, K.Henn, A.Lehrach, R. Maier,
D. Prasuhn, A. Schnase, R.Stassen, H. Stockhorst, R. Tölle

Beam time statistics

The scheduled beam time for COSY in the year 1998 has amounted 7172 hours. With an up-time of 6766 hours the accelerator complex has proven good reliability of nearly 94%. The maintenance time was additionally increased for three weeks due to vacuum foils (carbon fibre) burst in the large ANKE dipol chamber. The beam time distribution for the COSY operation is shown in Fig. 1.

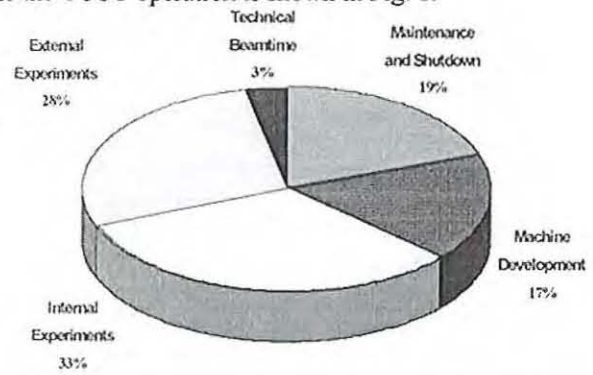

Fig. 1: Beam time distribution for COSY in the year 1998

Stochastic Cooling

Longitudinal stochastic cooling by the filter method and transverse cooling were routinely applied during COSY-11 experiment runs. This experiment located with a cluster target in one of the arcs of COSY demands besides a high luminosity a small diameter in the reaction zone in order to reconstruct the mass spectrum with high resolution. Without cooling a special optic of the COSY ring was necessary to create a small beam spot size at the target location. Furthermore, during the experiment the optical conditions had to be continuously adjusted in order to prevent the beam spot from moving away from the target due to energy loss. This becomes especially important during long time runs. Using stochastic cooling the optic is adjusted to optimum cooling conditions. Cooling of the transverse and longitudinal emittances simultaneously keeps a high beam quality during the whole time of the experiment. COSY had only to be refilled for a next spill due to losses coming from reactions between the target and the proton beam. Cycle lengths of more than one hour with an increased duty cycle are now possible and used for experiments. The performance of the cooling system could be further increased by replacing the electrical notch filter with an optical transmission line version. Developments to apply stochastic cooling in supercycles were carried out.

Polarized Proton Beam

The acceleration of a polarized proton beam up to the design momentum of COSY (3.3 GeV/c) was realised using the successfully commissioned tune jumping system. Correction dipoles or the solenoids of the electron cooler acting as partial snake have been used to conserve the polarization at the imperfection resonances by exciting total spin flips. The magnetic structure allows to adjust superperiodicity P = 6. Then only one resonance is excited which flips the spin with polarization losses. To conserve polarization at this resonance a tune jumping system was developed. To accelerate the beam to maximum energy the transition energy is shifted upwards with the horizontally foccussing quadrupoles in the arcs which leads to a reduced superperiodicity. Additional intrinsic resonances are excited which can be suppressed by tuning the vertically focussing quadrupoles in the arcs.

Stacking

To increase the intensity of the polarized proton beam in COSY tests with the electron cooler and a repetitive injection were carried out. The orbit bump in COSY for the stripping injection was deformed so that the incoming beam is not injected on the closed orbit. The resulting betatron oscillations as well as the emittance and momentum spread of the injected beam is cooled by the electron cooler. After five seconds of cooling the next stack is injected and cooled. Due to the deformed orbit bump the injected and cooled stacks do not hit the stripping target and survive the next bumper action. The intensity of the beam was reduced in front of the cyclotron to an intensity which is comparable to the polarized beam intensity. The result was an accumulated beam of $4 \cdot 10^9$ protons after about 180 seconds. The single injection leads to an intensity of $1 \cdot 10^9$ protons.

Commissioning of ANKE

In May 98 the spectrometer ANKE has been implemented into the COSY ring and commissioned. It is a universal facility for the studies of ejectiles which are emitted in forward direction in collisions of the proton beam with nuclear targets. The separation of the ejectiles from the circulating beam and the identification of their momenta and emission angles is achieved with the central large aperture dipole magnet (D2, 60 tons) of 20 cm gap width. The two other dipole magnets (D1 and D3, 15 tons each) serve for guiding the beam but also for studying reaction products which are emitted at 180 degrees with respect to the beam. The accelerating procedure of COSY has been adapted to the new situation with ANKE, i.e. altered orbit length, multipole components of the separator magnets during ramping. Al possible bending angles between zero and 10.6 degrees were successfully tested. First experiments were started (2.3 GeV, $3.8 \cdot 10^{10}$p).

Stochastic extraction

At COSY stochastic extraction is now used in the wide momentum range from 800 MeV/c to 3.3 GeV/c. A digital noise generator developed at COSY is used for stochastic extraction and beam shaping. An extraction efficiency of about 60% has been reached for momenta less than 3 GeV/c. The requested spill duration is up to several minutes.

The ANKE 3-Dipole Insertion in the COSY Ring

U. Bechstedt, N. Bongers, A. Lehrach, Th. Sagefka, M. Simon, H.J. Stein

The three dipoles D1, D2, D3 of ANKE form a triangular shaped chicane in the cooler telescope of the COSY ring . The maximum deflection of the beam in D1 is 10.6°. D1, and D3 are identical, therefore, the maximum deflection in D2 is 21.2°. This large orbit bump has to be precisely balanced in order to avoid orbit distortions at other positions of the ring. The first prerequisite for a proper operation of ANKE in COSY was the determination of the dipole characteristics of the three magnets. The dependences $B_{max}(I)$ in the center of the magnets were measured by an NMR probe. The $B(\ell)$ along the z axis was measured with Hall probe based field mapping machines [1]. Both magnet types revealed an appreciable saturation above one tesla. Also the effective length

$$\ell_{eff}(I) = (1/B_{max}(I)) \int B(I, \ell)\, d\ell$$

is reduced by a few percent at high field values or high currents, respectively. Both saturation effects were combined to the dependence of the currents on effective field values B_{eff} , Fig. 1. Using *Mathematica* [2], the numerical results of the measurements have been represented by interpolating functions and approximated by three polynomials of forth order which form the basis for controlling the D1,3 and D2 power supplies. B_{eff} for the two types of magnets is given by

$$B_{eff\ D1,3} = (B\rho\ \varphi) / (\ell_{effo\ D1,3}\ (\varphi/2)\ \sin(\varphi/2)\ \cos((\varphi/2)-\delta))$$
$$B_{eff\ D2} = (B\rho\ 2\varphi) / (\ell_{effo\ D2}\ (\varphi / \sin\varphi))$$

where ℓ_{effo} is the effective length at low current, $B\rho$ is the magnetic rigidity of the beam, φ is the deflection angle in D1, δ= 3.6 degree is the fixed position angle of D1 and D3.

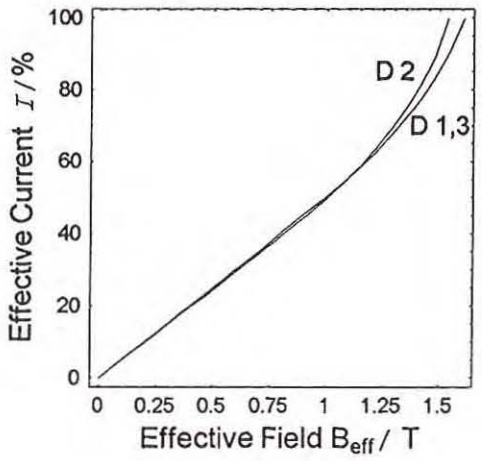

Fig. 1: D2 and D1,3 power supply currents comprising the saturation effects of $B_{max}(I)$ and $\ell_{eff}(I)$. The variable B_{eff} is determined by the beam momentum, the deflection angle, the effective length at low currents, and a geometrical correction taking into account the curved trajectory.

The trigonometric terms take into account the geometrical prolongation of the curved trajectory in the dipoles. To compensate different eddy currents in the vacuum chambers of ANKE, backleg windings at D1 and D3 are activated during acceleration.

The second prerequisite was the choice of an appropriate setting of the cooler telescope optics. The COSY telescopes shall preferably be operated in a 1:1–2π mode. The flexibility of the COSY ion optics allows various quadrupole settings to fulfill this requirement [3]. As a general rule, one should choose such a setting which yields the lowest β functions since magnetic field errors and disturbing insertions like the ANKE dipoles result in less distortion of the ion optical properties of the ring. In contrast to earlier studies [4], a setting with magnification M = 1 and common focus between the triplets [3] in the polarity configuration dffd-dffd / dffd-dffd is now used. The applied setting in the target telescope is M ≠ 1 in dffd-fddf / fddf-dffd polarity also yielding low enough β functions. With the assumption of ideal quadrupole properties, the corresponding plot of the lattice functions β_x, β_y, and D at injection energy is given in Fig. 2. The ANKE dipoles disturb the symmetry of the cooler telescope primarily due the edge focussing in the vertical plane. In the horizontal plane there is no focussing since the magnets are of the rectangular type. A slight influence on the optics is caused by the 0.068 m longer orbit which is to be compared to the distance of 6.456 m between the quadrupole triplets 7 and 8 where ANKE is located. Fig. 3 shows the lattice functions at injection with ANKE operating in the 10.6 degree position where the disturbances are maximal. In the vertical plane the periodicity P = 6 is lost as can be seen by the varying amplitudes of β_y in the six unitcells of the arcs. This is caused by an additional phase advance of 5% in the cooler telescope, however, the variation of the β_y function is still moderate. In the horizontal plane the very small value of 0.05% due to the 0.068 m longer orbit is negligible.

The β functions at the position of the ANKE target are in the range 3...4 m. These values at the target do not change much at flat top energy when γ transition shifting is applied in order to accelerate the COSY beam. However, the lattice functions around the ring are appreciably increased, see Fig. 4. Again, these distortions are minimized with the applied telescope setting. The beam target interaction is controlled by moving the beam into the strip target with the help of two vertical steerers in 2π phase distance. With the non-polarized p beam that will be used for the first set of measurements with a solid target no optical corrections are necessary.

The requirements for the polarized beam are much more stringent. It is desirable to maintain a high periodicity of the ring in order to avoid intrinsic depolarizing resonances. As can be seen by comparing Fig. 2 and 3, ANKE disturbs the 6 fold periodicity. In principle, the cooler telescope with ANKE can be adjusted such that in the vertical plane the phase advance is exactly 2π.

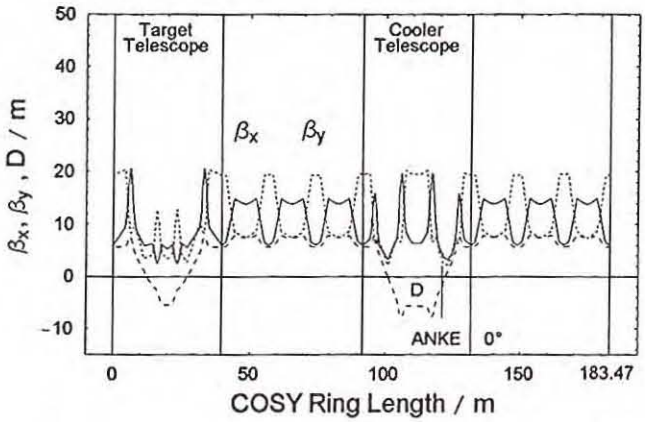

Fig. 2: Structure of the optical functions at injection with ANKE at zero degree position. The periodicity $P = 6$ in the arcs is maintained due to the telescopic 1:1–2π setting of the straight sections. Inner magnification M = 1 with dffd-dffd / dffd-dffd polarity in the cooler telescope. M ≠ 1 with dffd-fddf / fddf-dffd polarity in the target telescope.

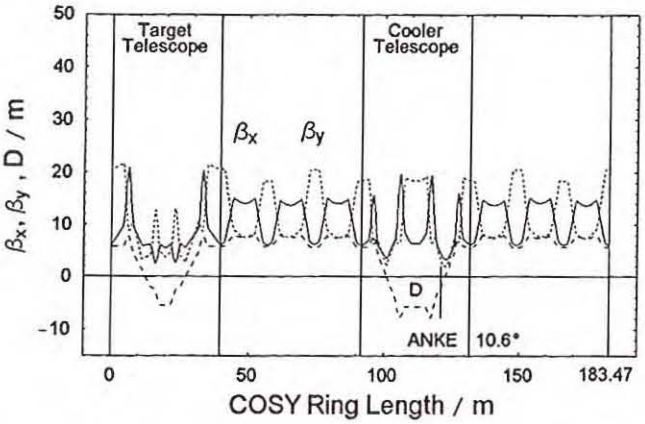

Fig. 3: Structure of the optical functions at injection with ANKE at the maximum angle position of 10.6°. The symmetry of the ring is broken due to 5% more than 2π phase advance in the cooler telescope resulting in a certain variation of the β_y function structure from one unit cell to the other.

However, this solution appears rather complicated since for the cooler telescope one would need six additional power supplies in order to control the triplets 7 and 8 as strongly asymmetric quadrupole triplets. A simpler alternative is indicated by lattice calculations which show that the β_y periodicity in the arcs can be maintained in good approximation by slightly reducing the current of the f quadrupoles in triplet 7 with an active shunt. However, the additional vertical phase advance is still 5%. Whether this can be tolerated is not yet clear [5] and is subject of further studies. It should be noted that as long as acceleration is performed using γ_{tr} shifting, a periodicity of only $P = 2$ can be obtained.

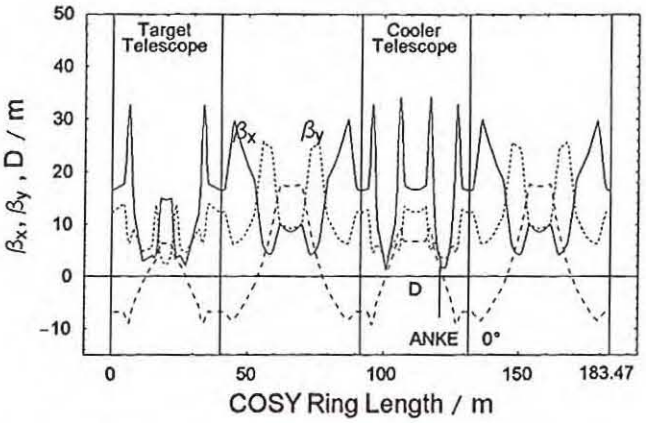

Fig. 4: Structure of the optical functions at flat top energy with ANKE at zero degree applying γ transition shifting during acceleration. The $P = 6$ periodicity is also lost, however, in an ideal lattice with 1:1–2π imaging in the telescopes, $P = 2$ is preserved at least.

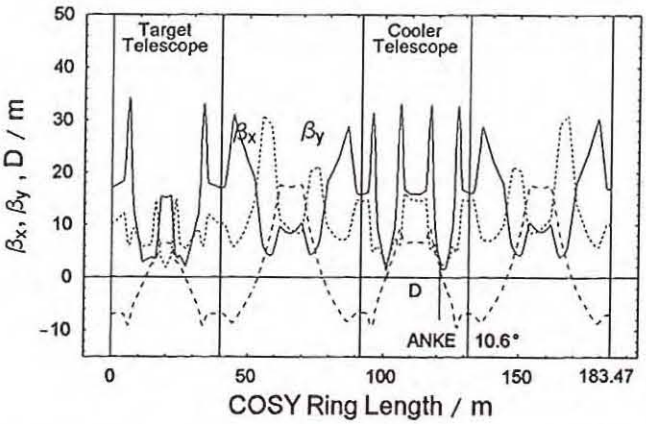

Fig. 5: Optical functions at flat top energy and ANKE at 10.6°. The $P = 2$ periodicity in β_y is completely lost. Using the polarized beam one has to deal with $P = 1$ if no means are found to obtain a higher periodicity.

References

[1] We thank the colleagues of GSI Darmstadt for providing us their large field mapping machine which was necessary to cover the extended measuring area of the D2 magnet.

[2] Stephen Wolfram, *The Mathematica Book*, 3rd ed. (Wolfram Media/Cambridge University Press, 1996)

[3] A. Lehrach et al., Tuning of the COSY Telescopes, IKP Annual Report 1996, Report Juel-3365 (1997) 228

[4] L.H.A.. Leunissen and H.J. Stein, Influence of ANKE on COSY Optics, IKP Annual Report 1997, Report Juel-3505 (1998) 158

[5] A. Lehrach et al., Development of the Polarized Beam at COSY, IKP Annual Report 1997, Report Juel-3505 (1998) 149

Operation of the tune jump system to preserve polarization at COSY

A. Lehrach, R. Gebel, R. Maier, D. Prasuhn

A tune jump allows to preserve polarization at intrinsic resonances by increasing the crossing speed during resonance crossing significantly due to a changing of the vertical betatron tune in the range of microseconds.

Introduction

In order to accelerate a polarized beam at the cooler synchrotron COSY to maximum energy a tune jump is needed to reduce polarization loss during crossing depolarizing resonances [1,2]. For intrinsic resonances the resonance frequency depends on the vertical betatron tune ν_y. The number of intrinsic resonances decreases with the superperiodicity P of the lattice given by the number of identical periods in the accelerator. As the betatron phase advance in the two straight sections of COSY is matched to 2π these sections are optically transparent and only the arcs contribute to the strength of intrinsic resonances. One obtains for the resonance condition:

$$\gamma G = kP \pm (\nu_y - 2),$$

where γG is the spin tune and k an integer. If the vertical betatron tune is changed abruptly as the precession frequency of the spin comes close to the resonance frequency the crossing speed on the resonance is increased significantly and the polarization loss is reduced.

Tune jumping system for COSY

A magnet system consisting of two iron free pulsed quadrupoles was developed and successfully used. This system has been specified for polarization losses of less than 5 % at the strongest intrinsic resonance and less than 1 % at all other intrinsic resonances in the energy range of COSY [3]. To achieve this aim a vertical tune jump of $\Delta\nu_y = 0.06$ in 10 µs is needed. Up to ten tune jumps with different polarities and amplitudes can be generated during one acceleration cycle.

Fig. 1 shows the polarization of the COSY beam measured during acceleration using the EDDA detector around the strongest intrinsic resonance ($\gamma G = 8\text{-}\nu_y$) at about 2090 MeV/c. This resonance excites a natural spin flip. The polarization loss is depending on the vertical emittance of the beam. Using a tune jump the polarization was almost preserved. During that beam time we were able to preserve the polarization up to a momentum of 2.7 GeV/c. For this prove of principle $5*10^7$ polarized protons were accelerated.

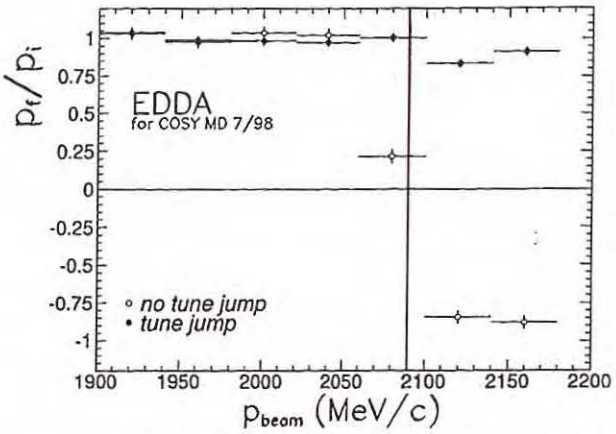

Fig 1: Normalized polarization during crossing the strongest intrinsic resonance at 2090 MeV/c with and without tune jump, P_i ist the initial polarization and P_f final polarization. The beam polarization was measured during acceleration using the EDDA detector [4].

Outlook

This tune jump system can be used at all intrinsic resonances of COSY, because they are more than a factor of three weaker than the strongest resonance. After establishing this method at COSY the polarized proton beam was accelerated to maximum momentum in November 1998.

Acknowledgment

We thank the EDDA collaboration for the measurement of the polarization during acceleration.

References

[1] A. Lehrach, 'Erarbeitung und Umsetzung eines Konzepts zur Beschleunigung polarisierter Protonen im Kühlersynchrotron COSY', PhD-thesis Jül-3501, Forschungszentrum Jülich.

[2] A. Lehrach et al., 'Status of polarized beam at COSY', 12th Symposium on High Energy Spin Physics, Amsterdam 1996.

[3] A. Lehrach et al., 'Tune jumping system for COSY', Annual Report (1995).

[4] V. Schwarz et al., 'EDDA as Internal High-Energy Polarimeter', 13th Symposium on High Energy Spin Physics, Protvino 1998.

Longitudinal Stochastic Cooling Improved by an Optical Notch Filter

R. Stassen, P. Brittner, R. Hartung (ZEL), F. Häsing (ZEL), R. Maier, D. Prasuhn, G. Schug, H. Singer, H. Stockhorst

Introduction

The stochastic cooling system was successfully established in the COSY ring and became a standard tool for beam cooling in the momentum range of 1.5-3.3 GeV/c. The stochastic cooling pickups also serve for precision measurements of the chromaticity.

First longitudinal Cooling

The installed vertical Band 1 system includes the possibility to switch between difference mode and sum mode at the pickup as well as at the kicker tank. This allows us to use the vertical Band 1 system for both transversal and longitudinal cooling including a notch filter in the sum path [1].

The longitudinal cooling has been used for the internal gas cluster target experiment COSY11. The cycle length has been increased up to 1 hour. Less than 10% of the stored protons were lost. The cooling system reached an equilibrium state after 20 minutes, where the energy loss of the protons through the gas target was compensated by the longitudinal cooling system (Fig. 1). The shape of the distribution remains unchanged until the end of the spill.

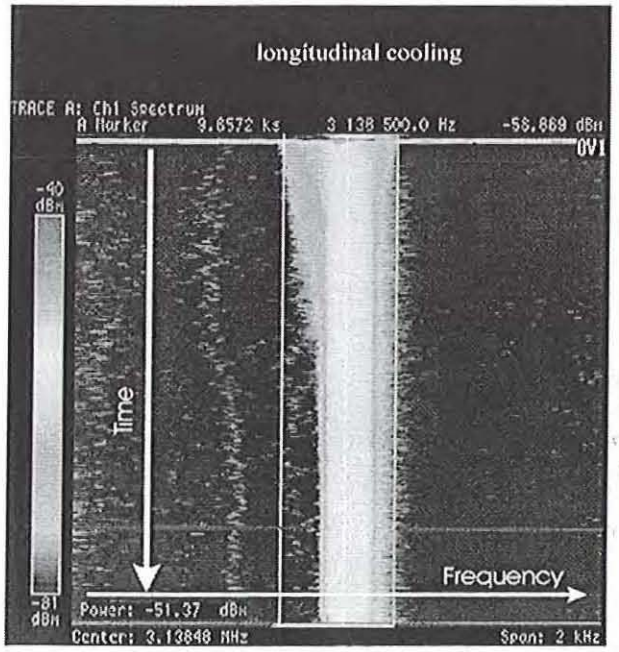

Fig. 1: Longitudinal schottky scan with cooling

Stochastic cooling in a 'supercycle'

The possibility to group up different machine settings within a 'supercycle' is a major advantage of COSY. The transversal stochastic cooling system has been upgraded using the COSY timing system to allow transversal cooling in all settings. The installed programmable delay-lines allow a change of proton momentum from 2.15 to 3.4 GeV/c in one supercycle with transversal stochastic cooling. Longitudinal cooling in a supercycle needs a system adjusting the length of the delay-line in the notch-filter. Both accuracy and resolution are required to be in the order of 1E-6. An envisaged realization using commercial RF components seems to consume too much time and costs. The solution transferring the RF signals into the terahertz region of a laser source was more praiseworthy [3].

Optical notch-filter

Our cooperation with colleagues of the ZEL produced an optical notch filter working at 1300 nm and 20 mW laser power. The first version of the notch-filter was fabricated in a similar structure like our coaxial notch-filter. The delay line has been substituted by an optical structure (Fig. 2). The modulator attenuates the laserlight synchronously to the longitudinal RF signal of the pick-up. The infrared signal is delayed by a fibre optic coil. The RF signal is afterwards reconstructed by the photodetector. The equal phase power divider [1] has been substituted by a hybrid having a better decoupling between the short and the long branch of the notch filter. The frequency dependence of the attenuation in the optical branch is neglectable because the small relative bandwidth required of the optical system is around 3E-6 at the RF frequency band of 1-1.8 GHz. Therefore the RF attenuator in Fig. 2 is now a frequency independent one. Equalizing the attenuation between the short and the long branch of the notch filter is simply fulfilled by regulating the power of the laser light.

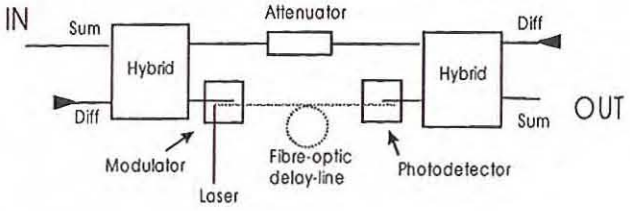

Fig. 2: First optical notch filter

The longitudinal cooling has been improved by the optically delayed notch filter in the following items:

- The notch depths over the whole frequency band excess values of 35 dB compared to 25 dB of the old RF delayed filter.
- The dispersion of the optical notch filter can be neglected.

Frequency shifts of only 25 Hz relating to the proton revolution frequency were measured at the RF band end caused by small phase deviations between both branches of the notch filter.

The dispersion of the coaxial line used for the delay in the old notch filter is essentially larger [2].

The horizontal Band 1 system has been extented by a new path for the longitudinal optical cooling system. Amplitude and phase of this new signal path have been adjusted by automated BTF measurements. The optical notch filter has been installed and tested with beam. After several minutes most of the particles are concentrated at the momentum given by the frequency of the notch filter. The resulting frequency distribution is smaller compared to the old notch filter. Both longitudinal cooling systems (the old notch filter of commercially available RF components and the optical one) were used alternately in a COSY11 run time at different energies.

In a later COSY11 run time the cycle lengths were successfully increased up to 2 hours with the aid of the optical notch-filter. After filling the COSY ring for the COSY11 experiment the beam of the cyclotron had been used for radionuclide production during this 2 hours.

Adjustable notch filter

We have added an adjustable delay line to the notch filter in order to use the longitudinal cooling system in a supercycle. Fig.3 shows the implemented changes of the optical delay line. The system for the fine adjust has been fabricated with a planned adjustable length of about 5m.

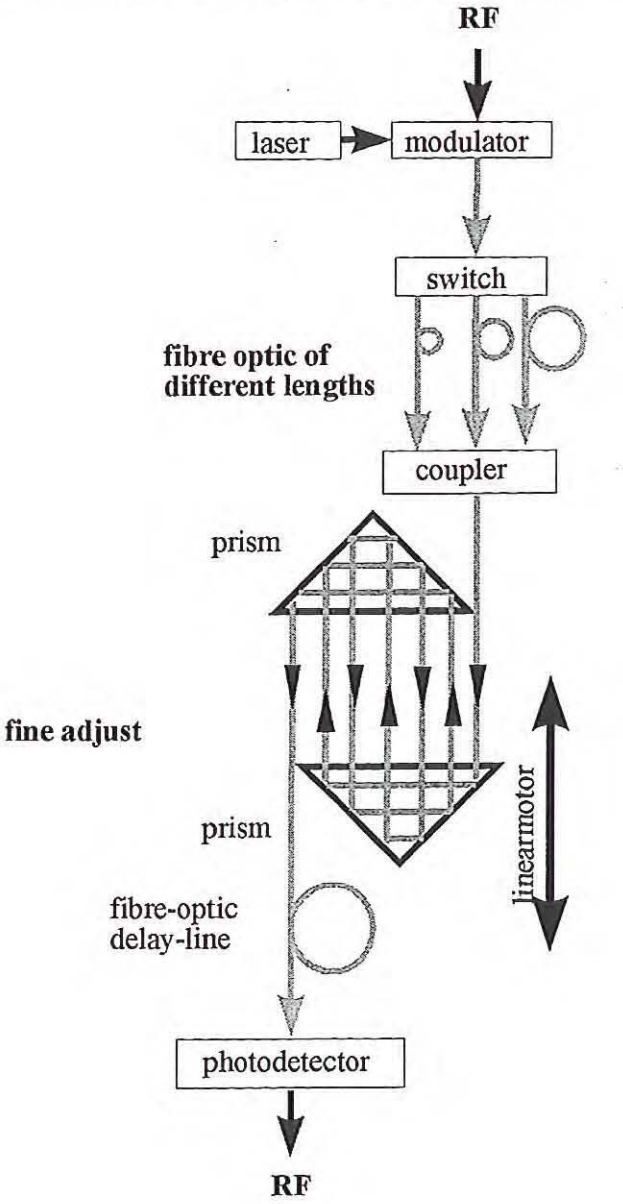

Fig. 3: Continuously adjustable delay line

This length difference is realized by an air section. This section is adjustable according to the beam travelling time with the aid of a motor-driven prism.

Fig. 4 presents the first measurements of the adjustable notch filter around the 900th-harmonic of the beam-revolution frequency. The motor-driven prism was moved 200 times over the moving range and back. 200 cycles are a realistic number at a COSY11 user run of a cycle length of 1 hour. We reached a reproducibility of 1.5E-6. This result encourages us to install the new system as soon as possible.

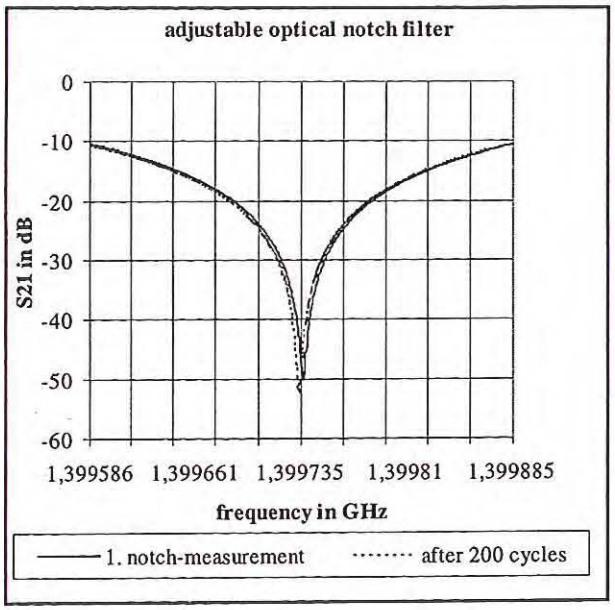

Fig. 4: Reliability of the adjustable notch filter

Outlook

The adjustable notch filter will be installed in the COSY ring at the beginning of 1999. First only the fine adjust will be used with a adjustable length of about 5m. This allows longitudinal cooling in the range from 3.4 GeV/c down to 2.6 GeV/c in one supercycle.

Acknowledgment

We would like to thank R.Hartung (FZJ-ZEL) and F.Häsing (FZJ-ZEL) for their great design and fabrication work.

References

[1] P.Brittner et al., Preparing the stochastic cooling system for the first operation in the COSY ring, IKP Ann.Rep. 1997, p.163

[2] H.Stockhorst et al, Commissioning of the Stochastic Cooling System and Application to an Internal Target Experiment, IKP Ann.Rep. 1997, p.160

[3] G.P.Jackson, A.Elliott, Optical Signal Acquisition and Processing in Future Accelerator Diagnostics

Optimising the Computed Noise for Slow Extraction

A. Schnase, F. -J. Etzkorn, H. Stockhorst

Motivation

The spill duration of the COSY proton beam to external experiments is in the range of some ten seconds to minutes. This is made possible by a better understanding of the extraction process, where the USE-system provides the noise for shaping and extraction of the beam [1]. One of the demands of the external experiments is to have an almost constant flux of particles. This is described with an integral parameter, the duty-factor. It is measured with a set-up shown in [2]. As the USE system influences the microscopic time structure of the spill, we improve the digital noise to have a more constant flux.

Technical Background

The digital noise for extraction is computed as a sequence of digital values which is continuously repeated with about 5.96 Hz rate [3]. Although there is no break in the sequence, the beam notices the repetitions. We measure this with the detector signals of the experimentators. When we decreased the periodicity of one of the noise generators by a factor of ten to get a repetition rate of about 0.596 Hz, we fed the signals of the extracted beam to a loudspeaker and it sounded like a heartbeat. Then we listened to the „sound" of the noise by means of a short-wave receiver tuned to the centre frequency of the noise, about 3.1 MHz at this time. Measurements with an analog spectrum analyser in zero span mode showed a relationship between the flux of the particles and the amplitude of the noise as a function of time.

Optimisation of noise sequences

We define the duty-factor of the extraction flux as:

$$\text{duty - factor} = \left(\frac{\text{mean flux}}{\text{rms flux}}\right)^2 = \frac{\text{dc power}}{\text{total power}}$$

The range of the duty-factor is between 0 and 1. The same definition is now applied to the amplitude of the digital noise. One condition is to maximise the duty factor of the amplitude. The other condition is to minimise the quotient of maximum amplitude divided by minimum amplitude.

The process of generating the digital noise sequences simulates a number of oscillators spaced in frequency by the repetition frequency. For instance: 168 oscillators are necessary for a 1 kHz wide rectangular noise distribution at 5.96 Hz repetition frequency. The initial phase of these oscillators is the free parameter. A bad choice would be to start the oscillators at equal phases. A better result is obtained by defining the initial phases by a pseudo-random sequence. The noise is optimised by the choice of a good initial value for the pseudo-random number generator. We analysed 44 spectra with different bandwidths: 50 Hz, 100 Hz, ..., 4000 Hz, 4.5 kHz, and 5.0 kHz.

For each of the spectra between 1000 to 10000 different sequences were generated and compared by the criteria outlined above. For a spectrum of 1 kHz bandwidth we need about 50s computing time to get full information and about 5s to get only the amplitude statistics. This brute force method was executed on several workstations under AIX, HP-UX and one PC operating with Linux. A typical plot for a spectrum of 4.5 kHz bandwidth is shown in fig. 1.

Simulations which performed well were then calculated for the USE-Targets, downloaded and checked with a spectrum analyser in zero span mode. The decision which spectrum to use can not be done by the computer only - the final decision (see fig. 1) has to be validated with the beam.

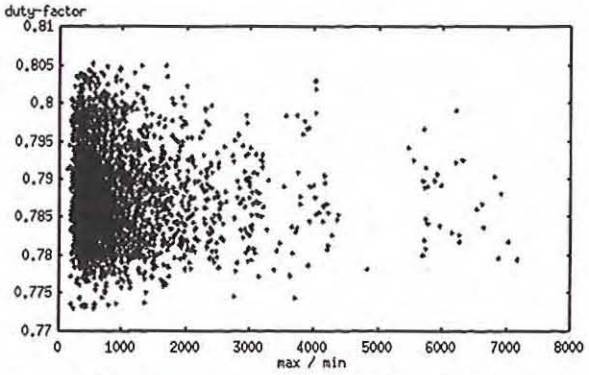

Fig. 1: Simulation pattern for a bandwidth of 4.5 kHz. Spectra in the upper left are good candidates.

The final result for the minimisation of the variation of the amplitude is shown in fig. 2a. The reduced quotient (Max / Min) means, that the peak amplitudes are reduced, and the amplitude will not go down to zero. The corresponding duty-factor of the amplitude is plotted in fig. 2b. For spectra up to 1 kHz bandwidth, the improvement is clearly shown, above it is of less importance. The reason for the convergence is that for spectra with higher bandwidth more numbers of the pseudo-random sequence are taken, so the distribution depends less on the initial value, which was taken for optimisation.

During one beam time, some of the improved noise sequences were applied to the COSY-beam. The third noise system (intended for the chimney) was operated with the improved spectra. The duty factor was increased by about 3% (from 40% to 43%). In no case, the duty factor of the beam was reduced. So, the noise sequences on all 3 system were updated.

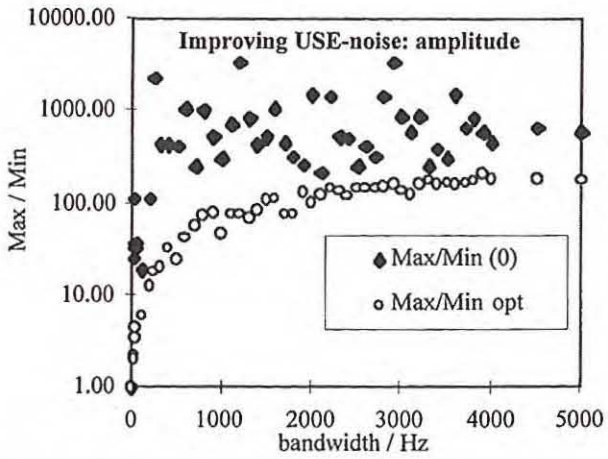

Fig. 2a: Amplitude variation as a function of bandwidth.

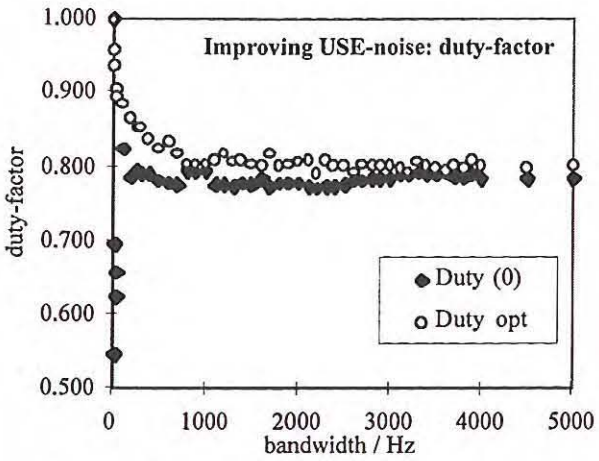

Fig. 2b: Duty factor of the amplitude as a function of bandwidth of the digital noise.

Chimney

The third noise generator of the USE-system is intended to synthesise a very narrow-band noise which is placed just over the resonance to increase the speed of the protons crossing the resonance on their way to the electrostatic septum. First experiments were performed, with a sample rate of the third noise generator one fourth of the „normal" digital noise resulting in a repetition rate of 1.49 Hz. We have changed it to one tenth (e.g. 0.596 Hz). This leads to an increase of the number of lines in the FFT-spectra of the measured spill. The decrease of the amplitudes of the Fourier-components influences the duty-factor quadratically. As a result, the duty factor can be improved by about 10 %. The effect of the chimney is demonstrated in frequency-domain with an FFT-vector analyser [4] connected to the detector of the external experiment TOF. The different gray levels correspond to the signal power. Every line in the following pictures represents a spectrum measuremt. Each new spectrum scrolls the picture upwards. Figure 3b shows that the third noise system smoothes the distribution of the extracted beam over time compared to fig. 3a.

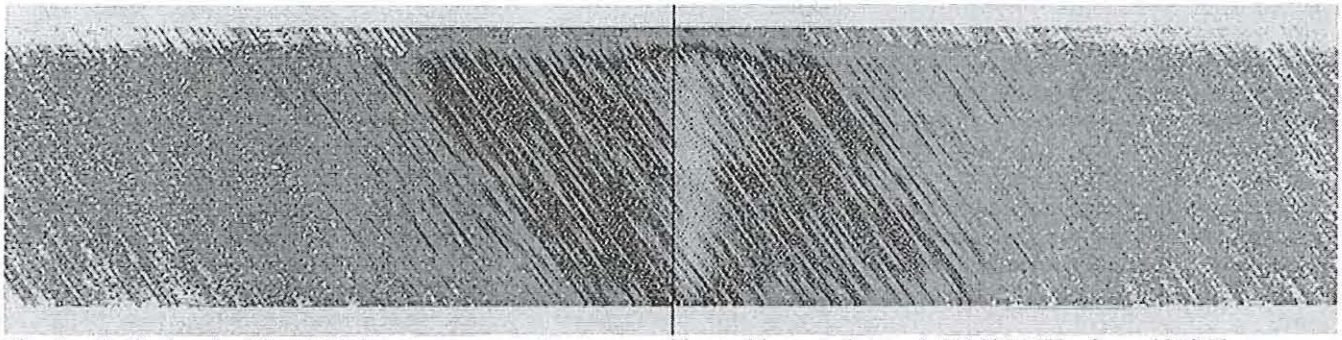

Fig. 3a: Spill-signal of the TOF-detector as a spectrogramm without chimney. Center 1.551425 MHz, Span 1953 Hz.

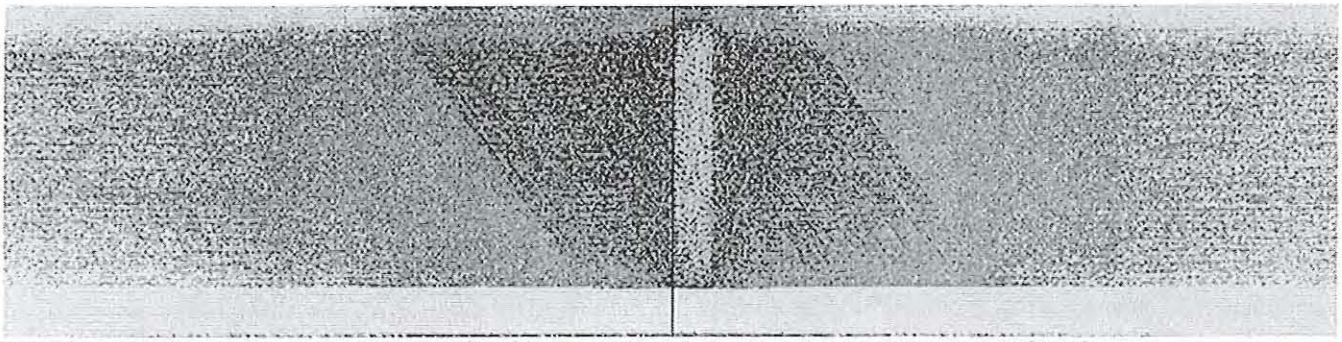

Fig. 3b: Spill-signal of the TOF-detector with chimney activated. Center 1.551425 MHz, Span 1953 Hz.

Results

The optimised noise sequences are now implemented and stored on the hard disks of the USE system. The improvement is small, but it is a step in the right direction. Further improvements are possible with longer noise sequences. For this we need faster VME-CPUs with more RAM and faster harddisks. We plan to base such a system on Linux.

The application of the third noise system as a chimney has been demonstrated. It has to be carefully adjusted to the other extraction parameters. Otherwise it will disturb the time structure of the spill. It is not a tool that can be simply switched on to improve extraction.

References

[1] A. Schnase, M. Böhnke, F.-J. Etzkorn, M. Simon, H. Stockhorst: „Developments for Extraction with USE: Revised User Interface & Computed Noise on CD", IKP Annual Report 1997, p. 186-187

[2] F.-J. Etzkorn, M. Böhnke, J. Dietrich, A. Schnase, H. Stockhorst: „DSP-based On-Line Spill measurement of Extraction", IKP Annual Report 1997, p. 190

[3] H. Stockhorst: „Beam Shaping Using a new Digital Noise Generator", Poster held at PAC 1995, Dallas, Texas

[4] A. Schnase et al.: „DSP based Accelerator Applications at the COoler SYnchrotron COSY", Poster held at EPAC 1998, Stockholm, Sweden

Measurements with the VXI-based Realtime Vectoranalyser

A. Schnase, F. -J. Etzkorn, H. Stockhorst

Introduction

In 1997 we introduced a measurement device operating from DC to 3.4 GHz for non-disturbing beam diagnosis [1]. A longitudinal measurement of a Schottky signal during a slow ramp of COSY indicated that longitudinal instabilities are removed by switching on the digital beam-phase loop.

Operational results

For acceleration of polarised beams we have to control the vertical tune to make sure that the polarisation is not lost. To study the betatron sidebands during acceleration we apply broadband-noise to a strip-line unit and measure the difference signal of a Schottky-pickup [2]. The two spectrograms show the measured spectrum versus time for a slow ramp during acceleration (fig. 1a) and deceleration (fig. 1b). Each line of the picture represents a full spectrum measurement of 2 MHz width with 1.25 kHz resolution and 10 averages. The shade of each pixel represents the measured spectral intensity. The bold line in the middle is the fundamental (h=1) during acceleration up to about 1.57 MHz. The two lines to the left and right are the vertical betatron sidebands. This type of measurement is limited by the dynamic-range of the pre-amplifiers and the analyser.

Another application is the optimisation of the extraction spill [3]. We analyse the detector signals of the external experiment. This helps to optimise the extracted proton beam and to adjust the 'chimney', a narrow band noise to smooth the extracted particle flux.

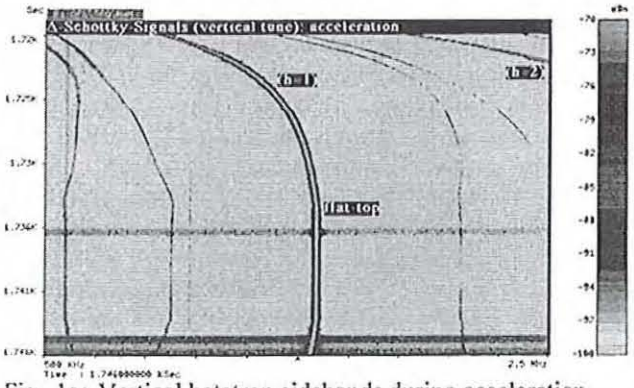

Fig. 1a: Vertical betatron sidebands during acceleration.

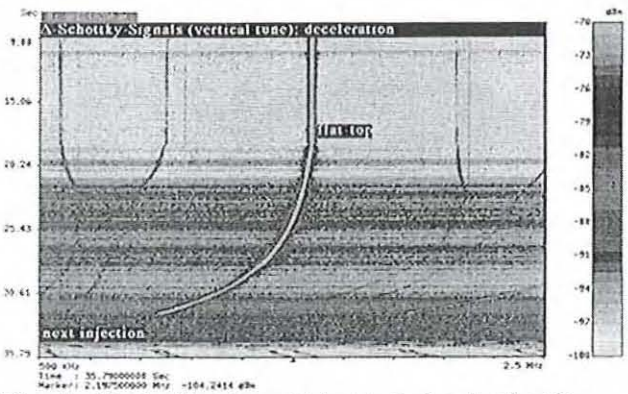

Fig. 1b: Vertical betatron sidebands during deceleration.

During beam-time for stochastic cooling, we measure the time variation of the longitudinal spectra. An example is given in fig. 2. The spectrogram in the upper trace shows the time evolution of the beam. The picture below represents a single spectrum as a snap-shot. In long machine cycles (one cycle per hour) the spectrum versus time shows that the beam is stable and stays on the target.

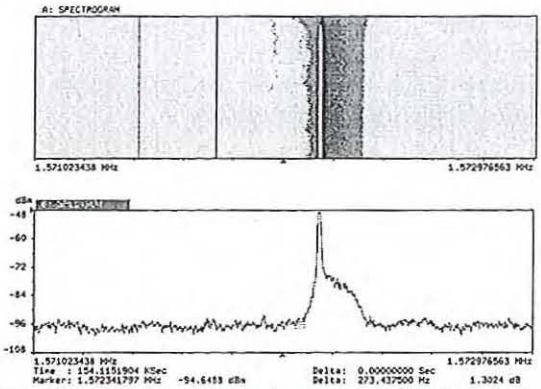

Fig. 2: Spectrogram and spectrum display during beam-time with stochastic cooling on.

Single shot acquisition

The analyser is able to measure the horizontal and vertical tune in 20 ms time intervals. For a 30s record as a single shot, 1500 spectra are stored, resulting in a 20 Mbyte data file. The result of such a measurement is plotted in fig. 3.

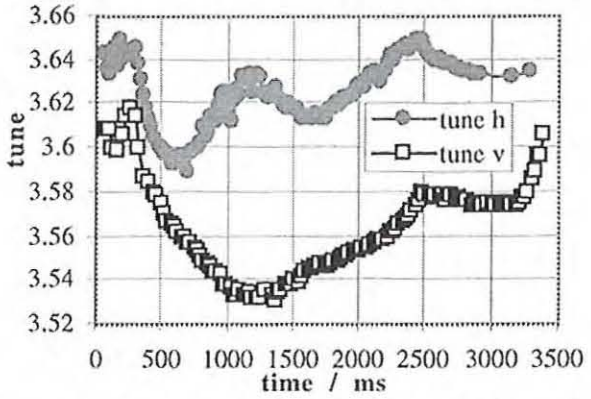

Fig. 3: Single-shot tune-measurement up to 2994 MeV/c.

Result

The VXI-based realtime vectoranalyser has proven to be a powerful tool to study and document the dynamic behaviour of COSY beam parameters.

References

[1] A. Schnase, J. Dietrich, F.- J. Etzkorn, R. Maier, H. Stockhorst: „VXI-based Realtime Vectoranalyser with embedded Risc-Workstation", IKP Annual Report 1997, p. 188

[2] A. Schnase et al.: „DSP based Accelerator Applications at the COoler SYnchrotron COSY", EPAC 1998, Stockholm, Sweden

[3] A. Schnase, F.-J. Etzkorn, H. Stockhorst: „Optimising the Computed Noise for Slow Extraction", this Report

Considerations for the Design of a New Schottky-Pickup

J. Bojowald, J. Dietrich

The two Schottky-pickups, with 1m length each and used until now in COSY, had to be removed mainly due to lack of free space for new installations (e. g. rf-cavity, experimental devices), the horizontal also due to limited aperture. At another position in COSY space of only 0.8m length is available. Therefore a new Schottky-pickup will be designed with utmost sensitivity and, if possible, with the opportunity (after switch over by coax-relays) to measure the Schottky-noise in both planes.

General remarks to monitor type and frequency range:

The Schottky-noise is preferably measured in the 10 – 60 MHz frequency range. This results from the fact, that the line widths in the Schottky-noise spectrum are proportional to the harmonic number with equal noise power per line. The narrow longitudinal lines are measured in the upper part of this frequency range, the in general much broader transversal lines at lower frequencies, because here the line structures yet don't overlap and, in particular, at higher frequencies the amplitudes can vanish in the noise level.

Because of the low power of the transversal signals an especially sensitive monitor is required, whose sensitivity will be enhanced further by resonant tuning. Despite of the gain of 20 – 30 dB by resonant tuning the sensitivity itself is very important and also its frequency dependence. Both, sensitivity and frequency dependence are influenced by the layout and the mode of operation.

Three monitor types are at disposal: inductive, capacitive and stripline-monitor. In the frequency range 10 – 60 MHz the capacitive monitor is well suited; the inductive monitor less, because the azimuthal magnetic field of the beam and hence the induced signal power is proportional to β^2 and Schottky-noise measurements at COSY must be performed also at low ß-values. The stripline monitor can be operated at high frequencies and it is able to separate the signals of particles travelling opposite to each other (directivity), as very useful in storage rings. But of this cannot be made use at COSY and the big disadvantage is the sinusoidal frequency dependence. The maximal sensitivity, obtained at frequencies with $\lambda/4$ corresponding to the monitor length, would be with 0.8m length at 94 MHz. In the 10 – 60 MHz range the sensitivity drastically falls down.

The amplitudes of the transversal Schottky signals are dependent on the square root of the ß-function. A suitable position in COSY with high ß-function values should be chosen, as is the case at the position now. In monitor design attention must be payed therefore to save the total aperture. For this purpose the electrodes must be arranged far outside, at best with beam tube diameter.

Design of the capacitive monitor and transfer impedance:

The capacitive monitor with high impedance preamplifier has the particular advantage of a flat frequency response within a band pass. The lower cutoff frequency is given by the electrode capacity and the preamplifier input impedance and can be realized to 10kHz. The upper cutoff frequency is determined by the bandwidth of the preamplifier and is larger than 100MHz, the proper frequency range.

The sensitivity or transfer impedance of one electrode with beam centred is

$$Z_{tr} = \frac{A_{el}}{2\pi r} \cdot \frac{1}{\beta c \cdot C_{el}} = \frac{\alpha_{el}}{2\pi} \cdot \frac{L}{\beta c \cdot C_{el}}$$

with: A_{el}=electrode plane, r=beam tube radius, L=monitor length and α=azimuthal angle of electrode. The first term is a geometrical factor, corresponding to the ratio of electrode plane to total monitor cylinder plane. The transfer impedance is maximal, if the electrodes together enclose the beam, i.e. if $\Sigma\alpha_{el}=2\pi$. For high sensitivity furthermore the electrode capacity C_{el} must be small, i.e. the distance to the beam tube cannot be to small. Therefore the vacuum tube should be broadened and the electrodes aligned in extension of the beam tube.

For the longitudinal or Σ- signal follows: $\Sigma(t) = n \cdot Z_{tr} \cdot i(t)$ with n=number of electrodes and i(t)=beam current. Important for the transversal or Δ- signals is the coupling capacity C_c between the electrodes, which reduces the amplitude, because

$$\Delta(t) = \frac{\Sigma(t)}{a/2} \cdot \frac{C_{el}}{C_{el} + 2C_c} \cdot (x - x_0)$$

with: a=electrode distance, x=displacement of beam from centre and x_0=monitor displacement from optical axis. The coupling capacity must be small in comparison to the electrode capacity. This means also, that the electrode capacity cannot be made as small as possible.

The geometry of the proposed Schottky pickup will have the schematic layout as shown in the figure. The apertures in horizontal (150mm diameter) and in vertical (60mm, rectangular) planes remain free, if the pickup diameter is made a little bit larger. The splitted structure into four electrodes, together surrounding the beam, makes possible, by proper switching of coax-relays, Schottky-noise measurements in horizontal and vertical plane. In order to realize a small coupling capacity (e.g. $C_c<C_{el}/10$), the slits in between cannot be made to narrow, so an azimuthal range of about 95% must be tolerated. The mechanical design of a test monitor for rf-measurements is in preparation.

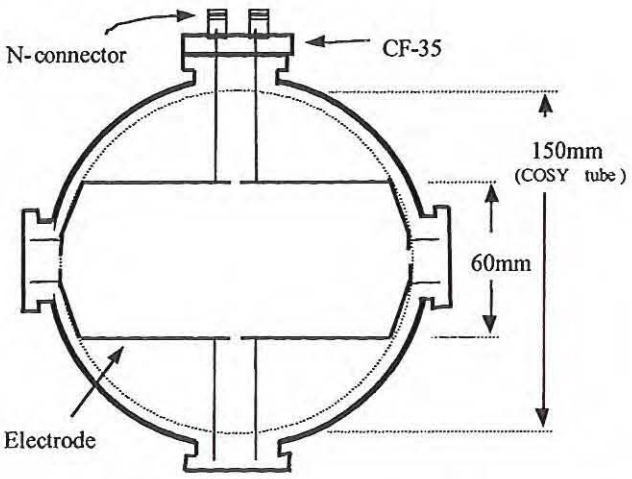

Fig.: Schematic view of the proposed Schottky pickup for measurements in horizontal and vertical plane (after proper switching of coax-relays).

Broadband Cavity with the Nano-crystalline material VitroPerm

M. Böhnke, F. -J. Etzkorn, U. Rindfleisch, A. Schnase, H. Stockhorst

Motivation for a new cavity

The higher harmonic cavity filled with VitroVac performs well [1], and TERA decided to buy it from SATURNE. At EPAC 1998 [2] we learned from KEK about a different material which is well suited for a broadband acceleration structure. This material is called FINEMET in Japan and we have found out that a comparable material is available in Germany which is called VitroPerm. This type of metglass is a nano-crystalline material compared to the amorphous material VitroVac. We started simulations and measurements with sample toroids and created a design which is optimised for operation at COSY. The frequency range will be from 400 kHz to 2 MHz without any tuning device. The broadband nature of this cavity allows non-sinusoidal waveforms for rf-gymnastics [3] like:

- improved capture of injected beam
- acceleration at different harmonics
- γ-transition crossing
- stochastic cooling of bunched beams
- high power shaped noise for stochastic extraction in seconds.

Comparison with a ferrite cavity and the VitroVac cavity

The cavity design does not follow all rules in the CERN yellow report on RF engineering. In fact it can not be described as a resonator. A better model will be that of a lossy inductor that isolates the acceleration gap from the environment. There are no gap-capacitors and no cooling plates. The magnetic material (VitroPerm 500F) is directly placed inside a water bath. The available space in the straight sections of COSY is limited. A new cavity with reduced longitudinal dimension is necessary in order to make room for devices used for spin gymnastics of polarised protons. The choice of material with different μ_r determines the length of a cavity:

- ferrite (h=1) cavity in use at COSY: 210 cm
- VitroVac 6025F loaded cavity (tested at SATURNE / for TERA): 140 cm
- VitroPerm 500 F (nano-crystalline): ≈ 80 cm.

The structure is shown in fig. 1.

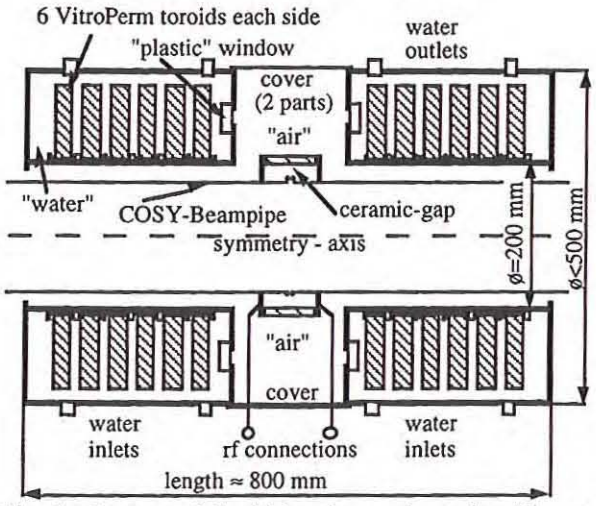

Fig. 1: Layout of the higher harmonic cavity. The vessel is made of stainless steel.

The advantages of the former tested VitroVac 6025F loaded cavity compared to a ferrite loaded cavity are:

- a smaller size due to higher permeability
- the broadband characteristic (low Q) allows higher harmonics

The disadvantage is that the lower impedance of ≈ 250 Ω gives less voltage at the same power. Still cooling plates and a tuning device are needed.

The application of VitroPerm 500 F offers advantages:

- a smaller size, due to high permeability
- the material is cheaper than ferrites or VitroVac
- the structure is broadband without tuning loop
- no cooling plates (direct water cooling)
- works with higher harmonics and noise
- impedance is between VitroVac 6025 F and ferrite
- the estimated maximum rf-amplitude will be 5 kV (2.5 kV for each half of the structure) with an rf-power of less than 50 kW.

There are also disadvantages: A protection against corrosion is needed - this coating is called „FIX" by the manufacturer. The cavity has to be protected against too high water pressure and the purity of water is important. As the size of the cavity is smaller than that of the amplifier, the latter has to be installed in some distance (3 to 7 m) which has to bridged with a high impedance transmission line of at least 200 Ω. For this we will need a coaxial air filled structure comparable to the copper transmission lines for the stochastic cooling system.

Measurements with material samples

We compared small toroids of VitroVac and VitroPerm. The size and the initial permeability at DC is given in the following table. The value in parentheses is estimated.

	VitroVac 6025	VitroPerm W531-51	VitroPerm W468-51	foreseen in new cavity
$ø_i$ / mm	35	50	76	200
$ø_a$ / mm	72	80	102	400
h / mm	25	20	25	25
L / nH	3.336	1.739	1.361	(3.2)
μ_r at DC	90000	30000	80000	80000
L/mH at DC	0.300	0.052	0.109	(0.25)

Impedance measurements were carried out with a network analyser at low power. We have also tested samples at higher rf-power to reach temperatures of 100 °C in a water bath. We have found no substantial change in impedance as a function of temperature. So we expect a good safety margin in operation between 20 to 50 °C. Fig. 2 shows the impedance as a function of frequency for one VitroVac toroid and the necessary power to get an rf-amplitude of 200 V. In fig. 3 the impedance of a combination of 4 VitroVac sample toroids in a test structure is plotted. The impedance of the test device is sufficient to get 2500 V amplitude. The material for the real cavity is scaled with this result. The impedance will be a bit higher, because we use 6 toroids for each side. The increased surface of the material allows to transfer the generated heat to the cooling water, so that the structure will operate with the estimated power.

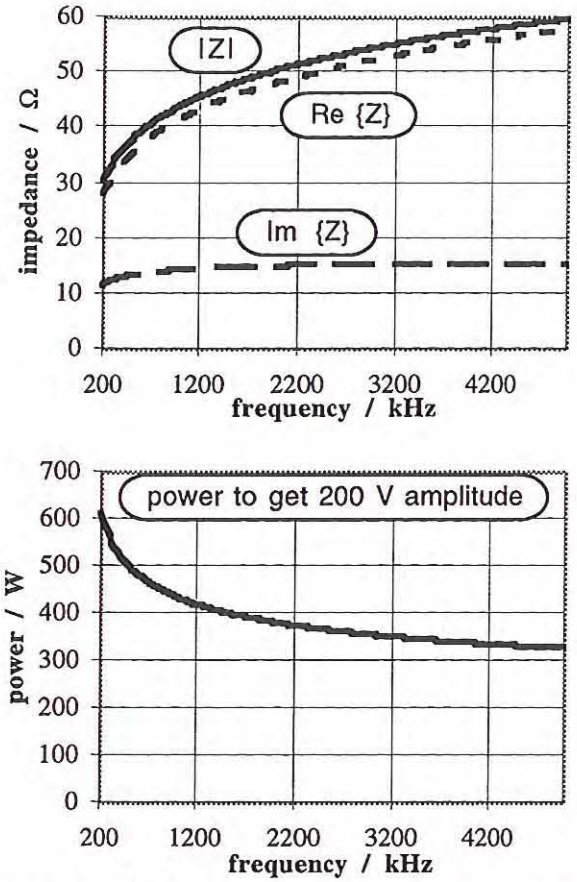

Fig. 2: VitroVac 6025F, $ø_a$ 80mm, $ø_i$ 50mm, h=25mm

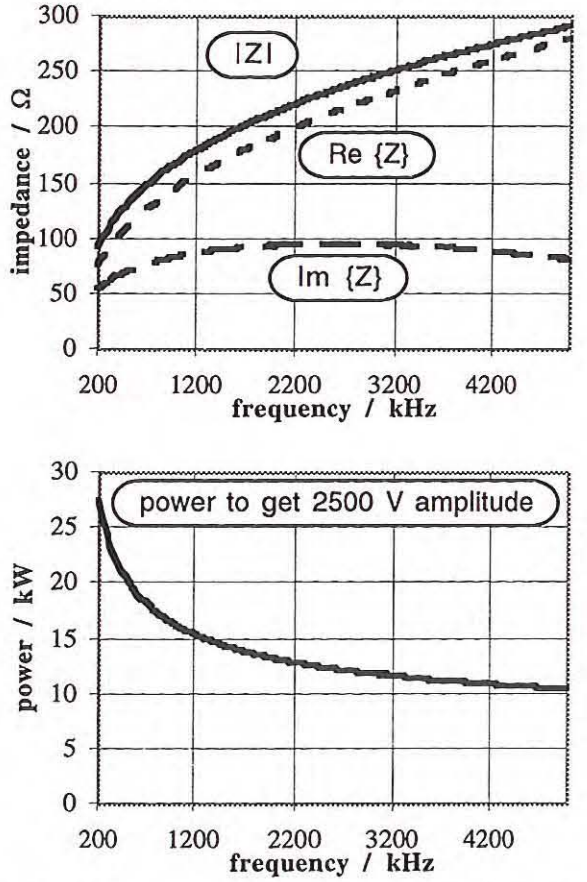

Fig. 3: Test structure with 4 samples of VitroPerm 500 F, dimensions of one toroid: $ø_a$=102mm, $ø_i$=76mm, h=25 mm

Application of higher harmonics to the test structure

To prove the principle of generating higher harmonics, we applied real signals at low power (5 ... 15 W) to the test structure with four toroids.

In fig. 4a and fig. 4b we tried a combination of fundamental and second harmonic adjusted to provide a flat zero-crossing. The broadband behaviour is clearly visible: the upper trace is the pre-distorted generator signal and the lower trace the voltage at the structure measured with a 1:10 probe. The difference between both measurements is the fundamental frequency, which was chosen to be 500 kHz in fig. 4a and 1500 kHz in fig. 4b.

The structure works with higher harmonics. This is proven in fig. 5a and fig. 5b where a second and a fourth harmonic are applied to synthesise a waveform with a flat-top. In fig. 5a the upper trace shows that at low frequencies the necessary pre-distortion is stronger. This is no surprise, because an inductor does not like to have a constant voltage at its terminals.

The synthesiser we used for these measurements [4] was not only able to generate these higher harmonics for fixed frequencies. It can perform a sweep while preserving the shape of the waveform, because the Fourier components can be adjusted in real time during the sweep.

For this test, there was only air-cooling. The water was added by means of a flexible plastic bag surrounding the toroids. With water cooling, where the toroids are placed directly inside the bath, the results may change, because we expect a capacitive effect of the order of some 100pF.

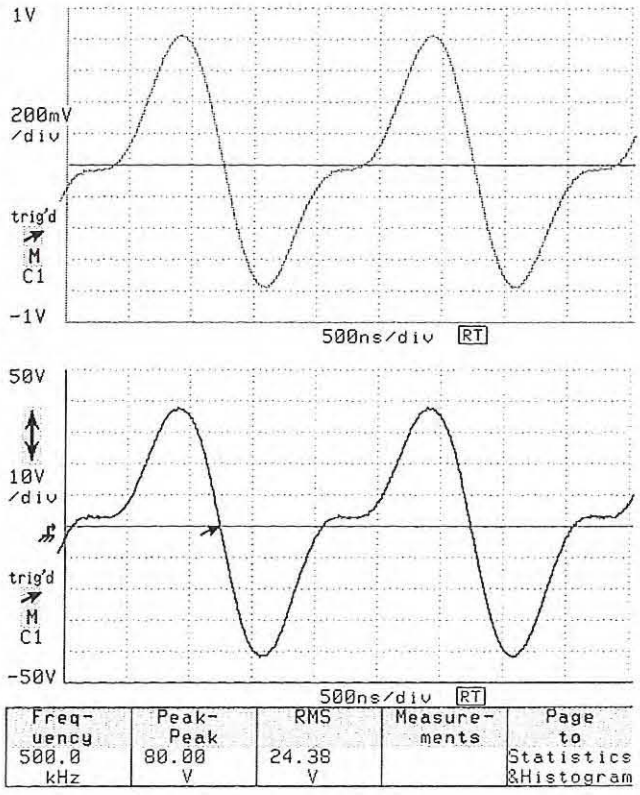

Fig. 4a: Waveform with flat zero-crossing using a second harmonic at 500 kHz fundamental, power ≈ 4W, Upper trace: low-level pre-distorted generator signal, lower trace: high level signal at gap.

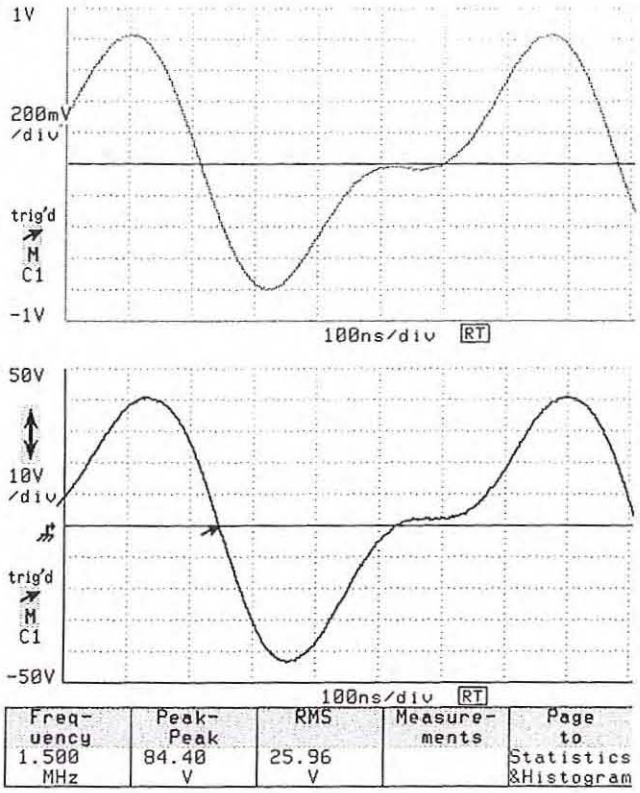

Fig. 4b: Waveform like fig. 4a at 1500 kHz fundamental, power ≈ 2.5W,

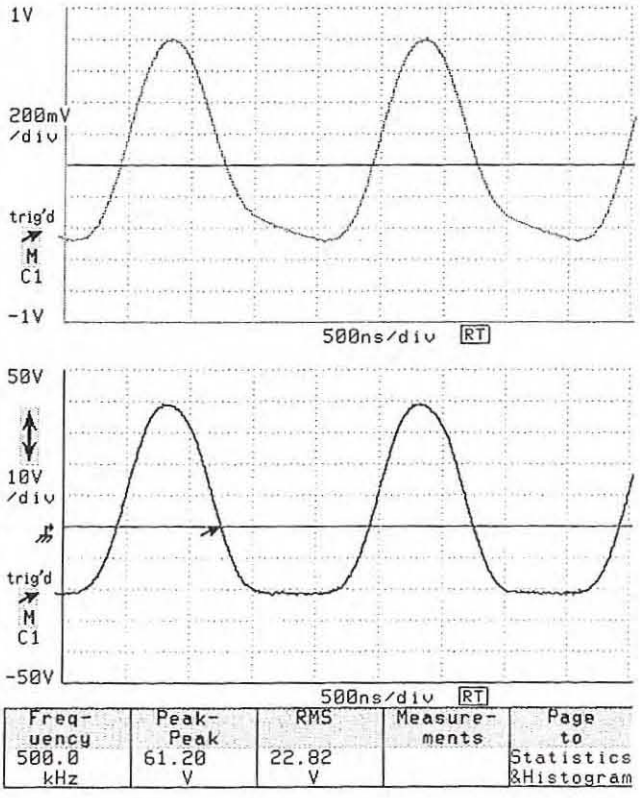

Fig. 5a: Waveform with flat top using a second and a fourth harmonic at 500 kHz fundamental, power ≈ 4W, Upper trace: low-level pre-distorted generator signal, lower trace: high level signal at gap.

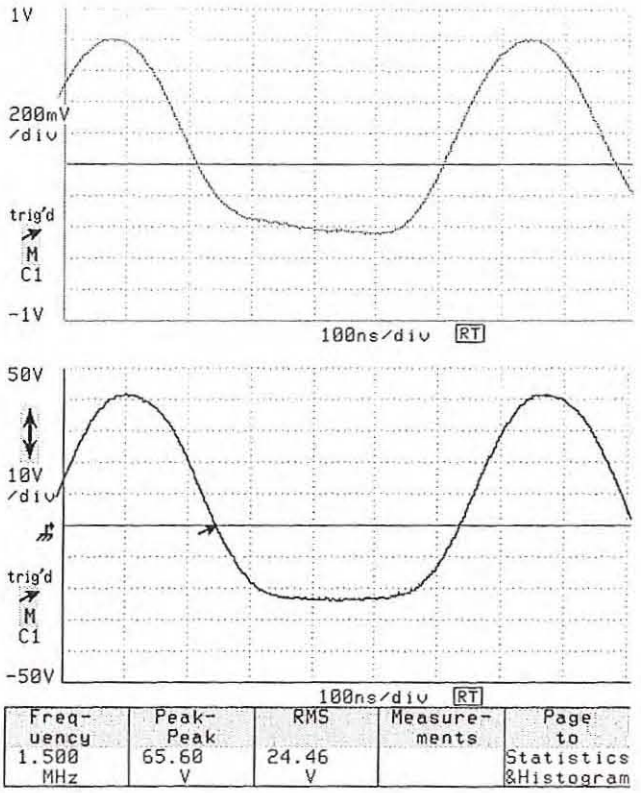

Fig. 5b: Waveform like fig. 5a at 1500 kHz fundamental, power ≈ 2.5W,

Results

The length of the new cavity is only about one third of the ferrite cavity now in operation at COSY. This allows the broadband cavity to be installed in another position of the ring to make room for new developments for the polarised beam. We prepare for an installation which allows to switch between the ferrite cavity and the higher harmonic cavity in reasonable time. Together with the fundamental we will apply higher harmonics (2nd or 4-th) adjusted in real time in amplitude and phase to bunch or to accelerate the proton beam with non-sinusoidal voltages. We will find out, if the impedance is high enough with water cooling, or if we have to rearrange the position of the cores inside the water tank.

References

[1] A. Schnase, M. Böhnke, F.-J. Etzkorn, H. Stockhorst, M. Crescenti, G. Primadei, A. Susini, C. Fougeron: „RF-gymnastics and recent developments", IKP Annual Report 1997, p. 195ff

[2] Y. Mori et al.: „A new type of RF cavity for high intensity proton synchrotron using high permeability magnetic alloy", EPAC 1998, Stockholm, Sweden

[3] H. Stockhorst: „Longitudinal Beam Dynamics in a Multiple Harmonic RF-System", IKP Annual Report 1994, p. 233ff

[4] F. J. Etzkorn, S. Papureanu, A. Schnase, H. Stockhorst: „Towards a cavity for higher harmonics", IKP Annual Report 1994, p. 221ff

Status of Application Programs and Accelerator Model

N. Bongers, R. Gebel, C. Haberbosch, M. Schaaf, R. Stassen, H. Stockhorst, R. Tölle

General activities

Activities in the realm of modeling were accelerator description as well as integration of the accelerator dedicated polarimeters into the control system. Analysis of data measured in machine development times was supported. Analysis usually is appended to the accelerator database and documentation pool. Presentation of the laboratory in the WWW was included.

Calculations with sextupole magnets

Calculations concerning the effective sextupole in the synchrotron and the chromaticity were improved and adapted to changes in the control system. As an example for chromaticity measurements the results for sextupole familiy MXL in the arcs is given. Data were taken using the pickups for stochastic cooling at the 1000th harmonic of the revolution frequency. Proton momentum was 2.62 GeV/c.

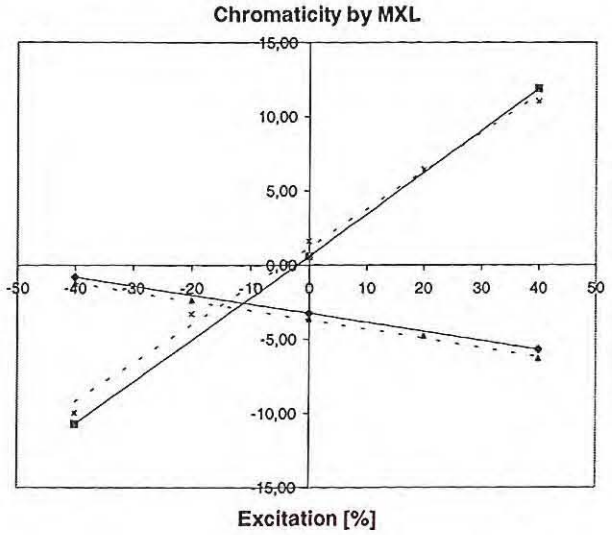

Fig. 1: Chromaticity measurement with sextupole family MXL in the arcs. Solid lines are calculated, dashed lines are measured. Positive slope refers to vertical chromaticity, negative slopes to horiztontal chromaticity. Values are $\Delta\xi$ / % = -0.0623 (-0.0613) and 25.9 (28.3) measured (calculated), respectively.

Effective sextupole calculations

For description of the extraction conditions the efective sextupole in the synchrotron has to be calculated. In nearly all cases an optic has been chosen with zero (horizontal) dispersion in the telescopes. Thus the sextupoles there do (almost) not contribute to chromaticity, but mainly change the amplitude of the effective sextupole. By experience, the calculation for good extraction conditions (sextupole setting, tune etc.) leads to reasonable starting values for the optimization process. Improvements depend on better knowledge of effective magnet lengths in real (iron) surroundings, depending on extraction momentum. Transportation of the beam from the electrostatic septum to the magnetic septum is included now into the calculations to check whether the beam possibly will pass the apertures. To gain flexibility for the betatron pase advance between the electrostatic and magnetic septum a second electrostatic septum can be used instead of the first one, and is integrated into the calculations as well.

Linear beamlines

Description of linear beamlines is now used on a routine basis to set up the transportation of extracted beam to the targets.

Accelerator dedicated polarimeter

Polarization development was supported by operating the low energy polarimeter in the injection beamline, installing in internal polarimeter in the synchrotron, and developing the user interface for the tune jumping system which is useful to rapidly cross depolarizing resonances.

Relyability of the low energy polarimeter was improved by splitting the 3 tasks of its VME-target: a) request for change of polarization, b) target movement, and c) detector readout are now indepentent of each other (as far as possible). Thus malfunctioning of one component only will usually not concern another one.

Comissioning of the internal polarimeter (together with University of Hamburg) started. First in situ dector and motor tests were performed.

The user interface for the tune jumping system was improved and streamlined according the standard of the COSY control system.

Magnets, Alignment and New Installations

U. Bechstedt, L. Conin, G. Krol, T. Sagefka

The year started with a lot of work to get the machine back into operation after the problems with the carbon foils at the ANKE facility [1]. As a consequence of the problems that had occurred aluminium foils wit a thickness of 500 μm were tested and approved to guarantee for the required safety. Furthermore the vertical beam position monitors between D1 and D2 as well as D2 and D3 were replaced by additional vacuum shutters to protect the rest of the vacuum system during work in the area of the D2 dipole magnet. As a third means to increase the security of the system it was decided to install a cage around the ANKE facility with doors protected by security contacts that switch off the power supplies when a door is opened.

After intensive tests of the vacuum windows and manufacturing of the vacuum components necessary to install the additional vacuum shutters the complete system was reinstalled into the COSY ring during weeks 20 and 21. In the following week first tests of the acceleration with the ANKE D2 in different angle positions were successful.

A modified electrostatic extraction septum was installed between dipoles 14 and 15 in the extraction arc of the COSY ring. This septum has modified end covers of the vacuum tank with an increased distance between the cathode and the end cover. This gives higher electrical fields during routine operation. Tests with the old configuration turned out that most of the sparking is between cathode and covers of the vacuum tank.

A polarimeter built by the university of Hamburg was installed between dipoles 9 and 11. To allow for the measurement of even the first depolarising resonance a vacuum chamber made of aluminium with a wall thickness of 1.5 mm was installed inside the polarimeter. Carbon and CH_2 fibre targets of the EDDA type are moved into the proton beam by means of a linear motor.

A storage cell for the polarised atomic beam source was installed at the EDDA experiment. Though it causes loss of beam during injection it should increase the event rate by a factor of four due to the higher effective target thickness.

A water leak occurred at one of the horizontal steering magnets. The coil with the leak was replaced by a coil of one of the vertical steering magnets that is not in routine operation. After repair of the coil it was reinstalled to the vertical steering magnet.

Another water leak occurred at a cooling plate of the acceleration cavity. We supported the rf-group when they changed the cooling plate and two of the ferrite rings.

Alignment activities were related to the re-installation of the ANKE facility and the other new installations into the accelerator. One of the measuring pillars had to be moved because it interfered with one of the motors of the new electrostatic septum. This as well as the disturbance of the grid by the ANKE installation initiated a new measurement of the measurement grid. It was possible to achieve error ellipses for the measurement pillars of a few hundreds of a millimetre.

References:

[1] Setup of the ANKE Facility, U. Bechstedt et al., IKP Annual Report 1997, p. 155

Review of Power Converters at the Accelerator Facility COSY

P. Birx, H. Borsch, K. Kruck, J. Schmitz, H. Schneider

All responsibilities concerning the ordering and maintenance of power converters used at the accelerator or the experimental facilities are handled by the power supply group. The up-time of these power converters is fundamental for the overall reliability of the accelerator and any repair has to be done without undue delay on a 24h/day basis. Our group has meanwhile a long standing experience but is on the other hand faced with the legacy of large power converters accumulated over the past twenty years. The main part originates from procurements in the late eighties when COSY was under construction. Due to the diversity of specifications that have been requested it has not been possible to use a single source for ordering. As a consequence one has to deal in quite a few cases with insufficient documentation and/or lack of service friendliness. In addition one is obligated to stock a plethora of spare parts of different manufacturers. This situation could have only be averted if the power converter crew had been large and had ample design know how. In this case they would have had the clout to team up with the manufactures to build power converters that adhere to stringent laboratory standards thus alleviating the complexity of maintenance and improving the overall reliability.

Stability requirements for the power converters vary greatly depending on the location:

10^{-6} cyclotron main magnet

10^{-5} extraction beam lines, BIG KARL

10^{-5} ramped power converters for COSY ring, modulation free with respect to 50 Hz harmonics

10^{-4} standard stability, ion sources, ion source beam line to cyclotron, injection beam line to COSY

Table 1 compiles the power converters according to maker. Reviewing a larger time reveals that this is not a static market. One has to face the fact that some companies wont be available after a certain time. This holds sometimes even in the case of renown large companies as often only smaller subdivisions are responsible for production and support. If they do no longer fit within the global outlook of the corporation their future looks bleak.
In such cases the local power supply group has to step in. In order to work effectively we had to design and build in some cases specialized test gear that did enable us to track malfunctions.

Failure incidents did happen roughly according to the bathtub curve with a high rate at the beginning that tended to flatten out with time. But one has to keep in mind that even with a leveled out rate of the mean-time-before-failure MTBF of four years one has to expect a failure every week due to the large number of power converters that are running continuously. This simple estimate has been approximately verified through our experience.

Table 1 Power Converters at COSY

Manufacturer	Number of devices	Support available	Out of business/ production discontinued
AEG now Alstom	3	X	
AMK	15	X	
Brandenburg now High Voltage Industries	2	X	
Bruker	39	X	
CERN	5		
Danfysik	43	X	
Delta	3	X	
EA	6	X	
FUG	23	X	
Földi	82		X
Heinzinger	21	X	
Holec now QtecQ	1	X	
HP	4	X	
Jema	6	X	
Kepco	4	X	
PPT	2	X	
Siemens	1	X	
Sorensen	3	X	
Waldorf	29		X
Rohrer	37	X	
Sum	329		

The power converter group has been also concerned with the modification of present power supplies to enable the control group to measure the actual output values for logging and verification. This included also the transmission of the values of ramped power supplies via fiber optic systems. Experience has shown that the behavior of the beam alone is in many cases not sufficient to trace problems. Tasks for the group included stability measurements down to 1 ppm/day and the measurement of the harmonic content down to very low levels as the beam is during extraction highly susceptible to even the smallest modulation.

For added transparency power converters have been retrofitted with additional status bits that are polled with SPS systems. The group is involved in the servicing of the embedded microprocessors and the firmware in the case of some power converters.

Based on our experience one should preferentially buy power converters at middle sized company that have a long standing history. In case of power converters above 0.5 MVA and highly sophisticated equipment a service contract is advised. One should specify complete remote ports and local control panels with the same functionality. An independent system should offer the actual values together with a complete status information. For fast switching of spare power supplies cross bars should be used.

500 MHz Narrowband Beam Position Monitor System of ELSA

J. Dietrich, J.Keil[1] and I.Mohos

The preservation of the polarization level during acceleration of the electron beam is currently the main topic at the Electron Stretcher Accelerator (ELSA) of the University of Bonn. The strength of one type of depolarizing resonances can be reduced by a good correction of the closed-orbit relative to the magnetic quadrupole centers using the method of beam-based alignment. Beam position monitor electronics, developed in the Forschungszentrum Jülich/IKP [1] for ELSA are integrated to form the 28 BPM orbit measurement equipment. The monitor station electronics consisting of an rf processing module and a data acquisition/control module plugged into a shielded crate, are placed close to the four-button monitor chambers. A serial field bus connects the stations to the host computer. The host controls the data acquisition and data preprocessing (sample rate, noise BW, etc.) by means of several commands and parameters, corresponding to the actual requirements. The stations send preprocessed data, the host performs higher level-analysis and displays the results. The RF part of the BPM electronics consisting of narrowband superhet RF electronics processes the fundamental bunch-frequency (number of bunches along the accelerator ring multiplied with the revolution frequency) components of the button signals. At the input low pass filters reject the higher harmonics, GaAs analog RF multiplexer scans sequentially the output of the filters. Low noise narrowband preamplifier (B=5MHz) amplifies the selected low level button-signal. For very high signal levels 30dB attenuation can be inserted. GaAs mixer transposes the desired frequency range to the intermediate frequency, where narrowband filters reduce the IF bandwidth to 220kHz and IF amplifier with controlled gain enhances the signal level appropriate for demodulation. On-board synthesizer generates the LO signal applied to the mixer. Its frequency determines the band-center frequency of the signal processing. Due to the low particle mass the revolution frequency is nearly constant in the acceleration ramp. Small frequency changes during the ramp within the IF bandwidth will be automatically tracked by the demodulator in real time. Band-center frequency adjustments for special measurement purposes can be achieved by synthesizer remote control in the range of 500MHz ± 2MHz with 50kHz steps. The output signal of the highly linear synchronous demodulator is proportional to the rms value of the fundamental component of the amplified button signal and carries also level changes with frequencies up to 500 Hz. The overall demodulation bandwidth can be selected by means of switched filters to frequencies between 0.1Hz and 500Hz in 13 steps. The gain control range of the processing chain is about 100 dB. Signal level dynamic between −80dBm and +10dBm is allowed. Scan timing and the step gain control are synchronized, four button signals will be measured in each cycle with the same gain, therefore consistent data can be used for position computing. The scan sequence of the button measurements is programmable. The data acquisition module consists of a 8bit microcontroller with 8kbyte EPROM and 32kbyte RAM and built-in timer, half-duplex 1Mbit/s asynchronous serial interface with galvanically decoupled twisted-pair transceiver for data communication, 12bit ADC for digitizing of the demodulated electrode signals and 12bit DAC for gain control, several bits for timing and bandwidth control and a 3-wire serial interface for synthesizer control. The timer of the microcontroller controls the RF multiplexer and the timing phases of the acquisition. After digitizing of the button signals, depending on the acquisition parameters, the microcontroller filters by means of a digital lowpass filter (0.1–500Hz) and/or averages the signal values for the presetted number (1-4096) of measuring cycles. The acquisition frequency is always 1kHz, the transfer rate can be set by remote command to 1-256ms corresponding to the selected lowpass filter. Data transfer begins after finishing of the averaging.

For the determination of BPM zero positions with respect to the magnetic axis of the quadrupoles beam based alignment was used to calibrate the system with an accuracy of better than 100 μm. The residual closed-orbit deviations after correction were 140 μm in both planes. Measured optics functions are in good agreement with theoretical predictions based on the analysis of the orbit-response matrix measured by the BPM system.

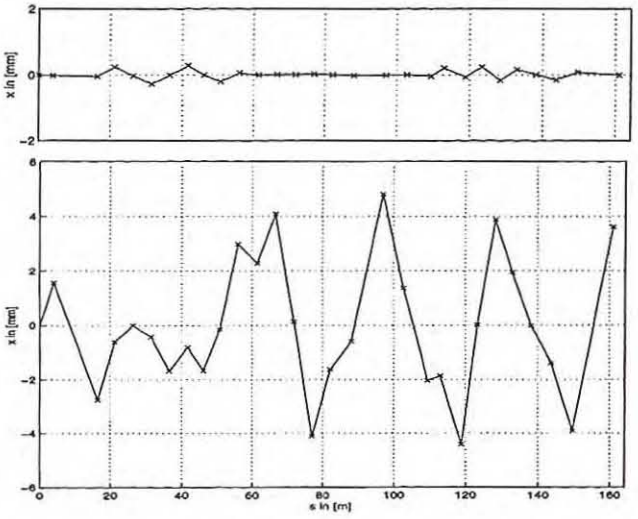

Fig. 1: Corrected and uncorrected horizontal closed orbit at ELSA (1.2 GeV).

[1]Physikalisches Institut, Universität Bonn

References

[1] I.Mohos and J.Dietrich, 500 MHz narrowband beam position monitor electronics, 8th Beam Instrumentation Workshop, Stanford, May 4-7, 1998

6. ION SOURCES AND BEAM TRANSPORT

Ion Sources and Low Energy Beam Transport

R. Gebel, O. Felden, N. Gad, M. Glende, A. Müller, P. von Rossen, N. Rotert

Ion source operation

The two unpolarized ion sources for COSY are multicusp H^--sources [1] and have demonstrated reliable operation in 1998. The scheduled operation of the polarized ion source was delayed two times by cesium leakage inside the cesium ionizer. The polarized beam was successfully used for studies to polarization conservation in the synchrotron up to the maximum beam momentum of 3.3 GeV/c [3].

Extension of the beam diagnosis in the source beam line

The beam diagnosis of the low energy beam in the transfer line to the injector cyclotron consists of five moveable copper plates with a thin potassium bromide surface for combined current measurement and optical analysis of the beam. The beam transport in the beam line is optimized for transmission, beam size and position. In front of the first cup an additional moveable grid has been installed. By means of a specially shaped grid it is possible to minimize the angle deviation of the beam at this position. The setup of the ion sources and ion optical elements were online corrected for minimum aberrations. Figure 1 shows the result of an artificially enhanced picture taken with a black and white CCD camera and stored by a PC based frame grabber and analysis system. Inverting and controlling brightness and contrast enhances the images.

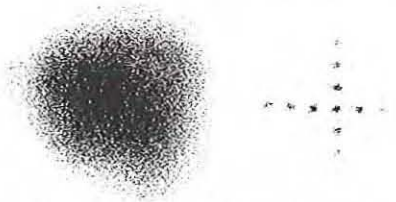

Fig. 1: Beam spots of a 200 µA unpolarized ion beam at the first cup in the source beam line without and with the grid in the beam path. The distance between two 0.5 mm apertures is 3 mm.

The Polarized Ion Source

The polarized ion source was built by a collaboration of the universities of Bonn, Cologne and Erlangen [2]. Polarized H^--ions for COSY are produced in a charge exchange reaction between a ground state nuclear polarized atomic hydrogen or deuterium beam and a fast neutral cesium beam. The nuclear polarization of the hydrogen beam is accomplished by rf transition units, they were developed for the polarized ion source and are also in use for the EDDA atomic beam target reaching there a polarization degree of over 90 % [4]. The polarization measured at the low energy polarimeter in the transfer beam line to COSY reaches 82 % for both spin states prepared with two separate rf transitions. Fig. 2 shows the rf resonator of the intermediate field transition unit after use in the polarized ion source. The fast neutral Cs beam damages the surfaces. For a misaligned and divergent Cs beam the quality factor of the resonator will decrease rapidly. By improving the geometry of the insulators and the rf coupling loops the sensitivity was substantially reduced.

Pulsed operation of the Cs ionizer

The picture of the rf structure shown in fig. 2 gives an impression of the effect of a temporal misalignment of the cesium beam during tuning and operation of the source. An uncontrolled and long-term aberration in continuous operation will lead to a reduced performance and uptime of various source components. Therefore, an investigation of a pulsed operation of the charged cesium beam part was started [5].

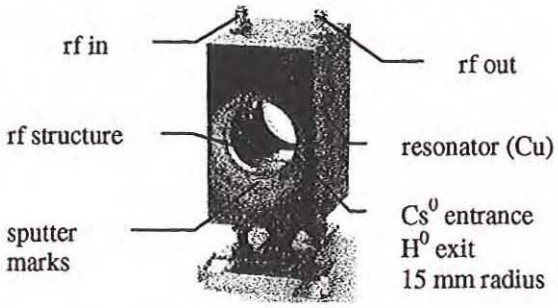

Fig. 2: The resonator of the 1.45 GHz transition unit after operation in the polarized ion source.

The setup of the new cesium ionizer [6] was modified for the installation of an additional electrode at the cesium beam potential. To implement of an electrical pulsing scheme at the present cesium ionizer the temperature of the cesium reservoir had to be reduced.

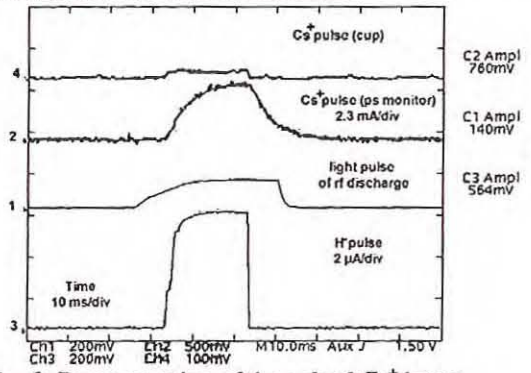

Fig. 3: Demonstration of the pulsed Cs^+ beam.

The length of the H^- output pulse of the polarized ion source on the first cup in the transfer beam line to the cyclotron is determined by the Cs^+ pulse with 20 ms pulse width. The 5.6 µA H^- peak current, Channel 3, corresponds to 3.5 mA Cs^+, measured at the power supply (ps) current monitor on channel 2. A photo diode, channel 1, detects the light of the rf discharge and the not neutralized fraction of the cesium beam is dumped after deflection in the cesium cup (channel 4). The slow rise and fall times of channel 2 are due to internal low pass filter of the power supply.

[1] H. Beuscher et al., IKP Annual Report (1996)
[2] P.D. Eversheim et al., IKP Annual Report (1996)
[3] A. Lehrach et al., this IKP Annual Report (1999)
[4] O. Felden, Ph.D. thesis, Bonn (1998)
[5] R. Gebel et al., IKP Annual Report (1998)
[6] M. Eggert, Ph.D. thesis, Köln (1998)

Operation of a Double gap Buncher with Complex Waveforms

W. Bräutigam, R. Brings, R. Gebel, H. Jungwirth, A. Müller, A. Schnase

Introduction

In addition to the existing resonant buncher for sinusoidal waveforms, the buncher system for complex waveforms described in [1] is installed. The buncher structure is placed inside the vacuum chamber of the Faraday-cup 5, which is just below the Cyclotron.

Tests with the initially designed structure showed beam losses due to a non sufficient aperture. The inner diameter was enlarged from 25 mm to 40 mm to match the beam size at this location. The original isolation of the centre electrode realised as a Teflon tube is replaced by three small stems made of POM. The grids made of small metal sheets are replaced by gold-coated tungsten wires of 40 µm diameter, to reduce capture of particles which move not perfectly parallel to the symmetry axis. An additional electrode detects particles off-axis. The electrical parameters of the structure remained almost unchanged.

The RF- layout

For the initial tests a not well adapted broadband amplifier had to be used because the specified amplifier was not delivered in time. We learned that more power and a better suppression of harmonics were required, which the available unit could not provide. Therefore we used two amplifiers in parallel: An ENI type A 300 provides the fundamental at 29.6 MHz with a maximum power of 300 W. The type AR 100W1000A amplifier provides the higher harmonics. The power, necessary for the sum of all higher harmonics up to 400 MHz is less than one tenth of the fundamental, e. g. max. 30 W. The broadband amplifier is able to deliver up to 100 W. At 30 W the distortions are low. We designed high- and low-pass filter networks to isolate the inputs and outputs of the amplifiers (Fig. 1). The components were selected for low losses: mica capacitors and inductors without cores made of silver-plated copper wire. We had to apply forced air cooling to the low-pass filter at the output of the 300 W amplifier, because we measured about 10 W rf-losses there, which destroyed a filter at the first tests. The detailed layout of the system is shown in fig. 2.

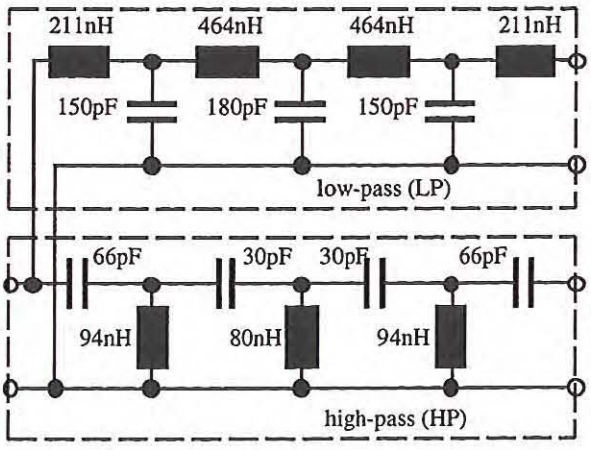

Fig. 1: Low-pass and high-pass filter design.

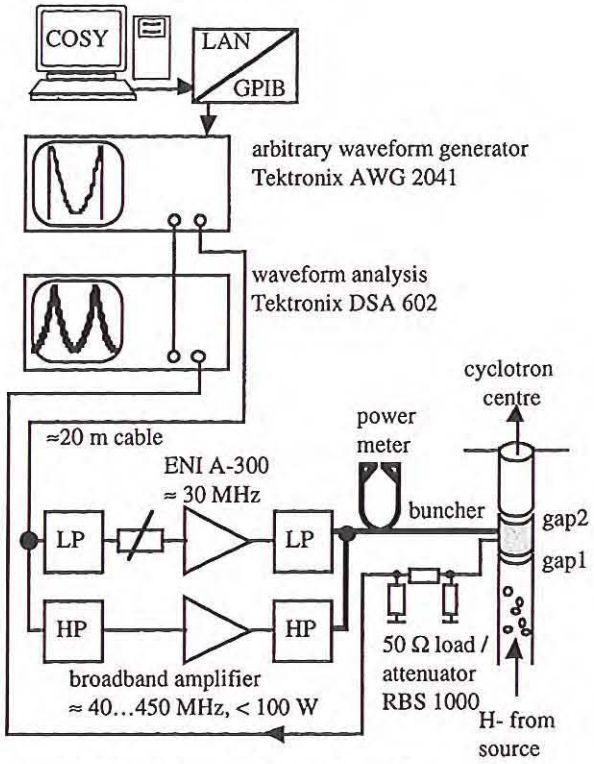

Fig. 2: Signal flow of the nonsinusoidal waveforms.

The combination of filters and rather long cables (20 m) makes it more difficult to provide the desired parabolic waveform at the buncher electrode. It is necessary to generate a pre-distorted signal at the output of the arbitrary waveform generator. The waveform at the generator is compared with the waveform at the buncher in fig. 3.

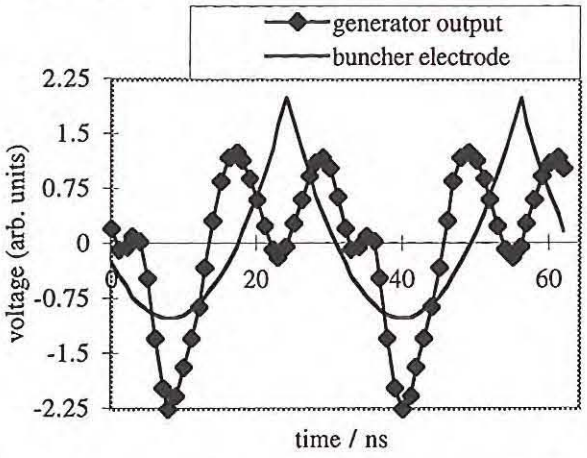

Fig. 3: Non-sinusoidal pre-distorted drive voltage to get a parabolic waveform at the buncher.

User interface

The buncher is controlled with a simple graphic user interface written in TCL (fig. 4), named „paraba". It communicates over network via a GPIB-LAN converter with the arbitrary function generator. It allows to switch the signal on or off, to change the trigger level which defines the phase, to control the amplitude, and to modify the waveform definition. The amplifiers are switched on manually.

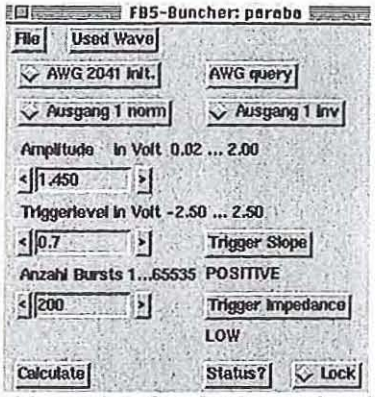

Fig. 4: Graphic user interface for the new buncher

Operation with unpolarised beam

A preliminary comparison of the buncher at FB5 with the resonant buncher was carried out with H^- beam. Without any buncher, the beam current at the exit of the cyclotron was 2.8 µA. The resonant buncher increased this value up to 5.2 µA, which corresponds to a bunching factor of 1.9. With the new buncher a bunching factor of 1.4 was obtained. The relation of the bunching factor to the trigger level (or phase) is shown in fig. 5a. The bunching factor at optimum phase as a function of power is plotted in fig. 5b. A combined operation of both bunchers resulted in the same bunching factor as the resonant buncher alone yields.

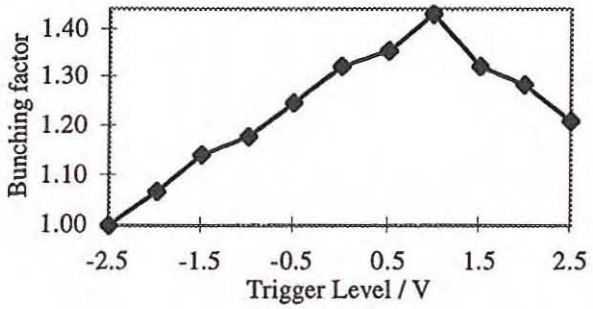

Fig. 5a: Bunching factor as a function of trigger level.

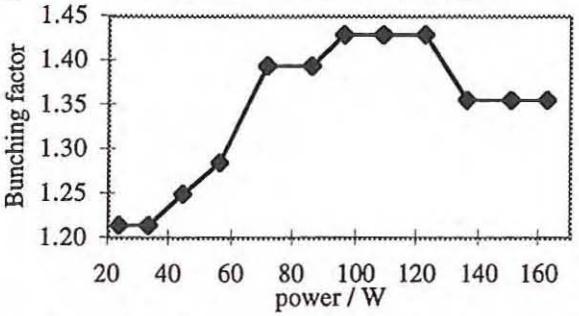

Fig. 5b: Bunching factor as a function of power (at 50Ω).

Operation with polarised protons

Measurements with polarised protons are difficult, because the beam is pulsed. As the current is much lower in this case, we use an internal target at maximum radius before extraction. The bunching factor for the resonant buncher as a function of phase shows fig. 6a. The relation between bunching factor and amplitude is plotted in fig. 6b. The results with the complex waveform buncher are plotted in fig. 7a and fig. 7b. Then we operated both bunchers together. The amplitude of the complex waveform was doubled (power 124W) and we obtained a combined bunching factor of 2.9. The resonant buncher alone yielded 1.8 and the complex waveform buncher another factor of 1.5. After the changes of the mechanical structure were carried out, we could improve the combined result to 3.6. The resonant buncher alone gave a factor of 2.

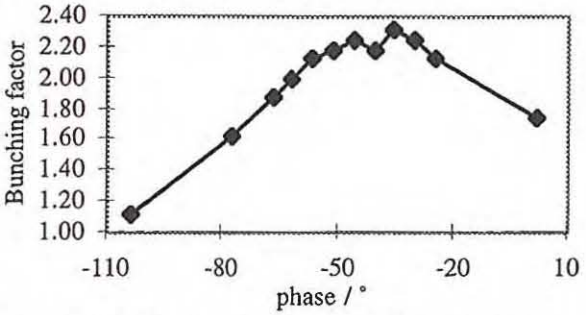

Fig. 6a: Bunching factor vs. phase at resonant buncher.

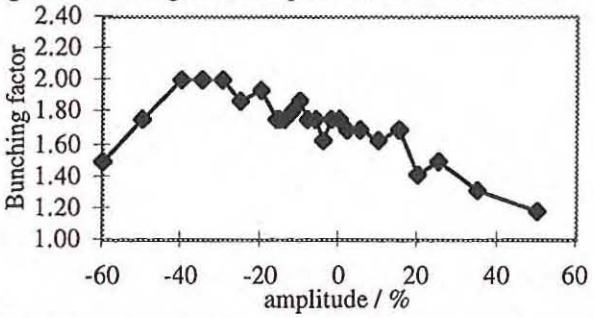

Fig. 6b: Bunching factor vs. amplitude at resonant buncher.

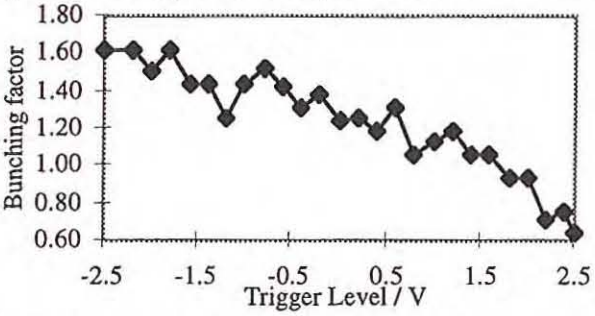

Fig. 7a: Bunching factor vs. phase at FB5 buncher.

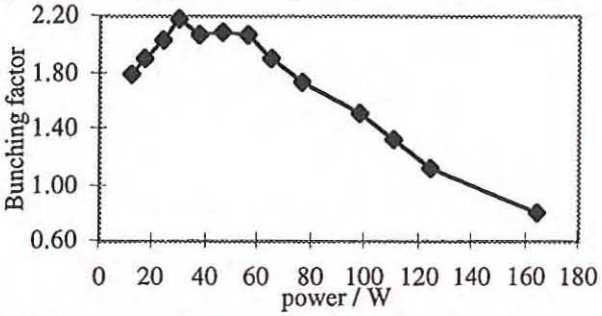

Fig. 7b: Bunching factor vs. power at FB5 buncher.

Results

In operation with unpolarised protons, the complex waveform buncher does not perform better than the resonant buncher alone. With a polarised beam the new buncher provides almost the same bunching factor as the resonant buncher alone. Both bunchers together with an optimised setting increase the bunching factor to almost the product of the single values. This is related to different beam parameters of the polarised source compared to the unpolarised ones. More experience is needed to understand this.

Reference

[1] W. Bräutigam, F.-J. Etzkorn, H. Jungwirth, A. Schnase: „Investigation of Bunchers for Injection into the Cyclotron", IKP Annual Report 1997, p. 210f

7. SPECTROMETER BIG KARL

Magnetic Spectrograph BIG KARL

J. Engel, R. Jahn, K. Kruck, H. Machner, R. Maier, P. v. Rossen, R. Tölle,
GEM- and MOMO-Collaboration

The magnetic spectrograph BIG KARL served experiments carried out by the GEM- and MOMO-collaboration as well as facilitated the calibration of detector systems used for a NASA mission. The scientific objective of this experiment, known as Gravity Probe-B, is to test special aspects of general relativity in space. Details to this space mission are found in a separate article in this report. Besides the routine maintenance to keep the experimental facility up to present technology standards a new small scattering chamber has been built according to the needs of experiments.

Another major addition was a set of two smaller position sensitive wire chambers together with a double set of scintillator hodoscopes to observe particles that exit at the side window of the first dipole. Originally this side window was conceived only as a narrow channel allowing the primary beam to leave the spectrometer without generating huge amounts of background for the focal plane detectors. The construction permitted to move this channel to accommodate a range magnetic rigidity ratios between the primary beam and the recorded ejectiles. Removing all iron shunts produces a window large enough to record ejectiles at this exit and at the same time in the focal plane creating an interesting option for a special class of experiments. This special mode works quite well as the optimal quadrupole setting is the same for recording of ejectile at both locations.

More generally the spectrometer has in this mode the option to measure particles with energies greatly exceeding the design values of the spectrometer if high energy resolution is not a primary concern. This opens the instrument to whole new class of experiments not within reach hitherto.

The MOMO collaboration took for the first time K^+K^- Data close to threshold (Q=56 MeV) in the reaction p d $\rightarrow$ ^{3}He K^+K^-. To ensure good kaon identification a 2 cm thick scintillator hodoscope consisting of 16 segments had been placed behind the scintillating fiber vertex wall. An additional movable scintillator paddle that could be put into the intensity reduced proton beam helped to heighten the normalization precision. Through an elaborate tuning the COSY crew managed to raise the intensity of the external beam to BIG KARL to $1*10^9$ protons/s at a momentum of 2.6 GeV/c with the halo down to a 10^{-4} level. This achievement was crucial to the success of the experiment looking at a low cross section process. In total 1700 twin kaon events have been recorded an a clear signal of the F-meson was observed. The further analysis is in progress.

Two separate runs were performed by the GEM experimenters. In one they looked at the reaction p+d $\rightarrow$ η ^{3}He at a proton momentum of 1650 MeV/c. Total and differential cross section have been deduced from the measured data. In the other run for the first time the reactions p+d $\rightarrow$ π^+ ^{3}H and p+d $\rightarrow$ π^0 ^{3}He have been investigated simultaneously. Employing this technique makes it possible to reduce to a large extend systematic errors that would otherwise spoil conclusions concerning isospin symmetry.

NASA Mission Gravity Probe-B - Detector Calibration at BIG KARL

S. Buchman*, J. Engel, R. Maier, D. Prasuhn, P. v. Rossen, P. Rusznyak**

Conclusions drawn from Einstein's general relativity theory have always inspired and enticed the experimenters to put them to a rigid test. In most cases they were confronted with extremely subtle effects which easily explains why these effects have for so long escaped the scrutinizing eye of experimental physics. After having established those effects the next barrier was to raise the accuracy bar in order to look for aberrations. Einstein's theory is no longer unchallenged and precision data would be decisive. Such is the case in the NASA mission Gravity Probe B which is a highly sophisticated scientific satellite scheduled to be launched in the year 2000. The roots of this experiment also called Relativity Mission, jointly performed by NASA and the Stanford University, date back to 1959 when Leonard Schiff published an article in the American Journal of Physics. The experiment will check with utmost precision minute changes in the directions of spin of four gyroscopes which are housed in a satellite orbiting over the Earth's poles in a distance of 400 miles.

These gyroscopes realize the latest in technological achievement and represent an almost perfect space-time reference system. They will allow to measure how space and time are warped by the presence of the Earth, and more profoundly, how the Earth's rotation drags space-time around with it. Although the effects are extremely small, they have far reaching implications for the nature of matter and the structure of the Universe.

This extremely small but vital frame-dragging effect never seen before could be measured with Gravity Probe B to a precision of 1% or better. The other effect albeit extremely small is large in comparison with the frame-dragging. The expected angular change in the direction of the gyroscopes exceed the frame-dragging by over a factor of 100. This enables one to reach a precision of 10^{-4} for this phenomenon and will then represent the most precise measured quantity predicted by general relativity.

At the heart of this experiment are super conducting gyroscopes. Perfect spheres of fused quartz with a diameter of 1.5 inch, coated with a thin layer of niobium and being held at a temperature of 1.8 K. These gyros exhibit a hitherto unmatched drift rate of 10^{-12} °/hour. Many aspects that could jeopardize the needed precision have to be carefully taken into account, one of which is the stream of high energy protons emitted irregularly by the sun. To deal with this influence a flight unit containing two silicon detector telescopes being at right angle and the associated electronics with data acquisition is on board of this mission satellite. The units are depicted in Fig. 1. As the relevant part of the energy spectrum reaches up to 500 MeV it is impractical to stop the protons, measuring thus their full energy. Instead a detector set of four silicon disks ranging in thickness from about 0.5 to 2 mm produces ΔE signals that can be calibrated to reflect the particle energy. To prove the functionality of this unit and obtain a reliable set of data points the units have been bombarded with protons from COSY that were filtered with the magnetic spectrograph BIG KARL. COSY did deliver to fixed energies namely 500 MeV and 300 MeV. All other energies down to 40 MeV were produced by degrading the primary beam energy and filtering the appropriate energy band with the spectrometer while the flight unit under test had been placed at the focal plane of the instrument.

The measurements did help to correct the initial calibration which had been performed with a pulser system. It also verified the full functionality under bombardment condition with protons over the envisioned energy range. Two flight units underwent successfully these tests one serving as a spare unit for the mission Gravity Probe B.

* Stanford University, California
** Space Technology, Ireland

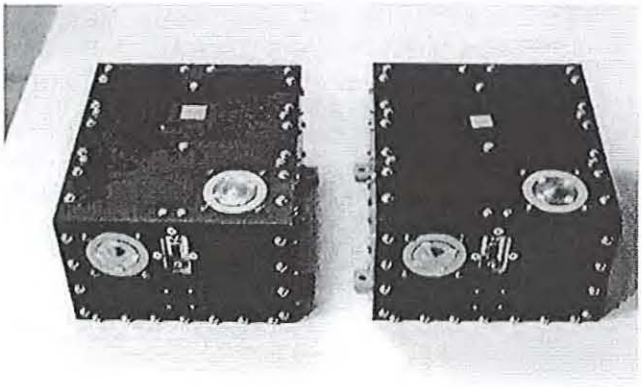

Fig. 1: The flight units tested for Gravity Probe B. The bright titanium disks have a diameter of approximately 5 cm and cover the openings of the silicon detector telescopes

8. RADIATION PROTECTION

Radiation protection

H.J. Probst, K. Krafft, J. Göbbels

For the beginning of 1998 the access to the inner hall of COSY is realized correspondingly to the new procedure, that means, the maximum local dose must not exceed the value of 1 mSv per week during presence of persons in the inner hall. An investigation of the maximum doses per week in 1998 showed maximum values of about 0.7 mSv so that no stops of the beam operation were necessary. The maximum value for a quarter of a year was 2.5 mSv. Simultaneously the neutron personal doses of the persons working in the inner hall of COSY were measured. The personal doses of a quarter of a year were so low that for a dosemeter sensibility of about 100 - 150 µSv no value was detectable. This result agrees with the measuring results of the last year. They showed that the personal doses of the persons working in the inner hall of COSY (close to the ANKE-electronic) not exceed 3% - 5% of the maximum local dose.

The existing radiation surveillance system was installed above all to interrupt the beam operation in case of unallowably high radiation levels, but it is also well suitable to determine and to document the dose rate outside of the shielding during long time intervalls. The figures 1 - 4 show for selected positions (NM 5: the middle of the northern section, NM 10: extraction septum, NM 15: injection/extraction beam line, NM 17: injection beam line, NM 20/NM 23/NM 26: begin, middle and end of the western bend section, NM 28: power supply room in the first floor, NM 29: access door to Big Karl, NM 32: measuring room behind the beam stop of TOF) the neutron dose rate (mean value of a week) for each week of 1998.

The injunctions of the authorities with respect to the announcement 1/97 (operation of the low energy polarimeter NEP in the injection beam line) were carried out before the first operation of NEP by the shielding and other measurements of the experts.

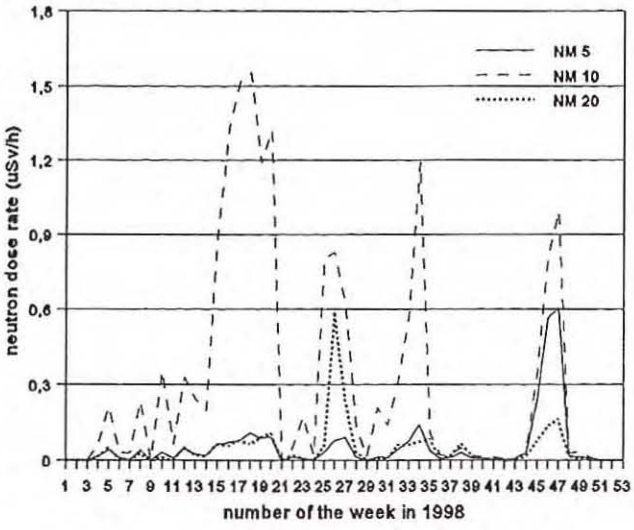

Fig. 1: Neutron dose rate (mean value of the week) outside of the shielding for the weeks in1998 on the positions of the neutron monitors NM 5, NM 10 and NM 20.

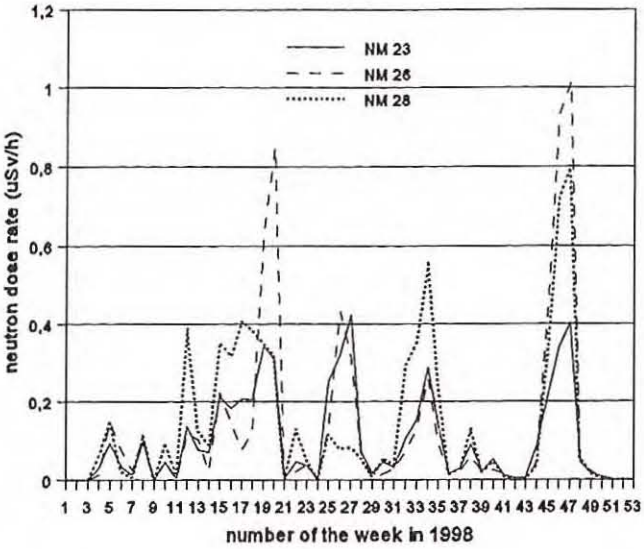

Fig. 2: Neutron dose rate (mean value of a week) outside of the shielding for the weeks in 1998 on the positions of the neutron monitors NM 23, NM 26 and NM 28.

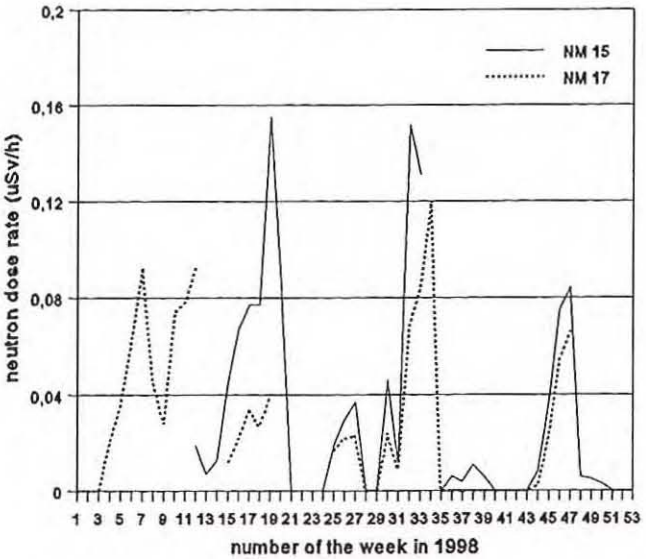

Fig. 3: Neutron dose rate (mean value of a week) outside of the shielding for the weeks in 1998 on the positions of the neutron monitors NM 15 and NM 17.

They had no objection to the modification of the personal safety system PSA. Moreover the dose rates in the COSY-ring during beam on NEP for a proton current of 1 µA and a proton energy of 40 Mev were ≤ 1 µSv/h, hence the background radiation was not significantly increased.

The neutron doses of a year resulting from the values of figures 1 - 4 are shown in figure 5.

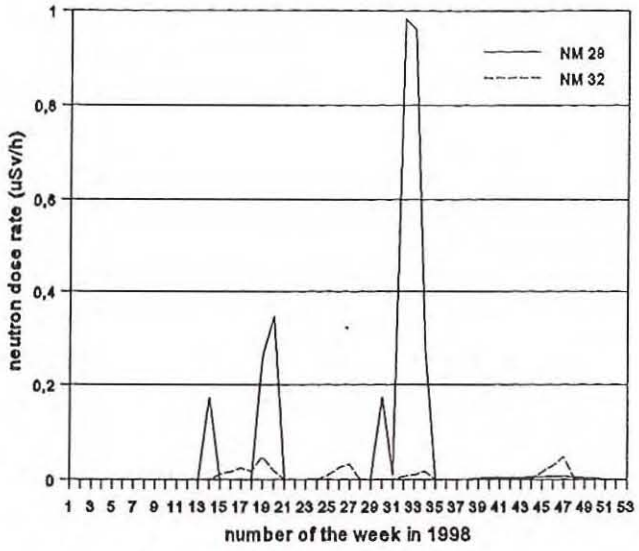

Fig. 4: Neutron dose rate (mean value of the week) outside of the shielding for the weeks in1998 on the positions of the neutron monitors NM 29 and NM 32.

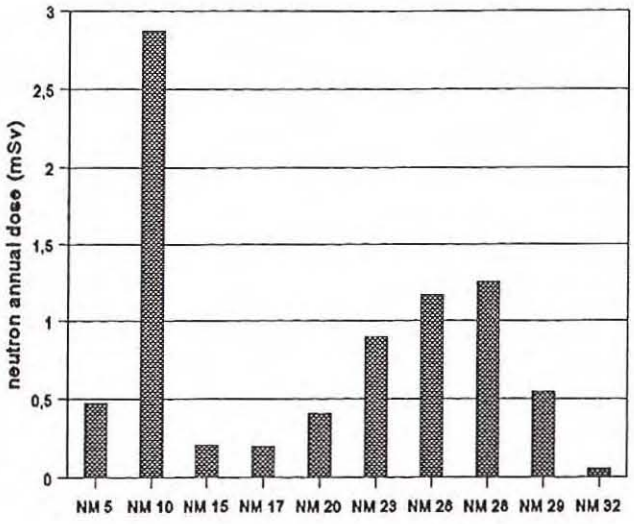

Fig. 5: Neutron annual doses in 1998 on the positions of the neutron monitors NM 5, NM 10, NM 15, NM 17, NM 20, NM 23, NM 26, NM 28, NM 29 and NM 32.

IV. EUROPEAN SPALLATION NEUTRON SOURCE (ESS)

9. TARGET PHYSICS

10. ACCELERATOR COMPONENTS

9. TARGET PHYSICS

Helium and Hydrogen Production cross sections for 1.2 GeV p+Fe,Au

The NESSI Collaboration: D.Filges, F.Goldenbaum, R.-D.Neef, K.Nünighoff, N.Paul, H.Schaal, G.Sterzenbach, A.Tietze(FZ-Jülich); M.Enke, C.Herbach, D.Hilscher, U.Jahnke(HMI-Berlin); J.Galin, A.Letourneau, B.Lott, A.Pèghaire(GANIL-Caen); L.Pienkowski(Univ. of Warsaw)

The comparison of many observables accessible in the experiment with results of high energy transport codes (e.g. HERMES[Clo88]) will give deep insights not only to the *inter*nuclear transport, but also to physical processes inside nuclei which might be described by *intra*nuclear cascade models [Ilj94, Cug87, Ber63, Clo88]. The latter aspect concerns the production of highly excited hot nuclei and the study of subsequent decay modes like multifragmentation, vaporization or conventional fission and evaporation.
As far as shielding requirements for the *E*uropean *S*pallation *S*ource ESS are concerned the angular and energetic distributions of neutrons have to be studied since published data for energies beyond 1 GeV incident proton energy are scarce and show large uncertainties. For the favored target material of ESS Hg, for instance, so far no data are known at all.

The experiment NESSI provides an important benchmark for obtaining key parameters necessary to design and construct the ESS. In summary NESSI is able to measure

- reaction cross sections
- neutron multiplicity distributions,
- charged particle (p,d,t,H,He,IMF) multiplicity distributions[Lot97],
- fission cross section,
- to some extend heavy residue production cross section,
- kinetic energies of charged particles and
- excitation energy *distributions* within approximately 10% accuracy.

Reaction particles released for each spallation process like neutrons, H- and He-isotopes, but also fission products and intermediate mass fragments are detected event by event by means of two 4π detectors—the 4π neutron ball and the 4π silicon ball [Hil98]. This eventwise detection allows measurements not only of average values, but also of charged particle and neutron *distributions* which represent much stronger constrains for the comparison with model calculations. Measurements have been carried out at the COSY facility in Jülich for 1.2 and 1.8 GeV proton induced reactions on target nuclei between Fe and U. In the present contribution we focus on using thin targets of 0.6 to 12.6 mg/cm^2, because the exact knowledge of production cross sections for light particles (p,d,t,H,He) is of special importance in respect to target-, structure- and window materials selected for ESS since the lifetime of window and target materials is directly associated to those cross sections. Furthermore, models describing composite particles might be validated or improved. The results for reaction cross sections σ_{reac} as well as for hydrogen and helium production are shown representative for Fe and Au nuclei in the following tables.

	HET		NESSI experiment
σreac.		1.692 b	1.760 b
σ(n)		19.99 b	19.10 b
σ(p)	6.44 b	9.5 b	2.400 b
σ(d)	2.19 b		
σ(t)	0.87 b		
σ(He-3)	0.25 b	2.44 b	1.280 b
σ(He-4)	2.19 b		

Figure 1: *Reaction cross section σ_{reac} as well as various production cross sections for 1.2 GeV p+Au. While for the HET-calculations $\sigma(n)$ is folded for the energy dependent detector efficiency, production cross sections for charged particles are neither corrected for efficiency nor detector thresholds.*

	HET		NESSI experiment
σreac.		0.782 b	0.800 b
σ(n)		2.54 b	2.95 b
σ(p)	3.042 b	3.51 b	1.320 b
σ(d)	0.390 b		
σ(t)	0.078 b		
σ(He-3)	0.081 b	0.322 b	0.440 b
σ(He-4)	0.241 b		

Figure 2: *Same as above, but for Fe.*

While especially for heavy targets we observe a good agreement between the model predictions [Clo88] and the preliminary experimental values for σ_{reac} and the neutron production cross sections, a significant deviation is obtained as far as the helium- and hydrogen production cross sections is concerned. The hydrogen yield was measured between 2.3 and 24 MeV for protons. In summary we have measured production cross sections for spallation reactions on thin targets for 1.2 and 1.8 GeV proton induced reactions and observed in particular for hydrogen considerable deviations between model predictions and the experimental results which are not yet fully understood.

References

[Clo88] P. Cloth et al.,HERMES, Report Juel 2203, ISSN 0366-0885, May 1988.

[Hil98] D. Hilscher et al., Nucl.Inst.&Meth. **A414**, 100 (1998).

[Ber63] H.W. Bertini et al., Phys.Rev. **134**, 1801 (1963).

[Cug87] J. Cugnon et al., Nucl.Phys. **A470**, 558 (1987).

[Ilj94] A.S. Iljinov et al., CRC Press, (1994).

[Lot97] B. Lott et al., Nucl.Phys.B **56a**, 114(1997).

Neutron Production in Spallation Target Materials

The NESSI Collaboration: D.Filges, F.Goldenbaum, R.-D.Neef, K.Nünighoff, N.Paul, H.Schaal, G.Sterzenbach, A.Tietze(FZ-Jülich); M.Enke, C.Herbach, D.Hilscher, U.Jahnke(HMI-Berlin); J.Galin, A.Letourneau, B.Lott, A.Pèghaire(GANIL-Caen); L.Pienkowski(Univ. of Warsaw)

In the framework of the ESS-Project[ESS] the international NESSI collaboration has initiated measurements at COSY in order to evaluate neutron production cross sections for proton-induced reactions for a variety of incident proton energies up to 2.5 GeV, different target materials like tungsten, mercury and lead and for various target geometries. Here essentially thick targets are used in order to benefit from particles emitted in the primary spallation reaction converting the original incident proton energy more effectively into neutron production by secondary, tertiary, etc. reactions [Hil98].
Reliable systematic data bases—especially for p-energies beyond 1 GeV—including *distributions* of neutron multiplicities are urgently needed in order to validate and improve the existing high energy transport codes like for instance HERMES[Clo88].

For measurements using the 4π berlin neutron ball BNB and thick targets of the order of several cm in diameter and length the key observables are the the neutron multiplicity M_n (measured event-wise!) and the reaction probability P_{reac}. Since we are counting all incident protons and the BNB provides also a prompt light signal with a rather low energy threshold (2 MeVee) even without the emission of any neutron, we are able to specify not only the neutron multiplicity per reaction, but also per incident proton—or P_{reac} related to the total reaction cross section. The survival probability ($1\text{-}P_{reac}$)

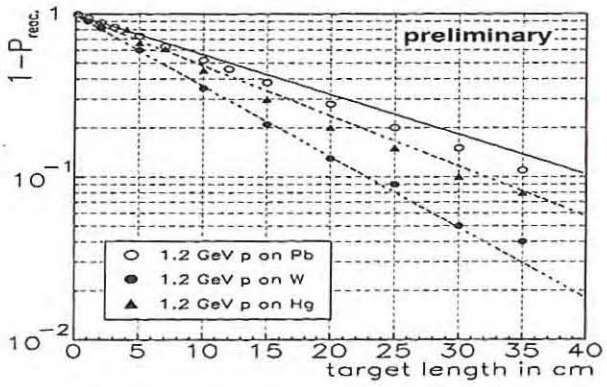

Figure 1: *Measured survival probability* $(1 - P_{reac})$ *for 1.2 GeV p+Pb, Hg and W-cylinders of 15 cm diameter (symbols). Straight lines are interpolations of HERMES calculations.*

as a function of target thickness is shown in Fig. 1 for 1.2 GeV proton induced reactions on Pb, Hg and W cylinders of 15 cm in diameter. The symbols presenting the measurements deviate slightly from the lines showing the result of HERMES calculations and following almost perfectly the exponential law $1 - P_{reac} = \exp(-L/L_{reac})$ where L is the target length and L_{reac} is the interaction length of 10, 14.1 and 17.9 cm for Pb, Hg and W, respectively.

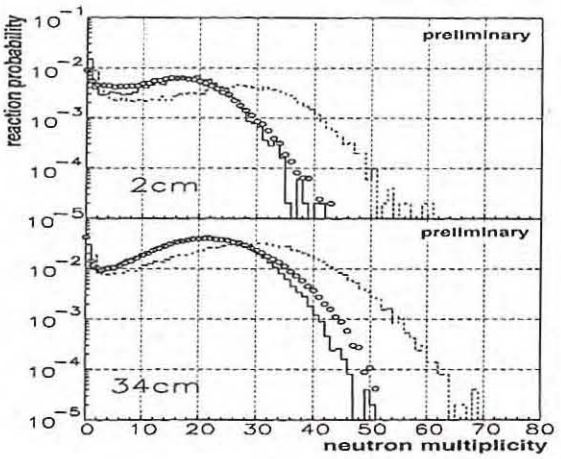

Figure 2: *M_n-distributions for 1.2 GeV p+Hg (for explanation cf. text)*

The average number of neutrons produced per incident proton N_n/p can be derived from the independently measured product of P_{reac} and $\langle M_n \rangle$. Differential cross sections or neutron multiplicity distributions are shown as an example for 1.2 GeV protons impinging on Hg cylinders of 15 cm diameter and 2 and 34 cm length, respectively. While the dashed line depicts the model-prediction(HERMES), the solid one is folded not only by the neutron kinetic energy dependent detector response, but also corrected for experimental dead time and can therefore be compared to the "as measured" experimental values presented by the open circles. It is worth mentioning that the experimental values are in good agreement with model predictions not only as far as the absolute values, but also the shape of the M_n-distributions is concerned. We obtain $\langle M_n^{exp} \rangle = 13.3$ and 19.6 for the experimental values to be compared to $\langle M_n^{model} \rangle = 13.8$ and 19.3 for the model predictions for 2 and 34 cm, respectively. The observed shift towards higher M_n for thicker targets is related to the increase of $\langle M_n \rangle$ due to secondary reactions and the increase of P_{reac} with target thickness.

In summary the experiment NESSI will provide systematic data and an important benchmark for testing high energy transport codes. The analysis of the data and a systematic comparison with model predictions is presently in progress.

References

[Clo88] P. Cloth et al.,HERMES, Report Juel 2203, ISSN 0366-0885, May 1988.

[ESS] Report ESS 95-30-M, ESS 96-53-M.

[Hil98] D. Hilscher et al., NIM**A414**, 100(1998).

Power Density Distribution in a Mercury Target

A. Tietze, R. D. Neef
For the NESSI Collaboration

The purpose of the experiment is to measure the energy depostion in a mercury target with the ESS proton energy of 1.334 GeV. The designed beam intensity of ESS generates an impuls of 100 kJ/pulse at the target which induces instantaniously temperature jumps. These temperature jumps produce pressure waves in the target material which stress the containment. Therefore it is necessary to know the power density distribution due to the proton pulse. Another reason to investigate the power density distribution is that we need this information for design the target station, in particular the cooling systems and the design of the density profile of the incident proton beam on the mercury target. At COSY we have the possibility to perform measurements with the ESS proton energy of 1.334 GeV, but its intensity is too low to determine an increasing temperature like the ASTE-Experiments.

To measure the spatial power density distribution in the target we use thermoluminescence detectors (TLDs) which are well-known from radiation protection where TLD measurements are perfomed routinely and the measurement technique is well established. One gets the energy deposition in the unit of Gy [J/kg] which depends on the TLD material.

Particle	Energy deposition [MeV/p]	Energy fraction
p	1.63 E-01	63%
$\mu^{\pm}$, $\pi^{\pm}$, d, t, He3, He4	5.49 E-03	2.1%
recoil energy	4.96 E-03	1.9%
exitation (submitted)	3.73 E-02	14.5%
n (submitted)	6.18 E-03	2.4%
π^0 (submitted)	4.08 E-02	15.9%
Σ	2.57 E-01	100%

Tab. 1: Calculated energy deposition in a TLD per 1.2 GeV incident p on mercury target, at 1.3 cm penetration depth

The first measurement in the mercury target was performed with protons of 1.2 GeV energy. The diameter of the target was 15 cm and the length 35 cm. We use Thulium (Tm) doped CaF_2-TLDs as detector.

The advantages of using thermoluminescence dosimeters are:

- the detector is very small and sensitive
- the detector does not disturb the flux of protons and secondary particles
- the doped CaF_2-TLDs produce two peaks, the low temperature peak to investigate effects like LET (linear energy transfer) and the high temperature peak to find out the deposited energy.

The stored energy in the TLD is proportional to the absorbed dose and the absorbed dose is proportional to the energy deposition in the surrounding material. The factor of proportionality between the energy deposition in CaF_2 and Mercury is in the order of 0.6.

By heating the TLD chip to a temperature of 350 ° C the stored energy is emitted by photons. A photomultiplyier amplifies the signal, so that we get a light signal proportional to the stored energy. We calibrated the detectors with the Co-60 source of the Institut für Medizin, FZ Jülich. To minimize the errors we repeat the calibration before and after measurement.

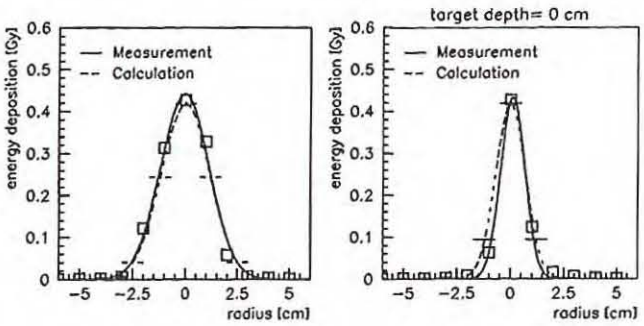

Fig. 1: Measured and calculated axial energy deposition in mercury target for 5 * 10^9 incident protons

For calculation we use the HERMES code-system. First we calculated the energy deposition of incident protons and secondary particles with the program HETC and the measured Gauß-distributed beam profile (see fig. 1). Protons, neutrons (above 20 MeV), $\pi^{\pm}$, $\mu^{\pm}$ are transported through the target whereas the energy of deuterons, tritons, He3, and He4 is deposited their energy at the position, where the particles are created. Table 1 gives an overview about the energy deposition by the different particles.

The energy depostion of the π^0 – decay is calculated by using the program EGS and the deexcitation of residual nucleus by using NDEM and EGS.

The comparison of measured and calculated energy distribution (see fig.2) shows reasonable agreement between calculation and experiment. Further measurements are planned with higher proton intensity to receive higher count rates for better accuracy.

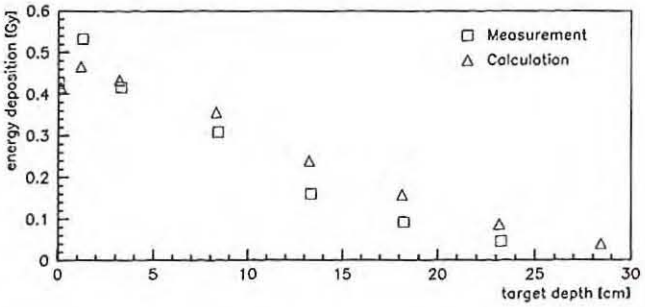

Fig. 2: Measured and calculated axial energy deposition in mercury target for 5 * 10^9 incident protons

The Preparation of a ESS-Target-Moderator-Reflector Mockup

W. Breuer, D. Filges, F. Goldenbaum, R.-D. Neef, K. Nünighoff, N. Paul, H. Schaal, G. Sterzenbach, A. Tietze
For the JESSICA Collaboration

1.) Introduction

JESSICA (Jülich Experimental Spallation Target Setup in COSY Area) is designed for prototyping experiments on the target / moderator / reflector system of the European Spallation Source (ESS). A full-size liquid Hg target will be placed in a short pulsed proton beam of COSY to produce a low intensity pulsed neutron beam. A variety of ambient temperature and cold moderators will be investigated at various positions relative to the target which is surrounded by a lead reflector. The aim is to validate the very complex simulation methods of particle production, interaction, and transport by experiments to optimize the technical layout of an ESS-type target-moderator-reflector system. This includes investigations of advanced cold moderators and development of scattering kernel data. With the JESSICA experiment we will measure the neutronic performance by means of neutron time of flight and scattering techniques. All results of the JESSICA experiment are important data to validate the simulation models and code systems– as CALOR, HERMES, LCS, NMTC-which are used to optimize the layout of high power spallation target systems.

The JESSICA initiative is an international joint collaboration of the world's leading laboratories producing and utilizing pulsed neutron beams.

A high power pulsed spallation source like ESS [1], injecting a 1.334 GeV / 75 A peak current pulsed proton beam on a liquid Hg target at a 50 Hz repetition rate has never before been realized. Only a limited amount of both theoretical and experimental data on the nuclear spallation process, cross-sections and reaction products are available for such a target station. Technical boundaries need to be pushed beyond present limits. New scientific data on advanced moderators and for thick target materials will be obtained.

COSY with its rather low intensity proton beam is of prominent importance for prototyping the high power ESS target. COSY is even more suitable for studying the neutronic performance of a liquid Hg target and advanced cryogenic moderators than any other facility, namely the existing medium power proton sources as ISIS or LANSCE.

Because of its low proton beam intensity COSY is particularly suitable for studying the neutron performance of advanced moderators, whereas radiolysis, high activation levels and background are negligible. Furthermore, only moderate shielding is necessary, this means the whole prototyping experiment is much easier to accomplish without any lack of scientific quality of the results. Not only can the proton beam energy be tuned from 0.8 - 2.5 GeV at COSY, the negligible activation rate enables easy modifications to the geometry, construction details and materials involved. On the other hand, using a realistic 1:1 mock-up model of the anticipated ESS target yields reliable data for the technical optimization process. All this makes JESSICA at COSY a virtually ideal experiment for direct measurements of the neutronic performance of target / moderator / reflector systems.

The JESSICA target is located downstream just in front of a proton beam dump. The ESS-type stainless steel target container is placed right in the beam and filled with approx. 35 litres of liquid Hg surrounded by a 1.5 m diameter Pb reflector providing space for 4 moderators and beam extraction tubes. One moderator position will be used for the various moderator types for high intensity spallation sources. The other three positions remain idle to simulate realistic neutron flux disturbance inside the reflector.The reflector consists of 4 tiers with 2-4 cm diameter lead rods. The gaps may be filled with polyethylene to simulate the coolant.

The moderators are located in wing geometry , i.e. the neutron beam tubes do not view the target through the moderator directly. This is to reduce the fast neutron background considerably. Furthermore, the moderator surfaces are oriented perpendicular to the neutron beam axes in order to conserve the time structure of the neutron pulse.

A complete description of the moderator performance is required for the optimized design of scattering instruments. The quantities to be studied include the neutron energy dependent intensity and the neutron energy dependent emission time distributions of the neutron beam. Therefore the experimental program of JESSICA includes studying different moderator concepts, as thermal and cold moderators.

Cold neutron moderators have come to be an essential ingredient for any new neutron source to be built in the future. The most effective cold moderator system known at present is based on solid methane which is better in intensity by a factor of two to three than conventionally used hydrogen and also has better slowing down properties. But due to problems of heat removal and radiation effects methane can be used so far only at low power neutron sources. Therefore, efforts were started in several countries to develop advanced cold moderator concepts.

From neutronic point of view methane (CH_4) is considered the best moderator. The candidate materials to be tested at 16 K are all methane based:

- solid methane in the shape of small pellets (methane has a melting point of 90.7 K at 1 bar)

-methane hydrate in pellet form (gas hydrates are ice-like crystalline structures of a water lattice with cavities which contain guest gases, e.g. methane. Gas hydrates belong to a

special family of inclusion compounds called clathrates methane hydrate is solid at 198 K and 1 bar.)

-methane adsorbed on zeolites (Zeolites are crystalline alumosilicates that are commercially fabricated with high porosities up to 40 %. Handling of this material is expected to be much easier than the other two materials.)

-isopentane (C_5H_{12}) has promising properties and is liquid between -160^0C and+29^0C shall also be tested, since a number of users are interested in intermediate temperature moderators (~100 K).

-liquid hydrogen at 16 K is the reference moderator material for all tests.

The neutrons slowed down in the moderators are extracted through beam holes of the JESSICA target-moderator-reflector mock-up. For both spectra and time structure measurements an evacuated and shielded time-of-flight tube of about 5 m length will be used.

Using the HERMES computer code system which is basis for all nuclear calculations for ESS we calculated the neutron production in the JESSICA target-moderator-reflector facility (Fig. 1) with an ambient water moderator. Furthermore, we performed time dependent calculations to study the time dependent neutron spectrum at the end of a flight path of 5 m in length (Fig.7.) The neutron TOF spectrum is normalised to 1 proton and the energy spectrum is collapsed into 4 groups, E>1.35 MeV, 1.35 MeV > E>1.86 eV, 1.86 eV > E >410 meV, 410 meV > E > 10 μeV, respectively.

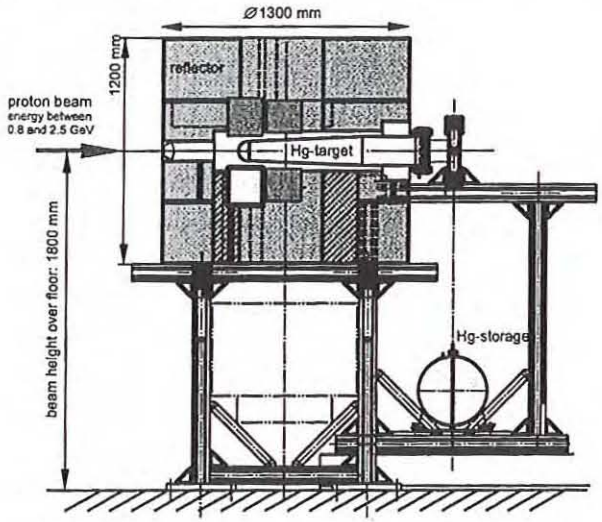

Fig. 1: JESSICA Target-Moderator-Reflector Test Facility.

Fast neutrons reach the detector at the end of the flight path in less than 10 μs after the proton pulse trigger. Epithermal neutrons (1.35 MeV > E > 1.86 eV) reach the detectors in less than 0.5 ms. Thermal neutrons in the upper energy range (0.41 eV > E > 1.86 eV) need 0.5 ms to 2 ms time-of-flight. The thermal neutrons (0.41 eV > E > 10 μeV) have flight times of 0.5 ms < tof < 5ms.

From Fig. 2 we can deduce directly the number of neutrons which we expect to count in a certain time interval: in the time interval 1ms<tof<2ms we expect 0.5 n/cm² per proton pulse of 10^7 protons.

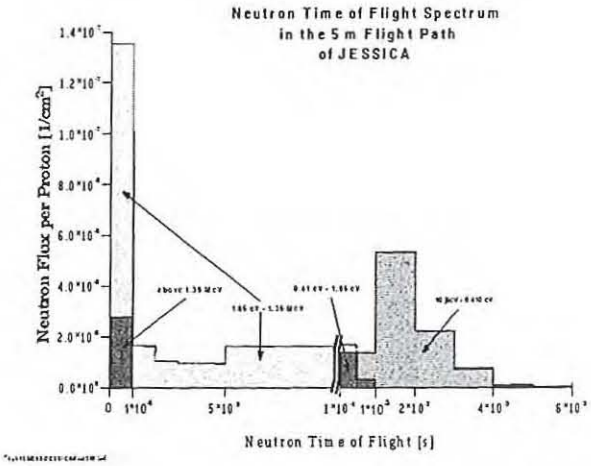

Fig. 2: Neutron Time of Flight Spectrum in the 5 m Flight Path of JESSICA

In the thermal energy range are 10^{-7} n/cm² per proton which reach the detector at the end of the flight path. If the detector has a surface of 100cm² and an efficiency of 1 and if a 1μs long proton pulse contains 10^7 protons we will measure a count rate of R=1.8x10^4n/s, but we will measure 100 thermal neutrons per proton pulse.

Reference

[1] G.S. Bauer et al., The European Spallation Source Study, Vol. III, ESS-96-53-M (Nov. 1996)

Validation of Energy Deposition Distribution in Mercury Target by a high Intensity Proton Pulse

W. Breuer, D. Filges, F. Goldenbaum, R.-D. Neef, K. Nünighoff, N. Paul, H. Schaal, G. Sterzenbach, A. Tietze
For the ASTE Collaboration

For ESS the important goal of the ASTE (AGS Spallation Target Experiment) collaboration is to verify experimentally the predictions with respect to power deposition and pressure wave buildup resulting from a short pulse of high energy content. The first experimental run in this collaboration was carried out at the AGS in Brookhaven in June 1997.

A 20 cm diameter, 1,2 m long cylindrical stainless steel container with a hemispherical front cap and filled with mercury was used as a spallation target in the experiment. In order to measure the spatial power distribution in the target, an array of 32 thermocouples were placed in the lower half-midplane of the cylinder. The 1.5 mm thick encapsulated Chromel-Alumel thermocouples (type K) were thinned down to 0,5 mm over the last 15 mm in order to improve their time response. The positions of the thermocouple tips inside the target were chosen on the basis of an assumed parabolic radial power distribution with a base width of r_s = 5 cm. The length of the cables between the thermocouples and the data logger was 50 m. The noise corresponded to roughly 0.5 K, in agreement with the specifications given by the manufacturer. Data recording was triggered from the pulse derived from the beam monitor.

For the beam intensity and profile measurement, an Al foil, 20 x 20 cm^2, 25 µm thick was placed on the beam axis in front of the target near the exit of the beam pipe.

The proton beam profile was measured by determining the proton induced ^{22}Na and ^{7}Be activity of the Al foil by cutting it into chips of 2 x 2 mm^2 and measuring their gamma activity. The beam axis was shifted to the target axis horizontically by 0.5 cm and vertically by 1.0 cm and the proton density profile was not very much like gaussian or parabolic. Therefore, for our energy deposition calculation we used the 100 x 100 measured values as input source distribution.

Two bunches of 24 GeV protons with 4 x 10^{12} protons in each bunch were injected into the target with 30 ms. The energy content of this pulse consisting of two bunches was therefore 30 kJ compared to 100 kJ in each ESS pulse. The measured temperature jump along the target axis compared with HERMES /1/ calculations is given in figure 1.

The maximum measured temperature jump is 3.5 K at 8 cm inside the mercury target. The dashed curve represents the results of a HET of HERMES calculation with the assumption that the π^0 energy can be deposited at the point of π^0 creation. The solid curve represents the same HET calculation, but the π^0 particles were input to the EGS code of HERMES which calculates π^0 decay, gamma and electron transport and energy deposition. The figure shows that for energy deposition determination the EGS calculation is necessary and we receive a good agreement between calculation and experiment.

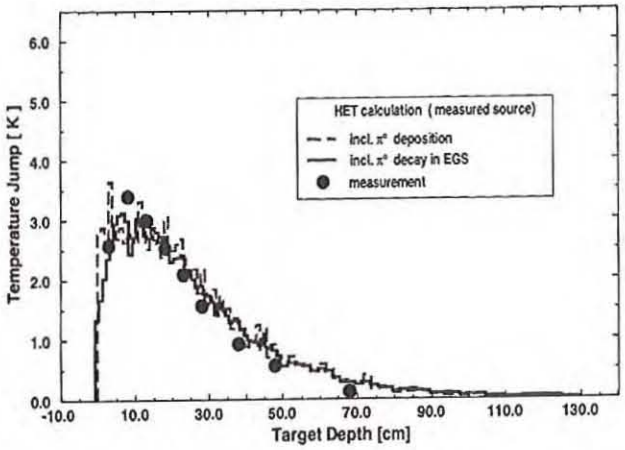

Fig. 1: Temperature jump in HG-target for $8x10^{12}$ protons in a pulse

After the proton pulse the temperature appears to stay more or less constant for almost 1 sec and then starts to drop rapidly. This drop must be attributed to the onset of convection because it cannot be explained in terms of the thermal conductivity of Hg. Calculations of the heat dissipation by conduction alone give a much slower temperature decrease, indicating that it would take minutes for the temperature to return to the original value. By contrast, the measured temperatures are back to their equilibrium values (22.4 °C) within less than 25 seconds. This clearly indicates the importance of convection in the system.

This preliminary experiment clearly showed that a set of thermocouples can be used to determine the power deposition in the Mercury target at the pulse levels available at the AGS. It also became obvious, how important information on the beam profile and position is in order to be able to evaluate the data properly. Although the Al-foil technique seems to have worked well in the present situation, a second method (wire scanner, giving digital readings directly) as foreseen for future runs will be of great value. Also, the possibility of steering the beam on the target and of measuring with more precision the total number of protons actually hitting the target will be indispensable in determining the confidence level of the experimental results.

While calculations on the stress levels expected on the basis of the current power deposition are in progress, it can be anticipated that the data obtained from future measurements will form a better basis to compare measured strain data with calculated stress levels and to provide valuable input for the nuclear and CFD-design of the targets and heat removal systems of future spallation neutron sources. Measurements at lower beam energies and more than two bunches per pulse seem, therefore, highly desirable.

Reference:

/1/ P. Cloth et al., HERMES A Monte Carlo Program System for Beam-Material Interaction Studies, Jül-2203 (May 1988)

Methods to Calculate Spallation Source Shields and Comparison with Experiments

H. Schaal, M. Isermann

The particles which cause the radiation problems of neutron spallation sources like ESS[1] are the deep penetrating neutrons with energies above 100MeV. They determine the dose rate at each point inside the shield because they produce there via cascade a neutron spectrum with energies down to thermal energies. That spectrum is far inside the shield more or less an equilibrium spectrum if the shielding material is not changed.

To calculate neutron spallation source shields different computational methods were developed:
One is the so called coupling procedure: In the vicinity of the neutron spallation target we use the Monte Carlo code HETC of our code system HERMES[2] to calculate the spatial and angular distribution of generated high energy neutrons. This distribution is handed over to the transport code ANISN[3], which calculates the attenuation of the high energy neutron flux with distance from the target. The neutron cross sections necessary for the ANISN calculations are data upgraded to 2.8 GeV neutron energy[4] for the shielding materials iron, concrete, and soil. The advantage of this calculation method is that it is not very time consuming and that in the target region the geometry can be described exactly and uncharged and charged particles can be treated.
Another method to combine different advantages of codes is to treat the geometry exactly, but to calculate the fast neutron flux and the induced dose rate via semiempirical equations using attenuation lengths and other parameters derived from transport calculations. The computer code with these features is named CASL[5]. The basic idea of CASL is that the high energy neutron flux is decreasing exponentially in the shield and that it determines the dose rate.

To check the computational methods with measurements we chose deep penetration experiments performed at different facilities and with different proton beam energies in the range from 230MeV up to 2700MeV:
- Loma Linda test area: For the proton beam energy of E_p=230MeV J. V. Siebers[6] described a series of neutron dose measurements for different detector positions inside thick concrete walls for the Loma Linda shielding study area at Fermilab. For the neutron dose determination we used the flux to dose conversion factors derived from ICRP51[7]. The comparison for detector positions perpendicular to the proton beam is given in fig. 1. Pure Monte Carlo results (denoted as HET-MORSE) are also given as far as reasonable statistics was achieved.

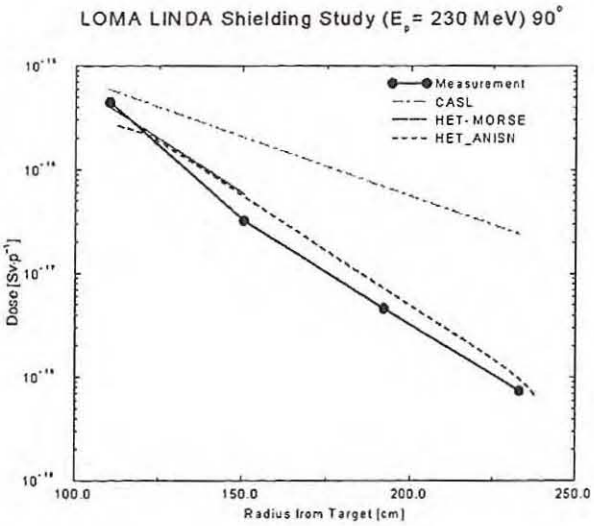

Fig.1: Dose rates of Loma Linda test shield at 90 degrees to proton beam direction

- ISIS: Y. Uwamino et al.[8] performed a shielding experiment at the target station of the ISIS facility (E_p=800MeV). The detector position is outside the shield of 291 cm cast iron and 96 cm concrete.
SATURNE: Bourgois et. al.[9] describe measurements in different directions behind a 3.6 m thick concrete wall at SATURNE in Saclay for E_p=2700MeV.

All comparisons show: The ANISN coupling method gives reasonable results and CASL always overestimates the experimentally determined neutron dose values.

References:
1. ESS - Vol. III, ISBN: 090 237 6659, (1996)
2. P. Cloth et al., HERMES, *KFA-Report Jül-2203*, (1988)
3. W. W. Engle Jr., ANISN, *K-1693,ORNL-TN*,(1967)
4. J. Moll, *KFA-Report Jül-2435, (1991)*
5. B. Wolfertz, *KFA-Report Jül-3197*, (1996)
6. J. V. Siebers, *PhD Thesis, The University of Wisconsin,* - Madison, (1990)
7. *ICRP Publication 51*, March 1987
8. Y. Uwamino et al., *Proceedings.. on Shielding Aspects,* Arlington, Texas, April 1994, pg. 185-194
9. L. Bourgois et al., *Health Physics*, Vol. 70, January 1996, pg. 36

Integration of the MC4 Monte Carlo Program into HERMES and further updates to MC4

G. Sterzenbach, R. D. Neef, D. Filges

MC4[1,2] is a Monte Carlo Program used to simulate the transport of high energetic hadrons in matter. The evolution of a hadronic cascade always implies the generation of leptons and of a large number of low energy particles. Both for leptons and for low energy hadrons there are no adequate models in MC4. The HERMES[3] program system provides a communication structure to submit particles falling out of the valid domain of a model to be picked up by other complementary programs. This communication structure has been implemented into MC4:
In the particle property table a general cutoff energy for each particle type has been added. A disposition tag indicates whether a particle should be killed or submitted reaching the energy cut. The default setting are shown in the table below.

Particle	Energy	Disposition
hadrons		
p, Λ, Σ	$< E_l$	kill
n	< 14.9 MeV	submit
π, K	$< E_l$	kill
others	any	kill
Leptons and γ		
γ	any	submit
$e^{\pm}$	any	submit
$\mu^{\pm}$	$> E_l$	transport without collisions
	$< E_l$	kill
$\tau^{\pm}$	any	kill
ν_e, ν_μ, ν_τ	any	kill
clusters from evaporation		
d, t, He^3, α	$> E_l$	transport without collisions
	$< E_l$	kill

In the table E_l means the lowest energy in the energy range table for a given particle in a given medium. These defaults can be overwritten using the ECUT command. A more specific control is provided by the use of detectors.
The detector concept of MC4 is adopted from HERMES. A detector is a structure which reacts to specific physical events in the life history of a particle. Whenever the detector is triggered, a contribution to a physical observable (like flux or energy deposition) is computed and added in the detector's data structure. Detector results are resolved by region, energy, angle, and time. The decision triggering the detector can also be used to request the submission of the triggering particle (and optionally remove it from the current Monte Carlo run). At the end of each event the observables gathered in the detector structures can be submitted too, to be collected and combined with the contributions detected in other Monte Carlo codes of the HERMES suite in the global analysis program STATIST.
Two new modules [4] have benn added to MC4:
The SPG module handles the generation of source particles. A set of commands is provided to describe the distribution of the various properties of source particles. Predefined distribution functions can be selected for source points, flight direction, energy or momentum and time from a set of commonly used shapes. Additionally measured (or other tabulated) distributions can be read in and even user written routines can be used in a well-defined interface structure. SPG can use the collision kernels of MC4 to simulate the effect of primary collisions. Since SPG is the most advanced source particle generator in HERMES, a special command has been introduced to directly record the particles produced on a HERMES submission file. Further development in source distributions can be concentrated in future in SPG exclusively.
The new ELAS[3,4] module is based on the work of T.W. Armstrong and B. Coleborn in HETC. It implements the elastic scattering of neutrons and protons on target nuclei in the energy range of 15 MeV up to 20 GeV. ELAS uses cross sections from the HILO and the NASA libraries which are interpolated in energy and target mass. The angular distribution follows a simple parameterization of the optical model. Kinematics is carried out in 4-momentum arithmetic.

[1]P.Cloth et. al. Proceedings of MC91 Workshop on detector and event simulation in high energy physics, Amsterdam, The Netherlands 1991
[2]P. Cloth et. al. Proceedings of MC93 International conference on Monte Carlo Simulation in High Energy and Nuclear Physics, Tallahassee, Florida USA 1993
[3]P. Cloth et. al. HERMES A Monte Carlo Program System for Beam-Material Interaction Studies, Report Jül 2203, (Mai 1988) ISSN 0366-0885
[4]G. Sterzenbach et. al. Proceedings of SARE4 International conference , Knoxville Tennesee USA 1998 (to be published)

10. ACCELERATOR COMPONENTS

A Superconducting Test Modul for the ESS

W. Bräutigam, O. Felden, S. Martin, G. Schug, E. Zaplatine

According to a proposed configuaration [1] at present state the accelerator complex of the European Spallation Neutron Source ESS will consist of two high intensity H^--ion sources (IS), their corresponding low energy beam transport systems (LEBT), the radio frequency quadrupol arrangements (RFQ) including the beam chopping in a parallel configuration (Fig.1). After acceleration up to 5 MeV by the RFQs the two separate beams with intensities of approximately 60 mA peak current each are combined to one beam of 350 MHz by a specially designed funneling system. The beam is accelerated to 70 MeV in a 350 MHz Drift Tube Linac (DTL) and then injected into a Coupled Cavity-Linac (CCL) operated at 700 MHz. The CCL accelerates the H^-- beam to the final energy of 1.334 GeV. It delivers almost the entire beam energy of 5 MW and will be by far the most expensive subsystem of the accelerator complex. Therefore it should be optimized very carefully in both design options, the normal and superconducting version.

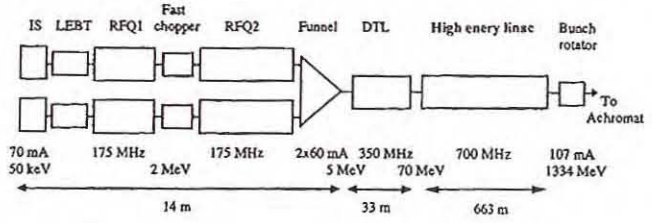

Fig. 1: The proposed ESS-LINAC scheme

The superconducting high energy linac proposed for the ESS [2] is expected to reduce the lenghth of this part from 663m (Fig. 1, normal conducting mode) to less than 300m. This is due to high field gradients of about 10MV/m. In addition to the reduced costs for the construction of buildings and shielding the very effective conversion of electrical power into RF accelerating-fields will result in a significant cost reduction for operation. - The superconducting CCL for the ESS [2] is formed by a total of 21 so called cryomodules; one cryomodul is composed of 4 cryo units; each cryo unit contains 2 cavities which results in a total number of 168 cavities each containing five cells. The length of one cell of a cavity is $\beta\lambda/2$ and therefore varies significantly along the proton linac. In order to reduce costs for development and construction the number of different cavity geometries have to be minimized. The cavity geometries have to be optimized with regard to important design parameters as there are ratio of the peak electric field to the effective accelerating field, ratio of maximum magnetic surface field to electric field, iris diameter, cell to cell coupling. Problems of multipacting, field emission etc. have to be investigated in detail. Additionally more technical aspects are also important as there are: microphonics, coarse and fine frequency tuning of the cavity and cryogenic problems. At present a test cavity is under construction which will be delivered in July 1999. It is specified for an operating frequency of 500 MHz for reasons of availability of RF power. Further specs are: $\beta = 0.75$, $E_{acc} > 5$ MV/m, $Q_0 = 2 \cdot 10^9$, T = 4.2K. Two RF ports are provided for the possibility of high power testing of RF couplers.

As the cavities in the ESS linac are operated in pulsed mode at a repetition rate of 50 Hz an elaborate control system is required for stabilizing amplitude and phase under all operating conditions, i.e. beam loading, Lorenz forces and microphonics have to be considered. It is planned to develop a control system on the basis of mainly digital techniques.

References:

[1] The ESS Technical Study Volume III, ESS-96-53-M

[2] Conceptual Design of the SC High Energy Linear H^--Accelerator for the ESS, ESS-96-60-L

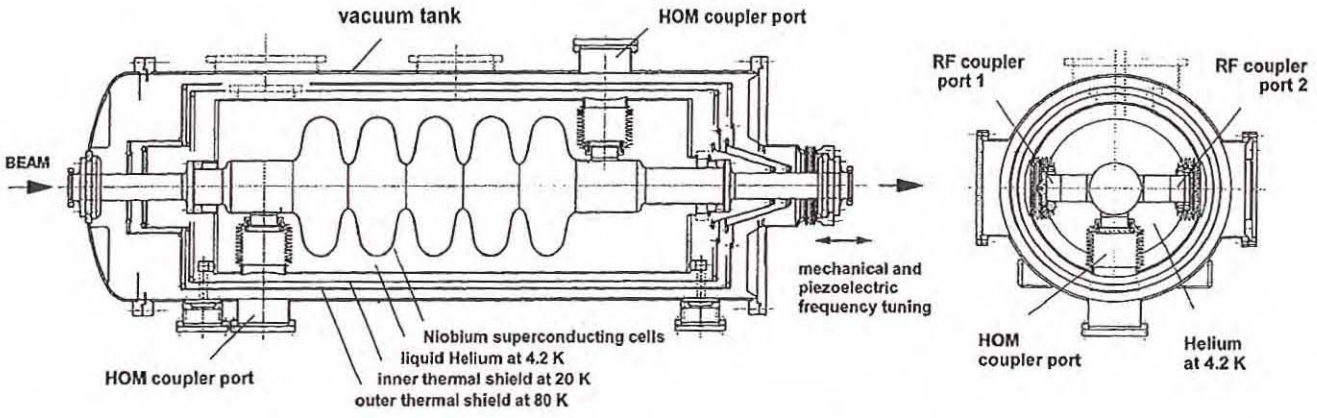

Fig. 2: Superconducting 5-cell test module built by ACCEL Instruments; specifications see text

Radiation Protection for ESS Prototype-Cavity Experiments

Gb.Schug, H. Singer, H.J. Probst, R. Stassen, P.v. Rossen, O. Felden, W. Bräutigam

ESS prototype cavity

The Nb-5-cell cavity [1] has been ordered for proton energies around 480 MeV (v/c=0,75). It will nominally work in π mode at E_0T = 4,4 MV/m at 4 K. The tests of the cavity at high electro-magnetic fields require shielding against Röntgen bremsstrahlung produced by field emission and acceleration of parasitic electrons [2-4]. The radiation shield must allow to operate the cavity at CW and the nominal gradient and intermittently at higher gradients.

Electron loading and bremsstrahlung

The standard textbooks on radiation shielding of particle accelerators do not include the estimation of Röntgen bremsstrahlung of accelerating cavities. This kind of radiation gets important only at VHF cavities and MV cell tensions as in our 500-MHz structure. Therefore, an approximation method was presented in a first internal memo [5]. Relevant results of that are included in the following.

Electrons will mainly be emitted near the irises of the cavity cells. Some typical electron trajectories beginning in the first cell are shown in Fig.1.

We have calculated the energy gains at some characteristic electron phases by direct integration. The electrons will maximally be accelerated up to 3 MeV at the nominal E_0T of 4,4 MV/m for protons (Tab.1). The total electron current of 10 µA was estimated via the low-field and high-field Q as guaranteed by ACCEL, Bensberg. This leads to a total bremsstrahlung power of 0,75 W [6]; the corresponding dose rates amount to 0,25 Sv/h at a distance of 1 m from the cavity surface along the cavity axis and 60 mSv/h perpendicular to the axis.

The rough formulae of [7] and [8] lead to forward-direction dose rates of 0,2 and 0,14 Sv/h assuming an 1-MV bremsstrahlung radiation of 10 µA electron current and 10 W electron power. The electron potential-gain distribution over the incremental electron current was assumed to reach the effective cell tension nearly homogeneously and to rapidly decrease at higher potential gains, similarly to [9]. The estimated angular photon-density distribution well matches that described in [10]. Both references treat 2/3 π structures at v/c =1, corresponding to an effective cell length of 2/3 half wavelengths, which is not too far from our value (3/4). The electromagnetic fields near the rounded irises resemble to those of our Nb cells. Tab.1 gives an overview of the photon-generating parameters.

Photon radiation and shielding design

The above estimated dose rate at the main radiation direction could virtually be generated by an equivalent radiation source. This results in a value between the activities of two standard nuclides of about 0,5 TBq Co-60 (20 Ci or ~20 mg; 1,17 and 1,33 MeV) and 3 TBq Cs-137 (100 Ci; 0,66 MeV of the daughter Ba-137-m). Hence, we can take advantage of the experimental curves in [11] and compare with calculated curves [12] and tables [13]. The point-source built-up factors [11,14,15] are therein included. The agreement was within a factor of 2 concerning the dose rates. A shielding vault will be built in the COSY Test Hall (former HHV). We avoid to categorise the hall as controlled area, as we guarantee the upper limit of 2,5 µS/h of the local dose rate outside the shielding.

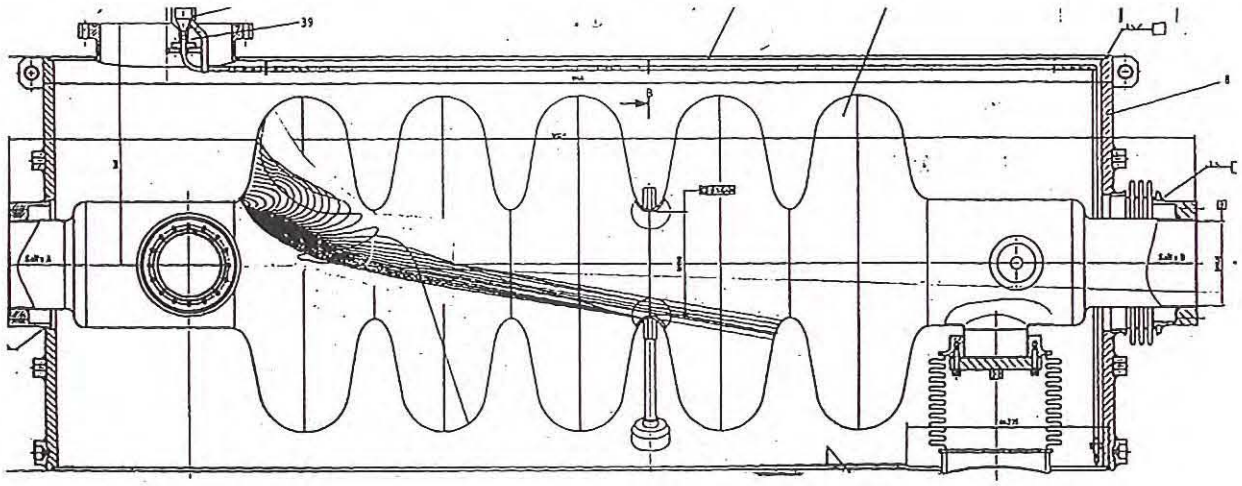

Fig. 1: Electron trajectories at π -mode field

This value had been accepted for COSY by the LAfA (Düsseldorf) and leads to maximum personal dose of 5 mSv per year (2000h) as required in §60 StrSchV (Betrieblicher Überwachungsbereich). The shielding design contains the following ray tracks

- direct axial radiation, attenuated by the shield
  ⇒ 1,10 m concrete equivalent, realised by 0,5m ordinary and 0,5 m barytes concrete;
- direct perpendicular radiation through the shield,
  ⇒ 0,9 m ordinary concrete;
- scattering (Compton, Albedo) through the maze,
  ⇒ necessity of at least 2 scattering steps and a closed door with a shielding of 3 mm Fe ;
- scattering (Compton, Albedo) by the hall walls after attenuation by the vault roof ,
  ⇒ 30 cm roof thickness (ordinary concrete);
- scattering by the air (photon sky shine) after attenuation by vault roof,
  ⇒ 20 cm roof thickness (ordinary concrete);
- direct radiation to high-floor bureau ("Olymp"), (20 m air path), attenuated by the roof,
  ⇒ 25 cm roof thickness (ordinary concrete);
- direct radiation to the cellar, attenuated by the concrete hall-floor (58 cm) at diagonal transmission and a stay factor of 10 % ,
  ⇒ the existent floor is sufficient as shield.

The inner of the vault will be a closed area. Its entrance door will be blocked at RF power-on state. Four radiation monitors near the vault surfaces will interrupt the RF power in case of a too high monitor signal for:

- axial radiation level ,
- radial level,
- roof radiation level
- entrance level.

The site in the hall and some estimated dose rates are shown in Fig.2.

cell number	5
cell length	0,225 m
field mode	π
nominal cell tension	1,24 MV
Nominal low-field Q_o (4,2 K)	2 E+9
Nominal high-field Q_o (4,2 K)	~3 E+9
Nominal proton energy	480 MeV
Relative proton velocity v/c	0,75
Nominal proton field E_oT	4,4 MV/m
Proton cell-transit-t. factor T	0,785
Electron cell-trans.-t.factor T1	0....0,875
Electron 5-cell-t.-t.factor T5	0....0,49
Electron energy by 1 cell	0...1,05 MeV
Electron energy by 5 cells	0 .... 3 MeV
Integr. el.current 0 ...1,05 MeV	10 µA
Integr. el.current 0,5 ...1,5MeV	8 µA
Integr. el.current 1,67 ...3 MeV	0,5 µA
Integr. el.current 2,22 ...3 MeV	0,05 µA
tot. Electron power in 5 cells	15 W
tot. Bremsstr.power in 5 cells	0,75 W
Equiv. dose rate on cav.surf.	≤4 Sv/h
Equiv. d. rate 1m from cav.surf.	≤ 0,25 Sv/h
Equiv. virt. Co-60 activity	0,5 TBq(~20Ci)
Equiv. virt. Cs-137 activity	3 TBq (~100Ci)
Concrete equivalent	0,9...1,2 m
Equiv. dose rate outside of vault	< 0,5 µSv/h
Neutr. dose rate outside of vault	< 3 pSv/h

Tab 1: Radiation-relevant parameters of the Nb-5-cell test cavity at 4K and CW operation

Here, the hall floor has a weight-carrying capability sufficient for the vault, because it is here provided with an basement floor.
This proposed shielding vault matches also the experience of similar Nb-cavity tests performed at Wuppertal [16].

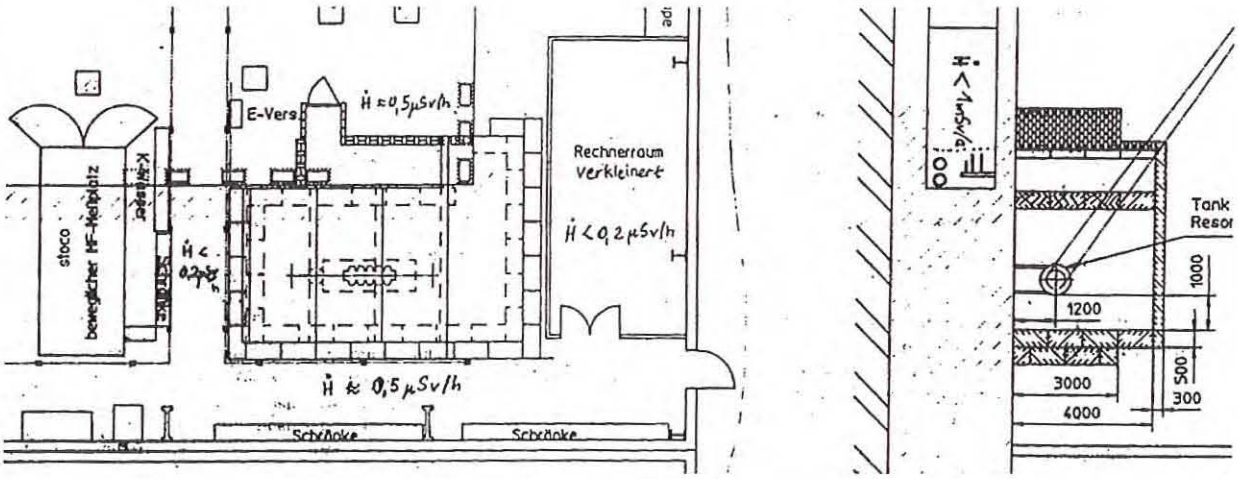

Fig.2: Site of the shielding vault and estimated dose rates

Neutron production and shielding

The photo-neutron production up to 3 MeV has not been treated in the standard accelerator shielding literature. The photon energies ≤ 3 MeV enable only 2 kinds of electro-disintegration processes, namely the (γ, n) reactions at Be-9 and D having thresholds of 1,67 and 2,23 MeV (stable isotopes of other elements have values > 4,9 MeV, the thresholds of (γ, 2n) and (e, ne') reactions are still higher, the lowest proton and quasi-deuteron thresholds occur at Li-6(γ, p) and (γ, np) at 4,6 and 3,7 MeV) [17,18,19]. But the additional neutron doses can be neglected because of the low Be and D contents of concrete (E-6) [26-29] and the low reaction cross sections (around 10 and 1 mbarn) [18-23] and the given 1 m shield [24,25].
Neutron dose and activation measurements at 8 and 6 MeV electron accelerators [30,31] confirm that statement.

Higher gradients

The electron current and the X-ray level will drastically increase at higher accelerating field strengths. An estimation for 7 MV/m leads to a 50 times higher radiation level. The above safety concept will also allow future tests at larger fields, at a duty factors near 10 % during the burn-in phase.

Acknowledgements

We are greatly indebted to thank our IKP colleagues H.Beuscher, D.Filges, D.Prasuhn, H.Schaal, Th.Sefzick and R.Wagner, for encouraging discussions and indicating helpful literature.

References

[1] A superconducting cavity for the ESS, IKP Ann. Rep. 1997, Jül-3505, FZ Jülich, Feb. 1998, p. 223

[2] W. Weingarten, Electron loading, in Proc. 2nd Wks. RF Supercond, CERN, 1984

[3] B. Bonin, Field emission in RF cavities, in CAS Hamburg 1995, CERN 96-03

[4] Bloess,D., Cavallari,G., Chiaveri,E., Hilleret,N., Tückmantel,J., Weingarten,W., Recent results from superconducting 350 MHz single cell cavities, CERN/EF 85-2 [20.May 1985]

[5] Gb. Schug (with the aid of H.J. Probst), Röntgenpegel Nb-5-Zeller, IKP internal memo, FZJ, Jülich, 6.2.98, revised at 11.9.98

[6] H.v.Seggern, Bremsstrahlungsausbeute bei vollständiger Abbremsung von Elektronen, in Kohlrausch, Praktische Physik, Band 3

[7] App. C, Rule of thumb No. 5, p. 319 of W.P. Swanson, Radiological Safety Aspects of the Operation of Electron Linear Accelerators, IAEA Techn. Rep. Ser. No. 188. Wien 1979

[8] Eq. (3.7), p. 83 of A.H. Sullivan, A Guide to Radi-ation and Radioactivity Levels near High-Energy Particle Accelerators, Nucl. Technol. Publ., Ashford, Kent

[9] Matsumoto,H., Fukushima,Y., Horiba,S., Horikoshi.G., Kimura,Y., Mizuno,H., Saito,Y., Sato,I., Shidara.T., Takata,K., Takeda,S., Terabayashi,N., Yamazaki..Y., Yoshioka,M. RF breakdown studies on S-band disk loaded structure, PAC [Wash., Mar.1987], IEEE Catalog No. 87CH2387-9, 1654...6

[10] Wang,J.W., Nguyen-Tuong,V., Loew,G.A., RF breakdown studies in a SLAC disk-loaded structure, Lin. Acc. Conf. [SLAC, 2-6.Jun.1986], SLAC-303 [Sep.86], 461...4

[11] P.F. Sauermann, K. Schneider, W. Voß, Experimentelle Untersuchungen zur Ermittlung von Aufbaufaktoren für Abschirmwände aus Beton, Interner Bericht 127, ZAS, KFA Jülich, 1969

[12] R. Dorner, H.-G. Vogt, Schwächung der Photonenstrahlen von Radionukliden, Zentraleinr.f.Strlsch.,Hannover 1982, Teil 4, Abschirmungsmaterial Barytbeton
Teil 5, Abschirmungsmaterial Normalbeton.
similarly: DIN 6844 (Nuklearmed. Betriebe)
Teil. 3 : Strahlenschutzberechnungen, Sep.1989
and DIN 25425 (Radionuklidlaboratorien)
Teil. 2 (Grundlagen für die Erstellung betriebs-interner Strahlenschutzregeln) BBl. 1: Hinweise zur Abschirmung von Photonen- und Betastrahlung, Juni 1989

[13] P.F.Sauermann, Strahlenschutz durch Abschirmung, Reihe Atomkernenergie Bd.11, Thiemig-Verl., München 1976
similarly: P.F.Sauermann, Interner Bericht 130, ZAS, KFA Jülich, 1970

[14] C.H.Eisenhauer, G.L.Simmons, Point isotropic builtup factors in concrete, N.S.E. 56 [1975], 263...70

[15] K. Takeuchi, S. Tanaka, Point isotropic builtup factors of gamma rays, including bremsstrahlung and annihilation radiation for water, concrete, iron and lead, N.S.E. 90 [1985], 158...64

[16] Prof. W.Hoffmann, U.Wuppertal, H.-P.Vogel, G.Peiniger, ACCEL, priv.comm.

[17] Chap. 2 of K.Wirtz, K.H.Beckurtz, Elementare Neutronenphysik, Springer 1958

[18] H.Goldstein, Photoneutrons, Chapt. 8.1.4 of E.P.Blizard, L.S.Abbott, Reactor Handbook, Vol. III, Pt. B, Shielding, Interscience Publ.,1962

[19] B.Bülow, B.Forkman, Photonuclear cross-sections in Hbk. on Nuclear Activation Cross-Sections, IAEA Techn. Rep. Ser. No. 156, Wien 1974

[20] C.P.Haigh, An analysis for deuterium based on the photoneutron effect, Nature 172 [Aug.1953], 359

[21] R.Nathans, J.Halpern, Excitation function for the photo-disintegration of Be, Phys. Rev. 92,4 [Nov.1953], 940...1

[22] R.Edge, The (γ, n) reaction in Be-9 at intermediate energies, Nucl. Phys. 2 [1956,1957], 485..495

[23] D.K.Trubey, Photoneutrons, Chapt. 2.3.2.3 and E.A.Burril, Shielding of electron accelerators, Chapt. 10.6 of R.G.Jaeger Engineering Compendium on Radiation Shielding, Vol. I [1968], Vol. II [1975], Vol. III [1970], Springer-Verl.

[24] R.W.Roussin, F.A.R.Schmidt, Adjoint S_n calculations of coupled neutron and gamma-ray transport through concrete slabs, N.E.D. 15 [1971], 319..343

[25] Abschirmung von Neutronen, in P.F.Sauermann, Abschirmpraxis, Interner Bericht, KFA, 1985

[26] H.J.Rösler, H.Lange, Geochem. Tabellen, VEB Grundstoffindustrie, Leipzig

[27] A.F.Holleman, E.Wiberg, N.Wiberg, Lehrbuch der anorganischen Chemie, DeGruyter, Berlin 1996

[28] G.V.Samsonov, Hbk. of the Physicochemical Properties of the Elements, IFI/Plenum, 1968

[29] C.J.Smithells, E.A.Brandes, Metals Reference Book, Butterworths Ed.

[30] D.Fehrentz, G.M.Hassib, B.Spyropoulos, Neutronen-verschmutzung in Röntgenstrahlen-bündeln von Elektronen-beschleunigern, Strahlenther. 159,11 [1983] 703..12

[31] R.G.Lane, B.R.Paliwal, D.D.Tolpert, Leakage radiation characteristics of an 18 MeV clinical linear accelerator, Health Phys. 35 [Sept.1978] 485..9

Design Considerations for a Superconducting Linac as an Option for the ESS

W. Bräutigam, S. Martin, G. Schug, E. Zaplatine

Motivation

An approach for a superconducting high-current proton linac for the ESS has been discussed as an option in the "Proposal for a Next Generation Neutron Source for Europe- the European Spallation Source (ESS)"[1,2]. The following work studies the technical and economic conditions for a superconducting linac at the high-energy end of the proposed accelerator system. The use of superconducting elliptical cavities for the acceleration of high-energetic particles $\beta = v/c \approx 1$ is certainly state of the art. This is documented by many activities (TJNAF, TESLA, LEP, LHC, and KEK). For low energy particles (β<<1) quarter wave type cavities [4] and spoke-type cavities [5] have been discussed. The main motivation for this study is the expectation of significant cost reduction in terms of operational and possibly investment cost.

Basic Parameters

The basic parameters of the system are given in tables 1,2,3.

Maximum energy	1334	MeV
maximum β=v/c	0.91	
injection energy	70	MeV
injection β	0.4	
average current	3.75	mA
peak current	104	mA
repetition rate	50	Hz
pulse length	1.2	ms
duty factor	6	%

Table 1: Basic data of the superconducting ESS linac

revolution frequency accumulator	1.67	MHz
revolution time accumulator	0.6	μs
chopping beam-on time	360	ns
chopping beam-off time	240	ns
intensity		
particles per pulse	$4.7\ 10^{14}$	
particles per RF bunch	$2\ 10^{9}$	

Table 2: Pulse micro structure

Energy gain per cavity

The energy gain in cavity is usually given by $\Delta W = eE_0T \cdot l \cdot \cos(\phi)$. Here, T is the transit time-factor and l the length of the cavity. $E_0T = E_{acc}$ is the accelerating field and ϕ is the phase distance of the synchronous particle to the crest at the centre of the cavity.

The matched length of one cavity cell is given by $\Lambda = \beta_\Lambda \cdot \lambda/2$ where $\beta_\Lambda = \beta = v/c$ the velocity factor of the synchronous particle. The cell transit-time factor is given by

$$T_\Lambda = \begin{cases} \dfrac{\pi}{2 \cdot \left(1 + \dfrac{2\Lambda}{\beta \cdot \lambda}\right)} & \text{for } \beta \approx \beta_\Lambda (\leq 3\%) \\ \cos\left(\pi \cdot \dfrac{\Lambda}{\beta \cdot \lambda}\right) \cdot \dfrac{1}{1 - \left(\dfrac{2\Lambda}{\beta \cdot \lambda}\right)^2} & \beta \neq \beta_\Lambda \end{cases}$$

These expressions neglect the changes of beam velocities within a cell. Therefore, the lower formula is in accordance with the theory of Wangler [3].We have set up an approximate relation in order to give the validity range of the phase ϕ. The relative T_Λ error holds less than 0.5% (1.5%) for $|\phi| < 76°\ (85°)$. This relation is valid up to the maximally occurring values of velocity mismatch (0.05) and the difference of the beam velocity factors within a cell (0.02).

frequency	700	MHz
RF wave length	0.428	m
data for a β=0.75 cavity		
length of a cell Λ	0.182	m
length of a 5-cell cavity	0.91	m
maximum surface electric field E_{peak}	25	MV/m
accelerating field E_{acc}	10	MeV/m
transit time factor per cell T_Λ	0.79	
maximum tension amplitude per cell	2	MV
maximum phase for acceleration	-20	degree

Table 3: Radiofrequency system

The energy gain of an N-cell cavity results as addition of gains of N single cells. Thereby, particular synchrotron phases of each cell have successively been calculated. This numerical method makes the base of future longitudinal particle tracking of the high-energy part of the linac.

The β-dependence of the energy gain of an N-cell cavity can be manifested using Wangler's formalism [3]. Here, the beam velocity along the N cells is set to be constant. The cavity transit-time factor T can then be factorised: $T = T_\Lambda \cdot T_S$.Where the synchronism factor is given by

$$T_S\left(N,\frac{\beta}{\beta_\Lambda}\right)=\begin{cases}(-1)^{\frac{N-1}{2}}\cdot\dfrac{\cos\left(\dfrac{N\pi\beta_\Lambda}{2\beta}\right)}{N\cdot\cos\left(\dfrac{\pi\beta_\Lambda}{2\beta}\right)}, & \text{N - odd}\\[2ex](-1)^{\frac{N}{2}+1}\cdot\dfrac{\sin\left(\dfrac{N\pi\beta_\Lambda}{2\beta}\right)}{N\cdot\cos\left(\dfrac{\pi\beta_\Lambda}{2\beta}\right)}, & \text{N - even}\end{cases}$$

where β is the centre velocity factor and β_Λ is the cavity geometric velocity factor. The number of cells per cavity has been chosen to be N=5.

The transit-time factor for such a 5-cell cavity is shown in the figure 1.

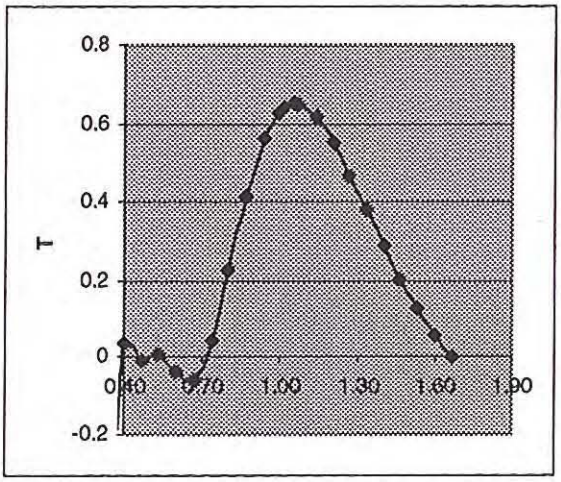

Figure 1: transit-time factor for a 5-cell cavity vs. the velocity ratio β/β_Λ

The maximum value occurs at the design velocity factor β_D, which is a little larger than the geometric velocity β_Λ.

β-grouping

The cell number N=5 have been chosen for ESS because of the smaller influence of the end cells compared to N=4. We have slightly rearranged the high energy linac part by fixing the maximal surface electric field to 25 MV/m.

The number of groups of identical cavities to be built should be as small as possible for an economic manufacturing. On the other hand, a criterion has been used to tolerate a maximum decrease of the transit-time factor of 10% at the ends of the groups of identical cavities. Hence, 5 different groups of identical cavities will be necessary to accelerate the beam in the linac from 70 MeV up to 1334 MeV. The geometric velocities for the 5 groups are β_Λ=0.353, 0.431, 0.526, 0.641, and 0.782.

We will create two additional cavity groups at the upper end because most of the energy will be gained at β=0.75 (480 MeV). Figure 2 shows as an example the energy gain per cell for a group of identical cavities.

The single-cell tracking method will be completed to include also power coupler and transverse beam dynamics aspects.

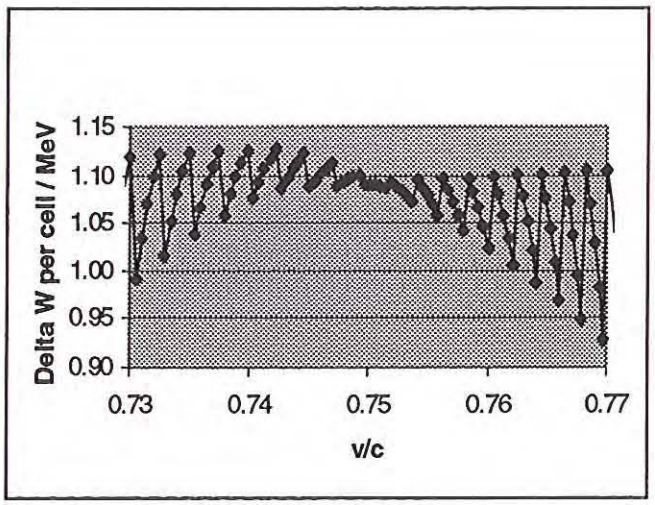

Figure 2: Energy gain per cell β_Λ=0.75 (crp. 480 MeV). The maximum phase ϕ is set to -20°.

REFERENCES

[1] J.Kjems, A.D.Taylor, J.L.Finney, H.Lengeler, U.Steigenberger (ed.), "ESS - A Next Generation Neutron Source for Europe", Vol III, "The ESS Technical Study", Copyright: ESS Council, March 1997

[2] B.Aminov, A.Gamp, E.Haebel, H.Heinrichs, H.Piel, J.Pouryamout, Th.Schilcher, D.L.Schrage, G.Schulz, S.Simrock, C.H.Rhode, and R.Röth, "Conceptual design of the Superconducting High Energy Linear H- Accelerator for the Future European Spallation Source (ESS)", ESS 96-60-L, December 1996

[3] T.P. Wangler, "Principles of RF Linear Accelerators", Wiley series in beam physics and accelerator technology, 1998

[4] G. Bisoffi, "Operational experience with sc low beta cavities",Inv. Talk at THE EIGHT WORKSHOP ON RF SUPERCONDUCTIVITY; Abano Terme, Italy, Oct. 1997

[5] K. Shepard, "Accelerator Development for a Radioactive Beam Facility Based on ATLAS",Inv. Talk at THE EIGHT WORKSHOP ON RF SUPERCONDUCTIVITY; Abano Terme, Italy, Oct. 1997

Accelerator Components for the European Spallation Source ESS

W. Bräutigam, J. Dietrich, O. Felden, R. Maier, S. Martin, A. Schnase, G. Schug, R. Stassen, E. Zaplatine

In 1993 a multinational study group, partitionally supported by the CEC, started to evaluate the feasibility for a next generation pulsed European Spallation Neutron Source (ESS). This conceptual study was completed in 1996 and a Reference Design was published [1] comprising a system of linear accelerators and storage rings, combined with very ambitious target technology. The beam is specified to have an average power of 5 MW at a repetition rate of 50 Hz and a pulse length of about 1μs. The entire energy gain is achieved by a combination of linear accelerators accelerating negative charged hydrogen ions up to a kinetic energy of 1.334 GeV.

Beside establishing a site independent cost estimation the Reference Design identified areas of research and development work, still necessary before such a facility can be realised. In an addendum to the final report [2] a superconducting option for the high energy part of the ESS LINAC was discussed.

The main motivation for analysing a superconducting option of the ESS linac in addition to the normal conducting reference design is the expectation of a significant cost reduction. This assumption is based on the reduced length of the linac, its reduced investment cost for the RF system and the savings in the costs for operation. The savings overcompensate the additional costs for refrigeration and the more expensive superconducting cavities.

Superconducting accelerator technology can announce great achievements in the last years. It has been applied successfully at various high intensity electron accelerators (TJNAF, CERN) or is under development in a number of laboratories (DESY, JAERI). So far there is no experience with superconducting accelerating structures at high intensity proton accelerators but several projects are under development (APT in USA, projects in Japan). R&D work is necessary to transfer the experiences made at electron accelerators into the world of proton LINACs.

It is planned to contribute to the application of superconducting technology at proton accelerators in theoretical and experimental way. At present a test cavity is under construction at ACCEL Instruments GmbH, Bensberg [3]. It will be delivered in July 1999 and then be the main subject of the experimental program.

An appropriate working group had to be established first for the ESS related accelerator R&D program. At the end of 1998 a total amount of about 7 staff-years is available for the program. Beside a number of members of the COSY department the group is supported by other institutes of FZJ (2 scientists) and completed by 2 scientists on guest- and HGF-positions respectively. Important tasks of this group at present time is the definition of the experimental programme and the preparation of the site for the superconducting test module. This includes calculation and design of the x-ray shielding for the system, mapping and compensation or shielding of magnetic fields (only a fraction of the earth field can be accepted), provision for the necessary RF power, installations for LHe inclusive the feedback of He gas to the liquefying station. This tasks are mostly on the way, significantly supported by the infrastructure of FZJ.

On the basis of original drawings some calculations were done in collaboration with an external expert to evaluate the dynamic characteristics (mechanical resonances) of the 5-cell test cavity. Vibrations significantly influence the RF resonance of superconducting systems, which are characterised by Q factors > 10^{10}.

In order to verify (and possibly optimise) the accelerator configuration of the Reference Design, especially the grouping of identical modules in the high energy part of the LINAC, software tools were developed or modified. A code segment, which supports the parameter-controlled design layout of multicell charge coupled structures was developed according to our specifications by an external contractor and is on-hand in a first version. Software packages like MAFIA, SUPERFISH, OPERA-3D inclusive TOSCA and SOPRANO are commonly accepted at many accelerator laboratories. Members of the group could effectively familiarise with this codes and achieved already reasonable results.

In order to optimise the total LINAC system, it is mandatory to analyse and possibly optimise also the low energy section. Recently novel so called IH- and CH-structures were proposed and partially already realised by scientists of GSI Darmstadt [4]. It has to be investigated, if these structures are applicable with advantage for the ESS. In addition we started to investigate also the characteristics of spoke type cavities; a 5-cell normal conducting test module of this type is ready for test.

The majority of the scientists and technicians in the ESS group had no experience with linear and i.e. with SC accelerator components. It is evident that contacts to institutes, universities etc. could significantly support the practice in a new field. So we are happy to have collaborations with the Universities of Frankfurt and Wuppertal, with GSI Darmstadt, DESY Hamburg, and internationally with RAL (England), LANSCE Los Alamos (USA), Saclay (France), Aarhus (Denmark), JAERI and KEK (both Japan) and companies like ACCEL Instruments, Bensberg, and CRYOELECTRA, Wuppertal.

References:

[1] The ESS Technical Study Volume III, ESS-96-53-M

[2] Conceptual Design of the SC High Energy Linear H^- Accelerator for the ESS, ESS-96-60-L

[3] A SC Test Module for the ESS, this Annual Report

[4] U. Ratzinger: Effizente HF-Linearbeschleuniger für leichte und schwere Ionen
Habilitationsschrift, GSI Darmstadt, Juli 1998

Design Study for SC Proton Linac Accelerating Cavities

E. Zaplatine, W. Braeutigam, S. Martin

Abstract

A 70-1334 MeV superconducting proton linac is under consideration as a possible version for the high energy part of European Spallation Source accelerator. In this paper we describe two alternative options of an accelerating structure (500 MHz) for this machine. First is the 5-cell elliptical cavities designed for the β=0.5-0.92. The second type is a spoke cavity extended to multigap design (β=0.3-0.5). A full scale SC elliptical cavity prototype is under construction in collaboration with ACCEL.

Introduction

In some recently launched projects[1]-[3] for high intensity proton beam acceleration the possibility to use superconducting cavities is under investigation. For this purpose a well established "elliptical" (Fig. 1) β=1 cavity shape is adapted for much slower proton beams with β range from 0.45 to 0.95. At the same time from mechanical calculations such type cavity use for β lower than 0.5 is accomplished with a need of serious mechanical structure stiffeners. As a possible alternative a so called spoke cavity[4] is under consideration. During past year, at Forschungszentrum Juelich, we have been looking at the possibility to use SC cavities in European Spallation Source project (ESS)[5].

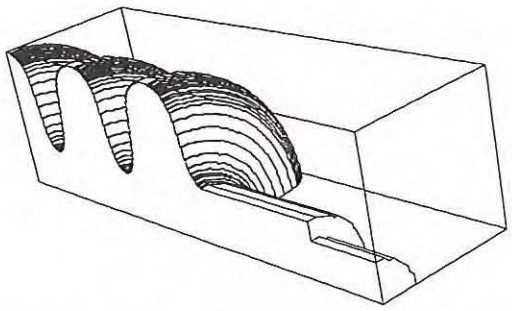

Figure 1: Elliptical Cavity Geometry (1/8 part is shown)

SC Cavity Study

Usually, an elliptical cavity design is a compromize between various geometric parameters which should define a most optimal cavity shape in terms of an accelerator purpose. Within a SC proton linac design there is a need of grouping of cavities with different $\beta = v/c$ values. It means that the process of cavity designs for SC linac becomes time consuming. Here we want to present some basics which can help to obtain rather fast the main cavity parameters and which we used for ESS project. A further cavity optimization can be made afterwards but we believe that an improvement will be within 10%.

The main advantage of any SC cavity is a possibility of high accelerating electric field maintaince (E_{acc}). There are two characteristics which limit in principle an acheivable value of E_{acc}. They are the peak surface electric field (E_{pk}) and the peak surface magnetic field (H_{pk}). H_{pk} is important because a superconductor will quench above the critical magnetic field. Thus H_{pk} may not exceed this level. E_{pk} is important because of the danger of field emission in high electric field regions. All these mean that to maximize the accelerating field first of all it is therefore important during a cavity design to minimze the ratios of peak fields to the accelerating field. There are some more figures of merit to compare different designs such as power dissipation P_c, a quality factor Q and shunt impedance R_{sh}. But these parameters are not so crucial to the cavity design and may be varied in some limits without any sufficient harm for a system in whole. Here we should mention also such figure like the cavity apperture (bore radius in elliptical cavity design R_i). This characteristic is obtained in conjuction with beam dynamic calculations and more or less is defined as a first. The choice of R_i limits in some extend E_{pk} and H_{pk}, defines cell-to-cell coupling in multicell cavity, influences the shunt impedance value and field flatness. That's why it should be changed if the first choice was wrong.

An elliptical cavity design should start with R_i definition. Now, as to concern the cavity shape design itself there are some geometric characteristics (dome radius R_{top}, slope angle α, ellipse axis) which should be defined for a most optimal cavity shape in terms of mentioned above RF parameters. And as a next step of design we suggest E_{pk}/E_{acc} and H_{pk}/E_{acc} investigation on slope angle α value. The reason of this is that an optimal value of α could be define unique if to consider dependences of E_{pk}/E_{acc} (a cavity frequency 500 MHz) (Fig. 2). Here as a parameter we use R_{top}. On Fig. 3 the similar set of H_{pk}/E_{acc} curves are shown. And already from these two grafs one may make a decision about a cavity shape. These calculations have been done by means of 2D cavity simulation code SUPERFISH[6]. The ellips parameters have been defined by program automatically to satisfy the fixed cell length $\beta\lambda/2$.

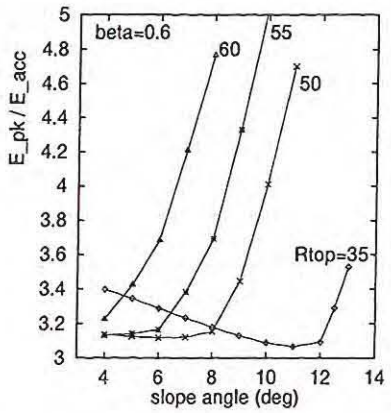

Figure 2: Maximum Electric Surface Field to Accelerating Field Ratio vs. Cavity Slope Angle α (R_i=65 mm)

The results of our calculations are presented on Fig. 4 along with results from other calculations[1]-[3]. These results reffer to the projects with quite different basic purposes and parameters (pulsed and cw, different final energies and RF frequencies). but these differences only emphasize the tendency of dependence on β.

Table 1 lists the main parameters of elliptical cavity de-

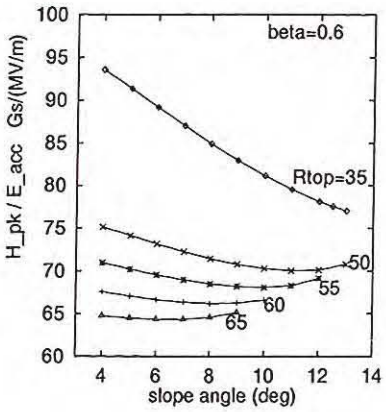

Figure 3: Maximum Magnetic Surface Field to Accelerating Field Ratio vs. Cavity Slope Angle α (R_i=65 mm)

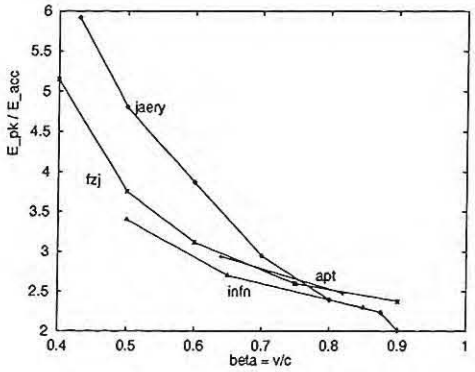

Figure 4: Maximum Electric Surface Field to Accelerating Field Ratio

signs for different β values.

Table 1: Some Parameters to Compare Elliptical Cavities with Different $\beta = v/c$

β	0.4	0.5	0.6	0.75	0.9
aperture R_i (cm)	6.5	6.5	6.5	6.5	6.5
dome R_{top} (cm)	2.5	3.5	5.5	6.5	9.5
slope α (deg)	6	7.5	6	10	10
cell-length (cm)	12	15	18	22.5	27
transit time factor	0.782	0.778	0.773	0.769	0.761
E_{pk}/E_{acc}	5.15	3.79	3.17	2.60	2.38
H_{pk}/E_{acc} (Gs/(MV/m))	115.8	87.5	69.6	62.1	52.5
$R_s * Q_0$ (Ohm)	102.8	132.1	171.2	200.1	245.3

As an alternative to the elliptical cavity for small β's a spoke cavity is under consideration (Fig. 5). This one cell cavity has been built and tested at high fields at Argonne National Lab. The advantages of such type cavity before elliptical ones are smaller dimensions and higher mechanical ridgidity. Table 2 lists some parameters for multycell spoke cavities. An accelerating π-mode electrical field is similar to the elliptical cavity accelerating mode but magnetic peak field on surface is defined by spoke diameter.

A multigap spoke cavity has a "cell-to-cell" magnetic coupling rather than an elliptical cavity with electric coupling. It means that a first frequency of a spoke cavity fundamental band is π accelerating mode which should simplify HOM damping.

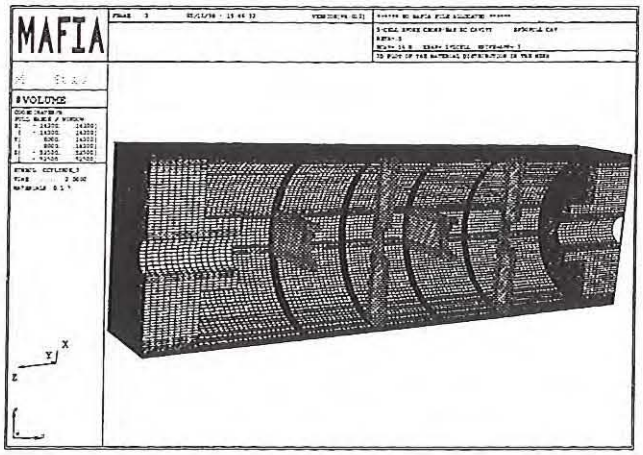

Figure 5: Spoke Cross Bar Cavity Geometry (1/2 part is shown)

Table 2: Some Parameters to Compare Spoke Cavities with Different $\beta = v/c$

β	0.3	0.5
cell-length (cm)	9	15
acc. gap (cm)	4.5	10
transit time factor	0.805	0.771
E_{pk}/E_{acc}	4.2	4.06
$R_s * Q_0$ (Ohm)	67.8	103.0

References

1. N. Ito et al., "Development of a Superconducting Cavity for the High Intensity Proton LINAC in JAERI",
2. F. L. Krawczyk et al., "Superconducting Cavities for the APT Accelerator",
3. D. Barni et al. "SC Beta Graded Cavity Design for a Proposed 350 MHz LINAC for Waste Transmutation and Energy Production", EPAC'98, Stockholm, p.1870 (1998).
4. J. R. Delayen et al., "Design and Test of a Superconducting Structure for High-Velocity Ions", LINAC'92, Ottawa, 1992.
5. W. Braeutigam et al., this proceeding.
6. J. H. Billen and L. M. Young, "POISSON/SUPERFISH on PC Compatibles", Proceedings of the 1993 Particle Acc. Conf., Vol. 2, p. 790..
7. M. Bartsch et al. "Solution of Maxwell's Equations", Computer Physics Comm., 72, 22-39 (1992).

V. Technical Developments

11. DATA ACQUISITION, ELECTRONICS, SEMICONDUCTOR DETECTORS, TARGETS

11. DATA ACQUISITION, ELECTRONICS, SEMICONDUCTOR DETECTORS, TARGETS

A Data Acquisition System for Small Experiments

T. Sefzick, M. Drochner*, P. Wüstner*, K. Zwoll*

The computer and data acquisition market is changing rapidly: many old PCs are replaced by faster systems and MS-DOS is out of fashion. Consequently, there is the need to replace the old PC-based CAMAC data acquisition systems used for small experiments and detector tests. Developing a completely new program is beyond any discussion, standard components should be used instead to minimize man power and programming effort. A new readout and visualization system is presented, combining i) the data acquisition concept developed by ZEL [1], ii) ported to Linux, and iii) the well-known CERN software package PAW [2].

the interface is based on the visual representation of a CAMAC crate, see Fig. 1. When starting the program the computer hardware is scanned for installed CAMAC interfaces, one can only start a server for existing hardware. After definition of the used converter modules and activation of the ADC or TDC channels, the trigger type (e.g. LAM trigger or triggering via a synchronisation module) can be selected. Data output can be chosen to be to file, tape, or Ntuple.

If Ntuple data output is chosen a PAW window is started automatically with access to a shared memory

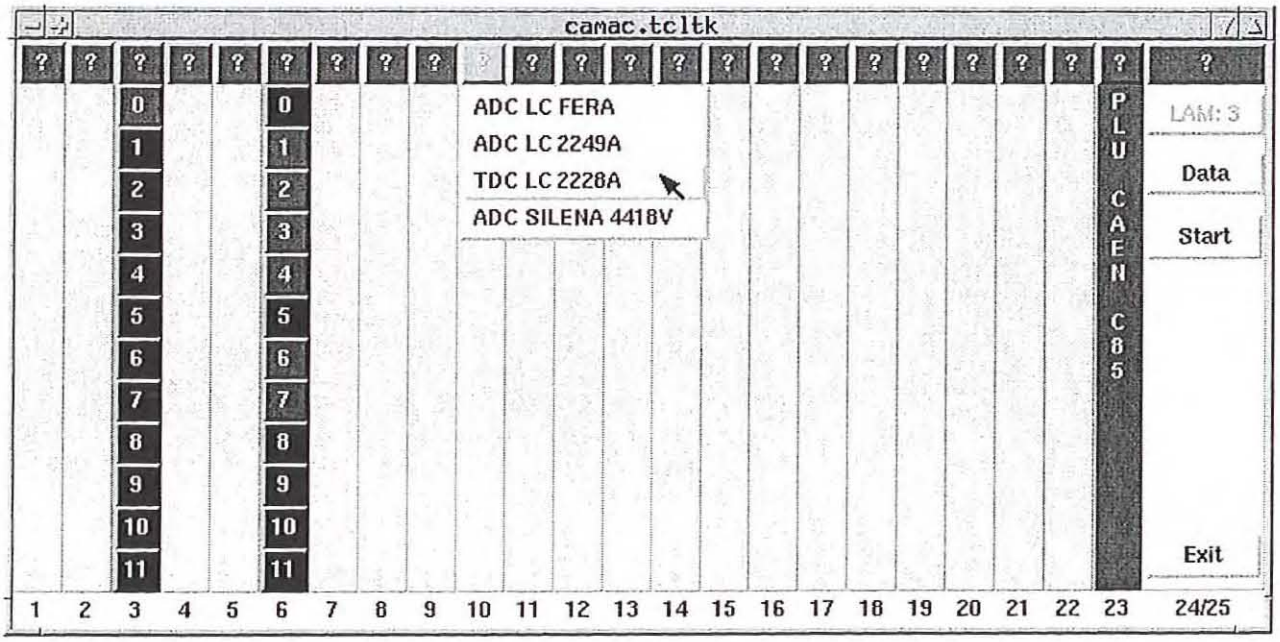

Figure 1: Screenshot of the TclTk window used for data acquisition setup and control

A typical simple data-acquisition system consists of a few CAMAC ADC and/or TDC modules, a CAMAC crate controller, and a PC. After porting the server part of the ZEL software to Linux additional drivers for various CAMAC controllers were re-written resp. adapted. The driver for the DSPT CC-SCSI/A CAMAC controller (internally a Jorway73a) consists essentially of the sjy73a package from Fermilab. The software for the DSPT 6001/6002 CAMAC (for ISA bus) controller was already existing. Only for the PCI-CAMAC controller (developed by ZEL) software porting from NetBSD to Linux needed to be done.

For data handling the EMS [3] data format is used, the event clusters are written to disk or tape directly, or are converted into Ntuples used for graphical representation and simple analysis under PAW. A circulating buffer assures that only the newest Ntuples are available for histogram filling.

The graphical user interface is written in TclTk using the normal window shell (wish) extended by EMS commands. The experiment setup is very easy because

section containing the continuously updated events. The user is free to fill histograms or scatterplots and apply cuts to the data for simple analysis.

After stopping the data acquisition, PAW windows are closed and the interface server is terminated, this is done to assure a well defined situation for the next acquisition.

The presented system is a good example for the simplicity and scalability of the redesigned ZEL data acquisition system [4] which will be installed at existing COSY experiments in a larger scale.

References

[1] M.Drochner, PHD thesis, Jül-3218, Jülich 1996
[2] CERN program library
[3] K.Zwoll et al., IEEE Trans.Nucl.Sci. 41(1), 37-44, 1994
[4] P.Wüstner, PHD thesis, Univ. Bochum 1998

* ZEL, Forschungszentrum Jülich

COSY Experiment Data Acquisition and Processing

K.H. Watzlawik, M. Karnadi

In collaboration with institutes inside the KFA and other research centers the activities due to the enforcement of COSY experiments have been proceeded /1,2/. The main topics in this intention are the cooperation with physicists in the realization of experiments at COSY as well as the providing of the data processing processing infrastructure.

At experiments, the buildup of data acquisition will be supported in the installation of various systems. These are in particular systems based on Motorola CAMAC, FASTBUS and VME CPUs running the OS9 operating system and such as based on Intel PCs using the NetBSD operating system. Therefor the installation and handling of Instrumentation Systems and different CAMAC and FASTBUS modules including the frontend CPUs, VICbus interfacing and networking will be provided.
At COSY11 experiment, the frontend hardware was reconfigured. The FASTBUS system was splitted into two crates each represented by one Instrumentation System. Additionally the readout of the DRAMS system was distributed at three DRAMS receiver modules. Therefore the dead-time of the data acquisition is reduced. The control system "Wendy" /3/ has been adjusted accordingly.
At the GEM experiment, the frontend CPUs were implemented in the OS9 cluster at the Unix server.
For the ANKE experiment, the data acquisition was buildup. To speedup the event data transfer and other network traffic a 10/100Mbps Ethernet network, consisting of two 3COM SuperStack II Switches connected by fiber cabels, has been installed. To one switch, located at the experiment, frontend PCs are connected by twisted pair cables. The other one is placed in the COSY Control room and supports the eventbuilder, experiment workstation and Linux PCs. Frontend PCs works in the 10Mbps mode, the eventbuilder, experiment workstation, Linux PCs and the switchinterconnection in the 100Mbps mode. The experiment workstation acts as a gateway to the institute wide network, the ikpnet. All frontend PCs (at now eleven) are implemented in the NetBSD cluster.
The NetBSD operating system has been upgraded to the version 1.3.2. For the data acquisition, the EMS server software, running at frontend PCs and the EMS client software, used at the experiment workstation under DigitalUnix, has been upgraded to the actual version. Further on, for data analysis the XD-Sorter base software and the GEM library have been implemented for DigitalUnix and Linux at the Unix server. The actual data analysis software is stored at the central Unix server and will be distributed to all collaboration partners from the ftp account of this server. For the data analysis at about 12 Intel Pentium PCs the operating system SuseLinux vers. 5.2 and 5.3 has been installed and the NFS access to all needed software at the Unix server has been established.

The providing of a data processing structure for COSY experiments comprises the buildup of the central Unix server and workstation groups as well as the sustaining of resources for the data acquisiton at experiments and for the analysis of experiment data. In operating systems, support is granted for DigitalUnix, ULTRIX, Linux, NetBSD, OS9 and VMS. Accordingly, the instruction of users is provided in the handling of operating systems and the software development.

One of the basic activities was the improvement of the central Unix server regarding to the multiuser operation, bootservice for frontend CPUs at the experiments and software service for workstations running DigitalUnix and ULTRIX as well as PCs under Linux and NetBSD operating systems. The server was extended regarding to the Memory and disk capacity. At now the server is equipped with 1GB Memory and 66GB disk storage capacity.

Various software products arranged according to the topics: data acquisition, data analysis, document preparation, network communication and software development were implemented or upgraded. The clusters for diskless frontend CPUs, namely the cluster for CAMAC, FASTBUS and VME CPUs running OS9 and the cluster for PC oriented ReadoutControllers in CAMAC and FASTBUS as well as the Eventbuilder using the NetBSD operating system were expanded and continuously supported for the COSY11, GEM, ANKE and LAMBDA experiments.

Due to the improvements of the EMS software, various versions of this product were implemented. Because of problems with the GNU C++ compiler at SuseLinux, the RedHat Linux, providing the egcs C++ compiler, has been installed to port the EMS software to Linux. At now, the last release of the EMS software is implemented and tested for DigitalUnix, Linux and NetBSD and is available at the Unix server. Thereby each configuration of data acquisition for experiments can be realized, distributed multicrate configurations with one NetBSD PC for each crate, one dedicated eventbuilder PC and Alpha Workstation or Linux PC for experimnt control, as well as single crate configurations for small systems.
On various Alpha workstations for data analysis at the IKPE1 and IKPE2 the DigitalUnix vers. 4.0d including the NFS access to products at the Unix server was installed.
The buildup of a cluster for Linux PCs is taken into account for the ANKE collaboration. Because of differences in the NFS implementation between DigitalUnix and Linux, in the current state of development, at this time the central Alpha Unix server cannot be used as server for such cluster. For the implementation of NetBSD software as well as for the buildup and development of data acquisition, a frontend PC with an appropriate CAMAC controller, both developed at ZEL, was put into operation.
In the local FastEthernet network, Alpha workstations and Linux PCs equipped with 100Mbps Ethernet interface were implemented.
The preparation of a reliable central backup service for Alpha workstations and Linux PCs at the Unix server is still in progress.

The old VAX cluster is continuously used by several scientists for offline processing, especially the preparation of COSY experiments.

References

/1/ IKP Annual Report 1997 (3505) p. 217
/2/ IKP Annual Report 1996 (3365) p. 267, 269
/3/ IEEE Transactions on Nuclear Science February 1996, Vol.43, No.1, p.44

Development of High-speed Digital Signal Processing Techniques for Gamma-ray Tracking

H. Brands, M. Rossewij, W. Gast, A. Georgiev[1], J. Stein[1]

For the next generation of high resolution multi-detector arrays for nuclear spectroscopy employing highly segmented tracking detectors, a new version of the Pulse Processing Analog to Digital Converter (PPADC) has been built. It is based on a PCI bus implementation developed by our industry partner target systemelectronic gmbh and aims at low cost per channel, compact size, and high computing power to allow a high number of processing channels as well as on-line pulse shape analysis.

1. Hardware

To allow an easy integration into different instrumentation systems a modular hardware structure was chosen. The present system consists of a PCI/ISA motherboard onto which up to eight PPADC processing channels can be plugged as daughterboards. In contrast to previous designs, each daughterboard contains all signal processing functions, whereas on the motherboard mainly the channel multiplexer, controler, on-line singles histogrammer, and readout are implemented.

a) Motherboard

A prototype of the PCI/ISA motherboard provided by target systemelectronic gmbh with four daughterboard connectors has been assembled and tested. As main components it contains a Digital Signal Processor (DSP) with integrated PCI/ISA interface, two PLDs for interfacing and multiplexing the processing channels, and various memory moduls for singles spectra histogramming, booting, etc.(see fig.1). For the first tests of the functionality of these components the ISA bus interface was used.

b)Daughterboard

The daughterboards, measuring only 84x66 mm, contain all hardware needed for large dynamic range, high resolution signal processing: the analog signal conditioning and triggering, a 12 bit, 20 Msps sampling ADC with integrated decimation and a maximum resolution of 16 bit at 2.5 Msps output data rate, and two high performance DSPs. Various Digital to Analog Converters (DAC) connected to the serial ESSI interface of the Motorola DSP are used for setup and control (see fig.2). A prototype of the daughterboard provided by target systemelectronic gmbh was assembled and tested. For the latter a test enviroment employing the host interface, the command converter, and the JTAG interface of the Motorola Application Development System (ADS) was installed.

2. Software

Various software modules for testing the hardware, controling the parameters, and establishing the communication between the different signal processing components have been developed on the basis of sample programs provided by target systemelectronic gmbh. Most of the software has been written in assembly language using the software tools delivered with the Motorola ADS package.

a) Motherboard

Various test routines were developed and downloaded to the DSP on the motherboard, to test the internal and external memory, the ports, and the interfaces of the DSP. For the download itself, a program provided by target systemelectronic gmbh to download Motorola assembler/linker output files via the ISA bus was used. After testing functionality of the DSP, software to setup the PCI interface was developed. A dual boot strategy [1] was implemented, which starts booting from the Flash EEPROM, in order e.g. to put the DSP into the proper operating mode with respect to the required clock frequency, and then continues booting via the PCI bus.

PC and DSP software modules employing the commercial available virtual device drivers from MTM [2] were written to establish the communication via the PCI bus. With these modules it is possible to download programs to the DSP and to read/write data from/to the DSP. Test measurements were performed to study the communication bandwidth as a function of the block size.

b)Daughterboard

The high sampling frequency of the ADC and the distribution of the real-time processing tasks in the PPADC requires a high communication bandwidth between the different signal processing components. DSP1 reads the ADC data using its memory interface (PORTA). After preprocessing the ADC data, the processed data are send from DSP1 to DSP2 via the DSP1 host interface and the DSP2 memory interface. Since the DSP cores are occupied with processing tasks, the DSP software had to make use of Direct Memory Access (DMA) channels for the ADC to DSP1 and DSP1 to DSP2 data transfers.

The common mode level, the offset, and the trigger level of the analog part as well as the operation mode of the ADC are adjusted by DACs, which are controled via the serial ESSI1 interface of DSP1. Software for serial communication via the ESSI interface has been written to establish the necessary control functions.

[1] target sytemelectronic gmbh, D-42651 Solingen, Kölner Str. 99, Germany

This work is supported by the EU in the framework of the TMR program under the contract ERB FMR XCT 970123, and by TTB in the framework of the technology transfer project TTB/V.292.03.92.

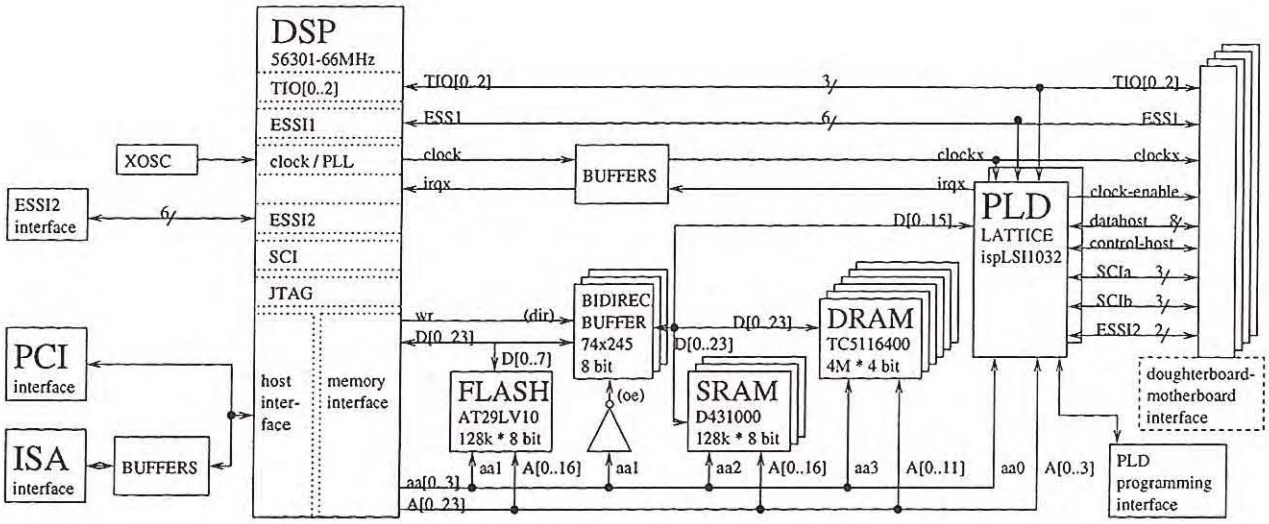

Figure 1: Blockdiagramm of the PPADC motherboard.

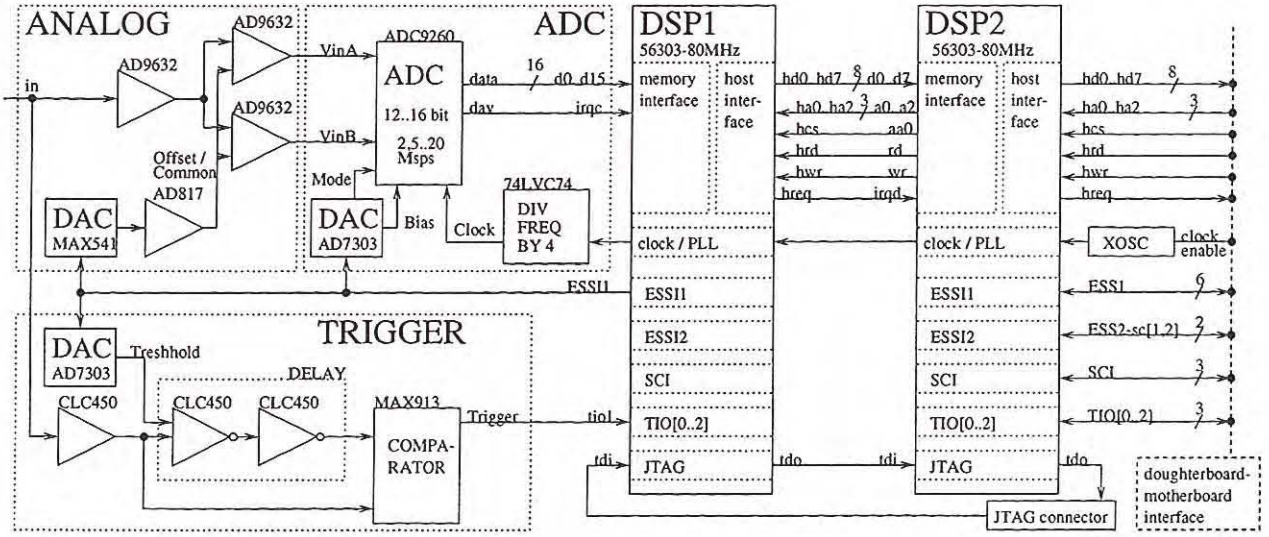

Figure 2: Blockdiagramm of the PPADC daughterboard.

References:

[1] Motorola Application Note AN1780/D, Rev.0, Nov. (1998)

[2] MTM User Ref. Manual MTM 563xx PCI DSP, Version 1.01, Oct. (1998)

J. Bojowald, H. Labus, E. Brökel, N. Dolfus, W. Ernst, G. Lürken, R. Nellen and K. Winkler

In the IKP-electronics laboratory activities were carried out for the COSY-region, here especially for the diagnostic instrumentations at COSY and the beamlines, and for the nuclear experiments with COSY-beam. Also external experiments at CERN and PSI were supported as well as one technological transfer project and first jobs for the ESS project. Among them were developments of electronic systems and devices, which are not commercially available, electronic support during running experiments, consultation and assistance for physicists, and common services like repairs, purchase and storage of electronic devices and components. Some of the developments were carried out in cooperation with the COSY-diagnostic group. In the following the representative activities are listed and briefly described.

Activities for COSY:

For the refitting of the source beam line 10 remote controllable current sources with crates and power supplies were designed and built.

For the pulsing of the ion optical elements of the polarised source 10 amplifiers were built with remote controlled amplification to toggle by a TTL signal between pre selectable reference currents .

The timing electronics of the source was modified to use the cyclotron beam for diagnostic purposes and isotope production during long COSY cycles. Furthermore the development of a logic system was started which allows by switches (locking switches in several apparatus or toggle switches on the front panel) or logical levels the control of interlock conditions for the additional beam pulses during the COSY cycle.

For current and energy measurements of the cyclotron beam with the capacitive pickups a VEE program was written to read and evaluate the data of the new fast VXI scope. The system will also be used for investigation of the cyclotron beam bunches.

Considerations and first steps for the layout of a new Schottky pickup are in progress. Special attention is given to construct an high sensitive monitor which is even able to measure Schottky noise in both planes by suitable switching of coax relays.

The electronic of one MWPC was modified to ten times higher sensitivity for low intensity measurements along the extraction beam line.

For the ESS project suitable methods of temperature measurements were searched to measure the super conducting cavity surface with resolution of <0.1K.

Activities for COSY-experiments:

ANKE: 80 analogue fan outs with special crates and power supplies were built. The hardware and software of the target control was modified several times.

COSY-11: A timing controller system was built to stop data acquisition and gas flow of the cluster target during injection and ramp times. The trigger is derived from the COSY timing and the control is performed by a VEE-program.

TOF: 200 splitters for the fast detector signals and flexible multiple coax cables with special multi point connectors were built to expand the energy calorimeter.

GEM: Fast limiting amplifiers were developed and merged into 16 fold NIM-Modules. They are needed for extension of the dynamic amplitude range due to the large energy range of the reaction particles.

ATRAP: The development of the fast front end signal processing electronics for the space sensitive photo multipliers with 16 cathode pixels consisting of fast amplifiers and discriminators was started. Rigid space limitations demand sophisticated lay out even with SMD components.

TOF and BIG-KARL: For the control of the liquid hydrogen target, which is now based on PC hardware with analogue and digital I/O interface boards and graphical programming with LABVIEW, a new hardware concept was studied based on FIELD-POINT, a modular distributed I/O-System from NI, by which future expansion of the experiment control to more sensors and other devices as pumps, valves, compressors etc. can be realised with less effort and liability to interferences.

Crystal Spectrometer: The old version of the experiment control is extended to several new functions as temperature control of the crystals and monitoring of different physical states of the detector. Also this job is done with the FIELD-POINT system mentioned above. The old software is transferred to the new LABVIEW version 5.1 with real time capabilities offering very comfortable programming strategies but must partly be rewritten and expanded to the additional functions.

Technology-Transfer: A Compton back scatter detector was developed to measure the specific weight of thin papers or foils using a photo multiplier with plastic scintillator and a strong AM241 gamma source which is embedded in the centre of the scintillator.

Semiconductor Detectors and Targets

G. Fiori, A. Hamacher, H. Metz, J. Pfeiffer, D. Protic

As during the last years the main activity of the laboratory was concentrated on the preparation of the detector system "Germanium Wall" for GEM-experiments at COSY [1]. Former regenerated detectors were placed into the second GEM-cryostat with improved Kapton-feedthroughs which now enable an easy exchange of the detectors: One Quirl-detector and two E-detectors with 32 sectors. At the end of the GEM-experiment in February 1998 the detectors showed serious radiation damage. After the annealing in the cryostat at ~ 380 K the detectors were tested in the laboratory with uncollimated γ-sources. The corresponding spectra did not show a significant influence of the former radiation damage. But even in the beginning of the second GEM-experiment in October 1998 the smaller E-detector could not deliver proper signals comming from a central area with a diameter of about 20 mm. The other detectors worked properly up to the end of the experiment.

These facts confirm again the difference between the detectors made from p- or n-type germanium. The smaller E-detector has been manufactered from n-type germanium which converted to the p-type during the thermal treatment at 670 K after the implantation of phosphorus ions. The larger E-detector with the Li-diffused contact has remained n-type after the manufacture. Very important conclusion is that the n-type germanium detectors are less sensitive to the radiation damage and easier to regenerate than p-type ones. Additional efforts have to be undertaken to establish a reliable way of manufacturing which will prevent the change of the n-type germanium into the p-type, especially during the treatment at higher temperatures.

Extensive investigations have been performed to control the depth of the boron implanted p^+-layers. The range of the boron ions implanted at the usual energy of 20 keV can be as long as 25 µm and almost independent on the crystal orientation. Due to its thickness such a p^+-contact is very rugged and can be easily handled. This is also one of the reasons to perform a position sensitive structure on it. Therefore the etched grooves needed for the electrical separation of the position elements must be more than 25 µm deep. Such a deep groove will be also quite wide. Thus the realization of finer structures is not possible. A new technique has been established which enables producing of a p^+-contact with the desired effective thickness. The crystaline structure of the surface layer can be easily destroyed by bombarding with argon ions. Such an amorphous layer prevents the deep penetration of the boron ions. Depending on the damage level, which is determined by the implantation dose of argon ions, one can vary the effective thickness of the p^+-contact in the range from ~ 2 to 20 µm. The former used method based on evaporation of a thin aluminum layer before the boron implantation led to similar results, but was hard to perform in our lab under clean room conditions.

Several strip detectors were manufactured from ~ 4 mm thick lithium drifted silicon and tested at COSY. One of them, with 80 strips on an area of 20 x 10 mm^2 and a pitch of 0.25 mm was installed in the ANKE target area as E-detector of a spectator-telescope. Preliminary tests were performed to investigate the energy and position resolution of spectator-protons up to 30 MeV. First results have been encouraging, but further investigations are necessary to improve the long term stability of the interstrip resistance in vacuum. A two-dimensional position sensitive detector system was developed for the diagnosis of the external COSY-beam. Two Si(Li) detectors, each having 39 strips on an area of 39 x 39 mm^2, have been mounted on a holder with Li-contact against Li-contact and strips under 90°. As in the case of the ANKE-detector the read out was performed by means of a resistive chain to which the detector strips had been connected. This system was tested at the chamber 4.5 in front of BIG KARL during the GEM-experiment in October 1998. Each detector delivered two analog signals taken at the ends of the corresponding resistor chain. With the help of a Camac based system a two-dimensional picture of the beam cross-section could be presented in COSY control room and at the GEM-experiment.

During the last experiments inside the CELSIUS-ring (0°-spectrometer, collaboration with the University of Stockholm) the E-detector of the germanium telescope was mounted in a modified holder with an improved protection of the intrinsic zone [2]. As expected, the increase of the leakage current in the course of the experiment was much less pronounced than before although the detector was as close as possible to the particle beam. This improvement will enable long measuring times without the need of heating up in next experiments [2].

A new collaboration was started with GSI-Darmstadt (Lamb-shift at heavy nuclei). For detection of x-rays up to 100 keV a germanium detector with 200 strips will be manufactured.

Diverse targets were produced for IKP-groups such as Mo^{95} and Mo^{96} for EUROBALL collaboration and carbon targets on PE-backing, Al-targets and tempered carbon foils for ANKE-experiments. A store of carbon targets was kept ready for the COSY-injection system. Various scintillators for TOF-experiments were covered with evaporated aluminium. A series of small glass plates were covered with evaporated copper of different thicknesses (H^0-diagnosis). Some parts of the COSY ion source were cleaned with the help of 0_2-plasma. A lot of IKP-groups were supported in solving diverse lab problems.

References:

[1] GEM-Collaboration, this Annual Report
[2] Annual Report IKP 1997, Jül-3505, p. 222

Cluster targets for COSY

H.H. Adam*, A. Khoukaz*, T. Lister*, C. Quentmeier*, R. Santo*, C. Thomas*

Cluster beams are of growing interest for accelerator experiments. Produced in Laval-nozzles, they can be used as windowless targets of very high purity. The absolute density can easily be varied over orders of magnitude by changing the nozzle temperature or the gas input pressure. Different to gas-jet beams they provide a spatially well defined target beam with a homogeneous density distribution.

In the IKP at Münster extensive studies on cluster beam production, especially of hydrogen, have been performed in the framework of designing optimized cluster targets for storage ring experiments [1]. Two cluster targets have been build for the COSY storage ring at the FZ-Jülich. The first one was installed in 1995 at the target place TP3 as part of the COSY-11 installation. Several months of beam time have been carried out using hydrogen cluster beams with areal densities of up to 10^{14} atoms/cm^2. Detailled information on this target can be found in [2, 3].

For experiments at the ANKE installation the second cluster target for COSY was build in 1998 in the IKP at Münster and moved to FZ-Jülich the same year. A sketch of the mechanical assembly of this cluster target is shown in Fig. 1. Test measurement with the ANKE target have been performed in the IKP at Münster and the FZ-Jülich and confirmed the expected performance comparable to the COSY-11 target. The installation of the cluster target is scheduled for week 31 in 1999, thus first experiments within the ANKE installation are planned for fall 1999.

For control purposes via ethernet a slow control system based on a LINUX PC-system was designed and built up in the IKP at Münster. This cluster target remote control allows to switch devices on or off and displays pressure values in the different pumping stages, nozzle temperature and gas input pressure as well as the status of target components like pumps, shutter and valves. Furthermore, two identical switch bords, one forseen at the target place and one outside of the storage ring, enable the manual control of the cluster target. The complete system was already set into operation.

During a test run of the COSY-11 cluster target it was shown that also deuterium can be used as target material which allows to provide neutrons as target. To avoid high operation costs during future beam times using the more expensive deuterium, a recuperation system is under construction in the IKP at Münster by collecting the gas after the pumping system. After cleaning of the gas by means of absorption filters it is compressed ($\leq$ 20 bar) and fed back to the existing gas supply system, which includes a hydrogen/deuterium palladium purifier for the final cleaning of the gas.

References:

[1] A. Khoukaz, T. Lister, C. Quentmeier, R.Santo, and C. Thomas, accepted for publication in Eur. Phys. Jour. D

[2] H. Dombrowski, D. Grzonka, W. Hamsink, A. Khoukaz, T. Lister, R.Santo, Nucl. Phys. **A 386**, 228 (1997)

[3] S. Brauksiepe et al., Nucl. Phys. **A 376**, 397 (1996)

* Institut für Kernphysik, Universität Münster, 59399 Münster, Germany

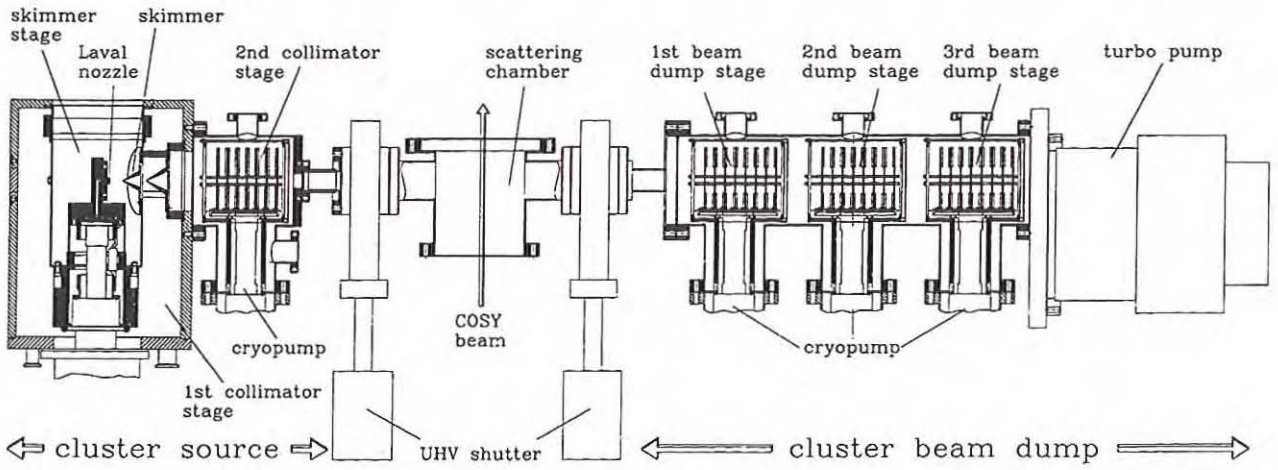

Fig. 1. Sketch of the cluster target for the ANKE experiment at COSY.

VI. SCIENTIFIC COUNCIL COSY

Prof. Dr. P. Braun-Munzinger	GSI Darmstadt
Prof. Dr. J. Cameron	Indiana University
Prof. Dr. L. Cardman	Thomas Jefferson Lab., VA
Prof. Dr. H. Coenen	INC, FZJ Jülich
Prof. Dr. D. Drechsel	University of Mainz
Prof. Dr. D. Husmann	University of Bonn
Prof. P. Paul (Chairman)	State University, New York
Dr. D. Reistad	University of Uppsala
Prof. Dr. D.O. Riska	University of Helsinki
Prof. Dr. B. Schoch	University of Bonn
Prof. Dr. Th. Walcher	University of Mainz
Prof. Dr. H. Wenninger	CERN, Genf

VII. ADVISORY COMMITTEES AT COSY (elected members)

PAC (Program Advisory Committee)

Prof. A. Boudard	CE Saclay, France
Prof. Dr. K. Goeke	University of Bochum
Prof. Dr. E. Grosse	GSI Darmstadt
Prof. Dr. C. Guaraldo	INFN Frascati
Prof. Dr. D. v. Harrach	University of Mainz
Dr. H. Herr	CERN, Genf
Prof. Dr. S. Kullander	University of Uppsala
Prof. Dr. H.O. Meyer	IUCF Bloomington, USA
Prof. Dr. U. Mosel (Chairman)	University of Gießen
Prof. Dr. K. Rith	University of Erlangen
Prof. Dr. E. Rössle	University of Freiburg
Prof. Dr. C. Wilkin	University College London

ENC (Exekutiv-Komitee zur Nutzung COSY)

Dr. K.W. Baurmann	WTA, FZJ Jülich
Dr. D. Grzonka	IKP, FZJ Jülich
Prof. Dr. D. Husmann	University of Bonn
Prof. Dr. K. Kilian	IKP, FZJ Jülich
Prof. Dr. T. Mayer-Kuckuk	University of Bonn
Prof. Dr. R. Maier	IKP, FZJ Jülich
Prof. Dr. U. Mosel	University of Gießen
DI U. Pfister	BD, FZJ Jülich
DK R. Scheid	FA, FZJ Jülich
Prof. Dr. K. Sistemich	IKP, FZJ Jülich
Prof. Dr. J. Speth	IKP, FZJ Jülich
Prof. Dr. H. Ströher	IKP, FZJ Jülich
Prof. Dr. J. Treusch	VS, FZJ Jülich
Prof. Dr. R. Wagner (Chairman)	VS, FZJ Jülich

MAC (Machine Advisory Committee)

Dr. N. Angert	GSI Darmstadt
Prof. Dr. D. Husmann (Chairman)	University of Bonn
Dr. D. Möhl	CERN, Genf
Prof. Dr. G. Mülhaupt	ESRF
Dr. F. Willeke	DESY Hamburg

VIII. COLLABORATIONS

COSY-EDDA-Collaboration*
Spokesmen: J. Bisplinghoff, F. Hinterberger, W. Scobel

R. Gebel, R. Maier, D. Prasuhn, P. v. Rossen:
Institut für Kernphysik, Forschungszentrum Jülich, D-52425 Jülich

M. Altmeier, J. Bisplinghoff, T. Bissel, M. Busch, R. Daniel, O. Diehl, H.J. Engelhardt, J. Ernst, P.D. Eversheim, O. Felden, R. Gross-Hardt, F. Hinterberger, T. Hüskes, R. Jahn, R. Maschuw, T. Mayer-Kuckuk, H. Rohdjeß, D. Rosendaal, M. Schulz-Rojahn, V. Schwarz, S. Thomas, H.J. Trelle, M. Walker, E. Weise, R. Ziegler:
Institut für Strahlen- und Kernphysik, Universität Bonn

F. Bauer, T. Bissel, R. Bollmann, K. Büßer, F. Dohrmann, J. Flammer, M. Gasthuber, J. Greiff, A. Gross, K. Hebbel, I. Koch, R. Langkau, T. Lindemann, J. Lindlein, M. Pfuff, B. Sanz, N. Schirm, W. Scobel, S. Steinbeck, A. Wellinghausen, K. Woller:
I. Institut für Experimentalphysik, Universität Hamburg

*supported by BMFT-Verbundforschung; University Program of Forschungszentrum Jülich

COSY-11 Collaboration*
Spokesman: W. Oelert

D. Grzonka, M. Hofmann, K. Kilian, W. Oelert, G. Schepers, T. Sefzick, S. Sewerin, M. Wolke:
Institut für Kernphysik, Forschungszentrum Jülich, D-52425 Jülich

H. Gutschmidt, M. Jochmann, M. Köhler, P. Wüstner:
Zentralinstitut für Elektronik, Forschungszentrum Jülich, D-52425 Jülich

H.H. Adam, A. Khoukaz, T. Lister, C. Quentmeier, R. Santo:
Institut für Kernphysi, Universität Münster

L. Jarczyk, P. Moskal, J. Smyrski, M. Sokolowski, A. Strzalkowski:
Institute of Physics, Jagellonian University, Cracow, Poland

J. Balewski, A. Budzanowski: Institute of Nuclear Physics, Cracow, Poland

C. Goodman: IUCF Bloomington, Indiana, USA

U. Seddik: NRC, Atomic Energy Authority, Cairo, Egypt

*supported by BMFT-Verbundforschung; International Bureau of the BMBF, DLR-Bonn; University Program of Forschungszentrum Jülich

COSY-13 Collaboration*
Spokesman: B. Kamys

W. Borgs, N. Dolfus, S. Geisler, H.R. Koch, P. Kulessa, R. Maier, H. Ohm, D. Prasuhn, U. Rindfleisch, O.W.B. Schult, H. Ströher:
Institut für Kernphysik, Forschungszentrum Jülich, D-52425 Jülich

L. Jarczyk, B. Kamys, St. Kistryn, K. Pysz, Z. Rudy, A. Strzalkowski:
Institute of Physics, Jagellonian University, Cracow, Poland

W. Cassing: Institut für Theoretische Physik, Universität Gießen

I. Zychor:
Soltan Institute for Nucl. Studies, PL-05400 Swierk

M. Matoba, Y. Uozumi:
Dept. of Nuclear Engineering, Kyushu University, Fukuoka 812, Japan

*supported by International Bureau of KfK Karlsruhe; TEMPUS-Program

ANKE* (0°-Facility)
Spokesman: K. Sistemich

U. Bechstedt, N. Bongers, G. Borchert, W. Borgs, W. Bräutigam, M. Büscher, J. Dietrich, D. Gotta, D. Grzonka, M. Hartmann, H. Junghans, M. Karnadi, H.R. Koch, K. Krude, H. Labus, R. Maier, S. Martin, R. Nellen, W. Oelert, H. Ohm, D. Prasuhn, H.J. Probst, R. Schleichert, A. Schneider, H. Schneider, G. Schug, O.W.B. Schult, H. Seyfarth, K. Sistemich, H.J. Stein, H. Ströher, K.-H. Watzlawik:
Institut für Kernphysik, Forschungszentrum Jülich, D-52425 Jülich

W. Klein: Institut für Schicht- und Ionentechnik, Forschungszentrum Jülich, D-52425 Jülich

F. Klehr, H. Stechemesser: Zentralabteilung Allgemeine Technologie, Forschungszentrum Jülich, D-52425 Jülich

R. Baldauf, M. Drochner, W. Erven, H. Kleines, H. Loevenich, H. Pohl, J. Sakardi, P. Wüstner, K. Zwoll:
Zentrallabor für Elektronik, Forschungszentrum Jülich, D-52425 Jülich

M. Dombrowski, N. Langenhagen, H. Müller, B. Prietzschk, B. Rimarzig, Chr. Schneider:
Zentralinstitut für Kernforschung, Rossendorf, D-01474 Dresden

J. Ernst: Institut für Strahlen- und Kernphysik, Universität Bonn, D-53115 Bonn

N. Koch, S. Lorenz, K. Rith, F. Rathmann, F. Schmidt, E. Steffens:
Physikalisches Institut II, Universität Erlangen-Nürnberg, D-91058 Erlangen

W. Cassing, A. Sibirtsev: Institut für Theoretische Physik, Universität Gießen, D-35392 Gießen

R. Eßer, H. Paetz gen. Schieck: Institut für Kernphysik, Universität Köln, D-50937 Köln

H. Adam, A. Khoukaz, Th. Lister, C. Quentmeier, R. Santo:
Institut für Kernphysik, Universität Münster, D-48149 Münster

U. Schwarz: Universität GH Paderborn, Abt. Soest, D-59494 Soest

L. Jarczyk, B. Kamys, St. Kistryn, P. Kulessa, K. Pysz, Z. Rudy, J. Smyrski, A. Strzalkowski:
Institute of Physics, Jagellonian University, Cracow, Poland

V. Abazov, V. Artemov, A. Chusin, S. Dymov, O. Gorchakov, A. Kacharava, N. Kadagidze, V.I. Komarov, V. Kruglov, A. Kulikov, V. Kurbatov, V. Leontiev, G. Macharashvili, S. Mercliakov, A. Petrus, E. Strokovsky, M. Sapozhnikov, Yu. Uzikov, A. Volkov, S. Yaschenko, B. Zalikhanov, N. Zhuravlev:
Joint Institute of Nuclear Research, Dubna, Russia

S. Trusov, V. Yazkov: Dubna Branch of the Moscow State University, Dubna, Russia

S. Barsov, S. Belostotski, O. Grebenyuk, V. Koptev, A. Kovalov, P. Kravfsov, M. Mikirtichyants, S. Mikirtichyants, V. Nelubin, H. Nekipelov, A. Vassiliev: Petersburg Nuclear Physics Institute, Gatchina, Russia

A. Gerasimov, V. Grishina, L. Kondratyuk, V. Tchernyshev:
Institute for Theoretical and Experimental Physics, Moscow, Russia

Ye.S. Golubeva: Institute for Nuclear Research, Russian Academy of Sciences, Moscow, Russia

C. Wilkin: Physics Department, Univ. College London, London WC1 6BT

N. Amaglobeli, B. Chiladze, Z. Menteshashvili, M. Nioradze:
High Energy Physics Institute, Tbilisi State University, Tbilisi, Georgia

H. Gruppelaar: ENC-Nuclear Energy, Petten, The Netherlands

A. Mussgiller: FH München, Fachbereich Elektronik, D-80335 München

I. Zychor: Soltan Institute for Nuclear Studies, PL-05400 Swierk, Polen

*supported by Land Nordrhein-Westfalen, BMFT (Verbundforschung; Forschungszentrum, WTZ mit Rußland), INTAS, Collaborators

COSY-GEM-Collaboration*
Spokesman: H. Machner

J. Bojowald, D. Filges, A. Hamacher, A. Hassan, K. Kilian, R. Klein, H. Machner, R. Maier, H.P. Morsch, D. Protic, P. v. Rossen, J. Stein:
Institut für Kernphysik, Forschungszentrum Jülich, D-52425 Jülich

M. Drochner, G. Kemmerling, K. Zwoll:
Zentralinstitut für Elektronik, Forschungszentrum Jülich, D-52425 Jülich

J. Ernst, R. Jahn, B. Razen:
Institut für Strahlen- und Kernphysik, Universität Bonn

D. Frekers, R. Garske, K. Grewer:
Institut für Kernphysik, Universität Münster

P. Hawranek, L. Jarczyk, S. Kistryn, W. Klimala, A. Magiera, J. Smyrski, A. Strzalkowski:
Jagellonian University, Cracow, Poland

A. Budzanowski, L. Freindl, S. Kliczweski, R. Siudak: Institute of Nuclear Physics, Cracow, Poland

H.S. Plendl: Physics Department, FSU, Tallahassee, Florida, USA

B.J. Lieb: Physics Department, GMU, Fairfax, Virginia, USA

L.C. Liu: LANL, T. Division, Los Alamos, USA

H. Nann: IUCF, Bloomington, Indiana, USA

M.G. Betigeri, A. Chatterjee, B.K. Jain, S.S. Kapoor, B.J. Roy:
BARC Trombay, Bombay, India

J. Ilieva, T. Kutsarova, E. Pentchev: Institute of Nuclear Research and Nuclear Energy, Sofia, Bulgaria

E. Friedman: Hebrev University, Racah Institute, Jerusalem, Israel

S. Mordechei: Ben Gurion University, Ber Sheva, Israel

S. Förtsch: National Accelerator Centre, Faure, South Africa

D. Kolev. R. Tsenov: Univ. Sofia, Sofia, Bulgaria

*supported by BMFT-Verbundforschung; University Program of Forschungszentrum Jülich & DLR, Bonn

COSY-TOF Collaboration*
Coordinator: E. Roderburg

U. Bechstedt, D. Filges, R. Geyer, U. Goldmann, H. Hadamek, A. Hassan, D. Hesselbarth, P. Jahn, K. Kilian, R. Klein, H. Machner, S. Marwinski, H.P. Morsch, K. Nünighoff, N. Paul, U. Rindfleisch, E. Roderburg, M. Rogge, M. Schmitz, T. Sefzick, F. Siegers, P. Turek, D. Völlmecke:
Institut für Kernphysik, Forschungszentrum Jülich, D-52425 Jülich

H. Nann: IUCF Bloomington, USA

P. Herrmann, H. Koch, J. Krug, W. Meyer, M. Steinke, A. Wilms, U. Zielinski:
Institut für Experimentalphysik, Ruhr-Universität Bochum, D-44780 Bochum

H. Dutz: Physikalisches Institut der Universität Bonn, D-53115 Bonn

A. Böhm, K. Brinkmann, H. Freiesleben, B. Hübner, L. Karsch, E. Kuhlmann, J.S. Lange, M. Richter, P. Schönmeier, M. Schulte-Wissermann, G.J. Sun, M. Würschig-Pörsel:
T.U. Dresden, D-01062 Dresden

M. Müller-Veggian: Fachhochschule Jülich

R. Bilger, H. Clement, A. Erhardt, J. Kreß, G.J. Wagner:
Physikalisches Institut, Universität Tübingen, D-72076 Tübingen

S. Dshemuchadse, P. Michel, K. Möller, B. Naumann, L. Naumann, A. Schamlott:
Institut für Kern- und Hadronenphysik, FZ Rossendorf, D-01314 Dresden

W. Eyrich, M. Fritsch, J. Hauffe, A. Metzger, W. Schroeder, F. Stinzing, M. Wagner, Wirth: Physikalisches Institut, Universität Erlangen-Nürnberg, D-91058 Erlangen

C. Fanara, A. Filippi, S. Marcello, A. Raimondo: INFN Torino, Italien

P. Zupranski: SINS Warschau

*supported by BMFT-Verbundforschung; University Program of Forschungszentrum Jülich

COSY-MOMO-Collaboration*
Spokesman: R. Jahn

H. Machner, P. v. Rossen, R. Tölle: Institut für Kernphysik, Forschungszentrum Jülich, D-52425 Jülich

F. Bellemann, A. Berg, J. Bisplinghoff, G. Bohlscheid, J. Ernst, F. Hinterberger, R. Ibald, R. Jahn, R. Joosten, R. Maschuw, T. Mayer-Kuckuk, G. Mertler, J. Munkel, D. Rosendaal, H. Schnitker:
Institut für Strahlen- und Kernphysik, Universität Bonn

P. v. Neumann-Cosel: Institut für Kernphysik, Technische Hochschule Damstadt

L. Jarczyk, A. Magiera, J. Smyrski, A. Strzalkowski:
Institute for Physics, Jagellonian University, Cracow, Poland

A. Kozela: University of Cracow, Poland

C. Wilkin: University of London, England

*supported by BMFT-Verbundforschung; University Program of Forschungszentrum Jülich;
International Bureau of the BMBF, DLR-Bonn

NESSI Collaboration (European Spallation Source (ESS))*
Spokesman: U. Jahnke

D. Filges, F. Goldenbaum, R.-D. Neef, K. Nünighoff, N. Paul, H. Schaal, A. Tietze:
Institut für Kernphysik, Forschungszentrum Jülich, D-52425 Jülich

D. Hilscher, U. Jahnke:
Hahn-Meitner-Institut Berlin, Bereich Festkörperforschung, D-14109 Berlin

J. Galin, A. Letourneu, B. Lott, A. Péghaire
GANIL (IN2P3-CNRS, DSM-CEA), BP 5027, F-14021 Caen-Cedex, France

L. Pienkowski: University of Warsaw, 02-097 Warszawa, Poland

J. Töke, W.U. Schröder: University of Rochester, Rochester, New York 14627, USA

P. Figuera: Instituto Nazionale di Fisica Nucleare, LNS, I-95123 Catania, Italy

*supported by EU-TMR-Program and Helmholtz Strategie fonds

JESSICA-Collaboration*
Spokesman: H. Tietze-Jaensch

B. Alefeld, H. Barnert-Wiemer, H. Conrad, J. Dietrich, D. Filges, F. Goldenbaum, B. Guttek, H. Klein, S. Martin, R.D. Neef, K. Nünighoff, D. Prasuhn, H. Schaal, H. Stechemesser, H. Tietze-Jaensch, U. Ullmaier:
Institut für Kernphysik, Forschungszentrum Jülich, D-52425 Jülich

P.K. Job, N. Watanabe : Argonne National Laboratory (USA)

Y. Oyama: JAERI (Japan)

M. Furusaka: KEK (Japan)

P. Ferguson, E. Pitcher, G. Russell: Los Alamos National Laboratory (USA)

T. Gabriel, T. Lucas: Oak Ridge National Laboratory (USA)

G.S. Bauer, H. Spitzer: Paul Scherrer Institut (Switzerland)

T. Broome, H. Jones: RAL (UK)

Y. Kiyanagi: University of Hokkaido (Japan)

*supported by EU-TMR-Program, Helmholtz Strategie fonds

TETHYS-Collaboration
Spokesmen: A. Boudard, D. Filges

D. Filges, K. Kilian, H. Machner, H.P. Morsch, R.D. Neef, E. Roderburg, H. Schaal:
Institut für Kernphysik, Forschungszentrum Jülich, D-52425 Jülich

M. Beyss, U. Ullmaier:
Institut für Festkörperforschung, Forschungszentrum Jülich, D-52425 Jülich

J. Cugnon: Liege University, Belgium

A. Boudard, J.E. Ducret, R. Legrain, S. Leray, Y. Terrien, C. Volant: DAPNIA/SPhN, CEA Saclay, France

J. Frehaut, Y. Patin: DPTA/SPN, CEA Bruyères-le-Chatel, France

R. Barna, V. D´Amico, A. Italiano, D. De Pasquale:
Dip. di Fisica, Univ. di Messina, Istituto Naz. di Fisica Nucl. Secione di Catania, Gruppo collegato di Messina, Italy

L. Jarczyk, B. Kamys, St. Kistryn, A. Magiera, J. Smyrski, A. Strzalkowski, M. Smoluchowski:
Jagellonian University, Cracow, Poland

J. Brzchczy, P. Pysz, W. Wlazlo: Inst. of Phys., Jagellonian Univ., Cracow, Poland

P. Zupranski: University of Warsaw, Poland

A. Budzanowski, M. Kistryn, St. Kliczewski, R. Siudak:
H. Niewodnicanski Inst. of Nucl. Phys., Jagellonian Univ., Cracow, Poland

G. Alkhazov, A. Prokofiev: PNPI Gatchina, Russia

PROMICE/WASA Collaboration*
Spokesmen: B. Höistad and S. Kullander

M. Blom, H. Calen, S. Dahlgren, K. Fransson, L. Gustafsson, S. Häggström, B. Höistad, A. Jansson, A. Johansson, T. Johansson, S. Kullander, J. Moehn, A. Mörtsell, R. Ruber:
Department of Radiation Sciencves, Uppsala, Sweden

K. Kilian, W. Oelert, T. Sefzick:
Institut für Kernphysik, Forschungszentrum Jülich, D-52425 Jülich

A. Turowiecki, Z. Wilhelmi, J. Zlomanczuk:
Institute of Experimental Physics, Warsaw, Poland

Z. Zabierowski:
Institute of Nuclear Studies, Lodz, Poland

A. Kupsc, A. Nawrot, J. Stepaniak:
Institute for Nuclear Studies, PL-00681 Warsaw, Poland

A. Bondar, G. Kolachov, A. Kuzmin, T. Purlatz, B. Shwartz, V. Sidorov, A. Suchanov:
Institute of Nuclear Physics, Novosibirsk, Russia

Z. Pawlowski:
Institut of Radioelectronics, Warsaw, Poland

D. Bogoslawsky, V. Dunin, L. Komogorova, A. Kuznetsov, B. Morosov, A. Povtorejko, A. Sandukovsky, A. Sukhanov, V. Tikhomirov, A. Zernov
Joint Institute for Nuclear Research Dubna, 101000 Moscow, Russia

D. Akimov, A. Bolozdynia, I. Chuviolo, L. Kondratyuk, A. Martemyanov, M. Shepkin, A. Sibirtsev, V. Sopov, V. Tchernyshev:
Institut of Theoretical and Experimental Physics, Moscow, Russia

H. Hirabayashi, A. Yamamoto, A. Yamaoka:
National Laboratory for High Energy Physics, Tsukuba, Japan

B. Chernyshev, M. Gornov, Y. Gurov, R. Shafigulin:
Moscow Engineering Physiccs Institute, Moscow, Russia

H. Ikegami, Y. Mizuno, Y. Yuasa:
Research Center for Nuclear Physics, Osaka, Japan

C. Ekström, D. Reistad:
The Svedberg Laboratory, Uppsala, Sweden

ATRAP Collaboration (Antihydrogen TRAP)*
Spokesman: G. Gabrielse

G. Gabrielse, T. Roach, J. Estrada, D. Hall, P. Yesley:
Department of Physics, Harvard University, Cambridge, MA 02138, USA

H. Kalinowsky: Univ. Bonn, ISKP, D-53115 Bonn

T.W. Hänsch, K. Eikema, J. Walz: Max-Planck-Institut für Quantenoptik, D-85748 Garching

J. Bojowald, W. Oelert, D. Grzonka, H. Hadamek, R. Nellen, T. Sefzick:
Institut für Kernphysik, Forschungszentrum Jülich, D-52425 Jülich

H. Herr: CERN, PPE-DED-Division, CH-1211 Genf 23

T. Hijmans: Dept. of Physics, Univ. of Amsterdam, NL-1018 XE, The Netherlands

W.D. Phillips, St.L. Rolston: National Institute of Standards and Technology, Gaithersburg, MD 20899, USA

J. Walraven: FOM Institute for Atomic and Molecular Physics, 100 DB Amsterdam, The Netherlands

W. Jhe: Department of Physics, Seoul National University, 151-742 Korea

D. Wineland, J. Bollinger: National Institute of Standards and Technology, Boulder, CO 80303, USA

*supported by BMFT-Verbundforschung, National Science Foundation (USA)

PS185/3 Collaboration*
Spokesman: K. Röhrich

R. Geyer, K. Kilian, W. Oelert, K. Röhrich, T. Sefzick:
Institut für Kernphysik, Forschungszentrum Jülich, D-52425 Jülich

B. Bassalleck, S. Eilerts, D.E. Fields, P. Kingsberry, J. Lowe, D. Wolfe:
Univ. of New Mexico, Albuquerque

H. Dutz, S. Görtz, A. Meyer, U. Plückthun, B. Schoch: Univ. Bonn, Institute of Physics, D-53115 Bonn

W. Meyer, G. Reicherz: Univ. Bochum, Institut für Experimentalphysik, D-44780 Bochum

A. Berdoz, G. Franklin, C.A. Meyer, K. Pascke, B. Quinn, R. Schumacher:
Physics Department, Carnegie-Mellon University, USA

H. Dennert, W. Eyrich, J. Hauffe, A. Metzger, M. Moosburger, F. Stinzing, St. Wirth:
Physikalisches Institut, Universität Erlangen, D-91058 Erlangen

H. Fischer, J. Franz, K. Königsmann, E. Kriegler, M. Ruh, H. Schmitt:
Fakultät für Physik, Universität Freiburg, D-79104 Freiburg

T. Johansson, S. Pomp: The Svedberg Laboratory, Uppsala, Sweden

B. Bunker, R.A. Eisenstein, D. Hertzog, T. Jones, R. Tayloe:
Physics Department, Loomis Lab. of Physics, University of Illinois, USA

*supported by BMFT-Verbundforschung, National Science Foundation (USA)

PS202 Collaboration*
Spokesman: M. Macri

R. Geyer, K. Kilian, W. Oelert:
Institut für Kernphysik, Forschungszentrum Jülich, D-52425 Jülich

D. Drijard, M. Ferro-Luzzi, R. Jones, B. Mouellic, S. Ohlsson, J.-M. Perreau:
CERN, Geneva, Switzerland

W. Eyrich, M. Moosburger, S. Pomp, F. Stinzing:
Physikalisches Institut, Universität Erlangen

H. Fischer, J. Franz, E. Rössle, H. Schmitt, H. Wirth:
Fakultät für Physik, Albert-Ludwigs-Universität Freiburg

P.T. Debevec, R.A. Eisenstein, Ph. Harris, D.W. Hertzog, S.A. Hughes, P.E. Reimer, J. Ritter:
Physics Department, Loomis Lab. of Physics, University of Illinois, USA

C. Evangelista, A. Palano: Physics Department, University degli Studi di Bari, Italy

A. Buzzo, K. Kirsebom, M. Lo Vetere, M. Macri, M. Marinelli, S. Passaggio, M.-G. Pia, A. Pozzo, E. Robutti, A. Santroni:
Istituto Nazionale di Fisica Nucleare, Genova, Italy

T. Johansson: The Svedberg Laboratory, Uppsala, Sweden

H. Korsmo: Department of Physics, University of Oslo, Norwegen

B. Stugu: Univ. of Bergen, Norwegen

*supported by BMFT-Verbundforschung; Department of Energy (USA); National Science Foundation (USA)

ZEUS Collaboration
Spokesman: R. Klanner, Deutsches Elektronen-Synchrotron (DESY), D-22603 Hamburg

D. Filges, R.D. Neef:
Institut für Kernphysik, Forschungszentrum Jülich, D-52425 Jülich
and 49 national and international institutions

EUROBALL-Collaboration

R.M. Lieder: Institut für Kernphysik, Forschungszentrum Jülich, D-52425 Jülich

P. von Brentano: Institut für Kernphysik, Universität zu Köln, D-50937 Köln

D. Schwalm: MPI für Kernphysik Heidelberg, Postfach 103980, D-69029 Heidelberg

J. Gerl: GSI Darmstadt, Postfach 110552, D-64291 Darmstadt

H. Hübel: Institut für Kernphysik, Universität Bonn, D-53115 Bonn

K.P. Lieb: II. Physikalisches Institut, Universität Göttingen, D-37073 Göttingen

F. Dönau: Institut für Kern- und Hadronenphysik, Forschungszentrum Rossendorf, D-01314 Rossendorf

J. Lisle: Department of Physics, Victoria University of Manchester, Manchester M13 9PL, UK

P. Nolan: Department of Physics, Univ. of Liverpool, Liverpool L69 3BX, UK

J. Simpson: Daresbury Laboratory, Warrington WA4 4AD, UK

C. Rossi-Alvarez: Istituto Nazionale di Fisica Nucleare, Padova, I-35131 Padova, Italy

G. deAngelis: Istituto Nazionale di Fisica Nucleare, Lab. Nazonali di Legnaro, I-35020 Legnaro, Italy

M. Pignanelli: Istituto Nazionale di Fisica Nucleare, Sezione di Milano, I-20133 Milano, Italy

P.G. Bizzeti: Istituto Nazionale di Fisica Nucleare, Sezione di Firenze, I-50125 Firence, Italy

B. Rubio: Instituto de Fisica Corpuscular, ES-46100 Burjassot (Valencia), Spain

C. Fahlander: Department of Physics, University of Lund, S-22362 Lund, Sweden

Ö. Skeppstedt: Department of Physics, Chalmers University of Technology Göteborg, S-41296 Göteborg, Sweden

A. Johnson: Manne Siegbahn Institute of Physics, S-10405 Stockholm, Sweden

J. Nyberg: The Svedberg Laboratory, S-75121 Uppsala, Sweden

B. Herskind: NBI, University of Copenhagen, DK-1350 Copenhagen, Denmark

H. Sergolle: Institut de Physique Nucleaire, IPN, F-91406 Orsay, France

H. Guerreau: Institut de Physique Nucleaire, GANIL, F-14021 Caen, France

F. Beck: Institut de Physique Nucleaire, IReS, F-67037 Strasbourg, France

F. Chemin: Institut de Physique Nucleaire, CENBG Bourdeaux, F-33170 Gradignan, France

F. Hannachi, Institut de Physique Nucleaire, CSNSM, F-91405 Orsay, France

IX. PERSONNEL

Scientific Staff:

Dr. D. Anagnostopoulos (E2)
until March 14, 1998

Prof. Dr. G. Baur (TH)
(a.o. Prof. at the Univ. of Basel)

DP V. Baru (TH)
since July 1, 1998

Dr. U. Bechstedt (LI)

R. Böckmann (TH)
until July 31, 1998

Dr. J. Bojowald (Ec)

Dr. K. Bongardt (LI)

Prof. Dr. G. Borchert (E2)
(apl. Prof. at the Univ. of Cologne)

DI W. Bräutigam (LI)

Dipl. W. Brands (E1)
until Dec. 31, 1998

W. Breuer (E1)
until Aug. 16, 1998

Dr. M. Büscher (E2)

Dr. P. Büttiker (TH)

Dr. J. Dietrich (LI)
(Priv. Dozent at the Univ. of Dresden)

Dr. A. Djaloeis (E1)

DP S.M. Abd El-Samad (E1)
since Oct. 1, 1998

DP E. Epelbaum (TH)

Dr. R. Eßer (E2)

Dr. O. Felden (LI)
since Sept. 01, 1998

DP N. Fettes (TH)

Prof. Dr. D. Filges (E1)
(apl. Prof. at the Univ. of Wuppertal)

A. Gasparian (TH)
since August 9, 1998

Dr. W. Gast (E1)

Dr. R. Gebel (LI)

Dr. R. Geyer (E1)

DP M. Glende (LI)

J. Goertz (LI)
since Sept. 15, 1998

Dr. F. Goldenbaum (E1)
since Sept. 1, 1998

Dipl. U. Goldmann (E1)
until Oct. 14, 1998

Dr. D. Gotta (E2)

Dr. F. Grümmer (TH)

Dr. D. Grzonka (E1)

Dr. J. Haidenbauer (TH)
(Univ. Doz. at the Univ. of Graz)

Dr. C. Hanhart (TH)

Dr. M. Hartmann (E2)

DP A.M. Hassan (E1)
since April 1, 1998
until June 30, 1998

Dr. T. Hemmert (TH)
since February 1, 1998

DI K. Henn (LI)

DP D. Hesselbarth (E1)

DP M. Hofmann (E1)
from Sept. 1 to Dec. 31, 1998

I. Ivanov (TH)
since July 1, 1998

Dr. P. Jahn (E1)

DP H. Junghans (E2)

DP H. Jungwirth (LI)
until March 31, 1998

Prof. Dr. K. Kilian (E1)
(Prof. at the Univ. of Bonn)

Dr. V. Klemt (TH)

Dr. H. R. Koch (E2)

DP O. Krehl (TH)

Prof. Dr. S. Krewald (TH)
(apl. Prof. at the Univ. of Bonn)

DP P. Kulessa (E2)

Dr. H. Labus (Ec)

H.-R. Langohr (E1)

Dr. H. Lawin (LI)

Dr. A. Lehrach (LI)

Prof. Dr. R.M. Lieder (E1)
(apl. Prof. at the Univ. of Bonn)

Dr. H. Machner (E1)

Prof. Dr. R. Maier (LI)
(Prof. at the Univ. of Bonn)

Dr. S. Martin (LI)

DP S. Marwinski (E1)

Prof. Dr. Ulf-G. Meißner (TH)
(Prof. at the Univ. of Bonn)

Dr. W. Melnitchouk (TH)

DP L. Mihailescu (E1)
until Oct. 31, 1998

I. Mohos (LI)

Dr. H.P. Morsch (E1)

Dr. Ch. Mosbacher (TH)

Dr. R.-D. Neef (E1)

Prof. Dr. N.N. Nikolaev (TH)

DI K.U. Nünighoff (E1)
since April 1, 1998

Prof. Dr. W. Oelert (E1)
(apl. Prof. at the Univ. of Bochum)

Dr. H. Ohm (E2)

DI N. Paul (E1)

Dipl. I.A. Pellmann (E1)
until June 15, 1998

Dr. A. Pineda (TH)
until July 17, 1998

Dr. D. Prasuhn (LI)

DP D. Protic (Dt)

Dr. B. Razen (E1)
until Feb. 28, 1998

Ch. Reul (E1)
until Feb. 23, 1998

Dr. E. Roderburg (E1)

Dr. M. Rogge (E1)

Dipl. G. Rosenwald (E1)
since Jan. 1, 1998

Dr. P. von Rossen (LI)

Dr. T. Sefzick (E1)

DP S. Sewerin (E1)

Dr. H. Schaal (E1)

DP W. Schäfer (TH)

Dr. G. Schepers (E1)
since June 1, 1998

Dr. R. Schleichert (E2)

Dr. M. Schmitz (E1)
since Nov. 1, 1998

Dr. A. Schnase (LI)

Dr. A. Schneider (E2)
until September 30, 1998

DI H. Schneider (LI)

DP W. Schneider (E1)

DI G. Schug (LI)

Prof. Dr. O. Schult (E2)
(Prof. at the Univ. of Cologne)
until March 31, 1998

Dr. H. Seyfarth (E2)

Ing.-Stud. F. Siegers (E1)
until Sept. 14, 1998

Dr. Th. Siems (E2)
until March 31, 1998

Prof. Dr. K. Sistemich (E2)
(apl. Prof. at the Univ. of Cologne)

Prof. Dr. J. Speth (TH)
(Prof. at the Univ. of Bonn)

DI R. Stassen (LI)

Dr. J. Stein (E2)

DP S. Steininger (TH)

G. Sterzenbach (E1)

Dr. H. Stockhorst (LI)

Prof. Dr. H. Ströher (E2)
(Prof. at the Univ. of Mainz)
since April 1, 1998
(Prof. at the Univ. of Cologne)
since September 1, 1998

Dr. R. Tölle (LI)

DI T. Vashegyi (LI)

Ing.-Stud. D. Völlmecke (E1)
until Sept. 14, 1998

Dr. R. Wagner (LI)

DP Z. Wang (TH)

Dr. K.-H. Watzlawik (Da)

Dr. M. Wolke (E1)
since March 1, 1998

Dr. E. Zaplatine (LI)
since May 1, 1998

Technical and Administrative Staff:

P. Birx (LI)
R. Bley (Ad)
H.G. Böge (LI)
M. Böhnke (LI)
W. Borgs (E2)
H. Borsch (LI)
R. Brings (LI)
G. Brittner (Ec)
P. Brittner (LI)
E. Brökel (Ec)
J. But (Ws)
M. Comuth (Ad)
since June 8, 1998
L. Conin (LI)
B. Dahmen (LI)
W. Derissen (Cd)
N. Dolfus (Ec)
G. D'Orsaneo (E2)
R. Enge (LI)
J. Engel (LI)
P. Engels (LI)
W.R. Ermer (E2)
W. Ernst (Ec)
K. Esser (Ad)
H.J. Etzkorn (LI)
H.P. Faber (LI)
G. Fiori (Dt)
H.-W. Firmenich (Ws)
G. Gad (LI)
D. Gehsing (LI)
S. Geisler (Cd)
G. Göbbels (Rp)
Ch. Haberbosch (LI)
H. Hadamek (Ws)
A. Hamacher (Dt)
M.G. Holona (Ws)
K.D. Jach (LI)
H.M. Jäger (E1)
H.J. Jansen (Ws)
R. Janssen (Ad)
M. Karnadi (Da)
R. Klein (E1)
K. Krafft (Rp)
M. Kremer (Ws)
G. Krol (LI)
K.P. Kruck (LI)
M. Küven (Ws)
K.G. Langenberg (LI)
W. Lorenz (Ad)
G. Lürken (Ec)
H. Metz (Dt)
A. Müller (LI)
M. Müskes (LI)
R. Nellen (Ec)
S. Papaspyrou (Ad)
until May 19, 1998
J. Pfeiffer (Dt)
H. Pütz (LI)
C. Reimert (Ad)
until May 15, 1998
A. Retz (Cd)
A. Richert (LI)
U. Rindfleisch (Cd)
G. Roes (Ad)
since June 15, 1998
B. Rogozik (LI)
N. Rotert (LI)
D. Ruhrig (LI)
Th. Sagefka (LI)
M. Schaaf (LI)
Jos. Schmitz (Ws)
Jürg. Schmitz (LI)
F. Schultheiß (Ws)
M. Simon (LI)
H. Singer (LI)
K. Sobotta (LI)
D.W. Spölgen (Ws)
J. Strehl (Ws)
E. Tesch (Ad)
K. P. Wieder (E2)
K. Winkler (Ec)
DI J.-D. Witt (LI)
H.W. Zens (LI)

(E1) Institute for Experimental Nuclear Physics 1
(E2) Institute for Experimental Nuclear Physics 2
(Th) Institute for Theoretical Nuclear Physics
(LI) Large Nuclear Physics Instruments
(Ad) Administration
(Cd) Construction and Design
(Da) Data Acquisition Group
(Dt) Detector and Target Laboratory
(Ec) Electronics
(Rp) Radiation Protection
(Ws) Mechanical Workshop

Research Visitors (IKP)
(for one week to six months):

Prof. Dr. I. Afnan (Th)
from June 1 to June 6, 1998
(Flinders University Adelaide, Australia)

Dr. V. Afonasiev (E2)
from November 15 to December 13, 1998
(Institute for Theoretical and Experimental Physics, Moskau)

Dr. G. Alkhazov (E1)
from March 8 to 15, 1998
(St. Petersburg Nucl. Phys. Inst., Gatchina, St. Petersburg)

Dr. V. Artemov (E2)
from February 1 to 22, 1998
(Joint Inst. for Nucl. Res., Dubna, Moskau)

Dr. S. Barsov (E2)
from July 8 to 22, 1999-02-18
from September to October 7, 1998
from October 21 to November 29, 1998
(St. Petersburg Nucl. Phys. Inst., Gatchina, St. Petersburg)

Prof. M.G. Betigeri (E1)
from Oct. 14 to Nov. 8, 1998
(BARC India)

C. Celiktas (E1)
from July 3 to Aug. 28, 1998
(Ege Universitzy, Izmir, Türkei)

Dr. A. Chatterjee (E1)
from Oct. 14 to Nov. 8, 1998
(BARC India)

Prof. V. Chernyshev (E2)
from October 19 to December 18, 1998
(Institute for Theoretical and Experimental Physics, Moskau)

Prof. M. Chumakov (E2)
from January 17 to February 15, 1998
from October 19 to November 15, 1998
(Institute for Theoretical and Experimental Physics, Moskau)

Dr. M. Chiapparini (Th)
from September 26 to September 30, 1998
(State University Rio de Janeiro, Brasil)

Dr. M. Debowski (E2)
from December 15 to 23, 1998
(FZ Rossendorf, BRD)

Prof. S. Drozdz (Th)
from February 9 to April 8, 1998
from October 1 to November 30, 1998
(University of Krakow, Poland)

Prof. J.W. Durso (Th)
from June 1 to July 31, 1998
(Mount Holyoke College, Hadley, USA)

Dr. V. Eletsky (Th)
from February 16 to February 20, 1998
(Universität Erlangen, Germany)

Salem Mohamed Abd El-Samad (E1)
until Sept. 30, 1998
Research Scholarship
(Atom Energy Agency, Cairo, Egypt)

C. Fanara (E1)
from Jan. 12 to Dec. 31, 1998
(INFN, Italien)

Dr. L. Freindl (E1)
from July 5 to Aug. 1, 1998
(Kernforschungszentrum Krakau, Poland)

G. Gellas (Th)
from September 19 to September 25, 1998
(University of Athen, Greece)

Ing. G. Georgiev (E1)
from Aug. 1 to 14, 1998
(Inst. for Nucl. Res. and Nucl. Energy, Sofia, Bulgaria)

Dr. A. Gerasimov (E2)
from March 23 to April 17, 1998
from August 2 to 30, 1998
(Institute for Theoretical and Experimental Physics, Moskau)

Prof. S. Gevorkyan (Th)
from March 9 to April 3, 1998
(Yerevan Phys. Inst., Armenia)

Dr. E. Golubeva (E2)
from January 18 to February 28, 1998
from June 28 to July 26, 1998
from November 16 to December 18, 1998
(Institute for Theoretical and Experimental Physics, Moskau)

Dr. V. Goryachev (E2)
from November 15 to December 13, 1998
(Institute for Theoretical and Experimental Physics, Moskau)

Dr. V. Grishina (E2)
from September 27 to November 8, 1998
(Institute for Theoretical and Experimental Physics, Moskau)

Dr. L. Gusev (E2)
from January 17 to February 15, 1998
(Institute for Theoretical and Experimental Physics, Moskau)

Moh. A.G. Hassan (E1)
until March 31, 1998
(Research sholarship)
(Atom Energy Agency, Cairo, Egypt)

P. Hawronek (E1)
from March 23 to April 5, 1998
from July 13 to 25, 1998
from Oct. 11 to Oct. 26, 1998
(Univ. Krakau, Poland)

Prof. Dr. B. Holstein (Th)
(AvH-Awardee)
from February 17 to June 15, 1998
(University of Massachusetts, USA)

Prof. Dr. B. Ioffe (Th)
(AvH-Awardee)
from September 6 to November 14, 1998
(ITEP Moscow, Russia)

Y. Ilieva (E1)
Research sholarship
(Inst. of Nucl. Res. and Nucl. Energy, Sofia, Bulgaria)

D. Ivanov (Th)
from November 6 to November 13, 1998
(Akademik Koptyuk, Novosibirsk, Russia)

DP Helge Jungwirth (LI)
from June 29 to July 10, 1998
(NAC, South Africa)

Prof. S. Kamerdzhiev (Th)
from September 17 to November 14, 1998
(IPPE, Obninsk, Russia)

Prof. B. Kamys (E2)
from February 8 to 21, 1998
from November 15 to 21, 1998
(Jagellonian University Cracow, Poland)

Dr. A. Katcharava (E2)
from July 5 to 26, 1998
from October 25 to December 6, 1998
(Joint Inst. for Nucl. Res., Dubna, Moskau)

V. Khokhloc (E2)
from March 23 to April 17, 1998
from August 2 to 30, 1998
(Institute for Theoretical and Experimental Physics, Moskau)

Dr. St. Kistryn (E1)
from March 23 to April 5, 1998
from July 13 to 28, 1998
(Univ. Krakau, Polen)

Dr. St. Kliczewski (E1)
from March 22 to April 8, 1998
from July 5 to Aug. 1, 1998
from Oct. 4 to 31, 1998
(Kernforschungszentrum Krakow, Poland)

W. Klimala (E1)
(Jagellonian Univ. of Krakow, Poland)

Dr. D. Kolev (E1)
from Feb. 10 to April 30, 1998
from July 9 to 30, 1998
from Oct. 1 to Nov. 13, 1998
(University of Sofia, Sofia, Bulgaria)

Prof. V. Komarov (E2)
from February 1 to April 20, 1998
from October 25 to November 22, 1998
(Joint Inst. for Nucl. Res., Dubna, Moskau)

Prof. L. Kondratyuk (E2)
from November 15 to 19, 1998
(Institute for Theoretical and Experimental Physics, Moskau)

Prof. V. Koptev (E2)
from June 28 to July 26, 1998
from September 6 to October 7, 1998
from October 18 to November 28, 1998
from December 9 to 20, 1998
(St. Petersburg Nucl. Phys. Inst., Gatchina, St. Petersburg)

Dr. A. Kovalev (E2)
from October 14 to November 11, 1998
(St. Petersburg Nucl. Phys. Inst., Gatchina, St. Petersburg)

Dr. S. Kulagin (Th)
from February 3 to February 28, 1998
(Russische Akademie d. Wissenschaften, Moscow, Russia))

Prof. Dr. A. Kudryavtsev (Th)
from August 15 to September 15, 1998
from November 10 to December 9, 1998
(ITEP Moscow, Russia)

Dr. A. Kulikov (E2)
from March 22 to April 12, 1998
from July 5 to 20, 1998
from September 26 to October 11, 1998
(Joint Inst. for Nucl. Res., Dubna, Moskau)

Prof. Dr. E. Kuraev (Th)
from January 12 to February 20, 1998
(JINR Dubna, Russia)

Dr. V. Kurbatov (E2)
from January 20 to February 17, 1998
from September 9 to October 11, 1998
from October 12 to November 8, 1998
(Joint Inst. for Nucl. Res., Dubna, Moskau)

Prof. T. Kutsarova (E1)
from Feb. 23 to March 9, 1998
(Acad. Science, Sofia, Bulgaria)

Prof. Dr. R. Lemmer (Th)
(AvH-Awardee)
from May 1 to July 31, 1998
(University of Witwatersrand, Johannisburg, South Africa)
Dr. V. Leontiev (E2)
from November 1 to December 6, 1998
(Joint Inst. for Nucl. Res., Dubna, Moskau)

Dr. G. Macharashvili (E2)
from March 22 to April 12, 1998
from October 25 to November 22, 1998
(Joint Inst. for Nucl. Res., Dubna, Moskau)

Dr. A. Magiera (E1)
from Jan. 27 to Feb. 28, 1998
from March 18 to April 8, 1998
from July 4 to 30, 1998
from Oct. 14 to Oct. 25, 1998
(Kernforschungszentrum Krakau, Poland)

J. Majewski (E1)
from March 9 to April 8, 1998
from May 2 to 30, 1998
from June 20 to July 20, 1998
from Aug. 15 to Sept. 14, 1998
from Oct. 17 to Dec. 16, 1998
(Jagellonian Univ. of Krakow, Poland)

Dr. S. Merzliakov (E2)
from September 20 to November 26, 1998
(Joint Inst. for Nucl. Res., Dubna, Moskau)

Dr. S. Mikirtytchiants (E2)
from June 28 to July 22, 1998
from September 20 to October 7, 1998
from October 18 to November 17, 1998
(St. Petersburg Nucl. Phys. Inst., Gatchina, St. Petersburg)

P. Moskal (E1)
from Jan. 26 to Feb. 20, 1998
(Jagellonian Univ. of Krakow, Poland)

U. Mostafa (E1)
from Feb. 15 to May 19, 1998
Research sholarship
(Atom Energy Agency, Cairo, Egypt)

Prof. Dr. K. Nakayama (Th)
from June 12 to August 20, 1998
(University of Georgia, Athens, USA)

Prof. V. Nelyubin (E2)
from June 14 to July 12, 1998
from October 18 to November 29, 1998
(St. Petersburg Nucl. Phys. Inst., Gatchina, St. Petersburg)

Prof. M. S. Nioradze (E2)
from July 5 to 25, 1998
from October 28 to November 7, 1998
(High Energy Phys. Inst., Tbilisi State University, Tbilisi, Georgien)

Prof. W.T. van Oers (E1)
from May 5 to Dec. 31, 1998
(Univ. of Manitoba, Canada)

Dr. L. Pentchev (E1)
from Oct. 5 to Oct. 31, 1998
(INRE, Sofia, Bulgaria)

Dr. O. Petrus (E2)
from January 1 to March 31,1998
from October 12 to November 8, 1998
(Joint Inst. for Nucl. Res., Dubna, Moskau)

H. du Plessis (LI)
from Sept. 21 to Oct. 8, 1998
(NAC, South Africa)

Dr. A. Prokofiev (E1)
from March 8 to 15, 1998
(St. Petersburg Nucl. Phys. Inst., Gatchina, St. Petersburg)

Dr. K. Pycz (E2)
from July 5 to 26, 1998
from September 23 to October 14, 1998
(Jagellonian University Cracow, Poland)

Prof. Dr. R.D. Ratna-Raju (Th)
from October 24 to November 1, 1998
(University of Visakhapatnam, India)

Dr. R. Rapp (Th)
from June 15 to July 12, 1998
(SUNY at Stony Brook)

Dr. Z. Rudy (E2)
from July 5 to 26, 1998
from September 21 to October 3, 1998
from November 2 to 21, 1998
(Jagellonian University Cracow, Poland)

Dr. T. Rzaca-Urban (E1)
from Aug. 17 to 30, 1998
(Inst. of Exp. Physics, Warsaw, Poland)

Prof. Dr. L.N. Satpathy (Th)
from September 12 to September 16, 1998
(Inst. of Physics, Bhubaneswar, India)

Dr. R. Siudak (E1)
from March 22 to April 8, 1998
from July 5, to Aug. 3, 1998
from Oct. 4 to 31, 1998
(Jagellonian Univ. of Krakow, Poland)

Dr. J. Smyrski (E1)
from Feb. 14 to 26, 1998
(Jagellonian Univ. of Krakow, Poland)

Dr. E. Strokovsky (E1)
from March 8 to 15, 1998
(JINR Dubna, Moscow)

Dr. A. Szczurek (Th)
(DLR-fellow)
from August 7 to September 4, 1998
from October 9 to November 10, 1998
(Univ. of Krakow, Poland)

Dr. P.-E. Tegner (E1)
from March 15 to 27, 1998
(University of Stockholm, Sweden)

Dr. G. Tertychny (Th)
(DFG-fellow)
from January 9 to March 7, 1998
from September 16 to November 14, 1998
(IPPE, Obninsk, Russia)

Dr. R. Tsenov (E1)
from Feb. 16 to March 5, 1998
(University of Sofia, Sofia, Bulgaria)

Dr. A. Vassiliev (E2)
from September 20 to October 21, 1998
from November 1 to 22, 1998
(St. Petersburg Nucl. Phys. Inst., Gatchina, St. Petersburg)

Prof. Dr. E. Veit (Th)
from June 15 to July 14, 1998
(University Rio Grande do Sul, Porto Alegre, Brasil)

Dr. Y. Venkova (E1)
from April 14 to June 15, 1998
(Bulgarische Akademie der Wissenschaften, Sofia,
Bulgarien)

Prof. C. Wilkin (E2)
from February 11 to 15, 1998
from August 17 to 29, 1998
(University College London, GB)

Dr. M. Wojcik (Th)
from February 25 to March 20, 1998
from October 1 to November 30, 1998
(University of Krakow, Poland)

Dr. S. Yaschenko (E2)
from December 3 to 24, 1998
(Joint Inst. for Nucl. Res., Dubna, Moskau)

Dr. B.G. Zakharov (Th)
(DFG-fellow)
from October 29, 1998 to January 19, 1999
(Landau Inst. for Theor. Phys., Moscow, Russia)

Dr. B. Zalikhanov (E2)
from December 3 to 24, 1998
(Joint Inst. for Nucl. Res., Dubna, Moskau)

Dr. N. Zhuravlev (E2)
from January 1 to February 15, 1998
(Joint Inst. for Nucl. Res., Dubna, Moskau)

Dr. V. Zoller (Th)
(DFG fellow)
from March 9 to April 28, 1998
from October 29 to December 23, 1998
(ITEP, Moskow, Russia)

P. Zupranski (E1)
from March 9 to 22, 1998
from Sept. 7 to 25, 1998
(Soltan Institute for Nuclear Studies, Warschau, Poland)

Dr. I. Zychor (E2)
January 5 to April 4, 1998
May 25 to June 24, 1998
September 14 to October 13, 1998
November 8 to 27, 1998
(Soltan Inst. for Nucl. Studies, Swierk-Otwock, Poland)

X. PUBLICATIONS

Journals

IKP-98-11-001
Achenbach, P., Altarev, I., Grimm, K., Hammel ,T., von Harrach, D., Hoffmann, J., Hofmann, H., Kabuß, E.-M., Köbis, S., Lopes Ginja, A., Maas. F.E., Schilling, E., Ströher, H.
Radiation Resistance and Optical Properties of Lead Fluoride Cherenkov Crystals
Nucl. Instr. Meth. A416 (1998) 357
20.50.0

IKP-98-11-002
Anagnostopoulos, D., Augsburger, M., Belmiloud, D., Borchert, G., Castelli, C., Chatellard, D., Daum, M., Egger, J.P., El-Khoury, P., Elble, M., Frosch, R., Gorke, H., Gotta, D., Hauser, P., Indelicato, P., Kirch, K., Lenz, S., Nelms, N., Rashid, K., Schult, O.W.B., Siems, Th., Simons, L.M.
High Precision X-ray Spectroscopy in Hydrogen-like Fermionic and Bosonic Atomic Systems
Proc. 3rd Euroconference on Atomic Physics with Stored Highly Charged Ions
Ferrara, Italy, 22.-26.9.1997
Hyperfine Interactions, 114, 157 (1998)
20.50.0

IKP-98-11-003
Anagnostopoulos, D., Augsburger, M., Belmiloud, D., Borchert, G., Chatellard, D., Daum, M., Egger, J.P., El-Khoury, P., Gorke, H., Gotta, D., Hauser, P., Indelicato, P., Kirch, K., Lenz S, Siems, Th., Simons, L.M.
A New Determination of the Mass of the Charged Pion
Phys. Rev. Lett. B 416 (1998) 50
20.50.0

IKP-98-11-004
Anagnostopoulos, D.F., Augsburger, M., Belmiloud, D., Borchert, G., Chatellard, D., Daum, M., Egger, J.-P., El-Khoury, P., Gorke, H., Gotta, D., Hauser, P., Indelicato, P., Kirch, K., Lenz, S., Siems, T., Simons, L. M.,
A New Determination of the Mass of the Charged Pion
Phys. Lett. B 416 (1998) 50
20.50.0

IKP-98-11-005
Anagnostopoulos, D.F., Amundsen, P.A., Borchert, G., Gotta, D., Jakubassa-Amundsen, D.H., Rashid, K.,
High Resolution Study of Ion Induced $K\alpha_{1,2}$ X-Ray Spectra from High-Z Elements
Phys. Rev. A 58 (1998) 2797
20.50.0

IKP-98-11-006
Anagnostopoulos, D.F., Augsburger, M., Borchert, G., Chatellard, D., Egger, J.-P., El-Khoury, P., Gotta, D., Hauser, P., Indelicato, P., Kirch, K., Siems, Th., Simons, L.M.
A New Precision Measurement of the Pionic Deuterium S-Wave Strong Interaction Parameters
Phys. Rev. C 58 (1998) 1869
20.50.0

IKP-98-11-007
Appenheimer, M., Averbeck, R., Charbonnier, Y., Diaz, J., Döppenschmidt, A., Hejny, V., Hlavac, S., Holzmann, R., Kugler, A., Löhner, H., Marin, A., Metag, V., Novotny, R., Ostendorf, R.W., Pleskac, R., Schubert, A., Schutz, Y., Simon, R.S., Ströher, H., Tlusty, P., Vogt, P.H., Wagner, V., Weiß, J., Wilschut, H.W., Wissmann, F., Wolf, A.R., Wolf, M.
Multistep Production of η and Hard π^0 Mesons in Subthreshold Au-Au Collisions
Phys. Rev. Lett. 80 (1998) 5281
20.50.0

IKP-98-11-008
Arbuzov, A.B., Krehl O, Kuraev E.A., Magar E., Shaikhatdenov B.G.
Radiative Corrections to the Background of $\mu \rightarrow e\gamma$ Decay
Phys. Lett. B432 (1998) 421-426
20.80.0

IKP-98-11-009
Balewski J.T., Budzanowski A., Dombrowski H., Goodman C., Grzonka D., Haidenbauer J., Hanhart C., Jarczyk L., Jochmann M., Khoukaz A., Kilian K., Kohler M., Kozela A., Liste T., Meißner Ulf-G., Moskal P., Nikolaev N.N., Oelert W., Quentmeier C., Santo R., Schepers G., Seddik U., Sefzik T., Smyrski J., Sokolowski M., Strzalkowski A., Thomas C., Wolke M., Wustner P., Wyrwa D.
η' Production in Proton-Proton Scattering Close to Threshold
Phys. Rev. Lett. 80 (1998) 3202-3205
20.80.0

IKP-98-11-010
Balewski, J.T., Daehnick, W.W., Doskow, J., Dzemidzic, M., Flammang, R.W., Haeberli, W., Lorentz, B., Meyer, H.O., Pancella, P.V., Pollock, R.E., von, Przewoski, B., Rathmann, F., Rinckel, T., Schwartz, B., Sperisen, F., Swapan, K., Saha, Tedeschi, D.J., Thörngren-Engblom, P., Wise, T., Wolanski, M.,
Dependence of $\vec{p}\vec{p} \rightarrow pp\pi^0$ near Threshold on the Spin of the Colliding Nucleons
Phys. Rev. Lett., 81, 3096 (1998)
20.50.0

IKP-98-11-011
Balewski, J. et al.
Low-energy Λ-p scattering parameters from the $pp \rightarrow pK^+\Lambda$ Reaction
Eur. Phys. J A2, 99-104 (1998)
20.50.0

IKP-98-11-012
Bargholtz, Chr.; Frannson, K.; Holmberg, L.; Lindh, K.; Sandberg, L.; Protic, D.; Sitnikova, I.; Tegner, P.-E.; Thörngren Engholm, P.; Weiss, G.; Wilhelmsen Rolander, K.
A Zero-Degree Spectrometer in CELSIUS and the $d(d,2\pi)^4$He Reaction Close to Threshold
Nucl. Phys. A626 (1997) 73c
20.20.0

IKP-98-11-013
Baur G., Hencken K., Trautmann D.
Photon-Photon Physics in Very Peripheral Collisions of Relativistic Heavy Ions
Topical Review, Journal of Physics G:
Nucl. Part. Phys. 24 (1998) 1657-1691
20.80.0

IKP-98-11-014
Beane S.R., Bernard V., Lee T.-S.H, Meißner Ulf-G.,
Isoscalar S-wave πN Scattering Length a^+ from π Deuteron Scattering
Phys. Rev. C57 (1998) 424-426
20.80.0

IKP-98-11-015
Beck, R., Döring, W., Mengel, K., Metag V., Novotny, R., Ströher, H.
Detection of Monochromatic Photons Between 50 and 790, MeV with a $PbWO_4$ Scintillator Array
IEEE Trans. On Nucl. Sci. 45 (1998) 681
20.50.0

IKP-98-11-016
Bernard V., Fearing H. ,Hemmert T., Meißner Ulf-G.
The Form-Factors of the Nucleon at Small Momentum Transfer
Nucl. Phys. A635 (1998) 121-145
20.80.0

IKP-98-11-017
Bertini M., Genovese M., Nikolaev N.N., Pronyaev A.V., Zakharov B.G.
Twist-4 Effects and Q^2 Dependence of Diffractive DIS
Phys. Lett. B422 (1998) 238
20.80.0

IKP-98-11-018
Bertulani C.A., Baur G.
Antihydrogen Production and Accuracy of the Equivalent Photon Method
Phys. Rev. D58 (1998) 034005
20.80.0

IKP-98-11-019
Bilger, R., Böhm, A. Brand, H., Brand, S. Brinkmann, K.-Th., Clement, H., Cloth, P., Dahmen, M., Dshemuchadse, S. Eyrich, W., Filges, D., Freiesleben, H., Fritsch, M., Geyer, R., Hassan, A., Hauffe, J., Herrmann, P., Hübner, B., Jahn, P. Kilian, K., Koch, H., Kress, J., Krug, J., Kuhlmann, E., Lange, J.S., Metzger, A., Michel, P., Möller, K., Morsch, H.P., Nake, Ch., Nann, H., Naumann, B., Naumann, L., Ringe, P., Roderburg, E., Rogge, M., Schamlott, A., Schönmeier, P., Schülke, A., Steinke, M., Stinzing, F., Turek,P., Wagner, G.J.,Wirth, S., Zielinski, U.
Proton-Proton Bremsstrahlung at 797 MeV/c
Phys. Lett. B 429 (1998) 195-200
20.45.0

IKP-98-11-020
Bilger, R., Böhm,.Brand, A., Brand, S., Brand,.H., Brinkmann, K.-Th., Clement, H., Cloth, P., Dahmen, M., Dellert, M., Dennert, H., Dshemuchadse, S. Eyrich, W., Filges, D., Freiesleben, H., Fritsch, M., Geyer, R., Hassan, A., Hauffe, J., Herrmann, P., Hübner, B., Jahn, P. Kilian, K., Kirsch, M., Koch, H., Kress, J., Krug, J., Kuhlmann, E., Lange, J.S., Metzger, A., Michel, P., Möller, K., Morsch, Moosburger, M., H.P., Nake, Ch., Nann, H., Naumann, B., Naumann, L., Ringe, P., Roderburg, E., Rogge, M., Schamlott, A., Schönmeier, P., Schülke, A., Sperl, R., Steinke, M., Stinzing, F., Turek, P., Wagner, G.J., Wirth, S., Zielinski, U.
Strangeness Production in the Reaction $pp \rightarrow pK^+\Lambda$ in the Threshold Region
Phys. Lett. B 420 (1998) 217
20 45 0

IKP-98-11-021
Blanpied, G., Blecher, M., Caracappa, A., Djalali, C., Giordano, G., Hicks, K., Hoblit, S., Khandaker, M., Kistner, O.C., Kuczewski, A., Lowry, M., Lucas, M., Matone, G., Preedom, B., Rebreyand, D., Sandorfi, A.M.,Schaerf, C., Sealock, R.M., Ströher, H., Thorn, C.E., Thornton, S.T., Whisnant, C.S., Zhang, H., Zhao, X.
The E2/M1 – Ratio in Delta Photoproduction
Nucl. Phys. A629 (1998) 171c
20.50.0

IKP-98-11-022
Borgs, W., Cassing, W., Hartmann, M., Hodde, H., Jarczyk, L., Kamys, B., Koch, H.R., Kulessa, P., Maier, R., Matoba, M., Ohm, H., Prasuhn, D., Pysz, K., Rudy, Z., Schult, O.W.B., Strzalkowski, A., Zychor, I.
K-Λ Production in p + Bi Interaction
Act. Phys. Pol. B, 29 (1998)
20.45.0

IKP-98-11-023
Borgs, W.; Cassing, W.; Hartmann, M.; Hodde, Kamys, B.; H.; Koch, H.R.; Kulessa, P.; Maier R.; Matoba M; Ohm, H.; Prasuhn, D.; Pysz, K.; Rudy, Z.; Schult, O.W.B.; Z.; Strzalkowski, A.; Zychor, I.
Measurement of the lifetime of heavy hypernuclei produced in the bombardment of Bi with protons
Nuclear Physics A639 (1998) 283c-286c
20.30.5

IKP-98-11-024
Borgs, W., Cassing, W., Hartmann, M., Hodde, H., Jarczyk, L., Kamys, B., Koch, H.R., Kulessa, P., Maier, R., Matoba, M., Ohm, H., Prasuhn, D., Pysz, K., Rudy, Z., Schult, O.W.B.,Strzalkowski, A., Zychor, I.,
Production of heavy hypernuclei in the p + Bi reaction and determination of their lifetime for fission induced by Λ, decay
Phys. Lett. B 427 (1998) 403
20.45.0

IKP-98-11-025
Borgs, W., Cassing, W., Hartmann, M., Hermes, T., Jarczyk, L., Kamys, B., Koch, H.R., Kulessa, P., Maier, R., Ohm, H., Prasuhn, D., Pysz, K., Rudy, Z., Stein, H.J., Strzalkowski, A., Schult, O.W.B., Uozumi, Y., Zychor, I.,
Investigation of production and fission decay of heavy hypernuclei at COSY Jülich
Nucl. Phys. A629 (1998) 416c
20.45.0

IKP-98-11-026
Borgs, W., Cassing, W., Hartmann, M., Hodde, H., Kamys, B., Koch, H.R., Kulessa, P., Maier, R., Matoba, M., Ohm, H., Prasuhn, D., Pysz, K., Rudy, Z., Schult, O.W.B.,Strzalkowski, A., Zychor, I.,
Measurement of the lifetime of heavy hypernuclei produced in the bombardment of Bi with protons
Nucl. Phys. A639 (1998) 283c
20.45.0

IKP-98-11-027
Borgs, W., Cassing, W., Hartmann, M., Hermes, T., Jarczyk, L Kamys, B., Koch, H.R., Kulessa, P., Maier, R., Ohm, H., Pfeiffer, J., Prasuhn, D., Pysz, K., Rudy, Z., Schult, O.W.B., Strzalkowski, A., Uozumi, Y., Zychor, I.
Measurement of the lifetime of heavy Λ hypernuclei with the recoil shadow method and internal targets in the storage ring COSY-Jülich
Nucl. Instr. Meth. A420 (1998) 356
20.45.0

IKP-98-11-028
Büttiker P.
Higher Threshold Parameters in $\pi\pi$ Scattering
Phys. Lett. B415 (1997) 402-410
20.80.0

IKP-98-11-029
Calén, H. et al.
Threshold Structure of the Quasifree p+n → d+η Reaction
Phys. Rev. Lett. 80, No. 10, (1998) 2069
20.45.0

IKP-98-11-030
Calén, H. et al.
Upper Limits for a Narrow Dibaryon in pp Collisions at 200 and 310 MeV
Phys. Lett. B 427 (1998) 248-253
20.45.0

IKP-98-11-031
Calén, H. et al.
Measurement of the Quasifree pn→pnη Reaction
Phys. Rev. C58 (1998) 2667
20.50.0

IKP-98-11-032
Chen B.Q., Grümmer F., Krewald S., Ma Z.Y.,
Relativistic Mean-field Theory of Proton Halos in the 2s1d Shell
J. Phys. G24 (1998) 97
20.80.0

IKP-98-11-033
Cloth, P.; Filges, D. and the members of the ZEUS Collaboration:
Measurement of the Diffractive Structure Function $F_2^{D(4)}$ at HERA
Eur. Phys. J. C 1 (1998) 81-96
20.48.0

IKP-98-11-034
Cloth, P.; Filges, D. and the members of the ZEUS Collaboration:
Dijet Cross Sections in Photoproduction at HERA
Eur. Phys. J. C 1 (1998) 109-122
20.48.0

IKP-98-11-035
Cloth, P.; Filges, D. and the members of the ZEUS Collaboration:
Measurement of jet shapes in Photoproduction at HERA
Eur. Phys. J. C 2 (1998) 61-75
20.48.0

IKP-98-11-036
Cloth, P.; Filges, D. and the members of the ZEUS Collaboration:
Charged Particles and Neutral Kaons in Photoproduced Jets at HERA
Eur. Phys. J. C 2 (1998) 77-93
20.48.0

IKP-98-11-037
Cloth, P.; Filges, D. and the members of the ZEUS Collaboration:
Elastic and Proton-Dissociative ρ^0 Photoproduction at HERA
Eur. Phys. J. C 2 (1998) 247-267/Report, DESY 97-237, Dec. 1997
20.48.0

IKP-98-11-038
Cloth, P.; Filges, D. and the members of the ZEUS Collaboration:
Measurement of the t Distribution in Diffractive Photoproduction at HERA
Eur. Phys. J. C 2 (1998) 237-246/ Report, DESY 97-238, December 1997
20.48.0

IKP-98-11-039
Cloth, P.; Filges, D. and the members of the ZEUS Collaboration:
High-E_T Inclusive Jet Cross Sections in Photoproduction at HERA
Eur. Phys. J. C 4 (1998) 591-606/Report, DESY 98-018, Feb. 1998
20.48.0

IKP-98-11-040
Cloth, P.; Filges, D. and the members of the ZEUS Collaboration:
Diffractive Dijet Cross Sections in Photoproduction at HERA
Eur. Phys. J. C 5 (1998) 41-56
20.48.0

IKP-98-11-041
Cloth, P.; Filges, D. and the members of the ZEUS Collaboration:
Forward Jet Production in Deep Inelastic Scattering at HERA
Eur. Phys. J. C 6, (1999) 239-252/Report, DESY 98-050, May 1998
20.48.0

IKP-98-11-042
Cloth, P.; Filges, D. and the members of the ZEUS Collaboration:
Event Shape Analysis of Deep Inelastic Scattering Events with a Large Rapidity Gap at HERA
Phys. Lett. B 421 (1998) 368-384
20.48.0

IKP-98-11-043
Cloth, P.; Filges, D. and the members of the ZEUS Collaboration:
Search for selectron and squark production in e^+p collisions at HERA
Phys. Lett. B 434 (1998) 214-230/Report, DESY 98-069, June 1998
20.48.0

IKP-98-11-044
Cloth, P.; Filges, D. and the members of the ZEUS Collaboration:
Measurement of the Diffractive Cross Section in Deep Inelastic Scattering Using ZEUS 1994 Data
Eur. Phys. J. C 6 (1999) 43-66/Report, DESY 98-084, July 1998
20.48.0

IKP-98-11-045
Cloth, P.; Filges, D. and the members of the ZEUS Collaboration:
Measurement of Inclusive $D^{*\pm}$ and Associated Dijet Cross Sections in Photoproduction at HERA
Eur. Phys. J. C 6 (1999) 67-83/Report, DESY 98-085, July 1998
20.48.0

IKP-98-11-046
Dezarn, W., A., Doskow, J., Dzemidzic, M., Haeberli, W., Hardie, J.G., Lorentz, B., Meyer, H.O., Pancella, P.V., Pollock, R.E., v.Przewoski, B., Rathmann, F., Rinckel, T., Sperisen, F., Wise, T.
Proton-proton analyzing power and spin correlation measurements between 250 and 450 MeV at 7°, ≤, $\theta_{c.m.}$, ≤, 90° with an internal target in a storage ring,
Phys. Rev. C 58, 1897 (1998)
20.50.0

IKP-98-11-047
Dezarn, W.A., Doskow, J., Dzemidzic, M., Haeberli, W., Hardie, J.G., Lorentz, B., Meyer, H.O., Pancella, P.V., Pollock, R.E., von, Przewoski, B., Rathmann, F., Rinckel, T., Sperisen, F., Wise, T.
Complete angular distribution measurements of pp spin correlation parameters A_{xx}, A_{yy}, and A_{xz} and analyzing power A_y at 197.4 MeV, \
Phys. Rev. C 58, 658 (1998)
20.50.0

IKP-98-11-048
Drochner, M., Ernst, J., Förtsch, S., Freindl, L., Frekers, D., Garske, W., Grewer, K., Igel, S., Jahn, R., Jarczyk, L., Kemmerling, G., Kilian, K., Kliczewski, S., Klimala, W., Kolev, D., Kutsarova, T., Lippert, G., Machner, H., Maier, R., Nake, C., Razen, B., von Rossen, P., Roy, B.R., Schok, K., Siudak, R., Smyrski, A., Strzalkowski, A., Tsenov, R., Zolnierczuk, A., Zwoll, K.
The $p+p\rightarrow\pi^{+}+d$ Reaction Close to Threshold at COSY
Nucl. Phys. A643 (1998) 55
20.45.0

IKP-98-11-049
Drozdz S., Nishizaki S., Speth J., Wojcik M.
Collectivity Embedded in Complex Spectra of Finite Interacting Fermi Systems: Nuclear Example
Phys. Rev. E57 (1998) 4016
20.80.0

IKP-98-11-050
Epelbaum E., Glöckle W., Meißner Ulf-G.
Low Momentum Effective Theory for Nucleons
Phys. Lett. B439 (1998) 1-5
20.80.0

IKP-98-11-051
Epelbaum E., Glöckle W., Meißner Ulf-G.
Nuclear Forces from Chiral Lagrangians Using the Method of Unitary Transformation, 1. Formalism
Nucl. Phys. A637 (1998) 107-134
20.80.0

IKP-98-11-052
Erven, W., Junghans, H., Koch, H.R., Langenhagen, H., Zwoll K.,
An Overall MWPC-Readout System Based on Chamber Mounted ASIC´s
IEEE Trans. On Nucl. Sci. 45 (1998)
20.45.0

IKP-98-11-053
Fettes N., Meißner Ulf-G., Steininger S.
Pion-Nucleon Scattering in Chiral Perturbation Theory, 1. Isospin Symmetric Case
Nucl. Phys. A640 (1998) 199-234
20.80.0

IKP-98-11-054
Hagedoorn, H.L.; Leunissen, L.H.A., Maier, R.
Measurement of third order Hamilton coefficients at COSY
ICFA Beam Dynamics Newsletter, No.16
20.30.0

IKP-98-11-055
Haidenbauer J., Speth J.
Meson-Meson and Meson-Nucleon Scattering and the Structure of Hadrons
Nucl. Phys. A629 (1998) 111c-120c
20.80.0

IKP-98-11-056
Haidenbauer J., Hanhart C., Speth J.
Threshold Pion Production in Nucleon-Nucleon Collisions
Nucl. Phys. A631 (1998) 515-518
20.80.0

IKP-98-11-057
Haidenbauer J. and the COSY-11 Collaboration
Total Cross Section of the Reaction $pp\rightarrow pK^{+}\Lambda$ close to Threshold
Phys. Lett. B420 (1998) 211-216
20.80.0

IKP-98-11-058
Hanhart C, Haidenbauer J., Hoffmann M., Meißner Ulf-G., Speth J.
The Reactions $pp\rightarrow pp\pi^{0}$ and $pp\rightarrow D\pi^{+}$ at Threshold: The Role of the Isoscalar πN Scattering Amplitude
Phys. Lett. B424 (1998) 8-14
20.80.0

IKP-98-11-059
Haidenbauer J. and the COSY-11 Collaboration
η-Production in Proton-Proton Scattering close to Threshold
Phys. Rev. Lett. 80 (1998), 3202-3205
20.80.0

IKP-98-11-060
Hanhart C., Haidenbauer J., Krehl O., Speth J.
Role of the Δ Isobar in the Reaction $NN\rightarrow NN\pi$ near Threshold
Phys. Lett. B 444 (1998) 25-31
20.80.0

IKP-98-11-061
Hemmert T., Holstein B.
Heavy Baryon Chiral Perturbation Theory with Light Deltas
J. Phys. G24 (1998) 1831-1859
20.80.0

IKP-98-11-062
Hemmert T., Meißner Ulf-G., Steininger S.
Strange Magnetism in the Nucleon
Phys. Lett. B437 (1998) 184-190
20.80.0

IKP-98-11-063
Hemmert T., Holstein B., Kambor J., Knochlein, G.
Compton Scattering and the Spin Structure of the Nucleon at Low-Energies
Phys. Rev. D57 (1998) 5746-5754
20.80.0

IKP-98-11-064
Holstein B., Donoghue J.F.
Improved Treatment of Loop Diagrams in SU(3) Baryon Chiral Perturbation Theory
Phys. Lett. B436 (1998) 331-38
20.80.0

IKP-98-11-065
Kamerdzhiev S., Liotta R., Litvinova E., Tselyaev V.
Continuum Quasiparticle Random Phase Approximation Description of Isovector E1 Giant Resonances
Phys. Rev. C58 (1998) 172
20.80.0

IKP-98-11-066
Kilian, K.
First Results from COSY
Nucl. Phys. A629 (1998) 303c-314c
20.45.0

IKP-98-11-065
Kilian, K., Meißner, U.-G., Speth, J.
Physik am Kühlersynchrotron COSY
Phys. Bl. 54 (1998) Nr. 10
20.45.0, 20.80.0

IKP-98-11-067
Kuraev E.V., Nikolaev N.N., Zakharov B.G.
Diffractive Vector Mesons beyond the s-Channel Helicity Conservation
JETP Lett. 68, 667 (1998)
20.80.0

IKP-98-11-068
Machner, H.
Low Energy Pion Reactions
Nucl. Phys. A 633 (1998) 341-354
20.45.0

IKP-98-11-069
Maier, R.; Prasuhn, D.; Röser, A.; Schilcher, R.B.; Schneeweiß, F.; Tölle, R.
Physikalische Rahmenbedingungen für die Bestrahlung von Zellkulturen mit 45 MeV Protonen am Zyklotron des Forschungszentrum Jülich
Strahlentherapie und Onkologie (1998); Sondernr. 1, 59
20.30.0

IKP-98-11-070
Meier H., Halabuka Z., Hencken K., Trautmann D., Baur G.
Relativistic Antihydrogen Production
The European Physical Journal C5 (1998) 287-291
20.80.0

IKP-98-11-071
Meier H., Hencken K., Trautmann D., Baur G.
Bremsstrahlung Pair Production in Relativistic Heavy Ion Collision
European Phys. J. c2 (1998) 741-746
20.80.0

IKP-98-11-072
Meißner Ulf-G., Steininger S.
Isospin Violation in Pion-Nucleon Scattering
Phys. Lett. B419 (1998) 403-411
20.80.0

IKP-98-11-073
Meißner Ulf-G.
Hadron Structure in the Non-Perturbative Regime of QCD: Isospin Symmetry and its Violation
Nucl. Phys. A629 (1998) 72c-81c
20.80.0

IKP-98-11-074
Melnitchouk W., Speth J., Thomas A.W.
Semi-Inclusive Pion Probes of the Large x d/u Ratio
Phys. Lett. B435 (1998) 420-426
20.80.0

IKP-98-11-075
Nakayama K., Szczurek A., Hanhart C., Haidenbauer J., Speth J.
Production of ω-Mesons in Proton-Proton Collisions
Phys. Rev. C57 (1998) 1580-1587
20.80.0

IKP-98-11-076
Nemchik J., Nikolaev N.N., Predazzi E., Zakharov B.G., Zoller V.R.
The Diffraction Cone for Exclusive Vector Meson Production in Deep Inelastic Scattering
J. Exp. Theor. Phys. 86, 1054 (1998)
20.80.0

IKP-98-11-077
Nemoto S., Chmielewski K., Schellingerhout N.W., Haidenbauer J., Oryu S., Sauer P.U.
Nucleon-Deuteron Scattering with Δ-Isobar Excitation I: Test of Separable Expansion
Few Body Systems 24, 1998
20.80.0

IKP-98-11-078
Nemoto S., Chmielewski K., Meyer U., Haidenbauer J., Oryu S., Sauer P.U.
Nucleon-Deuteron Scattering with Δ-Isobar Excitation II: Elastic Scattering
Few Body Systems 24, 1998
20.80.0

IKP-98-11-079
Nikolaev N.N., Pronyaev A.V., Zakharov B.G.
Predictions for the Forward Cone in Diffractive DIS
JETP Lett. 68, 604 (1998)
20.80.0

IKP-98-11-080
Nikolaev N.N.
Scaling Properties of Transverse Flow in Bjorken's Scenario for Heavy Ion Collisions
JETP Lett. 68, 191 (1998)
20.80.0

IKP-98-11-081
Oelert, W. et al.
Associated Strangeness Production in the Threshold Region
Nucl. Phys. A639 (1998) 13c
20.50.0

IKP-98-11-082
Oelert, W. et al.
Total Cross Section of the Reaction $pp \rightarrow pK^+\Lambda$ Close to Threshold
Phys. Lett. B420 (1998) 211
20.50.0

IKP-98-11-083
Oelert, W. et al.
η`Production in Proton-Proton Scattering Close to Threshold
Phys. Rev. Lett. 80 (1998) 3202
20.50.0

IKP-98-11-084
Oelert, W. et al.
Strangeness Production in the p+p Interaction at Threshold at the Experimental Facility COSY-11
Nucl. Phys. A629 (1998) 164c
20.50.0

IKP-98-11-085
Schütz C., Haidenbauer J., Speth J., Durso J.W.
Extended Coupled Channels Model for πN Scattering and the Structure of N*(1440) and N*(1535)
Phys. Rev. C57 (1998) 1464-1477
20.80.0

IKP-98-11-086
Speth J., Thomas A.W.
Mesonic Contribution to the Spin and Flavor Structure of the Nucleon
Advances in Nucl. Phys. Vol. 24, Plenum Press, NY 1998
20.80.0

IKP-98-11-087
Steininger S., Meißner Ulf-G., Fettes N.
On Wave Function Renormalization and Related Aspects in Heavy Fermion
J. High Energy Physics 9809 (1998) 008
20.80.0

IKP-98-11-088
Szczurek A., Nikolaev N.N., Speth J.
Leading Proton Spectrum from DIS at HERA
Phys. Lett. B428 (1998) 383-390
20.80.0

IKP-98-11-089
The JETSET Collaboration
Study of the Reaction $\bar{p}p \to \phi\phi$ from 1.1 to 2.0 GeV/c
Phys. Rev. C57 (1998) 5379
20.50.0

IKP-98-11-090
Thomas A.W., Melnitchouk W.
Deuteron Structure Functions in the Context of Few-Body Physics
Nucl. Phys. A631 (1998) 296-315
20.80.0

IKP-98-11-091
Tsushima K., Haidenbauer J., Saito K., Thomas A.W:
The Quark-Meson Coupling Model for Λ, Σ, and Ξ and Hypernuclei
Nucl. Phys. A630 (1998) 691-718
20.80.0

IKP-98-11-092
Zakharov B.G.
Light-cone path integral approach to the Landau-Pomeranchuk-Migdal effect
Phys. Atom. Nucl. 61 (1998) 838
20.80.0

IKP-98-11-093
Zoller V.R.
Coherent Neutrino Magnetic Conversion in Crystals
Phys. Lett. B416 (1998) 447
20.80.0

Proceedings, Reports

IKP-98-12-001
Anagnostopoulos, D., Augsburger, M., Belmiloud, D., Borchert, G., Chatellard, D., Daum, M., Egger, J.P., El-Khoury, P., Frosch, R., Gorke, H., Gotta, D., Hauser, P., Indelicato, P., Kirch, K., Lenz, S., Siems, Th., Simons, L.M.
High Precision Spectroscopy of Pionic and Muonic X-Rays to Extract a new upper Limit for the Muon-Neutrino Mass
Acta Phys. Pol. B 29 (1998) 131
20.50.0

IKP-98-12-002
Avdeenkov A.V., Kamerdzhiev S.
Distribution of Single-particle Strength in Odd Non-Magic Nuclei
Proc., Spring Seminar on Nuclear Physics „Highlights of Modern Nuclear Structure", Varenna, Italy, 18.-22.5.1998, World Scientific, Singapore, 1998
20.80.0

IKP-98-12-003
Balewski, J.T. for the COSY-11 Collaboration
Low-Energy 1-p Scattering Parameters from the $pp \rightarrow pK^+K$ Reaction
FZJ-IKP(I)-1998-2
20.45.0

IKP-98-12-004
Bechstedt, U.; Dietrich, J.; Henn, K.; Lehrach, A.; Maier, R.; Martin, S.; Prasuhn, D.; Schnase, A.; Schneider, H.; Stassen, R.; Stockhorst, H.; Tölle, R.
The stochastic cooling system and its application to internal experiments at the cooler synchrotron COSY
Proc. of EPAC 1998, Stockholm, Sweden, p. 553-556
20.30.0

IKP-98-12-005
Bechstedt, U.; Dietrich, J.; Henn, K.; Lehrach, A.; Maier, R.; Martin, S.; Prasuhn, D.; Schnase, A.; Schneider, H.; Stassen, R.; Stockhorst, H.; Tölle, R.
The Performance of COSY
Proc. of EPAC 1998, Stockholm, Sweden, p. 541-543
20.30.0

IKP-98-12-006
Bechstedt, U.; Dietrich, J.; Etzkorn, F.-J.; Henn, K.; Lehrach, A.; Maier, R.; Martin, S.; Prasuhn, D.; Schnase, A.; Schneider, H.; Stassen, R.; Stockhorst, H.; Tölle, R.
DSP based Accelerator Applications at the COoler SYnchrotron COSY
Proc. of EPAC 1998,
Stockholm, Sweden, p. 1595-1597
20.30.0

IKP-98-12-007
Betz M., Veit E.A., Haidenbauer J., Mull V.
Δ-Exchange Contribution to $p\bar{p}$ Annihilation into Three Pions
Relativistic Aspects of Nucl. Phys., eds. T. Kodama et al., World Scientific, Singapore, 1998, pp. 403-406
20.80.0

IKP-98-12-008
Bräutigam, W.; Dietrich, J.; Gebel, R.; Maier, R.; Martin, S.; Meads, P.F.; Schug, G.
Considerations of an improved Injector for the Cooler Synchrotron COSY at Jülich
Proc. of the 6th European Particle Accelerator Conference, 22. June to 26 June 1998
20.30.0

IKP-98-12-009
Bräutigam, W.; Brings, R.; Gebel, R.; Jungwirth, H.; Maier, R.; Schnase, A.
H^--Operation of the Cyclotron Julic as Injector for the Cooler Synchrotron COSY-Jülich
15th International Conference on Cyclotron an their Applications, Caen-France, 14th-19th June, 1998
20.30.0

IKP-98-12-010
Chen B.Q., Ma Z.Y., Grümmer F., Krewald S.
The Role of Fock Terms and Isovector Mesons in Relativistic Hartree-Fock Calculations for Neutron Rich Nuclei
Acta Physica Polonica B29 , No. 9 (1998) 2223-2229
20.80.0

IKP-98-12-011
Cloth, P.; Filges, D. and the members of the ZEUS Collaboration:
Measurement of Jet Shapes in High-Q^2 Deep Inelastic Scattering at HERA
Report, DESY 98-038, March 1998
20.48.0

IKP-98-12-012
Cloth, P.; Filges, D. and the members of the ZEUS Collaboration:
Measurement of Elastic Y Photoproduction at HERA
Report, DESY 98-089, July 1998
20.48.0

IKP-98-12-013
Cloth, P.; Filges, D. and the members of the ZEUS Collaboration:
Exclusive Electroproduction of p^0 and J/ψ at HERA
Report, DESY 98-107, August 1998
20.48.0

IKP-98-12-014
Cloth, P.; Filges, D. and the members of the ZEUS Collaboration:
ZEUS Results on the Measurement and Phenomenology of F_2 at Low x and Low Q^2
Report, DESY 98-121, August 1998
20.48.0

IKP-98-12-015
Cloth, P.; Filges, D. and the members of the ZEUS Collaboration:
Measurement of Three-Jet Distributions in Photoproduction at HERA
Report, DESY 98-162, October 1998
20.48.0

IKP-98-12-016
Dietrich, J.; Mohos, I.
Dynamical tune measurement at COSY-Jülich
8th Beam Instrumentation Workshop, Stanford, May, 4-7,1998:
20.38.0

IKP-98-12-017
Dietrich, J.; Mohos, I.
500 MHz narrowband beam position monitor electronics
8th Beam Instrumentation Workshop, Stanford,
May, 4-7,1998:
20.38.0

IKP-98-12-018
Dietrich, J.; Maier, R.; Mohos, I.
Online Phase Space Measurement with Kicker Excitation
8th Beam Instrumentation Workshop, Stanford, May 4-7,
1998
20.30.0

IKP-98-12-019
Dietrich, J.; Maier, R.; Mohos, I.
Husmann, D.; Keil, J.; Uni-Bonn
The new Beam Position Monitoring System of ELSA
Proceedings of the 6th European Particle Accelerator
Conference, 22. June to 26 June 1998
20.38.0

IKP-98-12-020
Dietrich, J.
Erzeugung und Beschleunigung von $Li3^+$ - Ionen am
Rossendorfer Zyklotron U-120
40-Jahre Rossendorfer Zyklotron U-120, FZR-234,
September 1998
20.30.0

IKP-98-12-021
Durso J.
Meson Exchange Model of Meson-Meson Interactions
Acta Physica Polonica B29, No. 9(1998) 2539-2546
20.80.0

IKP-98-12-022
Filges, D.; Neef, R.-D.; Sterzenbach, G.:
Experimental Validation of Nuclear Models for the
Optimization of the ESS Target System
Proc. 2nd Int. Topical Meeting on Nuclear Applications of
Accelerator Technology, AccApp´98, Gatlinburg, TN, USA,
Sept. 20-23, 1998
20.90.0

IKP-98-12-023
Garske, W., Betigeri, M.G., Bojowald, J., Budzanowski, A.,
Chatterjee, A., Drochner, M., Ernst, J., Förtsch, S.,
Freindl, L., Frekers, D., Grewer, K., Hamacher, A., Igel, S.,
Ilieva, I., Jahn, R., Jarczyk, L., Kemmerling, G., Kilian, K.,
Kliczewski, S., Klimala, W., Kolev, D., Kutsarova, T., Lieb,
B.J., Lippert, G., Machner, H., Magiera, A., Maier, R.,
Nann, H., Pentchev, E., Plendl, H.S., Prasuhn, D., Protic,
D., Razen, B., von Rossen, P., Roy, B., Siudak, R.,
Smyrski, J., Strzalkowski, A., Tsenov, R., Zolnierczuk,
P.A., Zwoll, K.
Meson Production Studied with the GEM Detector
Acta Physica Pol. B29 (1998) 3025
20.45.0

IKP-98-12-024
Gotta, D.
Experiments on Exotic Atoms Spectroscopy
Frontier Tests of QED and Physics of the Vacuum
eds. E. Zavattini, D. Bakalov, C. Rizzi, Heron Press, Sofia,
1998, p., 170, –, 187
20.50.0

IKP-98-12-025
Haidenbauer J., Melnitchouk W., Speth J.
Meson-Exchange Model for the YN Interaction
Proc. of the Sendai International Workshop on the
Spectroscopy of Hypernuclei, eds. H. Tamura et al.,
Tohoku University Press, Sendai, Japan, 1998, pp. 27-36
20.80.0

IKP-98-12-026
Hanhart C., Haidenbauer J., Speth J.
Pion Production in Proton-Proton Collisions
Acta Physica Polonica B29, No. 11 (1998) 3047
20.80.0

IKP-98-12-027
Holstein, B.
Low Energy Compton Scattering and Nucleon Structure
Acta Physica Polonica B29, No. 9 (1998) 2467-2475
20.80.0

IKP-98-12-028
Jarczyk, L., Drodz, S., Machner, H., Magiera, A.
Proc. of the Int. Konf. MESON '98, Krakau
Acta Physica Polonica B29, No. 11 (1998) 2963-3528
20.45.0

IKP-98-12-029
Kamerdzhiev S., Speth J., Tertychny G.
Effects of the Quasiparticle-Phonon Interaction in Magic
and Non-Magic Nuclei
Acta Physica Polonica B29, No. 9 (1998) 2231-2238
20.80.0

IKP-98-12-030
Klemt V.
On Self-Consistency in the Theory of Finite Fermi
Systems
Acta Physica Polonica B29, No. 11 (1998) 3375
20.80.0

IKP-98-12-031
Kobus, H.
Entwicklung eines Teilchentransport-Simulationsmodells
zur Bestrahlungsplanung und zur Kontrolle der
Bestrahlungssicherheit in der Protonentherapie
FZJ-Jül-Report 3507
20.48.0

IKP-98-12-032
Koptev, V.P., Kovalev, A.I., Kravtsov, P.A., Rathmann, F.,
Seyfarth, H., Vassiliev, A.A.
Optimization of the Vacuum system of the Atomic Beam
Source
PNPI Gatchina Report, EP-52-1998, no. 2266 (1998)
20.45.0

IKP-98-12-033
Krehl O., Krewald S., Speth J.
$\pi N \rightarrow \eta N$ Cross Sections and the Influence of Baryonic
Resonances
Acta Physica Polonica B29, No. 11 (1998) 3073
20.80.0

IKP-98-12-034
Krehl O., Speth J.
The Structure of Baryon Resonances in πN Scattering
Acta Physica Polonica B29, No. 9 (1998) 2477-2485
20.80.0

IKP-98-12-035
Krehl O., Rapp R., Janssen G., Wambach J., Speth J.
Proc. Workshop „Chiral Dynamics 1997: Theory and Experiment", Lecture Notes
Physics Vol. 513, Springer Verlag, Berlin, 1998
20.80.0

IKP-98-12-036
Lehrach, A.
Erarbeitung und Umsetzung eines Konzepts zur Beschleunigung polarisierter Protonen im Kühlersynchrotron COSY
Dissertation, Januar 1998
Jül-3501
20.30.0

IKP-98-12-037
Leunissen, L.H.A.
Non-linear transverse dynamics at the Cooler Synchrotron COSY
Dissertation, Januar 1998
ISBN 90-386-0617-6
20.30.0

IKP-98-12-038
Machner, H.
Symmetries in Low Energy Pion Physics and the πNN Coupling Constant
Acta Physica Pol. B29 (1998) 3025
20.45.0

IKP-98-12-039
Meißner Ulf-G.
Low Momentum Effective Theory for Few-Nucleon Systems
Acta Physica Polonica B29, No. 9 (1998) 2339- 2347
20.80.0

IKP-98-12-040
Meißner, Ulf-G.
Hadron Structure in the Nonperturbative Regime of QCD: Isospin Symmetry and its Violation
Proc. Conference „QULEN 97", Osaka, Japan, 20.-23.5.1997,
Nucl. Phys. A629 (1998) 72c-81c
20.80.0

IKP-98-12-041
Mosbacher C.A.
Hadronische Reaktionen am Deuteron im Δ-Resonanzbereich
Dissertation, November 1998
Jül-3609
20.80.0

IKP-98-12-042
Mosbacher, C.A., Osterfeld F.
The ΔN Interactions in Hadronic Reactions on a Deuteron Target
Acta Physica Polonica B29, No. 11 (1998) 3087
20.80.0

IKP-98-12-043
Nakayama K., Krewald S., Speth J.
Possible Role of the ρN Coupling in Pion Photo-Production
Acta Physica Polonica B29, No. 9 (1998) 2519-2526
20.80.0

IKP-98-12-044
Nikolaev N.N.
Soft and Hard Structure of Nucleons as Seen in Deep Inelastic Scattering at HERA
Acta Physica Polonica, B29, No. 11 (1998) 2415
20.80.0

IKP-98-12-045
Razen, B., Betigeri, M.G., Bojowald, J., Budzanowski, A., Chatterjee, A., Drochner, M., Ernst, J., Förtsch, S., Freindl, L., Frekers, D., Garske, W., Grewer, K., Hamacher, A., Hawash, M., Igel, S., Ilieva, I., Jahn, R., Jarczyk, L., Kemmerling, G., Kilian, K., Kliczewski, S., Klimala, W., Kolev, D., Kutsarova, T., Lieb, B.J., Lippert, G., Machner, H., Magiera, A., Maier, R., Nann, H., Plendl, H.S., Protic, D., von Rossen, P., Roy, B., Siudak, R., Smyrski, J., Strzalkowski, A., Tsenov, R., Zolnieczuk, P.A.
Beam Energy Calibration with Meson Production
Acta Physica Pol. B29 (1998) 3119
20.45.0

IKP-98-12-046
Rossi, G.; Morse, J.; Protic, D.:
Energy and Position Resolution of Germanium Microstrip Detectors at X-ray Energies 15 to 100 keV
IEEE Trans. Nucl. Scil, NS-
20.20.0

IKP-98-12-047
Schaal, H.; Filges, D.; Neef, R.D.; Sterzenbach, G.; Broome, T.:
ESS Target Station Shielding Aspects
Proc. 2nd Int. Topical Meeting on Nuclear Applications of Accelerator Technology, AccApp´98, Gatlinburg, TN, USA, Sept. 20-23, 1998
20.90.0

IKP-98-12-048
Sistemich K.
Proc. Intern. Workshop on Exiting Physics with New Accelerator Facilities, Spring 8, Japan, 11.-13.3.1997
(H. Toki, S. Daté, eds.), World Scientific, Singapore, p. 23
20.45.0

IKP-98-12-049
Sterzenbach, G.; Cloth, P.; Filges, D.; Neef, R.D.:
Models and Codes for the Nuclear Assessment of the ESS Target System
Proc. 2nd Int. Topical Meeting on Nuclear Applications of Accelerator Technology, AccApp´98, Gatlinburg, TN, USA, Sept. 20-23, 1998
20.90.0

IKP-98-12-050
Schwarz, V.; Bauer, F.; Büßer, K.; Lehrach, A.; Lindlein, J.; Rohdjess, H.
EDDA as internal high-energy polarimeter
13th International Symposium on High-Energy Spin Physics, Protvino (1998)
20.38.0

IKP-98-12-051
Vassiliev A.
Two Dimensional On-line Monitor of the Atomic Hydrogen (Deuterium) Flow
PNPI Gatchina Report, EP-46-1998, no. 2260 (1998).
20.45.0

IKP-98-12-052
Wojcik M., Drozdz S.
Configuration Mixing Effects in Isoscalar Giant Dipole Resonance
Acta Physica Polonica B29, No. 9 (1998) 2239-2244
20.80.0

Invited Talks

IKP-98-21-001
Baur G.
Photon-Photon and Photon-Hadron Physics in Peripheral Collisions at LHC
Workshop „Heavy Ion Physics with CMS", CERN, Geneve, Switzerland, 12.-12.6.1998
20.80.0

IKP-98-21-002
Baur G.
Two Photon Physics in pp and AA Collisions
Workshop „Photon Interactions and the Proton Structure", Lund, Sweden, 10.-13.9.1998
20.80.0

IKP-98-21-003
Baur G.
Photon-Photon and Photon-Hadron Interactions at Relativistic Heavy Ion Colliders
„International School of Nuclear Physics: Heavy Ion Collisions from Nuclear to Quark Matter",
Erice, Italy, 17.-25.9.1998
20.80.0

IKP-98-21-004
Epelbaum E.
Nuclear Forces from Chiral Lagrangians Using the Method of Unitary Transformation
Workshop „Effective Field Theories" Caltech, Pasadena, USA, 26.-27.2.1998
20.80.0

IKP-98-21-005
Epelbaum E.
Low-momentum Effective theory for Nucleons Using the Method of Unitary Transformation
Workshop „Few-Body Problems in Physics", Autrance, France, 1.-6.6.1998
20.80.0

IKP-98-21-006
Epelbaum E.
Low-momentum Effective Theory for Two Nucleons
Workshop „Chiral Effective Theories", Bad Honnef, Germany, 30.11.-4.12.1998
20.80.0

IKP-98-21-007
Fettes N.
Pion-Nucleon Scattering in Heavy Baryon Chiral Perturbation Theory
Workshop „Chiral Effective Theories"
Bad Honnef, Germany, 2.12.1998
20.80.0

IKP-98-21-008
Filges, D.:
European Spallation Source: Material Science Research Tool for the Next Millenium
APS/IPNS Joint Seminar, ANL Chicago, May 6, 1998
20.90.0

IKP-98-21-009
Filges, D.:
European Spallation Source, Challenges in the Target Station Design
IPNS Division Seminar, ANL Chicago, May 7, 1998
20.90.0

IKP-98-21-010
Filges, D.:
Die "Europäische Spallationsneutronenquelle (ESS)"
Lehrstuhl für Reaktorsicherheit und –Technik, RWTH Aachen, 19. Mai 1998
20.90.0

IKP-98-21-011
Gotta, D.
Experiments on Exotic Atoms Spectroscopy
Workshop on „Frontier Tests of Quantum Electrodynamics and Physics of the Vacuum",
Sandansky, Bulgaria, 10.-14.6.1998
20.50.0

IKP-98-21-012
Gotta, D.
Protonium X-ray Spectroscopy
Invited talk, workshop on „Exotic Atoms, Molecules and Muon Catalyzed Fusion", 19-24.7.1998, Monte Verità, Ascona, Switzerland
20.50.0

IKP-98-21-013
Grzonka, D.
The experimental program at COSY
Workshop on Future Directions in Quark Nuclear Physics, Adelaide, Australien, 9.-20.3.1998
20.45.0

IKP-98-21-014
Haidenbauer, J.
Meson Productions in Nucleon-Nucleon Collisions
Workshop „Future Directions in Quark Nuclear Physic", Adelaide, Australia, 9.-20.3.1998
20.80.0

IKP-98-21-015
Haidenbauer, J.
Pion Production in Proton-Proton Collisions
Workshop „MESONS98", Krakow, Poland, 26.5.-2.6.1998
20.80.0

IKP-98-21-016
Haidenbauer, J.
Vector Meson Production in Nucleon-Nucleon Collisions
Universität Gießen, Gießen, Germany, 29.10.1998
20.80.0

IKP-98-21-017
Haidenbauer J.
Polarization in Pion Productions Reactions
Workshop „Intermediate Energy Spin Physics", Jülich, Germany, 18.-20.11.1998
20.80.0

IKP-98-21-018
Haidenbauer J.
Meson Production in Nucleon-Nucleon Collisions
UERJ, Rio de Janeiro, Brazil, 29.11.1998
20.80.0

IKP-98-21-019
Hanhart C.
π Production near Threshold – Role of the Δ Resonance
Workshop „Pion Production near Threshold", Argonne Nat. Lab., Argonne, USA, 13.8.1998
20.80.0

IKP-98-21-020
Hanhart C.
π Production near Threshold – Role of the Δ Resonance
Workshop „Mesons-Nuclear Physics", Oberjoch, Germany, 29.9.1998
20.80.0

IKP-98-21-021
Hemmert T.
NN and NΔ Form-Factors viewed from CHPT
Lecture, Workshop „N* Physics and Nonperturbative QCD", Trento, Italy, 18.-29.5.1998
20.80.0

IKP-98-21-022
Hemmert T.
Recent Developments in the Physics of Nucleon Form-Factors
Particle Physics Seminar, University of Zürich, Switzerland, 24.6.1998
20.80.0

IKP-98-21-023
Hemmert T.
Muon Capture and the Pseudoscalar Form-Factor of the Nucleon
Conference „BARYONS 98", Bonn, Germany, 22.-26.9.1998
20.80.0

IKP-98-21-024
Hemmert T.
Strange Magnetism
Conference „BARYONS 98", Bonn, Germany, 22.-26.9.1998
20.80.0

IKP-98-21-025
Hemmert T.
Baryon CHPT and Nucleon Resonance Physics
WE-Heraeus Seminar „Chiral Effective Theories", Bad Honnef, Germany, 30.11.-4.12.1998
20.80.0

IKP-98-21-026
Hemmert T.
Effekte der Delta Resonanz bei niedrigen Energien
CANU-Meeting, Bad Honnef, Germany, 21.-22.12.1998
20.80.0

IKP-98-21-027
Kamerdzhiev S.
Compression Mode in Medium Mass Nuclei
Conference „Giant Resonances", Varenna, Italy, 11.-16.5.1998
20.80.0

IKP-98-21-028
Kamerdzhiev S.
Effects of the Quasiparticle-phonon Interaction in Magic and Non-magic Nuclei
Workshop „The Structure of Mesons, Baryons and Nuclei", Krakow, Poland, 26.-30.5.1998
20.80.0

IKP-98-21-029
Kamerdzhiev S.
Distribution of Single-particle Strength in Odd Non-magic Nuclei
Spring Seminar on Nuclear Physics „Highlights of Modern Nuclear Structure", S. Agata Sui Dui Golfi, Italy, 18.-22.5.1998
20.80.0

IKP-98-21-030
Kilian, K.
Associated Hyperon Production at COSY
MESON `98 Konferenz, Krakau, Polen, 27.5.-2.6.1998
20.45.0

IKP-98-21-031
Klemt V.
On Self-Consistency in the Theory of Finite Fermi Systems
Workshop, "MESON98", Krakow, Poland, 29.5.-2.6.1998
20.80.0

IKP-98-21-032
Krehl, O.
Nucleon Resonances in πN Scattering
DPG Frühjahrstagung, Bochum, Germany, 16.3.1998
20.80.0

IKP-98-21-033
Krehl, O.
$\pi N \rightarrow \eta N$ Cross Sections and The Influence of Baryonic Resonances
Workshop „MESON98", Krakow, Poland, 29.5.1998
20.80.0

IKP-98-21-034
Krewald S.
Bulk Properties of Nuclei derived from Medium-modified Meson-Exchange Interactions
„International Workshop of Nuclear Structure under Extreme Conditions", Xian, China, 23.-27.3.1998
20.80.0

IKP-98-21-035
Krewald S.
The Role of the Fock Terms and Isovector Mesons in Relativistic Hartree-Fock Calculations for Neutron-Rich Nuclei
Workshop „MESONS98", Kracow, Poland, 27.5.-2.6.1998
20.80.0

IKP-98-21-036
Kulessa P.
Determination of the Λ Lifetime in Heavy Hypernuclei
Kaon workshop, FZ Rossendorf, Dresden, 10.-11.12.98
20.45.0

IKP-98-21-037
Lehrach, A.
Polarized Proton Beam at COSY'
Beschleunigerseminar AGS, Brookhaven National Laboratory, NY, USA, 30.4.1998
20.30.0

IKP-98-21-038
Lehrach, A.
Polarized Proton Beam at COSY'
Beschleunigerseminar HERA, DESY Hamburg, 31.3.1998
20.30.0

IKP-98-21-039
Machner, H.
Isospin Symmetry in Hadronic Reactions
MESON `98 Konferenz, Krakau, Polen, 27.5.-2.6.1998
20.45.0

IKP-98-21-040
Maier, R.
Performance and perspective of the Cooler Synchrotoron COSY, National Accelerator Centre, South Africa, 7.10.1998
20.30.0

IKP-98-21-041
Maier, R.; Prasuhn, D.; Röser, A.; Schilcher, R.B.; Schneeweiß, F.; Tölle, R.
Evaluation of Radiation Physics for radiation of Cell Cultures using 45 MeV Cyclotron Protons at Forschungszentrum Jülich, 22.-25- Mai, Heidelberg
20.30.0

IKP-98-21-042
Maier, R.; Prasuhn, D.; Röser, A.; Schilcher, R.B.; Schneeweiß, F.; Tölle, R.
Physikalische Rahmenbedingungen für die Bestrahlung von Zellkulturen mit 45 MeV Protonen am Zyklotron des Forschungszentrum Jülich, 07.-10.11.98, Nürnberg
20.30.0

IKP-98-21-043
Meißner Ulf-G.
Pion Nucleon Scattering and Isospin Violation
Workshop „Future Directions in Quark Nuclear Physics", Adelaide, Australia, 9.-20.3.1998
20.80.0

IKP-98-21-044
Meißner Ulf-G.
Low Momentum Effective Theory for Few-Nucleon Systems
Workshop „The Structure of Mesons, Baryons and Nuclei", Kracow, Poland, 26.-30.5.1998
20.80.0

IKP-98-21-045
Meißner Ulf-G.
Chiral Symmetry and Parity – Violating Meson – Nucleon Interaction Regions
Workshop "Parity Violation in Hadronic and Nuclear Systems", INT, Seattle, USA, 22.-24.6.1998.
20.80.0

IKP-98-21-046
Meißner Ulf-G.
Thoughts about pion and Eta Production in Proton-Proton Collisions
INT, Workshop "Pion Production Near Threshold", Argonne National Lab, Argonne, USA, 8.-9.8.1998
20.80.0

IKP-98-21-047
Melnitchouk W.
Meson-Exchange Model for the YN Interaction
Workshop „Spectroscopy of Hypernuclei", Tohoku University, Sendai, Japan, 8.-10.1.1998
20.80.0

IKP-98-21-048
Melnitchouk W.
Quark Asymmetries in the Proton
Workshop „Future Directions in Quark Nuclear Physics", University of Adelaide, Adelaide, Australia, 9.-20.3.1998
20.80.0

IKP-98-21-049
Melnitchouk W.
Quark Asymmetries in the Proton
Workshop „National Trimonthly Medium-Energy Physics Meeting", University of Groningen, Groningen, The Netherlands, June 1998
20.80.0

IKP-98-21-050
Melnitchouk W.
Extraction of Twist-Four Matrix Elements of the Nucleon
„International Nuclear Physics Conference '98", Paris, France, 24.-28.8.1998
20.80.0

IKP-98-21-051
Melnitchouk W.
Can Deeply-Virtual Compton Scattering be Measured
„European Centre for Theoretical Studies Workshop (ECT*)", Trento, Italy, 1.-11.9.1998
20.80.0

IKP-98-21-052
Melnitchouk W.
Where is the Spin of the Nucleon
„International Workshop on Intermediate Energy Spin Physics", Technologiezentrum, Jülich, Germany, 18.-20.11.1998
20.80.0

IKP-98-21-053
Mosbacher, C.A.
The ΔN Interactions in Hadronic Reactions on a Deuteron Target
Workshop „MESON98", Krakow, Poland, 29.5.1998
20.80.0

IKP-98-21-054
Mosbacher C.A.
Hadronic Reactions on a Deuteron Target in the Δ Resonance Energy Region
Université Paris Sud, Orsay, France, 3.11.1998
20.80.0

IKP-98-21-055
Nikolaev N.N.
Soft and Hard Structure of Nucleons as Seen in Deep Inelastic Scattering at HERA
Workshop „The Structure of Mesons, Baryons and Nuclei", Krakow, Poland, 26.-30.5.1998
20.80.0

IKP-98-21-056
Nikolaev N.N.
Lightcone QCD and Diffractive DIS
„IX International Workshop on Small-x Physics and Light-Front Dynamics in QCD", St. Petersburg, Russia, 6.-15.7.1998
20.80.0

IKP-98-21-057
Nikolaev N.N.
Diffractive vector mesons and BFKL Pomeron
Workshop „BFKL", St. Petersburg, Gatchina, Russia, 21.-25.12.1998
20.80.0

IKP-98-21-058
Nikolaev N.N.
Intrinsic Transverse Momentum of Gluons in the Pomeron
„HERA Monte-Carlo Workshop", DESY, Hamburg, Germany, 1.9.1998
20.80.0

IKP-98-21-059
Nikolaev N.N.
Vector Meson Production
Workshop „Strukturfunktionen und hadronische Wellenfunktionen", Bad Honnef, Germany, 14.-18.12.1998
20.80.0

IKP-98-21-060
Oelert, W.
Physics at COSY – Experiments at COSY-11
WASA/PROMICE Main Meeting, Uppsala, 20.-23.3.1998
20.45.0

IKP-98-21-061
Schäfer, W.
The Tensor Structure Function $b_2(x,Q^2)$ of the Deuteron at small x
Workshop „Deep Inelastic Scattering and QCD (DIS98)", Brussels, Belgium, 5.4.1998
20.80.0

IKP-98-21-062
Schäfer, W.
Secondary Reggeons in Diffractive DIS: The Microscopic QCD Evaluation
Workshop „Deep Inelastic Scattering and QCD (DIS98)", Brussels, Belgium, 6.4.1998
20.80.0

IKP-98-21-063
Schäfer, W.
The Impact of NLO Corrections on the Determination of the $\bar{d}u, \bar{d}$ -Content of Nucleons from Drell-Yan Production
Workshop „Deep Inelastic Scattering and QCD (DIS98), Brussels, Belgium, 6.4.1998
20.80.0

IKP-98-21-064
Schäfer, W.
Nuclear Modifications of Parton Densities in the Deuteron
Workshop „Coherent QCD Processes with Nucleons and Nuclei (ECT)", Trento, Italy, 8.9.1998
20.80.0

IKP-98-21-065
Schnase, A.
Digitale Signalverarbeitung bei den HF-Systemen von COSY, GSI Darmstadt, 29. – 30.1.1998
20.30.0

IKP-98-21-066
K. Sistemich
Research at COSY
EU Meeting on Frontiers in Nuclear Physics and Astrophysics, Jyväskylä, Finland, 29.-30.6.1998
20.45.0

IKP-98-21-067
Speth J.
πN-Scattering and the Structure of the First Excited States of the Nucleon
Workshop „Future Directions in Quark Nuclei Physics", Adelaide, Australia, 10.3.1998
20.80.0

IKP-98-21-068
Speth J.
Meson-Baryon and Meson-Meson Interactions
Workshop "The Structure of Mesons, Baryons and Nuclei", Krakow, Poland, 26.-30.5.1998,
Acta Physica Polonica, Vol. B29 (1998) 2185-2560
20.80.0

IKP-98-21-069
Speth J.
Sea-quark Distributions in the Proton
Workshop „Strukturfunktionen und hadronische Wellenfunktionen"
Bad Honnef, Germany, 14.12.1998
20.80.0

IKP-98-21-070
Stein, H.J.
Application of Electron Cooling in COSY
Workshop „Medium Energy Electron Cooling"
JINR Dubna, Russia, 14.-15.9.1998
20.50.0

IKP-98-21-071
Steininger S.
Isospin Violation in Pion-Nukleon Interaction
Workshop „Electronuclear Physics with Internal Targets and the Bates Large Acceptance Spectrometer Toroid (BLAST– MIT-Bates), Cambridge, USA, May 1998
20.80.0

IKP-98-21-072
Stockhorst, H.
The Use of Noise for Stochastic Extraction and Cooling
DESY, Hamburg, 19. – 20.5.1998
20.30.0

IKP-98-21-073
Stockhorst, H.
Ultra Slow Extraction and Stochastic Cooling at COSY
Frühjahrstagung der Deutschen Physikalischen Gesellschaft, DPG, Bochum, 16.-20.3.1998
20.30.0

IKP-98-21-074
Stockhorst, H.
Formung des COSY Strahls
ELSA/COSY-Seminar am Physikalischen Institut der Universität Bonn, 27.1.1998
20.30.0

IKP-98-21-075
Ströher H.
Polarizabilities of Hadrons
Meson '98, Krakau (Polen), 2.3.1998
20.50.0

IKP-98-21-076
Zoller V.R.
The Running BFKL: Precocious Asymptopia for Charm and the $dF_2/d\log Q^2$-puzzle
Workshop „6th International Workshop on Deep Inelastic Scattering and QCD (DIS98), Brussels, Belgium, April 1998,
20.80.0

IKP-98-21-077
Zoller V.R.
Forward Cone in Exclusive Heavy Vector Meson Production
Workshop „6th International Workshop on Deep Inelastic Scattering and QCD (DIS98), Brussels, Belgium, April 1998,
20.80.0

Conference Contributions

IKP-98-22-001
Barsov, S., Brüggemann, R., Koch, N., Koptev, V., Lemaitre, S., Loevenich, H., Maier, R., Mikirtichyants, S., Nellen, R., Nelyubin, V., Paetz gen. Schieck, H., Pohl, H., Prasuhn, D., Rathmann, F., Schleichert, R., Schug, G., Schult, O.W.B., Seyfarth, H., Souslov, A., Steffens, E., Stein, H.J., Vassiliev, A., Zwoll, K.
The polarised Atomic Beam Source for the internal Gas Target at ANKE/COSY
DPG-Frühjahrstagung, Physik der Hadronen und Kerne, Bochum, 16.-20.3.1998
20.45.0

IKP-98-22-002
Barsov, S., Bechstedt, U., Bongers, N., Borchert, G., Borgs, W., Büscher, M., Eßer, R., Gotta, D., Hartmann, M., Junghans, H., Klehr, F., Koch, H.R., Maier, R., Ohm, H., Prasuhn, D., Schleichert, R., Schneider, H., Schneider, Chr., Schult, O.W.B., Seyfarth, H., Sistemich, K., Stein, H.J. für ANKE-Kollaboration
The spectrometer ANKE at COSY
DPG-Frühjahrstagung, Bochum, Germany, 22.-26.3.1998
20.45.0

IKP-98-22-003
Baur G.
Application of Coulomb Dissociation to Nuclear Astrophysics
Vortrag, Workshop „Hirschegg98", Hirschegg, Germany, 11.-17.1.1998
20.80.0

IKP-98-22-004
Baur G.
Photon-Photon Physik mit relativistischen Schwerionen-kollisionen
Vortrag, „DPG-Frühjahrstagung", Bochum, Germany, 16.-20.3.1998
20.80.0

IKP-98-22-005
Baur G.
Neue Möglichkeiten für Coulombdissoziationsexperimente zur nuklearen Astrophysik
Vortrag, „Arbeitstreffen Experimente „Nukleare Astrophysik", GSI, Darmstadt, Germany, 23.-24.4.1998
20.80.0

IKP-98-22-006
Baur G.
Coulombdissoziation: Anwendung auf Kernstruktur und Nukleare Astrophysik
Kernphysikalisches Kolloquium, Universität Gießen, Gießen, Germany, 9.7.1998
20.80.0

IKP-98-22-007
Bilger, R., Grossmann, R., Clement, H, Wagner, G.J. and the COSY-11 Collaboration
Search for the πNN Resonance d` at COSY-11 with the Reaction $pp \rightarrow pp\pi^-\pi^+$
Verhandlungen der DPG, Bochum, 16.-20.3.1998
20.45.0

IKP-98-22-008
Böckmann R.
$\pi\sigma$-Scattering and the Softening of the pNN Form Factor
Vortrag, DPG-Frühjahrstagung, Bochum, Germany, 16.-20.3.1998
20.80.0

IKP-98-22-009
Borchert, G.
High resolution X-ray spectroscopy in exotic atoms
KVI Groningen, 10.3.1998
20.50.0

IKP-98-22-010
Borchert, G., Drochner, M., Erven, W., Hartmann, M., Junghans, H., Koch, H.R., Langenhagen H., Ohm, H., Wüstner, P., Zwoll, K.
Economic MWPC-readout at ANKE: data reduction with chamber mounted highly integrated circuits and data processing with industrial PC´s
Nuclear Physics Spring Meeting, Bochum, Germany, 16.-20.3.1998, contribution HK 56.71
20.45.0

IKP-98-22-011
Borchert, G., Erven, W., Junghans, H., Koch, H. R., Langenhagen, H., Ohm, H., Zwoll, K.
Large area MWPCs with fast on-board readout for the spectrometer ANKE
DPG Frühjahrstagung, Bochum 16.-20.3.1998
20.45.0

IKP-98-22-012
Borchert, G.
High resolution X-ray spectroscopy in exotic atoms
PNPI Gatchina, 6.8.1998
20.50.0

IKP-98-22-013
Borchert, G.
What can we learn from high resolution X-ray spectroscopy in exotic atoms
ITEP Moskau, 19.8.1998
20.50.0

IKP-98-22-014
Borgs, W., Cassing, W., Hodde, H., Jarczyk, L., Kamys, B., Koch, H.R., Kulessa, P., Maier, R., Matoba, M., Ohm, H., Prasuhn, D., Pysz, K., Rudy, Z., Schult, O.W.B., Strzalkowski, A., Zychor, I.,
The lifetime of heavy hypernuclei produced in the $^{209}Bi + p$ reaction at COSY Jülich
DPG Frühjahrstagung, Bochum 16.-20.3.1998
20.45.0

IKP-98-22-015
Borgs, W., Cassing, W., Jarczyk, L., Hartmann, M., Hermes, T., Hodde, H., Kamys, B., Koch, H.R., Kulessa, P., Maier, R., Matoba, M., Ohm, H., Pfeiffer, J., Prasuhn, D., Pysz, K., Rudy, Z., Schult, O.W.B., Strzalkowski, A., Uozumi, Y., Zychor, I.,
Production of Λ-hypernuclei at COSY Jülich
Workshop on Perspectives of Strangeness and Hypernuclear Physics, GSI Darmstadt, 6.-7.4.1998
20.45.0

IKP-98-22-016
Bräutigam, W.
Superconducting LINAC Components for ESS
Accelerator Applications`98, Gatlinburg, TN, USA,
20.-23.09.98
20.30.0

IKP-98-22-017
Büscher M.
Planned studies of a a_0^+ -mesons using the reaction
$pp \rightarrow d a_0^+ \rightarrow K^+ \bar{K}^0$ at ANKE/COSY,
Spring Meeting of Nuclear Physics Sections, Bochum, Germany, 16.-20.3.1998
20.45.0

IKP-98-22-018
Büscher M.
Physics at the ANKE spectrometer at COSY-Jülich,
Institute of Theoretical and Experimental Physics, Moscow, Russia, 10.6.1998
20.45.0

IKP-98-22-019
Büttiker P
A Dispersive Analysis of $\pi\pi$ Scattering
DPG-Frühjahrstagung, Bochum, Germany 16.-20.3.1998
20.80.0

IKP-98-22-020
Dezarn, W.A., Doskow, J., Dzemidzic, M., Haeberli, W., Hardie, J.G., Lorentz, B., Meyer, H.O., Pollock, R.E., von Przewoski, B., Rathmann, F., Rinckel, T., Sperisen, F., Pancella P.V., Wise, T.,
Measurements of Spin Correlation Coefficients in pp Elastic Scattering between 200 and 450 MeV: Analysis, Results and Comparison to Theory
DPG-Frühjahrstagung, Physik der Hadronen und Kerne, Bochum, 16.-20.3.1998
20.50.0

IKP-98-22-021
Dietrich, J.
Beschleunigerphysikalische Messungen an COSY mit bunchsynchroner Abtastung
Winterseminar des Instituts für angewandte Physik der J.W. Goethe-Universität Frankfurt/Main, 22. – 28.2.1998
20.30.0

IKP-98-22-022
Epelbaum E.
Nuclear Forces from Chiral Lagrangians Using the Method of Unitary Transformation
DPG-Frühjahrstagung, Bochum, Germany, 16.-20.3.1998
20.80.0

IKP-98-22-023
Eßer, R., Hartmann, M., Ohm, H., Prietzschk, B., Rimarzig, B., Schleichert, R., Schneider, A.
A monitoring system for scintillation counters based on pulsed LEDs
DPG Frühjahrstagung, Bochum 16.-20.3.1998
20.45.0

IKP-98-22-024
Eyrich, W. for the COSY-TOF-Collaboration
Strangeness Production in the Reaction $pp \rightarrow K^+ \Lambda p$ Close to Threshold
Verhandlungen der DPG, Bochum, 16.-20.3.1998
20.45.0

IKP-98-22-025
Fettes N.
Inclusive and Deep Inelastic Scattering from a Dressed Nucleon
DPG-Frühjahrstagung, Bochum, Germany, 16.3.1998
20.80.0

IKP-98-22-026
Filges, D.; Neef, R.-D.; Schaal, H.; Sterzenbach, G.; for the NESSI-, ASTE-, JESSICA- and RECOIL Collaboration:
Radiation Physics and Nuclear Assessment of the Target Station of the European Spallation Neutron Source
4th Specialists´ Meeting on Simulation Accelerator Radiation Environments (SARE-4), Knoxville, Tennessee, 13.-16.9.1998
20.90.0

IKP-98-22-027
Filges, D.; Neef, R.-D.; for the NESSI-Collaboration:
Thin and Thick Target Benchmark Investigations to Validate Spallation Physics Models
4th Specialists´ Meeting on Shielding Aspects of Accelerators, Targets and Irradiation Facilities (SATIF-4), Knoxville, Tennessee, 17.-18.9.1998
20.90.0

IKP-98-22-028
Filges, D.:
Strategien zur Inkorporationsüberwachung an PET-Zentren am Beispiel des Forschungszentrums Jülich
30. Jahrestagung Radioaktivität in Mensch und Umwelt, Lindau im Bodensee, 28.9.-2.10.1998
20.48.0

IKP-98-22-029
Gast, W., Georgiev, A., Stein, J., van der Meer, E.A., Mihailescu, L. and Lieder, R.M.
Test of a Pulse-Shape Analyzer Based on Digital Signal Processing Techniques
Verhandlungen der DPG, Bochum, 16.-20.3.1998
20.10.0

IKP-98-22-030
Gebel, R.
Polarized Proton an Deuteron Ion Sources for COSY
Workshop on Intermediate Spin Physics, Jülich,
18. – 20.11.1998
20.30.0

IKP-98-22-031
Gotta, D.
Fifth Biennial Conf. on Low Energy Antiproton Physics (LEAP 98), Villasimius, Cagliari, Italy, 7.-12.9.1998
20.50.0

IKP-98-22-032
Gotta, D.
Protonium X-ray spectroscopy
Spring Meeting of the DPG, Bochum, FRG, 16.3.1998
20.50.0

IKP-98-22-033
Gotta D.
Strong interaction effects in pionic deuterium
Spring Meeting of the DPG, Bochum, FRG, 16.3.1998
20.50.0

IKP-98-22-034
Grewer, K. for the GEM-Collaboration
First Measurements with the Germanium Wall
Verhandlungen der DPG, Bochum, 16.-20.3.1998
20.45.0

IKP-98-22-035
Grzonka, D.
Physics at COSY
XIV International Seminar on High Energy Physics Problems, Dubna, 17.-22.8.1998
20.45.0

IKP-98-22-036
Haidenbauer J.
The Reaction pp→ppϕ and the Violation of the OZI-Rule
Vortrag, Conference „BARYONS98", Bonn, Germany, 22.-26.9.1998
20.80.0

IKP-98-22-037
Haidenbauer J.
Meson Production in Nucleon-Nucleon Collisions
UNESP, Sao Paolo, Brazil, 14.12.1998
20.80.0

IKP-98-22-038
Hanhart C.
π Production near Threshold – Role of the Δ Resonance
Vortrag, DPG-Frühjahrstagung, Bochum, Germany, 17.3.1998
20.80.0

IKP-98-22-039
Hanhart C.
π Production near Threshold – Role of the Δ Resonance
Seminar, University of Washington, Seattle, USA, 19.8.1998
20.80.0

IKP-98-22-040
Hanhart C.
π Production near Threshold – Role of the Δ Resonance
Vortrag, Conference „BARYONS98", Bonn, Germany, 23.9.1998
20.80.0

IKP-98-22-041
Hanhart C.
Meson Produktion nahe der Schwelle
Seminar, Universität Freiburg, Germany, 11.12.1998
20.80.0

IKP-98-22-042
Hanhart C.
Meson Produktion nahe der Schwelle
Vortrag, CANU-Meeting, Bad Honnef, Germany, 21.-22.12.1998
20.80.0

IKP-98-22-043
Hemmert T.
The Nucleon Form Factors at Small Momentum Transfer
Vortrag, DPG-Frühjahrstagung, Bochum, Germany, 16.-20.5.1998
20.80.0

IKP-98-22-044
Hemmert T.
Strange Magnetism in the Nucleon
Talk, Workshop „The Physics of Strangeness"
INT, Seattle, USA, 28.9.-4.12.1998
20.80.0

IKP-98-22-045
Hofmann, M. and ATRAP-Collaboration
A Detector System for the Observation of Cold Antihydrogen at AD/CERN
Verhandlungen der DPG, Bochum, 16.-20.3.1998
20.50.0

IKP-98-22-046
Hoffmann, W.; Bienen, J.; Filges, D.; Schmitz, Th.:
TLD 300 Dosimetry in a 175 MeV Proton Beam
12th Int. Conf. on Solid State Dosimetry, Burgos, Spanien, 5.-10.7.1998
20.48.0

IKP-98-22-047
Ilieva, I., Kutsarova, T., Machner, H.
Coulomb Corrections for pp→dπ$^+$ Cross Sections
Verhandlungen der DPG, Bochum, 16.-20.3.1998
20.45.0

IKP-98-22-048
Kamerdzhiev S.
Microscopic Description of Excitations of Odd Non-magic Nuclei
Seminar, Universität Köln, Köln, Germany, 20.1.1998
20.80.0

IKP-98-22-049
Kilian, K.
Future Strangeness Experiments at COSY
Senday Workshop on the Spectroscopy of Hypernuclei
Sendai, Tokyo, 8.-10.1.1998
20.50.0

IKP-98-22-050
Kilian, K.
Strangeness with Antiproton
Sendai Int. Workshop on the Spectroscopy of Hypernuclei, Tohoku University, Sendai, Japan, 8.-10.1.1998
20.45.0

IKP-98-22-051
Kilian, K.
Resultate von COSY
ISKP der Uni Bonn, 22.1.1998
20.45.0

IKP-98-22-052
Kilian, K.
Resultate und Perspektiven der Hadronenphysik an COSY
FZ Rossendorf, Dresden, 22.6.1998
20.45.0

IKP-98-22-053
Kilian, K.
Detector Equipment at COSY
FCG-Meeting, KVI Groningen, 10.-11.10.1998
20.45.0

IKP-98-22-054
Kilian, K.
Experiments at COSY
Int. KEK-Tanashi Symposium, Univ. of Tokyo, 14.-17.12.1998
20.45.0

IKP-98-22-055
Klimala, W. for the GEM-collaboration
Search for Pionic Atoms in $^{209}Bi(p,2p)^{208}Bi$ $\bar{p}p \rightarrow \phi\phi\pi$
Verhandlungen der DPG, Bochum, 16.-20.3.1998
20.45.0

IKP-98-22-056
Krewald S.
Ein Meson-Austausch Modell für die Pion-Nukleon Streuung
Vortrag, DPG Frühjahrstagung, Bochum, Germany, 16.-20.3.1998
20.80.0

IKP-98-22-057
Krewald S.
The Effect of Vector-meson Nucleon Channels in Pion Photoproduction
Seminar, George Washington University, Washington, USA, 8.10.1998
20.80.0

IKP-98-22-058
Krewald S.
Der Vektormeson-Nukleon Reaktionskanal und das Problem der weichen Formfaktoren in der Pion Photoproduktion
Seminar, TH Darmstadt, Darmstadt, Germany 3.12.1998
20.80.0

IKP-98-22-059
Lehrach, A.
Acceleration of Polarized Beams in COSY
Workshop on Intermediate Spin Physics,
Jülich, 18. – 20.11.1998
20.30.0

IKP-98-22-060
Lehrach, A.
Polarized Proton Beam at COSY
DPG Fruehjahrstagung Bochum, 16. – 20.3.1998
20.30.0

IKP-98-22-061
Lieder, R.M., Lunardi, S., Bazzacco, D., Falconi, G., Menegazzo, R. Pavan, P., Petrache, C.M., Rossi-Alvarez, C., Ur, C.A., Venturelli, R., DePoli, M., Gadea, A., de Angelis, G., Napoli, D.R., Podolyak, Z., Gast, W., Georgiev, A., Jäger, H.M., Jensen, H.J., Rzaca-Urban, T., Urban, W., Pytel, Z., Augsburg, M., Stabosta, K., Kalfas, C.A., Papadopoulos, C.T., Vlastou, R.
Search for the Decay-out of the Yrast Superdeformed Band in ^{144}Gd
Verhandlungen der DPG, Bochum, 16.-20.3.1998
20.10.0

IKP-98-22-062
Lieder, R.M.
Study of Superdeformation in Light Gd Nuclei with Large Gamma-Detector Arrays
Workshop on Nuclear Theory, Gueletchiza, Bulgarien, 15.-20.6.1998
20.10.0

IKP-98-22-063
Machner, H.
Symmetries in Low Energy Pion Physics
Workshop on Broken Symmetries, Schladming/Österreich, 27.2.-8.3.1998
20.45.0

IKP-98-22-064
Machner, H.
Symmetries in Low Energy Pion Physics
Workshop on Broken Symmetries, Schladming, Österreich, 27.2.-8.3.1998
20.45.0

IKP-98-22-065
Machner, H., Razen, B.
Symmetries in Low Energy Pion Physics
Verhandlungen der DPG, Bochum, 16.-20.3.1998
20.45.0

IKP-98-22-066
Machner, H.
Mesonenproduktion nahe der Schwelle in Proton-Proton- und Proton-Deuteron-Wechselwirkungen
Koll. des FB Physik der Uni GH Essen, 28.10.98
20.45.0

IKP-98-22-067
Maier, R.
Beschleunigerphysikalische Arbeiten mit dem und für das Kühlersynchrotron COSY
Universität Frankfurt, Seminar WS 97/98, 6.2.1998
20.30.0

IKP-98-22-068
Martin, S.
Beam Dynamics Considerations for a Superconducting High-Energy H-Linac for the ESS.
Accelerator Applications'98, Gatlinburg, TN, USA,
20.-23.09.98
20.38.0

IKP-98-22-069
Meißner Ulf-G.
Chiral Dynamics: Status and Perspectives
Vortrag, Conference „BARYONS98", Bonn, Germany, 22.-26.9. 1998.
20.80.0

IKP-98-22-070
Meißner Ulf-G.
Effective Field Theory Approaches to Pion Production in Proton Proton Collisions
Vortrag, Conference „BARYONS 98", Bonn, Germany, 22.-26.9.1998.
20.80.0

IKP-98-22-071
Melnitchouk W.
Quark Asymmetries in the Nucleon
Talk, University of Maryland, USA, July 1998,
20.80.0

IKP-98-22-072
Melnitchouk W.
Asymmetric Quarks in the Proton
Talk, University of Coimbra, Portugal, October 1998
20.80.0

IKP-98-22-073
Mosbacher, C.A.
Study of ΔN and ΔΔ Excitations in the Reactions $\pi^+ d \leftrightarrow pp$ and $(\pi\pi)^0 d \leftrightarrow np$
Vortrag, DPG-Frühjahrstagung, Bochum, Germany, 19.6.1998
20.80.0

IKP-98-22-074
Mosbacher, C.A.
Quantendynamik in Liouville-Raum
Vortrag, Sommerakademie, Studienstiftung des Deutschen Volkes, Molveno, Italy, 4.9.1998
20.80.0

IKP-98-22-075
Neef, R.D., Arai, M., Bauer, G., Carroll, A.S., Conrad, H., Filges, D., Futakawa, M. Glasgow, D., Haines, J., Hastings, J., Ikeda, Y., Jerde,, E., Kijanagi, Y., Nakashima, H., Spitzer, H., Stechemesser, H., Takada, H. Watanabe, N.:
Spallation Neutron Target Experiments at the AGS-BNL
DPG-Frühjahrstagung, Bochum, Germany, 16.-20.3.1998
20.48.0

IKP-98-22-076
Nikolaev N.N.
Diffractive DIS: Summary of the Diffractive Working Group Convener at the „6th International Workshop on Deep Inelastic Scattering and QCD (DIS98),
Brussels, Belgium, 4.-8.4.1998
20.80.0

IKP-98-22-077
Oelert, W. for the COSY-11-Collaboration
Strangeness Production into K^+K^- and K^+Y from pp Scattering at COSY
Verhandlungen der DPG, Bochum, 16.-20.3.1998
20.45.0

IKP-98-22-078
Oelert, W. together with the COSY-11 Collaboration
η`-Meson Production in the pp Scattering at COSY
Verhandlungen der DPG, Bochum, 16.-20.3.1998
20.45.0

IKP-98-22-079
Oelert, W. together with the COSY-11 Collaboration
Luminosity Determination at the Experiment COSY-11
Verhandlungen der DPG, Bochum, 16.-20.3.1998
20.45.0

IKP-98-22-080
Oelert, W. together with the COSY-11 Collaboration
A Measurement of $\bar{p}p \rightarrow \bar{\Lambda}\Lambda$ near Threshold
Verhandlungen der DPG, Bochum, 16.-20.3.1998
20.45.0

IKP-98-22-081
Oelert, W.
Physics at COSY – Experiments at COSY-11
WASA/PROMICE Main Meeting, Uppsala, 20.-23.3.1998
20.45.0

IKP-98-22-082
Oelert, W.
Strangeness Production Experiments at COSY-11, Status and Future
Working group at GSI, Darmstadt, 6.-7.4.1998
20.45.0

IKP-98-22-083
Oelert, W.
Strangeness Production on the Nucleon
Workshop on Perspectives of Strangeness and Hypernuclear Physics
GSI Darmstadt, 6.-7.4.1998
20.45.0

IKP-98-22-084
Oelert, W.
Große Maschinen für kleinste Teilchen der Grundlagenforschung
Journalistenseminar, Jülich, 11.-12.5.1998
20.45.0

IKP-98-22-085
Oelert, W.
Mesonenproduction an der Schwelle in der Proton-Proton Streuung
Gemeinsames kernphysikalisches Kolloquium beider Münchener Universitäten, München, 5.6.1998
20.45.0

IKP-98-22-086
Oelert, W.
K^+-Erzeugung in der Proton-Proton-Wechselwirkung
16. CANU-Arbeitstreffen, Bad Honnef, 21.-22.12.1998
20.45.0

IKP-98-22-087
Probst, H.J.
Gerätetechnischer Strahlenschutz und Sicherheitsmaßnahmen für Beschleunigerstrahlenschutz
RWTH Aachen, Haus der Technik, Essen, 7. – 10.9.1998

IKP-98-22-088
Probst, H.J.
Betriebsinterne Überwachung und Kontrolle, Wartung und Aufzeichnungen und Meldepflichten;
Spezialkurs für Beschleunigerstrahlenschutz
RWTH Aachen, Haus der Technik, Essen, 7. – 10.9.1998

IKP-98-22-089
Probst, H.J.
Arbeitsabläufe und Strahlenschutzplanung;
Spezialkurs für Beschleunigerstrahlenschutz
RWTH Aachen, Haus der Technik, Essen, 7. – 10.9.1998

IKP-98-22-090
Rathmann, F.
ANKE
Nuclear Physics Seminar, IUCF, 16.4.1998
20.45.0

IKP-98-22-091
Schaal, H.; Filges, D.; Sterzenbach, G.:
Methods to Calculate Spallation Source Shields and Comparison with Experiment
4th Specialists´ Meeting on Shielding Aspects of Accelerators, Targets and Irradiation Facilities (SATIF-4), Knoxville, Tennessee, 17.-18.9.1998
20.90.0

IKP-98-22-092
Schäfer, W.
The Impact of NLO Corrections on the Determination of the $\bar{d}u, \bar{d}$ -Content of Nucleons from Drell-Yan Production
Vortrag, DPG-Frühjahrstagung, Bochum, Germany, 22.-26.3.1998
20.80.0

IKP-98-22-093
Sewerin S.
Vergleich der Wirkungsquerschnitte für Λ- und Σ-Produktion im Schwellenbereich
16. CANU Arbeitstreffen, Bad Honnef, 21.-22.12.1998
20.45.0

IKP-98-22-094
K. Sistemich
German-Russian Research at ANKE/COSY
Workshop on Scientific Cooperation between JINR and German Research Centres
Dubna, 16.-17.11.1998
20.45.0

IKP-98-22-095
K. Sistemich
Access to COSY for New European Users
Mid-Term Review by the European Commission
Louvain-la-Neuve, Belgium, 21.10.1998
20.45.0

IKP-98-22-096
Speth J.
Compression Modes in Nuclei
Kolloquium, University of Witwatersrand, Witwatersrand, South Africa, 18.2.1998
20.80.0

IKP-98-22-097
Speth J.
Neutral Pion Production
Seminar, University of Witwatersrand, Witwatersrand, South Africa, 20.2.1998
20.80.0

IKP-98-22-098
Speth J.
Compression Modes in Nuclei
Kolloquium, University of Stellenbosch, Stellenbosch, South Africa, 24.2.1998
20.80.0

IKP-98-22-099
Speth J.
Compression Modes in Nuclei
Kolloquium, University of Captown, Captown, South Africa, 26.2.1998
20.80.0

IKP-98-22-100
Speth J.
Compression Modes in Nuclei
Kolloquium, University of Adelaide, Adelaide, Australia, 19.3.1998
20.80.0

IKP-98-22-101
Stassen, R.
Stochastische Kühlung am Speicherring COSY
DPG Früjahrstagung, Bochum, 16. – 20.3.1998
20.38.0

IKP-98-22-102
Steininger S.
Isospinverletzung in ππ- und πN-Reaktionen
Arbeitstreffen „Kernphysik" , Schleching, Germany, 25.2.-5.3.1998
20.80.0

IKP-98-22-103
Steininger S.
Isospin Violation in ππ and πN-Scattering
Seminar Talk, Indian Institute of Science, Bangalore, India, March 1998
20.80.0

IKP-98-22-104
Steininger S.
Virtual Photons in Chiral Perturbation Theory
Seminar Talk, University of Massachusetts, Amherst, USA, August 1998
20.80.0

IKP-98-22-105
Steininger S.
Isospin Violation in Pion-Nukleon Scattering
Workshop „BARYONS98", Bonn, 22.-26.9.1998
20.80.0

IKP-98-22-106
Steininger S.
Isospinbrechung in der Pion-Nukleon-Streuung
Studientage des Graduiertenkollegs „Die Erforschung subnuklearer Strukturen der Materie"", Adenau, 24.-27.11.1998
20.80.0

IKP-98-22-107
Steininger S.
Isospin-Violation in Pion-Nucleon Scattering
Workshop „Chiral Effective Theories", Bad Honnef, 30.11.-4.12.1998
20.80.0

IKP-98-22-108
Sterzenbach, G.; Cloth, P.; Filges, D.:
MC4 – A new Hadronic Monte Carlo Code for High to Medium Energies
4th Specialists´ Meeting on Simulation Accelerator Radiation Environments (SARE-4), Knoxville, Tennessee, 13.-16.9.1998
20.48.0

IKP-98-22-109
Ströher H.
Photonukleare Experimente an MAMI und anderswo
Graduiertenkolleg "Schwerionenphysik" Universitäten Frankfurt–Gießen
29.1.1998
20.50.0

IKP-98-22-110
Ströher H.
Polarisierbarkeiten von Hadronen
Schleching, 2.3.1998
20.50.0

IKP-98-22-111
Ströher H.
Die innere Struktur des Nukleons
Kolloquium GSI Darmstadt, 27.10.1998
20.50.0

IKP-98-22-112
Venkova, Ts., Lieder, R.M., Utzelmann, St., Gast, W., Schnare, H., Marti, G.V., Spohr, K., Hoernes, P., Georgiev, A., Bazzacco, D., Menegazzo, R., Rossi-Alvarez, C., de Angelis, G., Kaczarowski, R., Rzaca-Urban, T., Morek, T., Maier, K.H., Frauendorf, S.
Beobachtung einer $vh_{9/2}$ Bandenkreuzung in ^{180}Os
Verhandlungen der DPG, Bochum, 16.-20.3.1998
20.10.0

Poster

IKP-98-23-001
Mosbacher C.A.
Study of $\Delta\Delta$ Excitations in the Reaction $n+p \rightarrow d+\pi\pi$
Posterbeitrag, Conference „BARYONS98", Bonn, Germany, 22.-26.9.1998
20.80.0

IKP-98-23-002
Stassen, R.
The stochastic cooling system and its application to internal experiments at the Cooler Synchrotron COSY
EPAC 98, Stockholm, 22. – 26.6.1998
20.38.0

Patents

IKP-10
G. Heinrichs, H. Meuth, A. Schnase, H. Stockhorst
Patent P 43 42 520.8 - 35 "Schmalbandiger arbiträrer HF-Modulations- und Rauschgenerator" (Digitaler Rauschgenerator für die ultralangsame Extraktion an COSY)
Patent in Amerika unter der Nummer 5694094 erteilt: (Narrow Band Arbitrary HF Modulation and Noise Generator.)
20.30.0

Lectures at Universities

WS 97/98

IKP-98-4-001
Baur G.
Einführung in die allgemeine Relativitätstheorie
Universität Basel, V1
1.1 KPH

IKP-98-4-002
Borchert G. L.
Physik für Naturwissenschaftler II
Universität zu Köln, V 4
1.1 KPH

IKP-98-4-003
Borchert G. L.
Oberseminar Kernpysik
Universität zu Köln, S 2
1.1 KPH

IKP-98-4-004
Filges D.
Einführung von computergestützten Rechenverfahren/
Simulationsrechnungen mit Teilchentransportprogrammen
Universität Wuppertal, V 2, Ü 1
1.4 ESS

IKP-98-4-005
Krewald S.
Einführung in die Theorie der schwachen Wechselwirkung
Universität Bonn, V 4, Ü 2
1.1 KPH

IKP-98-4-006
Maier R.
Anwendung von Teilchenbeschleunigern
Universität Bonn
1.1 KPH

IKP-98-4-007
Meißner Ulf-G.
Quantentheorie I
Universität Bonn, V 4, Ü 4
1.1 KPH

IKP-98-4-008
Oelert, W.
Teilcenphysik I
Universität Bochum, V 4
1.1 KPH

IKP-98-4-009
Sistemich K.
Physik für Mediziner
Universität zu Köln, V 2
1.1 KPH

IKP-98-4-010
Sistemich K.
Oberseminar Kernphysik
Universität zu Köln, S 2
1.1 KPH

IKP-98-4-009
Speth J.
Quantentheorie I
Universität Bonn, V 4, Ü 4
1.1 KPH

SS 98

IKP-98-4-001
Baur G.
Kosmologie und allgemeine Relativitätstheorie
Universität Basel, V 1
1.1 KPH

IKP-98-4-002
Filges, D.
Ausgewählte Kapitel des Strahlenschutzes
Universität Wuppertal, V 2
1.4 ESS

IKP-98-4-003
Krewald S.
Einführung in die Theorie der schwachen Wechselwirkung
Universität Bonn, V 4, Ü 2
1.1 KPH

IKP-98-4-004
Machner, H.
Kern- und Teilchenphysik
Universität Essen, V 4, S 2
1.1 KPH

IKP-98-4-005
Meißner Ulf-G.
Relativistische Quantenmechanik und Vielteilchentheorie
Universität Bonn, V 4, Ü 4
1.1 KPH

IKP-98-4-006
Sistemich K.
Physik für Naturwissenschaftler
Universität zu Köln, V 2
1.1 KPH

IKP-98-4-007
Speth J.
Relativistische Quantenmechanik und Vielteilchentheorie
Universität Bonn, V 4, Ü 4
1.1 KPH

IKP-98-4-008
Ströher, H.
Physik I
Universität zu Köln, V6, Ü 2
1.1 KPH

IKP-98-4-009
Ströher, H.
Oberseminar über Kernphysik
Universität zu Köln, S 2
1.1 KPH

WS 98/99

IKP-98-4-001
Baur G.
Allgemeine Relativitätstheorie, schwarze Löcher und
relativistische Astrophysik
Universität Basel, V1
1.1 KPH

IKP-98-4-002
Borchert G. L.
Oberseminar Kernphysik
Universität zu Köln, S 2
1.1 KPH

IKP-98-4-003
Dietrich J.
Kompaktkurs Beschleunigerphysik
Institut für Kern- und Teilchenphysik
Technische Universität Dresden
1.1 KPH

IKP-98-4-004
Filges D.
Physik III, Kernphysik, Thermodynamik
Universität Wuppertal, V 2, U 2
1.1 KPH, 1.4 ESS

IKP-98-4-005
Krewald S.
Klassische Mechanik und Elektrodynamik für Lehramtsstudierende
Universität Bonn, V 4, Ü 2
1.1 KPH

IKP-98-4-006
Meißner Ulf-G.
Angewandte Quantenfeldtheorie
Universität Bonn, V 4, Ü 4
1.1 KPH

IKP-98-4-007
Sistemich K.
Oberseminar Kernphysik
Universität zu Köln, S 2
1.1 KPH

IKP-98-4-008
Speth J.
Angewandte Quantenfeldtheorie
Universität Bonn, V 4, Ü 4
1.1 KPH

XI. INDEX OF AUTHORS

Forschungszentrum Jülich

Jül-3640
February 1999
ISSN 0944-2952